

Physicochemical
Problems
of Mineral Processing
38 (2004)

Instructions for preparation of manuscripts

It is recommended that the following guidelines be followed by the authors of the manuscripts:

- Original papers dealing with the principles of mineral processing and papers on technological aspects of mineral processing will be published in the journal which appears once a year.
- The manuscript should be sent to the Editor for reviewing before February 15 each year.
- The manuscript should be written in English. For publishing in other languages an approval of the editor is necessary.
- Contributors whose first language is not the language of the manuscript are urged to have their manuscript competently edited prior to submission.
- The manuscript should not exceed 10 pages.
- Two copies of the manuscript along with an electronic version should be submitted for publication before April 15.
- There is a 80 USD fee for printing the paper. No fee is required for the authors participating in the Annual Symposium on Physicochemical Problems on Mineral Processing.
- Manuscripts and all correspondence regarding the symposium and journal should be sent to the editor.

Address of the Editorial Office

Wrocław University of Technology
Wybrzeże Wyspiańskiego 27, 50-370 Wrocław, Poland
Institute of Mining Engineering
Laboratory of Mineral Processing

Location of the Editorial Office:

Pl. Teatralny 2, Wrocław, Poland
Phone: (071) 320 68 79, (071) 320-68-78
Fax: 3448123

andrew@ig.pwr.wroc.pl

jan.drzymala@pwr.wroc.pl

<http://www.ig.pwr.wroc.pl/minproc>

Physicochemical
Problems
of Mineral Processing
38 (2004)

Z. SADOWSKI
(EDITOR)

www.ig.pwr.wroc.pl/minproc

WROCLAW 2004

Editors of the journal

Zygmunt Sadowski, Jan Drzymala, Andrzej Łuszczkiewicz

Editorial Board

Zofia Blaschke, Wiesław Blaschke, Marian Brożek, Stanisław Chibowski,
Witold Charewicz, Tomasz Chmielewski, Beata Cwalina, Janusz Girczys,
Andrzej Heim, Jan Hupka, Andrzej Krysztafkiewicz, Janusz Laskowski,
Janusz Lekki, Kazimierz Małysa, Paweł Nowak,
Andrzej Pomianowski (honorary chairman), Stanisława Sanak-Rydlewska,
Jerzy Sablik, Jan Szymanowski, Kazimierz Sztaba (chairman)

Reviewers

RM. Brożek, W. Blaschke, W. Charewicz, J. Drzymala, A. Heim, A. Krysztafkiewicz,
J.S. Laskowski, A. Lutyński, A. Łuszczkiewicz, P. Nowak, M. Sachambiński,
Z. Sadowski, A. Skłodowska, J. Szymanowski, W. Walkowiak

Technical assistance

Stefan Zawadzki

The papers published in *Physicochemical Problems of Mineral Processing* are abstracted
in *Chemical Abstracts*, *Metals Abstracts*, *Реферативный Журнал* and other sources

Wydanie publikacji dofinansował
Komitet Badań Naukowych

ISSN 0137-1282

OFICyna WYDAWNICZA POLITECHNIKI WROCLAWSKIEJ, WYBRZEŻE WYSPIAŃSKIEGO 27,
50-370 WROCLAW, POLAND

In honor of Professor Janusz S. Laskowski on the 40th Anniversary of the Physicochemical Problems of Mineral Processing	5
J.S. Laskowski, Testing flotation frothers	13
M.E. Holuszko, J.S. Laskowski, Use of pelletization to assess the effect of particle-particle interactions on coal handleability.....	23
M.T. Spyridopoulos, S.J.R. Simons, S.J. Neethling, J.J. Cilliers, Effect of humic substances and particles on bubble coalescence and foam stability in relation to dissolved air flotation processes	37
J. Drzymala, H. Ahmed, Effect of flotation procedure and composition of reagents on yield of difficult-to-float coal	53
V.A. Chanturiya, W.E. Vigdergauz, L.M. Savkissova, A.I. Dorofeev, The hydrophilic-hydrophobic transitions on chalcopyrite; electrochemical study.....	65
Z. Ekmekçi, A. Aslam, H. Hassoy, Effect of EDTA on selective flotation of sulphide minerals	79
L. Ergün, Z. Ekmekçi, Ö. Gülsoy, H. Benzer, The evolution of copper flotation plant performance by plant survey and laboratory tests.....	95
B. Beklioglu, A.I. Arol, Selective flocculation behavior of chromite and serpentinite.....	103
L. Gotfryd, J. Szymanowski, Recovery of zinc(II) from acidic sulfate solutions. Simulation of counter-current extraction-stripping process	113
M. Rozenblat, M. Regel-Rosocka, J. Szymanowski, Metal removal from spent pickling solutions of high zinc(II) concentration	121
M. Ulewicz, C. Kozłowski, W. Walkowiak, Removal Zn(II), Cd(II) and Cu(II) ions by polymer inclusion membrane with side-armed diphosphaza-16-crown-6ethers.....	131
P. Maciejewski, W. Walkowiak, Selective removal of cesium(I), strontium(II) and barium(II) cations with proton-ionizable lariat ethers in the ion flotation process.....	139
A. Heim, T.P. Olejnik, A. Pawlak, The effect of the number of contact points between grinding elements on the rate of grinding in ball mills.....	147
A. Heim, R. Kazimierczak, A. Obraniak, The effect of equipment and process parameters on torque during disk granulation of bentonite.....	157
A. Heim, T. Gluba, A. Obraniak, Bed dynamics during drum granulation	167
T. Gluba, A. Obraniak, E. Gawot-Młynarczyk, The effect of granulation conditions on bulk density of a product	177
L. Domka, M. Kozak, Tribochemically activated natural chalk as a filler for plasto- and elastomers	187
F. Ciesielczyk, A. Krysztafkiewicz, T. Jesionowski, Influence of precipitation parameters on physicochemical properties of magnesium silicates	197
K.St. Sztaba, Influence of grain size upon its falling velocity	207

A.S. Erdem, S.L. Ergün, A.H. Benzer, Calculation of the power draw of dry multi-compartment ball mills	221
L. Ergün, Z. Ekmekçi, Ö. Gülsoy, H. Benzer, Modeling and simulation of the grinding circuit in Madneuli copper concentrator	231
Ö. Genç, L. Ergün, H. Benzer, Single particle impact breakage characterization of materials by drop weight testing	241
P. Wodziński, Crude ore screening in copper industry	257
J. Farbiszewska-Kiczma, T. Farbiszewska, M. Bąk, Bioleaching of metals from Polish black shale in neutral medium	273
M. Pacholewska, Bioleaching of galena flotation concentrate.....	281
A. Uryga Z. Sadowski. A. Grotowski, Bioleaching of cobalt from mineral products	291
Ö.Y. Gülsoy, E.C. Orhan, Importance of magnet-steel configuration in dry high intensity permanent magnetic rolls: Theoretical and practical approach	301
M.H. Khedr, Effect of firing temperature and compacting pressure on the magnetic and electrical properties of nickel-ferrite	311
Z. Özdemir, G. Özbayoğlu, M. Kizilyalli, A. Yilmaz, Synthesis and characterization of lithium tetraborate	321
A. Muszer, Mineralogical characteristics of metallurgical dust in the vicinity of Glogow.....	329
T. Chrzan, Influence of mineral composition of melaphyre grits on durability of roadway surface	341
I. Polowczyk, Z. Sadowski, Effect of polymer-surfactant interaction onto the spherical agglomeration	351



**In honor of Professor Janusz S. Laskowski
on the 40th Anniversary
of the Physicochemical Problems of Mineral Processing**

Although officially the first Symposium took place on 18th of February of 1966, the truly first Symposium was held two years earlier in 1964 [see Wspomnienie, *Physicochemical Problems of Mineral Processing*, No. 27, pp. 9-11 (1993)]. The year 2004 thus marks the 40th anniversary of the Symposia, and it coincides with 45th anniversary of Professor Laskowski's scientific activities. It is the 20th year of publication of *Coal Preparation* international journal which was founded by Professor Laskowski. This year, he and his wife Barbara celebrated 40 years of

marriage. With all these facts in mind the Organizing Committee is pleased to announce that this 41st Symposium in the series Physicochemical Problems in Mineral Processing, which deals with all aspects of mineral processing and is the longest symposia series in Poland and probably in the Central and Eastern Europe, has been dedicated to Professor Janusz Laskowski.

Janusz Laskowski graduated B.Sc. in chemistry from the Silesian University of Technology in 1956, and obtained M.Sc. degree in chemical engineering in 1958. Following his father's advise who kept saying that "colloid chemistry is a future of mineral processing" he decided eventually that surface chemistry was what he wanted to go into more deeply. He had a good fortune to hear Academician Peter Aleksandrovich Rehbinder's lectures on colloid chemistry when he ended up as a postgraduate student at the Lomonosov University in Moscow in 1961/62. Peter Aleksandrovich quickly learned that his student from Poland was spending a lot of time in libraries studying everything that Rehbinder had ever published on wettability and he arranged a special program for his student with the experimental work carried out under the supervision of Professor V.I. Klassen at the Mining Institute of the USSR Academy of Sciences. Having forged a strong bond with Klassen, Janusz translated his monograph on "*Coal Flotation*" (the book was published in Poland by Slask in 1966). Under Professor Klassen's guidance he started working on his dissertation on *Coal Salt Flotation* which was defended at the Silesian University of Technology, Gliwice, in 1963. He completed his thesis of Habilitation in 1966. In 1967, Janusz Laskowski left Gliwice for a one-year postdoctoral period as a Leverhulme Trust Postdoctoral Research Fellow in Dr. J.A. Kitchener's surface chemistry lab in the Department of Mining & Mineral Technology, Imperial College, London. This, we think, explains pretty well the dedication in Professor Janusz Laskowski's recent monograph on *Coal Flotation and Fine Coal Utilization* (Elsevier, 2001) to my professors: Tadeusz Laskowski, Villi Ivanovich Klassen and Joseph A. Kitchener".

All good things must come to an end and not all of Janusz and Barbara's life has been roses. In 1971 their daughter died at the age of 4 years. But suddenly during this devastating period Professor Laskowski received an invitation from Professors Jorge Goldfarb and Carlos Diaz to join Universidad de Chile as a visiting professor. Warm welcome by Goldfarb's team of young enthusiasts, beauty and splendid climate of Chile, excellent wines, and a son, Kornel, brought back from Chile, played a decisive role in the long recovery process. Chile became a second motherland for Professor Laskowski and he has been maintaining up to now his contacts with this country and visits it quite frequently. Invited by Professor Jan Leja, on his return from Chile in 1972 he stopped over for a few

lectures at the University of British Columbia in Vancouver, the city which ten years later became his home.

In addition to building up active research groups first at the Silesian University of Technology and later at the Wrocław Technical University, he made a number of other important contributions. After launching the “*Physico-Chemical Problems of Mineral Processing*”(www.ig.pwr.wroc.pl/minproc/journal/) symposia (he was chairing the Organizing Committee until 1980) he kept putting together every year a proceedings volume (the first number of *Physicochemical Problems of Mineral Processing* appeared in Gliwice in 1967). In 1964, in collaboration with Dr. Bortel and Dr. Buntner he wrote a textbook on *Physicochemical Principles and Technology of Flotation* published by the Silesian University of Technology in 1964. In 1969, published his book on *Physical Chemistry in Mineral Processing*, Slask, 1969.

In Chile, he used this book to teach surface chemistry courses at Universidad de Chile in Santiago, and at Universidad de Concepcion where was invited by Dr. Fernando Concha. Following Professor Concha’s suggestion he updated his book which was then translated into Spanish and published by University of Concepcion in 1974 (*Fundamentos Physicoquimicos de Mineralurgia*). For many years he was a member of Mineral Processing Section of the Mining Committee of Polish Academy of Sciences, and Committee of Physical Chemistry of Surfaces. Since 1970, Professor Laskowski was a member of the International Committee for International Mineral Processing Congresses, chaired the 13th International Mineral Processing Congress in Warsaw in 1979 and edited the two-volume proceedings (*Mineral Processing – Proc. 13th Int. Mineral Processing Congress*, Elsevier, 1980) and three volumes of the round-table seminars.

The 13th International Mineral Processing Congress turned out to be a very important event for the Laskowski’s family. Directly after the 13th Congress Janusz Laskowski was invited by Professor Tom Meloy to attend his Engineering Foundation Conference, and invited by Professor Douglas Fuerstenau he joined University of Berkeley as a visiting professor. Because of the martial law in Poland he postponed his return to the homeland, in 1982 joined the University of British Columbia as a full professor of mineral processing, and settled in Vancouver with his wife Barbara and two sons Kornel (9 years) and Cyprian (3 years). His Vancouver career has been interspersed with several sabbatical leaves: with Prof. Jean Cases’s Surface Chemistry Group at Ecole Nationale Superieure de Geologie, Nancy, France in 1987/88, and with the Department of Chemical Engineering of the University of Cape Town in 1996.

On becoming a faculty member at UBC, Professor Laskowski entered a dynamic situation at the Department of Mining and Mineral Processing which with Professors Jan Leja, Andrew Mular and George Poling was one of the world

leading centers in the area of mineral processing. Professor Laskowski took over and totally revised teaching of the 3rd year flotation course making colloid chemistry fundamentals of an integral part of it. The new course included not only sulfide flotation as before, but also flotation of oxidized Cu-Zn-Pb ores, flotation of phosphates, and extremely important in western Canada potash ore flotation and coal flotation. He introduced a new elective courses “Coal Preparation” and “Surface Properties” and also a graduate course “Fine Particle Processing”. And then, again, he began the process of building from scratch his new research group. Several post-docs and visiting scholars participated in this process: Dr. Jaime Solari (from Chile, Ph.D. from Imperial College) Professor Sergio Castro from University of Concepcion (Chile), Dr. Suzan Partridge (Ph.D. from Bristol University), Dr. Qi Dai (Ph.D. from Tohoku University, Japan), Dr. S. Subramanian (from Indian Institute of Science), Dr. Qun Wang (Ph.D. from the Helsinki University of Technology), Dr. Alexander Lopez-Valdivieso (professor from Universidad Autonoma de San Luis Potosi, Mexico; Ph.D. from the University of Berkeley), Dr. Qi Liu (who obtained Ph.D. working under Professor Laskowski at UBC and after spending 5 years with the University of Wuhan, China, returned to Canada as a visiting scholar), Dr. Ana B. Garcia (from Instituto Nacional del Carbon, Oviedo, Spain), Dr. Agnieszka Sworska (from the University of Maria-Curie Sklodowska, Poland), Dr. Simon Yuan (Ph.D. from Lulea University of Technology), Dr. Feridun Boylu from Istanbul Technical University.

Professor Laskowski became a very active member of SME and since 1982 presented his papers at all SME Annual Meetings and organized and chaired many sessions. He served as a member of the SME Mineral Processing Fundamentals Committee and also chaired it. In Canada he became a very active member of the Metallurgical Society of Canadian Institute of Mining. In 1995, initiated a new series of UBC-McGill international symposia on Fundamentals of Mineral Processing and chaired the first Symposium on “Processing of Hydrophobic Minerals and Fine Coal”, Vancouver, August 1995; jointly with George Poling he edited the proceedings volume “*Processing of Hydrophobic Minerals and Fine Coal*” published by CIM Metallurgical Society in 1995. He chaired the 3rd Symposium on “*Polymers in Mineral Processing*”, Quebec City, 1999, and edited the proceedings volume which appeared under the same title. This year he is organizing and editing proceedings volume of the 5th UBC-McGill Int. Symposium on “*Particle Sized Enlargement in Mineral Processing*” (it will take place in Hamilton, Ontario, August 22-25, 2004). Over the last four years he chaired the Mineral Sciences and Engineering Section of the Metallurgical Society of CIM.

When J.A. Kitchener retired Janusz Laskowski jointly with John Ralston put together a special volume which appeared in 1992 under J.S. Laskowski and J. Ralston's editorship ("*Colloid Chemistry in Mineral Processing*", Elsevier, 1992). When Professor Jan Leja retired after 20 years with the University of British Columbia, Professor Laskowski edited a volume "*Frothing in Flotation*" in his honor (published by Gordon and Breach in 1989). This book was followed by "*Frothing in Flotation II*", edited jointly with E.T. Woodburn and published by Gordon and Breach in 1998. "*Frothing in Flotation III*", edited jointly with C.T. O'Connor and J.P. Franzidis, appeared as a special issue of International Journal of Mineral Processing, Vol. 64, Nos. 2-3 (2002).

Professor Laskowski jointly with Professor David Boger organized the Engineering Foundation Conference on "*Rheology in the Mineral Industry*", San Diego, February, 1997. The papers presented at this conference appeared in a special issue of Mineral Processing and Extractive Metallurgy Review (Vol. 20, Nos. 1-3, 1999), edited by D.V. Boger and J.S. Laskowski, and in a special issue of Coal Preparation (Vol. 18, Nos. 3-4, 1997) edited by J.S. Laskowski and H. Usui. This conference was followed by the 2nd Engineering Foundation Conference on "*Rheology in the Mineral Industry*", Hawaii, March, 1999, which he co-chaired.

In 1984, Professor Laskowski founded "*Coal Preparation*" international journal and has been its editor-in-chief since. Over years, he was a dedicated member of the Editorial Boards of several scientific journals (Minerals Science and Engineering, Colloids and Surfaces, Mineral Processing and Extractive Metallurgy Review, International Journal of Mineral Processing).

With Dr. J. Drelich (Michigan University of Technology) he co-chaired the Symposium "Apparent and Microscopic Contact Angles" held in conjunction with the 216th National American Chemical Society Meeting, Boston, August 24-27, 1998. Jointly with J. Drelich and K.J. Mittal he edited the volume "*Apparent and Microscopic Contact Angles*" published by VSP in 2000.

Since translating Klassen's monograph on Coal Flotation from Russian into Polish (in 1966) Professor Laskowski was collecting data for his own monograph on the subject which in comparison with Klassen's monograph was much enlarged and also includes fine coal utilization. The book appeared in 2001 ("*Coal Flotation and Fine Coal Utilization*", Elsevier in 2001).

In 2001, Professor Laskowski officially retired from University of British Columbia and we have noticed that now it is much more difficult to catch him in Vancouver. He developed a strong collaboration with Department of Chemical Engineering of the University of Cape Town (UCT website lists him as a visiting professor), and with the Helsinki University of Technology, and he maintains a very active group of graduate students at UBC. In all, he supervised: 10 Ph.D.

Theses in Poland, 1 Ph.D. Thesis and 1 M.Sc Thesis in Chile, 7 Ph.D. Theses and 5 M.A.Sc. Theses in Canada, and recently 1 M.Sc. Thesis in Argentina (Universidad Nacional de San Juan). We have learned that over the last few years Professor has been teaching many short-courses:

- *Use of Polymers in Mineral Processing*, Universidad Autonoma de San Luis Potosi, Mexico, May, 2004.
- *Use of Polymers in Mineral Processing*, University of Concepcion, Chile, December, 2003.
- *Coal Flotation and Fine Coal Utilization*, Mintek, Johannesburg, South Africa, November, 2003.
- *Use of Polymers in Mineral Processing*, Mintek, Johannesburg, South Africa, November, 2003.
- *Use of Polymers in Mineral Processing*, University of Cape Town, South Africa, October, 2003.
- *Surface Chemistry*, Helsinki University of Technology, Finland, May, 2003.
- *Surface Chemistry*, Helsinki University of Technology, Finland, May, 2002.
- *Flotation Fundamentals*, Saskatchewan Potash Corporation, Saskatoon, Canada, March 4-5, 2002.
- *Frothers and Their Use in Flotation*, Florida Institute of Phosphate Research, Lakeland, Florida, USA, August 9, 2001.
- *The Use of Polymers in Mineral Processing*, Outokumpu, Finland, September, 1999.
- *Coal Flotation: Fundamentals and Engineering*, Sparwood, B.C., Canada, April 3-4, 1997.

Professor Laskowski has published more than 200 papers in refereed journals and conference proceedings based on research conducted in Poland, Russia, Chile, USA, Canada, South Africa and Finland. Since the 10th International Mineral Processing Congress in 1973, Professor Laskowski has presented papers at all International Mineral Processing Congresses (with the exception of the 14th IMPC in 1982). Since the 10th International Coal Preparation Congress in Edmonton in 1986 he has presented papers at all Coal Preparation Congresses. Below we list some of his significant findings:

- improvement of froth flotation in the presence of salt results from collapsing of hydration layer shielding coal particles and nucleation of microbubbles on coal surface in concentrated salt solutions (various papers between 1962 and 2001)
- instability of water films of a certain thickness on hydrophobic solids is fundamentally due to a deficiency of hydrogen bonding in these films compared with liquid water (J.S. Laskowski and J.A. Kitchener, *The hydrophilic hydrophobic transition on silica*, *J. Coll. Interface Sci.*, 29 (1969), p.670. By some, this paper is considered “one of the most elegant

demonstrations of the inadequacy of the DLVO theory” (R.M. Pashley, in *Colloid Chemistry in Mineral Processing*, Elsevier, 1992, p.104).

- with Bern Klein developed a viscometer for studying unstable non-Newtonian suspensions (B. Klein, J.S. Laskowski and S.J. Partridge, *A New Viscometer for Rheological Measurements on Settling Suspensions*, *Journal of Rheology*, 39 (1995) p. 827) and using this equipment established with Y.B. The relationship between magnetite particle size distribution, and stability and rheology of magnetite aqueous suspensions, and the effect of rheological properties of such a system on separation efficiency of dense medium separators (R.Y. He and J.S. Laskowski, *Dense Medium Cyclone Separation of Fine Particles – Parts I and II*, *Coal Preparation*, 16 (1995) p. 1 and p. 27; and J.S. Laskowski, *Dense Medium Rheology and Its Effect on Dense Medium Separation*, *Advances in Gravity Concentration* (R.Q. Honaker and W.R. Forest, eds.), SME, 2003, pp. 55- 70).
- -in the 80’ he studied weak electrolyte type flotation collectors (e.g. fatty acids, primary amines) and described the properties of colloidal species that appear over given pH ranges in aqueous solutions containing such surfactants. These species exhibit clear iso-electric-points and depending on pH may either be positively or negatively charged. It was shown that the properties of the mineral systems with a weak electrolyte collector added cannot be explained without taking into account such species (S.H. Castro, R.M. Vurdela and J.S. Laskowski, *The Surface Association and Precipitation of Surfactant Species in Alkaline Dodecylamine Hydrochloride Solutions*, *Colloids and Surfaces*, 21 (1986) p. 87; J.S. Laskowski, *Weak Electrolyte Collectors*, *Advances in Flotation Technology* (B.K. Parekh and J.D. Miller, eds.), SME, 1999, pp. 59-82. By the way, for the latter work Professor Laskowski won the Arthur F. Taggart Award of SME in 2000.
- in the second half of the 1980’ initiated with Qi Liu, who was at that time his Ph.D. student, fundamental studies on the mechanism of adsorption of polysaccharides (dextrins) onto mineral surfaces. The postulated mechanism, which involves a chemical in nature interaction between OH groups on mineral surfaces and OH groups in glucose ring, has been confirmed by other researchers and may eventually lead to the development of non-toxic modifiers for flotation of polymetallic sulfide ores (Q. Liu and J.S. Laskowski, *The Role of Metal Hydroxides at Mineral Surfaces in Dextrin Adsorption – Parts I and II*, *Int. Journal of Mineral Processing*, 26(1989) p. 297; 27 (1989) p. 147; *Journal of Colloid and Interf. Sci.*, 130 (1989) p.101 and subsequent papers with G. Nyamekye, and with M. Subramanian).

- over the last five years in search for more scientific roots he has returned to the studies on the properties of flotation frothers carried out in the 70' with Janusz Lekki, and with Sam Cho introduced the concept of the critical coalescence concentration (CCC), described the correlation between CCC and DFI (Dynamic Foamability Index) (Y. S. Cho and J.S. Laskowski, Effect of Flotation Frothers on Bubble Size and Foam Stability, Int. J. Miner. Process, 64 (2002) p.69) and showed how these indices can be used to classify the flotation frothers (J.S. Laskowski, Fundamental Properties of Flotation Frothers, 22nd Int. Mineral Processing Congress, Cape Town, 2003, Vol. 2, pp. 788-797).

Janusz Laskowski's interests extend far beyond his professional life; he is an expert camper and hiker, good skier, lake swimmer and keen tennis player. After many years of studying impressionists at many art galleries around the world, a few years ago he decided to start painting for relaxation. According to his own words "he works in oil". He has recently told us that this brought about an acclamation of his neighbors and colleagues during the recent garden party in his house celebrating 40th Anniversary of his and Barbara marriage. The guests admired with interest the fresh painting of their house and on hearing that Janusz did it himself some commented that "this time this job was done much better than a few years ago", and some others were delighted that "Janusz finally found a well paid job".

More about Professor Laskowski and his accomplishments can be found at www.mining.ubc.ca/department/faculty/laskowski.

Andrzej Łuszczkiewicz
Jan Drzymala
Zygmunt Sadowski

Janusz S. LASKOWSKI*

TESTING FLOTATION FROTHERS

Received March 15, 2004; reviewed; accepted May 15, 2004

In practice, frothers are selected following general guidelines and verification by laboratory and/or plant tests. The terms “powerful” or “selective,” which are commonly used to characterize frothers, have intuitive rather than scientific meaning.

A research program has been set out to study fundamental properties of the flotation frothers and to identify the tests which can provide information needed to characterize and classify such flotation agents. Since flotation frothers are used to reduce bubble size and increase froth stability, in the procedures adopted in this paper they were characterized by their ability to reduce bubble size in a flotation cell and to increase foam stability. It has been shown that the developed frother classification system based on these two measurements is able to correctly distinguish the frothers known as being selective from those which are known to be powerful.

Key words: flotation frothers, dynamic foamability index, crystal coalescence concentration

INTRODUCTION

Froth flotation process commonly requires quite a large variety of flotation agents. Although it is believed that the most important are collectors, which are used to render valuable minerals hydrophobic, as the term froth flotation implies the process is inseparable from the froth. Froth generation requires the use of frothers which are utilized to facilitate air dispersion into fine bubbles, and to stabilize the froth. According to Leja-Schulman's penetration theory (Leja & Schulman, 1954; Leja, 1956/57), frothers accumulate preferentially at the water/gas interface and interact with collector molecules adsorbed onto solid particles in the particle-to-bubble collision and attachment.

The difficulties inherent in giving a comprehensive scientific analysis of flotation frothers were in depth analyzed by Wrobel 50 years ago (Wrobel, 1953). The situation

* Department of Mining Engineering, University of British Columbia, Vancouver, B.C., Canada,
JSL@apsc.ubc.ca.

50 years later is not that different and the terms “powerful” and “selective” are still commonly used to describe the properties of these flotation agents. The frothers that are purchased for commercial use usually come along with the information exemplified by Table 1.

Table I. Flotation Frother Characteristics as Provided by Manufacturers

Property	Frother 1	Frother 2	Frother 3
Molecular weight	200	250	400
Viscosity, cP	7	12	27
Density, g/cm ³	0.970	0.980	0.988
Freez point, °C	below -50	below -50	below -50
Flashpoint, °F	250	285	325

°F stands for Fahrenheit degrees.

While the information provided in Table I is important for handling these products it does not say anything about their flotation properties. Some manufacturers, therefore, provide some additional qualitative information in which these products may be further characterized as “selective” or “powerful”. So, what we - who have to use these products - do? Well, we develop a research program and screen the acquired products following some general guidelines which may vary depending on the school.

In the fundamental studies on flotation frothers there are many unknowns, and one known fact. It is well accepted that pure liquids do not foam. For a liquid to foam, it must be able to form a membrane around the gas bubble that opposes the thinning of the lamellae. Foaming does not occur in pure liquids because there exists no such mechanism for the retardation of lamellae drainage (Kitchener & Cooper, 1959). When surface active molecules are present, however, their adsorption at the gas/liquid interface serves to retard the loss of liquid from the lamellae and to produce a more mechanically stable system. This directly leads to a simple conclusion that relates frother activity to its surface tension. However, in the concentration ranges in which frothers affect foaming and bubble size the water surface tension is affected very little (Sweet et al., 1997). Recent results prove without any doubt that frothers control the size of bubbles by decreasing bubble coalescence (Cho & Laskowski, 2002a; Cho & Laskowski, 2002b), and that the bubble coalescence can be entirely prevented at frother concentrations exceeding the critical coalescence concentration (CCC).

The testing procedure described in this paper is based on the fundamental and well recognized fact that flotation frothers reduce the bubble size. Likewise, they are known to increase foam stability. These two measurements should then be employed to characterize fundamental flotation related properties of these agents.

EXPERIMENTAL PROCEDURES

MATERIALS

Since MIBC is the most common frother, the first series of tests included various n-hexanol isomers/derivatives (Cho and Laskowski, 2002a; Cho and Laskowski, 2002b). In the second series, the mono-alkyl ethers of propylene oxide, which include three important commercial frothers (DF-200, DF-250 and DF-1012) have been tested (Laskowski et al., 2003). The studied frothers are listed in Table II.

Table II. List of the tested frothers

Common name	Purity	Chemical formula	Molecular weight	HLB
MIBC	Technical	CH ₃ CHCH ₃ CH(OH)CH ₃	102.2	6.1
HEX	Reagent	C ₆ H ₁₃ OH	102.2	6.0
DEMPH	Technical	C ₆ H ₁₃ OH(EO) ₂ (PO)	248.4	6.6
DEH	Technical	C ₆ H ₁₃ OH(EO) ₂	190.3	6.7
MPDEH	Technical	C ₆ H ₁₃ OH(PO)EO ₂	248.4	6.6
(PO)1	Reagent	CH ₃ (PO)OH	90.12	8.3
(PO)2	Reagent	CH ₃ (PO) ₂ OH	148.12	8.15
DF-200	Technical	CH ₃ (PO) ₃ OH	206.29	8.0
DF-250	Technical	CH ₃ (PO) ₄ OH	264.37	7.8
DF-1012	Technical	CH ₃ (PO) _{6.3} OH	397.95	7.5

EO and PO are abbreviations for -OC₂H₄- and -OC₃H₆-, respectively.

BUBBLE SIZE

Quite a large variety of experimental methods have been introduced to measure the size of bubbles (Chen et al, 2001; Grau and Heiskanen, 2002). The bubble sizer developed at the University of Cape Town (O'Connor et al., 1990, Tucker et al., 1994), referred to as UCT bubble sizer, has been used in our measurements (Cho and Laskowski, 2002a; Cho and Laskowski, 2002b). Bubbles were generated in an Open Top Leeds Flotation Cell set at 1000 rpm and at air flow rate of about 5 dm³/min. The sampler of the UCT bubble sizer was positioned 50 mm above the stator. Distilled water was used to prepare solutions of the tested frothers.

DYNAMIC FOAMABILITY INDEX

The procedure that has been used follows the methodology developed by Malysa and his colleagues (Malysa et al., 1978; Czarnecki et al., 1982). This method requires determination of the retention time (rt) from the slope of the linear portion of the dependence of the total gas volume (V) contained in the system (solution and foam) plotted versus gas flow rate (Q).

$$rt = \frac{\Delta V}{\Delta Q} \quad (1)$$

The obtained rt values are then used to determine the DFI which is defined as the limiting slope of the rt -concentration plot for $c \rightarrow 0$:

$$DFI = \left(\frac{\partial rt}{\partial c} \right)_{c=0} \quad (2)$$

SURFACE TENSION

Du Noy Ring Tensiometer was used to measure the surface tension of aqueous solutions at varying frother concentrations.

RESULTS

Figs. 1 and 2 show the bubble size versus concentration curves plotted for polyglycol frothers and MIBC. The figures also indicate the critical coalescence concentration (CCC) determined graphically from the plots. At concentrations $c > CCC$, the bubbles cease to coalesce, the size of bubbles becomes constant and is not affected by frother concentration any more. The CCC values for the studied polyglycols are given in Table III. By normalizing frother concentration with regard to the CCC values for each frother it can easily be shown that all the curves converge on one single curve (Fig. 3).

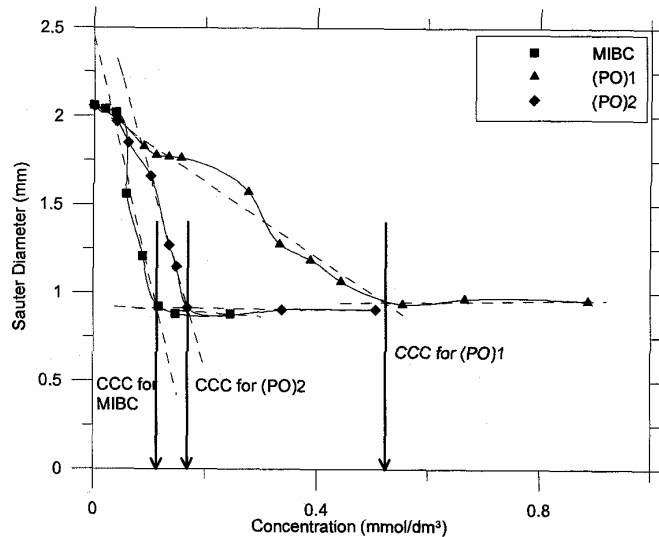


Fig. 1. Graphical evaluation on the CCC values for MIBC, (PO)1 and (PO)2

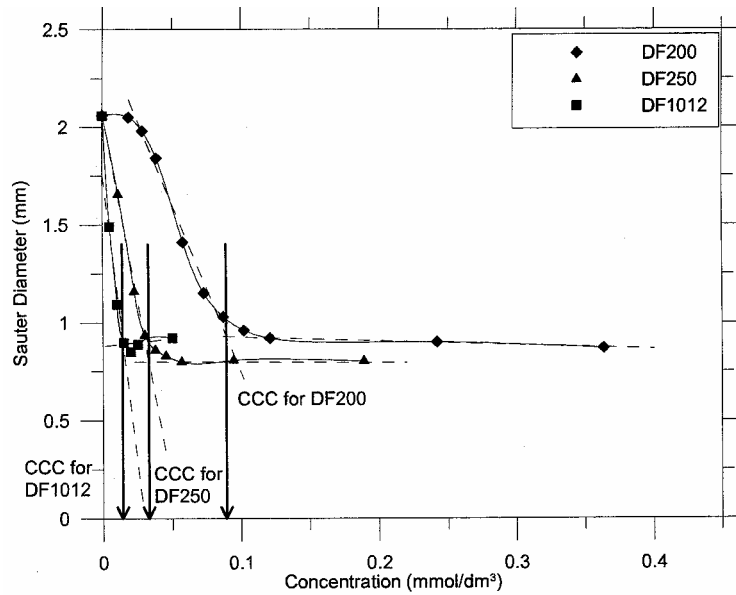


Fig. 2. Graphical evaluation on the CCC values for Dowfroths

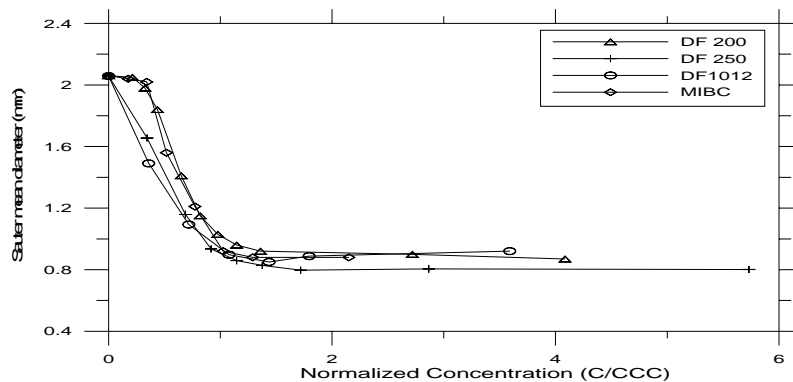


Fig. 3. Effect of the normalized concentration on bubble size

The obtained results indicate that with the increasing number of propylene oxide groups per molecule in the homologous series of polyglycol frothers, the ability of these compounds to reduce the bubble size improves (Laskowski et al. 2003). The frothers that produce finer bubbles also produce more stable dynamic foams as the correlation between DFI and CCC values suggest (Fig. 4.). This figure confirms that the frothers that are more efficient in reducing bubble size also produce more stable foam. Larger DFI values indicate more stable foam, the foam in which bubbles do not easily coalesce.

As already discussed (Laskowski, 2003), the DFI-CCC diagram (Fig. 4) can be used to classify frothers. Those situated in the left-upper corner of this diagram are very powerful frothers, while the ones situated in the right-bottom corner are weaker and more selective.

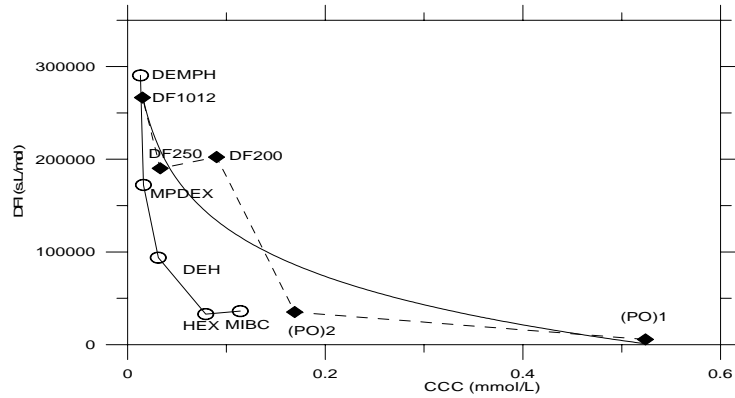


Fig. 4. Relationship between DFI and CCC values for the tested frothers

The results so far discussed have been obtained while working with two-phase systems (foams). It is still not clear how all this is related to the flotation performance of the frothers. To analyse it further, in my paper presented at the 22nd Int. Mineral Processing Congress (Laskowski, 2003) I compared Fig. 4 with Fig. 5.

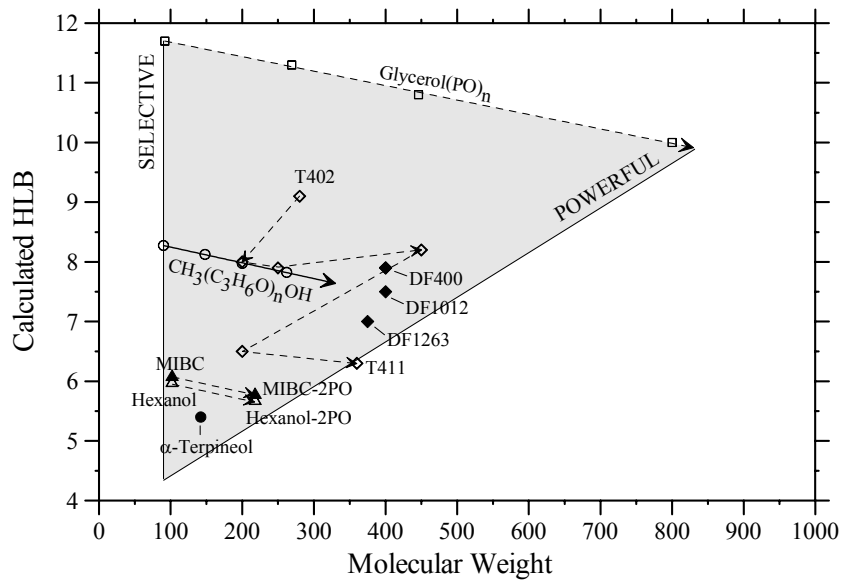


Fig. 5. The HLB-Molecular Weight diagram for flotation frothers

In the latter diagram, various frothers are positioned on the HLB – Molecular Weight plot (HLB stands for Hydrophile Lipophile Balance). As seen the frothers which fall on the left side of this diagram are known to be selective in flotation, while the ones which are situated far to the right from this line are known to exhibit properties of the strong flotation frothers. The former can be used in flotation of very fine particles, whereas the latter will provide higher recoveries and better performance in floating of coarser particles. Comparison with Fig. 4 explains that those which are selective are characterized by small DFI and large CCC values, while the powerful frothers are characterized by large DFI and small CCC values.

DISCUSSION

The results shown in this paper demonstrate that flotation frothers can be well characterized by the CCC and DFI values. These indices are easy to determine experimentally and they should be provided by frother manufacturers along with other characteristics of such agents. It has also been demonstrated that CCC values can be used in preparing frother blends (Laskowski et al., 2003).

Table III. CCC values for the investigated frothers

Frother	CCC	
	mmol/dm ³	ppm
MIBC	0.11	11.2
(PO)1	0.52	46.8
(PO)2	0.17	25.1
DF-200	0.089	18.4
DF-250	0.033	8.7
DF-1012	0.015	6.0

While there is no doubt that the CCC and DFI numbers are very valuable in characterization of flotation frothers, our understanding of these values is still not complete. This is quite obvious when comparison is made with the common surface tension measurements. Fig. 6 shows the surface tension isotherms (room temperature) for three Dowfrothers.

Comparison of the surface tension results with the CCC values given in Table III indicates that while for the DF-200 the surface tension at the CCC concentration for this forther (8.9×10^{-5} M) is almost that of pure water, the surface tension for DF-250 at its CCC value (3.3×10^{-5} M) is about 66 mN/m and for the DF-1012 (CCC= 1.5×10^{-5} M) it is about 61 mN/m. Since surface tension values are interrelated with adsorption via Gibbs adsorption isotherm this means that the adsorption of DF-1012 at its CCC is much larger than the adsorption of DF-250 at the corresponding CCC values for DF--250; in turn the adsorption of DF-250 is much higher than the adsorption of DF-200 at

their respective CCC values. Since the DF-1012 molecules are much larger than the molecules of DF-250 (which in turn are larger than DF-200 molecules) this indicates that the adsorption for larger molecules of polyglycols must be much higher to prevent bubbles from coalescence.

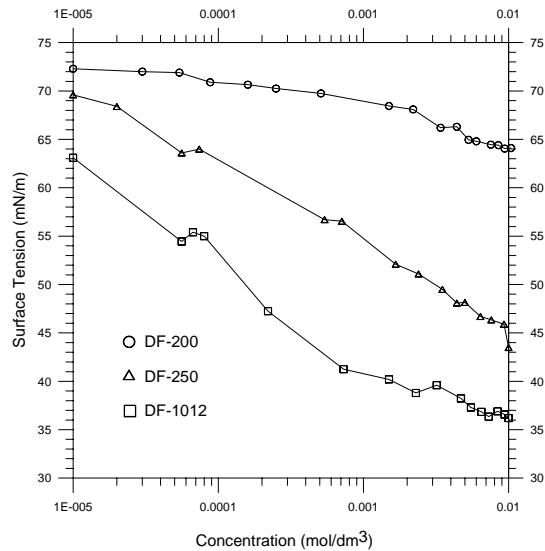


Fig. 6. Surface tension isotherms for DF-200, DF-250 and DF-1012 frothers

This is a very surprising result. It may as well indicate that the “static” surface tension measurements cannot be directly utilized in the analysis of the properties of dynamic systems, such as foams. These foams are very unstable, exist only during bubbling gas and collapse when the foam formation process is stopped. It is likely that the stability of such systems is determined by elasticity forces (Malysa, 1992). Under dynamic conditions the coalescence must then be related not so much to the frother adsorption as to the rate with which it can adsorb (Comley et al, 2002).

CONCLUSIONS

1. Flotation frothers can be characterized by the DFI and CCC values.
2. The diagram in which the DFI values are plotted versus CCC values can be used to classify frothers. The frothers which are situated in the upper-left corner of the diagram are very powerful, while those situated in the bottom-right corner are selective.
3. The CCC and DFI values should be provided for all commercial frothers by frother manufacturers.

ACKNOWLEDGEMENTS

The author thanks Mr. Francisco Melo for the surface tension measurements.

REFERENCES

- CHEN, F., GOMEZ, C.O., FINCH, J.A., (2001), *Bubble Size Measurement in Flotation Machines*, Minerals Engineering, Vol. 14, pp. 427-432.
- CHO, Y.S., LASKOWSKI, J.S., (2002a), *Effect of Flotation Frothers on Bubble Size and Foam Stability*, Int. J. Min. Proc. Vol. 64, pp. 69-80.
- CHO, Y.S., LASKOWSKI, J.S., (2002b), *Bubble Coalescence and Its Effect on Bubble Size and Foam Stability*, Canadian J. Chem. Eng. Vol. 80, pp. 299-305.
- COMLEY B.A., HARRIS P.J., BRADSHAW D.J., HARRIS M.C., (2002), *Frother Characterization Using Dynamic Surface Tension Measurements*, Int. J. Min. Proc., Vol. 64, pp. 81-100.
- CZARNECKI J., MALYSA K., POMIANOWSKI A., (1982), *Dynamic Frothability Index*, J. Coll. Interf. Sci. Vol. 86, pp. 570-572.
- GRAU R.A., HEISKANEN K., (2002), *Visual Technique for Measuring Bubble Size in Flotation Machines*, Minerals Eng., Vol. 15, pp. 507-513.
- KITCHENER J.A., COOPER C.F., (1959), *Current Concepts in the Theory of Foaming*, Quarterly Reviews Vol. 123, pp. 71-95.
- LASKOWSKI J.S., (2003), *Fundamental Properties of Flotation Frothers*, Proc. 22nd Int. Mineral Processing Congress, Cape Town, Vol. 2, pp. 788-797.
- LASKOWSKI J.S., TLHONE T., WILLIAMS P., DING K., (2003), *Fundamental Properties of the Polyoxypropylene Alkyl Ether Flotation Frothers*, Int. J. Min. Proc., Vol. 72, pp. 289-299.
- LEJA J., SCHULMAN J.H., (1954), *Flotation Theory: Molecular Interactions between Frothers and Collectors at SolidLiquidAir Interfaces*, Trans. AIME Vol. 199, pp. 221-228.
- LEJA J., (1956/57), *Mechanism of Collector Adsorption and Dynamic Attachment of Particles to Air Bubbles as Derived from Surface Chemical Studies*, Trans. IMM Vol. 66, pp. 425-437.
- MALYSA K., (1992), *Wet Foams: Formation, Properties and Mechanism of Stability*, Advances in Coll. Interf. Sci. Vol. 40, pp. 37-83.
- MALYSA K., CZUBAK-PAWLIKOWSKA J., POMIANOWSKI A., (1978), *Frothing Properties of Solutions and Their Influence on the Floatability*, Proc. 7th Int. Congress Surface Active Substances, Moscow, Vol. 3, pp. 513-520.
- O'CONNOR C.T., RANDALL E.W., GOODALL C.M., (1989), *Measurement of the Effects of Physical and Chemical Variables on Bubbles Size*, Int. J. Min. Proc. Vol. 28, pp. 139-149.
- SWEET C., VAN HOOGSTRATEN J., HARRIS M., LASKOWSKI J.S., (1997), *The Effect of Frothers on Bubble Size and Frothability of Aqueous Solutions*, Processing of Complex Ores – Proceedings of the 2nd UBC-McGill Int. Symposium (J.A. Finch, S.R. Rao and I. Houbec, eds.), Metallurgical Society of CIM, Montreal, pp. 235-245.
- TUCKER J.P., DEGLON D.A., FRANZIDIS J.P., HARRIS M.C., O'CONNOR C.T., (1994), *An Evaluation of Direct Method of Bubble Size Distribution Measurements in a Laboratory Batch Flotation Cell*, Mineral Eng. Vol. 7, pp. 667-680.
- WROBEL S.A., (1953), *Flotation Frothers, Their Action, Properties and Structures*, Recent Developments in Mineral Dressing, IMM, London, pp. 431-450.

Laskowski J.S., *Testowanie flotacyjnych odczynników pianotwórczych*, Physicochemical Problems of Mineral Processing, 38, (2004) 13-22 (w jęz. ang.).

W praktyce odczynniki pianotwórcze (spieniacze) dobierane są zgodnie z ogólnymi zasadami i sprawdzone w testach laboratoryjnych oraz przemysłowych. Określenia takie jak: „mocne lub „selektywny” są powszechnie stosowane dla scharakteryzowania speniacza. Mają one znaczenie raczej intuicyjne niż naukowe. Został przyjęty program badawczy dla zbadania podstawowych właściwości odczynników pianotwórczych stosowanych w flotacji, oraz dla ustalenia testów, które dostarczą koniecznych informacji potrzebnych dla scharakteryzowania i klasyfikacji odczynników pianotwórczych. Odczynniki pianotwórcze stosowane są w celu redukcji rozmiarów pęcherzyków i wzrostu stabilności. Procedury, jakie użyto w tej pracy, były weryfikowane przez ich zdolność do charakteryzowania redukcji wielkości pęcherzyków w komorze flotacyjnej i wzrostu stabilności piany. Zostało pokazane, że system klasyfikacji speniaczy, bazujący na dwóch zaprojektowanych parametrach, jest w stanie poprawnie rozróżnić speniacze zwane jako „selektywne” od tych, które znane są jako „mocne”.

M.E. HOLUSZKO, J.S. LASKOWSKI*

USE OF PELLETIZATION TO ASSESS THE EFFECT OF PARTICLE-PARTICLE INTERACTIONS ON COAL HANDLEABILITY

Received May 10, 2004; reviewed; accepted June 25, 2004

Although there is no widely accepted rigorous definition of handleability, the handling coal characteristics often referred to as handleability define whether a coal has the ability to flow unhindered through the processing and transportation systems. The handleability may be severely affected if fine coal particles tend to aggregate. In the pelletization process, the rolling action of the drum is applied to bring the individual particles into proximity with each other so that they can aggregate and form pellets. Because of apparent similarities between these two processes, the pelletization tests are carried out in parallel to the handleability tests in this project, and the pelletization results are used to explain coal handleability properties.

Key words: coal, pelletization, handleability

INTRODUCTION

British Columbia produces nearly 30 million tonnes of coal annually. Almost all of the produced clean coal is exported outside of the province, and transported by trains across the continent for the use in the eastern Canada or United States, and to other overseas destinations by cargo ships. Coals produced from western Canada have large amounts of fines and high surface moisture at the point of load, which affect these coals handleability characteristics. The western Canadian coals are also very friable and the content of very fine particles continues to increase during transportation.

Many handleability studies carried out over the years mostly related physical parameters of coal samples such as amount of fines, mineral matter type and moisture content on handling characteristics. The quality of fines in terms of surface properties has never been studied before to any significant extend. Neither the porosity of coal has been considered as a factor influencing behavior of fine particles in the presence of water.

* Department of Mining Engineering, University of British Columbia Vancouver, B.C., V6T 1Z4, Canada
JSL@apsc.ubc.ca.

The objective of this research project is to study the effect of surface properties of fines with the special emphasis on wettability, surface properties such as surface area, pore volume and relating these factors to the handleability of bulk coal. Pelletization experiments have been used as a method of testing fine coal particle interactions. The pellet strength is used as an evidence of forces acting on these particles owed to their surface properties. The surface properties of fines are then related to the bulk sample behavior in handling of the selected western Canadian coals.

BACKGROUND

HANDLEABILITY OF COAL

A number of techniques have been developed over the years to assess handleability; for example using specially designed cone to measure the flow of coal and referred to as Durham Cone (Brown, 1997; Cutress et al., 1960; Vickers, 1982; Brown et al., 1997). Other methods focused on either measuring the shear strength of fines (Jenike, 1961; Arnold, 1992; Barois-Cazenave, 1999) or tensile strength of fines, as in the method developed in Poland (Polish norms, 1982; Wawrzynkiewicz, 2003). Extrusion through Index method that was developed by Brown at the University of Nottingham aimed at measuring compressive strength of the bulk sample (Brown, 1997; Brown, Atkin, 2000). The advantage of this method being that, it actually measures the strength of the representative sample of the handled material not only the strength of fines.

The study by (Blondin et al., 2000) showed that handleability is determined by the content of clays and fine particles and developed their own handleability classification system based on these two parameters. (Mikka, Smitham, 1985) showed that bentonite effect on fine coal handleability is much larger than the effect of kaolin.

FACTORS INFLUENCING HANDLEABILITY OF COAL

Factors that influence handleability of coal are: moisture, ash, size distribution and fines content. In general, as the moisture content of coal increases the handleability deteriorates until it reaches a point where coal is so moist that behaves as a fluid. The same trend is observed with increase in fines content, the high fines content leads to deterioration of handleability. It was found that increase in fines content has greater effect on coal handleability than increase in moisture content (Arnold, 1992).

An increasing amount of fines (<0.5mm) can have similar effect as raising moisture content. Widening the spectrum of sizes in bulk coal improves handleability; larger particles counteract moisture effects (Mikka, Smitham, 1985; Holuszko, Laskowski, 2003). It has been shown that the effect of moisture is greater in the case of fines (<0.5mm) than in case of coarse coal (Wawrzynkiewicz, 2003). Mineral matter content has the greatest effect on handleability when clays are present. Clays tend to swell in presence of water and act as glue between particles leading to buildup of cohesiveness within the fines as well as coarse particles.

PELLETIZATION

Pelletization is the particle-enlargement process, in which tumbling of moist fines in drums, discs or in conical devices leads to formation of pellets. Physical forces, such as interfacial attraction, surface tension, van der Waals interactions, combined with the applied mechanical energy of tumbling, that bring particles together are responsible for pelletization (Sastry et al., 1982).

In an extensive study on pelletization of coals of various ranks by (Sastry and Fuerstenau, 1982), the fundamental principles of coal pelletization have been formulated. It was concluded that moisture addition is critical for successful pelletization and lies in a narrow range for each coal and it varies inversely with the content of ash.

There are apparent similarities between behavior of fine particles in pelletization and in a free flow that determine handleability. In both processes coal particles are subjected to mechanical forces; therefore the same phenomena should be responsible for their behavior. Using pelletization as the model for particle aggregation, it can be assumed that in the system where coal particles are subjected to mechanical movement due to rotation (pelletization) or flowing (handleability), the particles collide with each other. As the moist particles encounter each other, the aggregation of particles may take place. The same surface properties which lead to aggregation in pelletization will cause particles to stick together and build up cohesive strength affecting handleability of a bulk sample. Therefore, pelletization can be used as the method to elucidate fine coal particle behavior that determine coal handleability.

EXPERIMENTAL

SAMPLE CHARACTERISTICS

Five raw and two coal products were used for this study. Three coals were of metallurgical grade (LC3, LC 10BC, LC 10B) and two of thermal grade; one lower rank coal (LS20) and one higher rank (LC 8U). One of the raw coals was oxidized under laboratory conditions and used for testing (LC 3OXY). One metallurgical and one thermal sample represented product coals.

Two types of samples were used for testing. For bulk testing 10 kg samples were prepared in such a way that they were closely representing the coal in terms of the size distribution. All raw coal samples were crushed down to 100% passing 25.4 mm. For pelletization and surface properties characterization minus -0.5mm size fraction was sieved out from the bulk sample and used for evaluations. The product coals were used as received, and fine fraction of 0.5mm was also isolated from the bulk sample for surface properties characterization.

The coal analyses are given in Table I. The equilibrium moisture and transmittance are included to demonstrate different hydrophobicity (wettability) characteristics of selected coals. Equilibrium moisture indicates water-holding capacity and was

determined following ASTM D 1412-93. Transmittance values were determined following the ASTM D5263-93 method.

Table 1. Samples Characteristics

Coal Sample	Yield of 0.5mm fraction	Ash in Fines %	Ash in bulk Sample %	Equilibrium moisture %	Transmittance %
LC 3	36.0	12.61	30.12	1.30	95.25
LC 10BC	39.0	24.41	37.45	1.65	80.90
LC 10B	45.0	12.94	24.30	2.96	56.24
LC 8U	37.0	15.37	23.63	7.34	26.06
LS 20	22.0	33.7	35.00	8.02	34.80
LC met	44.0	12.66	9.77	1.56	99.02
LC thermal	45.0	15.86	15.15	2.09	50.63
LC 3 OXY	36.0	12.61	30.12	4.38	57.80

Penetration rate tests were used to characterize wettability of fines obtained from the studied coals. The gravimetric version of the method based on Washburn equation (15) was used as described by (Laskowski et al., 2003). In this method, 3 grams of coal was packed in a tube and compressed by a column-packing device under load of 5 kg. The tube with compacted material was then attached to a balance, contacted with water and the total weight of the column was monitored on-line using an electronic balance. The patterns of penetration for the studied coals are shown in Figure 1.

SIZE DISTRIBUTION OF THE FINES

Size analyses were performed using Malvern Mastersizer 2000. In this method laser beam is used to obtain scattering patterns of particles in order to determine the size distribution. Figure 2 presents cumulative size distribution of 0.5mm fractions from all seven coals.

N₂ SURFACE AREA AND PORE VOLUME DETERMINATION

Surface area was determined by Quantachrome Autosorb Automated Gas Sorption System using BET method with N₂ as an adsorbate at 77.35 K. The samples were dried at 120°C overnight in a vacuum oven and then outgassed at 50 °C . The BET surface area was calculated according to the Brunauer-Emmett-Teller equation. The total pore volume was derived using calculations from Density Functional Theory (DFT) and micropore volume was computed from Brauner MP method (Lowell et al. 1998).

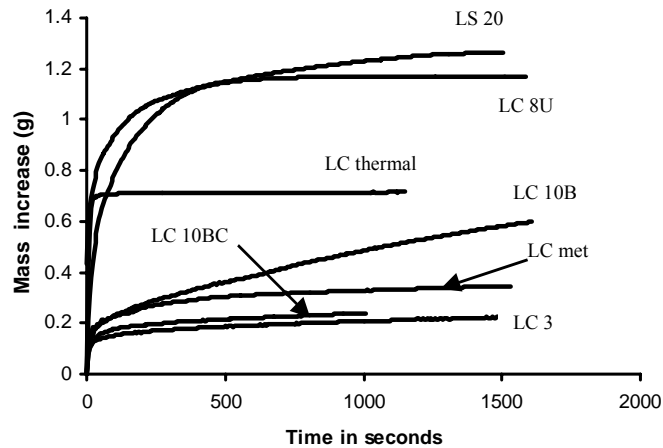


Fig. 1. Penetration rates for studied coals

PELLETIZATION

Pelletization was used as a method to characterize surface properties of fines (-0.5mm). The tests were set up for all the samples under the same operating conditions. Approximately 1kg of dry coal was placed onto the pelletizing disc (Syndron) rotating at 25 rpm and sprayed with water at a rate of 10 ml/min. The amount of water added to each sample was calculated from equation derived by (Sastry and Fuerstenau, 1982). Since the addition of water for each coal depends on the ash content, duration of pelletization run had to be adjusted accordingly. The pelletization tests were carried out until suitable pellets were formed and for most of the coals this was completed within 30 minutes. The pellets were collected and strength was measured using a Tritester tensiometer. The compressive strength of single pellet was measured by crushing the pellet between flat parallel surfaces and the loads at which failure occurred was recorded. The rate of loading was strictly controlled and was digitally set at 0.75mm per minute.

HANDLEABILITY TESTS

The handleability of bulk samples was tested with the use of Durham Cone (Cutress, et al., 1960). For each test 10 kg of coal was prepared and placed into the cone shaped container. The cone was vibrated for 30 seconds and then it was allowed to flow out through the opening. The time to discharge the coal from the vibrating cone was measured and flow rate in kg/s was calculated and referred to as Durham Cone Index. (DCI) The test was repeated for at least 10 times and average value of DCI was calculated.

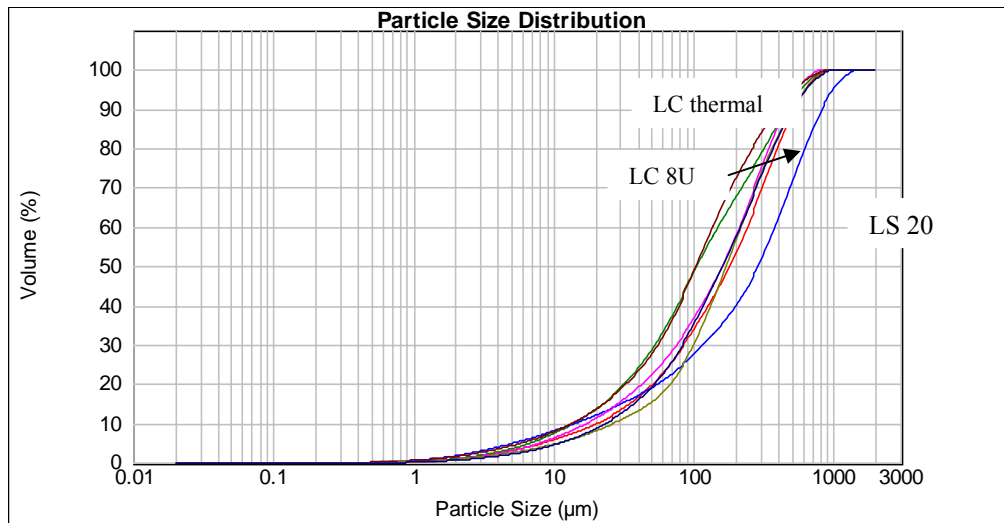


Fig. 2. Particle size distribution of 0.5mm size fractions for studied coals. The coarsest distribution is for LS 20 coal and the finest two are; LC thermal and LC 8U. Distributions for all the other coals are in between

RESULTS AND DISCUSSION

COAL SURFACE PROPERTIES CHARACTERIZATION

The surface properties of all studied coals are summarized in Table II. The selected coals were typical metallurgical coals from British Columbia. These coals were of medium volatile bituminous rank. LC thermal and LC met (metallurgical) were the coal products received from one of the local mines. The exception was LS 20 coal, which was the lower rank coal (high volatile A) from Alberta. These samples varied significantly in wettability characteristic, from very fresh to heavily oxidized, as observed from the transmittance values. The LC 3OXY sample was oxidized by heating at 180°C in the oven for eight weeks.

As Figure 1 shows, the penetration rate patterns for studied coals are in relatively good agreement with both equilibrium moisture and transmittance data. The surface area and pore volume data for studied coals are included in Table II.

As already indicated, in this study pelletization was used as a method of elucidating the effect of surface properties of coals which are responsible for aggregation of particles in presence of moisture. The strength of the resulting pellets was used to evaluate the effect of interparticle interactions on aggregation. However, from the strength and surface area data alone it will be difficult to judge what is causing formation of strong pellets for some coals.

PELLETIZATION

Pelletization of coal particulates is controlled by interfacial and capillary forces due to presence of a liquid phase (Kapur et al., 1966; Sastry et. al. 1977, 1981; Capes, 1980). For pelletization to take place, first liquid has to wet the surface of coal particles, the liquid bridges between particles must form, and the capillary forces must create the bonds between the particles.

Wetting of hydrophobic coal is difficult. Once the coal is covered with coalesced droplets of water, the bonds formed between particles of such a solid are not strong due to high interfacial tensions between liquid and solid. Although capillary state may be reached, the layer of water around aggregating particles remains relatively thick and unstable. As a result, strength of the formed pellet is much smaller. (Kaji et al., 1986) made an important observation that for some coals, adsorbed water occupies only ~30-75% of the total pore volume, while for other coals the adsorbed water exceeds by 2 to 3 times their pore volume.

Table 2. Surface Properties Characterization

Coal Sample	Ash in fines %	N ₂ BET Surface area m ² /g	Total pore Volume cc/g E-0.5	Micropore Volume cc/g E-0.5	Pellets strength g/cm
LC 3	12.61	0.390	32.4	2.6	8.5
LC 3 OXY	12.61	0.276	18.9	9.8	14.3
LC 10BC	24.41	0.652	45.2	4.2	13.8
LC 10B	12.94	0.376	24.1	0.8	11.6
LC 8U	15.37	1.440	97.3	2.9	20.0
LS 20	33.70	4.140	280.0	27.8	289.0
LC met	12.66	0.439	32.0	7.7	7.5
LC thermal	15.86	0.661	26.5	3.1	20.0

In case of hydrophilic coal, water penetrates quickly into the pores creating micro-capillary pressure from within. Once an excess of liquid appears on the surface of the particles, only at the moisture content exceeding the equilibrium moisture, an aggregation can proceed almost instantly to the capillary state. The stable layer of water on the surface of particles is much thinner; therefore, strength of pellets is much greater due to the strong capillary pressures from within the coal structure. To facilitate discussion the data from Table 2 will be analyzed as separate case studies.

Case 1. Comparison of the behavior of the LC 3 and LC 3OXY coal samples. Since the LC 3OXY sample was prepared by oxidizing the LC 3 sample, their ash contents

remain the same. Although the pore volume changes a little and the micropore volume is also smaller after the oxidation, the strength of the pellets almost doubled for the oxidized sample (LC 3OXY). Following our assumptions that for oxidized – hydrophilic coal, the strength of the pellets results from strong capillary forces due to surface hydrophilicity, porosity as well as the ash content and surface area, it is evident that decrease in hydrophobicity has a larger overall effect.

Case 2. Comparing LC met and LC thermal coals shows similar trend; much stronger pellets are produced from the hydrophilic LC thermal coal. Pore volume along with microporosity is much greater in LC met, however due to hydrophobicity of these coal particles, this does not have any significant effect and does not increase the pellet strength. The wetting water on the LC met coal is not able to penetrate the pores to create significant force for aggregation.

Case 3. Two coals LC met and LC 10BC of similar hydrophobicity (Figure 1), one gives pellets 1.83 times stronger than the other. In both cases, contribution of porosity to the force pulling particles together is apparently negligible; the only difference is in the ash content. In this case it appears that only the ash in the LC 10BC sample contributes to the strength of the pellets, and is almost exactly the same magnitude as the difference between the strength of the pellets formed for these two coals.

Case 4. The LC 8U and LS 20 are the two hydrophilic coals. Pellets formed from LS 20 are 14 times stronger than pellets formed from LC 8U. If we consider that LS 20 having twice as much ash content (2.2) and approximately three times as much greater surface area (2.8) and pore volume (2.9) as compared to LC 8U, this should give $(2.2 \times 2.8 \times 2.9 = 17.8)$ 17.8 times stronger pellets from LS 20 coal. According to penetration rate both coals have similar level of hydrophilicity with similar equilibrium moisture value. However, moisture requirement for pelletization predicted from (14) was based on the ash content of the fines and did not take into account surface area; as a result, it underestimated the amount of water required for pelletization of LS 20. The ratio of the underestimated amount of water is equal to 0.73, hence $17.8 \times 0.73 = 13$. Thus according to these calculations 13 times stronger pellets are expected to be formed from LS 20, which is very close (14 times) to the actual difference between strength of pellets from these coals.

Likewise, all the other cases seem to confirm our conclusion that the strength of the formed pellets is related to the hydrophilic/hydrophobic character of coal particles, and their porosity, microporosity and ash content. In summary, the effectiveness of pelletization is dependant on wettability. The wettability is the most important factor because it decides whether the porosity can create a strong capillary force that affects particle-to-particle adhesion. This capillary force and mineral matter on coal surface determine behavior of the water films between particles. In the case of hydrophobic coals, the strength of the pellets results only from the ash (mineral matter), since water will not penetrate into the pores, at least not to the great extent, to create strong pulling force from within coal pores.

HANDLEABILITY

During coal transportation, fine and coarse particles are tumbled together; however, fines are responsible for the cohesiveness of the whole mixture that affects coal handleability. Depending on the hydrophobic/hydrophilic character and ash content of coal, fine particles can strongly affect coal handleability.

If the same surface properties are responsible for fine particle behavior in handleability as in pelletization, then hydrophobic coals should be much easier to handle than hydrophilic ones. Further on, it can be concluded from the conducted pelletization tests that for hydrophobic coals only ash (mineral matter) content can influence their handling characteristics.

The handleability tests were performed using Durham Cone on the bulk samples of all seven coals. The tests were carried out varying moisture levels; flow rates at different moistures are plotted to examine the trends (Figure 3 and 4). The LC met, LC 10B and LC thermal coals have similar amount of fines (about 45% of 0.5mm material) and ash content with the exception of LC thermal (Table I). According to pelletization tests LC thermal sample should be ranked the most difficult to handle followed by LC 10B and LC met and indeed this is the case.

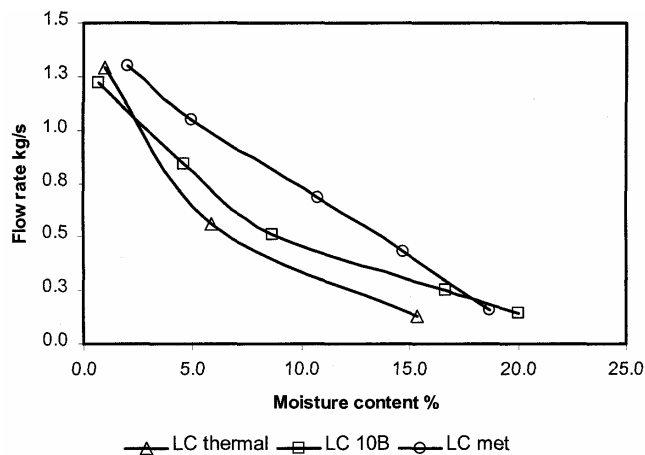


Fig. 3. Flow rates at different moistures content for LC thermal, LC 10B and LC met coals

For other four coals the trend is not so evident (Figure 4). Coals LS 20 and LC 8U have similar wettability characteristics (Figure 1) however, LS 20 has only 22.0% of fines (0.5mm fraction) as compared to 37.0% in LC 8U. Since the amount of fines is the most critical factor, it is not surprising that LS 20 has much better handleability than LC 8U. Both of these coals have their equilibrium moisture at about 8%; this implies that below that moisture content, there is no surface moisture present on the surface of particles which would lead to the aggregation. Thus, only at the moisture levels exceeding 8% the particles will start to aggregate or stick together. To

emphasize this effect, correlations shown in Figure 4 were replotted versus the surface moisture for these four coals (Figure 5). Surface moisture was calculated as the difference between actual moisture and equilibrium moisture.

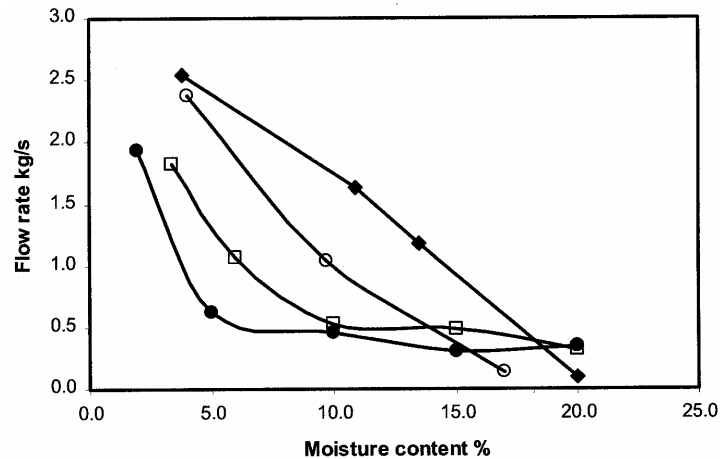


Fig. 4. Flow rates at different moistures content for LC 3, LC 10BC, LC 8U and LS 20 coal

Lines showing the trends of the flow rate change vs. surface moisture for LS 20 and LC 8U moved to the range of much reduced handleability (Figure 5). The LC 8U coal has the same amount of surface moisture as the LC 3 coal; the difference is that at 10% surface moisture this coal almost entirely stops to flow, while LC 3 is still handleable.

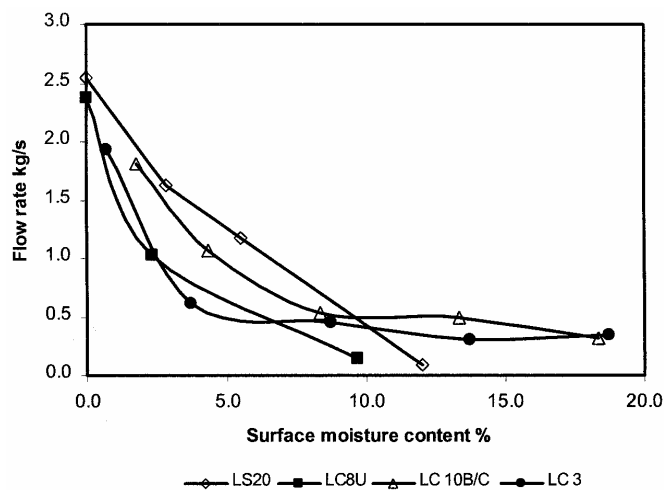


Fig. 5. Flow rate change vs. surface moisture for LC 3, LC 8U, LC 10BC and LS 20

The LC 10BC coal exhibits a very similar trend in flow rate vs. moisture to that of the LC 3 coal, suggesting that being hydrophobic it does not cease to flow at high moisture levels. However, both of these coals exhibit overall poor handleability characteristics. To clarify why these two coals have such bad handling properties, X-ray diffraction (XRD) of low-temperature ash (LTA) was carried out to learn more about mineral matter type in these samples. Table 3 presents XRD results for these coals.

As Table 3 indicates, both of these coals have very high amounts of clay minerals. The LC 3 coal has 5% more clays in total than LC 10BC. Based on this information it can be concluded that handling behavior of these two coals is hindered by the presence of high amount of clay material.

Table 3. Mineralogical Composition of LTA from LC 3 and LC 10BC

Mineral	LC 3%	LC 10BC %
Quartz	19.6	24.4
Kaolinite	36.4	26.1
Illite	24.1	27.8
Muscovite	18.9	20.7
Total clays	79.4	74.5
Pyrite	0.3	0.4
Dolomite	0.6	0.6

CONCLUSIONS

The following conclusions can be drawn from this project:

- Pelletization can be used as a method of characterizing surface properties of fines that affect behavior of these particles in handling. Testing coal for pelletization under controlled conditions can help to reveal the effect of surface properties (such as wettability, surface area and porosity) on ability of fine coal particles to aggregate. In general, easy to pelletize coals are difficult to handle.
- Equilibrium moisture is an important parameter that needs to be assessed in order to set the limits for good and bad handleability ranges for any given coal. For lower rank and oxidized coals, equilibrium moisture is usually much higher, therefore these coals can tolerate higher moisture levels before they start to be difficult to handle. However, at the moisture levels exceeding their equilibrium moistures, a rapid deterioration of their handling behavior is observed, leading practically to non-flowing conditions.

- In case of hydrophobic coals only the mineral matter and type of association with coal organic matter affects significantly these coals handleability. For such coals an increase in moisture content tends to affect handleability to certain level, but the coal does not cease to flow completely. Apparently high amount of clay material even in very hydrophobic coals can have very damaging effect on handleability.
- Since the amount of fines is the most critical factor influencing handleability, in order to see the effect of coal surface properties the tested samples must have the same size distributions, especially the levels of fines.

REFERENCES

- D.W. BROWN, 1997, *Factors Affecting the Handleability of Coal and its Measurement*, Coal International, July, 1997, 147-149.
- J. CUTRESS, J.C. SPROSON, J.M. RUNCIE, 1960, *Designs and Trials of Coal Handleability Machines*, Internal Report, National Coal Board, Durham and Northern Divisions, Scientific Department.
- F. VICKERS, 1982, *The Treatment of Fine Coal*, Colliery Guardian, Vol.230, 359-366.
- D.W. BROWN, B.P. ATKIN, N.J. MILES, D.S. CREAM, 1997, *Determination of the Handleability of a Coal Blend using an Extrusion Through*, Fuel, Vol.76, 1183-1186.
- JENIKE, A.W. JENIKE, 1961, *Gravity Flow of Bulk Solids*, Bull.108, the University of Utah, Engineering Experiment Station, USA.
- B.J. ARNOLD, 1992, *Coal Handleability - Addressing the Concerns of the Electric Utility Industry*, Mining Engineering, January, 1992, 84-89.
- A. BAROIS-CAZENAVE, P. MARCHAL, V. FOLK, L. CHAPLIN, 1999, *Experimental Study of Powder Rheological Behavior*, Powder Technology, Vol.103, 58-64.
- POLISH NORMS, 1982, *Determination of Transportability Index*, GIG, PN-82/G-04544.
- W. WAWRZYŃKIEWICZ, 2003, *Factors Influencing Transportability of Steam Coals*, Journal of the Polish Mineral Engineering Society.
- D.W. BROWN, B.P. ATKIN, *A Method for Rapid on-site Assessment of Handleability*, Coal Preparation, 2000, Vol. 21, 299-313.
- J. BLONDIN, M. GIRARDEAU, M. NOMINE, 1988, *Two Simple Tests for the Assessment of Wet Fine Coal Handleability*, Industrial Practice of Fine Coal Processing, Proceedings of the Conference at Hidden Valley, Somerset, PA, 25-28 September, 1988, 253-255.
- A. MIKKA, J.B. SMITHAM, 1985, *Coal Handleability Assessment*, Third Australian Coal Preparation Conference, Wollongong, pp. 12-27.
- M.E. HOLUSZKO, J.S. LASKOWSKI, 2003, *The effect of surface properties on fine coal handleability*, presented at Mineral Processing Research Unit conference, at the XXII IMPC 2003, September 28 – October 3, Cape Town, South Africa.
- K.V.S. SASTRY, D.W. FUERSTENAU, 1982, *Pelletization of fine coals*, Report EPRI CS-2198 Research Project 1030-, University of California, Berkeley, California.
- V.T. CROWL, W.D. WOOLDRIDGE, 1967, *A Method for the Measurement of Adhesion Tension of Liquids in Contact with Powders*, Wetting, Society of Chemical Industry, London, pp. 200-212.
- J.S. LASKOWSKI, M.E. HOLUSZKO, S. FINORA, 2003, *An Experimental Study of Wetting of Coal with Drilling Fluids*, Internal Report for Laskowski Research Inc.
- S. LOWELL, J. E. SHIELDS, 1998, *Powder Surface Area and Porosity*, Chapman and Hall, London.
- P.C. KAPUR, D.W. FUERSTENAU, 1966, *Size Distributions and Kinetics Relationship in the Nuclei Region of Wet Pelletization*, Ind. Eng. Chem. – Process Design and Development, Vol.5, 5-10.
- K.V.S. SASTRY, D.W. FUERSTENAU, 1977, *Kinetics and Process Analysis of Agglomeration of Particulate Materials*, in Agglomeration 77, Ed. K.V.S. Sastry, AIME, New York, 381-402.

K.V.S SASTRY, V.P. MEHROTRA, 1981, *Pelletization of Coal Fines: State-of-the-Art*, 3rd International Symposium, Nurnberg Partikel Technologie, Vol.2, H36-H51.

C.E. CAPES, 1980, *Particle Size Enlargement*, Elsevier Scientific Publishing Company, Amsterdam.

R. KAJI, Y. MURANAKA, K. OTSUKA, Y. HISHINUMA, 1986, *Water absorption by coals: effects of pore structure and surface oxygen*, Fuel, Vol. 65, 288-291.

Holuszko M.E., Laskowski J.S., *Peletyzacja jako metoda badania oddziaływań międzyziarnowych i ich wpływu na podatność transportową węgla*, Physicochemical Problems of Mineral Processing, 38, (2004) 23-35 (w jęz. ang.).

„Coal handleability”, termin, którego polskim odpowiednikiem jest “podatność transportowa węgla”, charakteryzuje przepływ węgla przez różne węzły technologiczne i opisuje zachowanie się drobnego węgla podczas transportu, składowania i dozowania. Podatność transportowa węgla zależy w bardzo dużym stopniu od agregacji ziarn węgla. W procesie peletyzacji ruch obrotowy bębna/dysku powoduje stykanie się drobnych ziarn, które w wyniku tego mogą tworzyć kuliste pelety. Ta sama podatność ziarn do tworzenia agregatów w trakcie ich transportu powoduje agregację ziarn, co zasadniczo wpływa na podatność transportową takiego materiału. W tej pracy badano równolegle podatność transportową różnych próbek węgla i peletyzację tych próbek. Wyniki peletyzacji zostały użyte do scharakteryzowania właściwości drobnego węgla, które określają jego podatność transportową.

Michael SPYRIDOPOULOS, Stefaan SIMONS, Stephen NEETHLING*
and Jan CILLIERS**

EFFECT OF HUMIC SUBSTANCES AND PARTICLES ON BUBBLE COALESCENCE AND FOAM STABILITY IN RELATION TO DISSOLVED AIR FLOTATION PROCESSES

Received April 20, 2004; reviewed; accepted May 31, 2004

In this paper the effect of humic substances (natural surfactants), electrolytes and solid particles on bubble coalescence, and as a consequence on froth stability, have been investigated. We formed two bubbles of equal size and forced them to collide using a novel experimental apparatus. The interactions were recorded by a high-speed camera, the images of which helped to determine the coalescence frequency and the coalescence time, as well as the mechanisms of the interactions. Two types of humic substances were used, along with three different electrolytes. Humic substances appeared to have a considerable effect on bubble coalescence, while the effect of electrolytes was minimal. Moderate and high hydrophobic glass spheres were used between two bubbles. Very hydrophobic spheres promoted fast bubble coalescence, while moderate hydrophobic spheres had no effect. We present data of coalescence frequency and time, as well as images of the coalescence events. The coalescence frequency was used to validate a parameter, P_f , known as the film failure frequency, used in a simulation model to predict foam height in a gas-sparged vessel. Predictions determined using P_f were then validated by experimentation.

Key words: bubbles, coalescence, flotation, surfactants, electrolytes, particles, froths, foams

INTRODUCTION

The formation and stability of froth is important in many industrial processes. For instance, in flotation processes, during which air bubbles capture solid particles from the bulk liquid and subsequently rise to the surface, where they form a froth layer. A great deal of work has been published attempting to establish the influence of various parameters on this phenomenon, such as the characteristics of the surfactants,

* Colloid and Surface Engineering Group, Department of Chemical Engineering, University College London, Torrington Place, London WC1E 7JE, UK, stefaan.simons@ucl.ac.uk.

** Froth and Foam Research Group, Department of Chemical Engineering, UMIST, P.O. Box 88, Manchester, M60 1QD, U.K.

electrolytes and solid particles (Bhakta and Ruckenstein, 1997; Darton and Sun, 1999; Dippenaar, 1982a; Pugh, 1996; Ross, 1991). With an increased interest in the application of dissolved air flotation (DAF) to the purification of drinking water, a fundamental understanding of the effect of various operational conditions on froth formation and stability is vital for process optimisation and control, since the efficiency of this process depends heavily on this phenomenon.

With regards to drinking-water treatment, DAF was first used in 1965 in Finland (Heinänen et al., 1995) and since 1970 in South Africa (Haarhoff and van Vuuren, 1995). It is now widely used in many more countries, such as Belgium and The Netherlands (van Puffelen et al., 1995), in Asia and Australia (Edzwald, 1995), while it is an emerging technology in North America (Schmidt et al., 1995; Nickols et al., 1995; Adkins, 1997). In the UK, DAF plants appeared in the 1970's, initially at a limited number of sites. Nowadays, the number of DAF plants in the UK is probably more than 90 (Gregory, 1997). DAF is very effective for natural waters rich in algae and humic substances (coloured waters) and is very important because of existing and proposed regulations that require filtration of surface waters and increased removal of protozoa cysts such as *Cryptosporidium* and *Giardia* (Edzwald, 1995).

This paper is concerned with the influence of the basic constituents of water in DAF tanks in the drinking-water purification treatment on the formation and stability of froth. These constituents include humic substances, electrolytes and solid particles.

Humic substances (HSs) are a form of the natural organic matter in water, accounting for 40% - 90% of the dissolved organic carbon. They are high molecular weight, coloured, polyelectrolytic, organic acids (Thurman, 1985). Usually, they are divided into two fractions: (a) the fulvic acid, which is of lower molecular weight (500-2000) and soluble in water under all pH, and (b) the humic acid, which is of higher molecular weight (2000 – 5000) and it is not soluble in water under acidic conditions ($\text{pH} < 2$) but is soluble at higher pH values. HSs are important constituents of water because they appear to be present in all natural waters and play a vital role in determining many aquatic processes. The concentration of HSs varies for different natural waters; streams, rivers, and lakes contain from 0.5 to 4.0 mgC/l, and coloured rivers and lakes have much larger concentrations of HSs, from 10 to 30 mgC/l. HSs, as with other natural organic compounds, possess hydrophobic and hydrophilic functional groups. As a result they reduce the surface tension of water and exhibit similar to synthetic surfactants, surface activity (Anderson et al., 1995), and this is the reason why people refer to them as natural surfactants.

Electrolytes are added in natural water just before the water to enter the DAF tank, in order to encourage the particulate matter contained in it to coagulate and flocculate in larger particles. In the literature there are some papers demonstrating the inhibition effect of electrolytes on bubble coalescence (Oolman T.O. and Blanch, 1986; Lessard and Zieminski, 1971; Pashley and Craig, 1997; Deschenes et al., 1998, Laskowski et al., 2003), though there is not a clear explanation for this effect.

Solid particles, that is the matter that its removal from drinking water is aimed, can also play a role on froth stability. In fact, previous workers studying froth stability in the presence of particles have found that particles can promote or inhibit froth stability (Dippenaar, 1982a; Dippenaar, 1982b; Johansson and Pugh, 1992; Spyridopoulos and Simons, 2004). It can be said that the shape, the number, and, perhaps most importantly, the hydrophobicity of the particles play a crucial role on the bubble coalescence and the subsequent phenomenon of froth stability. Dippenaar (1982a) found that a particle caused the rupture of the liquid film -formed between two liquid-air interfaces- when the two three-phase lines were forced to migrate to the same point on the particle. Smooth spherical particles with a contact angle of $\theta > 90^\circ$ ruptured the liquid films when the films thinned for the particles to bridge them. Particles with irregular shapes could rupture the films even when $\theta < 90^\circ$. Johansson and Pugh (1992) found that particles in the size range 26 - 40 μm , showed the following behaviour:

- For less hydrophobic particles ($\theta < 40^\circ$), there was little influence on froth stability.
- Particles of intermediate hydrophobicity increased froth stability.
- Particles of high hydrophobicity ($\theta > 80^\circ$) the particles ruptured the liquid film.

We have studied the effect of HSs, electrolytes and solid particles on froth formation and stability by conducting bubble coalescence experiments using a novel instrument, known as a Micro-Force Balance (MFB), developed in our laboratory. Bubbles of diameter up to 1 mm are grown on opposing nozzles inside a glass cell filled with an aquatic solution. The bubbles are brought together by the expansion of a piezoelectric tube. The rate of expansion and the resulting collision are controlled by software, which control the frequency and the value of the signals sent to a micromanipulator. For the cases where the HSs and the electrolytes were examined, we have observed the conditions under which the bubbles coalesce, e.g. coalescence frequency, type and concentration of HS/electrolyte, and bubble size. For the cases where we had coalescence, we measured the coalescence time, using high-speed video. The effect of solid particles on bubble coalescence was conducted by using glass spheres of different degrees of hydrophobicity. By attaching a glass sphere to the bottom of a bubble and pushing another bubble underneath we could record the particle influence on bubble coalescence. In this paper we present data of coalescence frequency and coalescence time, as well as images of the coalescence events.

To describe foam or froth stability, the frequency of failure of films must be described as a function of any number of applicable variables. In a two-phase system, the three most important variables are the chemical conditions (amount and type of surfactant in the films), the radius of curvature of the Plateau borders and vertices, r_{PB} , (and hence the pressure exerted on the films) and the size of the films themselves (which is directly related to bubble size, r_{bubble}).

In an earlier paper, we have defined the film failure frequency, P_f , to describe film failure, where $P_f = (\text{average lifetime of a film})^{-1} = f(r_{\text{PB}}, r_{\text{bubble}}, \text{chemical conditions})$

(Cilliers et al., 2003). Coalescence is the failure of the film (lamella) between two neighbouring bubbles and results in the formation of a single, larger bubble. Coalescence results in a loss of lamella surface, and of Plateau border length. The rate of coalescence is determined by the stability of lamellae between bubbles in the froth. Immediately after the film between two bubbles has failed, surface tension will straighten the remaining lamellae. Some of the liquid from the lost Plateau border will remain trapped in the single lamella that is formed out of the two lamellae that existed before. Due to the relatively sharp curvatures associated with the relic of the previously existing Plateau border, this liquid will rapidly enter and thickening the new lamella. Coalescence therefore wets the new, larger film that is formed. It is possible that the lamella straightening will precipitate failure and lead to cascades of coalescence events. This can sometimes be observed in practice.

While the film failure frequency function may be obtained purely by experimental means, it is useful to consider the functional forms for P_f suggested by different coalescence mechanisms. The two dominant mechanisms are; the time taken for the film to thin beyond its failure limit and the mechanical vibrations required to rupture a film that is at its equilibrium thickness. The first results in an expression for P_f shown in equation (1), whilst the second results in two slightly different expressions depending on the nature of the disturbances acting on the film. The expressions are discussed in detail in Neethling et al. (2002). In this paper we show how experimental measurement of P_f indicated that the former theory best describes foam stability.

$$P_f = \frac{K_1}{r_{\text{bubble}}^n} \times \left(\frac{1}{r_{\text{PB}}} - \frac{1}{r_{\text{PB(Critical)}}} \right) \quad (1)$$

where n takes a value between 1 and 2 and K_1 is proportional to the fluid viscosity, but also depends on surface chemistry since it affects the film thickness at which rapid, van der Waal's induced failure occurs.

EXPERIMENTAL

BUBBLE COALESCENCE MEASUREMENTS

Materials

A sample of fulvic acid (FA) extracted from a sitka Spruce stand at Rumster in Caithness, UK, was provided by Thames Water Plc (Kempton, UK), one of the major water companies of the UK and collaborators in this project. A second sample of FA, from the Cairgorms region in Scotland, was purchased from the Macaulay Institute (Aberdeen, UK). Thames Water also provided two samples of different molecular weight polymaleic acid (PMA), which is a synthetic polymer that resembles humic and fulvic acids. The samples were stored in glass containers inside a glass desiccator, due to the tendency of the HSs to absorb water from the atmosphere.

Solutions of the HSs were prepared by dissolving a specific quantity of the sample in AnalaR-grade water (BDH, Dorset, UK). Though the HSs were supposed to be soluble in water (since they were FA), they contained traces of non-soluble matter, such as silica, which had to be removed by passing the solutions through a filter paper with pore size of 0.2 μm . The pH of the aquatic solutions was adjusted to 5.0-5.5, the pH usually encountered in drinking-water treatment, using a few drops of (for acidic solutions) NaOH 0.1N or (for basic solutions) HCl 0.1N (BDH, Dorset, UK).

Three electrolytes, potassium chloride (KCl), calcium chloride dihydrate ($\text{CaCl}_2 \cdot 2\text{H}_2\text{O}$) and lithium chloride (LiCl), were purchased from BDH Laboratories Supplies (Poole, UK) and were of AnalaR grade. The solutions of the electrolytes were prepared by simply dissolving the salt in AnalaR-grade water, with no further treatment.

Repelcote VS was purchased from BDH (Dorset, UK). Methanol and ethanol were obtained from Fluka (Dorset, UK). Lead-glass spheres were purchased from Plowden & Thompson Ltd (, UK), with diameters in the range 20-100 μm . Microscope slides were purchased from BDH (Dorset, UK).

Measurement of surface tension

The measurements of the surface tension of the HS solutions were conducted with the Wilhelmy-plate method, using a Krüss K-12 tensiometer (Krüss GmbH, Hamburg, Germany). For each concentration and sample, three measurements were taken and the average taken as the surface tension of the solution.

Silanisation of spheres

The spheres were cleaned by immersing them in a 1:1 MeOH-HCl solution for 30 mins and thoroughly rinsing with distilled water. This procedure has been found to produce fairly clean glass surfaces (Cras et al., 1999). Finally, the spheres were rinsed with AnalaR-grade water and were dried in a furnace for 24 hrs. The spheres were hydrophobised by reaction in a silanising solution, Repelcote VS. The detailed procedure is described elsewhere (Fairbrother, 1998). The spheres remained immersed for ten minutes in the solution and subsequently were rinsed with EtOH before placing in the furnace at 150 °C for 24 hrs to dry.

Measurement of contact angles

The contact angles of the glass spheres in AnalaR water were determined by conducting the measurements on glass slides that had undergone the same procedure with the glass spheres. Prior to measurement, the slides were rinsed in AnalaR water and dried in an oven. The measurements were carried out with a Krüss K-12 tensiometer GmbH (Hamburg, Germany), which makes use of the Wilhelmy-plate method. With this instrument, the values of the advancing and the receding contact angles were taken. The contact angle of the solid surface was taken the average of these values. For each glass sphere (untreated/silanised/glass type) three slides were tested, three measurements per slide.

The apparatus

A schematic representation of the apparatus is shown in Figure 1. It comprises the Micro-Force Balance (MFB), where the bubble interactions take place, a complex visual system, and a personal computer, which is used to control the electronic components of the apparatus and to carry out the analysis of the recorded images.

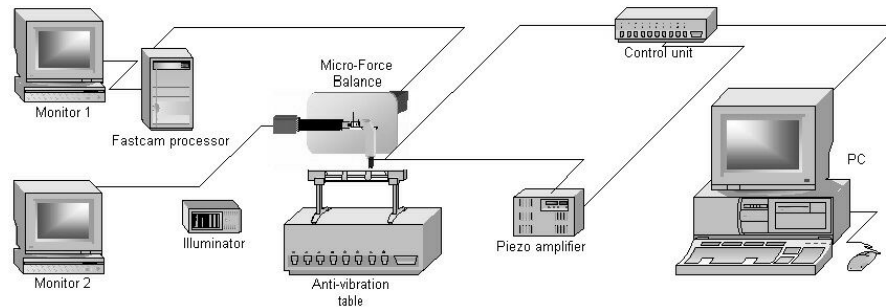


Fig. 1. Schematic representation of the experimental apparatus

The bubble interactions take place in the MFB. In the MFB there is an optical clear glass cell, which is filled with an aquatic solution. The tips of two glass micropipettes are immersed in the aquatic solution, one opposite the other. A bubble is formed at the tip of the lower micropipette by carefully compressing the air inside a flexible tube. The upper micropipette is then moved down to pick up the bubble. A second bubble of the same size is formed similarly at the lower tip. The result of this procedure is the formation of two bubbles, opposite to each other and separated by a liquid film of a few microns. The time needed for this procedure is less than 30 seconds.

The bubbles are forced together by the expansion of a piezoelectric crystal located in a micromanipulator, connected to the lower micropipette. In this way, the lower bubble can move towards the upper bubble and collide with it. An application executed in the computer and written in the VEE Pro programming environment (Agilent Technologies Inc., USA) sends the instructions to a 16-bit multifunction board (Data Translation Inc., MA, USA) to provide the piezoelectric crystal with successive voltages in order to expand it according to the desired rate and expansion. Due to the intrinsic non-linearity of piezoelectric crystals, a Linear Variable Differential Transformer (LVDT) is used to follow the expansion and refer the correct position of its edge with accuracy. The same application in VEE Pro is used for control and data acquisition.

Bubble interactions are monitored and recorded by a high-speed camera, PHOTRON FASTCAM Super 10K (Photron Ltd, San Diego, CA, USA), capable of recording images between 30 and 3000 frames per second (fps). A second CCD camera from Sony Corp. (Tokyo, Japan) is placed at a right angle to the high-speed camera, while both the cameras lay on the horizontal plane. This configuration helps

in the vertical alignment of the bubbles. Each camera is coupled to a single-tube microscope (Edmund Scientific Ltd, York, UK) fitted with a plan achromatic objective lens from Olympus Optical Co, Ltd (Tokyo, Japan). Illumination is provided by a Stocker & Yale Inc. (Salem, USA) M1000 illuminator coupled with a liquid light guide. The high-speed camera fitted with a 10x objective gave an optical resolution of 0.854 $\mu\text{m}/\text{pixel}$. Recorded images are transferred to the computer for image analysis.

The measurement

For bubble coalescence experiments in aquatic solutions of HSs or electrolytes, the following procedure takes place. After the formation of the bubbles, their vertical alignment and their positioning to a separation distance of about 10 μm , the piezoelectric crystal is expanded at a rate of 10 $\mu\text{m}/\text{s}$ and the high-speed camera is triggered to record the event. The event ends either with the coalescence of the bubbles, or when the piezoelectric tube has reached its maximum expansion, 100 μm . In the last case, the bubbles have been squeezed but not coalesced. At least 10 repetitions are conducted for each case (bubble size, concentration and type).

It should be noted here that what is being studied is the bubble coalescence behaviour in the froth, not that in the bulk suspension. Since the velocity of the bubbles in the froth is very low, almost static, the conditions used in our experiments are seen as a reasonable approximation to that experienced by bubbles entering from the underside of the froth and then coalescing as they are forced together.

Bubble coalescence in the presence of a solid particle is carried out as follows: The micromanipulator-held bubble (the upper bubble) is transferred to the bottom of the cell, where glass spheres are resting. By aligning the bubble over one sphere, and lowering carefully the micromanipulator, the bubble captures the sphere. In practice, hydrophilic spheres are more difficult to capture, but moderate or highly hydrophobic glass spheres are captured almost immediately. The bubble-particle aggregate is lifted to the proximity of the other micropipette tip. Squeezing further the air inside the lower micropipette, a second bubble is formed. Afterwards, the bubble-particle is moved on top and at the centre of this bubble to a distance of about half the diameter of the sphere. The high-speed camera is triggered to record the interaction, which starts once the piezo starts expanding, forcing the lower bubble to the bubble-particle aggregate. The experiment ends whenever stable agglomerate resulted or bubble coalescence occurred, at which point the camera stops recording.

All the experiments and measurements take place at room temperature, 21-23 $^{\circ}\text{C}$.

FOAM EXPERIMENTS

Foams (i.e. structures without particles present) were formed by sparging air at rates increasing from 0.1 to 0.2 cm/s into an aqueous solution of 500 mg/l polymaleic acid in a vertical 2cm diameter tube. The height of the foam in the column was then measured.

RESULTS AND DISCUSSION

EFFECT OF HSs AND ELECTROLYTES ON BUBBLE COALESCENCE

Measurements of the surface tension of aquatic solutions of the HSs used in this work confirmed that the presence of HSs in water lowers its surface tension. The decrease was of the order of 10% of the surface tension of pure water at 23 °C (72.75 mN/m), for solutions of FAs at 100 mg/l. These measurements showed, also, that the surface tension of the aquatic solutions of HSs drops gradually with time, not reaching immediately its final value (see Fig.2). The PMA with MW < 500 Da appeared to drop the surface tension, but less than the two FAs. Electrolytes appeared not to have any great effect on the surface tension of water, increasing marginally its value.

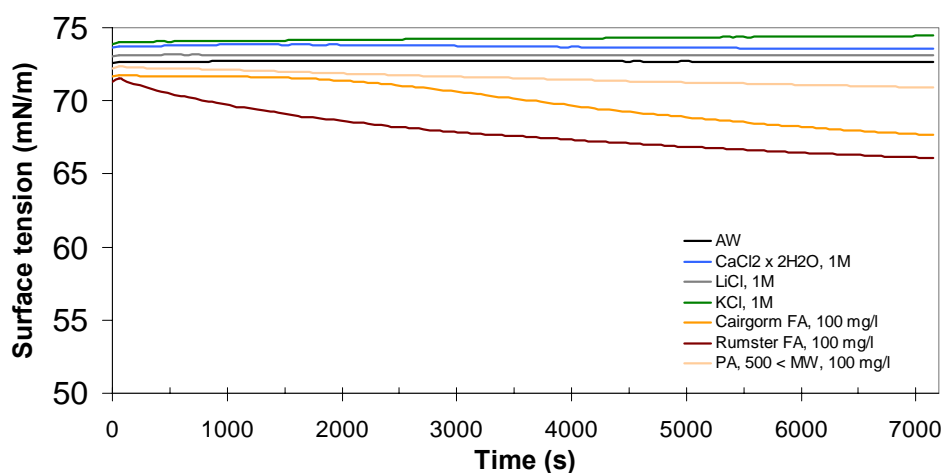


Fig.2. Surface tension of various aquatic solutions at 21-23 °C (pH: 5.0 - 5.5 as the HSs were concerned)

Bubble coalescence experiments were made using pairs of 275- μ m and 550- μ m diameter bubbles (about \pm 25- μ m standard deviation) in water and solutions of electrolytes and HSs. The bubbles were forced to collide at 10 μ m/s, while their separation was decreasing about 6 nm for every expansion of the piezoelectric crystal. In this work, we used a recording rate of up to 500 fps, so the uncertainty was at least 2 ms; as will be shown below, this uncertainty is not significant, judging by the coalescence times that we measured.

The results for the coalescence frequency for the solutions concerned are shown in Fig. 3. As was expected, there was always bubble coalescence in AnalaR water. There was also 100% coalescence frequency, when the interactions took place in electrolyte solutions, even at high concentration (1M). This was not expected, since published works on the effect of electrolytes on bubble coalescence had shown that electrolytes

could considerably decrease bubble coalescence above a certain concentration (Lessard and Zieminski, 1971). The concentrations were reported to be much less than the concentrations employed in this study. The only explanation that we can give for this discrepancy is the difference in the manner in which the experiments were carried out. In this study, the two bubbles collided coaxially and at low velocity and the liquid film between them was encouraged to thin by the expansion of the piezoelectric crystal, which forced the lower bubble towards the upper. In other studies, the bubbles collided either in bubble columns (e.g. pair of free-to-move bubbles collided at high velocities in a solution) (Deschenes et al., 1998) or in cells, where they had been grown in adjacent nozzles (Lessard and Zieminski, 1971; Oolman T.O. and Blanch, 1986). Double layer repulsions may be more important under such conditions, whereas in our experiments they are overcome by physically pushing the bubbles together.

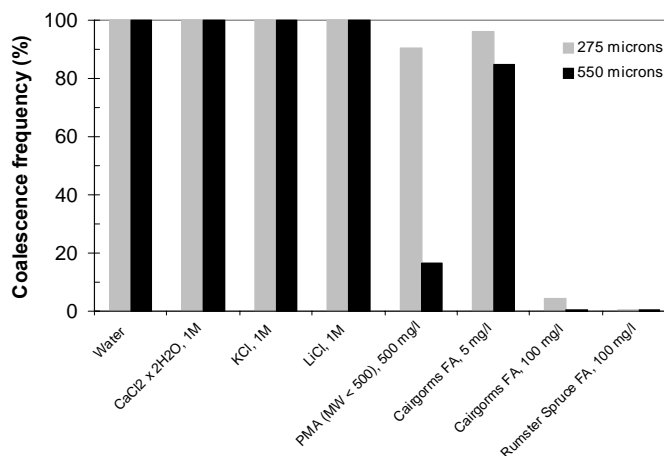


Fig. 3. Coalescence frequencies for bubbles interacting in water and in solutions of electrolytes and HSs

Contrary to the electrolytes, the HSs tested in this work appeared to have a great effect on bubble coalescence. At low concentrations, the coalescence frequency decreased marginally. At higher concentrations, though, the two FAs essentially inhibited the coalescence of bubbles (see). These observations seem to be in accordance with the measurements of the surface tension, where the HSs appeared to be surface active. The inhibition effect of HSs is possibly due to their macromolecules, which raise the steric interaction between colloidal particles (Gregory, 1993).

The coalescence times for the interactions that led to the rupture of the liquid film initially separating the two bubbles are reported in Table 1. Although the values for the case of AnalaR water seem to be much higher than those mentioned in literature

(Oolman T.O. and Blanch, 1986; Tse et al., 1998), this could be due to the use of a different method to collide the bubbles. Indeed, we have conducted bubble coalescence at higher collision rates (30 and 100 $\mu\text{m/s}$) and we have found that the coalescence times decreased to just a few ms (data not presented here). Bubbles colliding in electrolytes solution needed about the same time to coalesce as in water. In solutions of HSs, however, the coalescence times were much higher, confirming the great effect of HSs on bubble coalescence.

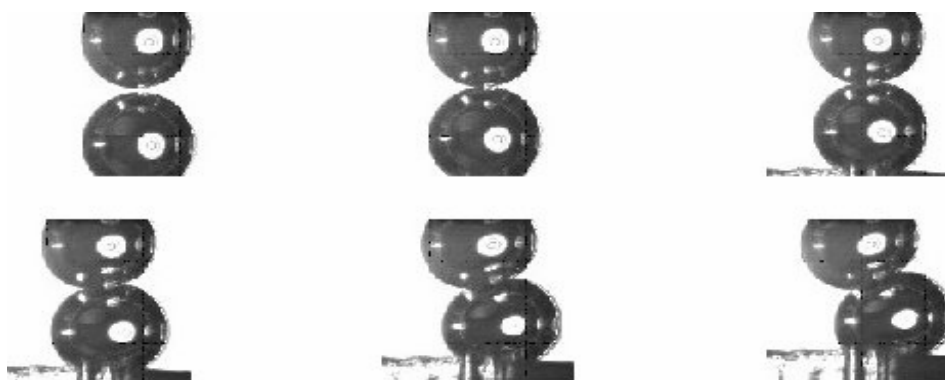


Fig. 4. Two bubbles (275 μm in diameter) are colliding in aquatic solution of FA from Rumster, 100 mg/l, at 10 $\mu\text{m/s}$. No coalescence. Recording rate: 30 fps. Frame numbers: 0, 60, 120, 180, 240 and 300.

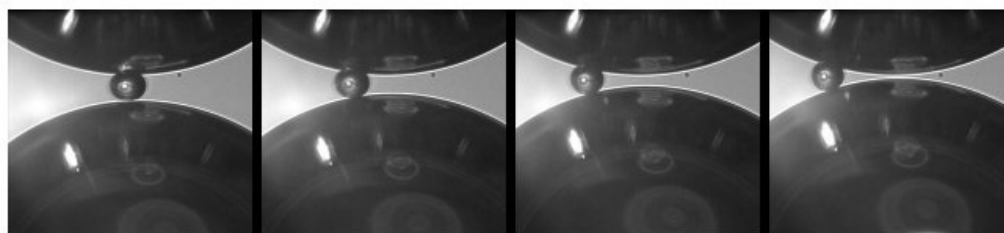
Table 1. Coalescence times of bubbles in water and aquatic solutions of electrolytes and HSs

Liquid	Coalescence time (ms)	
	275- μm bubbles	550- μm bubbles
AnalaR water	66.2	46.6
CaCl ₂ ·2H ₂ O, 1M	48.5	89
LiCl, 1M	72.4	124.6
KCl, 1M	46.9	114.1
Polymaleic acid (MW < 500 Da), 50 mg/l	90.8	175.5
Polymaleic acid (MW < 500 Da), 100 mg/l	94.8	-
Cairgorms FA, 5 mg/l	595.3	663
Cairgorms FA, 100 mg/l	1400.0	Non-coalescence
FA from Rumster, 100 mg/l	Non-coalescence	Non-coalescence

EFFECT OF SOLID PARTICLES ON BUBBLE COALESCENCE

The glass spheres that were tested involved lead glass spheres. Cleaning these spheres just with water resulted in a contact angle of about 30 °C. Thus, these spheres were characterised as moderate hydrophobic. After the silanisation of these spheres, the contact angle of water increase to 105 °C, which means that the surface of the glass spheres was very hydrophobic.

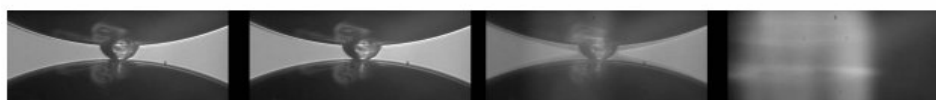
Fig. 5 shows a moderate hydrophobic sphere between two approaching bubbles. Initially, the sphere is hanging from the upper bubble, while the lower bubble is moving upwards. Upon attachment of the sphere with the lower bubble, the sphere did not form a second TPL (e.g. the sphere did not penetrate the lower liquid-air interface), but instead started sliding between the spheres. The bubbles kept approaching each other, as the sphere had no effect on it. The two bubbles coalesced when their apexes touched (image not shown here).



$t_0 = 0 \text{ s}$ $t_1 = 1.17 \text{ s}$ $t_2 = 2.34 \text{ s}$ $t_3 = 3.5 \text{ s}$

Fig.4. A moderate hydrophobic sphere ($d_{\text{sphere}} = 60 \mu\text{m}$, $\theta = 32^\circ$) slides between the approaching bubbles ($d_{\text{bubble}} = 900 \mu\text{m}$): no effect on bubble coalescence. The two bubbles will coalesce (the interaction took place in water) once they will touch each other

However, when the sphere was very hydrophobic, as the sphere shown in the sequence of images in Fig. 5, the situation was different. Almost immediately after the lower bubble came into contact with the sphere, a second TPL was formed. The two TPLs (the first formed between the upper bubble and the sphere, the second between the lower bubble and the sphere) moved to the same line on the surface of the sphere (Fig. 5, image 3). The meeting of the two TPLs resulted to the rupture of the liquid film and the subsequent bubble coalescence (Fig. 5, image 4). The whole interaction took place in less than 6 ms, which shows how a very hydrophobic particle, even of a regular shape, can lead to very fast bubble coalescence.



$t_0 = 0 \text{ ms}$ $t_1 = 2 \text{ ms}$ $t_2 = 4 \text{ ms}$ $t_3 = 6 \text{ ms}$

Fig. 5. A very hydrophobic sphere ($d_{\text{sphere}} = 78 \mu\text{m}$, $\theta = 105^\circ$) forms immediately a 2nd three-phase contact line (TPC) upon attachment with the lower bubble ($d_{\text{bubble}} = 1000 \mu\text{m}$). The two TPLs meet at the same line on the bead (image 3) and the liquid film that initially separated the bubbles ruptures.

The interaction took place in water

It has to be noted at this point that the interactions took place in pure water. It remains to be seen what the effect is of particles, both moderately and highly hydrophobic, on bubble coalescence in other aquatic environments, especially those containing surfactants, such as HSs.

DETERMINING P_f

The coalescence frequencies described above were used to calculate P_f . Since the film formed between the two bubbles was essentially flat and the overall bubble deformation small, the exerted pressure is inversely proportional to the radii of the bubbles being forced together. Figure 7 shows P_f as a function of the pressure exerted (each point is the average of many experiments).

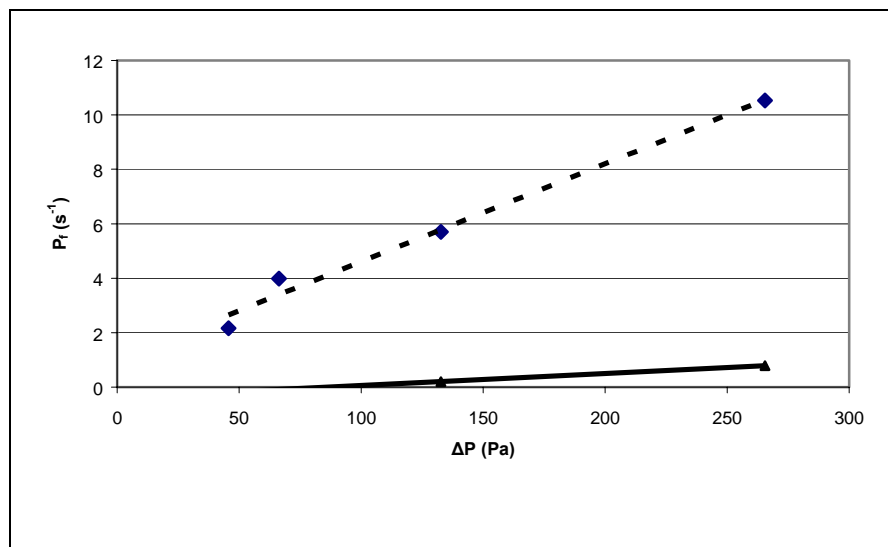


Fig. 7: P_f vs pressure exerted from micro-manipulation experiments (----- PA 50 mg/l, — PA 500 mg/l)

Figure 7 clearly shows that the relationship between P_f and the applied pressure is linear, as would be expected from film drainage theory (equation 1). The intercept is approximately zero for the low concentration experiments, which indicates virtually no electric double layer barrier, while the higher concentration experiments suggest at least some pressure barrier to coalescence.

FOAM EXPERIMENTS AND SIMULATIONS

The high film failure frequencies shown in Figure 7 indicate that, even for the higher concentration, polymaleic acid foams will be very unstable. The foam height results are plotted with results from the simulations in Figure 8. For both the experimental and simulated results a near-linear relationship between foam depth and air rate is observed.

Note that the simulations suggest a strong dependency between the incoming bubble size and the equilibrium foam depth, with larger bubbles producing deeper foams. This foam is very unstable, with only a few layers of bubbles existing. Unfortunately, in these experiments, the accurate measurement of the incoming bubble size was not possible, but the incoming bubble size was in the range of 1.5mm to 2.5mm, which, as shown in Figure 8, gives close correspondence between experiment and theory.

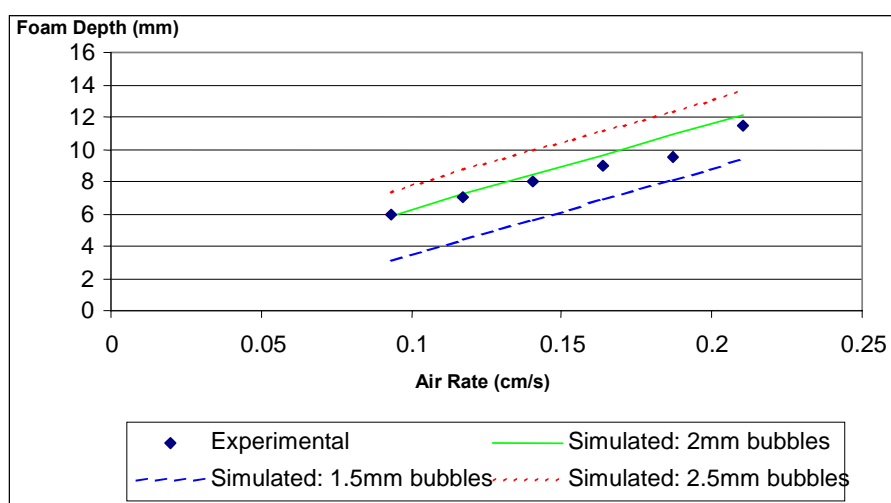


Fig. 8: Experimental and simulated results for 500 mg/l polymaleic acid solution

CONCLUSIONS

Humic substances can have an effect on bubble coalescence, and as a consequence on froth stability. Humic substances at low concentrations will retard bubble coalescence, while at high concentrations can prevent coalescence completely, due to the steric interaction brought about by the macromolecules of humic substances. On the other hand, the electrolytes appear not to have any considerable impact on bubble coalescence under the experimental conditions used (i.e. at low velocity collisions). The presence of humic substances in natural water may partly interpret the stability of froths in DAF tanks in water-treatment plants. If not all the humic substance has been coagulated before entering the DAF tank, it will contribute to the stability of froth, along with other impurities also present in natural water.

By direct observation and recording of the behaviour of glass spheres between two bubbles in pure water, the following conclusions can be drawn:

- Spheres of moderate hydrophobicity ($\theta \sim 30^\circ$) could not form a TPL with the second bubble. When they were pushed against it, they slid along the surface of the bubble.

- As long as the low hydrophobic spheres were between the two bubbles, no film rupture occurred and the bubbles remained intact. When the spheres eventually slipped completely from the space between the bubbles, the bubbles then came in contact and, depending on the purity of the liquid film, immediately coalesced.
- Highly hydrophobic glass spheres ($\theta > 100^\circ$) penetrate the lower bubble, forming a second TPL. The bubbles coalesced because the two TPLs moved on the same position over the surface of the sphere.

The form for the drainage time limited case of P_f was experimentally verified and simulations of the height of foam columns using this form showed close correspondence to experimental results. Further investigation on the effect of solid particles on bubble coalescence is needed, particularly testing their effect when the interaction takes place in aquatic solutions of surfactants, and not just in water, as the case in this study.

ACKNOWLEDGMENTS

The authors would like Mr Joe Hague of Thames Water Plc for providing the humic substances used in this work, as well as for the continuous information about the application of the DAF process in drinking-water treatment. Dr Len Fisher (University of Bristol, UK) collaborated in the development of the MFB. This work was funded by the Engineering and Physical Sciences Research Council, under joint grants GR/M98647 and GR/M98685.

REFERENCES

- ADKINS, M.F., (1997), *Dissolved Air Flotation and the Canadian Experience*. Proc CIWEM, pp 289-307.
- ANDERSON, M.A., HUNG, A., MILLS, D., SCOTT, M.S. (1995), *Factors affecting the surface tension of soil solutions of humic acids*. Soil Science, vol 160, no 2, pp 111-116.
- BHAKTA, A., RUCKENSTEIN, E. (1997), *Decay of standing foams: drainage, coalescence and collapse*. Advances in Colloid and Interface Science, vol 70, pp 1-124.
- CILLIERS, J.J., NEETHLING, S.J., SPYRIDOPOULOS, M.T., SIMONS, S.J.R. (2003), *The failure of thin films between bubbles – from micromanipulation to foam stability*. Flotation and Flocculation: From Fundamentals to Applications, Kona, Hawaii, 29th July – 2nd Aug.
- CRAS, J.J., ROWE-TAITT, C.A., NIVENS, D.A., LIGLER, F.S. (1999), *Comparison of chemical cleaning methods of glass in preparation for silanization*. Biosensors & Bioelectronics, vol 14, no 8-9, pp 683-688.
- DARTON, R.C., SUN, K.-H. (1999), *The effect of surfactant on foam and froth properties*. Transaction of the Institution of Chemical Engineers Part A, vol 77, pp 535-542.
- DESCHENES, L.A., BARRETT, J., MULLER, L.J., FOURKAS, J.T., MOHANTY, U. (1998), *Inhibition of bubble coalescence in aqueous solutions. 1. Electrolytes*. Journal of Physical Chemistry B, vol 102, pp 5115-5119.
- DIPPENAAR, A. (1982a), *The destabilization of froth by solids. I. The mechanisms of film rupture*. International Journal of Mineral Processing, vol 9, pp 1-14.
- DIPPENAAR, A. (1982b), *The destabilization of froth by solids. II. The rate-determining step*. International Journal of Mineral Processing, vol 9, pp 15-27.

- EDZWALD, J.K. (1995), *Principles and applications of dissolved air flotation*. Water Science and Technology, vol 31, no 3-4, pp 1-23.
- FAIRBROTHER, R. J. (1998), *A Microscopic Investigation of Particle-Particle Interactions in the Presence of Liquid Binders in Relation to the Mechanisms of "Wet" Agglomeration Processes*. PhD Thesis, University College London.
- GREGORY, J. (1993), *The role of colloid interactions in solid-liquid separation*. Water Science and Technology, vol 27, no 10, pp 1-17.
- GREGORY, R., (1997), *Summary of general developments in DAF for water treatment since 1976*. Proc CIWEM, pp 1-8.
- HAARHOFF, J., van VUUREN, L.R.J. (1995), *Design parameters for dissolved air flotation in South Africa*. Water Science and Technology, vol 31, no 3-4, pp 203-212.
- HEINANEN, J., JOKELA, P., ALA-PEIJARI, T. (1995), *Use of dissolved air flotation in potable water treatment in Finland*. Water Science and Technology, vol 31, no 3-4, pp 225-238.
- JOHANSSON, G., PUGH, R.J. (1992), *The influence of particle size and hydrophobicity on the stability of mineralized froths*. International Journal of Mineral Processing, vol 34, pp 1-21.
- LESSARD, R.R., ZIEMINSKI, S.A. (1971), *Bubble Coalescence and Gas Transfer in Aqueous Electrolytic Solutions*. Industrial Engineering.Chem.Fundam., vol 10, no 2, pp 260-269.
- LASKOWSKI, J.S., CHO, Y.S. AND DING, K. (2003), *Effect of Frothers on Bubble Size and Foam Stability in Potash Ore Flotation Systems*, Canadian J. Chemical Engineering, Vol. 81, 63-69.
- NEETHLING, S.J., LEE, H.S., CILLIERS, J.J. (2002), *A foam drainage equation generalised for all liquid contents*, Journal of Physics: Condensed Matter, 14, 331-342
- NICKOLS, D., MOERSCHHELL, G.C., BRODER, M.V. (1995), *The first DAF water treatment plant in the United States*. Water Science and Technology, vol 31, no 3-4, pp 239-246.
- OOLMAN T.O., BLANCH, H.W. (1986), *Bubble coalescence in stagnant liquids*. Chemical Engineering Communications, vol 43, pp 237-261.
- PASHLEY, R.M., CRAIG, V.S.J. (1997), *Effects of Electrolytes on Bubble Coalescence*. Langmuir, vol 13, pp 4772-4774.
- PUGH, R.J. (1996), *Foaming, foam films, antifoaming and defoaming*. Advances in Colloid and Interface Science, vol 64, pp 67-142.
- ROSS, V.E. (1991), *The Behavior of Particles in Flotation Froths*. Minerals Engineering, vol 4, no 7-11, pp 959-974.
- SCHMIDT, P.D., TOBIASON, J.E., EDZWALD, J.K., DUNN, H. (1995). DAF treatment of a reservoir water supply: comparison with in-line direct filtration and control of organic matter. *Water Science and Technology*, vol 31, no 3-4, pp 103-111.
- SPYRIDOPOULOS, M.T., SIMONS, S.J.R., (2004), *Direct Measurement of Bubble-Particle Adhesion Forces on the Effects of Particle Hydrophobicity and Surfactants*, Transaction of the Institution of Chemical Engineers Part A, 82, 490-498.
- THURMAN, E. M. (1985), *Organic Geochemistry of Natural Waters*. Martinus Nijhoff/Dr W.Junk Publishers. Dordrecht, 361p.
- TSE, K., MARTIN, T., MCFARLANE, C.M., NIENOW, A.W. (1998), *Visualisation of bubble coalescence in a coalescence cell, a stirred tank and a bubble column*. Chemical Engineering Science, vol 53, no 23, pp 4031-4036.
- van PUFFELEN, J., BUIJS, P.J., NUHN, P.N.A.M., HIJNEN, W.A.M. (1995), *Dissolved air flotation in potable water treatment: the Dutch experience*. Water Science and Technology, vol 31, no 3-4, pp 149-157.

Spyridopoulos M., Simons S., Neethling S., Cilliers J., *Wpływ substancji humusowych i cząstek ciała stałego na koalescencję pęcherzyków powietrza i stabilność piany w odniesieniu do zdyspergowanego powietrza w procesie flotacji*, Physicochemical Problems of Mineral Processing, 38, (2004) 37-52 (w jęz. ang.).

W pracy przeprowadzono badania nad wpływem substancji humusowych (naturalne surfaktanty), elektrolitów i cząstek ciała stałego na koalescencję pęcherzyków powietrza, a w konsekwencji na stabilność piany. Nowa aparatura została wykorzystana do pomiarów sił oddziaływań między dwoma pęcherzykami o jednakowym kształcie. Oddziaływania zostały zarejestrowane przez specjalną kamerę. Obrazy z kamery pozwoliły określić częstotliwość i czas koalescencji, jak również mechanizmy oddziaływania. Dwa rodzaje substancji humusowych użyto do badań oraz trzy rodzaje elektrolitów. Okazało się, że substancje humusowe miały istotny wpływ na koalescencję pęcherzyków. Wpływ elektrolitów był minimalny. Kule szklane o średnim i wysokim stopniu hydrofobowości powierzchni były umieszczane między pęcherzykami. Kule o dużej hydrofobowości powierzchni powodowały szybszą koalescencję pęcherzyków, podczas gdy, kule o średniej hydrofobowości powierzchni nie wykazywały tego efektu. W pracy przedstawiono dane dotyczące częstotliwości koalescencji. Te dane zostały użyte do weryfikacji parametru P_b , określanego jako częstotliwość rozerwania filmu. Parametr ten został użyty w modelu symulacyjnym, który określał wysokość piany w naczyniu. Otrzymane wartości parametru P_f na podstawie modelu, zostały eksperymentalnie zweryfikowane.

Hussin A.M. AHMED and Jan DRZYMALA*

EFFECT OF FLOTATION PROCEDURE AND COMPOSITION OF REAGENTS ON YIELD OF A DIFFICULT-TO-FLOAT COAL

Received May 10, 2004; reviewed; accepted June 25, 2004

The paper discusses two procedures of flotation of difficult-to-float oxidized coal. The first one is the normal flotation procedure which relies on wetting coal with water followed by addition of flotation reagents (dodecane, dodecyl tetraoxyethelene ether (C₁₂E₄), and 1-pentanol). The second, direct contact procedure consists of mixing pure reagents with dry coal followed by addition of water. Investigation showed that for both procedures and applied chemicals, the yield – reagent dosage curves reached a plateau. The yield plateau level was 10 g/kg for normal flotation and 20 g/kg for direct contact flotation. At the plateau dosage, normal flotation provided a maximum clean coal yield of only 70% with mixed two-reagent (C₁₂E₄ + 1-pentanol). The second procedure resulted in a maximum clean coal yield of ~94 % using the same two reagent but at a higher dosage. It was also concluded that always two-reagent systems provided better flotation yields compared to one-reagent and three-reagent systems. Thus, flotation of difficult-to-float oxidized coal can be successfully accomplished by applying the direct contact flotation procedure with appropriate reagents.

Key words: flotation, flotation reagents, difficult-to-float materials, oxidized coal

INTRODUCTION

Flotation is one of the most effective techniques for upgrading coals (Davis, 1948; Aplan, 1977 and 1997; Vamvuka and Agridiotis, 2001). For low rank and oxidized coals, however, the process requires certain improvement (Chander, et al, 1994). Various modifications have been proposed to increase flotation of difficult-to-float oxidized coals. The most important include the use mixtures of reagents (collector – co-collector, collector – promoter and collector – promoter-surfactant systems) and two-stage addition of emulsified oily-collector with frother (Firth et al, 1979; Fuerstenau, 1981; Majka-Myrcha and Sobieraj, 1987; Moxon and Keast-Jones, 1986;

* Wrocław University of Technology, Wybrzeże Wyspińskiego 27, 50-370 Wrocław,
jan.drzymala@pwr.wroc.pl

Diao and Fuerstenau, 1992; Aktas and Woodburn, 1994). The use of certain reagent mixtures (oils + ionic collectors or oils + non-ionic surfactants) has been well-documented in literature (Moxon et al. 1988; Chander et al. 1996; Vamvuka and Agridiotis, 2001; Murat et al., 2003). The success of such mixtures to achieve acceptable results was explained by co-adsorption with formation of a mixed film at the tested material surface, which improves adsorption density and increases hydrophobicity (Rao and Frossberg, 1997; Jia, et al., 2000).

Studies related to modification of flotation procedure to improve coal flotation are rare (Mohanty et al. 1998). For this reason, the aim of this work is to improve flotation of highly oxidized coals by modification of the way the reagents are contacted with coal coupled with changing the composition of the chemical reagents used in flotation.

EXPERIMENTAL

REAGENTS

Three categories of reagents were used for flotation of coal: hydrocarbon (dodecane), alcohol (1-pentanol), and dodecyl tetraoxyethelene ether ($C_{12}E_4$). The hydrocarbon usually serves as the collector, alcohol as frother while C_xE_y as modifier. They all were of commercial grades and were used without further purification. The properties of the used reagents are listed in Table 1. Stock solutions of reagents used in the experiments were prepared fresh everyday.

SOLID MATERIALS

Coal used in this investigation was obtained from the Kazimierz Juliusz Mine in Sosnowiec, Poland. It was an oxidized and difficult-to-float material. The bulk sample approximate chemical analysis reflected 3.5% ash content and 10.8 % moisture. The size distribution of coal used in flotation tests is shown in Table 2.

Table 1. Manufacturer properties of the different used reagents at 25°C

Reagent	Producer	M.W. (g/mol)	Phase	Solubility in water	Density g/cm ³
Dodecane ($C_{12}H_{26}$)	Fluka	170.34	Colorless liquid (boils at 216 °C)	Insoluble	0.749
$C_{12}E_4$ ($C_{20}H_{42}O_5$)	Fluka	362.23	Viscous liquid (viscosity 35 cP)	Insoluble (self-dispersed acts as emulsifier)	1.109
1-pentanol ($C_5H_{12}O$)	Fluka	88.15	Colorless liquid (boils at 137.3 °C)	Moderately soluble (22.66 g/dm ³)	0.811

Table 2. Size distribution and ash analysis of the investigated flotation feed

Size, mm	Wt. %	Ash %
-0.500+0.250	13.69	1.56
-0.250+0.150	15.81	2.36
-0.150+0.106	12.78	2.52
-0.106+0.075	17.87	3.62
-0.075	39.85	4.50
Total	100.0	3.35

METHODS OF FLOTATION

Flotation tests were carried out in a mechanical sub-aeration laboratory flotation machine equipped with a 1-dm³ capacity cell, fed with 100 g dry coal resulting in a solid / liquid ratio of 10 % during flotation. After determining the intended operating conditions, the test was run according to two different procedures called here normal and direct contact flotation, respectively. At the test end, clean coal concentrate and residual tailings were filtered, dried at 90-100 °C, and weighed.

The normal flotation was run by the standard well-known flotation procedure, in which coal surface was cleaned first by agitation at high solid percentage (65%) in water for three min. Flotation reagents were used as one, two and three-reagent systems. Achieving the required reagents dosage was accomplished by addition of the needed dosage of hydrocarbon (dodecane), C₁₂E₄ (nonionic surfactant), and finally alcohol (1-pentanol). The required dosage of each reagent, calculated on the bases of grams of used reagent per kg of dry coal, was taken from 1 % (wt.) stock solution or emulsion in double distilled water, followed by 3 min conditioning after each reagent addition. Flotation pH was natural. Flotation time was 10 min.

In the second procedure, called here the direct contact flotation, pure reagents were mixed with the dry coal sample manually. Sequence of reagents addition was started with the intended dosage of C₁₂E₄ followed by required dodecane dosage and finally 1-pentanol dosage was added. To ensure complete adsorption of the reagent on the coal surface, mixing was continued until no aggregates of coal with reagents were noticed. It took usually from 1 to 3 min after each reagent addition. The reagent-coated coal was transferred into the flotation cell, diluted with tap water, and conditioned for 0.5 min. Finally, aeration was started for initiation of the flotation. Flotation time was kept constant and was 10 min.

Comparing the results obtained from different series was performed by direct plotting the measured response (yield) against variable under investigation. In case of using three reagents simultaneously, the plot was done using the Gibbs triangle. In this plot, the apex of the triangle represents one reagent flotation, while the outside borders represents different ratios of two-reagent mixtures, and finally the interior of the triangle shows flotation results with three-reagent mixtures (Hussin, 2004).

RESULTS AND DISCUSSION

NORMAL FLOTATION PROCEDURE

Flotation results of a difficult-to-float coal using different doses of one-reagent and two-reagent mixtures approach at selected compositions of the mixture are shown in Fig. 1. It is clear from this series that a single-reagent normal flotation procedure leads to a maximum yield of about 37% at a dosage of 10 g/kg $C_{12}E_4$ in spite of the moderate success of using such kind of nonionic surfactants for flotation of other oxidized coals (Jia et al. 2000). At the same time, increasing the reagent dosage above 10g/kg level did not provide any improvement. This reflects the high oxidation state of the coal surface, and the difficulty of its flotation using one-reagent normal flotation procedure. On the other hand, two-reagent systems (dodecane and 1-pentanol, dodecane and $C_{12}E_4$, as well as 1-pentanol and $C_{12}E_4$) at a total dosage of 10 g/kg provided a maximum clean coal yields of ~ 50%, 45 and 61% , respectively. These yields are higher than those obtained with one-reagent. Such an increase is usually attributed to the interactions between reagents leading to their improved adsorptions on the coal surface.

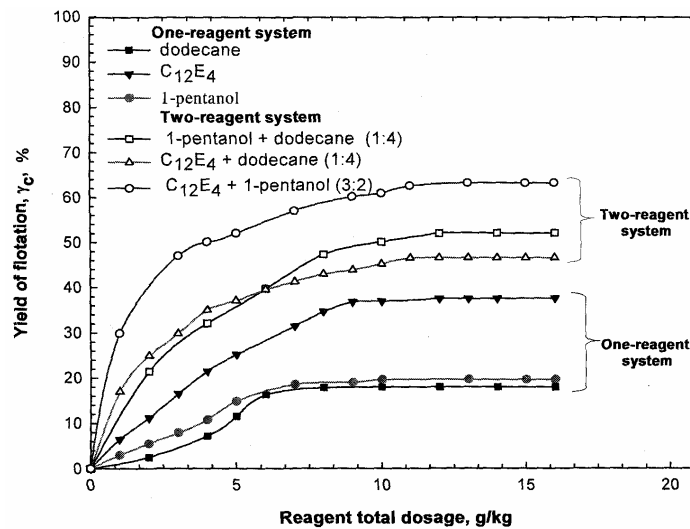


Fig. 1. Effect of one reagent and two-reagent dosage on flotation yield of coal using normal flotation procedure

It can be seen from Fig.1 that in each case there is a maximum yield (plateau), which can be achieved with a given composition of reagents, and the yield is never greater than about 60%. To see whether the yield can be higher in the presence of the three-reagents used in this work, another series of tests was carried out with the oxidized coal at the total dosage of the three-reagent mixtures of 10 g/kg. The results

of this series together with the selected data from Fig.1 are presented as the Gibbs triangle in Fig. 2. The plot has the studied reagent combinations marked as circles and the obtained yield values written as numbers beside the circles. From Fig. 2, one can notice that a maximum yield of the clean coal was ~ 61% and was obtained at 6 g/kg C₁₂E₄ together with 4 g/kg of 1-pentanol, which is a two-reagent system. Thus, lower clean coal yields were obtained applying one-reagent or three-reagent combinations.

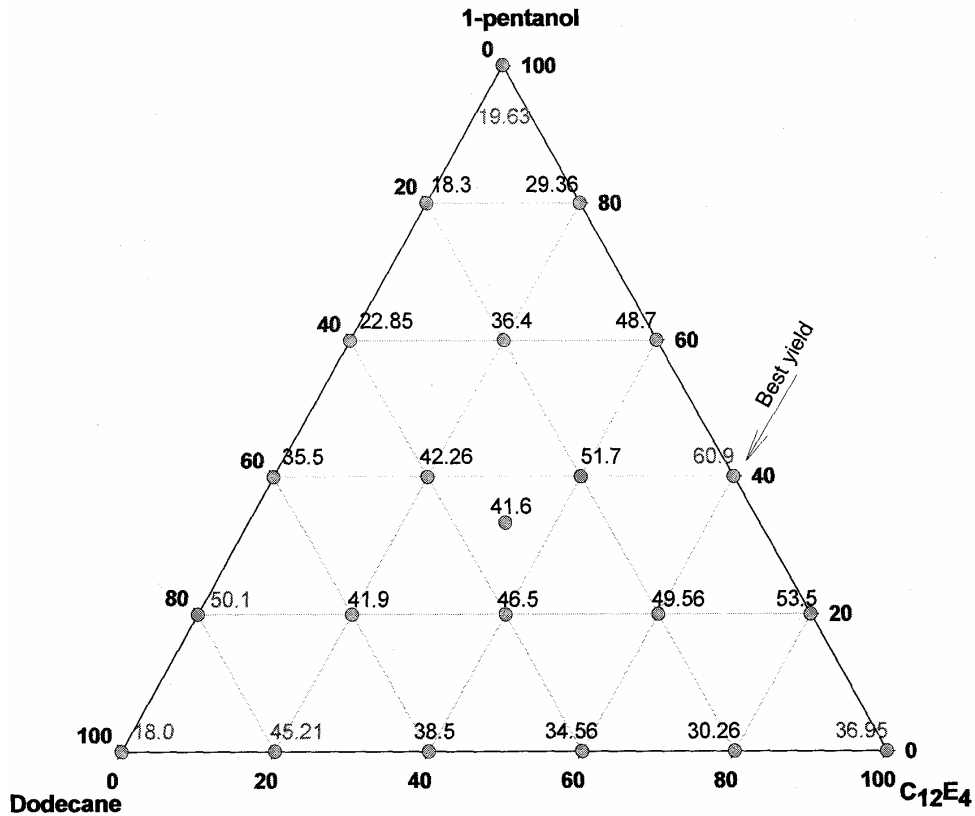


Fig. 2. Effect of dodecane - C₁₂E₄ - 1-pentanol combinations on clean coal yield, at a total dosage of 10 g/kg using normal flotation procedure. Ratios among the three reagents are the same as read from ternary plot. Circles represent studied points, numbers show clean coal yield

The relatively poor results obtained applying the normal procedure of flotation with the investigated coal can be attributed to many different factors. The main two parameters seem to be a high oxidation of the coal surface and / or the different not-enough-hydrophobic structures (micelles, emulsions, microemulsions, liquid crystals) formed from the used mixed reagents. Thus, the approach of increasing number of reagents is not successful. Therefore, further investigations were conducted with another procedure of flotation.

DIRECT CONTACT FLOTATION PROCEDURE

Oxidized coals are easy wetted with water and adsorption of hydrophobization reagents is hindered. Therefore we assumed that adsorption of the same chemicals on dry coal surface would be much more efficient and further addition of water to the system would only partially decrease the adsorption. To evaluate the effect of the direct contact procedure in comparison to the normal flotation procedure, we used the same flotation reagents in the tests.

Effect of dosage of one-reagent and two-reagent flotation systems

Figure 3 depicts clean coal yield using different reagents applying the direct contact flotation procedure. The chemicals used were the same as in the normal flotation tests. It can be noticed from Fig. 3 that changing the dosage of one-reagent using direct contact procedure leads to a better flotation yield than applying the normal flotation procedure.

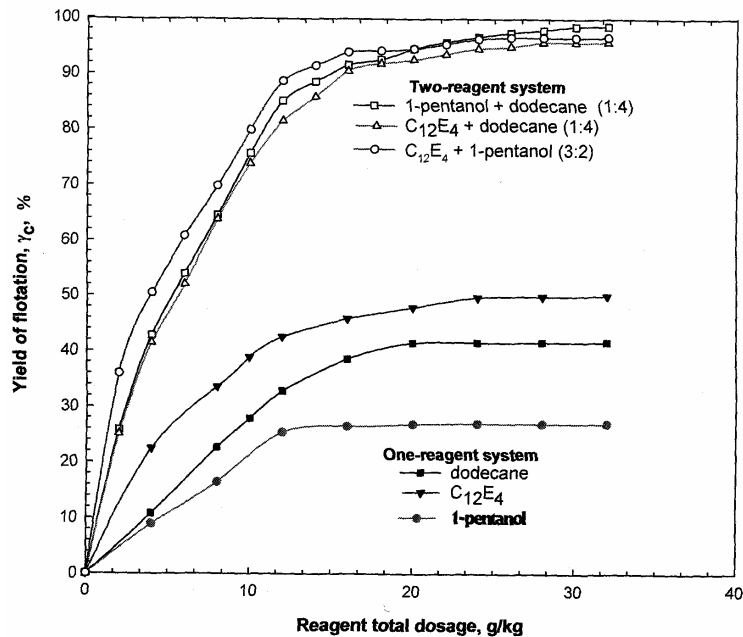


Fig. 3. Effect of one reagent and two-reagent dosage on the flotation yield of coal using direct contact flotation procedure

A maximum flotation yield of ~41.5% at 20 g/kg dodecane was obtained in comparison with a maximum flotation yield of ~18 % at a dose of 10 g/kg when using normal flotation procedure. In the case of nonionic surfactant (C₁₂E₄), a maximum yield of ~50% at (20 g/kg) was obtained compared to 37 % at a dosage of 10 g/kg,

which also reflects superiority of the direct contact flotation procedure. Reagent interactions in the two-reagent systems investigated in this series reflected a significant positive synergistic effect (Fig. 3). When using dodecane + 1-pentanol, dodecane + $C_{12}E_4$, and 1-pentanol + $C_{12}E_4$ systems, at a total dosage of 20 g/kg, maximum clean coal yields of 94.5, 92.56 and 94.5% were noticed compared to ~ 50%, 45 and 61% for the same systems using the normal flotation procedure. The high yields reflect the negative effect of water during normal flotation of highly oxidized coals. In general, one can draw a conclusion that using single reagent or two-reagent mixtures in the direct-contact flotation procedure leads to an improvement in the clean coal yield but on the expense of reagent dosage used. The high reagent consumption needed by this procedure can be attributed to particles roughness and / or porosity in addition to the thickness of the formed reagent film on the solid surface. It is explained on the proposed adsorption model shown in Fig. 4.

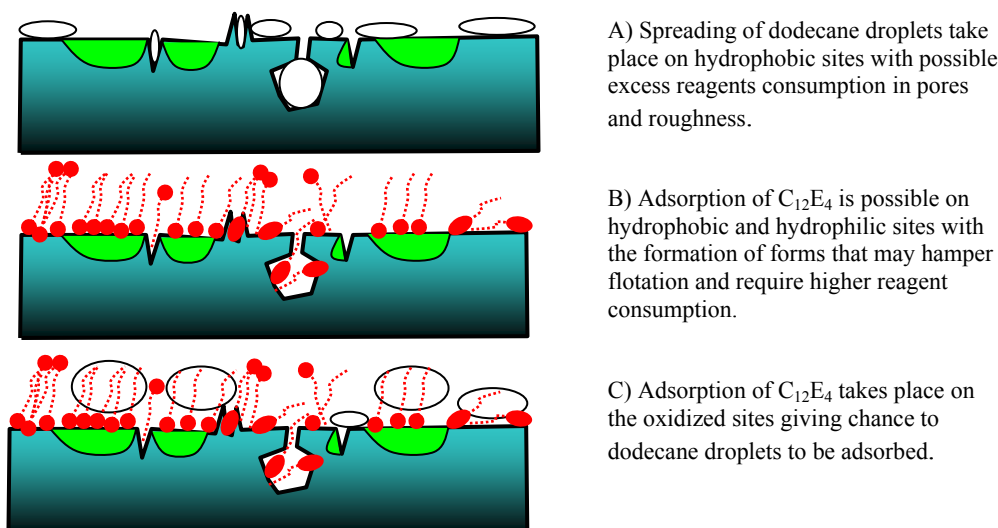


Fig. 4. Hypothetical model showing adsorption / spreading of reagents in case of direct contact flotation procedure

○ dodecane droplets ◐ oxidized sites ● nonionic surfactant

Despite the higher consumption of reagents, when applying the direct contact flotation procedure, it can be considered as successful because it provides greater yields. Further modification of the direct contact flotation for reduction of the reagents is very likely possible. One of the approaches can be the use of a third reagent, as it was done in the previous chapter using the normal flotation method.

Effect of three-reagent mixtures

The presented results showed that there exist two critical dosages of reagents: 10g/kg which represents maximum effective dosage in case of normal flotation, and 20 g/kg in direct contact flotation procedure. For this reason, the same three-reagent combinations used in normal flotation were investigated using direct contact flotation procedure at two different dosage levels, that is at 8 and 16 g/kg, just below the maximum dosage for each procedure.

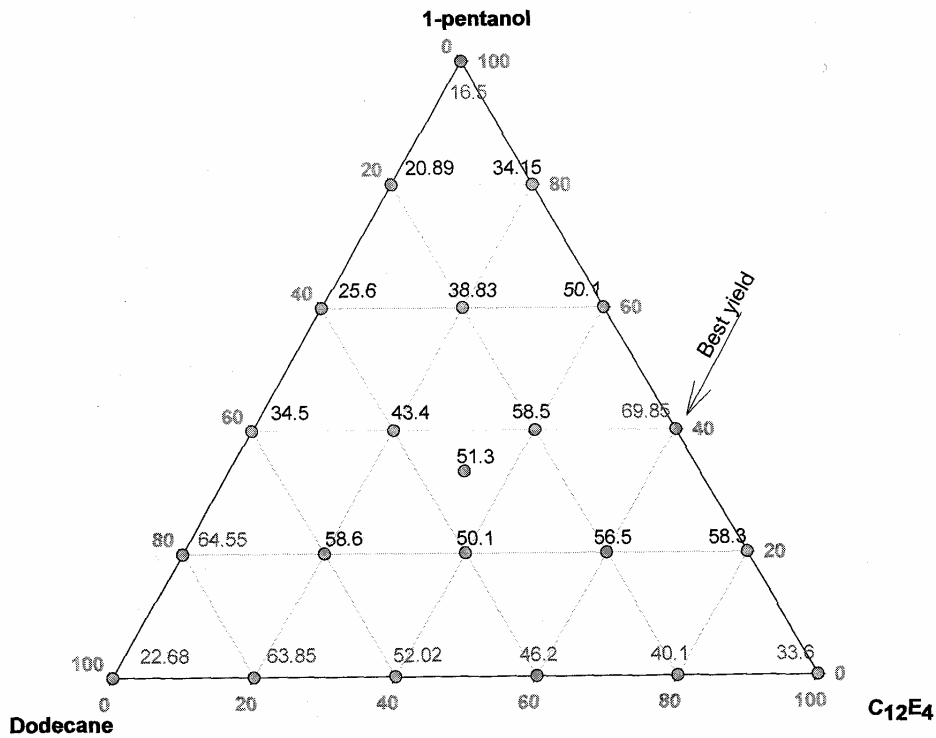


Fig. 5. Effect of dodecane - C₁₂E₄ - 1-pentanol combinations on clean coal yield, at a total dosage of 8 g/kg using direct contact flotation procedure. Ratios (in wt. %) among the three reagents are the same as read from ternary plot. Circles represent studied points, numbers show clean coal yield

Figure 5 illustrates the Gibbs triangle plot for the yield obtained from the different combinations at the lower dosage of 8 g/kg. The maximum clean coal yield obtained in both procedures was encountered at the same two-reagent system (C₁₂E₄ + 1-pentanol at the ratio of 3:2). The higher maximum yield in case of direct contact (~70%) compared with that obtained in normal flotation (~61%) can be understood taking into account the adsorption model shown in Figure 4. At the same time, all of the studied combinations (using direct contact at 8g/kg) provided higher yields

compared to that obtained by normal flotation procedure (at 10 g/kg) except the case of using 1-pentanol only. The lower yield obtained in such a case can be attributed to adsorption of too short chain length of 1-pentanol on coal pores and roughness. Thus, its consumption in coal pores is higher than the other studied reagents. Figure 6 shows yields obtained at the higher dosage level. A maximum yield of 93.85% was obtained at 9.6 g/kg $C_{12}E_4$ together with 6.4 g/kg of 1-pentanol. It confirms the superiority of the $C_{12}E_4$ - 1-pentanol system. It is also clear that the three-reagent combinations did not result in encouraging results even for the direct contact procedure. This is because in all the studied systems and combinations, the highest yield of the cleaned coal was obtained on the lines of the Gibbs plot representing two-reagent combinations.

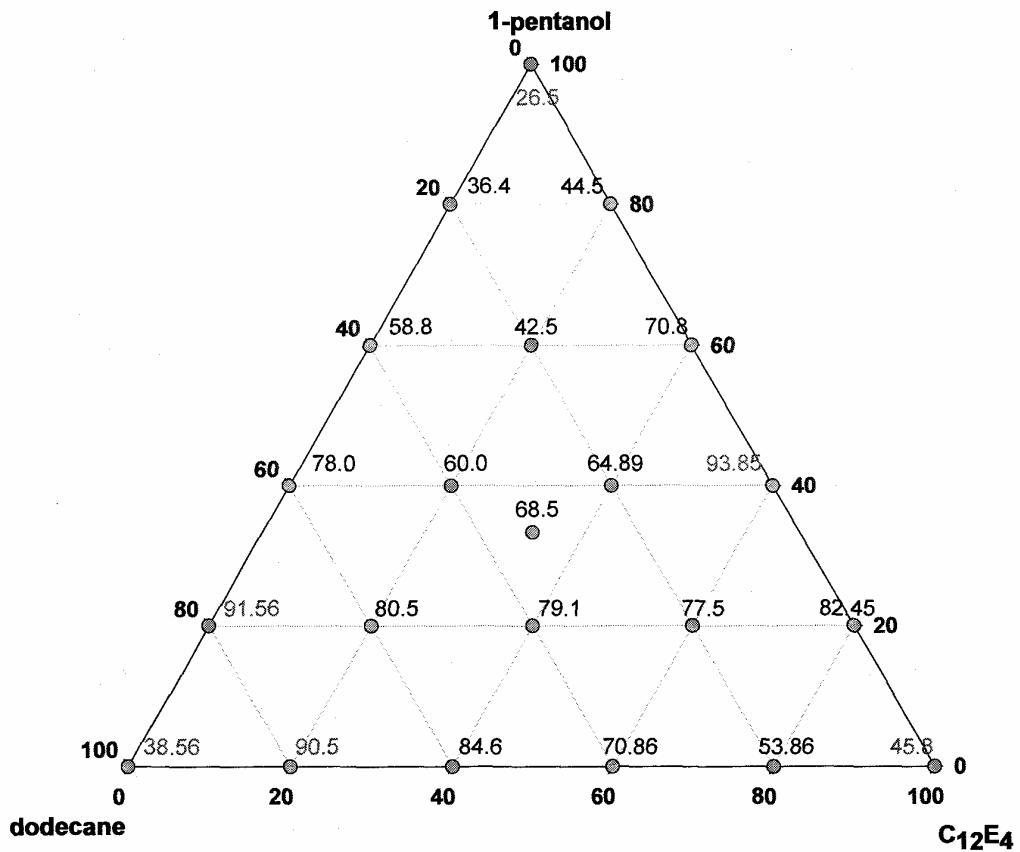


Fig. 6. Effect of dodecane - $C_{12}E_4$ - 1-pentanol combinations on clean coal yield, at a total dosage of 16 g/kg using direct contact flotation procedure. Ratios (in wt. %) among the three reagents are the same as read from ternary plot. Circles represent studied points, numbers show clean coal yield

CONCLUSIONS

From this study one can draw the following conclusions:

1. One-reagent flotation resulted in poor clean coal yields for both normal and direct contact flotation procedures.
2. After a certain dosage of the reagent under study, 10 g/kg in normal flotation and 20 g/kg in direct contact flotation, the further improvement in clean coal yield can be considered insignificant.
3. Using a two-reagent system improves flotation. Flotation improvement was higher in case of the direct contact flotation.
4. For both of the studied flotation procedures, three-reagent combinations provided relatively poor clean coal yields.
5. The maximum yield of cleaned difficult-to-float coal was ~94% for 9.6 g/kg C₁₂E₄ mixed with 6.4 g/kg of 1-pentanol for direct contact flotation, while in normal flotation procedure the maximum clean coal yield was ~70%.

REFERENCES

- AKTAS, Z., WOODBURN, E.T., 1994, *The adsorption behaviour of non-ionic reagents on two low rank British coals*, Miner. Eng. 7 9, 1115.
- APLAN, F., 1997, *The historical development of coal flotation in the United States*, In: Parekh, B.K., Miller, J.D. (Eds.), *Advances in Flotation Technology*. SME, Littleton, CO, pp. 269–287.
- APLAN, F.F., 1977, In: *Use of the flotation process for desulfurization of coal*, Wheelock, T.D. Ed. , Coal Desulfurization, ACS Symposium Series 64 American Chemical Society, Washington, DC, pp. 70–82.
- CHANDER, S., POLAT, H., MOHAL, B., 1994, *Flotation and wettability of a low rank coal in the presence of surfactants*, Miner. Metall. Process. 55, Feb.1994.
- CHANDER, S., POLAT, H., POLAT, M., 1996, *Mechanism of coal flotation by insoluble collectors in the presence of PEO/PPO/PEO block copolymers*, In: Kemal, M. (Ed.), *Proceedings of VI. IMPS*. Balkema, Rotterdam, pp. 461–467.
- DAVIS, D.H., 1948, *Froth flotation of minus 48-mesh bituminous coal slurries*, Trans. AIME 177, 320–337.
- DIAO, J., FUERSTENAU, D.W., 1992, *Characterization of coal oxidation and coal wetting behavior by film flotation*, Coal Preparation 10, 1–17.
- FIRTH, B.A., SWANSON, A.R., NICOL, S.K., 1979, *Flotation circuits for poorly floating coals*, Int. J. Miner. Process. 11, 321–334.
- FUERSTENAU, D.W. (Ed.), 1981, *Mathematical Models of Flotation. Mineral Coal Flotation Circuits—Their Simulation and Control*, Elsevier, New York, vol. 3, pp. 57–70.
- HUSSIN A.M. AHMED, 2004, *Graphical representation of flotation results affected by up to three variables*, Prace Naukowe Instytutu Górnictwa Politechniki Wrocławskiej journal 107, Konferencje 39, 249-261.
- JIA, R., HARRIS, G.H., FUERSTENAU, D.W., 2000, *An improved class of universal collectors for the flotation of oxidized and/or low-rank coal*, Int. J. Miner. Process. 58, 99–118.
- MAJKA-MYRCHA, B., SOBIERAJ, S., 1987, *The effect of ionic flotation reagents and the oxidation of the surface upon the flotation of hard coal by means of an apolar collector*, Trans. Tech. Univ. Silesia, 45, Series: Mining No. 160.
- MOHANTY, M.K., HONAKER, R.Q., HO, K., 1998, *Coal flotation washability: development of an advanced procedure*, Coal Preparation 19, 51–67.

- MOXON, N.T., KEAST-JONES, R., 1986, *The effect of collector emulsification using non-ionic surfactants on the flotation of coarse coal particles*, Int. J. Miner. Process, 18, 21–32.
- MOXON, N.T., KEAST-JONES, R., ASTON, J.R., 1988, *Increased coarse coal yield from flotation using non-ionic frothers*, Int. J. Miner. Process. 24, 295–305.
- MURAT EROL, CIGDEM COLDUROGLU, ZEKI AKTAS, 2003, *The effect of reagents and reagent mixtures on froth flotation of coal fines*, Int. J. Miner. Process. 1637, 1–15.
- RAO HANUMANTHA K., AND FROSSBERG K. S. E., 1997, *Mixed Collector System in Flotation*, Int. J. of Mineral Processing, Vol. 51, pp. 67-79.
- VAMVUKA, D., AGRIDIOTIS, V., 2001, *The effect of chemical reagents on lignite flotation*, Int. J. Miner. Process. 61, 209–224.

Ahmed Hussin A.M., Drzymała J., *Wpływ procedury flotacyjnej i składu reagentów na wychód trudno flotowalnego węgla*, Physicochemical Problems of Mineral Processing, 38, (2004) 52-63 (w jęz. ang.).

W artykule przedstawiono dwie różne procedury flotacyjne stosowane we flotacji trudno flotowalnego, utlenionego węgla. Pierwsza procedura jest to tradycyjna procedura flotacyjna, która polega na zmieszaniu węgla z wodą, a następnie dodaniu odczynników (dodekan, eter dodecyloetraoksylenu $C_{12}E_4$ i 1-pentanolu). Druga procedura polega na bezpośrednim kontakcie mieszaniny czystych odczynników z suchym węglem, a następnie dodawaniu wody. Badania pokazały, że dla obu zastosowanych procedur, krzywe obrazujące zależność wychodu od ilości dodanego reagentu osiągnęły plateau. Wartość plateau dla normalnej flotacji wynosiła 10 g/kg i 20 g/kg dla flotacji z bezpośrednim kontaktem reagentu. Przy dodatku odczynników odpowiadającym plateau, flotacja prowadzona zgodnie z normalną procedurą dostarcza węgiel z wydajnością 70% w przypadku mieszaniny odczynników ($C_{12}E_4$ + 1-pentanol). Zastosowanie drugiej procedury pozwala uzyskać wydajność czystego węgla ~94% przy zastosowaniu tej samej mieszaniny odczynników, ale w większej ilości. Ustalono, że układy składające się z dwóch odczynników zapewniają lepszy wychód węgla w porównaniu do układów z jednym lub trzema odczynnikami. Flotacja trudno flotowalnego węgla może być z powodzeniem zrealizowana przy użyciu procedury bezpośredniego kontaktu odczynników z węglem.

V.A. CHANTURIYA, V.E. VIGDERGAUZ, L.M. SARKISOVA, A.I. DOROFEEV*

THE HYDROPHILIC-HYDROPHOBIC TRANSITIONS ON CHALCOPYRITE: ELECTROCHEMICAL STUDY

Received March 14, 2004; reviewed; accepted May 15, 2004

The properties of chalcopyrite were studied by the methods of cyclic voltammetry, potentiometry, X-ray photoelectron spectroscopy and various techniques of the evaluation of wettability. Results of an experimental study of the potential and pH dependencies of the various characteristics of chalcopyrite hydrophobicity: detachment force, contact angle, gas evolution pressure and floatability, are discussed. It is shown that the detachment force/potential polarization curves are similar in shape for the case of the absence of xanthate and for the presence of all xanthates studied. The electrochemical polarization leads to generation of hydrophilic compounds and increases wettability of the mineral. A formation of the hydrophilic layer of iron hydroxide is a reason for decrease of hydrophobicity and floatability under oxidative conditions. Xanthate desorption leads to hydrophilisation of the mineral surface and depression under flotation in the cathodic area.

Key words: chalcopyrite, flotation, induction time, wettability cyclic, voltammetry

INTRODUCTION

Chalcopyrite is one of the most important for industry and therefore well-studied sulfide mineral [Gardner, Woods, 1979; Trahar, 1983; Finkelstein et al., 1975; Heyes, Trahar, 1977; Ammou-Chokroum et al. 1979; Peters, 1977; Eddington, 1977]. Electrochemical reactions of chalcopyrite are important for its processing by a wet mechanical dressing, flotation, and hydrometallurgy. Common practice of the operating with ores includes regulations of its redox-conditions for an optimal treatment. Fig.1 [Chanturiya, Vigdengrauz, 1993] illustrates changes of the immersed in slurry platinum electrode potential under the influence of air dissolution, sodium sulfide and potassium xanthate additions.

Irreversible changes of chalcopyrite surface composition during its polarization are well documented. In the presence of water and oxygen, chalcopyrite is thermodynamically unstable, but its oxidation is a rather slow process. This is the

* Institute of Complex Exploitation of Mineral Resources, Russian Academy of Sciences, IPKON RAN, 4 Kryukovsky, 111020 Moscow, Russia, e-mail address: vigderg@mail.com

reason for the existence of chalcopyrite in ore bodies and even in flotation tails stored for many years. There has been general agreement regarding the species responsible for rendering chalcopyrite hydrophobic and floatable. In the case of natural floatability, it is elemental sulfur and for the case of xanthate-induced flotation, it is dixanthogen and copper xanthate [Gardner, Woods, 1979; Trahar, 1983; Finkelstein et al., 1975; Heyes, Trahar, 1977; Eddington, 1977; Chanturiya, Vigdergauz, 1993].

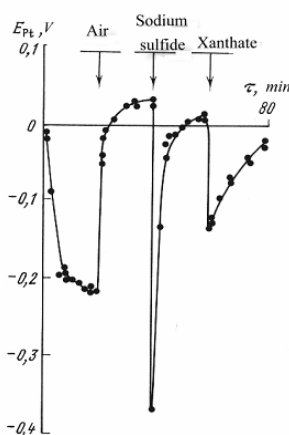


Fig. 1. Influence of reagents on the pulp potential of copper sulfide flotation

Polarization of solid electrodes changes the surface tension or surface free energy at the solid-liquid interface (γ_{sl}) that leads to the alteration of the angle of wettability. A method for the determination of the point of zero charge for metals that is based on this phenomenon is widely known [Frumkin et al., 1952]. Metal wettability has a minimum at this point. It is reasonable to assume that for the mineral-solution interface, γ_{sl} and therefore contact angle will also depend on the surface charge. As long as the charge on the mineral surface depends on the H^+ and OH^- ion concentrations, it is attractive to study pH dependences of minerals' wettability. In this paper, a summary is presented of the pH and potential dependencies of chalcopyrite wettability and possible reasons for these phenomena are proposed. There are discussed results of electrochemical studies of redox-transitions, sorption activity, wettability and flotation response of a chalcopyrite.

EXPERIMENTAL

REAGENTS PREPARATION

For the preparation of borate and phosphate buffer solutions with ionic strength $5 \cdot 10^{-2} M$, commercial salts of analytical purity were used. Potassium xanthates were obtained as commercial products from Hoechst. They were purified according to the standard procedure of two precipitations from acetone by addition of hexane.

MINERAL USED AND SURFACE PREPARATION

All experiments were carried out with n-type chalcopyrite from Kafan (Armenia) that was described earlier [Chanturiya, Vigdergauz, 1993]. Some characteristics are: Cu content 22.6; Fe content 39.0; conductivity – $3.7 \cdot 10^{-3} \Omega\text{m}^{-1}$. For flotation experiments, chalcopyrite was hand-selected, ground dry with an agate mortar and pestle, sized to $-0.16+0.08$ mm, rinsed with water to remove fines, dried, and stored in an dessicator. For cyclic voltammetry (CV), potentiometric and rotating disk (RD) experiments, a chalcopyrite disc with a diameter of 5 mm was mounted in a fluoroplast holder. The working surface was dry-polished in stages using alumina down to $0.05 \mu\text{m}$ and rinsed with distilled water or sometimes with ethanol between polishing stages. The surface was repolished immediately before using.

APPARATUS AND PROCEDURE

The mineral surface was studied by X-ray photoelectron spectroscopy (XPS) and electrochemical techniques (potentiometry, electrophoretic mobility measurements, CV and RD techniques). The X-ray photoelectron spectra were recorded with an X-ray photoelectron spectrometer IE-1 “Varian” at room temperature and pressure of 10^8 Pa with Al K α (1486.6 eV) as photon source, at 20 eV electron analyzer pass energies. Binding energies were calculated using the C 1s peak as a reference. Quantitative estimations of surface atomic ratios of Cu, Fe and S were made with integrated peak areas.

Electrochemical cells with a three-electrode system were used in CV, air bubble detachment force (DF), air bubble induction time (IT), air bubble evolution pressure (EP) and potentially controlled flotation experiments. Potentials were measured and reported versus a silver-silver chloride reference electrode, which had a potential of +0.22V against the standard hydrogen electrode. The potential of platinum mesh or chalcopyrite disc electrodes was controlled by a PI 50 potentiostat programmed with a sweep generator PR-8 (Izmeritel, Gomel, Byelorussia). A wire connected the working electrode to the external electrical circuit. The reference electrode was connected to the main compartment through a Lugging probe capillary. Current passed between the working electrode and a platinum counter electrode, which was housed in the compartment, separated from the main cell by a sintered glass disc. An X-Y recorder was used for recording cyclic voltammograms. To study xanthate sorption, spectral measurements were used [Chanturiya, Vigdengrauz, 1993].

For the evaluation of surface wettability under conditions of pH change and potentiostatic polarization the measurements of contact angle, IT, DF and EP were used. Experimental details of the measurements of an air bubble induction time, detachment force and contact angles were described earlier [Chanturiya, Vigdengrauz, 1993; Vigdergauz, Nedosekina, 1998; Vigdengrauz et al., 1996]. A torsion balance and a modified Sven-Nilsson device were used in DF and IT experiments. Induction time was defined as the minimum time necessary for the attachment of an air bubble

to the chalcopyrite surface. Air bubbles for measurements were deposited on the holder from a small diameter flat-nosed needle positioned below the holder. The bubble formation and size were controlled using a combination of plug and needle. The movement of the bubble was observed through the wall of the cell, the latter being illuminated by an electric lamp. The DF measurements were made a few seconds after the gas front had ceased to advance across the mineral surface. A freshly polished surface was used for each new series. The standard deviations of the DF values with five repeated measurements were confirmed to be less than 0.2 dyne.

For the studies of the beginning of air bubbles evolution under decompression was used the set-up that is schematically illustrated in Fig. 1.

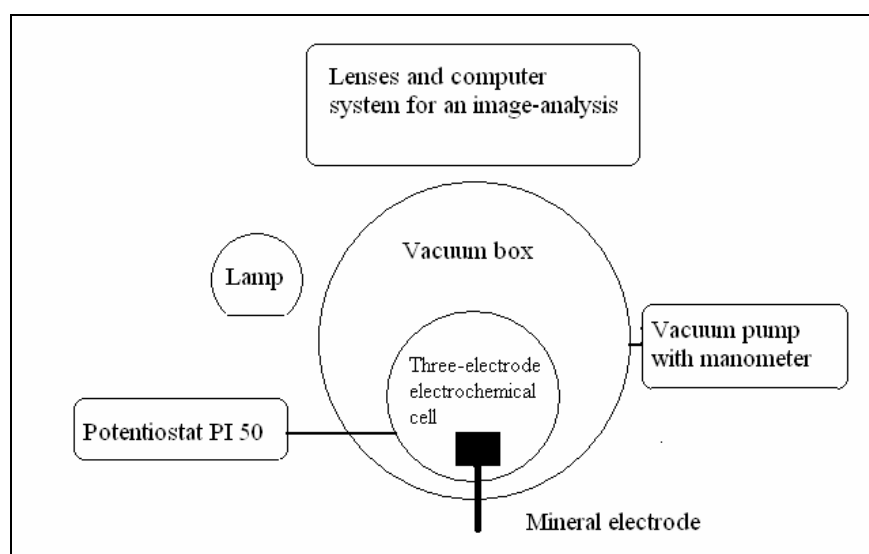


Fig. 2. Set-up for the EP-experiments

This set-up included vacuum box with vacuum pump and manometer, potentiostat, programmed with a sweep generator, electrochemical cell with a three-electrode system and photo lens with computer for an image analysis. Under potentiostatic control, the current passed between the mineral disc and a platinum counter electrode, which was housed in the compartment, separated from the main cell by a sintered glass disc. The wetting behavior can therefore be monitored over a range of anodic as well as cathodic polarization. An air bubbles evolution under decompression could be used for an evaluation of differences of surface properties of minerals. Device for the study of an electrochemical polarization influence on air bubbles evolution under decompression is a unique observatory that enables a direct view of the wetting process.

Flotation experiments were carried out in an electrochemical cell based on the Hallimond tube, Fig.3 [Chanturiya, Vigdergauz, 1993].

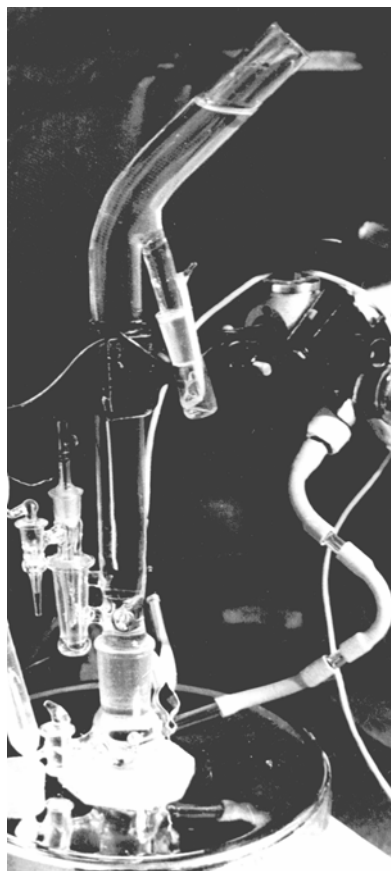


Fig. 3. The Hallimond tube cell for flotation with electrochemical treatment

The potential of the platinum mesh electrode was controlled with a potentiostat. The Hallimond tube cell design permits flotation without any frother. The usual procedure was to fill the cell with 7 ml of borate solution, load 250 mg of mineral, and condition the mineral suspension for 10 min at the desired potential prior to adding the collector. Floatability was determined by weighing the floated fraction. All flotation experiments were done with the new portions of chalcopyrite.

RESULTS AND DISCUSSION

REDOX STATE, SURFACE COMPOSITION AND REACTIVITY

X-ray photoelectron spectra of air-ground chalcopyrite show that the Fe(2p)_{3/2} spectra includes the major peak positioned at 711.7 eV associated with Fe³⁺ in a sulfide phase. The S(2p) spectra includes an intense peak arising at 162.33 eV that is usually attributable to sulfide species. One can conclude when comparing the Fe(2p) Cu(2p), and S(2p) spectra obtained with literature data [Putnis, McConnel, 1976] that

the oxidation state of the iron is 3+, that of copper is 1+, and that of sulfur is 2-. Thus, CuFeS_2 is a double sulfide of Fe_2S_3 and Cu_2S . It must also be pointed out that the position of the S(2p) maximum (about 162 eV) in the spectrum implies that elemental sulfur and sulfate are not present on the surface, even in the case of CuFeS_2 not polished.

CV study of redox-transitions on the chalcopyrite surface under cathodic and anodic polarization leads to the conclusion that both cationic and anionic sites participate in them simultaneously. It could be clearly demonstrated by a comparison of the CV-curves on the Fig. 4 [Radyushkina et al., 1986]. Rotation of the electrode leads to the removing of the maximums attributed to the reduction of copper ions and to the oxidation of hydrogen sulfide.

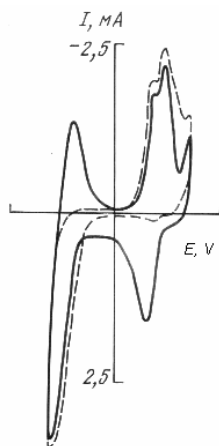


Fig. 4. Influence of rotation on the cyclic voltammograms of chalcopyrite in acid solution (pH 1.3) under potential sweep 25 mV/sec: 1 – solid curve without rotation; 2 – dotted curve under rotation 60 rev/sec

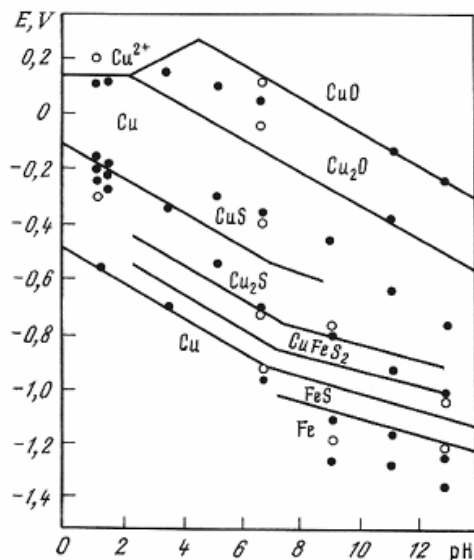


Fig. 5. Some lines of the Cu-Fe-S- H_2O diagram and potentials of the cathodic maxima of CV curves of chalcopyrite(●) and chalcocite (o)

Figure 5 shows the open-circuit potentials and the potentials of the cathodic maxima of CuFeS_2 , and Cu_2S as functions of solution pH. The same figure shows some lines from the potential-solution pH diagram of the copper-iron-sulfur system [Chanturiya, Vigdergauz, 1993].

With increasing pH the hydroxides of the metals become ever more important in the surface redox reactions of chalcopyrite. Fig.6 shows a shift of the stationary potential of the chalcopyrite electrode during long time conservation under water.

Impulse electrochemical methods (CV and impedance measurements) reflect an existence of the cationic and anionic centers on mineral surfaces. Surface of sulfide minerals is electrochemically heterogeneous and there are could be simultaneously represented cathodic and anodic areas. It was clearly shown by Plaksin and Shafeev with the help of microradiographic technique [Plaksin, Shafeev, 1959]. Moreover these surfaces are chemically heterogeneous and wettability measurements could reflect this heterogeneity. On the fresh non-oxidized surface of chalcopyrite, there are sulfur and metall sites with non-compensated negative and positive charges successively. These charges could be compensated both by regulation of pH and electrochemical potential according to the follow simplified schemes [Vigdergauz, 2001]:

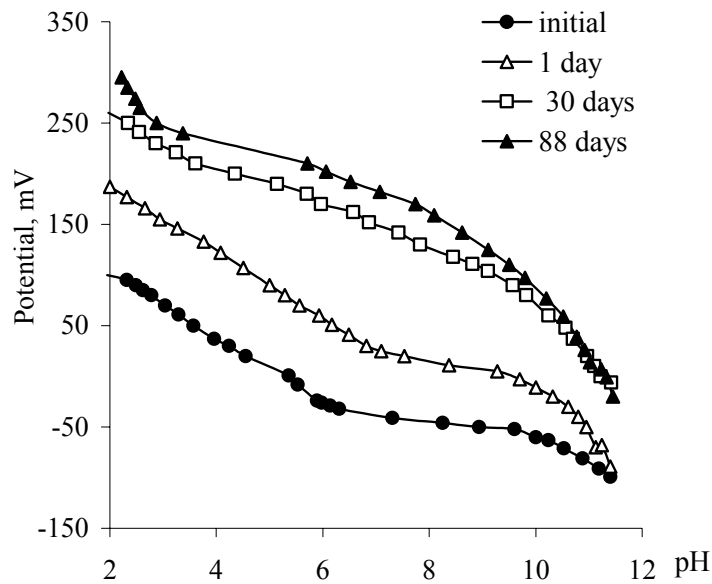
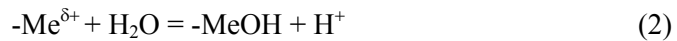
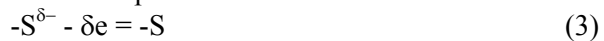


Fig. 6. Time dependence of the electrochemical potential – pH curves for chalcopyrite:
 - initial; - 1 day; - 30 days; - 88 days

I. By regulation of pH:



II. By regulation of an electrochemical potential:



EVALUATION OF WETTABILITY

Self-induced wettability was determined and also wettability induced by xanthates of different alkyl chain length. A combination of wettability measurements with electrochemical techniques has the advantage of controlling the surface oxidation state and the nature and amount of surface species present. Study of chalcopyrite wettability was carried out at various potentials of electrochemical polarization in buffer solutions with various pH.

Induction time measurements. Table 1 presents the dependence of induction time on the potential of electrochemical polarization in borate buffer solutions.

TABLE 1 The influence of the potential of chalcopyrite electrode and the length of xanthate carbon chain on the air bubble-mineral attachment and the induction time values^a

	Potential of chalcopyrite electrode, V																			
	-0.7	-0.6	-0.5	-0.4	-0.3	-0.2	-0.1	0	0.1	0.2	0.3	0.4	0.5	0.6	0.7	0.8	0.9	1.0	1.1	1.2
Xanthate	IT,sec																			
Ethyl	no ^b	no	no	no	no	no	no	2.5	0.7	0.8	0.8	0.8	0.8	2.0	2.0	no	no	no	no	no
Butyl	no	no	no	no	no	5.0	5.0	3.0	0.02	0.02	1.5	3.5	4.5	4.5	4.5	4.5	no	no	no	no
Amyl	no	no	no	no	no	no	4.0	2.0	2.0	2.0	2.5	1.5	2.0	2.0	1.5	0.4	1.5	1.5	2.5	1.5
Hexyl	no	5.0	3.5	3.5	2.5	2.0	1.5	1.5	1.5	0.1	0.45	1.5	1.5	0.6	0.02	0.02	0.004	0.004	0.004	0.5

^a Xanthate concentration, - 50 mg /dm³ or 312, 265, 248 and 231 μM for ethyl, butyl, amyl, and hexyl xanthates, respectively.

^bNo attachment

The result of increasing the carbon chain of xanthate was as a rule a decreasing IT and an expanding of the area of adhesion potentials. These data are in accordance with the well known fact that in increase in the alkyl chain of xanthate collectors leads to more rapid flotation [Vigdergauz, 2001]. In the experiments with hexyl-xanthate, we observed a cathodic shift of adhesion area of about 500 mV in comparison with the amyl-xanthate experiment. Due to the narrow adhesion interval, ethyl and butyl xanthates as collectors have an advantage for the electrochemical regulation of selective flotation processes.

From the above results, it is clearly seen that a process of bubble attachment to a planar surface is a rather slow one. It was shown that an induction time in the experiments with flat surfaces is two orders of magnitude bigger in comparison with the values determined in the experiments with powders [Sutherland, Wark, 1955]. So IT results could only be used for the approximate comparison of surface wettability and preliminary evaluation of its influence on flotation response.

Air bubble detachment force and calculated contact angles. Detachment force/potential polarization curves are similar in shape for the absence of xanthate and for the presence of all the xanthates studied, Fig.7. The qualitatively similar character of the dependences of hydrophobicity functions with and without collector leads to the conclusion that xanthate ions block metal sites that give an input to the total hydrophobicity, but the basic influence is the self-induced hydrophobicity of chalcopyrite due to the influence of S-sites.

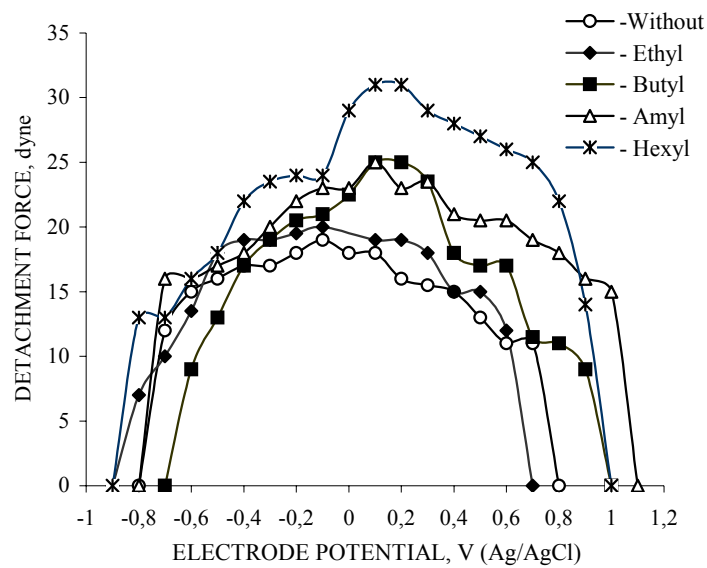


Fig. 7. DF dependences on the potential of chalcopyrite electrode

For the comparison of the observed DF results with the data on contact angles, a procedure was developed for the approximate evaluation of a contact angle from the measured force of detachment. DF data could be recalculated to give contact angles by Eq. 5 [Drzymala, Vigdergauz, 2001]:

$$F_d = 2\pi r_k \gamma_{lv} (1 - \cos \theta) = 4\pi r_k \gamma_{lv} \sin^2 (\theta/2) = 2\pi R \gamma_{lv} (1 - \cos \theta) \sin \theta \quad (5)$$

Eq.5 is based on the process of detachment with the formation of new interfaces while the use of equations which describe the process of rupture of the bubble from the surface and account capillary forces only does not explain the experimental values of the detachment force. Example of contact angles calculation from the experimental DF is given earlier for pyrite [Vigdergauz, 2001].

In the presence of butyl, amyl and hexyl xanthates the main DF maximum is observed near a potential of 0.2 V. This potential corresponds to that of dixanthogen layer formation on the surface. The maximum value of the detachment force changes

between 20 and 32 dyne with the increase in length of the alkyl chain of the collector. Minimum and maximum values were observed for ethyl and hexyl xanthates, respectively. Cathodic shift of DF maximums with an increasing of the length of apolar group of xanthate, Fig.7, correlates with the similar shift of IT minimums, Table 1. As it was mentioned above chalcopyrite is roughly a double sulfide of copper and iron $\text{Cu}_2\text{SFe}_2\text{S}_3$ and its DF-potential curves are in first approximation a superposition of similar curves for individual sulfides of copper and iron.

Gas evolution under decompression. Micro bubbles are produced on the mineral surface under decompression and preferably they will be appear on the hydrophobic sites. Consequently, surface wettability could be estimated by a comparison of a pressure decrease that will be enough for micro bubbles production.

Fig. 8 illustrates bubbles evolution under decompression on the surfaces of pyrite and chalcopyrite.

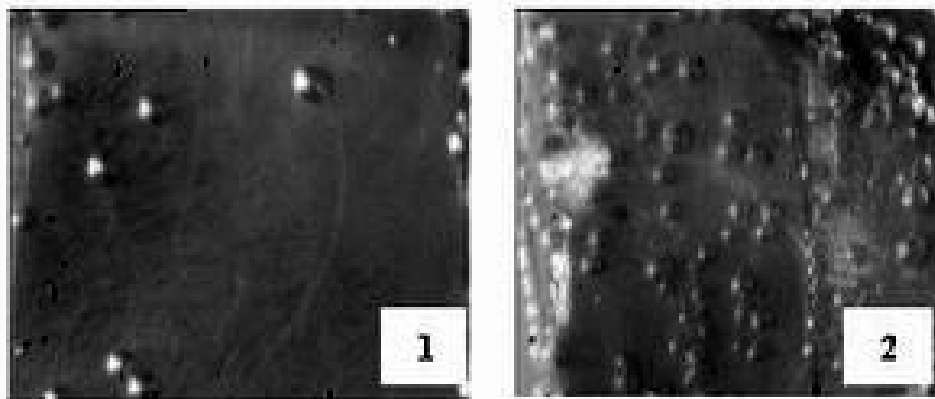


Fig. 8. Bubbles evolution under decompression (500 mm Hg) on the surfaces of pyrite (1) and chalcopyrite (2): pH 12.2 and butyl xanthate concentration 30 mg/l

Influence of an electrochemical polarization on a vacuum that leads to an emanation of bubbles on the chalcopyrite surface in weak alkaline buffer solution under butyl xanthate concentration 10 mg/l is demonstrated in Fig.9.

Area of the potentials of maxima hydrophobicity, Fig.9, corresponds with DF – potential results, Fig.7. Cathodic polarization leads to desorption of xanthate compounds from the surface of chalcopyrite electrode decreases DF and puts an end to bubble formation. Similar effects are observed under anodic polarization due the formation of hydrophilic layer of iron oxides.

Figure 2 [Vigdergauz, Panova, 2001] shows pH influence on the DF and EP values for chalcopyrite.

Comparison of Taggart's evaluation of the suction behind the blades of the impeller of an agitation-froth machine [Taggart, 1927] and EP data on chalcopyrite,

Figs.7-10, shows that gas evolution will be observed in the range of 1300-2700 revolutions of impeller per minute for hydrophobic and hydrophilic surfaces successively.

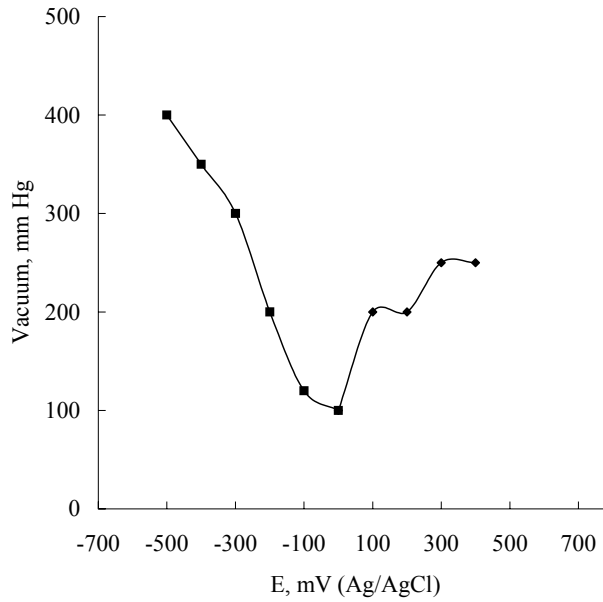


Fig. 9. Potential dependence on the decomposition of the beginning of bubbles evolution on chalcopyrite: pH 9.2 and butyl xanthate concentration 10 mg/l

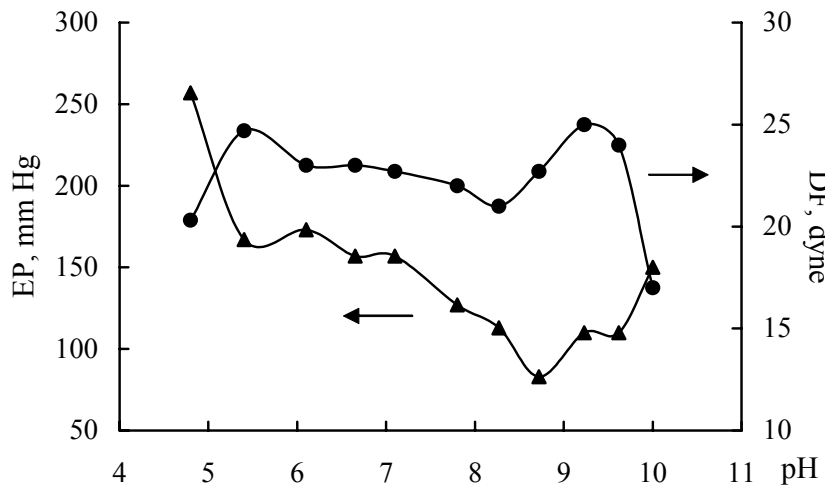


Fig. 10. DF and EP dependences on the pH for chalcopyrite

Floatability. Fig. 11 shows floatability-potential curves for chalcopyrite flotation without xanthate and in the presence of butyl xanthate [Chanturiya, Vigdergauz, 1993].

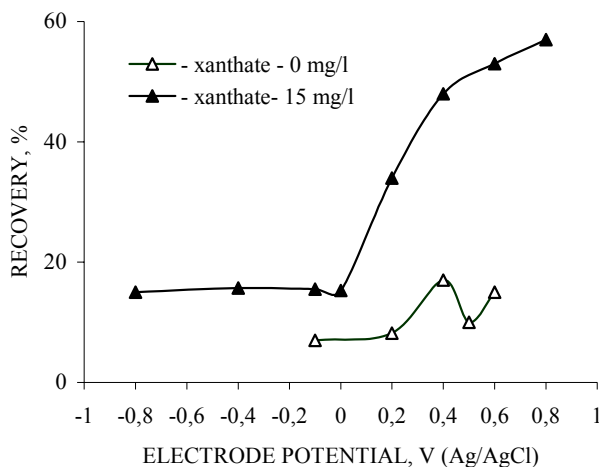


Fig. 11. Chalcopyrite floatation dependence on the potential of Pt mesh

Curves are similar in shape for the potentials of Pt mesh less than 0.4 V. Dixanthogen formation at potentials of +0.4 V and above leads to considerable increase of floatability in the experiments with xanthate.

SUMMARY

Presented results show that chalcopyrite surface is covered by cationic and anionic centres with charges that could be compensated by regulation of pH or an electrochemical potential value. Chalcopyrite surface hydrophobicity is a result of an input of hydrophilic and hydrophobic sites. Heterogeneity of the chalcopyrite surface determines the existence of pH and potential dependencies of hydrophobicity and flotation. In the case of xanthate induced hydrophobicity, a maximal hydrophobicity of chalcopyrite was observed on the stationary potential values at pH 5.5 and 9.2, and on the pH 9.2 at potentials of 0-0.2 V. A general agreement is observed between the pH of maximal hydrophobicity of bulk chalcopyrite determined by DF and EP experiments. There is also a general agreement between the potentials of maximal hydrophobicity of the bulk chalcopyrite electrode and the potentials of electrochemically-conditioned flotation of chalcopyrite. Under the conditions of froth flotation, it is necessary to account for the hydrophobicity of surface sites of major and minor influences to predict the observed phenomena. Resultant wettability reflects wettabilities of atomic or ionic sites and sorbed molecules and could be calculated through the energies of hydration of these sites.

ACKNOWLEDGEMENT

Special thanks to the Russian Foundation of Basic Researches for research grants No 00-05-64094 and 02-05-64225.

Grant of the Mr. President of the Russian Federation (No NSh 472.2003.5) is gratefully acknowledged.

REFERENCES

- GARDNER J.R., WOODS R. (1979) *An electrochemical investigation of the natural flotability of chalcopyrite*, Int.J.Minor.Process. V.6. P.1-16.
- TRAHAR W.J. (1983) *A laboratory study of the influence of sodium sulphide and oxygen on the collectorless flotation of chalcopyrite*, Int.J.Minor.Process. V.11. P.57-74.
- FINKELSTEIN N.P., ALLISON S.A., LOVELL V.M. et al. (1975) *Natural and induced hydrophobicity in sulphide mineral systems*, Advances in Interfacial Phenomena of Particulate/ Solution/ Gas Systems. Application to Flotation Research/ Ed. P.Somasundaran and R.G.Grievies. Am.Inst.Chem.Eng. Symp.Ser. N 150. V.71. P.165-175.
- HEYES G.W., TRAHAR W.J. (1977) *The natural flotability of chalcopyrite*, Int.J.Minor.Process. V.4. P.317-344.
- AMMOU-CHOKROUM M., SEN P.K., FOUQUES F. (1979) *Electrooxidation of chalcopyrite in acid chloride medium: kinetics, stoichiometry and reaction mechanism*, Proc. XIII Int. Miner. Process. Congr. Warsaw Polish Scientific Publishers. V.1. P.527-561.
- PETERS E. (1977) *The electrochemistry of sulfide minerals*, Trends in electrochemistry, Ed. Bockris J.O'M., Rand D.A.J., Welch B.J., N.Y.: Plenum Press. P.267-290.
- EDDINGTON P. (1977) *Study of oxidation layers on surfaces of chalcopyrite by use of Auger electron spectroscopy*, Inst.Min. Metall.Trans./ Sect.C. V.86. P.186-189.
- CHANTURIYA V.A., VIGDERGAUZ V.E. (1993) *Electrochemistry of Sulfides: Theory and Practice of Flotation*, (in Russian), Nauka, Moscow.
- FRUMKIN A.N., BAGOTSKI V.S., IOFA E.A., KABANOV B.N. (1952) *Kinetics of Electrode Processes*, (in Russian) MGU, Moscow.
- VIGDERGAUZ V.E., NEDOSEKINA T.V. (1998) *The Wettability of Electrodes Made of Natural Metal Sulfides*, J. Solid State Elchem., 2, 50.
- VIGDERGAUZ V.E., CHANTURIYA V.A., NEDOSEKINA T.V. (1996) *Pyrite Surface Hydrophobicity: Electrochemical Study*, Physicochemical Problems of Mineral Processing, 30, 187-192.
- PUTNIS A., MCCONNELL J.D.C. (1976) *The transformation behavior of metal-enriched chalcopyrite*, Contrib. Miner. And Petrol., 58, 127-136.
- RADYUSHKINA K.A., VIGDERGAUZ V.E., TARASEVICH M.R., CHANTURIYA V.A. *Electrochemistry of sulfide minerals: Surface redox-transitions chalcopyrite and chalcocite in aqueous solutions of electrolytes*, Soviet Electrochemistry, 22, 1491-1496 (1986).
- PLAKSIN I. N., SHAFEEV R. Sh. (1959) *In question about beginning of electrochemical heterogeneity of the surface of sulfide minerals (in Russian)*, Dokl. Akad. Nauk SSSR. V. 125, №3, P. 599-600.
- VIGDERGAUZ V.E. (2001) *Electrochemically Modified Wettability of Natural Metal Sulfides and Flotation*, Proceedings of IX Balkan Mineral Processing Conference, G.Onal, S.Atak, A.Guney, M.S.Celik and A.E.Yuce, Editors, p.187, Beril, Istanbul.
- SUTHERLAND K.L., WARK I.W. (1955) *Principles of Flotation*, Australas. Inst. Mining Met., Melbourne.
- YE Y., KHANDRIKA S.M., MILLER J.D. (1989) *Int. J. Mineral Processing*, 25, 221.

- DRZYMALA J., VIGDERGAUZ V.E. (2000) *Work and Force of Bubble-Particle Detachment as a Measure of Contact Angle in Flotation Systems*, Scientific Papers of Technical University of Wrocław, 87, 3.
- VIGDERGAUZ, V.E., PANOVA, M.V. (2002). *Air bubbles evolution on the mineral surface under decompression: 1. Pyrite, chalcopyrite, galena*, Proc.Int.Conf. Plaks. Chten., vol. 3, pp 97-98.
- TAGGART A.F. (1927) *Handbook of Ore Dressing*, Wiley & Sons, New York.

Chanturiya V.A., Vigdergauz V.E., Sarkisova L.M., Dorofeev A.I., *Zmiany hydrofobowo-hydrofilowe chalkopiryty: Badania elektrochemiczne*, Physicochemical Problems of Mineral Processing, 38, (2004) 65-78 (w jęz. ang.).

Fizykochemiczne właściwości chalkopiryty, zwłaszcza zwilżalność powierzchni zostały przebadane z wykorzystaniem takich technik badawczych jak: woltamperometria cykliczna, potencjometria, spektroskopia fotoelektryczna i inne. Przeprowadzono obszerną dyskusję otrzymanych wyników, które obejmowały zależność stopnia hydrofobowości chalkopiryty od potencjału i pH, a także siłę odrywu, kąta zwilżania, zmiany ciśnienia gazu i flotowalność. Zostało wykazane, że krzywe obrazujące zależność siły odrywu od potencjału polaryzacji wykazują podobny kształt dla przypadków braku ksantogenianu jak dla przypadku obecności ksantogenianu w układzie. Elektrochemiczna polaryzacja prowadzi do powstania hydrofilnych związków i wzrostu zwilżalności powierzchni badanego minerału. Utworzenie hydrofilnej warstwy wodorotlenku żelaza jest przyczyną obniżenia stopnia hydrofobowości i flotowalności w warunkach utleniających. Desorpcja ksantogenianu prowadzi do hydrofilizacji powierzchni i depresji we flotacji prowadzonej w warunkach katodowych.

Zafir EKMEKÇİ*, Alp ASLAN**, Hakan HASSOY*

EFFECTS OF EDTA ON SELECTIVE FLOTATION OF SULPHIDE MINERALS

Received April 21, 2004; reviewed; accepted June 21, 2004

Unwanted activation of sphalerite and pyrite by copper ions dissolved from copper minerals (mainly chalcopyrite) hampers flotation selectivity. Galvanic interaction between the sulphide minerals is considered as the main cause for such activation. Therefore, a complexing agent, EDTA, was used to prevent unwanted activation of sphalerite and pyrite by copper ions in the presence and absence of collector. In this study, unwanted activation of sphalerite and pyrite by copper ions and inhibition of this activation by using EDTA was investigated by using cyclic voltammetry and microflotation techniques. The influence of galvanic interaction between chalcopyrite-pyrite and chalcopyrite-sphalerite on flotation selectivity and the effect of EDTA were determined with microflotation tests performed with single mineral and mineral mixtures. The results pointed out dual effect of EDTA as preventing activation of sphalerite and pyrite by copper ions, but at the same time enhancing their collectorless flotation by removing the metal hydroxides from their surfaces.

Key words: flotation, sulphide minerals, activation, EDTA

INTRODUCTION

Oxidation of sulphide minerals is inevitable during processing in plant conditions. Every sulphide mineral is influenced at different degrees of oxidation by its chemical composition, crystal structure and most important its electrochemical reactivity (Ekmekçi et al. 2003). It is very well known that the flotation behaviour of a sulphide mineral, when mixed with other sulphide minerals in an ore, can be substantially different from that predicted by single and mixed mineral studies.

* Hacettepe University, Mining Engineering Department, Ankara, Turkey, zafir@hacettepe.edu.tr.

** Çayeli Bakır İşletmeleri A.Ş., Rize, Turkey.

The reasons suggested for this behaviour were attributed to galvanic interactions between sulphide minerals (Nakazawa and Iwasaki 1985; Yelloji Rao and Natarajan 1989; Ekmekçi and Demirel 1997). Unwanted activation and flotation of sphalerite in a complex lead/zinc ore or copper/zinc ore is an example to this type of behaviour. Therefore, determination of the degree of oxidation, surface species and their influence on flotation behaviour is necessary to develop processing strategies to minimize the negative effect of oxidation on flotation.

Clarke et al. (1995) has suggested some techniques to remove oxidation products, particularly metal hydroxides, from mineral surface. These techniques can be either chemical (dissolution by changing the pH, extraction by EDTA) or mechanical (sonification and attrition with quartz). Pulp pH can be adjusted to values outside the range of metal hydroxide formation and therefore mineral recovery can be improved. This method was found to prevent formation and precipitation of metal hydroxides rather than removing the previously formed oxidation products. Sonification is also considered as a potential method for selectively removing oxidation products from mineral surfaces. Preferential adsorption of metal ions dissolved from mineral surfaces on to quartz particles increased flotation performance significantly. However, it has been recognized by numerous workers (Shannon and Trahar 1986; Grano et al. 1988; Rumball and Richmond 1996) that EDTA has the ability to solubilize the oxidation products of sulphide minerals.

The negative effect of galvanic interaction in selective flotation, in enhancing the activation of pyrite by copper ions, has already been emphasized. This interference from metal ions can be prevented by the use of EDTA as a complexing agent to extract metal ions from the mineral surfaces and form complex compounds with the dissolved ions in the pulp. In this work, unwanted activation of sphalerite and pyrite by copper ions and inhibition of this activation by using EDTA was investigated by using cyclic voltammetry and microflotation techniques. The influence of galvanic interaction between chalcopyrite-pyrite and chalcopyrite-sphalerite on flotation selectivity and the effect of EDTA were determined by using mineral mixtures in microflotation scale.

MATERIALS AND METHODS

MINERALS

Natural samples of sulphide minerals of high purity were used in this study. Chalcopyrite and sphalerite were supplied by Wards Natural Science Establishment and pyrite crystals were obtained from Murgul (Artvin, Turkey) copper ore deposit.

Bulk analysis of the samples was performed by using Atomic Absorption Spectrometer at Mining Engineering Department of Hacettepe University. The results are given in Table 1. In addition to the chemical analysis, XRD analysis of the three mineral samples was also performed. The results confirmed purity of the samples (Ekmekçi et al. 2002).

Table 1. Results of bulk analysis of the natural mineral samples used in this study

Element (%)	Pyrite (FeS ₂)	Chalcopyrite (CuFeS ₂)	Sphalerite (ZnS)
Fe	44.67	29.14	1.22
Cu	0.16	35.28	0.065
Pb	0.016	0.006	0.57
Zn	0.004	0.028	60.68
S	54.13	33.30	33.61
Total	98.98	97.754	96.145

CYCLIC VOLTAMMETRY EXPERIMENTS

A conventional three-electrode system was used for electrochemical measurements in which a saturated calomel electrode, a platinum foil electrode with 1 cm² area and a mineral electrode were used as reference, counter and working electrodes respectively. The chalcopyrite and pyrite electrodes were prepared from highly mineralized massive specimens. A section of mineral with a rectangular cross-section was cut and mounted in a glass tube with an electrochemically inert epoxy resin. However, a different method was used to prepare sphalerite electrode due to its high resistivity compared to chalcopyrite and pyrite. Therefore, sphalerite was dry ground and the -100+150 µm fraction was mixed with carbon paste for electrode fabrication as proposed by Yoon and Chen (1996). The carbon paste was composed of graphite and conductive binder. The carbon paste was softened with ethyl ether and sphalerite particles were mixed at a ratio of 1/3 (mineral/paste). The homogenized mixture was then pressed into a glass tube and dried for one day for hardening. Therefore, current changes occurring at sphalerite surface were transferred with the aid of conductive carbon paste to a copper wire and then to a potentiostat.

Surface of the mineral electrodes was polished wet using 800-grit silicon carbide paper and then 1 µm diamond paste. After polishing the surface, the electrode was rinsed with distilled water and quickly transferred to the electrochemical cell. Depending on the experimental conditions CuSO₄ is first added and then EDTA into the electrochemical cell. The electrodes were conditioned for 5 minutes for each reagent addition and then scanning was started. All the experiments were performed in borate buffer solution of pH=9.2. Bank Elektronik Wenking PGS95 potentiostat/galvanostat was used for the cyclic voltammetry experiments. All the potentials reported in this paper have been converted to the standard hydrogen electrode (SHE).

MICROFLOTATION TESTS

Borate buffer solution of pH=9.2 was used in the microflotation tests. The tests were performed in a modified Hallimond tube. The mineral particles were dry ground and the fraction of -150+100 μm was used in the tests. Before conditioning, high purity (%99.99) nitrogen gas was intensively bubbled in the cell to remove dissolved oxygen. The same gas was also used for flotation. For each reagent addition the conditioning was taken as 2 minutes. Flotation was carried out for a total of 8 minutes with concentrate samples collected after 1, 3, 5 and 8 minutes of flotation. The flotation concentrates and the tail were filtered, dried and the mass of the mineral, and hence the recovery, was calculated for single mineral experiments. However, the concentrates were analyzed for Cu, Zn and Fe in the tests performed with mixtures of minerals. Calculation of the mass of mineral present in each fraction could then be made. Conditioning was performed in the following order depending on the number of reagents added; copper ions, EDTA and KEX.

RESULTS AND DISCUSSION

VOLTAMMETRY

SPHALERITE (ZnS)

Voltammograms of sphalerite taken with and without Cu^{2+} and EDTA at pH=9.2 are given in Figure 1. The scanning was commenced from the cathodic region and performed between -500 mV and +500 mV. Figure 1 shows that there is no significant electrochemical activity in this potential range in the absence of reagents. However, as the sphalerite electrode was treated with 10^{-4} M CuSO_4 , an anodic peak appeared at about 300 mV. This anodic peak corresponds to oxidation of CuS type compounds formed as a result of copper activation.

It is very well known that majority of copper ions added into alkaline solutions precipitate in the form of $\text{Cu}(\text{OH})_2$ (Fuerstenau and Fuerstenau 1982). Copper hydroxide can rapidly adsorb on sphalerite surface. However, copper sulphide may form in the following stages due to low stability of $\text{Cu}(\text{OH})_2$. At the end of activation process, sphalerite surface may be transformed into (Zn, Cu)S form. Surface analysis of copper activated sphalerite in alkaline solution by XPS has shown CuS like surface (Clarke 1997). Therefore, the anodic peak observed at about 300 mV may correspond to oxidation of CuS-like species to copper oxide and polysulphides.

After copper activation, sphalerite electrode was conditioned in the presence of 10^{-3} M EDTA to remove the adsorbed copper ions from the surface (Figure 1). The anodic peak remained in the presence of EDTA under stirred conditions, confirming formation of copper sulphide rather than copper hydroxide as an end product even at pH 9.2.

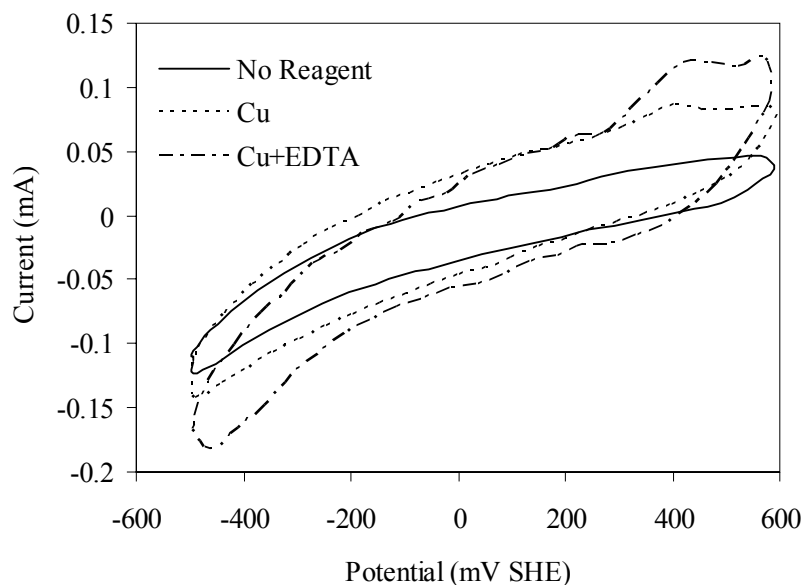
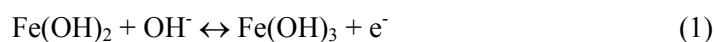


Fig. 1. Voltammograms of sphalerite with no reagent (—), 10^{-4} M Cu^{2+} (.....) and 10^{-4} M Cu^{2+} and 10^{-3} M EDTA (-.-.-) at pH=9.2. (Scan rate=50 mV/s)

PYRITE (FeS_2)

Voltammograms of pyrite taken with and without Cu^{2+} and EDTA are illustrated in Figure 2. One anodic and one cathodic peak were observed in the potential range of -500 mV and +500 mV. The anodic peak, having the maximum current at about 0 mV, corresponds to oxidation of ferrous hydroxide to ferric hydroxide form (reaction 2). This process is a reversible process and the cathodic peak corresponds to reduction of ferric hydroxide to ferrous hydroxide in the reverse direction of reaction 2.



Reversible potential of this reaction was calculated as 8.3 mV for pH 9.2, which is fairly close value to that observed in Figure 2.

Activation of pyrite by copper ions was also investigated using cyclic voltammetry. The voltammogram of pyrite taken in the presence of 10^{-4} M Cu^{2+} is given in Figure 2. It appears that in addition to the anodic and cathodic peaks showing oxidation/reduction of iron hydroxide, a new anodic appeared at about 300 mV after copper activation. It should be noted that this anodic peak appeared at the same potential to that observed with sphalerite after copper activation (Figure 1), corresponding to oxidation of CuS (reaction 1).

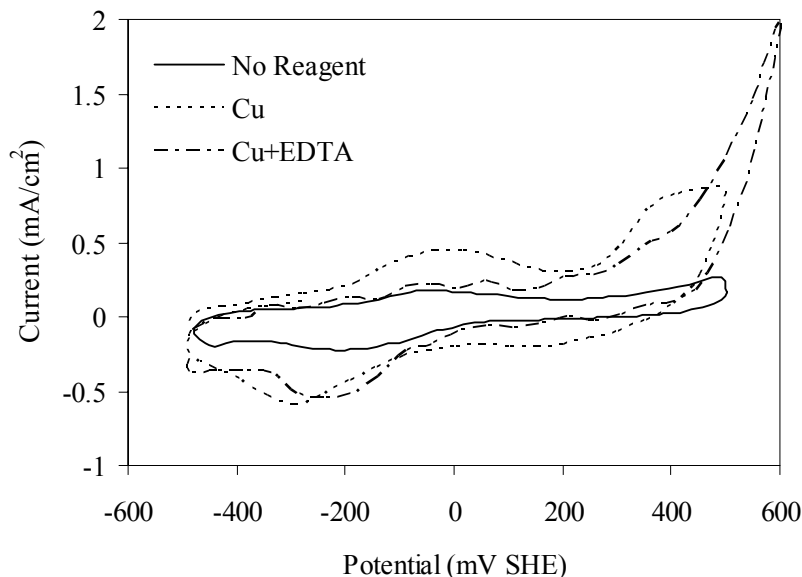


Fig. 2. Voltammograms of pyrite with no reagent (—), 10^{-4} M Cu^{2+} (.....) and 10^{-4} M Cu^{2+} and 10^{-3} M EDTA (-·-·-) at pH=9.2. (Scan rate=50 mV/s)

Voltammogram of copper activated pyrite in the presence of EDTA showed that the anodic peak showing oxidation of ferrous iron to ferric iron almost disappeared. It is well known that EDTA can easily remove the iron hydroxide species and therefore disappearance of the anodic peak at about 0 mV was anticipated. In addition to that current density of the second anodic peak, observed after copper activation, decreased substantially, in spite of the fact that CuS has higher stability than Cu-EDTA complex and therefore should not be affected by addition of EDTA. This may be related to kinetics of copper activation of pyrite, which may be slower than with sphalerite. Therefore, a large portion of copper ions might not replace iron in pyrite and still remained as $\text{Cu}(\text{OH})_2$ in the vicinity of the surface. Addition of EDTA may remove these species and resulted in considerable decrease in the current intensity of the corresponding anodic peak.

CHALCOPYRITE (CuFeS_2)

Voltammograms of chalcopyrite in the absence and presence of 10^{-4} and 10^{-3} M EDTA is illustrated in Figure 3. There were no changes in the shape of chalcopyrite voltammograms in spite of excess EDTA concentration. This result showed that EDTA did not affect chalcopyrite surface, as the anodic peak observed at about 300 mV corresponds to oxidation of chalcopyrite producing CuS at the surface.

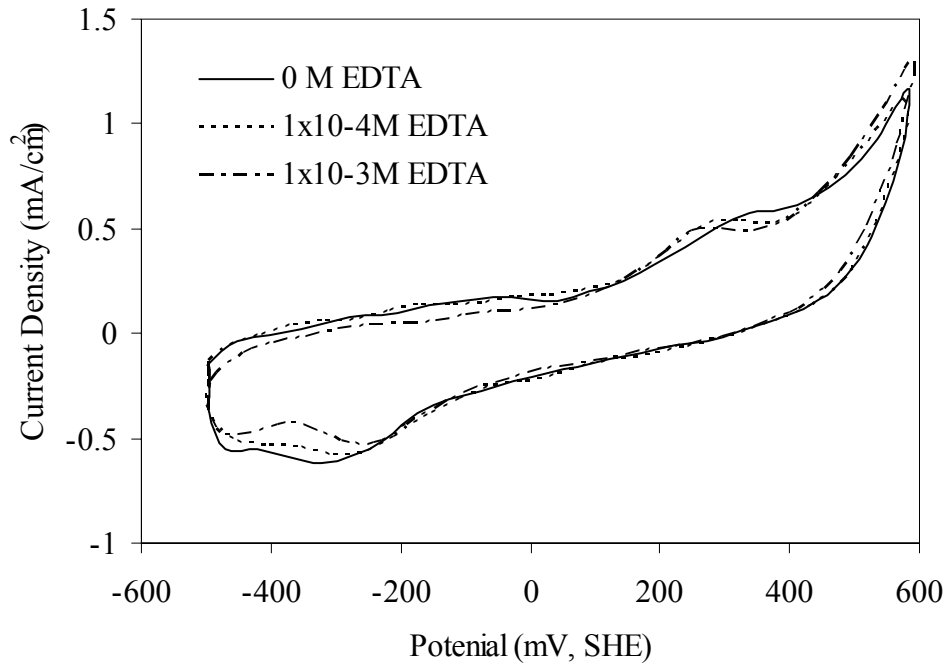


Fig. 3. Voltammograms of chalcopyrite with no reagent (—), 10^{-4} M EDTA (-----) and 10^{-3} M EDTA (- · - · -) at pH=9.2. (Scan rate=50 mV/s)

MICROFLOTATION EXPERIMENTS

Microflotation experiments give valuable information about the nature of the species, as hydrophobic or hydrophilic, which is very important for flotation. In this study flotation behaviour of the minerals were tested as single mineral and mineral mixtures (chalcopyrite-sphalerite and chalcopyrite-pyrite) in the absence and presence of ethyl xanthate (KEX). Therefore, effects of galvanic interaction and EDTA on selective flotation were investigated.

SINGLE MINERAL

SPHALERITE

Results of sphalerite flotation in the absence and presence of copper and EDTA are shown in Figure 4. Flotation recoveries of sphalerite in the absence and presence of copper ions were very low due to formation of hydrophilic $Zn(OH)_2$ and $Cu(OH)_2$ species respectively at pH 9.2. However, addition of EDTA after copper activation increased the recovery drastically from about 10 % up to 40 %.

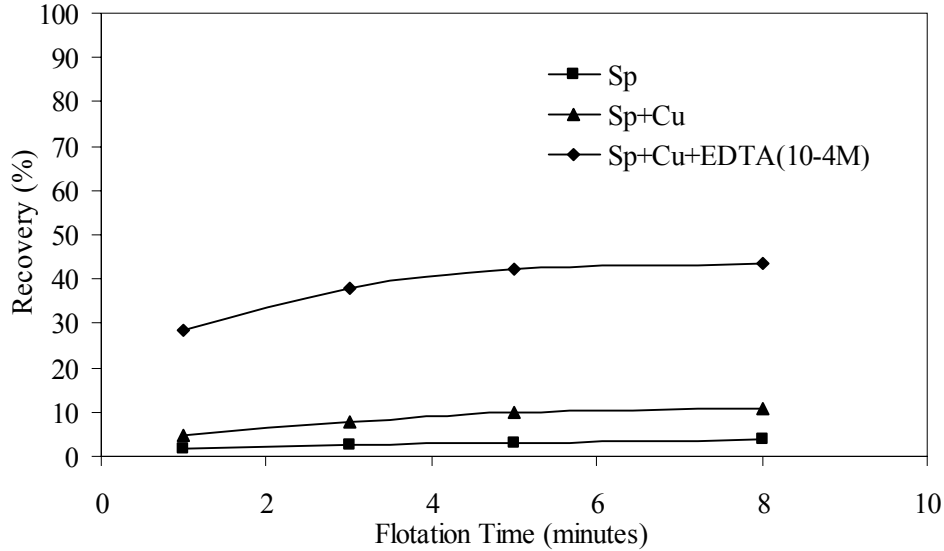


Fig. 4. Collectorless flotation of sphalerite in the absence and presence of copper and EDTA at pH 9.2

The increase in the recovery after EDTA addition was attributed to removal of copper and zinc hydroxide species and exposure of elemental sulphur or polysulphides, which made sphalerite hydrophobic to some extent. As it has been mentioned above, the copper ions are found in the form of $\text{Cu}(\text{OH})_2$ in alkaline solutions. These species can be first physically adsorbed or precipitate on to sphalerite surface and then proceed with electrochemical adsorption through reduction of Cu^{2+} to Cu^+ (reaction 2). As a result of that sulphide (S^{2-}) ions at the surface of sphalerite are oxidized into elemental sulphur or polysulphides (reaction 3) (Finkelstein 1997). Therefore, after removal of metal oxides by EDTA from the surface, a hydrophobic surface exposed and the recovery increased.



Addition of 10^{-4} M KEX did not increase the recovery of sphalerite in the absence of copper ions (Figure 5). As it is very well known that solubility of Zn-EX (4.9×10^{-9}) is considerably higher than $\text{Zn}(\text{OH})_2$ (1.62×10^{-17}) and therefore xanthate can not adsorb on sphalerite. Therefore, copper activation is essential for flotation of sphalerite and as it is shown in Figure 1, sphalerite can easily be activated by copper ions even in alkaline solutions. Addition of KEX resulted in formation of strongly hydrophobic CuEX, and thus very high recoveries.

Addition of 10^{-4} M EDTA did not affect the recovery. This is in agreement with the cyclic voltammetry results (Figure 1) showing no effect of EDTA addition to copper activated sphalerite. However, as EDTA concentration was increased to 10^{-3} M, the recovery and flotation rate decreased significantly. The decrease in the recovery after excess EDTA addition may be due to break down of the collector species adsorbed at the surface and/or precipitation of EDTA complexes at the surface.

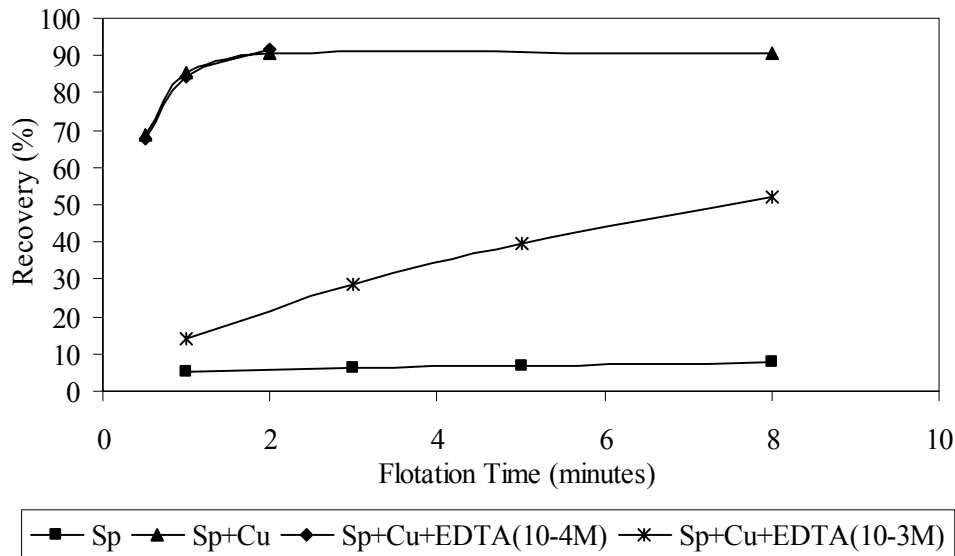


Fig. 5. Flotation of sphalerite with 10^{-4} M KEX in the absence and presence of copper and EDTA

PYRITE

Collectorless flotation behavior of pyrite in the absence and presence of copper ions and EDTA is illustrated in Figure 6. Collectorless flotation of pyrite is very low due to formation of hydrophilic iron oxide/hydroxide species in alkaline solution. Addition of copper ions increased the recovery slightly due to formation of elemental sulphur or polysulphides to some extent as also observed in the case of sphalerite (Figure 4). Addition of EDTA, however, increased the recovery considerably due to removal of hydrophilic ferric hydroxide species and exposure of sulphur rich hydrophobic layer at the surface.

Addition of KEX did not affect pyrite recovery significantly (Figure 7). Flotation of pyrite strongly depends on formation of dixanthogen which also depends on the presence of oxygen in the pulp. However, the flotation experiments were performed in the absence of oxygen by bubbling nitrogen gas prior to flotation. Therefore, absence of oxygen in the solution might inhibit formation of dixanthogen and resulted in low recovery of pyrite.

Addition of copper ions increased the recovery drastically up to 75 %. This was apparently due to activation of pyrite by copper ions, as shown by cyclic voltammetry in Figure 2, and formation of CuEX species upon addition of collector. However, addition of EDTA after copper activation could remove the adsorbed copper ions largely as shown by voltammetry experiments. Therefore, addition of EDTA before xanthate addition removed most of the pre-adsorbed copper ions and therefore prevented formation of CuEX at pyrite surface. In spite of that the recovery was still around 50 %. It was clear that addition of EDTA inhibited collector adsorption, but at the same time removed metal hydroxide species and resulted in exposure of sulphur rich hydrophobic surface, as observed with collectorless flotation (Figure 6).

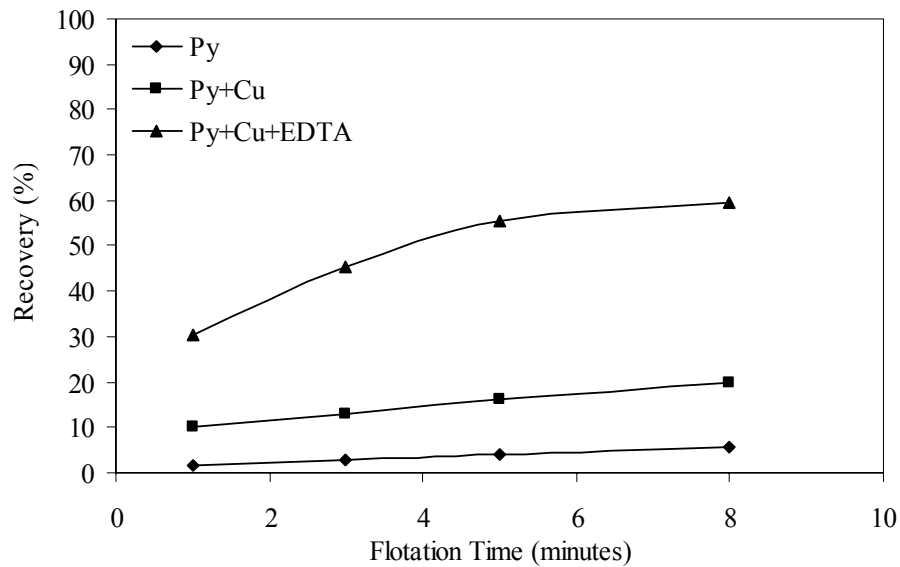


Fig. 6. Collectorless flotation of pyrite in the absence and presence of copper ions and EDTA

CHALCOPYRITE

In this section, only influence of EDTA on collectorless flotation of chalcopyrite was discussed since chalcopyrite was not affected by EDTA at all in the presence of KEX. Addition of EDTA increased the collectorless flotation recovery from about 30 % up to about 90 % (Figure 8). Electrochemical experiments showed that oxidation of chalcopyrite in alkaline solutions resulted in formation of ferric hydroxide at moderately oxidizing potentials and copper hydroxide at higher potentials. These hydrophilic metal hydroxide species cover the mineral surface and prevent its collectorless flotation. Addition of EDTA removed all of these metal hydroxide species and brought about exposure of a sulphur rich hydrophobic layer, as observed with collectorless flotation of both sphalerite and pyrite.

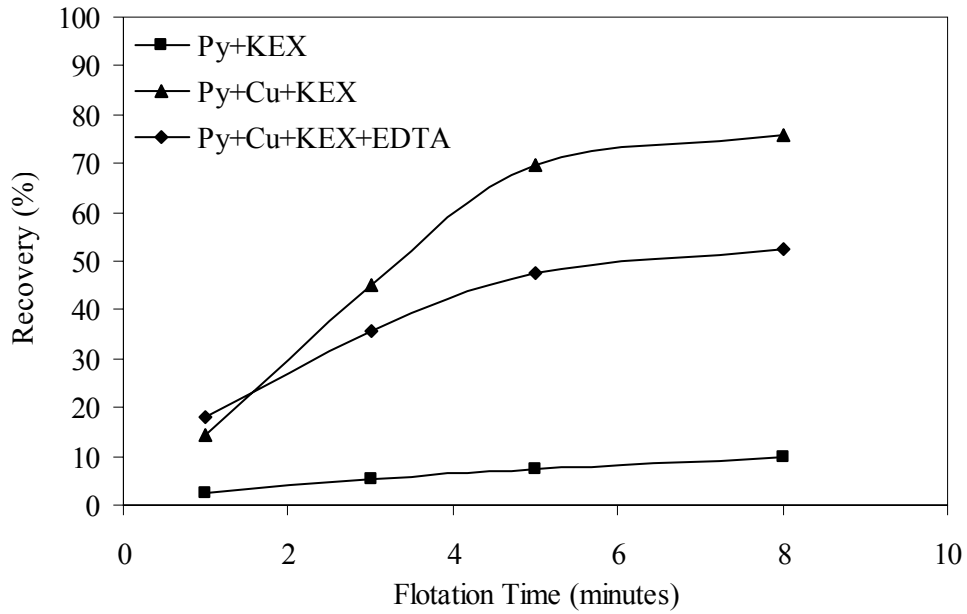


Fig. 7. Flotation of pyrite with 10^{-4} M KEX in the absence and presence of copper ions and EDTA

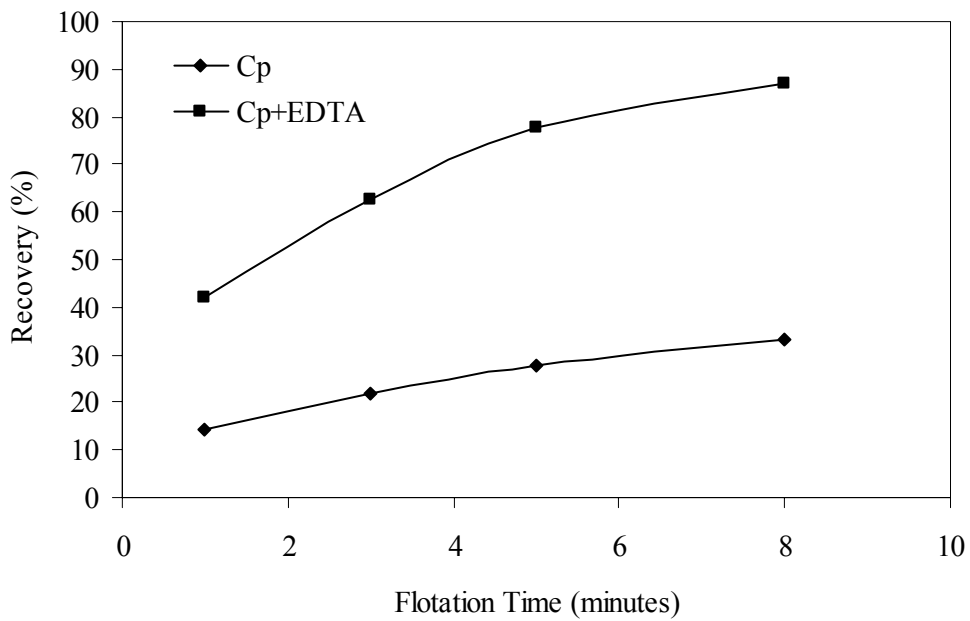


Fig. 8. Collectorless flotation of chalcopyrite in the absence and presence of 10^{-4} M EDTA at pH 9.2

MINERAL MIXTURES

Effects of galvanic interaction on activation and flotation of sphalerite and pyrite were investigated with microflotation experiments performed using chalcopyrite-sphalerite and chalcopyrite-pyrite mineral mixtures. It is very well known that galvanic interaction between these minerals cause dissolution of copper ions from chalcopyrite and thus unwanted activation of sphalerite and pyrite by these copper ions, which deteriorates the selectivity. Therefore, EDTA was tested as a complexing agent to prevent activation of sphalerite and pyrite in these experiments.

The results of collectorless flotation of chalcopyrite and sphalerite in the absence and presence of EDTA are illustrated in Figure 9. Presence of chalcopyrite did not affect sphalerite recovery in the absence of EDTA. However, as EDTA removed the metal hydroxide species from surface of both minerals, their recovery increased considerably, as it was also observed with single mineral experiments.

Addition of KEX increased flotation recovery of sphalerite in the mineral mixture (Figure 10). This was attributed to activation of sphalerite by copper ions dissolved from chalcopyrite as a result of galvanic interaction. However, addition of EDTA decreased the recovery in the order of 10 %. The final sphalerite recovery in the presence of EDTA was still about 30 %. EDTA was considered to have dual effect as preventing activation of sphalerite by copper ions, but at the same time enhancing its collectorless flotation by removing the metal hydroxides from the surface. Therefore, selective flotation could not be achieved at satisfactory level in the existing experimental conditions. The influence of pH and particularly EDTA concentration on selectivity must be investigated in detail.

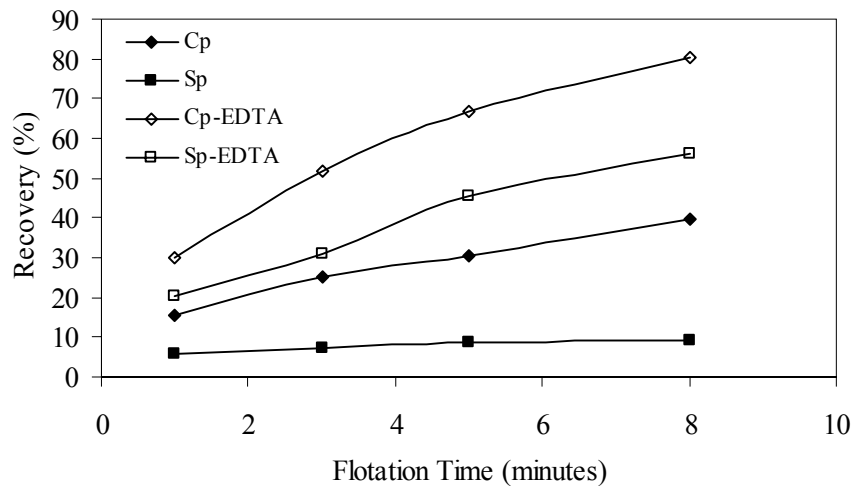


Fig. 9. Collectorless flotation of chalcopyrite and sphalerite in mineral mixture in the absence and presence of EDTA

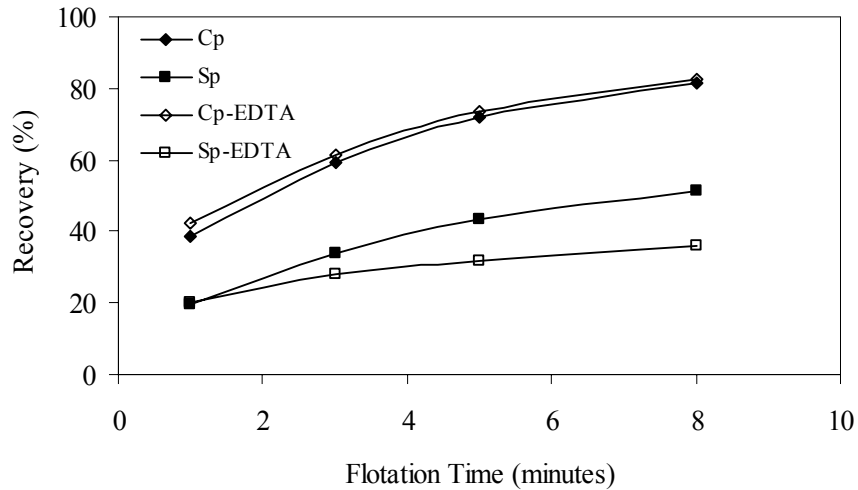


Fig. 10. Flotation of chalcopyrite and sphalerite in mineral mixture with 10^{-4} M KEX in the absence and presence of EDTA

Similar flotation behaviour was also observed with chalcopyrite-pyrite mixture in the absence and presence of KEX (Figures 11 and 12). Collectorless flotation of both chalcopyrite and pyrite in mineral mixture was not significantly different from that in single mineral experiments. However, addition of EDTA removed the metal hydroxide compounds for their surfaces and increased recovery of both minerals.

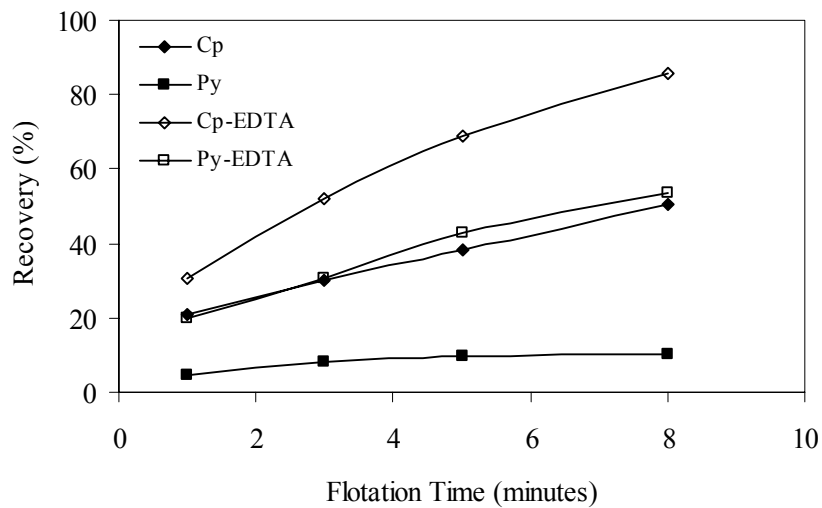


Fig. 11. Collectorless flotation of chalcopyrite and pyrite in mineral mixture in the absence and presence of EDTA

Recovery of pyrite in the presence of KEX increased to about 40 % due to galvanic interaction between chalcopyrite and pyrite. Dissolution of copper ions enhanced due to galvanic interaction. The dissolved copper ions may adsorb/precipitate on pyrite and form CuEX compounds after KEX addition. Addition of EDTA removed the copper ions from pyrite surface and prevent formation of CuEX, but it also removed the metal hydroxides and led to collectorless flotation of pyrite. Flotation of chalcopyrite was not affected by addition of EDTA in the existing experimental conditions.

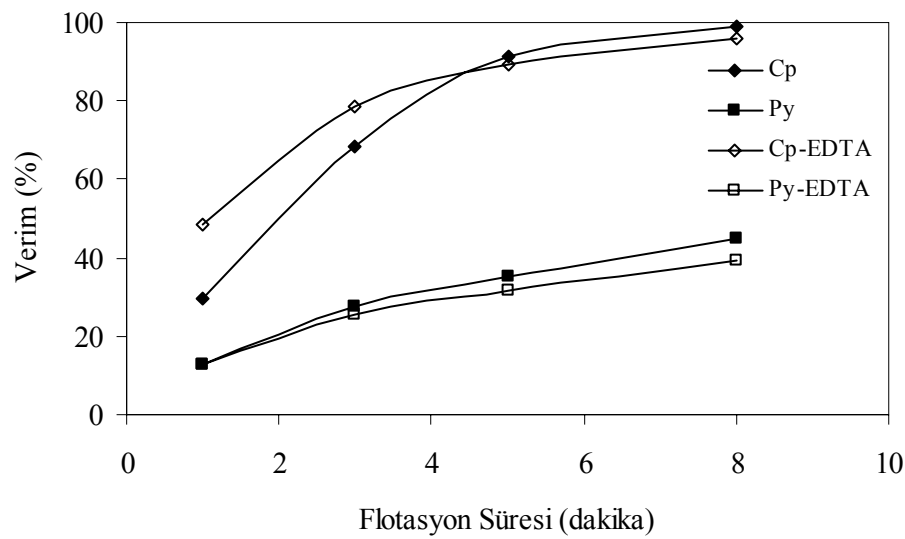


Fig. 12. Flotation of chalcopyrite and pyrite in mineral mixture with 10^{-4} M KEX in the absence and presence of EDTA

CONCLUSIONS

Unwanted activation of sphalerite and pyrite by copper ions dissolved from copper minerals (mainly chalcopyrite) hampers flotation selectivity. Galvanic interaction between the sulphide minerals is considered as the main cause for such activation. Therefore, a complexing agent, EDTA, was used to prevent unwanted activation of sphalerite and pyrite by copper ions in the presence and absence of collector.

Cyclic voltammetry experiments showed that sphalerite and pyrite can be activated by copper ions at pH 9.2, forming CuS like compounds at the surface. Addition of EDTA did not affect the newly formed CuS layer with sphalerite, but decrease the current intensity with pyrite. The activated copper layer was weakly adsorbed onto pyrite surface, presumably due to slower adsorption kinetics of copper on pyrite compare to sphalerite.

The results of collectorless flotation revealed that flotation of chalcopyrite, pyrite and sphalerite was significantly affected by the presence of metal hydroxide at their surface. The use of EDTA removed these hydrophilic metal hydroxide species thereby exposing a sulphur rich hydrophobic surface. Similar effects were observed with both single mineral and mineral mixture experiments. This effect increased the overall recovery and did not improve the selectivity.

The flotation experiments in the presence of collector showed that galvanic interaction resulted in unwanted activation of both sphalerite and pyrite by copper ions, thereby resulting in formation of CuEX layer at their surface. This situation increased their recovery and hampers the flotation selectivity. EDTA was used to prevent copper activation. However, the flotation recovery of both sphalerite and pyrite remained almost the same in the presence and absence of EDTA. EDTA was considered to have dual effect as preventing activation of sphalerite and pyrite by copper ions, but at the same time enhancing their collectorless flotation by removing the metal hydroxides from their surfaces.

ACKNOWLEDGEMENT

The authors gratefully acknowledge the financial support of this research by The Scientific and Technical Research Council of Turkey (TUBİTAK Project No: 199Y037).

REFERENCES

- CLARKE, P., FORSENARIO, D., RALSTON, J., SMART, R. St. (1995), *A study of the removal of oxidation products from sulphide mineral surfaces*, Minerals Engineering, 8(11), 1347-1357.
- CLARKE, P.C. (1997), *The interactions of metal ions and their hydrolysis products with sulphide mineral surfaces*, PhD Thesis, University of South Australia.
- EKMEKÇİ, Z., DEMİREL, H. (1997), *Effects of galvanic interaction on collectorless flotation behaviour of chalcopyrite and pyrite*, Int. J. Miner. Process., 52, 31-48.
- EKMEKÇİ, Z., ASLAN, A., HASSOY, H. (2002), *Effects of electrochemical parameters on selective flotation of chalcopyrite-sphalerite in complex sulphide ores*, TUBİTAK, Project No:199Y037, unpublished report, 72p.
- EKMEKÇİ, Z., BRADSHAW, D. J., HARRIS, P.J., ASLAN, A., HASSOY, H. (2003), *The value and limitations of electrochemical measurements in sulphide flotation*, Sixth International Symposium on Electrochemistry in Mineral and Metal Processing, Paris, France.
- FINKELSTAIN, N.P. (1997), *The activation of sulphide minerals for flotation: a review*, Int. J. Miner. Process., 52, 81-120.
- FUERSTENAU, D.W., FUERSTENAU, M.C. (1982), *The flotation of oxide and silicate minerals*, Principles of Flotation, (Ed. R.P. King), South African IMM, Johannesburg.
- GRANO, S.R., RALSTON, J., JOHNSON, N.W. (1988), *Characterisation and treatment of heavy media slimes in the Mount Isa Mines Lead-Zinc Concentrator Part I: Grinding media effects*, Minerals Engineering, 1(2), 447-459.
- NAKAZAWA, H., IWASAKI, I. (1985), *Effect of pyrite-pyrrhotite contact on their floatabilities*, Miner. Metall. Process., 2, 206-211.
- RUMBALL, J.A. RICHMOND, G.D. (1996), *Measurement of oxidation in a base metal flotation circuit by selective leaching with EDTA*, Int. J. Miner. Process., 48, 1-20.
- SHANON, L.K., TRAHAR, W.J. (1986), *The role of collector in sulphide ore flotation*, Proceedings on Advances in Mineral Processing, 408-426.

YELLOJI RAO, M.K., NATARAJAN, K.A. (1989), *Effect of electrochemical interactions among sulphide minerals and grinding medium on chalcopyrite flotation*, Miner. Metall. Process., August, 146-151.

YOON, R.H., CHEN, Z. (1996), Electrochemical aspects of copper-activation of sphalerite, Int. Symp. Electrochemistry in Mineral and Metal Processing IV, Electrochem. Soc., Pennington, NJ, 38-47.

Ekmekçi Z., Aslan A., Hassoy H., *Wpływ EDTA na selektywną flotację minerałów siarczkowych*, Physicochemical Problems of Mineral Processing, 38, (2004) 79-94 (w jęz. ang.).

Proces aktywacji sfalerytu i pirytu przez jony miedzi, znajdujące się w roztworze, ma niekorzystny wpływ na selektywność procesu flotacji. Procesy galwaniczne są rozpatrywane jako główna przyczyna powodująca aktywację. Odczynnik kompleksujący- EDTA- został użyty w celu przeciwdziałaniu aktywacji sfalerytu i pirytu. Badania z wykorzystaniem EDTA prowadzone były bez i z udziałem kolektora. Metody cyklovoltamperometrii i mikroflotacji zostały wykorzystane dla zbadania efektów wynikających z dodania EDTA. Dla układów chalkopiryt-sfaleryt i chalkopiryt-piryt określono wpływ EDTA na zjawiska galwaniczne i na selektywność flotacji. Otrzymane wyniki wskazują, że dodanie EDTA zapobiega aktywacji sfalerytu i pirytu jonami miedzi, a także podwyższa bezkolektorową flotację tych minerałów przez usunięcie wodorotlenków metali z ich powierzchni.

Levent ERGÜN*, Zafir EKMEKÇİ*, Özcan GÜLSOY*, Hakan BENZER*

THE EVALUATION OF A COPPER FLOTATION PLANT PERFORMANCE BY PLANT SURVEY AND LABORATORY TESTS

Received May 12, 2004; reviewed; accepted June 28, 2004

In this study the performance evaluation study of Georgia Madneuli Copper Ore flotation plant was performed using the data obtained from the detailed survey at the flotation circuit. The solids contents of the streams around the circuit were measured and the particle size distribution of the samples taken from the plant was determined. Mass balancing studies were performed using JKSimmet software. Mass balance results provided the flow rates and the chemical assays around the circuit. Therefore using the flow rates around each stream, the recovery of every unit in the circuit was calculated. The laboratory flotation tests were performed to obtain the optimum flotation conditions. For this purpose the flotation rate constants were determined for the different ore types processed at the circuit. Using the data obtained from plant and laboratory, a new circuit design was proposed.

Key words: flotation, flotation rate, mass balance, flotation test

INTRODUCTION

Madneuli-Georgia Copper Concentrator processes mainly three different ore types (named as sulphide ore, complex ore and oxidized ore). The plant consists of three different grinding and flotation circuits. Flotation circuit consists of two stages of rougher, two stages of scavenger and two stages of cleaner circuits. In the circuit studied, the plant capacity was found as 85.4 t/h. According to the design capacity, 1.600.000. t/y, the circuits must be operated at the capacity of 100 t/h. Therefore it is revealed that, the plant is performing with 85 % of the design capacity.

The flotation circuit consists of rougher, scavenger and cleaning circuits. The volumetric size of the cells in the rougher, scavenger and cleaner circuits are 6.3 m³,

* Hacettepe University, Department of Mining Engineering, 06532, Beytepe, Ankara, Turkey;
e-mail: ogulsoy@hacettepe.edu.tr

3.25 m³, and 3.25 m³ respectively. The flotation feed comprises 33-36 % solids with 1% Cu content. The concentration method is the selective flotation of the chalcopyrite. The pH value is kept around 11.5 for pyrite depression. Potassium isobutyl xanthate is used as the collector with the dosage of 25-32 g/t.

During the sampling survey, the average Cu grade of the flotation feed was 0.89 % and the concentrate grade was approximately 21 %. But the average Cu concentrate grade was approximately 18%.

In this study, the performance evaluation of Georgia Madneuli Copper Ore flotation plant was performed using the plant data and laboratory test results. For this purpose, pulp samples were taken from the flotation circuit. All samples were dried, weighed and sieved. Size distribution of each sample was determined down to 6 µm. Each size fraction was assayed for Cu, Fe and insoluble contents in the flotation circuit. Mass balancing of both grinding and flotation circuits was performed to calculate the flow rates in each stream.

Laboratory flotation tests were also applied to the ore samples taken from feed of the primary grinding mill to determine the best flotation conditions and to compare the laboratory results with existing conditions. This study provided the required information to enhance the existing circuit and operation conditions.

SAMPLING AND ORE CHARACTERIZATION STUDIES

To evaluate the performance of flotation circuit, pulp samples were taken from the points marked in Fig. 1.

The samples taken from flotation circuit were dried, weighed and sieved. Size distribution of each sample was determined. Flotation feed fineness was determined as d₈₀=300 µm in the existing circuit. Each size fraction was assayed for Cu, Fe and insoluble contents.

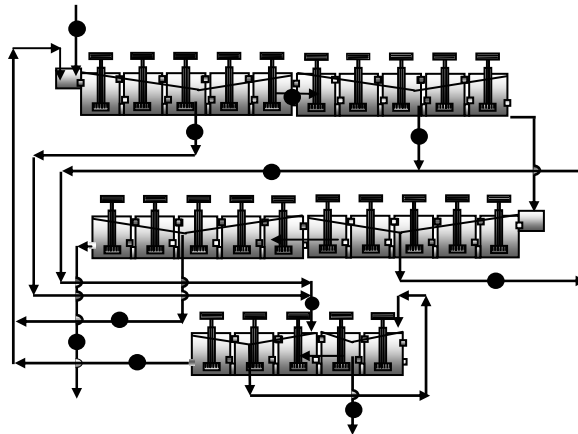


Fig. 1. Flotation circuits sampling points

In the plant mainly three different ore types (named as sulphide ore, complex ore and oxidized ore) are processed. Mineralogical compositions of the samples were determined by microscopic examination of the polished sections for sulphide minerals and X-Ray diffraction for non-sulphide minerals. The ore consists of mainly pyrite (FeS₂), chalcopyrite (CuFeS₂), traces of chalcocite (Cu₂S), covellite (CuS) and bornite (Cu₅FeS₄) as sulphide minerals and, quartz and clay minerals as non-sulphides. General chemical compositions of the ores are given in Table 1.

Table 1. Chemical compositions of the ores

Contents	Flotation feed	Oxidized ore	Sulphide ore	Complex ore
Cu	% 0.89	% 0.7	% 1.3	% 0.5
Fe	% 6.28	% 3	% 5.2	% 3.6
Zn	% 0.02	% 0.01	% 0.02	% 0.02
Pb	<50 ppm	<50 ppm	<25 ppm	<50 ppm
SiO ₂	% 80.58	% 76.38	% 79.89	% 87.18
Al ₂ O ₃	% 3.78	% 15.12	% 5.67	% 3.78

MASS BALANCING

Flow rates of each stream were calculated and balanced by using Cu and Fe assays of the head samples. Fig. 2 represents the balanced flow rates and Cu grade of the every sampling point around the flotation circuit.

The results showed that, during the survey, Cu recovery of the circuit was 89%. But Cu recovery of the circuit is between 63 and 82 % in regular measurements during the operation.

Flotation behavior of size fractions in the circuit was also investigated using the following kinetic model. The flotation rate of the size fractions was investigated in the rougher flotation bank. The relationship between flotation rate parameters and particle size is given in Fig. 3.

$$k\lambda=R/(1-R) \tag{1}$$

where; k is the flotation rate parameter, λ is the retention time, R is the recovery.

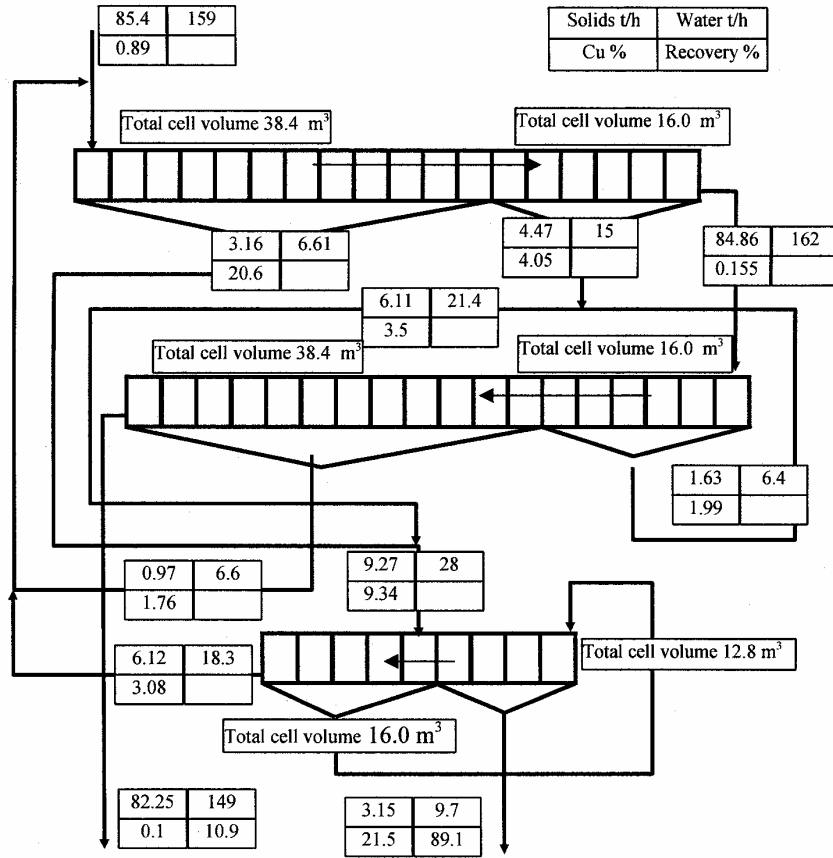


Fig. 2. Balanced flow rates, grades around the flotation circuit at actual operating condition

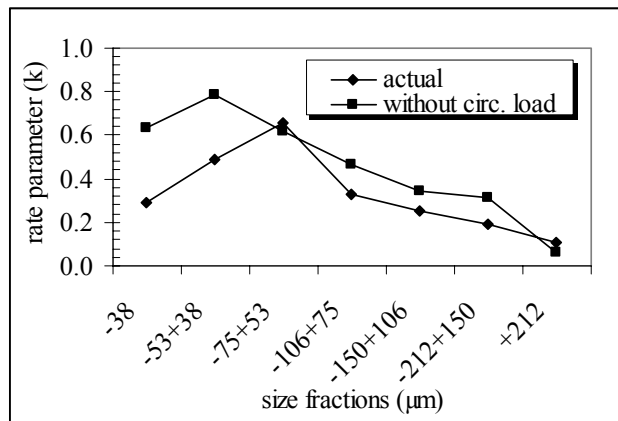


Fig. 3. Rate parameters obtained from plant data

Cu recoveries and flotation rate parameters of each size fraction were also calculated by using flow rates and Cu assays of the size fractions. It was observed that especially Cu recoveries of the fine size fractions were greater than that of the coarse sizes.

LABORATORY STUDIES

To obtain the best flotation behavior of the ore a series of laboratory flotation tests were carried out following the procedures given in Fig. 4.

In the laboratory Cu recovery higher than 94 % could be obtained in the rougher stage and the grade of this concentrate was increased to 26 % Cu by 3 stage cleaning. Although locked cycle tests were not performed, the Cu recovery was approx. 80% after cleaning.

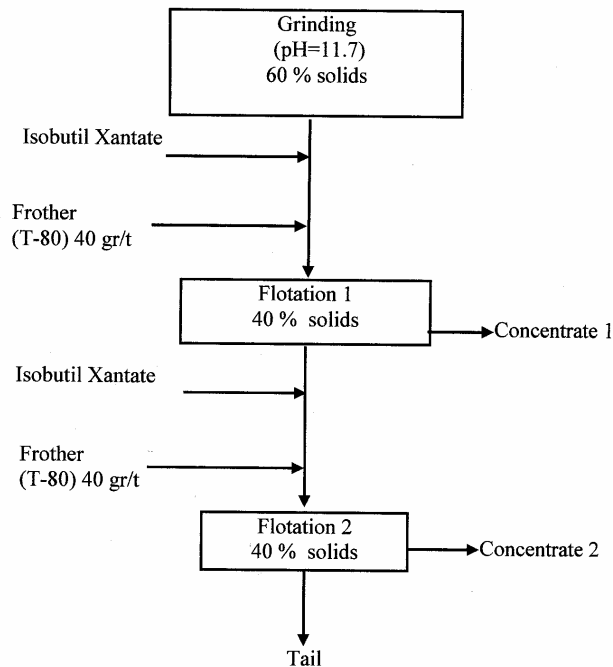


Fig. 4. Laboratory flotation test procedure

Finally, the laboratory studies showed that it is possible to obtain higher Cu recovery and grade by finer grinding.

In the laboratory, depending on the kinetic test results, retention times for each stage on the plant were estimated. By using the retention time values and flow rates, the required cell volumes and the number of cells were calculated. The laboratory revealed that different ore types showed different flotation behavior. The flotation behavior of different ores is illustrated in Fig. 5.

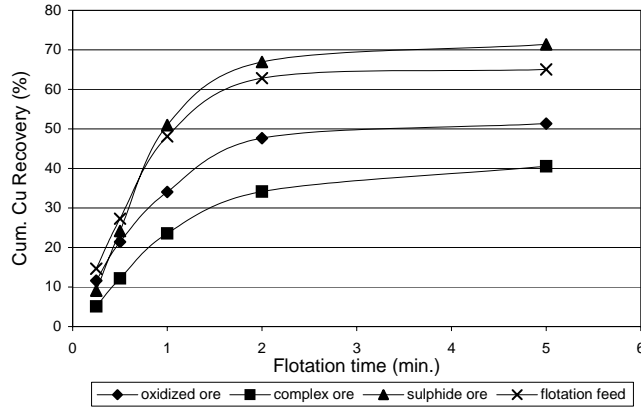


Fig. 5. Flotation behavior of the different ore types

The recovery and flotation rate of complex and oxidized ores were substantially lower than the sulphide ore. This was attributed to excessive oxidation of the sulphide minerals in these ore types. Therefore the flotation feed was prepared as a blend containing mainly sulphide ore and small amounts of oxidized and complex ores. Special flotation procedures and reagent schemes should be proposed for affective flotation of these problematic ore types.

The flotation behavior of the size fractions was also investigated. The relationship between flotation rate parameters and particle size is given in Fig. 6.

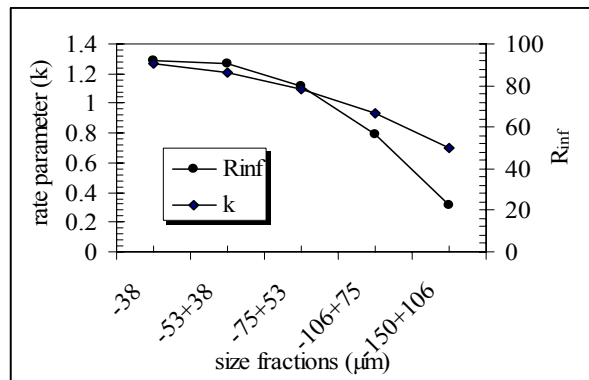


Fig. 6. Rate parameters obtained in laboratory study

To investigate the effect of feed fines on the flotation performance, two different samples ($d_{80} = +312 \mu\text{m}$ and $d_{80} = -312 \mu\text{m}$) were prepared and used in laboratory flotation tests. In these tests, the copper recovery was increased from 89.79% to 94.56 for coarse ($d_{80} = +312 \mu\text{m}$) and fine ($d_{80} = -312 \mu\text{m}$) feed respectively. The concentrate Cu grade was reached to 26.07% after 3 stages cleaning for fine feed. This

indicated that it is possible to increase the Cu grades by cleaning easily. Therefore the recovery must be as high as possible.

Consequently, the laboratory tests and plant scale studies showed that it is possible to obtain a concentrate with higher Cu recovery and grade by finer grinding.

Based on the results of the kinetic tests, retention time of the pulp was estimated for each stage in the plant. By using the retention time values and flow rates, required cell volumes and the number of cells were calculated using the following equation.

$$V_i = (Q \cdot \lambda \cdot S) / (60 \cdot a) \tag{2}$$

where Q is pulp volume m^3/h , λ is retention time, S is scale up factor (1.7 for lab. batch test) a is aeration factor (0.85).

Using the actual plant data and the laboratory test results a new circuit layout was developed in order to increase the performance of the circuit. The proposed circuit is given in Fig. 7. Therefore the number of cells in the circuit was increased from 18 to 24 for rougher, from 18 to 24 for scavenger and from 11 to 13 for cleaning circuits. In addition to that, the number of cleaning stages was increased from 2 to 3 to increase the Cu grade of the concentrate.

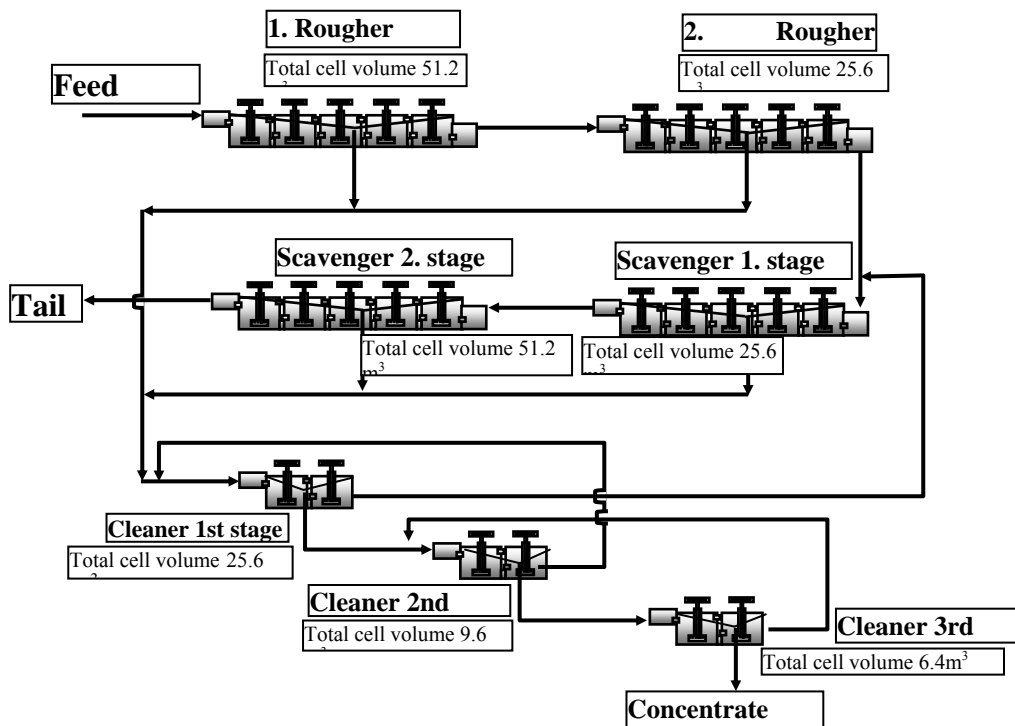


Fig. 7. Proposed flowsheet

CONCLUSIONS

The performance evaluation studies of the flotation circuit indicated that it is possible to obtain 21 % Cu copper concentrate with 90 % recovery. During the sampling survey flow rates of the flotation feed and the copper concentrate were measured as 85.4 t/h and 3.15 t/h respectively. According to these results annually 1.610.000 tons of ores would make 60.000 tons of concentrate.

Performance evaluation and laboratory test results showed that an improvement can be obtained by finer grinding of the ore and some changes in the circuit design. In the plant, the ore could not be ground to even design values, and retention time is not enough to handle the capacities greater than 85 t/h. Therefore, the required total number of cells was increased to handle the longer retention time after fine grinding. In addition to this, instead of 2 stages of cleaning as in the existing circuit, 3 stages cleaning were proposed to obtain higher Cu grade. Flotation studies revealed that the grinding circuit must be optimized to produce finer flotation feed.

Ergün L., Ekmekçi Z., Gülsoy O., H. Benzer H., *Poprawa pracy zakładu flotacji na podstawie opróbowania i testów laboratoryjnych*, Physicochemical Problems of Mineral Processing, 38, (2004) 95-102 (w jęz. ang.).

W pracy przedstawiono wyniki badań mające na celu poprawę pracy instalacji flotacyjnej w kopalni miedzi Madneuli w Gruzji. Węzeł flotacji został opróbowany, określone zostały przepływy, skład ziarnowy i zawartość części stałych. Badania bilansu masowego węzła flotacji przeprowadzono z wykorzystaniem programu komputerowego JKSimmet. Otrzymane wyniki pozwoliły określić właściwe prędkości przepływów oraz wychody. Przeprowadzone zostały także laboratoryjne badania flotacyjne w celu określenia optymalnych warunków flotacji rudy miedzi. Określono na podstawie testów laboratoryjnych stałe flotacji dla poszczególnych rodzajów rud. Otrzymane dane z optymalizacji zakładu i z testów laboratoryjnych pozwoliły na zaproponowanie nowej instalacji do prowadzenia procesu flotacji.

Baris BEKLIOGLU, Ali Ihsan AROL*

SELECTIVE FLOCCULATION BEHAVIOR OF CHROMITE AND SERPENTINE

Received May 5, 2004; reviewed; accepted 24 June, 2004

Application of selective flocculation using starch to separate chromite from serpentine has been investigated. It was determined that starch has a specific affinity towards chromite which can be exploited in selective flocculation. However, it was found that this could only be achieved when the amount of serpentine in the chromite-serpentine mixture is below 30% by weight and in the presence of a dispersant such as sodium silicate or ultrasonic treatment of the pulp.

Key words: selective flocculation, chromite, serpentine, starch

INTRODUCTION

Concentration separation of finely ground minerals has been a common industrial practice for a long period. Slimes, defined as $-20\ \mu\text{m}$ particles, are an unseparable part of such operations and may contain significant amounts of valuable minerals. Conventional techniques, such as gravity concentration, magnetic separation and flotation, are generally ineffective in treating slimes. Thus, slimes are usually discarded prior to concentration. Discarded slimes are not only an economical loss but their disposal may be an environmental concern and costly to manage as well. Many techniques have been developed to treat slimes. Among them are shear flocculation, selective flocculation, carrier flotation, high gravity separators, etc.

Selective flocculation is one of the techniques applicable to the enrichment of slime fraction. The technique is based on the preferential adsorption of an organic flocculant on the mineral particles to be flocculated, leaving the rest of the minerals suspended. Separation is brought about by the different settling rates of mineral particles controlled by the effective diameter which can be altered by flocculation or dispersion of a particular mineral. For a successful selective flocculation process, the pulp must

* Middle East Technical University Mining Engineering Department, 06531 Ankara, Turkey
arol@metu.edu.tr

be fully dispersed prior to the addition of the flocculant. Considerable success has been achieved in applying this technique for the separation of finely disseminated valuable minerals from ores on experimental as well as commercial scale (Yarar and Kitchener, 1970; Read, 1971; Attia, 1977; Lien and Morrow, 1978; Drzymala and Fuerstenau, 1981; Pradip and Moudgil, 1991; Moudgil and Mathur, 1994; Weissenborn et al., 1994; Sworska et al., 2000).

Chromite ores are usually concentrated by gravity concentration methods based on differences between specific gravities of chromite and gangue minerals, i.e., olivine and serpentine. Considerable amount of fine chromite is lost in the conventional gravity separation plants as a result of the process and/or equipment inefficiency in the fine particle size range. As much as 3×10^6 Mt of fine chromite tailings having upto 20% Cr_2O_3 have been accumulated in several disposal sites in Turkey (Anon.; Güney and Önal, 2000). Several researchers, employing gravity separation, flotation and magnetic separation have attempted to recover the chromite values from these sites with limited success (Doğan et al., 1996; Çiçek et al., 1998; Güney and Önal, 2000).

The mineral chromite is the main valuable mineral in chromite ores. It belongs to the spinel group and has the chemical formula of FeCr_2O_4 . The gangue mineral, serpentine, is a magnesium hydroxysilicate mineral with a chemical formula of $\text{Mg}_3\text{Si}_2\text{O}_5(\text{OH})_4$. Replacement of the cations in both minerals is a common occurrence in natural deposits.

Starch is a natural polymer and known to have a specific affinity towards iron bearing minerals (Iwasaki, et al., 1969; Balajee and Iwasaki, 1969; Dogu and Arol, 2004). This affinity has been related to a complex formation and hydrogen bonding between metal ions on the mineral surfaces and starch molecules (Khosla, et al., 1984; Laskowski, et al., 1991; Ravishankar, et al., 1995 and Weissenborn, et al., 1995). Because of this property, starch and its derivatives have been used in the commercial application of flotation and selective flocculation to iron ores (Lien and Morrow, 1978; Balajee and Iwasaki, 1969; Iwasaki et al., 1969).

The facts that chromite has iron oxide in its structure and that starch has a specific affinity towards iron oxide were exploited in the present study. Possibility of applying selective flocculation to chromite-serpentine mixture using starch, in a similar fashion to the selective flocculation of iron oxide-silica system, was explored.

MATERIALS AND METHODS

Both the chromite and serpentine samples were obtained from the Kavak Chromite Mine, Eskişehir, Turkey. The final size of both samples were reduced to $-45\mu\text{m}$ by stage crushing and grinding. The grinding was carried out on $-150\mu\text{m}$ roller crusher product wet in a porcelain mill. The $-45\mu\text{m}$ material was washed with distilled water 5 times to remove the dissolved species from the mineral surfaces, drained and dried at 105°C , and kept in plastic bags to be used in the experiments. The size and specific surface areas, analyzed by Sympatec Helos Laser Sizer (H1305), chemical and

mineralogical compositions of the samples, determined by XRF and XRD methods, are given in Table 1.

The commercial corn starch of Cargill, Turkey, was used as the flocculant. Reagent grade NaOH and HCl were used for pH adjustments. Distilled water was used in all experiments.

Table 1. Chemical, physical and mineralogical properties of chromite and serpentine

Property	Chromite	Serpentine
%80 passing size, μm	25	18
Specific surface area, cm^2/g	1.63	2.91
Specific gravity	4.71	2.70
Cr_2O_3 , %	57.6	0.8
Fe_2O_3 , %	19.0	12.5
Al_2O_3 , %	8.0	2.5
SiO_2 , %	3.0	47
MgO , %	8.5	29.0
CaO , %	0.2	2.5
Mineralogical composition	Chromite, γ -hematite, magnetite, olivine	Serpentine, chlorite, smectite, hematite, calcite, amorphous silicate

Starch was dissolved by cooking in distilled water for 30 min. in an autoclave at 140°C and 207 kPa. The cooked starch was homogenized in a Waring Blender and stored in 1mg/mL concentration. The starch solution was freshly prepared daily to avoid degradation (Iwasaki et al., 1969).

Starch adsorption of minerals was determined by mixing 2.5 g of minerals with a starch solution of known concentration for 10 minutes. The mixture was centrifuged to separate the solids. Starch remaining in solution was analyzed by sulfuric acid-phenol method (Dubios et al., 1956).

Flocculation and single stage selective flocculation tests were performed in a 250 ml graduated glass cylinder of 35 mm in diameter. In multiple stage selective flocculation experiments, tests were carried out in 1000 ml graduated cylinder of 6,5 cm diameter. All flocculation experiments were performed at a pulp density of 5% solids by weight. After adjusting the pH, starch was added in three equal increments and the cylinder was inverted 3 times after each addition and 5 times after the last addition. The pulp was allowed to settle for 60 seconds and the supernatant of the upper 80 % part of the cylinder was siphoned off, dried and weighed to determine the suspended solid and Cr_2O_3 content. For the multiple stage selective flocculation tests, the same procedure was followed up to the first stage flocculation. The subsequent flocculation tests were carried out by adding a make-up water to the settled portion of the previous stage. This allows the cleaning of the flocs. All the suspended and settled products were collected, weighed and analyzed for Cr_2O_3 . Complete details of the tests are given else where (Beklioglu, 2002).

RESULTS AND DISCUSSION

It is well known that selective flocculation can be applied to ores which are fully dispersed prior to polymer addition, and one of the minerals selectively adsorbs the polymer and flocculates after polymer addition. Flocculation-dispersion behavior as well as polymer adsorption characteristics of chromite and serpentine were investigated to determine under which conditions these prerequisites are achieved. As known coagulation-dispersion behavior of minerals in the absence of salts and polymers is dependent on the pulp pH governing the surface charge of the minerals. Dispersion behaviors of chromite and feldspar as a function of pH, expressed in terms of percentage of solids settled, are given in Figure 1. As seen from the amount of settled solids in the figure (also visually observed during the tests), neither chromite nor serpentine fully settled at any pH as a result of coagulation. Normally, a coagulated suspension would lead to around 90-100 % settling. Relatively higher amounts of settled fraction for chromite is a result of higher density as well as coarser size distribution of that mineral than serpentine.

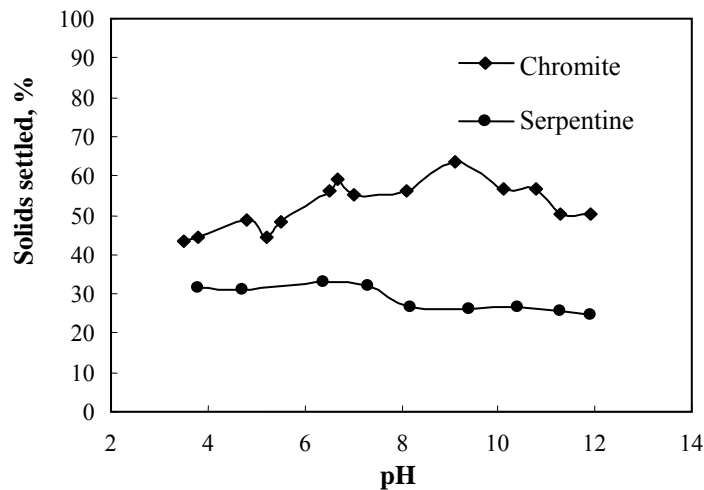


Fig. 1. Flocculation-dispersion behavior of chromite and serpentine as a function of pH

Adsorption of starch as a function of pH is another factor in selective flocculation. It is known that to have a successful selective flocculation process, starch must be adsorbed on one of the minerals while the other mineral adsorbs little or no starch. Starch adsorption as a function of pH was determined at a constant starch addition of 150 mg/mL at all pH values. As seen in Figure 2, in acidic and neutral pH values both chromite and serpentine adsorbed substantial amount of starch. In fact, in acidic pH range, serpentine adsorbed more starch than chromite. However, above pH 9, while chromite did still adsorb starch, adsorption by serpentine sharply decreased. It has been reported that pzc values of chromite and serpentine is around pH 5.5 and 8.7,

respectively (Sobieraj and Laskowski, 1973; Akdemir, 1995). Thus, adsorption by the respective minerals below these pH values can be partly attributable to the electrostatic attraction between the positively charged minerals and the negatively charged starch molecules (Iwasaki et al., 1969; Drzymala and Fuerstenau, 1987). Adsorption of starch by chromite above the pzc value of pH 5.5 may be explained by a specific affinity of chromite which contains iron in its crystal lattice towards starch in a similar fashion to iron minerals reported by many investigators (Iwasaki et al., 1969; Hanumantha, et al., 1985; Hanumantha and Narasimhan, 1985; Bagster and McIlveny, 1985; Weissenborn et al., 1994 & 1995; Ravishankar, et al., 1995 and Doğu, 2002).

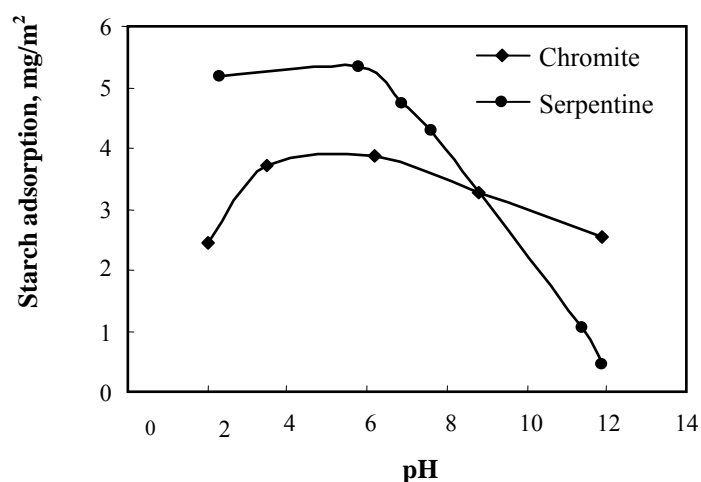


Fig. 2. Adsorption of starch by chromite and serpentine as a function of pH (initial starch concentration of solution: 150 mg/L)

Starch adsorption behavior of serpentine and chromite as a function of starch concentration were conducted at pH 5.5 and 11.9 in order to understand the nature of adsorption. The results are given in Figure 3. It was found that starch adsorption by serpentine was strongly pH dependent. At pH 5.5, serpentine completely adsorbed starch from solution at low concentration level and reached surface saturation with regard to starch above around 4 mg/m² adsorption density. However, at pH 11.9, very little starch was adsorbed at all starch concentration levels tested. Chromite, on the other hand, exhibited a different behavior. Its starch adsorption behavior was pH independent. At low starch concentration levels, the amounts of adsorption for both pH values were virtually the same. Starch adsorption at higher starch concentration levels at pH 11.9 was slightly lower than those at pH 5.5. From these results, it can be concluded that starch has a specific affinity towards chromite but not towards serpentine and selectivity can be achieved at around pH 11-12.

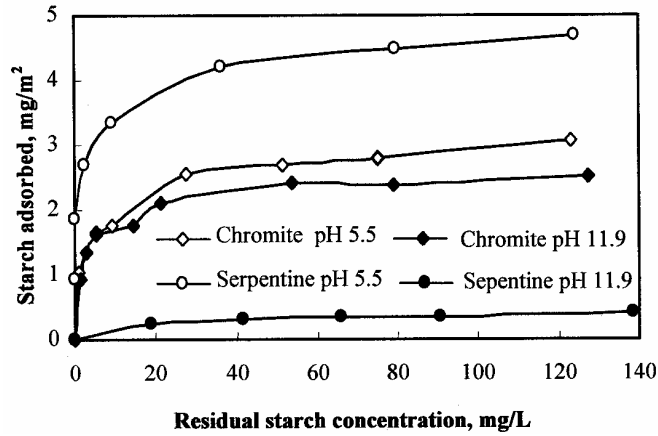


Fig. 3. Starch adsorption characteristics of chromite and serpentine as a function of starch concentration at pH 5.5 and 11.9

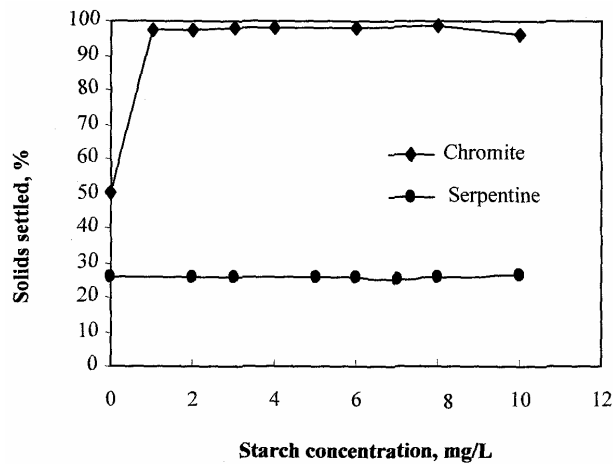


Fig. 4. Flocculation behavior of chromite and serpentine alone as a function of starch addition at pH 11.9

Based upon the above findings, flocculation tests were conducted for chromite and feldspar alone at pH 11.9 as a function of starch addition. As seen from the results presented in Figure 4, chromite starts to flocculate at a relatively low starch concentration with almost complete settling of chromite particles which are suspended with no starch addition. However, serpentine remained dispersed regardless of the starch addition level. Such behavior of the individual minerals is a prerequisite for a successful selective flocculation process.

The flocculation tests indicated that selective flocculation can be applied to an ore consisting of chromite and serpentine using starch as flocculant at pH 11.9. Thus, selective flocculation tests for artificial mixtures of chromite and serpentine were run

to observe the behavior of such mixtures. Two different chromite:serpentine ratios, namely 50%:50% by weight (the first value refers to chromite and the second to serpentine throughout this paper) and 70%:30% by weight, were tested. The results are given in Figures 5 and 6 as grade vs recovery curves. In such plots, a line extending along the full dispersion line shows dispersion; a line to the right of the full dispersion line indicates some degree of selectivity (the farther to the right, the more selective is the separation) in flocculation and all data points at around the feed means indiscriminate flocculation.

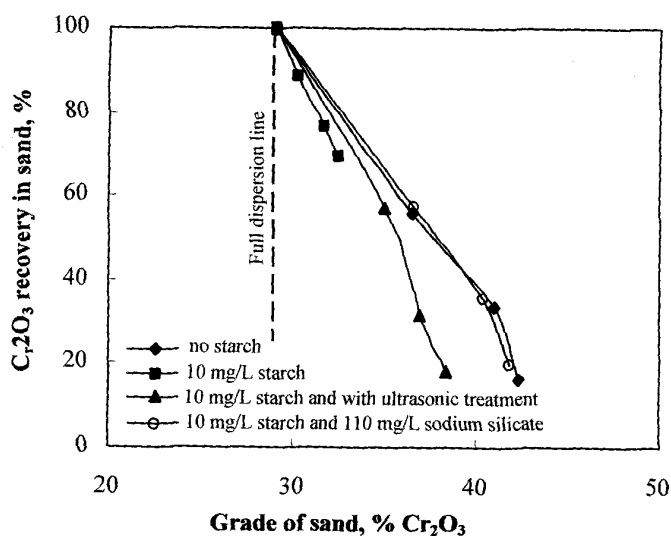


Fig. 5. Selective flocculation of chromite-serpentine mixture (50%:50% wt), pH 11.9

The selective flocculation tests yielded rather unexpected results, Figure 5 and 6. Both mixtures had some selectivity of separation with no starch addition. This can be attributed to the different settling velocities of denser chromite particles and lighter serpentine particles, Table 1. However, upon 10 mg/L starch addition for 50%:50% mixture and 14 mg/L starch addition for 70%:30% mixture, the pulp indiscriminately flocculated. Obviously, an interaction between chromite, serpentine and starch occurred. Although the nature of this interaction was not investigated in this study, it can be postulated that chromite and serpentine heterocoagulated and as starch flocculates chromite, both chromite and serpentine flocculated. A similar occurrence has been reported for the hematite-montmorillonite mixture (Arol and Iwasaki, 1986). The remedy for the adverse effect of a heterocoagulating solid is to remove it from the surface of the mineral to be flocculated. Use of a dispersant is a common practice and ultrasonic treatment of the pulp, albeit less common, can be applied (Heerema et al., 1982; Krishnan and Iwasaki, 1984; Arol and Iwasaki, 1987; Manukonda and Iwasaki, 1987).

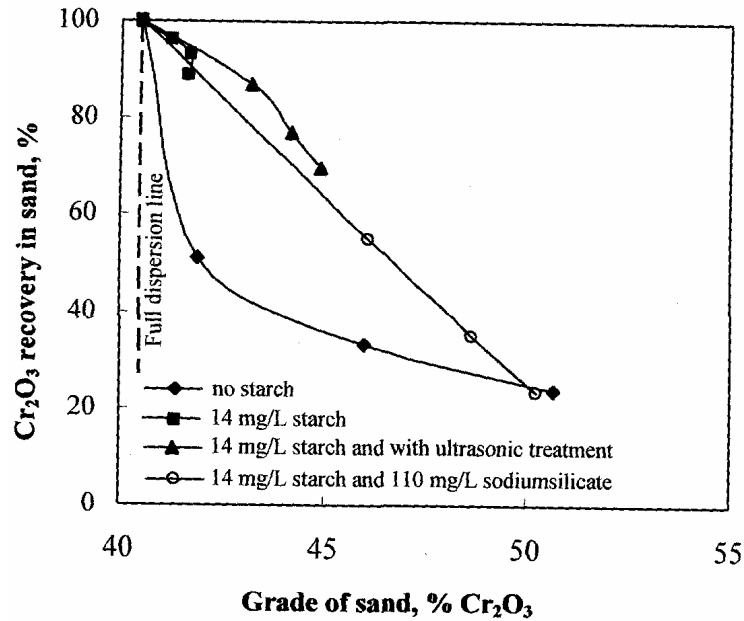


Fig. 6. Selective flocculation of chromite-serpentine mixture (70%:30% wt), pH 11.9

In this study, both methods were tried. As dispersant, 110 mg/L sodium silicate was added to the pulp prior to the starch addition. In another series of selective flocculation tests, the pulp was subjected to ultrasonic treatment for 60 seconds with a horn type sonication device after the starch addition. The results reported here were obtained under optimized conditions (Beklioglu, 2002) and are also included in Figures 5 and 6. As seen in Figure 5, both sodium silicate and ultrasonic treatment restored some selectivity lost by starch addition. However, there was no improvement over what was obtained with no starch addition. It is likely that both sodium silicate and ultrasonic treatment did prevent heterocoagulation but too many serpentine particles crowded the environment and hampered bridge formation between chromite particles by starch. When the amount of serpentine in the mixture was reduced to 30%, Figure 6, better selectivity was obtained with sodium silicate and ultrasonic treatment as the separation curves moved to the upper right direction. Improved selectivity can be attributed to the lessening of the crowding effect by serpentine particles. This behavior of chromite-serpentine mixture in the presence of sodium silicate and with ultrasonic treatment is also similar to the hematite-montmorillonite mixture (Arol and Iwasaki, 1987). Thus, it could be stated that selective flocculation of chromite from a chromite-serpentine mixture could only be possible at lower concentration of serpentine.

CONCLUSION

It was determined that starch has a specific affinity towards chromite but not serpentine. At above pH 11, chromite alone can be flocculated with starch while serpentine alone remains dispersed. When mixed, chromite and serpentine heterocoagulate which makes it difficult to separate the two minerals. Selective flocculation of chromite from a chromite-serpentine mixture is only possible in the presence of lower amounts of serpentine. A dispersant (sodium silicate) or ultrasonic treatment must be used to have a successful separation. Higher amounts of serpentine in the pulp leads to crowding which prevents any separation at all.

REFERENCES

- AKDEMİR, Ü.: 1995, *Shear flocculation of chromite and serpentine fines*, Ph.D. Thesis, Middle East Tech. Univ. Mining Eng. Dept., Ankara.
- ANONYMOUS, 2003, *Personal communication*.
- AROL, A.I. and Iwasaki, I.: 1986, *Effect of montmorillonite on the selective flocculation of iron ores*, Miner. Metall. Process., 3(4), pp. 231-236.
- AROL, A.I., Iwasaki, I.: 1987, *Control of montmorillonite via complexation and ultrasonics in the selective flocculation of iron ores*, Miner. Metall. Process., 4(2), pp. 82-87.
- ATTIA, Y.A.: 1977, *Development of a selective flocculation process for a complex copper ore*, Int. J. Miner. Process., 4(3), pp. 209-225.
- BAGSTER, D.F., MCILVENY, J.D.: 1985, *Studies in the selective flocculation of hematite from gangue using high molecular weight polymers, Part 1: Chemical Factors*, Int. J. Miner. Process., 14, pp. 1-20.
- BALAJEE, S.R., IWASAKI, I.: 1969, *Adsorption mechanism of starches in flotation and flocculation of iron ores*, Trans. AIME, 244, pp. 401-406.
- BEKLIÖGLU, B.: 2002, *Effect of ultrasonic treatment on selective flocculation of chromite*, M.Sc. Thesis, Middle East Tech. Univ. Mining Eng. Dept., Ankara.
- ÇIÇEK, T.; CÖCEN, I., SAMANLI, S.: 1998, *Gravimetric concentration of fine chromite tailings*, in Innovations in Mineral and Coal Processing, Ed.: Atak, Önal&Çelik, Balkema, Rotterdam, pp. 731-736.
- DOĞAN, M.Z., ÖNAL, G., GÜNEY, A., YÜCEL, A.E.: 1996, *New developments in processing of chromite tailings in Turkey*, in Mineral Processing and Environment, NATO Advance Study Institute, Director. G.P. Gallios, 18-30 August, Varna, Bulgaria.
- DOĞU, I., AROL, A.I.: 2004, *Separation of dark colored minerals from feldspar by selective flocculation using starch*, Powder Technology, 139, pp. 258-263.
- DUBOIS, M., GILLES, K.A., HAMILTON, J.K., REBERS, P.A. AND SMITH, F.: 1956, *Colorimetric method for determination of sugars and related substances*, Anal. Chem., 28, pp. 350-356.
- DRZYMALA, J., FUERSTENAU, D.W.: 1981, *Selective Flocculation of Hematite in the Hematite-Quartz-Ferric Ions-Polyacrylic Acid System. Part I. Activation and Deactivation of Quartz*, Inter. Min. Process. Journal, 8, 265-277.
- DRZYMALA, J., FUERSTENAU, D.W.: 1987, *Adsorption of Polyacrylamide, Partially Hydrolyzed Polyacrylamide and Polyacrylic Acid on Ferric Oxide and Silica*, Process Technol.Proc., Flocculation in Biotechnology and Separation Science, 45-60.
- GÜNEY, A., ÖNAL, G.: 2000, *Application of a new beneficiation method to ultrafine-size chromite*, in Mineral Processing on the Verge of 21st Century, Ed.: Özbayoğlu et al., Balkema, Rotterdam, pp. 299-303.

- HANUMANTHA, K.R., NAYAK, A., MAHAPATRA, S.N., NARASIMHAN, K.S.: 1985, *Selective flocculation for the recovery of iron in Kudremukh tailings*, Mining Engineering, 37, pp. 1312-1315.
- HANUMANTHA, K.R., NARASIMHAN, K.S.: 1985, *Selective flocculation applied to barsuaan iron ore tailings*, Int. J. Miner. Process. 14, 67-75.
- HEEREMA, R. H., LIPP, R.J., IWASAKI, I.: 1982, *Complexation of calcium Ion in selective flocculation of iron ores*, Trans. SME-AIME, 272, pp.1879-1884.
- IWASAKI, I., CARLSON, W. J., PARMETER, S.S.: 1969, *The use of starch and starch derivatives and depressants and flocculants in iron ore beneficiation*, Trans. AIME, 244, pp. 88-98.
- KHOSLA, N.K., BHAGAT, R.P., GANDHI, K.S., BISWAS, A.K.: 1984, *Calorimetric and other interaction studies on mineral-starch adsorption systems*, Colloids Surf., 4(8), pp. 321-336.
- KRISHNAN, S. V., IWASAKI, I. 1984, *Pulp Dispersion in Selective Desliming of Iron Ores*, Int. J. Miner. Process., 12(1), pp. 1-13.
- LASKOWSKI, J.S., LUI Q., BOLIN N.J.: 1991, *Polysaccharides in flotation of sulphides: Part 1. Adsorption of polysaccharides onto mineral surfaces*, Int. J. Miner. Process., 33(1-4), pp. 223-234.
- LIEN, H.O., MORROW, J.G.: 1978, *Beneficiation of lean iron ores solely by selective flocculation and desliming*, CIM Bulletin, 71(798), pp.109-120.
- MANUKONDA, V. R. AND IWASAKI, I.: 1987, *Control of calcium ion via chemical precipitation-ultrasonic treatment in selective flocculation*; Minerals & Metallurgical Processing, 4(4), pp. 217-222.
- MOUDGIL, B.M., MATHUR, S.: 1994, *Removal of dolomite and silica from apatite by selective flocculation*, Miner. Metall. Process., 11(4), pp. 217-22.
- PRADIP, R.A., MOUDGIL, B.M.: 1991, *Selective flocculation of tribasic from mixtures with quartz using polyacrylic acid flocculant*, Int. J. Miner. Process., 32(1-2), pp. 271-281.
- RAVISHANKAR, S.A., PRADIP, KHOSLA, N.K.: 1995, *Selective flocculation of iron oxides from its synthetic mixtures with clays: A comparison of polyacrylic acid and starch polymers*, Int. J. Miner. Process., 43(3-4), pp. 235-247.
- READ, A.D.: 1971, *Selective flocculation separations involving hematite*, Inst. Min. Metall. Trans., Section C, 80, pp. 24-31.
- SOBIERAJ, S., LASKOWSKI, J.: 1973, *Flotation of chromite: 1-early research and recent trends; 2-flotation of chromite and surface properties of spinel minerals*, Trans. IMM, Sec.C., 82, C207-C213.
- SWORSKA, A., LASKOWSKI, J.S., CYMERMAN, G.: 2000, *Flocculation of the Syncrude fine tailings Part I: Effect of pH, polymer dosage and Mg²⁺ and Ca²⁺ cations*, Int. J. Miner. Process, 60(2), pp. 143-152.
- WEISENBORN, P.K., WARREN, L.J., DUNN, J.G.: 1994, *Optimization of selective flocculation of ultrafine iron ore*, Int. J. Miner. Process., 42(3-4), pp. 191-231.
- WEISENBORN, P.K., WARREN, L.J., DUNN, J.G.: 1995, *Selective Flocculation of Ultrafine Iron Ore. I. Mechanism of Adsorption of Starch on Hematite*, Colloids and Surf. A: Physicochem. Eng. Aspects, 99(1), pp. 29-43.
- YARAR, B., KITCHENER, J.A.: 1970, *Selective flocculation of minerals: 1- Basic principles, 2- Experimental investigation of quartz, calcite and galena*, Inst. Min. Metall. Trans., Section C, 79, pp.23-33.

Bekhtoglu B., Arol A.I., *Selektywna flokulacja chromitu i serpentynitu*, Physicochemical Problems of Mineral Processing, 38, (2004) 103-112 (w jęz. ang.).

Metoda selektywnej flokulacji z użyciem skrobi jako flokulanta, została użyta do oddzielenia chromitu od serpentynitu. Zostało ustalone, na podstawie badań, że skrobia wykazuje specyficzne powinowactwo do chromitu, który dzięki temu może ulec selektywnej flokulacji. Okazało się jednak, że selektywny rozdział jest możliwy do osiągnięcia w warunkach, gdy ilość serpentynitu w chromicie nie przekracza 30% wagowych. Proces separacji został zrealizowany w obecności dyspersanta - krzemianu sodu, a zawiesina była traktowana ultradźwiękami.

Leszek GOTFRYD*, Jan SZYMANOWSKI**

RECOVERY OF ZINC(II) FROM ACIDIC SULFATE SOLUTIONS. SIMULATION OF COUNTER-CURRENT EXTRACTION-STRIPPING PROCESS

Received April 29, 2004; reviewed; accepted June 5, 2004

Cyanex 272 and di(2-ethylhexyl)phosphoric acid (DEHPA) were used for extraction of zinc(II) from sulphate solutions. Counter-current extraction-stripping process was simulated. The simulation enabled CYANEX 272 to be selected for the recovery of zinc(II) from acidic sulphate solutions. A higher selectivity of zinc(II) extraction was the main benefit of using CYANEX 272. Technologically significant conclusions could be arrived at only when process solutions with metal contaminants were used for the studies and several extraction-washing-stripping cycles were carried out. The studies of individual extraction and/or stripping using model solutions could be only considered as an initial step and were of a limited technological value.

Key words: zinc(II) extraction, CYANEX 272, di(2-ethylhexyl)phosphoric acid, counter-current extraction-stripping process simulation

INTRODUCTION

Pyrometallurgy of zinc, especially of secondary resources, gives several dust streams of which further pyrometallurgical processing is difficult and very inconvenient. Such wastes could be processed by hydrometallurgical methods (Dutrizac et al. 1998). Zinc could not be directly electrowinned from leach solutions because of the presence of metal contaminants. The contaminants should be separated in an extraction-stripping process. Acidic extractants, especially those containing dialkylphosphoric acid and dialkylphosphinic acid, are convenient for such separation (Gega et al. 1991, Sastre et al. 1984).

* Institute of Nonferrous Metals, Gliwice.

** Poznan University of Technology, Institute of Chemical Technology and Engineering,
pl. M. Skłodowskiej-Curie 2, 60-965, Poznan, Poland, jan.szymanowski@put.poznan.pl

The fundamental technological problems of zinc(II) extraction were discussed in several reviews (Bart, 2000, Jha et al. 2002, Mishonov et al. 2002). In most of the published papers, model feed solutions were used and either single extraction or the stripping stage was studied. Such results were very important for basic studies but they were of a limited value for designing the extraction-stripping process. Such basic studies should be verified using actual process solutions containing metal contaminants. Moreover, the process should be verified in a continuous multistage counter-current extraction-stripping process.

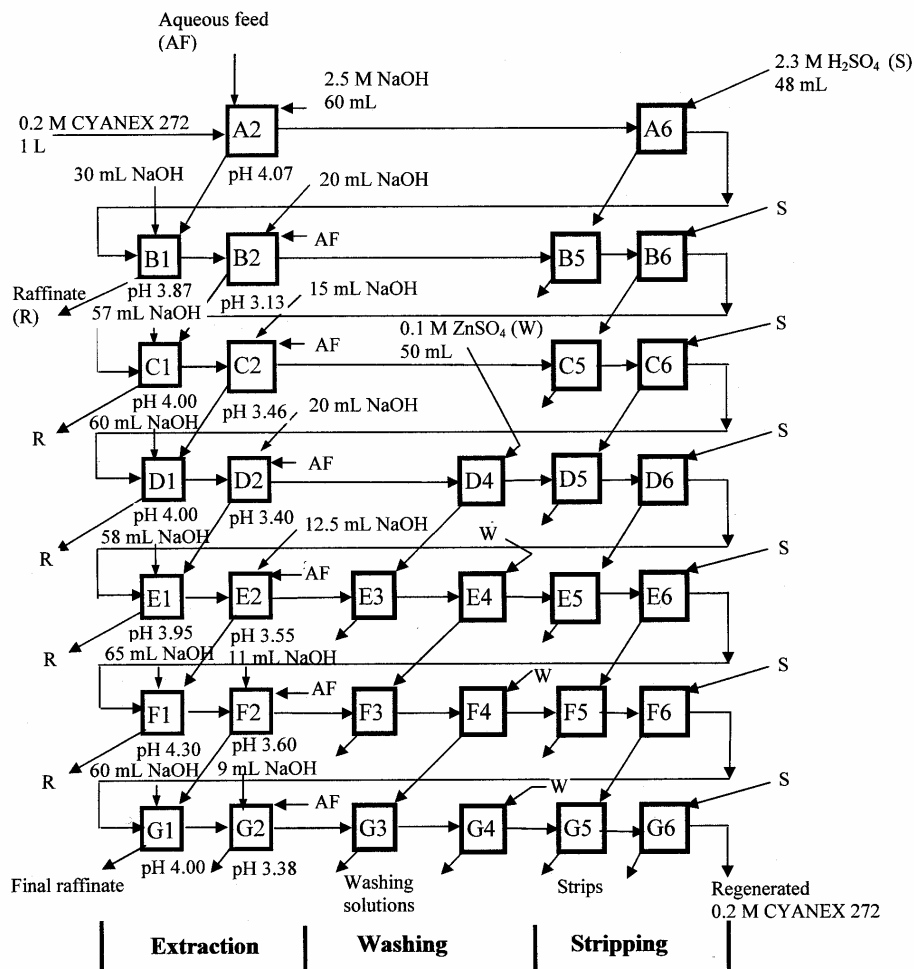


Fig. 1. Simulation of counter-current extraction-stripping process. 0.2 M CYANEX 272 as extractant (99.5 mL of the aqueous feed (AF) used for extraction in each cycle A2-G2, 45 mL of 2.3 M sulfuric acid (S) used for stripping in each cycle A6-G6, different volumes of 2.5 M NaOH (N) used for pH adjustment in each extraction, 50 mL of 0.1 M $ZnSO_4$ (W) used for washing in each cycle D4-G4)

The aim of this work was to simulate a counter-current extraction-stripping process in a laboratory scale using an actual sulphate process solution containing zinc(II), and contaminated with Cu(II), Cd(II), Na(I), K(I), Mg(II), Ca(II) and As(V). These studies were considered as the first step in the design of the counter-current extraction-stripping step working in a continuous mode.

EXPERIMENTAL

The aqueous feed was obtained by leaching electric furnace dust obtained from a copper smelter, Glogow, Poland, with sulphuric acid. Silica was removed from the leach solution by changing its pH value with sodium carbonate solution, and precipitation. The feed contained (in g/L): Zn 68.6, K 9.40, Na 4.4, Mg 3.05, Cu 3.4, Cd 0.38, Cl approx. 1 and As 0.053. 0.2 M solutions of CYANEX 272 (Cytec Inc., Canada) and di(2-ethylhexyl)phosphoric acid (DEHPA, SIGMA-Aldrich, Germany) in ESCAID 120 (Esso/Exxon, USA) were used for the extraction.

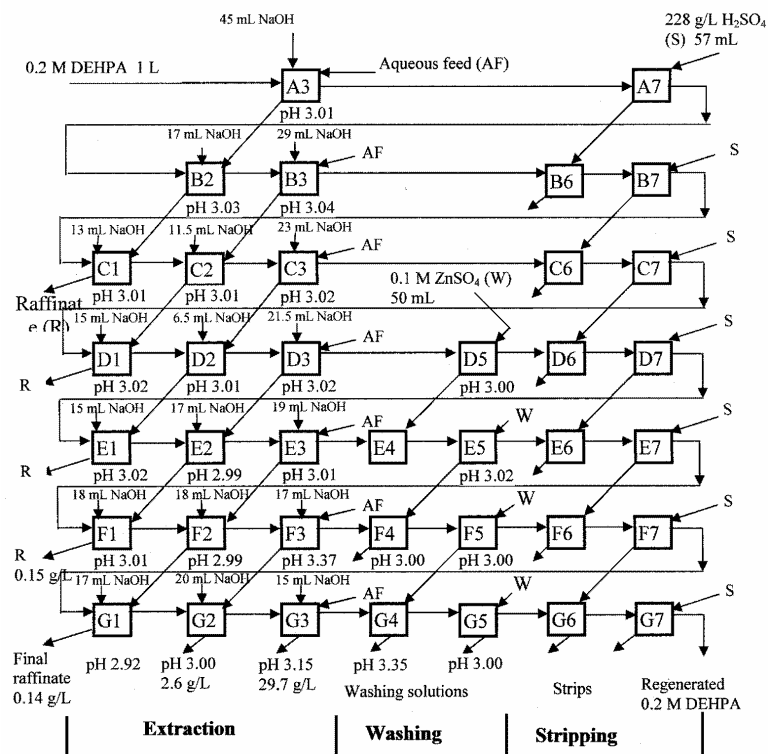


Fig. 2. Simulation of counter-current extraction-stripping process. 0.2 M DEHPA as extractant (117.5 mL of the aqueous feed (AF) used for extraction in each cycle A3-G3, 57 mL of 2.3 M sulphuric acid (S) used for stripping in each cycle A7-G7, different volumes of 5 M NaOH (N) used for pH adjustment in each extraction, 50 mL of 0.1 ZNSO₄ (W) used for washing in each cycle D5-G5)

The extraction-stripping process (2-2-2 and 3-2-2 for CYANEX 272 and DEHPA, where the subsequent digits denote the numbers of stages in extraction, washing and stripping, respectively) were simulated by contacting phases for 10 minutes in beakers (up to 2 L volume) and separating the phases in separatory funnels at a room temperature. pH was adjusted with 2.5 or 5 M NaOH to 3.5 and 4.0 in the first and second extraction stages with CYANEX 272, and to pH 3 in each extraction step with DEHPA. The same volume of 2.3 M (228.3 g/L) sulphuric acid was used for stripping in each stage (48 and 57 mL from CYANEX 272 and DEHPA, respectively). 0.1 M $ZnSO_4$ was used for washing. Actual equilibrium pH values in each extraction stage are given in Figs. 1 and 2.

The simulation was carried out in the manner presented in Figs. 1 and 2. Seven extraction cycles (A-G) were carried out. The raffinate obtained in the first cycle (A2) was used as an aqueous feed in the second stage (B1) of extraction of cycle B, in which the regenerated organic phase (after stripping in A6) was used. Next the organic phase was contacted with the fresh feed solution in B2. In the same second cycle B, both the aqueous phase from the first cycle (A6→B5) and fresh sulphuric acid (in B6) were used for stripping. Washing was started from the fourth cycle (D) and was carried out in two stages in each subsequent cycle.

Atomic absorption spectroscopy was used to determine the contents of the components in the aqueous phases.

RESULTS AND DISCUSSION

Initial experiments showed that equilibria of extraction stripping were obtained in 5 minutes of phase contact. The phases separated completely both in extraction and stripping.

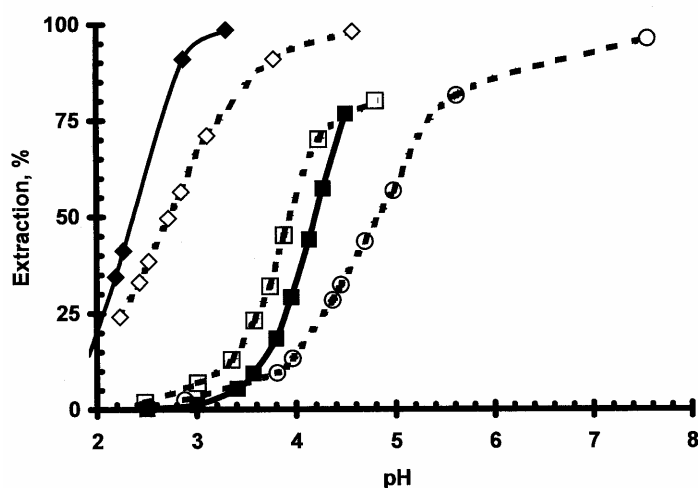


Fig. 3. Effect of pH on extraction of selected metal cations with 0.2 M CYANEX 272

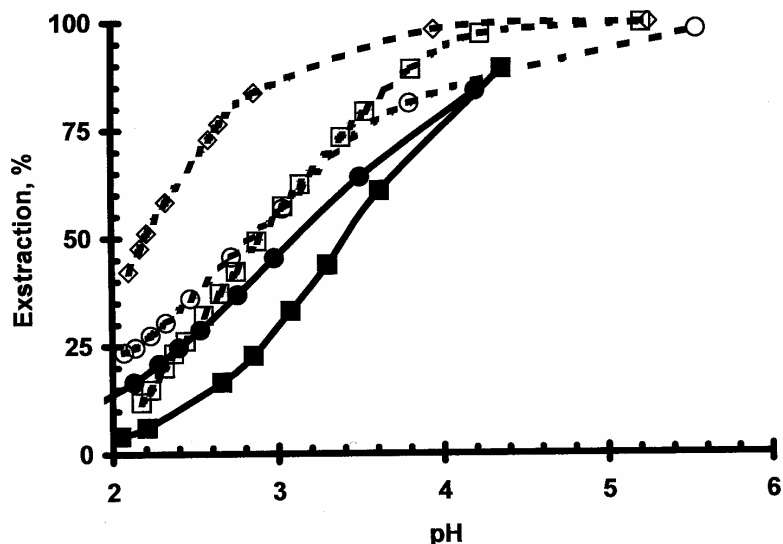


Fig. 4. Effect of pH on extraction of selected metal cations with 0.2 DEHPA

Figures 3 and 4 show the effect of equilibrium pH on the extraction of selected metal cations with 0.2 M solutions of CYANEX 272 and DEHPA. Such relationships are usually given in reagent catalogues. However, the position of the curves of % extraction vs. pH depends on the extraction conditions, i.e., concentrations of reagents in both phases and the diluent. The isotherms given in Figs. 3 and 4 correspond to the experimental conditions used in this work. In the both considered systems, zinc(II) was better extracted than other cations. DEHPA extracted zinc(II) at lower pH than did CYANEX 272. $pH_{0.5}$ values determined for metal sulphate concentration equal to 0.5 M amounted as follows: 0.2 DEHPA – Zn 2.21, Cd 2.83, Cu 2.90 and 0.2 M CYANEX 272 – Zn 2.72, Cd 4.82, Cu 3.93. Bigger gaps between the curves of % extraction vs. pH were observed for CYANEX 272.

Extraction isotherms of zinc concentration in the organic phase versus zinc concentration in the aqueous phase (Fig. 5) indicated that the loading capacities of the organic phases (0.2 M) were in the range 6-8 g/L for the considered equilibrium pH. Such low capacities indicated that i) the organic phase could easily be totally loaded with zinc(II) and, due to the crowd-out effect, the selectivity of zinc extraction could be improved, and ii) a significant volume excess of the organic phase would be needed to efficiently recover zinc(II) from concentrated aqueous feeds (68.6 g/L Zn(II)). The extraction should then be carried out in 2-3 counter-current stages.

The compositions of the selected aqueous phases and recoveries of contaminated components are given in Tables 1 and 2. A higher recovery of zinc(II) (99.997%) was obtained using DEHPA. However, the final aqueous phase contained significant amounts of metal contaminants. About 50% Cu(II), 30% Cd(II), 20% K(I) and 3.5%

Mg(II) present in the aqueous feed was transferred to the final strip. The content of sodium increased drastically from 4.4 g/L up to 7.6 g/L. That high concentration of sodium could result from the great difference in the volumes of phases in the stripping (1 L of organic phase and 57 mL of strip phase). The organic phase was not totally loaded with zinc(II) and accumulated sodium. Additional washing with a diluted acid should be necessary to remove sodium. However, some amounts of zinc(II) would be also washed out as a result.

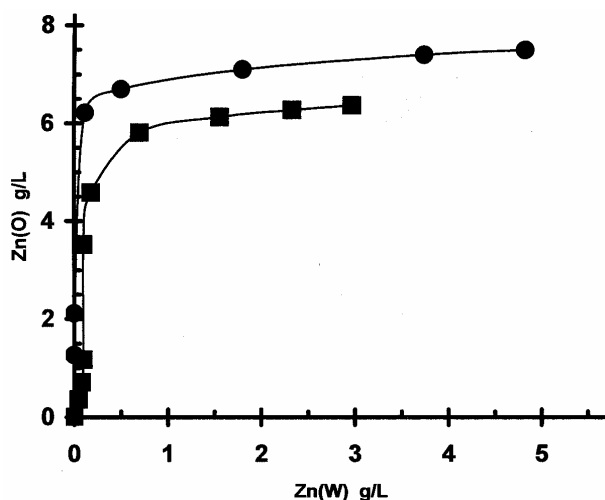


Fig. 5. Extraction isotherms for zinc(II) extraction with 0.2 DEHPA (pH 3.0) and 0.2 M CYANEX 272 (pH 4)

Table 1. Composition of selected aqueous phases and recoveries from the feed. 0.2 M CYANEX 272 as extractant

Solution		Concentrations, g/L							
		Cu	Cd	K	Na	Mg	As	Fe	Zn
Aqueous feed		3.4	0.38	9.4	4.4	3.05	0.053		68.6
F5	Strip	0.026	0.0034	0.14	0.94	0.036	0.013	0.006	110
G5	Strip	0.011	0.0021	0.10	1.01	0.018	0.010	0.004	140
F1	Raffinate	1.99	0.22	5.49	27.4	1.78	0.027	-	2.00
G1	Raffinate	1.98	0.22	5.50	26.2	1.79	0.028	-	4.25
G2	Raffinate	-	-	-	-	-	-	-	54.0
		Recovery, %							
F5	Strip	0.37	0.43	0.72	-	0.57	11.8	-	94.8
G5	Strip	0.16	0.27	0.51	-	0.28	8.9	-	89.4

CYANEX 272 extracted less zinc(II) (near 90%) but transferred significantly less metal contaminants. Thus, the use of CYANEX 272 was preferred because the reagent coextracted 150-300 times less copper(II), 70-100 times less cadmium(II), 35-45 times less potassium, 9-12 times less magnesium(II) and 6-8 times less sodium than DEHPA. Only the level of arsenic(V) was 1.3 times higher when CYANEX 272 was used.

Table 2. Composition of selected aqueous phases and recoveries from the feed. DEHPA as extractant.

Solution		Concentration, g/L						
		Cu	Cd	K	Na	Mg	As	Zn
Aqueous feed		3.4	0.38	9.4	4.4	3.05	0.053	68.6
F6	Strip	3.95	0.25	4.75	7.63	0.33	<0.007	150
G6	Strip	3.63	0.22	4.50	5.75	0.22	<0.007	150
F1	Raffinate	1.00	0.175	4.79	19.1	1.95	0.033	0.14
G1	Raffinate	1.12	0.187	4.94	19.2	2.02	0.034	0.15
G2	Raffinate	-	-	-	-	-	-	2.6
G3	Raffinate	-	-	-	-	-	-	29.7
		Recovery, %						
F5	Strip	56.4	31.9	24.5	-	5.25	<6.5	99.997
G5	Strip	51.8	28.1	23.2	-	3.50	<6.5	99.997

A higher selectivity of zinc(II) extraction with CYANEX 272 was obtained, although the equilibrium pH of the aqueous phases in the extraction (3.1-4, mainly near 4) was near 1 unit higher in comparison with the process in which DEHPA was used (near 3). At the same pH the advantage of using CYANEX 272 would be significantly higher. However, the strip solution needed further purification before electrowinning to reduce the content of Cu(II) and Cd(II) down to the level of 0.0001-0.0005 g/L. Such purification could be accomplished by cementation with zinc.

The use of Cyanex 272 was also more convenient because the formation of cruds was not observed. Contrary, the cruds were formed after a few cycles of extraction and stripping when DEHPA was used. The DEHPA organic phase became more viscous than the phase containing CYANEX 272.

CONCLUSIONS

The simulation of the counter-current extraction-stripping process enabled CYANEX 272 to be selected for the recovery of zinc(II) from acidic sulphate solutions. A higher selectivity of zinc(II) extraction was the main benefit of using CYANEX 272. Technologically significant conclusions could be arrived at only when process solutions with metal contaminants were used for the studies and several extraction-washing-stripping cycles were carried out. The studies of individual extraction and/or stripping using model solutions could only be considered as an initial step and were of a limited technological value.

REFERENCES

- BART H. J. 2000, *Reactive Extraction*, Springer, Berlin.
 DUTRIZAC J. E., GONZALES J. A., BOTTON G. L., HANCOCK P. (Eds.) 1998, *Zinc and Lead Processing*, Canadian Institute of Mining, Metallurgy and Petroleum, Montreal.
 GEGA J., WALKOWIAK W. 1991, *Organophosphorus compounds in extraction of metals*, Rudy Metale, Vol. 36, pp. 27-32 (in Polish).

- JHA M. K., KUMAR V., SINGH R.J. 2002, *Solvent extraction of zinc(II) from chloride solutions*, Solvent Extr. Ion Exch., Vol. 20, pp. 389-405.
- MISHONOV I. V., SZYMANOWSKI J. (2002), *Recovery of zinc(II) from primary and secondary chloride solutions by solvent extraction*, J. Appl. Chem., Vol. 46, pp. 187-207.
- SASTRE A. M., MUHAMMED M. 1984, *The extraction of zinc(II) from sulphate and perchlorate solutions by di(2-ethylhexyl)phosphoric acid dissolved in Isopar H*, Hydrometallurgy, Vol. 12, pp. 177-193.

ACKNOWLEDGMENTS

The work was partially supported by the EC - TREWAT Project (Contract No. IC15-CT-98 0146) as part of the INCO-Copernicus Programme. One of the authors (JS) appreciates the support of DS grant 32/044/2004.

Gotfryd L., Szymanowski J., *Odzysk cynku(II) z kwaśnych roztworów siarczanowych. Symulacja przeciwprądowego procesu ekstrakcyjno-reekstrakcyjnego*, Physicochemical Problems of Mineral Processing, 38, (2004) 113-120 (w jęz. ang.).

Cyanex 272 oraz kwas di(2-etyloheksylo)fosforowy (DEHPA) zastosowano do ekstrakcji cynku(II) z procesowych roztworów siarczanowych zawierających dodatkowo Cu(II), Cd(II), Na(I), K(I), Mg(II), Ca(II) i As(V). Symulowano przeciwprądowy proces ekstrakcyjno-reekstrakcyjny. Symulacja pozwoliła wytypować Cyanex 272 jako odpowiedni ekstrahent do selektywnej ekstrakcji cynku(II) wobec występujących zanieczyszczeń. Tylko zastosowanie prawdziwych roztworów technologicznych i prowadzenie pełnego cyklu ekstrakcji – przemywania i reekstrakcji umożliwia wyprowadzenie technologicznie rozsądnych wniosków. Badanie indywidualnego etapu ekstrakcji lub reekstrakcji posiada ograniczone technologiczne znaczenie.

Marta ROZENBLAT, Magdalena REGEL-ROSOCKA, Jan SZYMANOWSKI*

METAL REMOVAL FROM SPENT PICKLING SOLUTIONS OF HIGH ZINC(II) CONCENTRATION

Received April 29, 2004; reviewed; accepted May 15, 2004

The extraction of zinc(II), iron(III) and iron(II) with TBP from hydrochloric acid solutions containing high zinc(II) concentration is studied. Two technological approaches for the separation are considered. Firstly, the selective extraction of iron(III) (iron(II) is oxidized to iron(III)) over zinc(II) with TBP deficiency. Secondly, iron(III) reduction to iron(II) followed by zinc(II) selective extraction with an excess of TBP. The total removal of iron(III) needs several successive extractions with fresh TBP portions. Such a process is not technologically reasonable. Stripping both of zinc(II) and iron(III) can be effectively accomplished with water but is not selective. Prior stripping, the organic phase can be washed with small amounts of water. Scrubbing of TBP solutions containing iron(III) contaminated with zinc(II) gives always a mixture of zinc(II) and iron(III) which must be recycled to the extraction step in continuous process. Scrubbing of TBP solutions containing zinc(II) and iron(II) enables the removal of iron(II) with some amounts of zinc(II). Again, the solution must be recycled. Scrubbing is more advantageous than multistage extraction with small volume of TBP. The following technological concept is proposed: reduction of iron(III) to iron(II), extraction of zinc(II) with 5-10 volume excess of TBP, washing of TBP phase contaminated with iron(II) with small volumes of water and recycling of the scrubbing and stripping of zinc with water.

Key words: extraction, zinc(II), iron(III), iron(II), tributyl phosphate, spent pickling solutions

INTRODUCTION

Regeneration of spent pickling solutions from hot-dip galvanizing is an important and still unsolved problem. Hot-dip galvanizing in 96.5-99% purity zinc, carried out at 445-465 °C (Maass, 1998), needs the pure surface of iron goods. The rust is removed by the pickling with 20% HCl carried out at room temperature.

Pickling solutions are considered as spent solutions when hydrochloric acid concentration decreases by 75-85%, and metal content increases up to 150-250 g/L

*Institute of Chemical Engineering and Technology, Poznan University of Technology,
pl. M. Skłodowskiej - Curie 2, 60-965 Poznan, Poland, jan.szzymanowski@put.poznan.pl

(Maass 1997, Anielak 1987). The spent pickling solution content depends on the origin plant and pickling method applied there. Spent pickling solutions from steel pickling contain zinc(II), iron (mainly iron(II)), traces of lead, chromium and other heavy metals (max. 500 mg/L) and hydrochloric acid. Zinc(II) passes to the spent solution due to removal of bad covered zinc layers, dissolution of covered with zinc(II): racks, chains and baskets used for transportation of galvanized elements. As a result, zinc(II) concentration increases even up to 130 g/L, while iron content does not exceed 10 g/L (Maass 1997).

The use of several techniques was proposed to regenerate spent pickling solutions but they were not implemented into industrial practice (Lo, 1991). One of the possibilities is the use of solvent extraction. Fundamental problems of such separation were described in our previous papers (Regel et al. 2001, Cierpiszewski et al. 2002, Regel-Rosocka et al. 2002, Regel-Rosocka et al. 2003). However, problem concerned spent pickling solutions containing low amounts of zinc(II) and high amounts of iron.

It is the aim of the work to study the effect of phase ratio on selectivity of zinc(II) or iron(III) extraction with tributyl phosphate from spent pickling solution containing high zinc(II) concentration.

EXPERIMENTAL

Tributyl phosphate (TBP) (Merck, Germany) was used as an extractant. The reagent was used as delivered without any purification and was applied as undiluted and diluted (80%) with low aromatic kerosene Exxsol D 220/230 (ESSO A.G., Germany).

Extraction was carried out in small scale (separatory funnels) using different volume ratios equal to (organic/water) 1:10, 1:5, 1:1, 5:1, 8:1, 9:1 and 10:1. Phases were mechanically shaken for 10 minutes and left for phase separation. Contents of the model aqueous feed was near to a real solution from "Belos" galvanizing plant in Bielsko-Biala and contained 100 g/L Zn(II), 29 g/L Fe(II), 1 g/L Fe(III) 2.5 M HCl, 6.5 M Cl⁻. Stripping from loaded TBP was carried out with deionized water at volume ratio 1:1. Scrubbing of loaded TBP was carried out with deionized water at w/o ratio 1:5 and 1:10.

In the second part of the experiments the aqueous phase containing 120 g/L Zn(II), 30 g/L Fe(III), 4 M HCl, 6.5 M Cl⁻ (Feed1) was extracted with 80% TBP in several stages until iron(III) was removed completely. Three volume ratios were used o/w 1:2, 1:5, 1:10. After first extraction, the organic phase was contacted with the fresh aqueous feed (Feed2: 120 g/L Zn(II), 30 g/L Fe(III), 4 M HCl, 6.5 M Cl⁻) and after each further extraction the organic phase was contacted with raffinate (R_{2i}) to load TBP with iron(III) and to push up zinc(II) from the organic phase. The way of carrying out the experiment is shown in Fig. 1.

Zn(II) concentration in the aqueous phase was determined by amperometric titration with 0.05 M K₄[Fe(CN)₆]. HCl content in aqueous phase was determined by

potentiometric titration (702 SM Titrino, Metrohm, Switzerland) with 0.1 M NaOH. The content of Fe(II) and Fe(III) was determined by titration with $K_2Cr_2O_7$ (Fe(III) was reduced to Fe(II) with 5% solution of $SnCl_2$). The content of water in the organic phase was determined by the Karl - Fischer titration.

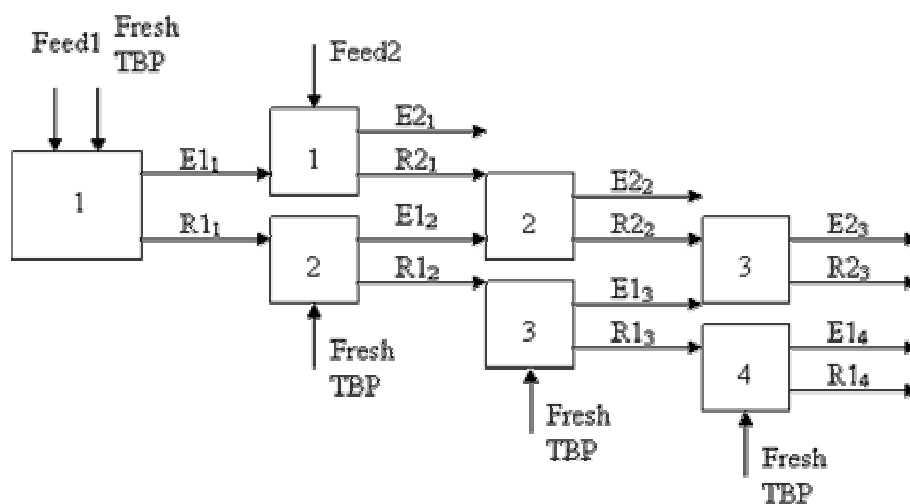


Fig. 1. Scheme of multistage extraction experiment (E and R denote extract and raffinate, respectively; capital digit succeeding R or E stands for feed 1 and 2; subscripts denote extraction step)

RESULTS AND DISCUSSION

The real solution from “Belos” galvanizing plant in Bielsko-Biala contains 120 g/L Zn(II), 30 g/L Fe(II), 1 g/L Fe(III), 2.5 M HCl, 6.5 M Cl⁻. In the considered system of high chloride concentration, metal ions exist mainly in the form of chlorocomplexes.

The computing results of chlorocomplexes distribution, presented in previous work (Bartkowska et al. 2002), suggest that in the initial aqueous feed only iron(II) is present in cationic forms (Fe^{2+} and $FeCl^+$) and can not be extracted by TBP. Both iron(III) and zinc(II) form higher chlorocomplexes which are extracted effectively.

Two technological approaches for the separation were considered. Firstly, the selective extraction of iron(III) over zinc(II) with small portions of TBP. Thus, it was assumed that prior extraction iron(II) would be oxidized to iron(III), e.g., with hydrogen peroxide. Secondly, iron(III) reduction to iron(II) with iron wool followed by zinc(II) selective extraction with an excess of TBP. Taking into account a high concentration of zinc(II), the first option seems technologically more sound.

The extraction depends on the phase ratio. Fig. 2 indicates that percentage of zinc(II) extraction increases significantly with increasing organic phase volume. For 10-folded excess zinc(II) extraction reaches almost 100%. Similar behavior is observed for iron(III). However, iron(III) extraction is high even for small organic

phase volume. Iron(II) extraction increases with increasing o/w volume, too. It can be explained with iron(II) oxidation to iron(III) or iron(II) transport in hydrophilic cores of reverse micelles to the organic phase.

In fact zinc(II) concentration in feed is near 100 times higher than iron(III) concentration. Thus, the content of zinc(II) in the organic phase is higher than iron(III) concentration, even for small organic phase volumes. Real view of zinc(II) and iron(III) extraction is better expressed as selectivity characterized by the ratio of distribution coefficients, e.g.:

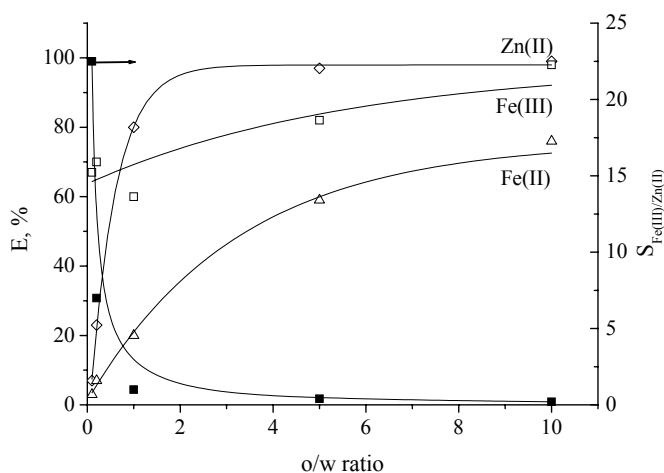


Fig. 2. Effect of organic/water volume ratio on percentage of zinc(II) (\diamond), iron(II) (\triangle) and iron(III) (\square) extraction and selectivity (\blacksquare) of iron(III) extraction over zinc(II) with 100% TBP. (Feed: 100 g/L Zn(II), 29 g/L Fe(II), 1 g/L Fe(III), 2.5 M HCl, 6.5 M Cl⁻)

$$S_{Fe(III)/Zn(II)} = \frac{D_{Fe(III)}}{D_{Zn(II)}} \quad (1)$$

The results in Fig. 2 indicate that good extraction selectivity of iron(III) over zinc can be obtained only for small o/w ratios (up to 1:2).

Table 1. Zinc(II) and iron(III) extraction with 80% TBP for different volume ratios (Feed: 100 g/L Zn(II), 30 g/L Fe(III), 2.5 M HCl, 6.5 M Cl⁻).

o/w ratio	$E_{Zn(II)}$ %	$[Zn(II)]_o$ g/L	$E_{Fe(III)}$ %	$Fe(III)_o$ g/L
1/10	0.37	3.7	11.4	34.2
1/5	0.81	4.1	22.3	33.4
1/2	0.78	1.6	42.0	25.2

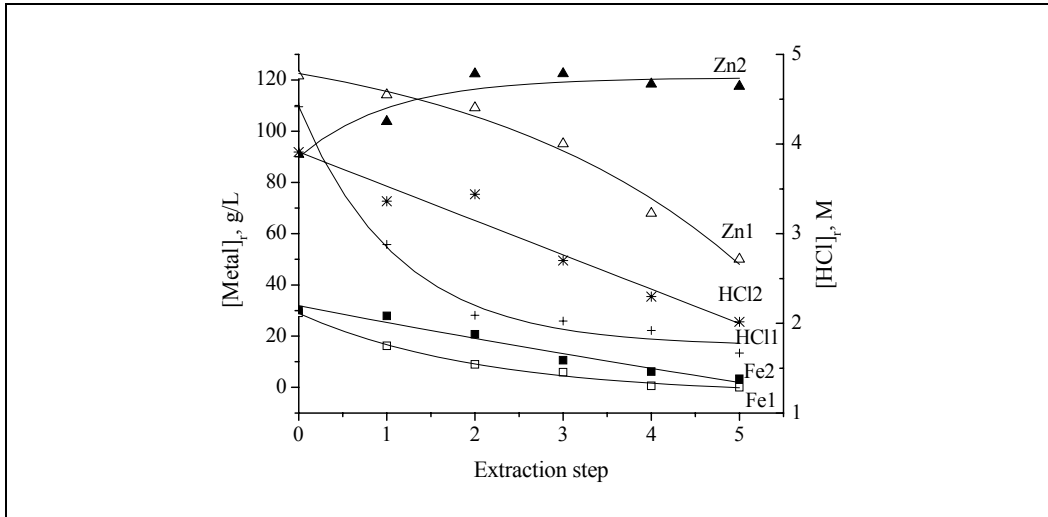


Fig. 3. Scheme of multistage extraction experiment (E and R denote extract and raffinate, respectively; capital digit succeeding R or E stands for feed 1 and 2; subscripts denote extraction step)

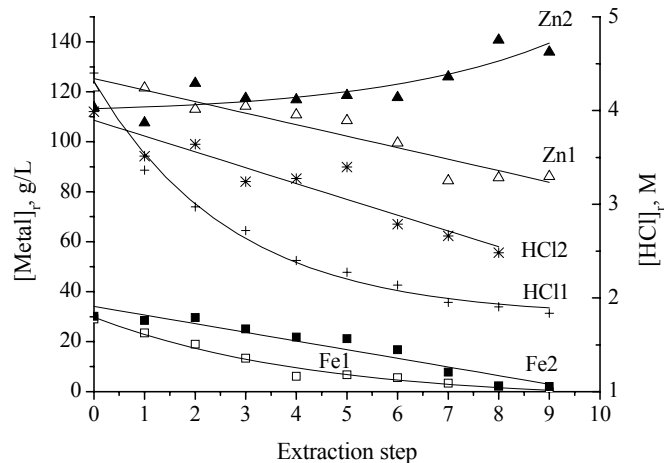


Fig. 4. Iron(III) (■, □), zinc(II) (▲, △) and HCl (*, +) concentrations in raffinate R1; (□, △, +) and R2; (■, ▲, *) in nine steps of extraction at o/w = 1:5 (Feed: 120 g/L Zn(II), 30 g/L Fe(III), 4 M HCl, 6.5 M Cl⁻; Organic: 80% TBP)

The loading capacities of 80 and 100% TBP are equal to 36 and 45 g/L Fe(III) respectively. The organic phase after single extraction with the volume ratio o/w changed from 1:10 to 1:5 contains over 30 g/L Fe(III) and 3-4 g/L Zn(II) (Table 1). Thus, the total removal of iron(III) (after oxidation of Fe(II)) needs several successive extractions with fresh TBP portions. Such process is not technologically reasonable.

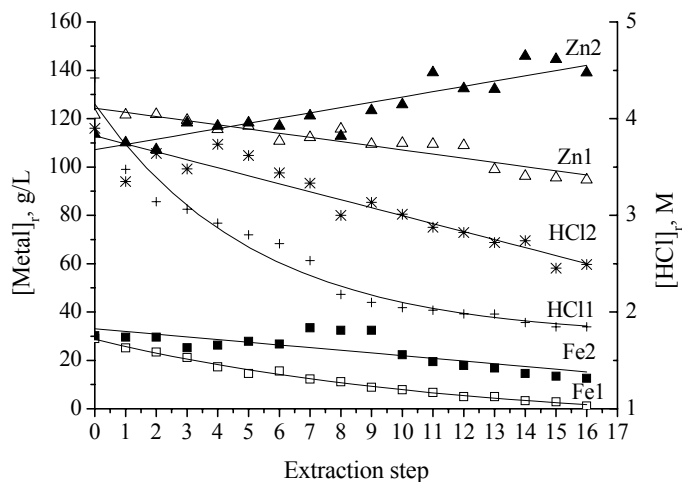


Fig. 5. Iron(III) (■, □), zinc(II) (▲, △) and HCl (*, +) concentrations in raffinate R1_i (□, △, +) and R2_i (■, ▲, *) in five steps of extraction at o/w = 1:2 (Feed: 120 g/L Zn(II), 30 g/L Fe(III), 4 M HCl, 6.5 M Cl⁻; Organic: 80% TBP)

The separation of iron(III) over zinc(II) is enhanced with an excess of the aqueous feed due to the crowd effect, i.e. when the organic phase is saturated with metal species then weaker complexes are replaced by the stronger ones. Such a phenomenon takes place in case of the second extraction (see Fig. 1 with extraction scheme), where raffinate after the extraction is richer in Zn(II). It is observed for all o/w ratios 1:2, 1:5 and 1:10 in Figs. 3–5, respectively. Iron(III) concentration in both raffinates (Fe1, Fe2 in R1_i and R2_i) decreases almost to 0 g/L. However, zinc(II) concentration (Zn1) in raffinate R1_i also decreases in each successive step of extraction. It means that Zn(II) is co-extracted to the organic phase. However, after contacting the loaded TBP with the second raffinate R2_i, Zn(II) concentration (Zn2) increases in each step and finally amounts to at least initial value in feed. HCl extraction plays important role in zinc(II) and iron(III) extraction. A dramatic decrease of HCl concentration (HCl1), from over 4 to 2 M, is observed in first three, six and nine steps in raffinate R1_i for o/w = 1:2, 1:5 and 1:10, respectively. Then, HCl transport is not significant. HCl concentration decreases continuously in the raffinate R2_i.

The results indicate that the “double extraction” carried out according to the scheme given in Fig. 1 enables the extraction of iron(III) in the presence of zinc(II) which accumulates in the aqueous phase (Fig. 6). Unfortunately, too many stages are needed.

Stripping both of zinc(II) and iron(III) can be effectively accomplished with water which, however, is not selective, i.e., both Fe(III) and Zn(II) are stripped. Prior stripping, the organic phase can be washed with small amounts of water (Table 2). For

w/o = 1:5 near 30% of zinc(II) is scrubbed from loaded TBP with water and almost 40% with Fe(III) solution. Fe(III) solution is used to increase crowd effect and to cause higher zinc(II) transfer to the aqueous phase. However, no visible impact is observed.

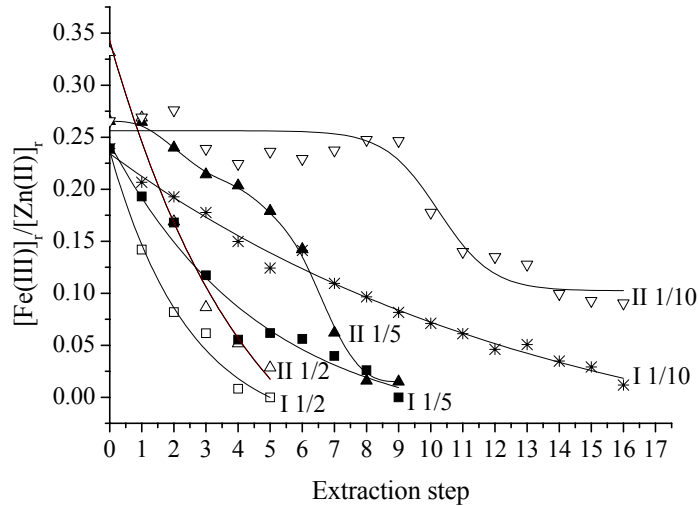


Fig. 6. Ratio of Fe(III) and Zn(II) concentrations in raffinate R_{1i} (□, ■, *) and R_{2i} (△, ▲, ▽) after each extraction step at o/w = 1:2 (□, △); 1:5 (■, ▲) and 1:10 (*, ▽).

Table 2. Zinc(II) and iron(III) scrubbing from two times loaded 80% TBP (E_{2i}) (Sc stands for scrubbing, o₁ and o₂ denote organic phase before and after scrubbing, respectively)

Scrubbing phase	w/o	[Zn(II)] _{o1} g/L	[Fe(III)] _{o1} g/L	Sc _{Zn(II)} %	Sc _{Fe(III)} %	[Zn(II)] _{o2} g/L	[Fe(III)] _{o2} g/L
water	1:5	47.2	16.3	27.5	20.4	34.3	13.0
water	1:5	31.7	42.2	28.4	18.0	22.9	34.6
4.5 g/L Fe(III)	5:1	18.3	23.2	100	71.3	0	6.62
4.5 g/L Fe(III)	1:5	19.4	22.1	39.4	15.8	11.7	18.6

Table 3. Zinc(II) and iron(II) extraction for different volume ratios and TBP concentrations (Feed: 100 g/L Zn(II), 30 g/L Fe(II), 2.5 M HCl, 6.5 M Cl⁻)

[TBP] %	o/w before extraction	E _{Zn(II)} %	E _{Fe(II)} %	[Zn(II)] _o g/L	[Fe(II)] _o g/L	o/w after extraction
100	8:1	99.4	15.9	11.9	0.55	20:1
	9:1	99.8	42.1	10.3	1.3	37:1
80	8:1	98.3	12.4	11.7	0.44	16:1
	9:1	99.0	14.9	10.9	0.49	20:1

An excess of scrubbing phase causes high Fe(III) washing out. Unfortunately, in case of small water amounts iron(III) is also scrubbed. Thus, it is impossible to wash out zinc(II) selectively without loss of iron(III). Scrubbing solution is always a mixture of zinc(II) and iron(III) and it must be recycled to the extraction step in continuous process. However, scrubbing is more advantageous than multistage extraction with small volume of TBP.

Results presented in Table 3 show very effective zinc(II) extraction (over 98%) in the presence of iron(II) at high excess of the organic phase. On the other hand, iron(II) is extracted significantly (over 10%). It is probably result of water transfer to the organic phase and iron(II) physical transport. o/w ratio after extraction confirms a dramatic decrease of the aqueous phase volume, especially in case of 100% TBP. Practically such continuous process can be carried out only with recycling of the aqueous phase from the settler to the mixer of the same contactor to keep the phase ratio in reasonable range $o/w = 2:1-1:1$.

Table 4. Zinc(II) and iron(II) scrubbing with water from loaded 80% TBP (Sc stands for scrubbing, o1 and o2 denote organic phase before and after scrubbing, respectively)

w/o	[Zn(II)] _{o1} g/L	[Fe(II)] _{o1} g/L	Sc _{Zn(II)} %	Sc _{Fe(II)} %	[Zn(II)] _{o2} g/L	[Fe(II)] _{o2} g/L
1:5	12.7	0.42	15.3	100	10.7	0
1:5	11.3	0.43	16.1	100	9.4	0
1:10	12.7	0.42	5.1	50.6	12.09	0.21
1:10	11.3	0.43	6.5	78.4	10.56	0.09

Scrubbing of TBP solutions containing zinc(II) and iron(II) enables the removal of iron(II) with some amounts of zinc(II) (Table 4). 100% of iron(II) is washed out from 80% TBP at w/o volume ratio 1:5. Using of higher volume ratio decreases amount of scrubbed iron(II). Again, the solution must be recycled because some amounts of zinc(II) (5-16%) are washed out. The removal of iron(II) by scrubbing with water supports the idea of unspecific iron(II) transfer in the cores of reverse micelles.

CONCLUSIONS

Two technological approaches for the separation are considered: the selective extraction of iron(III) over zinc(II) with TBP deficiency, and zinc(II) selective extraction with an excess of TBP after iron(III) reduction to iron(II). None of the both versions enables selective extraction of iron(III) or zinc(II). The total removal of iron(III) needs several successive extractions with fresh TBP portions. Zinc(II) can be quantitatively recovered using 5-10 volume excess of TBP.

Stripping both of zinc(II) and iron(III) can be effectively accomplished with water but is not selective. Prior stripping, the organic phase can be washed with small amounts of water. Scrubbing of TBP solutions containing iron(III) contaminated with zinc(II) gives always a mixture of zinc(II) and iron(III) which must be recycled to the

extraction step in continuous process. Scrubbing of TBP solutions containing zinc(II) and iron(II) enables the removal of iron(II) with some amounts of zinc(II) (5-16%). Again, the solution must be recycled. The removal of iron(II) by scrubbing with water supports the idea of unspecific iron(II) transfer in the cores of reverse micelles.

The following technological concept is proposed: reduction of iron(III) to iron(II), extraction of zinc(II) with 5-10 volume excess of TBP, washing of TBP phase contaminated with iron(II) with small volumes of water and recycling of the scrubblings and stripping of zinc with water.

REFERENCES

- ANIELAK A., CIEŚLIK G., (1987), *Analiza Studialna Metod Oczyszczania Ścieków Potrawiennych i Galwanicznych*, Monografia nr 8, Politechnika Częstochowska, Częstochowa.
- BARTKOWSKA M., REGEL-ROSOCKA M., SZYMANOWSKI J., (2002), *Extraction of Zinc(II), Iron(III) and Iron(II) with Binary Mixtures Containing Tributyl Phosphate and Di(2-Ethylhexyl)Phosphoric Acid or Cyanex 302*, Physicochem. Problems Min. Proc., Vol. 36, pp.217-224.
- CIERPISZEWSKI R., MIESIAC I., REGEL-ROSOCKA M., SASTRE A.M., SZYMANOWSKI J., (2002), *Removal of Zinc(II) from Spent Hydrochloric Acid Solutions from Zinc Hot Galvanizing Plants*, Ind. Eng. Chem. Res., Vol. 41, pp. 598-603.
- LO T.C., BAIRD M.H.J., HANSON C., (1991), *Handbook of Solvent Extraction*, Krieger Publishing Company, Malabar, Florida.
- MAASS P., PEISSKER P., (1998), *Cynkowanie Ogniowe*, Agencja Wydawnicza Placet, Warszawa.
- REGEL M., SASTRE A.M., SZYMANOWSKI J., (2001), *Recovery of Zinc(II) from HCl Spent Pickling Solutions by Solvent Extraction*, Envir. Sci. Technol., Vol. 35, pp. 630-635.
- REGEL-ROSOCKA M., MIESIAC I., SASTRE A.M., SZYMANOWSKI J., (2002), *Screening of Reagents for Recovery of Zinc(II) from Hydrochloric Acid Spent Pickling Solutions*, Proc. ISEC'2002, Chris van Rensburg Publ. Ltd., Cape Town, South Africa, Vol. 2, pp. 768-773.
- REGEL-ROSOCKA M., ZAWISTOWSKI P., SASTRE A.M., SZYMANOWSKI J., (2003), *Selection of Extractants for Dispersive Extraction of Zinc(II) from Hydrochloric Acid Solutions*, Pol. J. Appl. Chem., Vol. 47, pp. 83-94.

ACKNOWLEDGEMENT

The work was supported by DS grant 32/044/2004.

Rozenblat M., Regel-Rosocka M., Szymanowski J., *Usuwanie metali z roztworów potrawiennych o wysokim stężeniu cynku*, Physicochemical Problems of Mineral Processing, 38, (2004) 121-129 (w jęz. ang.).

Badano ekstrakcję cynku(II), żelaza(II) i żelaza(III) za pomocą fosforanu tributylu (TBP) z roztworów potrawiennych kwasu solnego o wysokim stężeniu cynku. Rozpatrzono dwa podejścia technologiczne. Pierwsze: selektywną ekstrakcję żelaza(III) (żelazo(II) utleniono do żelaza(III)) wobec cynku(II) niedomiarem TBP. Drugie: redukcję żelaza(III) do żelaza(II), a następnie selektywną ekstrakcję cynku(II) nadmiarem TBP. W celu całkowitego usunięcia żelaza(III) należy zastosować kilka do kilkunastu stopni ekstrakcji świeżym TBP. Reekstrakcję zarówno cynku(II), jak i żelaza(III) za pomocą wody można przeprowadzić wydajnie, ale nie jest ona selektywna. Przed reekstrakcją należy przemyć fazę organiczną niedomiarem wody. Odmycie z TBP naładowanego cynkiem(II) i żelazem(II) pozwala na całkowite usunięcie żelaza(II) i pewnych ilości cynku(II). Odmywanie jest korzystniejsze niż wielostopniowa ekstrakcja niedomiarem TBP. Zaproponowano następującą koncepcję technologiczną: redukcję żelaza(III) do żelaza(II), ekstrakcję cynku(II) nadmiarem objętościowym TBP 5-10, odmycie TBP zanieczyszczonego żelazem(II) małą ilością wody i zawrócenie roztworu wodnego po odmyciu, reekstrakcję cynku(II) wodą.

Małgorzata ULEWICZ*, Cezary Kozłowski**, Władysław WALKOWIAK***

REMOVAL OF Zn(II), Cd(II) AND Cu(II) IONS BY POLYMER INCLUSION MEMBRANE WITH SIDE-ARMED DIPHOSHAZA-16-CROWN-6 ETHERS

Received March 15, 2004; reviewed; accepted May 27, 2004

Competitive transport of Zn(II), Cd(II), and Cu(II) ions from aqueous chloride source phase ($c_{Me} = 0.01$ M) through polymer inclusion membranes (PIMs) containing cellulose triacetate (support), *o*-nitrophenyl pentyl ether (plasticizer) and side-armed lariat ether-type derivative of diphosphaza-16-crown-6 (ion carrier) has been investigated. The influence of the group attached type to the PNP-lariat ether molecule on the selectivity and efficiency of Zn(II), Cd(II), and Cu(II) transport through polymer inclusion membranes is studied. The removal of metal ions by transport through PIM's from acid aqueous phase into 0.1 M CH_3COONH_4 , NH_4OH or EDTA aqueous solution (receiving phase) is presented. The selectivity coefficient of Cd/Zn and Cd/Cu decreases with Cl⁻ concentration increase in source phase for transport with bis-lariat ether, whereas for mono-lariat ether the selectivity coefficients are not changed.

Key words: polymer inclusion membrane, zinc(II), cadmium(II), copper(II), PNP-crown ethers

INTRODUCTION

Recently a remarkable increase in the applications of liquid membranes for separation processes was found. The use of liquid membranes containing ion carriers is an alternative to solvent extraction for selective separation and concentration of metal ions from source aqueous phase, in which the concentration of metal ionic species is $> 1 \cdot 10^{-4}$ M (Bartsch and Way 1996). A new type of membrane system, called polymer inclusion membrane (PIM), has been developed which provides metal

*Department of Chemistry, Czestochowa University of Technology, 42-200 Czestochowa, Armii Krajowej 19 Street, e-mail: ulewicz@mim.pcz.czyst.pl.

**Institute of Chemistry and Environment Protection, Pedagogical University of Czestochowa, 42-200 Czestochowa, Armii Krajowej 13.

***Institute of Inorganic Chemistry and Metallurgy of Rare Elements, Wrocław University of Technology, 50-370 Wrocław, Wybrzeże Wyspiańskiego 27.

ion transport with high selectivity, as well as easy setup and operation (Bond et al., 1999).

Crown ethers as ion carriers were successfully used for metal ions separation in solvent extraction, transport through liquid membranes and ion exchange systems. A few papers deal with the selective removal of Zn(II) and Cd(II) ions with neutral crown ethers. Katsuta et al. (Katsuta et al., 2000) has studied the extraction of Zn^{2+} and Cd^{2+} cations with benzo-18-crown-6 (B18C6) into benzene organic phase in the presence of picric acid. Compared with Cd^{2+} , B18C6 extracts Zn^{2+} more effectively although the size of Zn^{2+} cation is less suited for the cavity of crown ether. Billah and Hohjo (Billah and Hohjo, 1997) extracted the mixture of cadmium(II) and zinc(II) from aqueous solutions as their thenyltrifluoroacetone (TTA) complexes with dibenzo-18-crown-6 (DB18C6) into *o*-dichlorobenzene. At pH 4.9 only Zn(II) was extracted quantitatively, whereas Cd(II) remained in the aqueous solution.

A reverse selectivity in Zn^{2+} and Cd^{2+} separation was obtained in transport across liquid membranes containing 18-membered crown ethers. In competitive transport of Zn(II) and Cd(II) through emulsion liquid membrane containing dicyclohexane-18-crown-6, near quantitative selectivity for Cd(II) over Zn(II) and Hg(II) has been achieved (Izatt et al., 1987). This can be explained by the preferential transport of neutral cation-anion moieties of CdA_2 from Zn^{2+} and HgA_2^{2-} , where A = SCN^- , I^- , Br^- or Cl^- (Izatt et al., 1986). Cho et al. (Cho et al., 1988, 1991, 1995) found out that a single transport of Cd^{2+} across emulsion liquid membranes by diazo-18-crown-6 (DA18C6) from 0.4 M SCN^- aqueous solutions is much more effective in comparison with Zn^{2+} . On the other hand, Dadfarnia and Shamsipur (Dadfarnia and Shamsipur 1992) discovered quantitatively transport of zinc(II) and only 1 % of cadmium(II) across bulk liquid membrane by DA18C6 and hexadecanoic.

We now present results for competitive transport of zinc(II), cadmium(II), and copper(II) ions from dilute aqueous solutions by side-armed PNP 16-crown-6 derivatives. PNP-lariat ether were used for separation of zinc(II) and cadmium(II) ions by ion flotation (Ulewicz et al., 2003). We have shown that the selectivity of cadmium(II) and zinc(II) separation with use of the PNP-lariat ethers depends upon pH of aqueous solution and the nature of the substituents at the N_3P_3 ring, playing part of the side arms. Present work deals with the separation of zinc(II), cadmium(II) and copper(II) metal ionic species ($c_{Me} = 0.01M$) from chloric aqueous solutions containing equimolar mixture of these metals by polymer inclusion membranes. Effects of structural modification of crown ethers upon the efficiency and selectivity of ions transport is now reported.

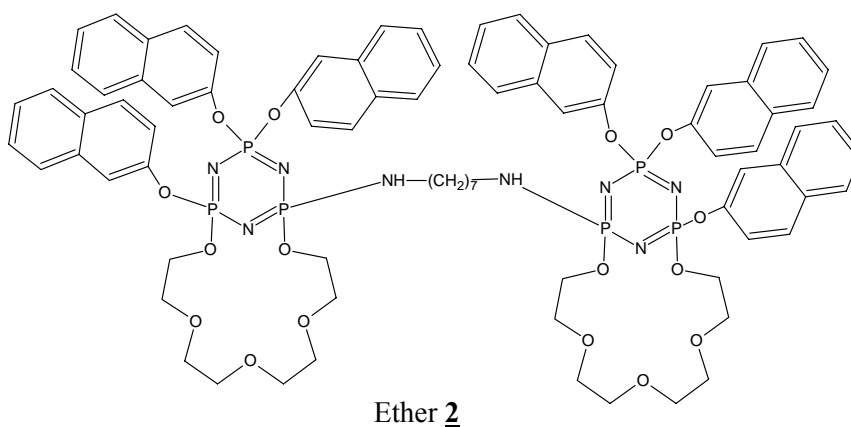
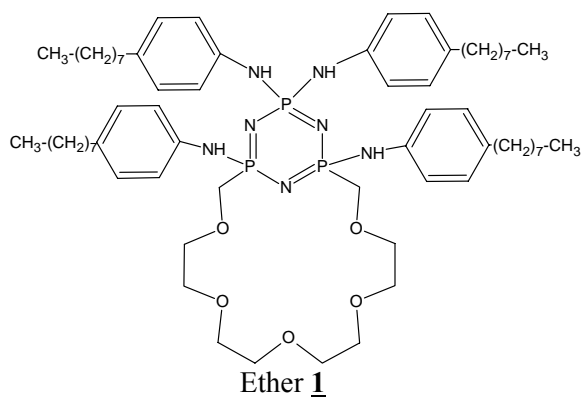
EXPERIMENTAL

POLYMER INCLUSION MEMBRANE PREPARATION

A solution of cellulose triacetate as the support, *o*-nitrophenyl pentyl ether as the plasticizer, and crown ethers **1** and **2** as the ion carriers in dichloromethane as the organic solution was prepared. A specified portion of this organic solution was poured

into a membrane mold comprised of a 9.0 cm glass ring attached to a plate glass with cellulose triacetate - dichloromethane glue. The dichloromethane was allowed to evaporate overnight and the resulting membrane was separated from the glass plate by immersion in cold water. Next, the membrane was soaked in 0.1 M aqueous solution of hydrochloric acid for 12 hours. Two samples of membrane were cut from the same membrane for duplicate transport experiments. The membrane contained 2.6 cm³ ONPPE / 1g CTA, and 0.1M crown ether based on plasticizer.

The inorganic chemicals, i.e. zinc(II), cadmium(II), copper(II) chlorides and hydrochloric acid were of analytical grade and were purchased from POCh (Gliwice, Poland). The organic reagents, i.e. cellulose triacetate (CTA), *o*-nitrophenyl pentyl ether (ONPPE) and dichloromethane were also of analytical grade and were purchased from Fluka and used without further purification. The density of plasticizer, i.e. *o*-nitrophenyl pentyl ether was 1.085 g/cm³. The aqueous solutions were prepared with double distillation water, which conductivity was 0.1 μS/m. Crown ethers **1** and **2** were synthesized in Institute of Polymer Chemistry, Polish Academy of Sciences, Zabrze (Poland).



TRANSPORT STUDIES

Transport experiments were conducted in a permeation cell in which the membrane film (at surface area of 4.9 cm²) was tightly clamped between two cell compartments. Both, i.e. the source and receiving aqueous phases (45 cm³ each) were mechanically stirred at 600 rpm. The receiving phase was 0.1 - 0.5 M aqueous solution of ammonium acetate, EDTA or ammonium hydroxide. The PIM transport experiments were carried out at the temperature of 20 ± 0.2 °C. Small samples (0.1 cm³ each) of the aqueous receiving phase were removed periodically via a sampling port with a syringe and analyzed to determine zinc and cadmium concentrations by atomic absorption spectroscopy method (AAS Spectrometer, Solaar 939, Unicam). The source phase acidity was controlled by pH meter (pH meter, CX-731 Elmetron, with combine pH electrode, ERH-136, Hydromet, Poland) and pH was kept constant by adding periodically small amounts of 1.0 M HCl aqueous solution.

The kinetics of PIM transport can be described by a first-order reaction in metal ion concentration:

$$\ln\left(\frac{c}{c_i}\right) = -kt \quad (1)$$

where c is the metal ions concentration (M) in the source aqueous phase at some given time, c_i is the initial metal ions concentration in the source phase, k is the rate constant (s⁻¹), and t is the time of transport (s).

To calculate the k value, a plot of $\ln(c/c_i)$ versus time was prepared. The rate constant value for the duplicate transport experiment was averaged and standard deviation was calculated. The relationship of $\ln(c/c_i)$ vs. time was linear, which was confirmed by high values of determination coefficient (r^2), i.e., from 0.9974 to 0.9912.

The initial flux (J_i) was determined as equal to:

$$J_i = -\frac{V}{A}k \cdot c_i \quad (2)$$

where V is volume of the aqueous source phase, and A is an effective area of membrane.

To describe the efficiency of metal removal from the source phase, the recovery factor (RF) was calculated:

$$RF = \frac{c_i - c}{c_i} \cdot 100\% \quad (3)$$

The selectivity coefficient, S was defined as the ratio of initial fluxes for $M1$ and $M2$ metal ions, respectively:

$$S = J_{i,M1} / J_{i,M2} \quad (4)$$

RESULTS AND DISCUSSION

Previously it was found that competitive transport of zinc(II) and cadmium(II) ions through PIM with tri-*n*-octyl amine (TOA) as the anionic carrier (Kozłowski et al., 2000), allows to remove both metals from acidic chloride aqueous solutions. Now we applied lariat ethers with cyclophosphazene subunits for zinc(II), cadmium(II), and copper(II) removal from chloride aqueous solutions. The mono- and bis-lariat ethers (**1**, **2**) were synthesized for the purpose of this study with diphosphaza-16-crown-6 rings and different sets of substituents.

The kinetic parameters and selectivity orders of metal ions transport through PIM from aqueous source phase containing equimolar mixture of all metal ions are shown in Table 1. The initial fluxes of all investigated cations increase with acidity of the feed phase increase. The selectivity order was as follows: Cd(II) \geq Zn(II) $>$ Cu(II). The selectivity coefficients of Cd/Cu and Zn/Cu for PIM decreases with HCl concentration increase in source phase. The highest values of $S_{Cd(II)/Cu(II)}$ and $S_{Zn(II)/Cu(II)}$ was observed for lariat ethers **2** – the selectivity coefficients of Cd(II)/Cu(II) were 8.7, 6.6 and 5.4 for 0.1, 0.3 and 0.5M HCl, respectively.

Table 1. The values of initial fluxes, selectivity coefficients and selectivity orders for competitive transport of Zn(II), Cd(II), and Cu(II) through PIM

Source phase: solution of Cd(II), Zn(II), Cu(II) at concentration 0.01M in 0.1÷0.5 M HCl;

Receiving phase: 0.1 M CH₃COONH₄; Membrane: 2.6 cm³ ONPPE / 1g CTA, 0.1 M crown ether

Crown ether	[HCl], M	Cation	Initial flux, (μmol/m ² s)	Selectivity orders and selectivity coefficient of Cd to other metals
1	0.1	Cd(II)	3.52	Cd \geq Zn , Cu 1.8
		Zn(II)	1.97	
		Cu(II)	1.92	
	0.3	Cd(II)	5.75	Cd \geq Zn \geq Cu 1.1 1.9
		Zn(II)	5.25	
		Cu(II)	3.04	
	0.5	Cd(II)	48.1	Cd \geq Zn \geq Cu 1.8 1.9
		Zn(II)	26.9	
		Cu(II)	24.3	
2	0.1	Cd(II)	17.4	Cd \geq Zn $>$ Cu 1.2 8.7
		Zn(II)	14.1	
		Cu(II)	2.01	
	0.3	Cd(II)	39.5	Cd \geq Zn $>$ Cu 1.0 6.6
		Zn(II)	38.1	
		Cu(II)	6.02	
	0.5	Cd(II)	76.7	Cd \geq Zn $>$ Cu 5.4
		Zn(II)	73.8	
		Cu(II)	14.3	

The results of metal ions removal, i.e. zinc(II), cadmium(II), and copper(II) from aqueous solutions containing equimolar mixture of metals ($c_{Me} = 0.01M$) with lariat ethers **1** and **2**, are shown in Fig.1. As it comes from Fig.1a using mono lariat ethers **1** all metal ions are removed from aqueous solutions in the comparable percent. Removal of metal ions increased with the increase of acidic solutions. Using bis-lariat ether **2** Cd(II) and Zn(II) ions are removed better than Cu(II) from 0.1 and 0.3M HCl solutions, but from 0.5M HCl solutions cadmium, zinc and copper ions are removed comparable. In the presence of chlorides at concentration $> 0.3 M$ all metals studied are in the form of chloride complex anions (Stability constants, 1982), which are attached to donor nitrogen atoms of ether **2**. As the effect of ion pairs formation zinc(II), cadmium(II) and copper(II) are transported across polymer inclusion membranes with **2** (Fig.1b). The recovery factor of all investigated metals with ether **2** was higher than for ether **1**. This suggests that formed ion pair between metal ion and ligand is determined by number of nitrogen atoms in the ring and sidearm of ligand (Bartsch et al., 2002).

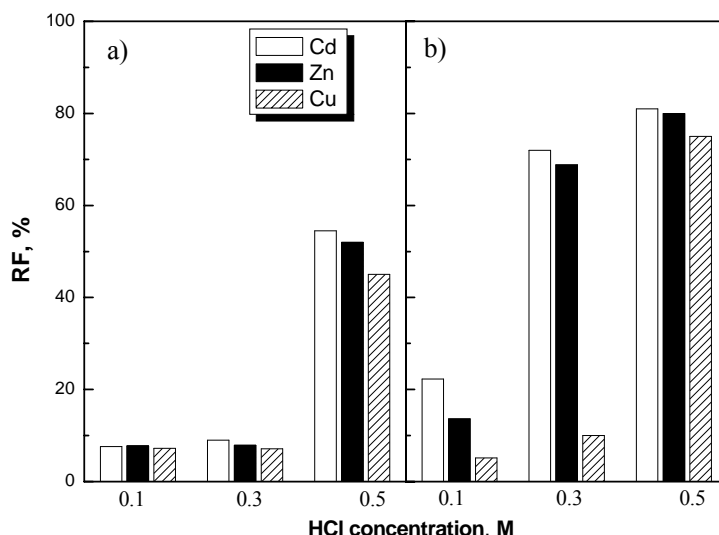


Fig. 1. Recovery factor (%) after 8 hours of transport for Zn(II), Cd(II), and Cu(II) ions from chloride aqueous solutions through polymer inclusion membrane with **1** (a) and **2** (b).

Source phase: solution of Cd(II), Zn(II), Cu(II) at concentration 0.01M in 0.1–0.5 M HCl; Receiving phase: 0.1 M CH_3COONH_4 ; Membrane: 2.6 cm³ ONPPE / 1g CTA, 0.1 M crown ether

Type of receiving aqueous phase also influences on the process transport of metal ions through PIM's. The maximal percent metal removal from chloride aqueous solutions into different receiving phases is shown in Fig.2. As it comes from this figure removal of metal ions increased in the sequence: $CH_3COONH_4 > EDTA > NH_4OH$.

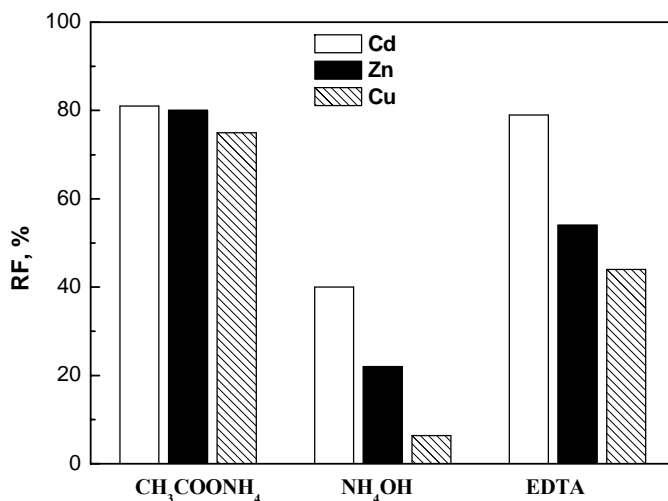


Fig. 2. Recovery factor (%) after 8 hours of transport through PIM with **2** of Zn(II), Cd(II), and Cu(II) ions from chloride aqueous solutions; Source phase: Cd(II), Zn(II), Cu(II) at concentration 0.01M in 0.5 M HCl; receiving phase: 0.1 M solution of CH₃COONH₄, NH₄OH or EDTA

CONCLUSION

Zinc(II), cadmium(II), and copper(II) ions can be effectively removed from aqueous chloride solutions in hydrometallurgical processes of polymer inclusion membranes. Competitive transport of zinc(II), cadmium(II) and copper(II) ($c_{Me} = 0.01$ M) from an aqueous chloride source phase through polymer inclusion membranes containing derivatives of PNP-crown ethers as ion carriers into aqueous ammonium acetate solutions allows removal of zinc(II), cadmium(II) and copper(II). The selectivity coefficients of Cd/Cu and Zn/Cu for PIM decreases with HCl concentration increase in source phase.

ACKNOWLEDGMENT

The authors would like to thank the Polish Science Foundation for financial support of this research (grant 4 T09B 107 22). We would also like to thank dr Iwona Porwolik-Czomperlik from Institute of Polymer Chemistry, Polish Academy of Sciences, Zabrze for synthesis of PNP-crown ethers.

REFERENCES

- BARTSCH R. A., WAY J., Eds. (1996), *Chemical Separation with Liquid Membranes*, ACS Symposium Series 642, Amer. Chem. Soc., Washington, DC
 BOND H., DIETZ M. L., ROGERS R.D., Eds. (1999), *ASC Symposium Series 716*, Washington, DC.
 KATSUTA S., TSUCHIYA F., TAKEDA Y. (2000), *Equilibrium studies on complexation in water and solvent extraction of zinc(II) and cadmium(II) with benzo-18-crown-6*, *Talanta*, 51, 637 - 644.

- BILLAH M., HONJO T. (1997), *Separation and determination of cadmium and zinc as their thenoyltrifluoroacetone complexes with dibenzo-18-crown-6 by means of synergistic extraction and atomic absorption spectrometry*, J. Fresenius, Anal. Chem., 357, 61 - 64.
- IZATT R. M., BONALD R. L., GENG W., CHO M. H., CHRISTENSEN J. J. (1987), *Separation of bivalent cadmium, mercury and zinc in a natural macrocyclic-mediated emulsion liquid membrane*, Anal. Chem., 59, 2405 - 2409.
- IZATT R. M., LINDCH G. C., BRUENING R. L., BRADSHAW J. S., LAMM J. D., CHRISTENSEN J. J. (1986), *Design of cation selectivity into liquid membrane systems using macrocyclic carriers*, Pure Appl. Chem., 58, 1453 - 1460.
- CHO M. H., SEON-WOO K. H., HEO M. Y., LEE I. C., YOON C. J., KIM S. J. (1988), *Studies on the macrocycles mediated transport in bulk liquid membrane system of transport metal ions*, Bull. Korean Chem. Soc., 9, 292 - 295.
- CHO M. H., CHUN H. S., KIM J. H., RHEE Ch. H., KIM S. J. (1991), *Study on separation of heavy metal ions in a natural macrocycle-mediated emulsion liquid membrane system*, Bull. Korean Chem. Soc., 12, 474 - 477.
- CHO M. H., SHIN S. Ch. (1995), *Studies on the macrocycle-mediated transport of divalent metals ions in a supported liquid membrane system*, Bull. Korean Chem. Soc., 16, 33 - 36.
- DADFARNIA S., SHAMSIPUR M. (1992), *Highly selective membrane transport of zinc(2+) ion by a cooperative carrier composed of 1,10-diaza-18-crown-6 and palmitic acid*, Bull. Chem. Soc. Jpn., 65, 2779 - 2783.
- ULEWICZ M., WALKOWIAK W., BRANDT K., PORWOLIK-CZOMBERLIK I. (2003), *Ion flotation of zinc(II) and cadmium(II) in the presence of side-armed diphosphaza-16-crown-6-ethers*, Sep. Sci. Technol., 38, 633 - 645.
- KOZŁOWSKI C., ULEWICZ M., WALKOWIAK W. (2000), *Separation of zinc and cadmium ions from aqueous chloride solutions by ion flotation and liquid membranes*, Physicochemical Problems of Mineral Processing, 34, 141-151.
- BARTSCH R. A., LEE E. K., CHUN S., ELKARIM N., BRANDT K., PORWOLIK-CZOMPERLIK I., SIWY D., LACH D., SILBERRING J. (2002), *Structure –alcalimetal cation complexation relationships for macrocyclic PNP-lariat ether ligands*, J. Chem. Soc., Perkin Trans, 2, 442 - 448.
- STABILITY CONSTANTS OF METAL-ION COMPLEX; Part A: Inorganic Ligands, Pergamon Press, New York, 1982.

Ulewicz M., Kozłowski C., Walkowiak W., *Wydzielanie jonów Zn(II), Cd(II) i Cu(II) przez polimerowe membrany inkluzyjne przy użyciu pochodnych PNP-dipozphaza-16-korony-6*, Physicochemical Problems of Mineral Processing, 38, (2004) 131-138 (w jęz. ang.).

Zbadano selektywność procesu wydzielania jonów cynku(II), kadmu(II) i miedzi(II) z wodnych roztworów chlorkowych zawierających równomolową mieszaninę tych trzech metali ($c_{Me}=1,0 \cdot 10^{-2}$ M) w procesie transportu przez polimerowe membrany inkluzyjne (PIM) przy użyciu w roli przenośników jonów eterów PNP-difosfazakoronowych. Membrany typu PIM zbudowano z trójocianu celulozy (nośnik), eteru *o*-nitrofenylopentylowego (pastyfikator) i eteru koronowego (przenośnik jonów); stężenie eteru w przeliczeniu na plastyfikator wynosiło 0,1 M. Współczynniki separacji Cd/Cu i Zn/Cu przez PIM przy użyciu mono-lariat eteru były porównywalne, podczas gdy przy użyciu bis-lariat eteru malały wraz ze wzrostem stężenia jonów Cl⁻ w fazie zasilającej. Współczynniki separacji Cd/Cu wynosiły odpowiednio 8,7; 6,6 i 5,4 dla roztworu 0.1; 0.3 i 0.5 M HCl, natomiast współczynniki separacji Zn/Cu dla tych roztworów wynosiły odpowiednio 7.0; 6.3 i 1.2. Tak więc współczynniki separacji jonów kadmu do miedzi były wyższe niż jonów cynku do miedzi. Separacja jonów Cd/Zn nie zachodzi. W pracy przedstawiono ponadto wyniki transportu badanych jonów przy zastosowaniu różnych faz odbierających, tj., roztworu octanu amonu, wodorotlenku amonu i EDTA. Najwyższy procent wydzielania jonów badanych metali uzyskano przy zastosowaniu CH₃COONH₄ (RF ≈ 80 %).

Paweł MACIEJEWSKI*, Władysław WALKOWIAK**

SELECTIVE REMOVAL OF CESIUM(I), STRONTIUM(II) and BARIUM(II) CATIONS WITH PROTON-IONIZABLE LARIAT ETHERS IN THE ION FLOTATION PROCESS

Received March 15, 2004; reviewed; accepted May 27, 2004

An experimental investigation is presented on competitive flotation of cesium(I), strontium(II) and barium(II) cations from dilute aqueous solutions with proton-ionizable lariat ethers in the presence of foaming agent. The influence of aqueous solution pH on the flotation rate and efficiency with lariat ethers possessing DB-16-C-5 cavity and four different acidic groups, i.e. sulfonamide (**1**), sulfonic (**2**), carboxylic (**3**), and phosphonic (**4**) was studied. It was found that, the ion flotation of Cs(I), Sr(II) and Ba(II) cations with dibenzo-16-crown-5 derivative **1** from dilute aqueous solutions was fast and selective, which might have a practical meaning for the decontamination of industrial (toxic, radioactive) aqueous solutions.

Key words: ion flotation, cesium(I), strontium(II), barium(II), proton-ionizable crown ether

INTRODUCTION

The ion flotation process is a simple and an effective method for removal and separation of metals ions from dilute aqueous solutions ($c < 1.0 \cdot 10^{-4}$ M). In this process, an ionic surface active compound (collector) is introduced to the aqueous solution to transport non-surface active colligend of the opposite charge from a bulk aqueous solution to the interface of solution and vapour. Counter ions must be co-adsorbed to neutralize the charge. If a sufficiently large aqueous solution / gas interface is provided by sparging gas through the solution, the colligend ions can be concentrated and removed along with the collector in a foam phase. The rate and efficiency of the ion flotation process separation is a function of many factors but the most important is the composition of aqueous solutions from which ions are to be floated

* Tadeusz Kościuszko Military Academy, 54-150 Wrocław, Czajkowskiego 107 Street, Poland

** Institute of Inorganic Chemistry and Metallurgy of Rare Elements, Wrocław University of Technology, 50-370 Wrocław, Wybrzeże Wyspiańskiego 27, e-mail: walkowiak@ichn.ch.pwr.wroc.pl

[Sebba, 1959; Grieves, 1975; Lemlich, 1972; Golman, 1982; Walkowiak, 1992; Zouboulis and Matis, 1987; Matis, 1987; Okamoto and Chou, 1997].

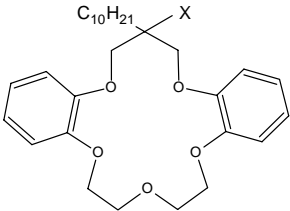
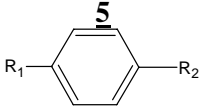
Selectivity of a process is not so high, when the ions of the same charge are being removed. This is reason why inclusion compounds having a cage, such as crown ethers, calixarenes or cryptands, and their derivatives have been investigated in recent years for many systems of metal ions selective removal. Since discovery in 1967 by Pedersen (1967) the first crown ether, i.e. dibenzo-18-crown-6, the macrocyclic compounds hold great interest and potential and were successfully applied for many metal ions separations in solvent extraction, transport across liquid membranes, and ion-exchange systems [Bond et al., 1999; Bartsh and Way, 1996]. Macrocycles, which exhibit metal ion molecular recognition, can be also regarded as being a novel inclusion-type surfactants (collectors) if they have sufficient solubility in water and can adsorb quantitatively onto aqueous - air interfaces. The recent advances of the crown ethers chemistry have been reviewed [Ludwig, 2000]. The general area covering the binding of all types of macrocycles in molecular cavities often is referred as host-guest chemistry. Structural modifications lead to macrocycle compounds with improved selectivity and efficiency in metal ions separation [Walkowiak et al., 1990; Talanowa et al., 1999, Deng et al., 1995]. There are only few papers which deals with application of macrocycles in the ion flotation process. Koide et al. (1996) used phosphate ethers of C-undecylcalix[4]resorcinarenes for uranium flotation from seawater and calix[4]arenes derivatives for alkali metal cations flotation [Koide et al., 1993]. Schulz and Warr (1998) applied cryptand 222, and 18-crown-6 together with anionic surfactant, i.e. bis(2,2')-ethylhexylsulfosuccinate (AOT) for alkali metal cations separation. Another approach to application of macrocycles for flotation of metal cations was done by Charewicz et al. (2001). They used as macrocycles proton-ionizable lariat ethers with sulphonic, phosphate and carboxylic acid groups for flotation of Sr^{2+} and Cs^+ cations. Ulewicz and Walkowiak (2003) used proton-ionizable lariat ethers with foaming agent for flotation of Zn(II) and Cd(II) ions from aqueous solutions.

We now present results for the selective removal of cesium(I), strontium(II) and barium(II) cations with proton-ionizable lariat ethers in the ion flotation process from dilute aqueous solutions in the presence of nonionic foaming agent. We have shown that the selectivity of cations flotation is a function of pH of aqueous solution and kind of acidic group attached to the dibenzo-16-crown-5 cavity.

EXPERIMENTAL

The flotation experiments were carried out in a glass column 45.7 cm in high and 2.4 cm in diameter. The argon gas was saturated with water, and the flow rate was maintained at 12 cm³/min. through a sintered glass sparger of 20-30 μm nominal porosity. The initial volume of each feed solution was 100 cm³. Concentrations of Cs(I), Sr(II) and Ba(II) in aqueous solutions were 1.0 · 10⁻⁵ M. All aqueous solutions were prepared using double distilled water of conductivity 10 μS at 20 °C. As the

lariat ethers were used four dibenzo-16-crown-5 derivatives with following acidic groups: sulfonamide (with terminal $-\text{CF}_3$ group) (**1**), sulfonic (**2**) carboxylic (**3**) and phosphonic (**4**).

	X	<i>Ether no.</i>	<i>nonionic foaming agent</i>  $R_1 = -\text{C}_8\text{H}_{17}$ $R_2 = -\text{O}(\text{CH}_2\text{CH}_2\text{O})_{10}\text{H}$
	$-\text{OCH}_2\text{CONHSO}_2\text{CF}_3$	1	
	$-\text{O}(\text{CH}_2)_3\text{SO}_3\text{Na}$	2	
	$-\text{OCH}_2\text{COOH}$	3	
	$-\text{OCH}_2\text{PO}(\text{OH})(\text{OC}_2\text{H}_5)$	4	

The metal cations concentration in the bulk solution (c) versus time was recorded continuously during ion flotation experiments by means of radioactive analytical tracer and gamma radiation spectrometry following a procedure described previously by Charewicz and Niemiec in 1969 and modified by Walkowiak and Ulewicz (2003). A single channel, gamma radiation spectrometer was used as the detector of radiation intensity of specific energy. In the present work the gamma radioactive isotopes, i.e., Cs-137, Sr-85, Ba-133, were used. They were of sufficiently high specific activity to neglect the effect of carrier concentration. The isotopes were purchased from the Atomic Energy Institute (Świerk, Poland). Proton-ionizable lariat ethers (**1-4**) were synthesized by Richard Bartsch research group from Texas Tech University. Octylphenyl decyl (ethylene glycol) ether (**5** -Triton X-100), a nonionic foaming agent was obtained from Merck (USA). Analytical grade CsNO_3 , $\text{Sr}(\text{NO}_3)_2$, $\text{Ba}(\text{NO}_3)_2$, all from POCH (Poland), were used to prepare the initial solutions of desired composition for each flotation experiment.

The kinetic rate constant of flotation was calculated from the general equation [Rubin, 1968; Rubin et. al., 1966]:

$$\frac{dc}{dt} = -\frac{c_i}{c_i - c_r} k(c - c_r)^n \quad (1)$$

where c_i – stands for the initial ion concentration, c_r – denotes the metal ion concentration in the residual solution and n – order of flotation.

The equation (1) after integration leads for $n = 1$ to the expression,:

$$k = -\frac{c_i - c_r}{c_i t} \ln \frac{c - c_r}{c_i - c_r} \quad (2)$$

The maximal percent removal (W) was described by the equation:

$$W = \left(1 - \frac{c_r}{c_i}\right) \cdot 100\% \quad (3)$$

RESULTS AND THEIR DISCUSSION

The preliminary experiments revealed that lariat ethers **1** and **3** exhibited insufficient foaming ability, so that they had to be used together with a foaming agent **5**. On the other hand, crown ethers with sulfonic (**2**) and phosphonic acidic groups (**4**) behaved like a regular ion flotation collector and they had a sufficient foaming ability. The flotation of studied cations without lariat ethers but in the presence of nonionic foaming agent only does not occur. The preliminary flotations of Cs(I), Sr(II) and Ba(II) were performed from dilute aqueous solutions containing single metal cations with crown ethers **1-4** in the presence of foaming agent as a function of aqueous solution pH. The percent removal versus pH for Sr²⁺ cations is shown in fig. 1. The maximal removal of metals depends upon pH of aqueous solution, for crown ether carboxylic derivative (**3**) especially. The percent removal for the others ethers were high and they increased with pH increase up to 7.0 and then remain constant.

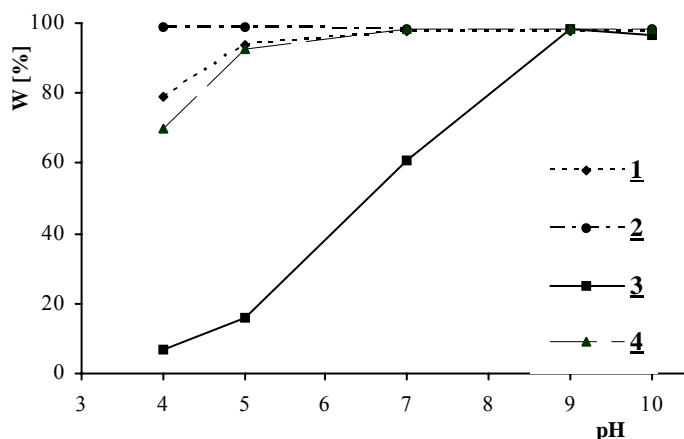


Fig. 1. The maximal percent removal of Sr(II) with crown ethers **1-4** at initial concentration of metal = $1.0 \cdot 10^{-5}$ M, [Lariat ether] = $5.0 \cdot 10^{-5}$ M, [Triton X-100] = $2 \cdot 10^{-5}$ M

The rate constant values (k) for first-order kinetics equation (2) and maximal percent removal for competitive ion flotation of Cs(I), Sr(II) and Ba(II) cations from dilute aqueous solutions with crown ethers **1 - 4** in the presence of foaming agent (Triton X-100) are presented in Tab.1. For all crown ethers with cavity size of 16-crown-5 removal of floated ions is quit high, however a selectivity of process using ethers **2-4** is low. The comparison of studied lariat ethers possessing the same

cavity size (DB-16-C-5) and lipophilic part (-C₁₀H₂₁) indicates that attachment to sulfonamide (trifluoromethyl -CF₃) increases the selectivity of ion flotation process with selectivity order: Sr²⁺ < Cs⁺ < Ba²⁺ (Tab. 1). As can be seen from this table also the kinetic rate constant for barium(II) are higher than for others cations. The high values of determination coefficient indicate that the ion flotation process runs according to first order kinetics as was previously suggested by Rubin et. al. [Rubin, 1968; Rubin et. al., 1966]. Flotation kinetic curves of Cs(I), Sr(II) and Ba(II) for competitive ion flotation of those metals from aqueous solutions with crown ethers derivative **1** in the presence of foaming agent are shown in Fig. 2. As can be seen from these curves flotation of Cs⁺ Sr²⁺ and Ba²⁺ is fast and after 5-6 min. final removal is reached.

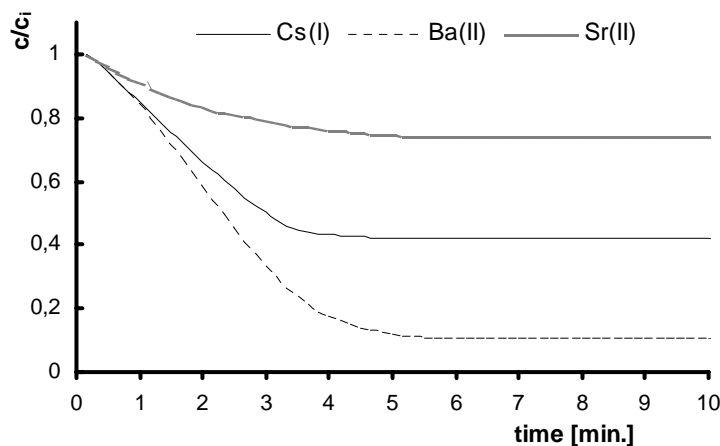


Fig. 2. The kinetic curves of competitive flotation of of Cs(I), Sr(II) and Ba(II) with crown ether **1** at equimolar initial concentration (1.0·10⁻⁵ M) of each metal. [Lariat ether] = 5.0·10⁻⁵ M, [Triton X-100] = 1·10⁻⁵ M, pH = 10,0

It was found that, the ion flotation of Cs(I), Sr(II) and Ba(II) with dibenzo-16-crown-5 derivative **1** from dilute aqueous solutions was fast, selective and efficient process, which might have a practical meaning for the decontamination of industrial (toxic, radioactive) aqueous solutions.

CONCLUSION

Cesium(I), strontium(II) and barium(II) cations can be effectively removed from aqueous solutions in process of ion flotation. The flotations of Cs(I), Sr(II) and Ba(II) from dilute aqueous solutions containing single metal cations with lariat ethers **1** - **4** in the presence of foaming agent indicate that the maximal percent removal of metals depends upon pH of aqueous solution, for crown ether carboxylic derivative (**3**) especially. The percent removal for the other lariat ethers were high and

increased with pH increase up to 7.0. Competitive flotation of Cs(I), Sr(II) and Ba(II) at equimolar initial concentrations ($c_{Me} = 1.0 \cdot 10^{-5} M$) from a dilute aqueous solutions with crown ether **1** allows for selective removal of floated metals, with selectivity order: $Sr^{2+} < Cs^{+} < Ba^{2+}$. Proton-ionizable crown ether derivatives of sufficient surface activity and water solubility could be a new generation of specific collectors for selective flotation of cations, such as Cs^{+} , Sr^{2+} , Ba^{2+} from dilute aqueous solutions.

Table 1. The flotation parameters for Cs(I), Sr(II) and Ba(II) competitive flotation with crown ethers **1** - **4**. Initial concentrations of Cs(I), Sr(II) and Ba(II) = $1.0 \cdot 10^{-5} M$, [Lariat ether] = $5.0 \cdot 10^{-5} M$, [Triton X-100] = $1 \cdot 10^{-5} M$

Ether no.	pH	Cs(I)	Sr(II)	Ba(II)
		k [min ⁻¹] / r ^{2*} / W[%]		
1	10.0	0.0824	0.0306	0.1821
		0.9990	0.9933	0.9992
		58.0	26.1	89.4
2	4.0	0.1495	0.1899	0.2431
		0.9990	0.9990	0.9987
		83.4	91.6	97.1
3	10.0	0.1219	0.1946	0.5661
		0.9991	0.9994	0.9983
		75.0	91.6	100.0
4	4.0	0.0737	0.1087	0.1183
		0.9982	0.9991	0.9986
		56.1	74.5	81.3

*Determination coefficient

ACKNOWLEDGMENT

Financial support of this work was provided by Polish Science Foundation Grants – grant no. 4T09A 176 24.

REFERENCES

- BARTSCH R. A., WAY J. D., (Eds.), 1996, *Chemical Separations with Liquid Membranes*, ACS Symposium Series 642, Washington, DC.
- BOND H., DIETZ M. L., ROGERS R. D., (Eds.), 1999, *Metal-Ion Separation and Preconcentration, Progress and Opportunities*, ACS Symposium Series 716, Washington, DC.
- CHAREWICZ W., GRABOWSKA J., BARTSCH R. A., 2001, *Flotation of Co(II), Sr(II), and Cs(I) cations with proton-ionizable lariat ethers*, Sep. Sci. Technol., 36, 1479.

- CHAREWICZ W., NIEMIEC J., 1969, *Flotation of anions using cationic surfactants, I. Flotation of molybdates*, Nukleonika, 14, 17.
- DENG Y., SACHLEBEN R. A., MOYER B. A., 1995, *Equilibrium and ring size aspects of the extraction of CsNO₃ by Dicyclohexano-21-crown-7, Dibenzocrown-7, and Bis-[tert-alkylbenzo]-21-crown-7*, J. Chem. Soc., Faraday Trans., 91, 4215.
- GOLMAN A. M., 1982, *Ionnaja flotacija*, Nedra, Moskva.
- GRIEVES R. B., 1975, *Foam separation: A review*, Chem. Eng. J., 9, 93.
- KOIDE Y., OKA T., IMAMURA A., SHOENJI H., YAMADA K., 1993, *The selective flotation of cesium ion with resorcinol type calix[4]arenes with alkyl side chains*, Bull. Chem. Soc. Jpn., 66, 2137.
- KOIDE Y., TERASAKI H., SATO S., SHOENJI H., YAMADA K., 1996, *Flotation of uranium from sea water with phosphate ethers of C-undecylcalix[4]resorcinarene*, Bull. Chem. Soc. Jpn., 69, 785.
- LEMLICH R., 1972, *Adsuble methods. In: Recent development in Separation Sciences*, Chem. Rubber Co. Press, Cleveland 1, 113.
- LUDWIG R., 2000, *Foam separation*, Fresenius J. Anal. Chem., 367, 103.
- OKAMATO Y., CHOU E.J., 1997, *Foam separation processes*, Handook of Sep. Tech. Chem. Eng. (3rd Ed), 2, 173.
- PEDERSEN C. J., 1967, *Cyclic polyethers and their complex with metal salts*, J. Am. Chem. Soc., 89, 2495.
- RUBIN A. J., 1968, *Removal of trace metals by foam separation process*, J. Amer. Walter Association, 60, 822.
- RUBIN A. J., JOHNSON J. D., LAMB J. C., 1966, *Ind. Eng. Chem., Process Design Develop.*, 5, 368.
- SCHULZ C., WARR G. G., 1998, *Comparison of variables in ion and precipitate flotation*, Ind. Eng. Chem. Res., 37, 2807.
- SEBBA F., 1959, *Concentration by ion flotation*, Nature, 184, 1062.
- TALANOVA G. G., ELKARIM N. S. A., HANES JR. R. E., HWANG H. S., ROGERS R. D., BARTSCH R. A., 1999, *Extraction selectivities of crown ethers for alkali metal cations: differences between single species and competitive solvent extractions*, Anal. Chem., 71, 672.
- ULEWICZ M., WALKOWIAK W., BRANDT K., PORWOLIK-CZOMPERLIK I., 2003, *Ion flotation of zinc(II) and cadmium(II) in the presence of side-armed diphosphaza-16-crown-6 ethers*, Sep. Sci. Technol., 38, 633.
- ULEWICZ M., WALKOWIAK W., JANG Y., KIM J. S., BARTSCH R.A., 2003, *Ion flotation of cadmium(II) and zinc(II) in the presence of proton-ionizable lariat ethers*, Anal. Chem., 75, 2276.
- WALKOWIAK W., 1992, *In: Innovation in ion flotation technology*, Ed. Marvos P. and Matis K. A., NATO ASI Series, Series E, Kluwer Acad. Publ. London, 455.
- WALKOWIAK W., KANG S. I., STEWART L. E., NDIP G., BARTSCH R. A., 1990, *Effect of structural variations within lipophilic dibenzocrown ether carboxylic acids on the selectivity and efficiency of competitive alkali metal cation solvent extraction into chloroform*, Anal. Chem., 62, 2018.
- ZOUBOULIS A. I., MATIS K. A., 1987, *Ion flotation in environmental technology*, Chemosphere, 16, 623.

Maciejewski P., Walkowiak W., *Selektywne wydzielenie kationów cezu(I), strontu(II) i baru(II) w procesie flotacji jonów z zastosowaniem jonizowalnych eterów lariatowych*, Physicochemical Problems of Mineral Processing, 38, (2004) 139-146 (w jęz. ang.).

Zbadano selektywne wydzielenie jonów cezu(I), strontu(II) i baru(II) z wodnych roztworów zawierających równomolową mieszaninę metali ($c_{Me}=1,0 \cdot 10^{-5}$ M) w procesie flotacji jonowej z użyciem czterech jonizowalnych eterów lariatowych o koronie DB-16-C-5; posiadających decylową grupę lipofilową, różniących się natomiast grupą kwasową, tj. z grupą sulfonoamidową **1** (z rodnikiem CF₃)

sulfonową **2**, karboksylową **3** lub fosfonową **4**. Flotacje prowadzono z zastosowaniem ww. eterów lariatowych o stężeniu $5 \cdot 10^{-5}$ M, w obecności spiniacza niejonowego, tj. Triton X-100, o stężeniu $1 \cdot 10^{-5}$ M, przy pH optymalnym dla danej grupy kwasowej. Badano wpływ pH flotowanego roztworu w zakresie pH od 4,0 do 10,0 stwierdzając, że procent wydzielenia metali wzrasta z wzrostem pH, szczególnie dla pochodnej karboksylowej. Dla pozostałych pochodnych badanych eterów, zależność ta jest słabsza. Wyniki uzyskane dla pochodnej sulfonowej **2** i karboksylowej **3** eterów lariatowych charakteryzują się podobnym, wysokim wydzieleniem dla wszystkich flotowanych jonów, co jest niekorzystne z punktu widzenia selektywności procesu. Dla pochodnej fosfonowej **3** eteru uzyskano nieco gorsze kolektywne wydzielenie. Dopiero zastosowanie pochodnej sulfoamidowej **1** umożliwia selektywne wydzielenie baru(II) a uzyskane procenty wydzielenia wynoszą: bar(II) – 89 %, cez(I) – 58 % i stront(II) – 26 %.

Andrzej HEIM, Tomasz P. OLEJNIK, AGNIESZKA PAWLAK*

THE EFFECT OF THE NUMBER OF CONTACT POINTS BETWEEN GRINDING ELEMENTS ON THE RATE OF GRINDING IN BALL MILLS

Received April 14, 2004; reviewed; accepted June 15, 2004

Results of studies aiming at the determination of the effect of the number of contact points of grinding media on the rate of grinding in ball mills are discussed in the paper. Studies covered batch mills operating in industrial conditions. Wet grinding in a water solution with the addition of anti-emulsifiers was carried out for typical raw materials applicable in industrial production of ceramic tiles. The process of grinding was investigated for three industrial ball mills with different numbers and sizes of corundum grinding media. In the tested mills the rate of grinding of particular size groups was specified. The change of ground material particle size distribution in time was analysed, and the effect of ball size, frequency of drum revolutions and the number of grinding media on the process rate was reported. This rate is variable during grinding and the effect of the above mentioned factors is different in consecutive periods of the process.

Key words: ball mill, point of contacts

INTRODUCTION

In ceramic industry, advantage is most often taken of grinding equipment whose operating principles are based on the use of free energy of grinding media. The simplest design solution are ball mills with steel or corundum grinding media. Grinding of material particles in these mills proceeds mainly between grinding elements and to a lesser extent between grinding media and the inner drum surface [Drzymala 1992, Mattan 1971]. Particles of the ground material which are between the surfaces of adjacent balls moving against each other (this motion may result from both translational motion and rotations of the balls) will be mainly abraded and sheared with possible crushing [Lynch 1974, Lowrison 1974]. In the cataract motion of balls

* Technical University of Lodz, Faculty of Process and Environmental Engineering,
90-924 Lodz, Stefanowskiego 12/16, Poland, olejnik@p.lodz.pl

(very desirable in ball mills), the striking mechanism of falling balls will be involved additionally [Shipway, Hutchings 1993]. Moreover, the particular mechanisms of grinding are affected by the size of balls and their number. It is obvious that at the same volume of the bed of balls (the same degree of drum filling with balls) the bigger are the balls the smaller is their number. Bigger balls mean a bigger mass of a single ball and higher forces of interactions. A related smaller number of balls means a fewer points of contact, hence a decrease of mini-regions in which in a given moment there can be loads breaking the particles of material being ground. Selection of ball diameters depends on the strength of material being ground and the diameter of raw material particles. In general, for bigger particles, which require bigger forces to be destroyed, bigger balls should be used, while in the case of smaller particles (of weaker materials) better results are obtained when the number of the points of ball contact increases, hence when this number grows at the cost of diameter. Results of grinding in three industrial ball mills operating in the plants that manufacture ceramic tiles were analysed from this point of view.

Simple construction of the mill does not correspond with grinding efficiency. Low efficiency of the process makes technologists search for such ball composition in which mean particle diameter decreases most quickly. This will enable the mill operation time to be more economical.

PROCESS AND EQUIPMENT PARAMETERS OF GRINDING

Changes of particle size distribution of ground material in time were investigated in three industrial mills. Mills A, B and C, were characterised by similar size and kinematic parameters (Table 1). The process of wet grinding was carried out in a water suspension with the addition of anti-emulsifiers. The feed consisted of a mixture of minerals, mainly feldspar and clay. Tables 2 to 4 show the compositions of feed ground in the tested mills.

Table 1. Main parameters of industrial mills

Industrial mills	A	B	C
Inner diameter, [m]	3	2.5	3.15
Total volume, [m ³]	34	38	38
Frequency of rotations, n[min^{-1}]	13	12.65	13
Critical frequency, n_{cr} [min^{-1}]	24.43	26.76	23.84
n/n_{cr}	0.53	0.47	0.54
Number of grinding balls, [thousand]	620	400	400

Slight differences in feed composition for the tested mills followed from different technologies of production. This was related to the application of ground product in manufacturing of ceramic materials that would meet special requirements. The ground product from each of the three mills was used in the production of two types of ceramics. Wall tiles are burnt from a material called monoporosis (mill A, B) and silica (mill C). In the production of floor tiles quarry tiles are used (mills A, B and C).

Table 2. Feed composition for silica quarry tiles in mill A.

	Monoporosis	Quarry tiles
Solid components, [kg]	18 000	18 000
- including feldspar, [kg]	5 220	9 540
- clay, [kg]	7 740	7 020
- quartz, [kg]	2 880	1 440
- carbonates, [kg]	2 160	-
Liquid components, [kg]	1 095	1 064
- including water, [kg]	1 000	1 000
- sodium tripolyphosphate, [kg]	15	24
- water glass, [kg]	80	40

Table 3. Feed composition for monoporosis and quarry tiles for mill B.

	Monoporosis	Quarry tiles
Solid components, [kg]	21 300	22 000
- including feldspar, [kg]	3 834	11 660
- clay, [%]	11 502	7 700
- dolomite, [%]	1 704	1 980
- calcium carbonate, [%]	1 704	-
- scrap metal, [%]	-	660
Liquid components, [kg]	2 100	2 600
- including water, [kg]	2 051	2 550
- sodium tripolyphosphate, [kg]	49	50

Table 4. Feed composition for silica and quarry tiles in mill C.

	Silica	Quarry tiles
Solid components, [kg]	20 000	20 000
- including feldspar, [kg]	6 000	10 000
- clay, [kg]	14 000	10 000
Liquid components, [kg]	1 500	1 500
- including water, [kg]	1 422	1422
- flumix, [kg]	20	20
- water glass, [kg]	68	68

Filling of mills with grinding media, in all three mills equal to ca. 45% batch-wise, was composed of corundum balls of different sizes. Particular ball size fractions in the tested mills are presented in Table 5.

Table 5. Composition of balls and their sizes

Mill	A	B	C
Ball diameter, [mm]	Mass of balls, [kg]		
19,05	1700	-	925
22,23	2750	-	1625
25	-	4000	-
25,4	4150	-	2500
30	-	8000	-
31,75	8000	-	5050
38,1	1800	-	1400
40	-	8000	-
44,45	3050	-	2300
45	-	6500	-
50,8	4550	-	3450
63,5	-	-	5750
Altogether	26000	26500	23000

The grinding was a batch process. After feeding the mill with raw material, in determined intervals (every 60 min) samples were taken for analysis of particle size distribution. The analyses were made using a FRITSCH laser particle size analyser ANALYSETTE 22. Table 6 gives examples of the results of particle size analysis for quarry tiles in mill A.

On the basis particle size analysis the rate of grinding of particular size fractions was calculated. In the calculations, equation (1) proposed by Gardner and Austin was used in the differential form for discrete values of fractions, under the assumption of an ideal mixing of the ground material.

$$\frac{dw_i(t)}{dt} = -S_i w_i(t) + \sum_{j=1, i>1}^{i-1} S_j b_{i,j} \cdot w_j(t) \quad (1)$$

Rate coefficients S_i in equation (1) for grinding of quarry tiles in mills A, B and C are given in Table 7.

Table 6. Particle size composition of quarry tiles for mill A

Size fraction i , [μm]		Grinding time, [min]							
		60	120	180	240	300	360	420	480
		Size fraction w_i , [%]							
1	0,21÷0,28	0,73	0,69	0,67	0,64	0,64	0,65	0,66	0,68
2	0,28÷0,36	0,95	0,92	0,89	0,86	0,86	0,88	0,91	0,92
3	0,36÷0,47	1,33	1,31	1,28	1,25	1,25	1,28	1,33	1,35
4	0,47÷0,62	1,91	1,90	1,87	1,84	1,85	1,9	1,96	2
5	0,62÷0,8	2,59	2,61	2,56	2,55	2,56	2,62	2,72	2,78
6	0,8÷1,05	3,18	3,22	3,16	3,16	3,18	3,26	3,39	3,47
7	1,05÷1,37	3,66	3,72	3,66	3,67	3,70	3,79	3,94	4,04
8	1,37÷1,78	3,97	4,04	3,98	4	4,04	4,14	4,31	4,42
9	1,78÷2,32	4,13	4,21	4,15	4,18	4,24	4,33	4,52	4,63
10	2,32÷3,03	4,22	4,31	4,26	4,31	4,36	4,46	4,66	4,78
11	3,03÷3,95	4,37	4,50	4,46	4,54	4,58	4,68	4,91	5,04
12	3,95÷5,16	7,73	4,96	4,92	5,03	5,07	5,2	5,45	5,62
13	5,16÷6,73	5,25	5,64	5,60	5,75	5,83	6	6,31	6,56
14	6,73÷8,78	5,5	6,09	6,08	6,24	6,46	6,69	7,07	7,42
15	8,78÷11,45	5,16	5,93	5,97	6,12	6,60	6,86	7,33	7,80
16	11,45÷19,94	4,54	5,48	5,60	5,74	6,50	6,77	7,34	7,92
17	14,94÷19,48	4,16	5,29	5,54	5,72	6,57	6,88	7,49	8,13
18	19,48÷25,42	4,15	5,46	5,98	6,33	6,81	7,22	7,60	8,01
19	25,42÷33,16	4,37	5,87	6,81	7,49	7,07	7,55	7,32	7,02
20	33,16÷43,25	4,71	6,53	7,91	8,91	7,51	7,87	6,83	5,48
21	43,25÷56,42	3,1	4,65	5,51	5,24	4,53	3,78	2,57	1,21
22	56,42÷73,60	3,44	4,35	4,78	3,60	3,04	1,68	0,68	0,13
23	73,60÷96,01	5,33	3,95	3,03	1,85	1,49	0,62	0,11	0,01
24	96,01÷125,24	6,2	2,56	0,69	0,37	0,42	0,16	0,01	0
25	125,24÷163,38	4,8	0,98	0,06	0,03	0,09	0,03	0	0
26	163,38÷213,12	1,98	0,15	0	0	0,02	0,01	0	0
27	213,12÷278,01	0,52	0,01	0	0	0,01	0,03	0,01	0
28	278,01÷362,67	0,11	0	0	0	0,04	0,03	0,1	0
29	362,67÷473,09	0,06	0,01	0	0	0,06	0,04	0,1	0
30	473,09÷617,14	0,15	0,06	0	0,02	0,03	0,03	0	0
31	617,14÷791,42	0,12	0,02	0	0	0,06	0,04	0,01	0

Table 7. Rate coefficients S_i for grinding of quarry tiles in mills A, B and C

Mill A		Mill B		Mill C	
d_i	S_{iA}	d_i	S_{iB}	d_i	S_{iC}
617,14÷791,42	0,000713	-	-	-	-
473,09÷617,14	0,000859	-	-	473,09÷617,14	0,0165
362,67÷473,09	0,00107	-	-	362,67÷473,09	0,0313
278,01÷362,67	0,00187	278,01÷362,67	0,00709	278,01÷362,67	0,0481
213,12÷278,01	0,00219	213,12÷278,01	0,0167	213,12÷278,01	0,0464
163,38÷213,12	0,00194	163,38÷213,12	0,0212	163,38÷213,12	0,0353
125,24÷163,38	0,0016	125,24÷163,38	0,0238	125,24÷163,38	0,0264
96,01÷125,24	0,00121	96,01÷125,24	0,0242	96,01÷125,24	0,0178
73,60÷96,01	0,000703	73,60÷96,01	0,0198	73,60÷96,01	0,0119
56,42÷73,60	0,000428	56,42÷73,60	0,0144	56,42÷73,60	0,00997
43,25÷56,42	0,000266	43,25÷56,42	0,0127	43,25÷56,42	0,00694
33,16÷43,25	0,000101	33,16÷43,25	0,0041	33,16÷43,25	0,00262
25,42÷33,16	7,53E-03	25,42÷33,16	0,002	25,42÷33,16	0,00187
19,48÷25,42	4,48E-03	19,48÷25,42	0,0015	19,48÷25,42	0,00134
11,45÷19,48	2,16E-03	11,45÷19,48	0,00123	11,45÷19,48	0,00107
8,78÷11,45	1,09E-04	8,78÷11,45	0,00105	8,78÷11,45	0,000835
6,73÷8,78	-6,06E-04	6,73÷8,78	0,000982	6,73÷8,78	0,000649
5,16÷6,73	6,75E-04	5,16÷6,73	0,00088	5,16÷6,73	0,000525
3,95÷5,16	2,00E-04	3,95÷5,16	0,00068	3,95÷5,16	0,000475
3,03÷3,95	1,60E-04	3,03÷3,95	0,000513	3,03÷3,95	0,000448
2,32÷3,03	-2,14E-04	2,32÷3,03	0,000419	2,32÷3,03	0,000346
1,78÷2,32	-2,67E-04	1,78÷2,32	0,000384	1,78÷2,32	0,000198
1,37÷1,78	-5,08E-04	1,37÷1,78	0,000305	1,37÷1,78	7,41E-05
1,05÷1,37	-7,01E-04	1,05÷1,37	0,000236	1,05÷1,37	-0,00011
0,8÷1,05	-8,38E-04	0,8÷1,05	0,000134	0,8÷1,05	-0,00025
0,62÷0,8	-8,97E-04	0,62÷0,8	8,00E-04	0,62÷0,8	-0,00044
0,47÷0,62	-8,74E-04	0,47÷0,62	5,80E-05	0,47÷0,62	-0,0005
0,36÷0,47	-6,61E-04	0,36÷0,47	0,000621	0,36÷0,47	-0,00059
0,28÷0,36	-1,84E-05	0,28÷0,36	0,000199	0,28÷0,36	-0,00068
0,21÷0,28	0	0,21÷0,28	0,00144	0,21÷0,28	-0,00134

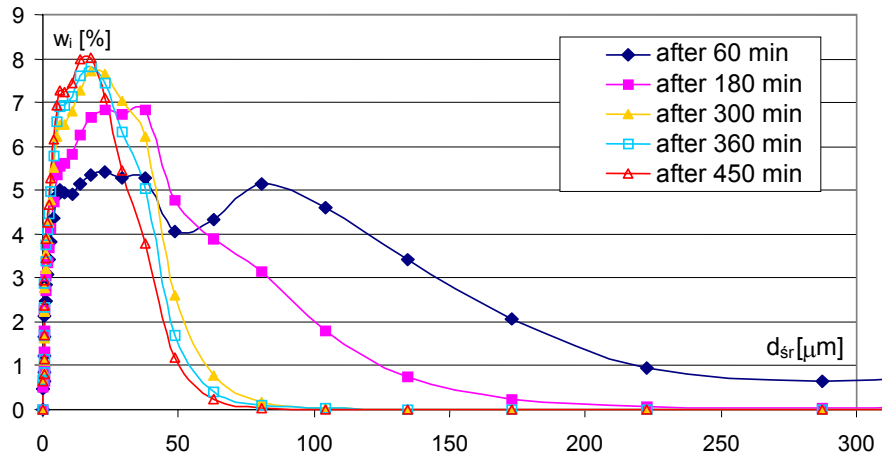


Fig. 1. Change of particle size composition of material ground in mill A in time

Knowing the particle size composition, mean particle size was calculated from the formula

$$d_{sr} = \sum_{i=1}^n d_{sr i} \cdot x_i \quad (2)$$

This enabled a graphical representation (Fig. 2) of grinding kinetics in the form of a relation between mean particle size and grinding time: $d_{sr} = f(t)$.

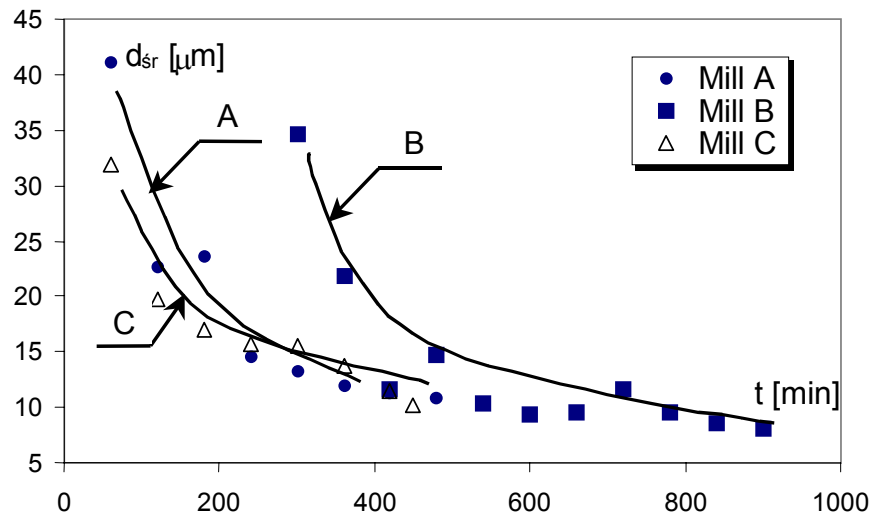


Fig. 2. Change of mean particle size d_{sr} during grinding

RESULTS AND DISCUSSION

Diagrams in Fig. 2 show clearly that in the first period of grinding, when raw material particles are big, the process of grinding is the fastest in mill C. Already, after 60 min of grinding, the mean size of particles ground in this mill is about 32 μm . Decay rates of size fractions between 699 and 109 μm are the biggest for mill C (Table 7) reaching about 0.04 min^{-1} . A worse result was achieved in mill A, because after the same time $d_{\text{sr}} = \sim 41 \mu\text{m}$. Rate S_{iA} for so big size fractions (362,67 to 73.6 μm) in mill B is almost twice as small as rate S_{iC} for the same fractions in mill C. For the mentioned size range the mean value of S_{iB} for mill B is around 0.02 min^{-1} . To obtain a mean size of particles of ground material $d_{\text{sr}} = 45 \mu\text{m}$, the process should be carried out in mill B for 300 min. These results can be explained by two factors. The first one is the size of grinding balls. The biggest balls in mill B had the diameter 45 mm, while in mill A the balls had the diameter 50.8 mm, and in mill C even 63.5 mm. Another parameter is the relative frequency of drum rotations which in mill B was much lower than in the two other mills (Table 1). This made that the energy of grinding balls in mill C was the highest (the highest relative rate and the biggest balls), while in mill B this energy was definitely the lowest. For these reasons, with big particles in the first period of grinding the process rates are so differentiated in particular mills. In the second period of grinding, shown in Fig. 2, which starts when the mean particle size of ground material reaches dozen micrometers, the process rate is determined not by the size of balls but their number to which the number of points of contact between balls is proportional. As was reported above, the probability that a particle of ground material can appear in the region where it is destroyed, thus in the region near the contact point of two balls, is proportional to the number of these contact points. In mills B and C the number of balls is the same and a time-dependent change of the mean particle size proceeds in a similar way. The values of S_{iB} and S_{iC} for the size fraction below 5.84 μm are similar (Table 7) and are equal to around 0.0004 min^{-1} . In mill A filled with a bigger number of balls (a bigger number of contact points) the rate of decreasing the mean particle size is bigger in the second period of grinding when only small particles occur.

CONCLUSIONS

The following conclusions can be drawn from the results discussed above:

1. In the first period of grinding in ball mills, when raw material particles are relatively big, the process depends on ball size and rotational speed of the mill, which determines the forces with which balls act on each other.
2. In the second period of grinding, when particle size of the ground material is much smaller, the effect of the number of balls and consequently the number of the points of contact of grinding elements between which material particles are comminuted, becomes more evident.

LIST OF SYMBOLS

- d_{sr} – mean (arithmetic) particle size in size interval i
 x_i – mass fraction of particles from the size interval i
 $w_i(t)$, $w_j(t)$ – weight fraction of particles from interval i or j after grinding time t ,
 S_i , S_j – specific rate of grinding of particles from interval i or j called also the distribution parameter,
 $b_{i,j}$ – distribution function defined as this part of ground material from size fraction j , which passed to size interval i .

REFERENCES

- DRZYMAŁA Z. i inni, 1992, *Badania i podstawy konstrukcji młynów specjalnych*. PWN. Warszawa.
LOWRISON G. C., 1974, *Crushing and grinding*. Butterworth, London.
LYNCH A.J., 1974, *Mineral crushing and grinding circuits*. Amsterdam, Oxford, New York.
MATTAN J., 1971, *How to step up ball mill efficiency*. Rock Products, Nr 5.
SHIPWAY P. H., HUTCHINGS I. M., 1993, *Attrition of brittle spheres by fracture under compression and impact loading*. Powder Tech. 76, 23-30.
SHIPWAY P. H., HUTCHINGS I. M., 1993, *Fracture of brittle spheres by fracture under compression and impact loading. I. Elastic stress distribution*. Phil. Magaz. A, 67, 1389-1404.

ACKNOWLEDGEMENTS

This study was carried out within research project no. 3T0C 005 23 financed by the State Committee for Scientific Research in the years 2002-2005.

Heim A., Olejnik T.P., A. Pawlak A., *Wpływ liczby punktów kontaktu młynników na szybkość mielenia w młynach kulowych*, Physicochemical Problems of Mineral Processing, 38, (2004) 147-155 (w jęz. ang.).

W pracy przedstawiono wyniki badań, których celem było określenie wpływu liczby punktów kontaktu młynników na szybkość mielenia w młynach kulowych. Badania prowadzono dla trzech młynów o działaniu okresowym pracujących w warunkach przemysłowych. Młyny posiadały zbliżone wymiary geometryczne. Przemiał prowadzono na mokro (w zawiesinie wodnej z dodatkiem antyemulgatorów) dla typowych surowców, mających zastosowanie w przemysłowej produkcji płytek ceramicznych, którymi były mieszaniny skalenia oraz ilów w odpowiednich udziałach masowych. Zbadano przebieg procesu mielenia dla trzech przemysłowych młynów kulowych, różniących się liczbą i wielkościami młynników korundowych. Dla każdego z przemiałów, co 60 minut pobierano próbki do analizy granulometrycznej. Określono szybkość rozdrabniania poszczególnych klas rozmiarowych w oparciu o równanie Gardnera Austina. Analizowano zmianę w czasie składu granulometrycznego mielonego materiału, stwierdzając wpływ na szybkość procesu wielkości kul, częstości obrotowej bębna oraz liczby młynników. Szybkość ta jest zmienna w czasie mielenia, a wpływ w/w czynników jest różny w poszczególnych okresach procesu.

Praca wykonana w ramach projektu 3T0C 005 23, finansowanego przez Komitet Badań Naukowych w latach 2002-2005.

Andrzej HEIM, Robert KAŻMIERCZAK, Andrzej OBRANIAK*

THE EFFECT OF EQUIPMENT AND PROCESS PARAMETERS ON TORQUE DURING DISK GRANULATION OF BENTONITE

Received April 15, 2004; reviewed; accepted June 14, 2004

Changes of torque during foundry bentonite granulation in disk granulators were studied. Variable parameters were the diameter and inclination angle of the granulator disk and filling of the disk with granular material. The bed of loose material was wetted drop-wise during tumbling, at a constant volumetric liquid flow, by a sprinkler that ensured uniform supply of the wetting liquid. In every trial the instantaneous values of net torque were measured. The effect of the disk diameter, its angle of inclination, filling with raw material and moisture content of the granulated bed on torque changes was assessed. A correlation equations was proposed to describe the effect of the above parameters on the reduced torque change.

Key words: disk granulation, torque

INTRODUCTION

For majority of operations that take place in rotary granulators the type of bed motion characterises and determines the process [Kapur 1992]. Granular bed dynamics in tumbling granulators, i.e. the motion of granules and particles and forces with which the bed and disk interact, determines the angle of bed inclination [Heim et al. 1995] and net torque [Heim et al. 2000], and consequently, the power of a driving motor [Gluba et al. 1995]. The inertial and friction forces in the discussed system are determined by such equipment and process parameters as the diameter and inclination angle of the apparatus [Chadwick and Bridgwater 1997], its filling with raw material [Kantorowicz 1959] and rotational speed [Heim et al. 1995]. The effect of these parameters on the dynamics of a model granular bed during mixing in a horizontal rotary drum [Koroticz 1961, Heim et al. 1995], during grinding in ball mills [Harris et

* Technical University of Lodz, Faculty of Process and Environmental Engineering,
90-924 Lodz, Stefanowskiego 12/16, Poland, heim@wipos.p.lodz.pl

al. 1985, Tarjan 1981] and during granulation in a horizontal drum granulator [Obraniak 2002] has already been studied. However, there are no studies on bed dynamics during disk granulation in a broad range.

AIM OF THE STUDY

The aim of this study was to determine the effect of selected process and equipment parameters, namely bed moisture content, disk filling and diameter and angle of disk inclination on torque.

RANGE OF STUDIES

The variable parameters were:

- disk diameter $D = 0.5, 0.75, 1.0$ m,
- filling of the granulator with granular bed $k = 3\% - 7\%$,
- angle of disk inclination $\alpha = 45^\circ - 53^\circ$.

The torque was measured on line during wet disk granulation.

MEASURING EQUIPMENT and METHODS

The experimental set up is shown in the photograph in Figure 1. The disk was driven by a motoreducer by means of a belt transmission and flexible coupling. A smooth change of disk rotational speed was obtained using an inverter, and the speed was controlled by a speedometer. Instantaneous values of torque were measured by a torquemeter, converted by a reader and recorded by a computer. The granular bed placed in the disk was wetted dropwise by a sprinkler which ensured a uniform liquid supply. The sprinkler was mounted on a stand independent of the granulator. The wetting liquid (distilled water) was supplied from a tank located on the level 2.5 m above the disk surface, and its constant flow rate ($Q=0.7 \cdot 10^{-6} \text{ m}^3/\text{s}$) was controlled by a rotameter. For the whole time of testing a constant liquid level was kept in the tank which ensured constant pressure of the supplied liquid. The granular bed was wetted until final moisture content was equal to $w_k=0.29$. Every 60 s or 120 s a sample was taken and bulk density and the angle of natural repose were measured. After that it was returned to the disk. The process of granulation was carried out batch-wise for each of the three disk dimensions at steady-state process and equipment parameters, i.e. filling of the disk and inclination angle of the granulator axis.

Results of measurements of instantaneous values (at time intervals 1s) of net torque M were converted to the reduced torque M^* according to equation (1).

$$M^*(t) = \frac{M(t) - Mj}{m_s + Q \cdot \rho_w \cdot t} \quad (1)$$

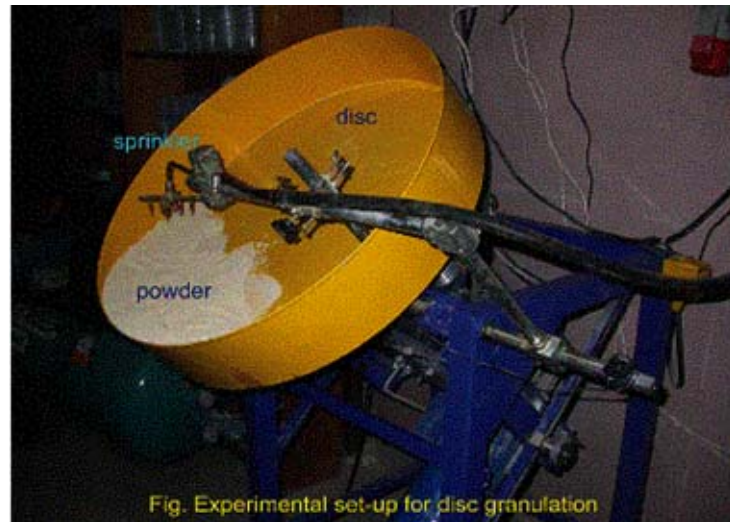


Fig. 1. Experimental set-up

Next, mean values of torque were calculated for 10-second periods (from 10 consecutive values). Variability of the reduced torque in time, when the wetting liquid is supplied continuously at a constant flow rate, is identical to the change of torque as a function of feed moisture content. This moisture content in a given moment “*t*” is calculated from the equation:

$$w = \frac{m_w}{m_s} = \frac{Q \cdot t \cdot \rho_w}{m_s} \quad (2)$$

RESULTS

An example of the dependence of reduced torque M^* averaged for 10-second periods on moisture contents is illustrated in Fig. 2. When analysing the diagrams three ranges can be distinguished each time for which different functions were obtained. In the first range, dependence of the torque on time is in the form of an increasing function, in the second range a decrease of the torque is observed, while in the third one it is stabilised.

Particularly interesting is the initial growth of the torque and its further steady state. This character of torque changes can be explained by changes in the parameters that characterise the granulated bed during the process. Then, the particle size distribution changes and due to water supply, the mass and moisture content of the entire bed and individual granules as well as the bulk density and inner friction angle at certain stages of the process also change.

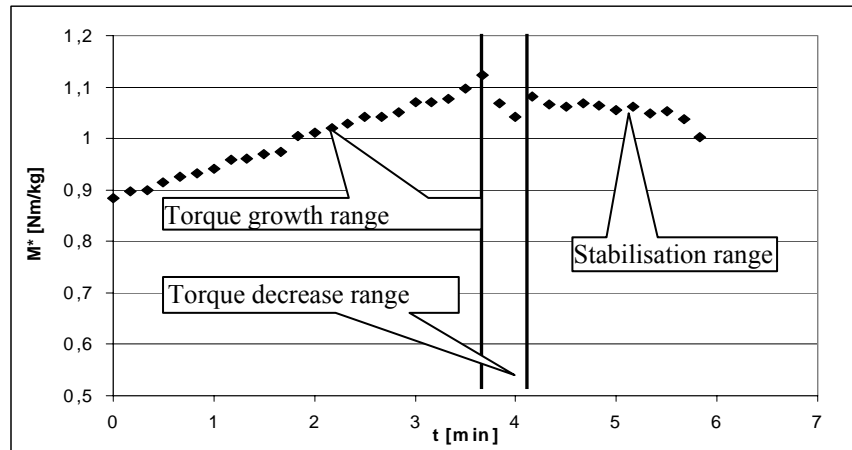


Fig. 2. Example of the dependence of reduced torque on wetting time, ($D=0.5$, $k=5\%$; $\alpha=45^\circ$)

It follows from Fig. 2 that after reaching some boundary value of bed wetting, the further liquid supply causes a decrease of the torque, and next the torque is on a stable level which is a result of steady state of the parameters that characterise the processed material (bulk density, angle of natural repose).

Analysis of results obtained in the studies indicates that the torque during bed wetting (granulation) in the rotating disk depends also on the equipment and process parameters, i.e. the degree of filling of the granulator k , disk diameter D and its angle of inclination α .

Figure 3 shows an example of comparison of reduced torque changes during bed wetting for different levels of disk filling k . On the basis of the results obtained it can be concluded that the reduced torque decreases with an increase of disk filling. This tendency is observed in the whole wetting range; from the starting point, through the stage of growth, until torque stabilisation. This is most probably related to a decreasing (with an increase of filling) distance of the point of application of the resultant force of friction (between the bed and disk surface) from the axis of the disk rotation. Owing to the arm of the force this has an effect on the torque coming from the resultant force of friction. Analysis of the relationships obtained allows us to conclude that different values of coefficient k , (due to changes in raw material mass) affect the wetting time and agglomeration rate, which in Fig. 3 is revealed by both total process duration and different time points in which characteristic stages of granulation occur.

To confirm the observed tendencies and to explain the effect of filling degree k , changes of torques in Fig. 3 are shown in Fig. 4 as functions of averaged bed moisture content changing during the process. Relations obtained show that for tests made at all degrees of filling k , the maximum unit torque is obtained for similar bed moisture contents. The torque is also stabilised for similar moisture contents.

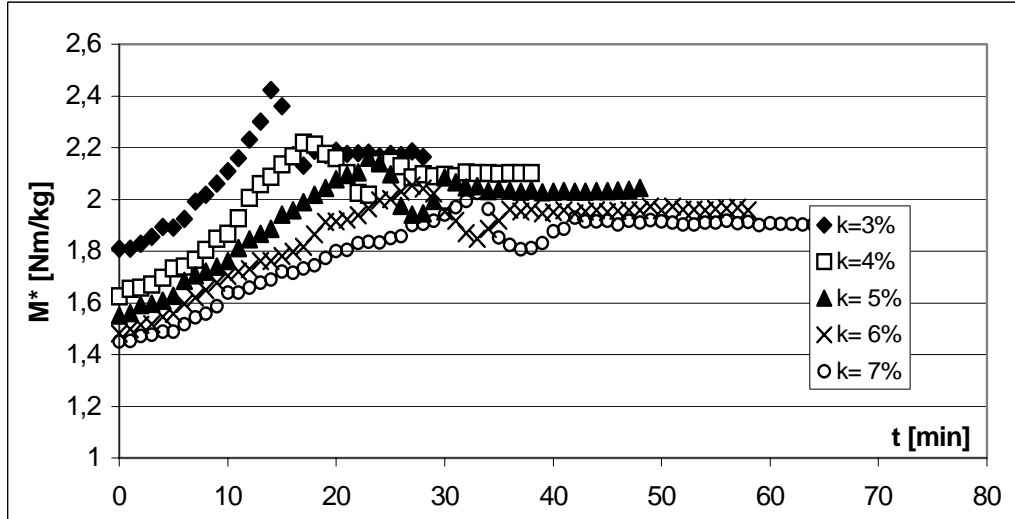


Fig. 3. Example of changes in reduced torque as a function of time for different values of disk filling k ($D=1$ m; $\alpha=47$)

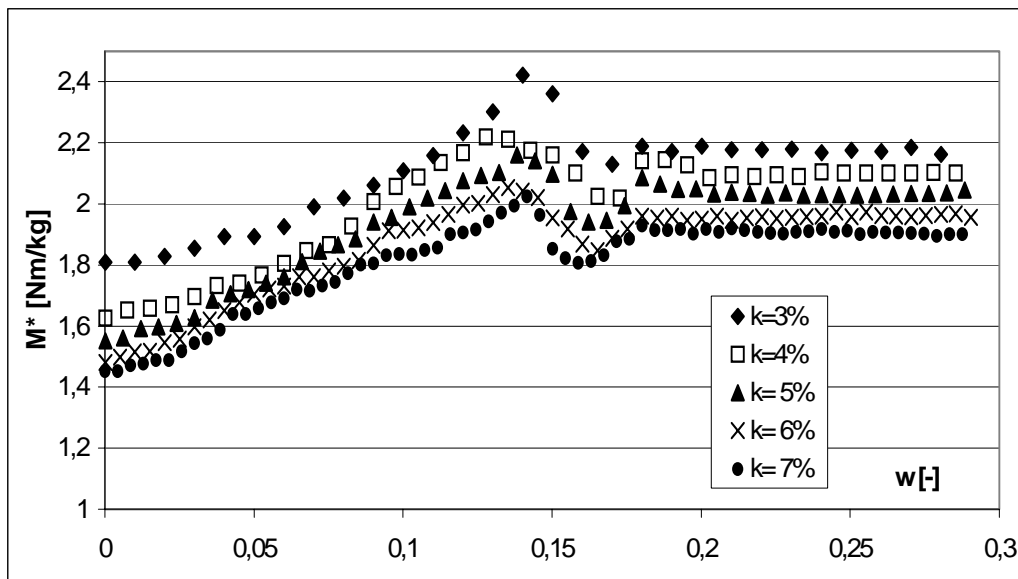


Fig. 4. Example of changes in reduced torque as a function of bed moisture content for different values of disk filling k ($D=1$ m; $\alpha=47$)

This provides an evidence of the effect of changes in disk filling only on the system dynamics. There is no such influence on changes of the granulated bed properties, i.e. process kinetics. Similar conclusions can be drawn from the analysis of changes in reduced torques during granulation in three disks with different diameters.

The effect of the next parameter – the disk diameter on reduced torque as a function of moisture content is shown in Fig. 5.

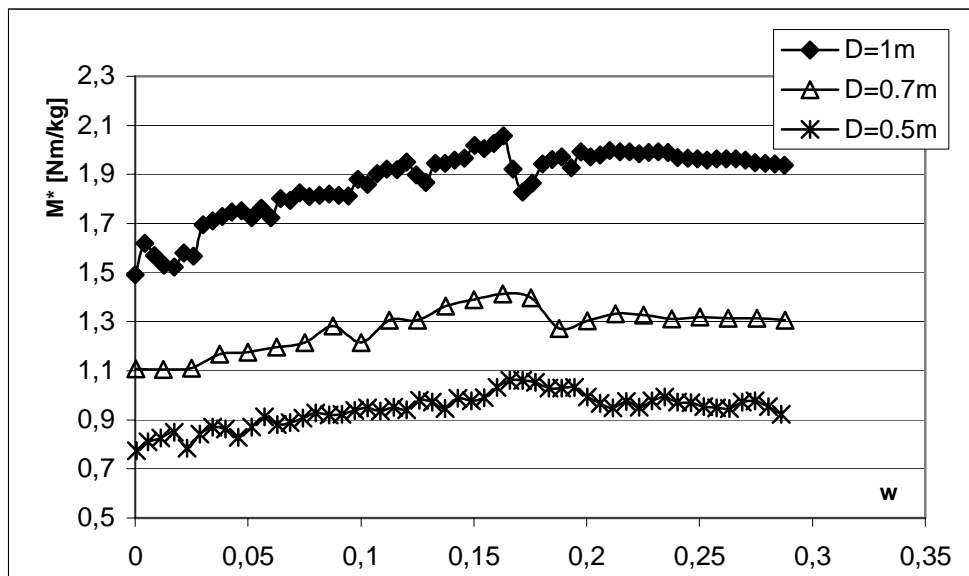


Fig. 5. Example of changes in reduced torque with bed moisture content for three disk diameters ($k=7\%$, $\alpha=45^\circ$)

It follows that for a disk with bigger diameter, the values of M^* are higher. An increase of the reduced torque is probably caused by a growing distance of the point of application of the resultant force of friction between the bed and disk surface, and hence by increasing the arm of this force which gives resistance to the torque.

An example of a diagram representing the reduced torque as a function of wetting time for five angles of disk axis inclination is shown in Fig. 6. When analysing the relations it was found that in the whole range of granulation, the values of reduced torque M^* are the higher the lower are the values of α . The influence of the disk inclination angle on the torque is connected with the components of forces of bed pressure on the disk bottom and edge. This has an effect on the resultant force of friction. Moreover, it can be observed that the disk inclination affects the duration of subsequent periods of granulation, and consequently on the agglomerate formation rate (process kinetics). This is revealed by differences in the duration of particular granulation periods at a changing inclination angle.

Owing to the presence of three ranges that differ in the character of reduced torque changes, it is difficult to correlate its values and the granulator operation parameters (disk diameter, filling of the granulator, angle of axis inclination) with one general equation. Hence, separate relations were proposed to describe the reduced torque as a function of equipment and process parameters for two ranges, in the first one the torque was growing and in the last one it assumed constant values. For the range of a small decrease after reaching a maximum, due to short duration no such relations were proposed.

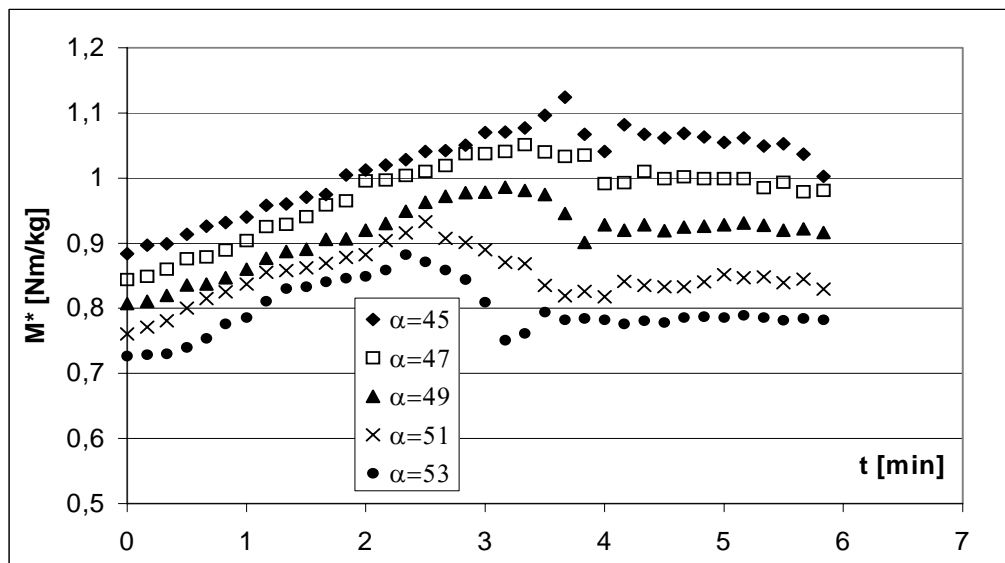


Fig. 6. Comparison of changes in the reduced torque as a function of moisture content for five angles of disk inclination ($D = 0.5$, $k = 5\%$)

For the range in which the reduced torque was kept on a constant level, the following equation was obtained:

$$M_{st}^* = 10^{0.62} \cdot D^{1.08} \cdot k^{-0.15} \cdot \cos \alpha^{1.28} \quad (3)$$

This relation was obtained for the value of the correlation coefficient $R^2=0.99$.

It follows from this relation that the angle of granulator axis inclination and disk diameter has the biggest influence on the torque, while the degree of filling affects the torque to a lesser extent.

A graphic comparison of the values obtained from measurements and the proposed correlation is illustrated in Fig. 7.

In the range of torque growth, beside the effect of equipment and process parameters a dependence of the reduced torque on bulk density, i.e. a parameter characterising changes in the processed bed properties, was observed. Additionally, a negligibly small effect of the angle of natural repose was found. The following relation was obtained:

$$M_w^* = 10^{0.71} \cdot D^{0.93} \cdot k^{-0.12} \cdot \cos \alpha^{0.47} \cdot \rho_n^{-0.23} \quad (4)$$

A graphic comparison of values obtained from measurements and correlation (4) is shown in Fig. 8.

The above relation was obtained at the correlation coefficient $R^2=0.95$.

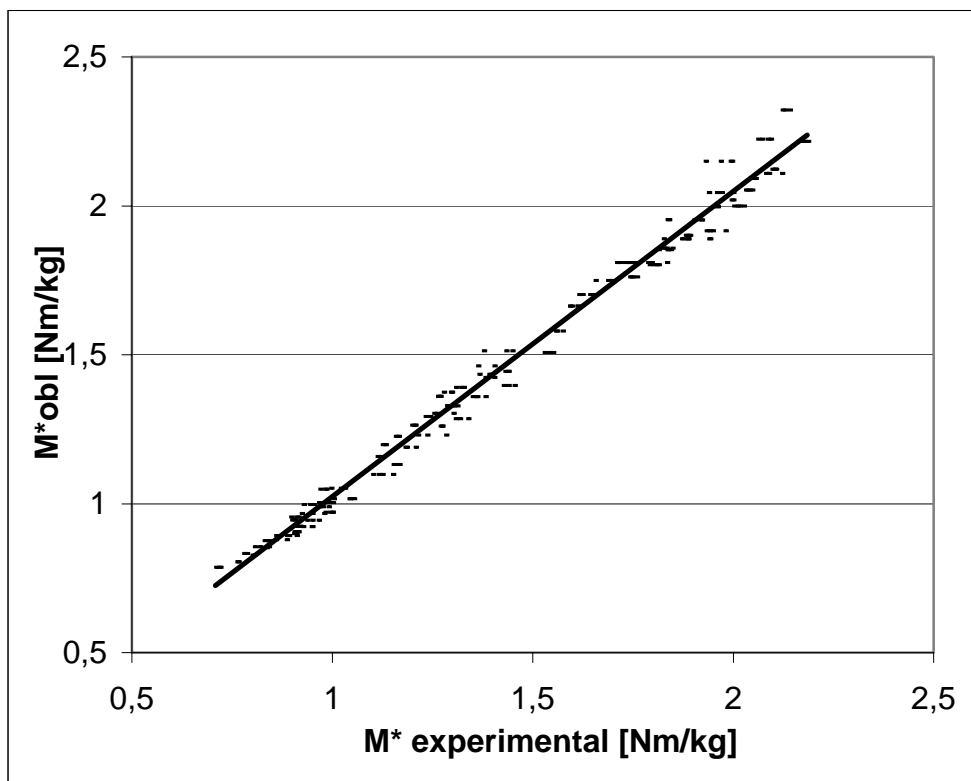


Fig.7. Comparison of values obtained from measurements and resulting from equation (3)

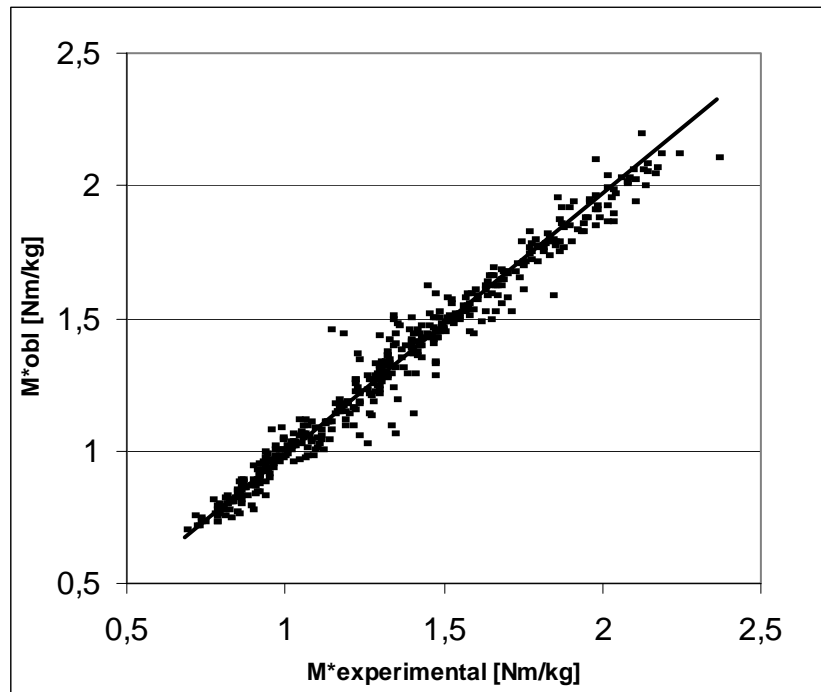


Fig. 8. Comparison of values obtained from measurements and resulting from relation (4)

CONCLUSIONS

1. Reduced torque M^* increases with an increase of bed moisture content only in the initial period of disk granulation to settle down after a certain decrease.
2. The reduced torques are higher for disks with bigger diameters.
3. The value of reduced torque decreases with an increase of disk filling with granular material.
4. A significant effect of the angle of disk inclination on the reduced torque was observed.
5. Changes in the values of torque during granulation can be described by correlation equations.

ACKNOWLEDGEMENT

The work was carried out under research project W-10/21/2004/BW.

LIST OF SYMBOLS

m_s – mass of loose material on the disk [kg]
 $m_w = Qtp_w$ – mass of wetting liquid added [kg]

M – net torque [Nm]
 M_j – torque of idle run for empty disk [Nm]
 M^* – reduced torque [Nm/kg]
 M^*_{obl} – calculated reduced torque [Nm/kg]
 w – moisture content of the bed [kg/kg]
 D – disk diameter [m]
 k – level of filling the disk with granular material [%]
 α – angle of inclination of the disk axis [deg]
 ρ_n – bulk density of the bed [kg/m³]
 t – wetting time [s]
 Q – volumetric flow rate of wetting liquid [m³/s]
 ρ_w – water density [kg/m³]
 n – rotational speed [1/s]

LITERATURE

- CHADWICK P.C., BRIDGWATER J., 1997, *Solids flow in disk granulators*, Chemical Engineering Science, Vol. 54, No. 15, 2497-2509.
- GLUBA T., HEIM A., KOCHAŃSKI B., OBRANIAK A., ZAŁUGA T., 1995, *Badania dynamiki wsadu ziarnistego w obrotowym bębnie*, XV Ogólnopolska Konferencja Naukowa Inżynierii Chemicznej i Procesowej, Gdańsk 1995, vol. I.
- HARRIS C.C., SCHNOCK E.M., ARBITER N., 1985, *Grinding mill power consumption*. Miner. Process. Technol. Rev., 1, 297-345.
- HEIM A., GLUBA T., KOCHAŃSKI B., OBRANIAK A., ZAŁUGA T., 1995, *Kształt przekroju poprzecznego warstwy ziarnistej w bębnie obrotowym*, Inż. Chem. i Proc., 1, 95-116.
- HEIM A., GLUBA T., OBRANIAK A., 1995, *Zapotrzebowanie mocy do napędu granulatora bębnowego*, V Ogólnopolskie Sympozjum GRANULACJA, Puławy.
- HEIM A., GLUBA T., OBRANIAK A., 2000, *The effect of the process and equipment parameters on the value of torque during the drum granulation*, Zeszyty Naukowe PL, No. 28, 91-99, Lodz.
- KANTOROWICZ Z.B., 1959, *Maszyny przemysłu chemicznego*, PWT, Warszawa.
- KAPUR P.C., RANJAN S., FUERSTENAU D.W., 1992, *A cascade-cataract charge flow model for power draft of tumbling mills*, Int. J. Of Miner. Proc., 36, 9-29.
- KOROTICZ W.I., 1961, *Dvizhenije sypuchevo materiala vo vrashchayushchemsa barabanie*, Stal, 8, 680-686.
- OBRANIAK A., 2002, *Dynamika złoża ziarnistego w poziomych bębnach obrotowych*, Praca doktorska, Wydział Inżynierii Procesowej i Ochrony Środowiska PŁ.
- TARJAN G., 1981, *Mineral Processing*, vol. 1, Akademia Kiado, Budapest.

Heim A., Kaźmierczak R., Obraniak A., *Wpływ parametrów aparaturowo-procesowych na wartość momentu obrotowego w procesie granulacji talerzowej bentonitu*, Physicochemical Problems of Mineral Processing, 38, (2004) 157-166 (w jęz. ang.).

Przeprowadzono badania zmian momentu obrotowego podczas procesu granulacji bentonitu odlewniczego w granulatorach talerzowych. W badaniach zmieniano: średnicę i kąt pochylenia talerza granulatora oraz stopień wypełnienia talerza materiałem ziarnistym. Złoże materiału sypkiego nawilżano kropłowo w czasie jego ruchu przesypowego, przy stałym objętościowym natężeniu dopływu cieczy, za pomocą zraszacza zapewniającego równomierne podawanie cieczy zwilżającej. Podczas każdej próby mierzono chwilowe wartości momentu obrotowego na wale granulatora. Przeprowadzono ocenę wpływu średnicy aparatu, jego kąta pochylenia, stopnia wypełnienia talerza oraz wilgotności granulowanego złoża ziarnistego na zmianę momentu obrotowego. Zaproponowano dwa równania korelacyjne opisujące wpływ w/w parametrów na zmianę zredukowanego momentu obrotowego.

Andrzej HEIM, Tadeusz GLUBA, Andrzej OBRANIAK*

BED DYNAMICS DURING DRUM GRANULATION

Received April 14, 2004; reviewed; accepted June 15, 2004

Results of investigations of a granulated bed dynamics during agglomeration in rotating drums were discussed. The investigations were carried out in granulators with continuous wetting of the bed with water, thus making no difference whether the wetting time or bed moisture content was assumed as an independent variable. The variable parameters were: drum diameter D ranging from 0.25 to 0.4 m, drum filling with raw material k in the range from 5 to 20% of inner drum volume and rotational speed of the drum $n = 10$ to 32 rpm. During granulation the torque value was measured on the granulator shaft. Every minute a sample was taken from the drum, the angle of natural repose of the product, and its bulk density were determined. A dimensionless equation describing the bed dynamics during granulation process was proposed.

Key words: drum granulation, torque, power number, Froude number

INTRODUCTION

The problems of granular bed dynamics were discussed in the literature most thoroughly for ball mills. Much fewer are the studies on mixing, granulation and other unit operations. Dirge (1990) claimed that the value of torque generated by forces of gravity of the bed in the ball mill depends on mill dimensions and properties of the bed. To describe this phenomenon Rose and Sullivan (1958) used dimensional analysis that included many parameters, while Gao (1990) proposed a formula which allowed him to calculate the power demand. Assuming that balls filling the drum are a continuous medium, which circulates in cascades, after a critical value of the angle of inclination has been reached on the free surface, Hogg and Fuerstenau (1972) calculated the work required to lift the balls that moved along circular trajectories from the lower to upper equilibrium point. As a result, they found that power required to drive the drum depended on the drum dimensions, rotational speed, filling with material and on the mass of this filling. Arbiter and Harris (1982) obtained similar results by equilibrating the moment of peripheral (driving) force with the moment of

* Technical University of Lodz, Faculty of Process and Environmental Engineering,
90-924 Lodz, Wólczajska 213/215, Poland, heim@wipos.p.lodz.pl

braking force of the load. On the basis of experiments, Kapur (1992) obtained the dependence of torque (treated as an energy parameter) on time. A characteristic property of this dependence published in a graphical form, is that the torque is constant in some range, it does not change with time and proceeding granulation. The range of constant torque was also confirmed by the investigations of mixing and granulation carried out by Heim et al. (1999). Weidenbaum (1958) introduced the Froude number to his relations as a parameter characterising the bed dynamics. The Froude number was used also in the description of material motion during granulation by Gusiev (1966) and Korotich (1966), who gave it as a function of a subsequent dynamic parameter – the angle of natural repose. A detailed analysis of the bed dynamics was proposed by Kantorowicz (1959) who studied the distribution of forces acting on granules. After making many simplifying assumptions he found the angle of bed inclination was equal to the angle of natural repose. When analysing the action of forces on grains of the bed and their velocities (both for granulation and mixing) Heim et al. used in the description of dynamics such parameters as bed inclination angle β (1995), moment on the drum shaft (1994), supplied power (1995) and grain velocity (1997).

AIM OF THE STUDY

The aim of the study was to describe bed dynamics during granulation using dimensionless numbers, and to determine the effect of process and equipment parameters (granulator drum diameter, its filling with raw material, rotational speed of the granulator and granulation time), and parameters characterising the granulated product (bulk density, friction angle) on the absolute torque value.

SCOPE OF INVESTIGATIONS

Experiments were carried out in a laboratory rig for drum granulation for the following range of variable parameters:

- granulator drum diameter $D = 0.25$ to 0.40 m,
- drum filling with a granular bed $k = 5\%$ to 20% ,
- the ratio of rotational speed of the drum to critical velocity $n/n_{kr} = 0.15$ to 0.375 .

The tested material was foundry bentonite with grain size ranging up to 0.16 mm and bulk density $\rho_n = 865$ kg/m³.

MODEL FORMULATION

During formulation of the model the following assumptions were made:

- the bed of granular material is a rigid body,
- the circulation of granular material in rotating drum is caused by the moment M_t generated by friction forces.

Considering the bed dynamics for an elementary sector of surface area dF , we can determine the value of the moment M_t . Figure 1 shows the distribution of forces acting on the granulated bed and its elementary sector. The following forces act upon element ABED.

- friction forces of the bed lifting – dT ,
- gravity force – $dP = \rho_n g L dF$,
- centrifugal force $dB = \omega^2 R dP / g$.

The friction force is connected with the centrifugal force and the radial component of the gravity force. It is determined by the formula:

$$dT = f \cdot dP \left[\frac{\omega^2 \cdot R}{g} + \cos(\beta_0 + \varphi) \right] = f \rho_n L g dF \left[\frac{\omega^2 R}{g} + \cos(\beta_0 + \varphi) \right] \quad (1)$$

According to Fig. 1, the elementary surface dF is

$$dF = R^2 \cos \varphi (\cos \varphi - \cos \alpha) d\varphi \quad (2)$$

Taking eqs. (1) to (2) the moment of friction force distributed along the arc on which material is in contact with the drum wall, is determined by the integral

$$M_t = \int_{-\alpha}^{+\alpha} R dT = R^3 L f \rho_n g \int_{-\alpha}^{+\alpha} \left[\frac{\omega^2 R}{g} + \cos(\beta_0 + \varphi) \right] \cdot (\cos^2 \varphi - \cos \alpha \cos \varphi) d\varphi \quad (3)$$

Upon integration we have:

$$M_t = f g L R^3 \rho_n \left[\frac{\omega^2 R}{g} \left(\alpha - \frac{\sin 2\alpha}{2} \right) + \cos \beta_0 \left(\frac{4}{3} \sin \alpha - \frac{1}{6} \sin 2\alpha \cos \alpha - \alpha \cos \alpha \right) \right] \quad (4)$$

Because the central angle α is a parameter which defines the drum filling with granular material k (and bulk density ρ_n , and angle β_0 is proportional to the inner friction coefficient f , the obtained formula can be simplified to the form

$$M_t = A L D^3 \rho_n^c \left[\frac{\omega^2 D}{2g} \cdot k^a \right] \cdot t g \beta^b \quad (5)$$

where A is constant.

Because power is defined by the formula

$$N = M_t \cdot \omega \quad (6)$$

After dividing both sides of the equation (5) by $\omega^3 \rho_n D^5$ and taking into account the definition of dimensionless numbers, we obtain the following relation

$$\frac{N}{\omega^3 \cdot \rho \cdot D^5} = A \cdot \frac{g}{\omega^2 D} \cdot \frac{L}{D} \cdot k^a \cdot \operatorname{tg} \beta^b \cdot \rho_n^{c-1} \quad (7)$$

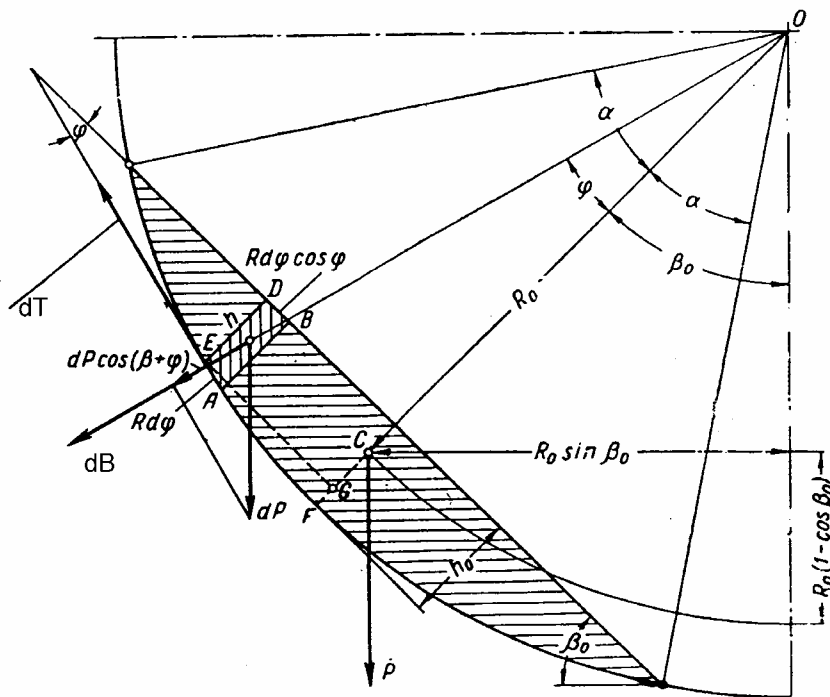


Fig. 1. Forces acting upon the elementary sector of the granulated bed

Upon substituting the symbols of dimensionless numbers: power number (N_e) and Froude number (F_r) we obtain

$$N_e = A \cdot \frac{1}{F_r} \cdot \frac{L}{D} \cdot k^a \cdot \operatorname{tg} \beta^b \cdot \rho_n^{c-1} \quad (8)$$

MEASURING EQUIPMENT AND METHODS

Experiments were carried out using an experimental rig for drum granulation. Drums of length $L = 0.24$ m, were driven by motoreducer by means of a belt transmission and a coupling. A smooth change of the rotational speed of the drum was obtained by means of inverter, and was controlled by a revolution counter.

Instantaneous values of the torque were measured by torque meter, read using reader and processed and recorded by computer. The granular bed placed in the drum was wetted drop-wise by sprinkler inserted axially into the granulator. The sprinkler was mounted on a separate stand.

The wetting liquid was supplied from tank, located 2.5 m above the drum axis and its flow rate was controlled by rotameter. During the experiment the liquid in the tank was maintained at a constant level, which guaranteed a constant flow rate of the liquid $Q = 10^{-6} \text{ m}^3/\text{s}$. The wetting liquid was distilled water, and the sprinkler ensured its uniform distribution along the entire drum length. The granular bed was wetted at a constant rate of the liquid discharge, until overwetting of the material which caused that the bed got stuck to the inner wall of the granulator. The process was carried out batch-wise, each time at steady process and equipment parameters, i.e. drum filling, rotational speed of the granulator and drum diameter. In the experiments drums of diameters 0.25, 0.3, 0.35 and 0.4 m were used. To be able to compare the results obtained for different drum diameters, we used in the experiments the values of relative velocity n_w , i.e. the rotational speed n related to the drum critical velocity n_{kr} . The relative velocity n_w was changed in the range which ensured an avalanche character of motion of the bed tumbling in the drum. Samples were taken in 60 s time intervals. On this basis bulk density of the bed and the angle of natural repose were determined. Prior to each experimental trial the torque was measured for the idle run of the apparatus.

RESULTS

The reduced moment M^* , described by the following formula, was proposed to define the processed bed dynamics

$$M^* = \frac{M - M_j}{m_s + m_w} \quad (9)$$

Examples of changes in the reduced moment M^* during granulation (wetting), i.e. with a change of bed moisture content are shown in Fig. 2. The points were obtained by averaging 60 subsequent readings of the torque made every 1 s.

Analysis of the relation $M^* = f(w)$ resulted in the determination of three ranges of the moment. The first one for the value growing approximately with the square function, until reaching a maximum, the second one – a short-term decrease called a transient range, and the third one, when the values of reduced moment are constant. To describe the effect of parameters on changes in the absolute values of torque ($M - M_j$) used for bed circulation during granulation, it was decided that – because of a different character of the relations in particular ranges – correlations should be prepared separately for two ranges of the torque change:

- for the first one in which there is an increase of the reduced moment M^* , (increase range),
- for the range in which the torque values are constant (stabilisation range).

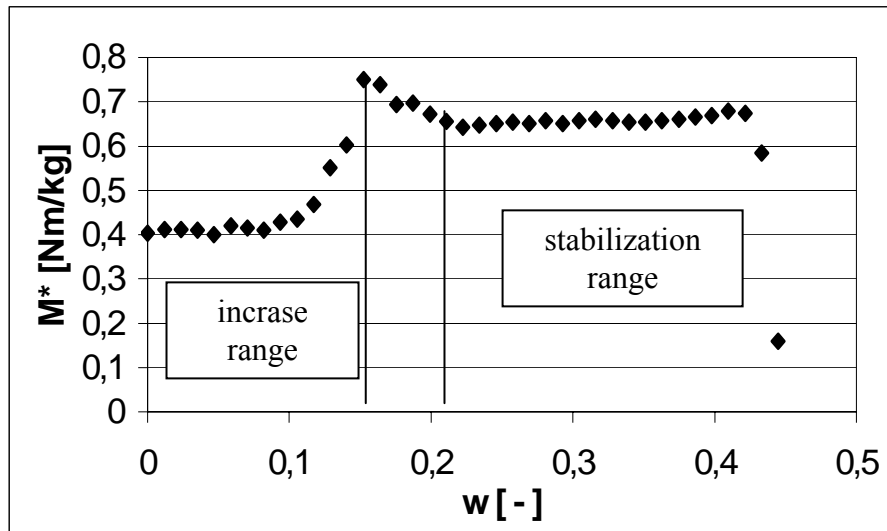


Fig. 2. Examples of changes in the reduced moment value with changing bed moisture content

Two correlation equations were obtained to calculate the torque value and analogously, two dimensionless equations describing the bed dynamics for the two mentioned stages of the process.

The effect of the tested parameters on the torque value was described by the equations:

- for the stabilisation range

$$M_{st} = 100 \cdot D^{2.87} \cdot n^{0.15} \cdot k^{0.75} \cdot \rho_n^{-0.5} \quad (10)$$

at correlation coefficient $R^2 = 0.96$

- for the increase range

$$M_{kw} = 10^{1.44} \cdot D^{2.13} \cdot n^{-0.1} \cdot k^{0.5} \cdot \rho_n^{-2.13} \cdot \text{tg}\beta^{1.21} \quad (11)$$

at correlation coefficient $R^2 = 0.905$.

Upon transformation, formulae (10) and (11) can be used to calculate power demand for granulation if the final product density is known.

Analysis of the above relations shows that in the “increase range” the torque value is affected strongly by the parameters that characterise the produced granulated material. Properties of the granular material change rapidly, so the bed tumbles irregularly which has an influence on fluctuations and an abrupt increment of the torque value. For the “stabilization range” the equipment and process parameters have a stronger effect on the bed dynamics.

Additionally, on the basis of the results obtained the values of dimensionless numbers Ne and Fr in the previously described model were calculated. This allowed us to generate the following dimensionless equations.

– For the “stabilization range”

$$Ne = \frac{100}{E_1} = f(Fr) = \frac{100}{Fr} \cdot \frac{1}{\left(\frac{D}{L}\right)^{1.2} \cdot \rho_w^{1.5} \cdot k^{-0.75}} \quad (12)$$

where relative density $\rho_w = \rho/\rho_p$

A dimensionless relation was obtained at $R^2 = 0.98$.

For the “increase range” the relation in a similar form was obtained:

$$Ne = \frac{53}{E_2} = \frac{53}{Fr} \cdot \frac{1}{\left(\frac{D}{L}\right)^{1.8} \cdot \rho_w^{3.2} \cdot \text{tg}\beta^{-1.2} \cdot k^{-0.55}} \quad (13)$$

at correlation coefficient $R^2 = 0.94$.

The above formulae of functions confirm the character of relationships between dimensionless numbers proposed in the dynamics model. The relations $Ne=f(Fr)$ for both considered ranges are presented graphically in Fig.3 and Fig. 4.

The dimensionless equations describing the process have the same character of relationship and a similar range of changes in the Euler and Froude numbers for both ranges considered. They differ only in the slopes of the straight lines, which depend on the exponents of dimensionless simplexes ($D/L, k, \rho_w$). This is a result of a different influence the particular parameters have on both granulation ranges.

For the increase range, which occurs at the beginning of the granulation when the bed movement is still unsteady, there is a much more distinct effect of the parameters that characterise the granulated bed. The value of the correlation coefficient and the scatter of points from the mean value confirm that the operation of the apparatus in this range is less stable. This is induced by an uneven tumbling of the granulated bed, which after being lifted to some height detaches and falls down suddenly in a way similar to a slope creep.

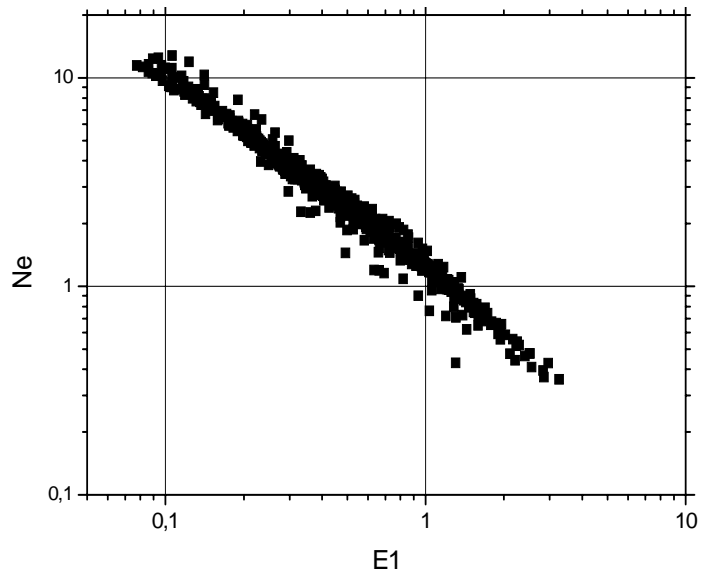


Fig. 3. Dependences of the power number on the value of E_1 describing the effect of Froude number on process dynamics for the stabilization range

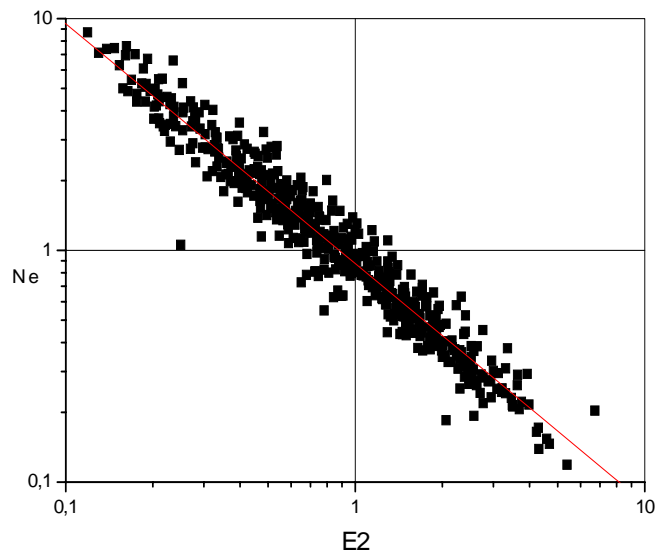


Fig. 4. Dependences of the power number on the value of E_2 describing the effect of Froude number on process dynamics for the increase range

In the case of the stabilisation range a much lesser scatter of the values from the centre line can be observed which gives evidence of a smooth operation and a stronger influence of parameters connected with the values that describe the process conditions.

CONCLUSIONS

1. The proposed model of the process and experimental results show that the bed dynamics during drum granulation can be described by the dimensionless equations presenting relationships between power number, Froude number and dimensionless parameters characterising the granulated product, and also process and equipment parameters. The increment of power number is inversely proportional to changes in the Froude number for all stages of the process.
2. Analysis of changes of the reduced moment M^* (parameters of the dynamic process) shows that it increases on the initial stage of granulation and then it assumes constant values. Changes of the granulated product properties at this stage of the process do not affect significantly the behaviour of the entire bed.
3. Correlations in which the torque depends on the operating parameters and granulated product properties were obtained. They are useful in designing the energy aspect of the apparatus.

ACKNOWLEDGEMENT

The work was carried out under research project W-10/21/2004/BW

NOMENCLATURE

m_s	– mass of loose material placed in the drum [kg]
$m_w = Q t_n \rho_n$	– mass of the wetting liquid added [kg]
M	– moment on the granulator shaft [Nm]
M_j	– moment of idle run for [Nm]
M^*	– moment reduced on the granulator shaft [Nm/kg]
N	– power supply [W]
t_n	– wetting time [s]
Q	– volumetric flow rate of wetting liquid [m^3/s]
ρ	– density [kg/m^3]
$\rho_w = \rho / \rho_p$	– relative density [kg/m^3]
ρ_p	– powder density [kg/m^3]
β	– angle of natural batching
ω	– angular velocity of the apparatus [s^{-1}]
n	– rotational speed of the apparatus [rpm]
w	– moisture content
A	– constant
Ne	– power number
Fr	– Froude number
$E_{1,2}$	– parameters describing bed dynamics during granulation

REFERENCES

- ARBITER N., HARRIS C.C., 1982, *Scale-up and dynamics of large grinding mills – a case study*. In: A.L. Mular and G.V. Jergensen II (Editors), *Design and Installation of Comminution Circuits*. AIME, New York, Ch. 26, pp. 491-508.
- DIRGE M., SANDVIK K.L., *Mineralteknikk*. NTH, Trondheim 1990 and earlier editions back to 1968. (In Norwegian).
- GAO M.W., 1990, *Optimization scale up and simulation of tumbling mills.*, Thesis. Luela University of Technology.
- GUSIEW J.I., 1966, *Dwizenie materiała w granulatorach barabannowo typu*. Chemiczeskoe i neftanoe maszynostroenie. Nr 11.
- HEIM A., GLUBA T., KOCHAŃSKI B., OBRANIAK A., ZAŁUGA T., 1995, *Kształt przekroju poprzecznego warstwy ziarnistej w bębnie obrotowym*, Inż. Chem. i Proc., 1, 95-116.
- HEIM A., GLUBA T., OBRANIAK A., 1995, *Zapotrzebowanie mocy do napędu granulatora bębnowego*, V Ogólnopolskie Sympozjum GRANULACJA, Puławy.
- HEIM A., GLUBA T., KOCHAŃSKI B., OBRANIAK A., ZAŁUGA T., 1994, *Warunki pracy bębna obrotowego z wypełnieniem ziarnistym*, XIV Ogólnopolska Konferencja Teorii Maszyn i Mechanizmów.
- HEIM A., GLUBA T., OBRANIAK A., 1997, *Prędkość ziaren wsadu w warstwie przyściennej bębna obrotowego*, Inż. Chem. i Proc., 18, 1, 133-141.
- HEIM A., GLUBA T., OBRANIAK A., 1999, *Investigation of torque during drum granulation*, Fizykochemiczne Problemy Mineralurgii, XXXVI Symposium, Wrocław, in Polish.
- HOGG R., FUERSTENAU D.W., 1972, *Power relationships for tumbling mills*. Trans. SME-AIME, 252: 418-423.
- KAPUR P.C., RANJAN S., FUERSTENAU D.W., 1992, *A cascade-cataract charge flow model for power draft of tumbling mills*. Int. J. of Miner. Proc., 36: 9-29.
- KANTOWOWICZ Z.B., 1959, *Maszyny przemysłu chemicznego*, PWT W-wa.
- KOROTICZ W.I., 1966, *Teoreticzeskije osnovy okomkowania żelezorydnych materiałow*. Metallurgia.
- ROSE H.E., SULLIVAN R.M.E., 1958, *Treatise on the Internal Mechanics of Ball, Tube and Rod Mills*. Chemical Publishing Co., New York.
- WEIDENBAUM S.S., 1958, *Mixing of Solids*, Advances in Chemical Engineering, Vol. 2 Acad. Press Inc., New York.

Heim A., Gluba T., Obraniak A., *Dynamika złoza podczas granulacji bębnowej*, Physicochemical Problems of Mineral Processing, 38, (2004) 167-176 (w jęz. ang.).

W pracy przedstawiono wyniki badań dotyczących dynamiki granulowanego złoza podczas prowadzenia procesu aglomeracji w bębnach obrotowych. Badania prowadzono w granulatorach przy ciągłym nawilżaniu złoza wodą, co powodowało, że przyjęcie jako zmiennej niezależnej czasu nawilżania bądź wilgotności złoza było tożsame. Jako parametry zmienne stosowano: średnicę bębna D od 0.25 do 0.4 m, stopień wypełnienia bębna surowcem k w zakresie 5-20% objętości wewnętrznej bębna, prędkość obrotową bębna w zakresie $n=10-32$ obr/min. Podczas granulacji mierzono wartości momentu obrotowego na wale aparatu. W stałych odstępach czasowych równych 1 min. pobierano z bębna próbki, na podstawie których określano kąt naturalnego usypu uzyskanego produktu, a także jego gęstość nasypową. W pracy zaproponowano również kryterialne opisujące dynamikę złoza w trakcie procesu granulacji.

Tadeusz GLUBA, Andrzej OBRANIAK, Estera GAWOT-MŁYNARCZYK*

THE EFFECT OF GRANULATION CONDITIONS ON BULK DENSITY OF A PRODUCT

Received April 15, 2004; reviewed; accepted June 8, 2004

Changes in bulk density of a bed during wet granulation of silica flour in a batch drum granulator were studied. Three size fractions of the flour were used in the studies. They differed in the particle size composition and mean particle dimension. Variable parameters were the wetting conditions (droplet diameter, degree of bed saturation) and particle size composition of the raw material. The bed of loose material was wetted while tumbling, at a constant volumetric flow rate, using a system of two pneumatic spray nozzles. In each trial at determined time intervals feed samples were taken from the drum to specify the particle composition and bulk density of granulated material at a given stage of the process. The effect of droplet diameter, mean size of raw material particles and the saturation of granulated bed on changes in the bulk density of a product was estimated. A correlation equation describing the effect of tested parameters on bulk density changes was proposed.

Key words: drum granulation, bulk density

INTRODUCTION

One of significant parameters that describe properties of granular materials is their bulk density. For granulated materials this parameter is of special importance. By selecting proper conditions of granulation process a product of possibly high density can be obtained, which has an influence on a better utilisation of storage area and means of transport. Bulk density of a granulated product depends both on raw material properties (density, particle size composition), concentration of particles in the formed granules (granule porosity), and on the obtained particle size distribution on which the volume of intraparticle space depends [Gluba and Grabowski (2001), Podczeczek and Lee-Amies (1996)]. In the process of granulation bulk density of the processed bed undergoes systematic changes that are related both to the mechanisms of formation

* Technical University of Lodz, Faculty of Process and Environmental Engineering
Stefanowskiego 12/16, 90-924 Lodz, Poland, gluba@wiposp.lodz.pl

and growth of agglomerates, their concentration, and also the mechanisms of destruction. Problems related to the effect of granulation conditions on bulk density of a product are not frequently discussed in literature. Obraniak (2002) presented changes in bulk density of granulated material produced from foundry bentonite in reference to process and equipment parameters and wetting time. He obtained a linear relation of bulk density changes with the time of granulation. Zuurman et al. (1995) conducted studies on the effect of a binding agent on bulk density and compactibility of granules of two types of lactose, using two different wet granulation techniques. They found that efficiency of the binder increased with a decrease of bulk density of the granulated bed. Yu et al. (1995) studied the effect of moisture content on coal agglomeration and bulk density. They observed among the others that the density of agglomerates increased with an increase of moisture content to a certain maximum, and next it started falling down, while bulk density of the bed decreased with an increase of moisture content to some minimum and then it started growing.

So far, the bulk density of a granulated bed has been investigated for selected groups of materials, which made it impossible to propose general relations. Additionally, there are no studies in which the effect of other parameters (beside moisture content) that characterise bed wetting is taken into account.

AIM OF STUDIES

The aim of studies was to assess the effect of bed wetting conditions and particle size of raw material on changes in the bulk density of feed during wet drum granulation.

EXPERIMENTAL SET-UP AND METHODOLOGY

Granulation was carried out batch-wise in a horizontal drum of diameter $D=0.5$ m and length $L=0.4$ m. The drum was driven by an electric motor through a toothed gear and belt transmission. In the entire series of investigations a constant rotational speed of the granulator $n=20$ rpm was applied and a constant volumetric degree of drum filling with the raw material $k=0.1$, determined in reference to the bulk density of loosely packed material was used. A tested material consisted of three size fractions of silica flour from Strzeblowska Mine of Mineral Raw Materials at Sobótka. Particular fractions denoted by the symbols MK 0,056, MK 0,075 and MK 0,10 differed in the maximum particle size and range of particle size composition. For each raw material the basic physical properties were determined. The particle size distribution was estimated by means of a laser particle analyser ANALYSETTE 22, and on this basis the mean particle size d_z was determined. Raw material density ρ_s and bulk densities in the material loosely packed ρ_{bl} and concentrated to the minimum volume ρ_{bc} were also determined. Fine-grained material placed in the drum was wetted while tumbling by means of two pneumatic spray nozzles introduced axially into the drum. Constant

flow rate of the wetting liquid (distilled water) through the nozzles, equal to $Q_w=12 \cdot 10^{-3} \text{ m}^3/\text{h}$ was applied. Changes in the wetting liquid dispersion (droplet size) were obtained by changing the rate of air flow through the nozzles in the range $Q_p=1$ to $3 \text{ m}^3/\text{h}$. Droplet size distribution in the dispersed stream at specified parameters of nozzle operation, characterised by the dispersion degree $q=Q_w/Q_p$, was measured by a DANTEC laser analyser. On the basis of these distributions, the mean droplet diameters d_k obtained at given parameters of nozzle operation were calculated. The operating parameters of the nozzle used in the investigations are given in Table 1. Each time, a determined volume of the binding liquid was supplied to the bed. The volume was determined for a specified value of feed saturation degree S , taken as a ratio of the volume of the added liquid to the volume of intraparticle space in the loosely packed material in the drum. Granulation was studied at three degrees of saturation $S = 0.32, 0.34$ and 0.36 . After wetting the process of granulation was continued until the moment when water pressed from the granules onto their surface caused intensive sticking to the drum walls hampering in this way a further process. In determined moments samples were taken from the drum and on their basis properties of the formed granulated product were specified. The first sample was taken immediately after the wetting had been finished ($t_g=0$), and the last one after completing the process. The particle size composition was determined on the basis of screen analysis and bulk density was calculated on the basis of the mass and volume of a sample placed in a measuring cylinder (after subtracting the mass of water contained in it).

Table 1. Operating parameters of spray nozzles

Q_w	Q_p	q	d_k
$[\text{m}^3/\text{h}]$	$[\text{m}^3/\text{h}]$	$[-]$	$[\mu\text{m}]$
0.012	1.0	0.0120	235.70
0.012	1.5	0.0080	211.90
0.012	2.0	0.0060	194.11
0.012	2.5	0.0048	154.16
0.012	3.0	0.0040	143.90

RESULTS AND DISCUSSION

On the basis of analysis of samples taken immediately after finishing the wetting it was found that the bed contained both non-granulated raw material and a specified percent of nuclei and still weak granules. Mutual quantitative proportions between the finest fraction (of dimensions $< 1 \text{ mm}$), containing non-granulated material and nuclei of granules and bigger agglomerates appeared to be dependent on the bed wetting conditions and also on particle size of the raw material. Percentage of the smallest size fraction in the bed was in the range from 40 to 60%. Structure of the bed formed after

wetting had an immediate influence on its bulk density. The effect of particle size of the raw material and wetting parameters on the bulk density of the bed (after wetting) was described by the power function of several variables. As a result of regression, equation (1) with the correlation coefficient $R = 0.93$ was obtained:

$$\rho_{bn} = A \cdot d_k^{0,32} \cdot d_z^{0,37} \cdot S^{-1,8} \quad (1)$$

where A is constant.

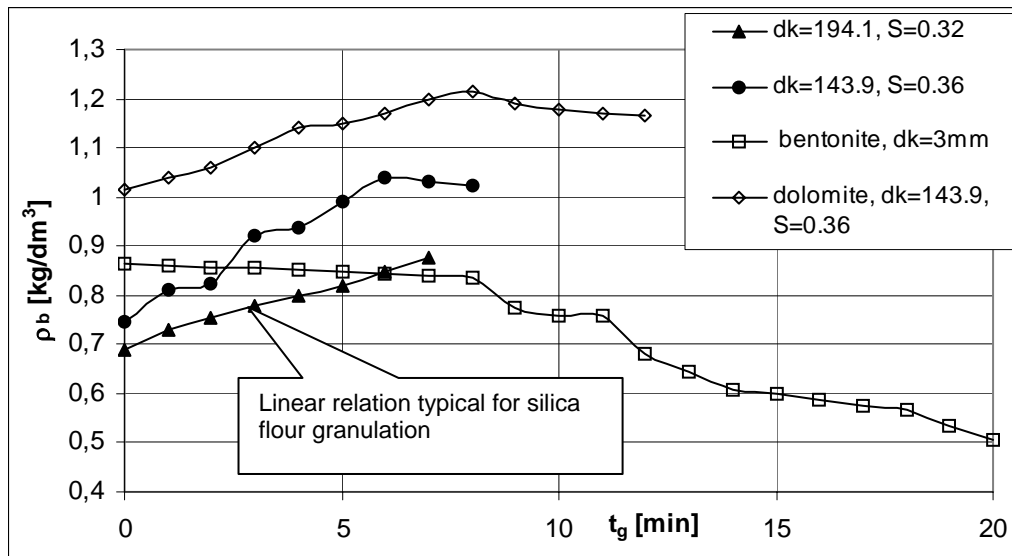


Fig. 1. Examples of changes in the bulk density of the bed during granulation

At the further stage of the process (granulation) systematic changes in the granulated bed properties took place leading to changes in bulk density of the bed. An example of changes in bulk density of the granulated bed of silica flour compared to the results obtained for other materials (dolomite and foundry bentonite) [Gluba (2003), Obraniak (2002)] is shown in Fig. 1. For most trials with silica flour a linear increase of bulk density with granulation time was obtained. In certain process conditions when a longer time of granulation was required, changes of bulk density in time departed from linearity (e.g. for $d_k=0.1439$). Analogous relations were obtained during dolomite granulation in similar wetting conditions. The required granulation time for this material was usually longer than for silica flour, which had an effect on the character of changes in bulk density (the presence of an extremum). A different character had the changes observed during bentonite agglomeration. In this case the process mechanism was different; in the whole granulation period wetting liquid in the

form of droplets with uniform size (about 3 mm) was supplied to the bed at low wetting intensity.

The differences observed in particular cases are a consequence of the dominance of various mechanisms of formation and growth of agglomerates at different stages of the process. To explain this problem some theoretical analysis should be made.

Bulk density of the feed during granulation can be determined on the basis of its mass m and volume V using the formula:

$$\rho_b = \frac{m}{V} \quad (2)$$

The mass of processed feed m is a sum of solid mass m_s and the mass of supplied wetting liquid m_w , while the volume of the bed consists of the volume of material particles V_s , binding liquid volume V_w and air volume V_p , hence:

$$\rho_b = \frac{m_s + m_w}{V_s + V_w + V_p} \quad (3)$$

The mass of raw material particles m_s is constant during the process, but the proportions between the mass of particles that form agglomerates and the mass of still non-granulated powder are changing continuously. A total volume of all particles in the bed V_s has also a constant value. The volume of air contained in the bed prior to wetting can be determined on the basis of the bulk density of a given raw material ρ_{bs} and specific density ρ_s . Changes in this volume during the process are very complex and difficult to describe because of a simultaneous interaction of many mechanisms that determine the formation, growth and also destruction of agglomerates.

From the practical point of view important is the bulk density of a dried product. In this case, when air of the same volume replaced the evaporated liquid, bulk density can be defined by the equation:

$$\rho_b = \frac{m_s}{V_s + V_w + V_p} = \frac{m_s}{\frac{m_s}{\rho_s} + \frac{m_w}{\rho_w} + V_p} \quad (4)$$

Substituting the relation for bed moisture content into equation (4)

$$w = \frac{m_w}{m_s} \quad (5)$$

form (6) is obtained:

$$\rho_b = \frac{1}{\frac{1}{\rho_s} + \frac{w}{\rho_w} + \frac{V_p}{m_s}} \quad (6)$$

Due to constant value of the final bed moisture content w (in a given trial) and raw material mass m_s and taking into account that specific powder density ρ_s and water density ρ_w do not change during the process, the above relation shows that changes in bulk density of the granulated bed ρ_b at the stage of granulation depend only on changes in the volume of air contained in the bed V_p .

To determine monotonicity of the above relation, the differential should be calculated:

$$\frac{d\rho_b}{dt} = \frac{-1}{\left(\frac{1}{\rho_s} + \frac{w}{\rho_w} + \frac{V_p}{m_s}\right)^2} \cdot \frac{1}{m_s} \cdot \frac{dV_p}{dt} \quad (7)$$

In order to set up the sign of this relation the differential dV_p/dt should be analysed.

The air in the granulated bed can be contained in the formed granules (V_1), between these granules (V_2) and between particles of still non-granulated raw material (V_3).

Hence:

$$\frac{dV_p}{dt} = \frac{dV_1}{dt} + \frac{dV_2}{dt} + \frac{dV_3}{dt} \quad (8)$$

Owing to the fact that the percentage of non-granulated particles decreases with the process, the value of V_3 decreases which brings about a negative value of derivative of this component after the granulation. Along with the granulation time the formed agglomerates are concentrated which results in a systematic decrease of pore size inside the granules leading to negative dV_1/dt . Changes in the volume V_2 are a result of changes in granule compactibility in the bed which depends on its homogeneity. Results of investigations on drum granulation obtained in this study as well as those presented by other authors [Gluba and Heim (2000)] show that with the granulation time grows monodispersity of the processed bed (Fig. 2) which causes that spaces between the formed granules increase. This is confirmed by the presented relation of changes in bed homogeneity coefficient s/d with the granulation time (where s – standard deviation, and d – mean particle size). It can be observed that despite decreasing values of the coefficient s/d (the bed homogeneity increase) bulk density determined for both dry and wet product increases.

Summing up the above considerations, the character of the effect of particular volume components can be presented in the form of inequality:

$$\frac{dV_2}{dt} > 0, \quad \frac{dV_1}{dt} < 0, \quad \frac{dV_3}{dt} < 0 \quad (9)$$

Taking the above into account, it can be stated that during the process of wet tumbling granulation changes in the bulk density may be both increasing and decreasing – depending which of the mentioned derivatives has a decisive influence in a given stage of granulation. So, it can be concluded that the character of changes depends both on the loose material properties and process parameters. To explain the impact of particular parameters applied in the investigations the obtained results should be analysed thoroughly.

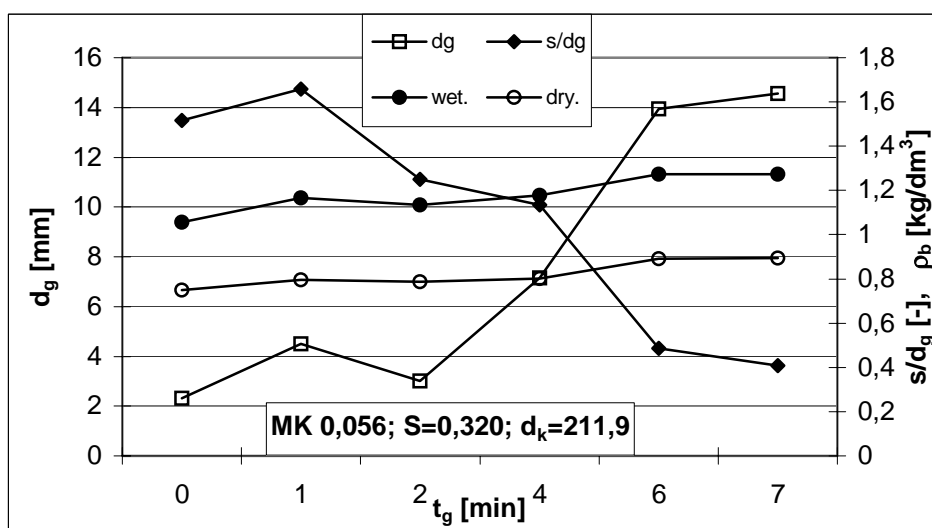


Fig. 2. Comparison of changes in bulk density of wet and dry granular material, variability coefficient and mean granule diameter during granulation

When considering changes of the bulk density as a function of granulation time (Fig. 3), for materials of different particle size composition, at constant saturation and the same droplet size it was found that for the materials with bigger particles, the bulk density is higher. This character of the obtained relations is related both to the compactibility of the particles in the formed granules, to the packing of the granules in the bed, and to the mean distance between the particles of non-granulated raw material. Fine-grained materials used in the study were characterised by a growing range of particle size composition with an increase of the mean particle size (a simultaneous growth of d_z and s/d_z). For these materials, with an increase of the mean

particle size, it is possible to reach denser packing of particles in the granules, which is followed by a general increase of the bed bulk density. The study has shown that during the process of granulation there is a systematic unification of the particle size composition (a decrease of variability coefficient s/d_g) which in turn has an effect on the compactibility of granules in the bed. It was observed that with an increase of the mean size of raw material particle the bed in the same process conditions becomes less homogeneous (s/d_g increases). This means that the bed obtained from the material of bigger particles is characterised by a denser packing of granules, which influences its bulk density increase.

Results of the studies revealed also a significant effect of dispersion of the wetting liquid stream (droplet size) on the process of granulation and consequently on the bulk density of the processed bed. A comparison of changes in the bulk density of feed during the process of granulation for different mean size of droplets is shown in Fig. 4. It follows that the feed bulk density increases with an increase of wetting liquid droplets [Gluba (2002)]. Bigger droplets enable formation of stronger liquid bridges which as a result leads to bigger condensation of particles in the granules. Additionally, the bed wetted with bigger droplets is characterised by higher polydispersity. These two factors have an influence on the increase of bulk density of the bed with an increase of droplet size during wetting.

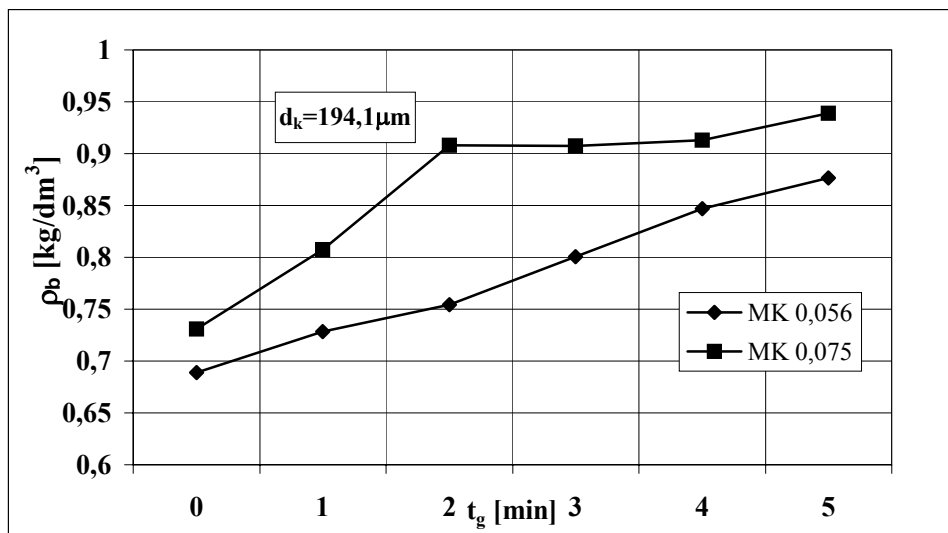


Fig. 3. Comparison of bulk density changes during granulation for the same droplet size and two types of raw material ($S = 0.320$)

On the stage of granulation, after wetting, continuous transformations induced by the mechanisms of formation, growth and destruction of agglomerates take place in the bed. A result of these transformations is an increase of the size of granules,

condensation of their inner structure and change in the particle size composition. These transformations being a determined function of granulation time lead also to specific changes in the bed bulk density. The change in bulk density of the bed in time is a combination of these transformations of the bed properties dependent on the properties of raw materials and process parameters.

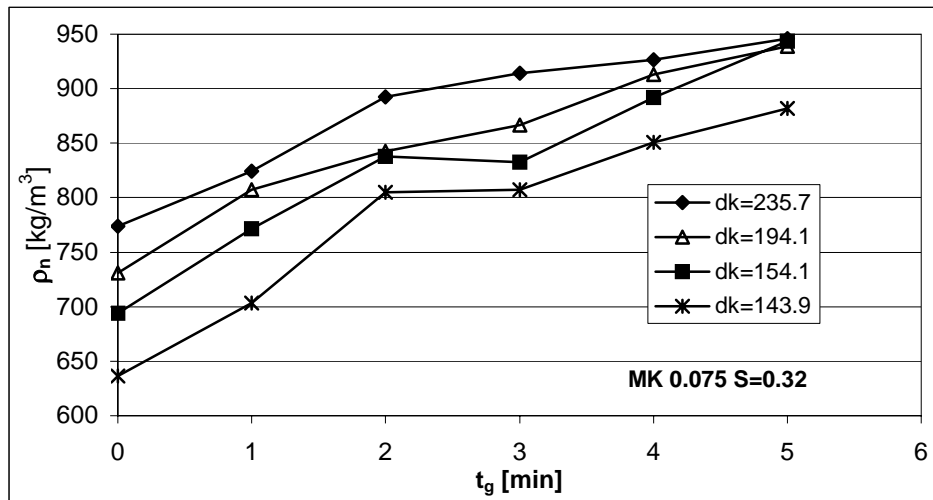


Fig.4. Comparison of bulk density changes during granulation for different droplet sizes

The effect of tested parameters on the increment of the bed bulk density at the stage of granulation is described by the power relation:

$$\rho_b - \rho_{bn} = B \cdot d_k^{0,3} \cdot d_z^{3,5} \cdot t \quad (10)$$

where B is constant.

The above relation was obtained at the correlation coefficient $R = 0.96$.

CONCLUSIONS

1. During wet drum granulation of silica flour, bulk density of the processed bed increases linearly in time;
2. The value of bulk density after wetting depends on the conditions of bed wetting (dimensions of the wetting liquid droplets and bed saturation) and on the size of raw material particles;
3. An increase of bulk density of the bed during granulation depends on the size of raw material particles and wetting liquid droplets;
4. The effect of tested parameters on the increase of bulk density of the bed during the process can be described by the power equation.

ACKNOWLEDGEMENT

The study was carried out within the research project no. 4 T09C 023 22 sponsored by KBN in the years 2002-2005.

REFERENCES

- GLUBA T. (2003), *The effect of wetting droplet size on the growth of agglomerates during wet drum granulation*, Powder Technology 130, 219-224
- GLUBA T. (2002), *The effect of bed wetting conditions on the quality of a product obtained during drum granulation*, 15th International Congress CHISA
- GLUBA T., GRABOWSKI R. (2001), *The effect of wetting conditions on granule porosity*, Prace Naukowe Instytutu Górnictwa Politechniki Wrocławskiej 95, Konferencje 31, 15-24
- GLUBA T., HEIM A. (2000), *Wzrost aglomeratów w procesie mokrej granulacji bębnowej surowca mineralnego o różnym składzie ziarnowym*, Inż. Chem. i Proc., 21, 329-344
- OBRANIAK A. (2002), *Dynamika złoża ziarnistego w poziomych bębnach obrotowych*, Praca doktorska, Wydział Inżynierii Proc. i Ochrony Środowiska PŁ
- PODCZECK F., LEE-AMIES G. (1996), *The bulk volume changes of powders by granulation and compression with respect to capsule filling*, International Journal of Pharmaceutics, 142, 97-102
- YU A.B., STANDISH N., LU L. (1995), *Coal agglomeration and its effect on bulk density*, Powder Technology, 82, 177-189
- ZUURMAN K., BOLHUIS G.K., VROMANS H. (1995), *Effect of binder on the relationship between bulk density and compactibility of lactose granulations*, International Journal of Pharmaceutics, 119, 65-69

Gluba T., Obraniak A., Gawot-Młynarczyk E., *Wpływ warunków granulacji na gęstość nasypową produktu*, Physicochemical Problems of Mineral Processing, 38, (2004) 177-186 (w jęz. ang.).

Przeprowadzono badania zmian gęstości nasypowej podczas procesu granulacji mączki kwarcowej w granulatorach bębnowych. W badaniach parametrami zmiennymi były: parametry nawilżania tzn.: średnica kropli, współczynnik saturacji oraz skład ziarnowy surowca. Złoże materiału sypkiego nawilżano kropłowo w czasie jego ruchu przesypowego, przy stałym objętościowym natężeniu dopływu cieczy, za pomocą zestawu dwóch dysz pneumatycznych zapewniającego równomierne podawanie cieczy zwilżającej. Podczas każdej próby mierzono w stałych odstępach czasowych skład ziarnowy i gęstość nasypową granulatu na danym etapie procesu. Przeprowadzono ocenę wpływu średnicy kropeł, średniego wymiaru surowca oraz saturacji granulowanego złoża ziarnistego na zmianę gęstości nasypowej produktu. Zaproponowano równanie korelacyjne opisujące wpływ w/w parametrów na zmianę gęstości nasypowej.

Ludwik DOMKA^{*}, Maciej KOZAK^{**}

TRIBOCHEMICALLY ACTIVATED NATURAL CHALK AS A FILLER FOR PLASTO- AND ELASTOMERS

Received May 24, 2004; reviewed; accepted 29 June, 2004

Physicochemical evaluation of chalk limestone subjected to tribochemical activation with or without a promoter of adhesion and strengthening is given. The powder materials processed in an electro-magneto-mechano-chemical reactor have undergone evident transformations, which increased their capacity to react and which involved:

- creation of additional network effects,
- formation of new surfaces which, due to deformations, are particularly reactive,
- development of additional network deformations due to the increased surface to volume ratio.

Dispersion and particle morphology were studied by scanning electron microscopy (SEM) and dynamic light scattering (DLS), moreover tap and bulk density, capacities to absorb water and dioctyl phthalate were evaluated. The chalk samples ground in the electro-magneto-mechano-chemical reactor demonstrated highly uniform granule size, usually smaller than 1 μm , measured by SEM and DLS.

Key words: chalk, chemical and mechanical modification of surface, microstructure

INTRODUCTION

In cases of plastics, ground natural chalks, limestone and various types of precipitated calcium carbonate can be used as fillers (Wypych, 1999). The precipitated calcium carbonates in particular exceed other CaCO_3 - based fillers in respect to whiteness and, first of all, in respect to the extent of disintegration. The application of

^{*}Technological Centre, A.Mickiewicz University, Grunwaldzka 6, 60-780 Poznań, mkozak@amu.edu.pl

^{**}Department of Macromolecular Physics, A. Mickiewicz University, Umultowska 85, 61-614 Poznań

modified chalk and carbonate fillers clearly improves physicomechanical properties of plasto- and elastomers (Wypych, 1999; Gächter and Müller, 1987). The modifiers can be fatty acids or their derivatives (Tabtiang and Venables, 2000; Domka et al., 1999), surfactants (Domka et al., 2002), coupling agents (Demjén et al., 1997; Plueddemann, 1991; Mittal, 1992; Domka, 1993, Domka, 1994) and, in particular, titanate proadhesive compounds (Domka, 1996). Recently, the surface modification with a combination of action of modifying agent and the mechano-chemical effect of ultrafine grinding was studied in surface modification of calcium carbonate particles by polymer grafting (Wua and Lu, 2003).

In processing of plastics, chalks are most frequently used as fillers. Due to the relatively low adsorption of plasticisers and stabilisers on the chalk surface, the latter may be introduced to plastics in relatively high amounts. The amount of the introduced filler may vary from 5 to 100 weight parts per 100 weight parts of polymers, depending upon the required physical properties of the product (Domka, 1979). Chalks used in polymer processing should be fully neutral towards the plastic and the applied supplements, should be thermostable, capable of rapid and easy formation of a dispersion in the plastic, should exhibit low adsorption of softeners, should not exert negative effects on mechanical properties of the plastic, should be white in colour, possibly homogeneous and relatively inexpensive (Wypych, 1999; Ishida, 1988; Katz and Milewski, 1987). Also the particle size distribution of filler is one of the most important parameters in the reactivity of such materials. Therefore, development of new grinding methods such as Hicom mill (Braun et al., 2002; Hoyer and Morgan, 1996; Hoyer, 1999) or electro-magneto-mechanical mill (Binczyk et al., 2001) is highly relevant.

EXPERIMENTAL

The studies were performed on the chalk limestone from the Sobków deposits, near Kielce (Poland). The limestone was subjected to processing by liquid classification, by removal of particles of the larger size. For the studies the chalk was dried and passed through the 6.3 μm sieve. The applied chalk consisted of:

- CaCO_3 - 96.8%,
 - MgCO_3 - 2.3%
 - insoluble residue (IR) - 0.70%,
 - Fe - 0.03%,
 - Mn - 0.02%,
 - Cu, Pb - traces,
 - H_2O - 0.15%,
- and showed:
- specific gravity - 2.59 g/cm^3 ,
 - specific area - 8.6 m^2/g ,

- bulk weight - 0.74 g/cm³,
- dominating crystal structure - calcite type.

The Sobków chalk was modified with fatty acids (maleic acid and stearic acid) and acrylic acid. The natural chalk was modified in two ways: in the electro-magneto-mechano-chemical reactor (Domka et al., 1999; Polechonski et al., 1996) and by depositing of the adhesion promoter from the solution (Domka et al., 2002; Domka, 1993; 1994; 1996). Each time, the modifier (adhesion promoter) was deposited on the chalk in the below described way (1 weight part of the modifier was used per 100 weight parts of the chalk). The carboxylic acids were dissolved in the mixture of methanol or isopropanol and water (at the ratio of 1:1 or 3:2). The final acids concentration in modification solution was 1% (w/v). The modification was performed in a spherical flask of 500 cm³ capacity, in a vacuum evaporator, in 1 h at room temperature. Subsequently, the samples of the chalk with the solution were left for 24 h. Then, the solvent was evaporated in an evaporator, at an increased pressure, at approx. 80 °C and the modified chalk was dried in a stream of hot air, at 100 °C. If needed, the chalk aggregates were disintegrated in a mortar and passed through a sieve of a mesh diameter 6.3 μm. The modification was performed also in an electro-magneto-mechano-chemical reactor (Binczyk et al., 2001; Polechonski et al., 1996). The reactor used the energy field generated in the reactive chamber by a rotating electromagnetic field and a ferromagnetic dipole movement. The reactor permits intensification of a number of technological processes due to a simultaneous and complex action on the processed media of several varying physical energy fields, including the electric, magnetic, acoustic, temperature fields, high pressures and friction. The media processed, contained in the reactive chamber, i.e. in the zone of moving ferromagnetic dipoles, are subjected to intense mixing and dispersion due to strong ultrasonic fields, high pressures and friction. In parallel, the media are affected by the heat field, variable electric and magnetic fields of pronounced gradients and intensities which evoke a number of complex electrochemical and magnetochemical phenomena. This causes that in several technological processes application of the reactor is of a unique significance and practically cannot find an equivalent in the other equipment known and applied till now (Binczyk et al., 2001).

The size distribution of the chalk particle agglomerates and aggregates was estimated using a lab-made system by dynamic light scattering (DLS) method with a laser light source of 635 nm.

Morphology of the filler was observed by scanning electron microscopy. SEM micrographs were taken using Philips SEM 515 field emission scanning electron microscope. The beam voltage used was 12 - 15 kV. The powdered sample, intended for the studies, was dispersed in t-butanol and, following sedimentation on a microscope holder, it was coated with gold in an ionisation chamber.

Surface areas of the chalk powders were determined by nitrogen adsorption (the BET method) using an ASAP 2010 instrument (Micrometrics Instrument

Corporation). The sizes of the pores of the fillers were also examined. All samples prior to the measurements were heated at 120 °C for 2 hours.

RESULTS AND DISCUSSION

Some physicochemical properties of the chalk samples after their modification are listed in Table 1.

Table 1. Principal physicochemical properties of the tested chalk samples

Parameter	Natural chalk	Chalk ground for 30 s	Chalk ground for 60 s
Bulk density (g/dm ³)	740	540	500
Tap density (g/dm ³)	1480	624	630
Whiteness (%)	90.0	90.8	91
Specific area (m ² /g)	8.6	10.5	11.1

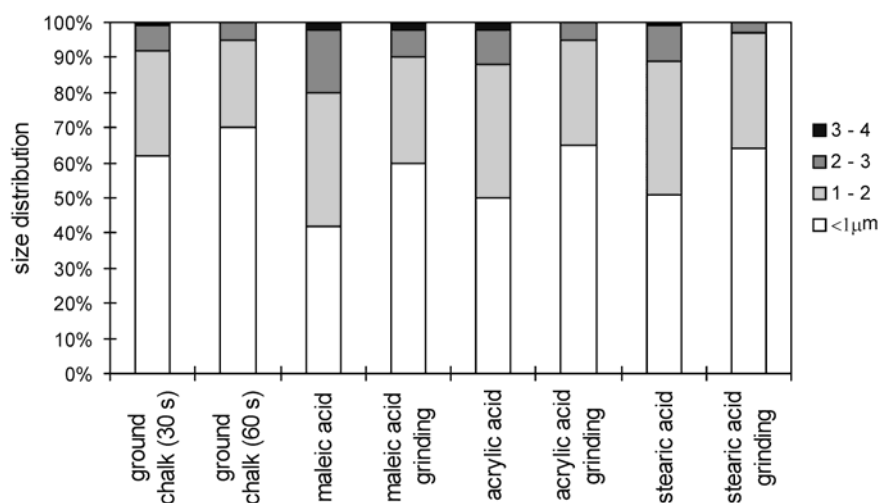


Fig. 1. Chalk granule size distribution determined using electron microscope photograms

As indicated by the Table 1 data, tribochemical modification promoted alteration of the surface character (evident increase in specific area and decrease in size of CaCO₃ particles - lowered tap density). The chalks modified with various acids contain also particle aggregates of significant size, linked to the preparation of the granule surface. However, the aggregates did not have much significance and disintegrated in the equipment used to homogenise the filler with the polymer.

The size distributions of chalk granules, determined using electron microscopy photograms, are shown in Figures 1 and 2.

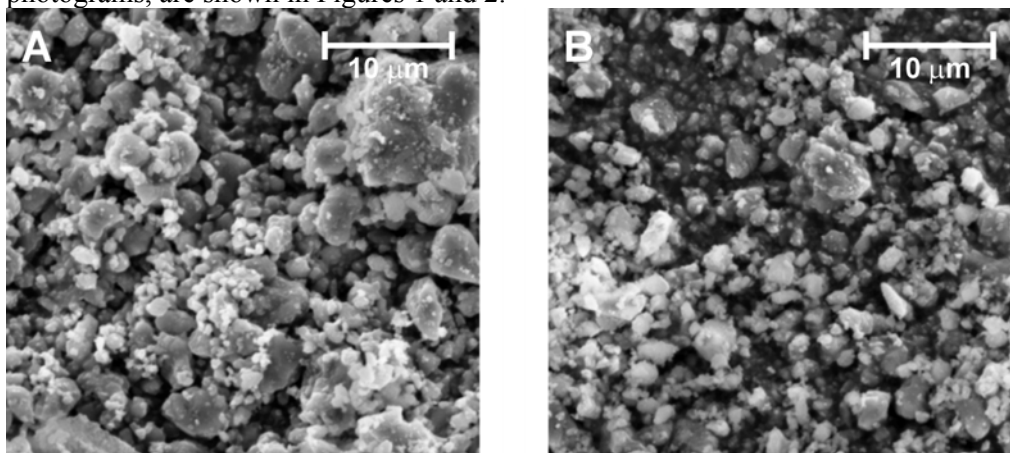


Fig. 2. SEM micrographs of natural chalk (A) and after grinding (60 s) in the electro-magneto-mechanico-chemical reactor (B)

The size distributions of the chalk particles before and after tribochemical activation with and without a coupling agent, determined by DLS, are presented in Table 2 and Figure 3. In the natural chalk, the small (primary) particles form a strong band (particle diameter range 780 – 1150 nm). The maximum intensity (100) corresponds to a particle diameter of 1010 nm. Also, as demonstrated in Figure 2, the electron micrograph shows some primary agglomerates of particles (aggregates). The mean diameter of the particles of unmodified chalk was 910 nm and the polydispersity was 0.112. Between 2110 and 3200 nm there was a band (maximum intensity of 21 at 2330 nm) which could be ascribed to secondary agglomerates in the chalk.

In the particle size distribution of the tribochemically modified chalk (after grinding for 30 s), the strongest band was present within the range of 720 to 1064 nm (a maximum intensity of 100 corresponded to a particle diameter of 905 nm). The second band was observed between 1890 and 2810 nm (with maximum intensity of 17 at 2205 nm). The mean diameter of the particles of tribochemically modified chalk was 892 nm and the polydispersity was 0.099.

The chalk after 60 s grinding was characterised by two other bands: 641 to 1020 nm (maximum at particle diameter 822 nm) and 1905 to 2688 nm (maximum intensity of 9 at 2109 nm). The mean diameter of the chalk particles was 835 nm and the polydispersity was 0.092. The detailed analysis of the change in the mean particle diameter and polydispersity of the chalk modified with various proadhesive compounds (Table 2) clearly shows that these values decreased significantly on modification in the electro-magneto-mechano-chemical reactor.

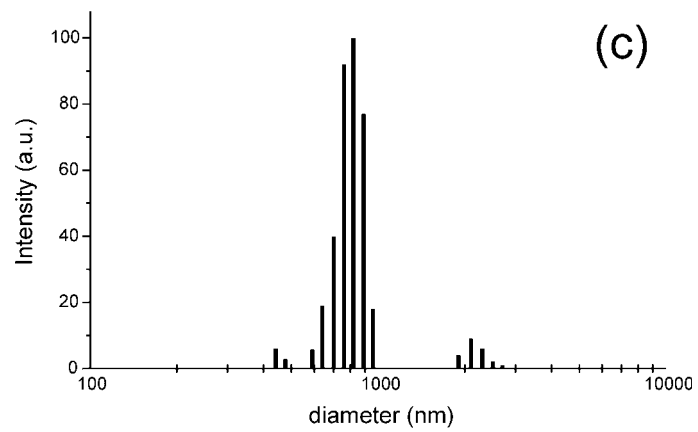
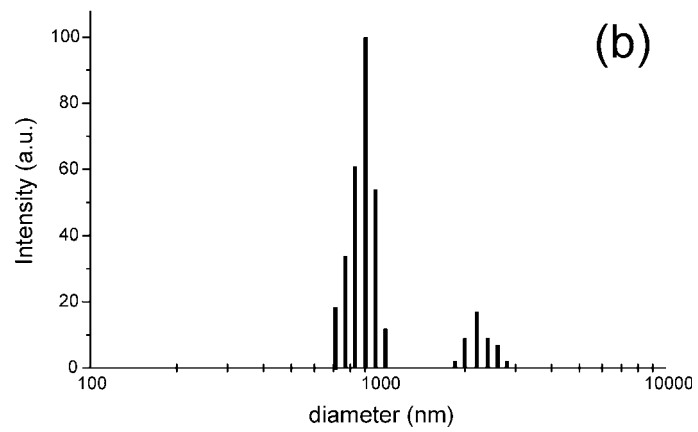
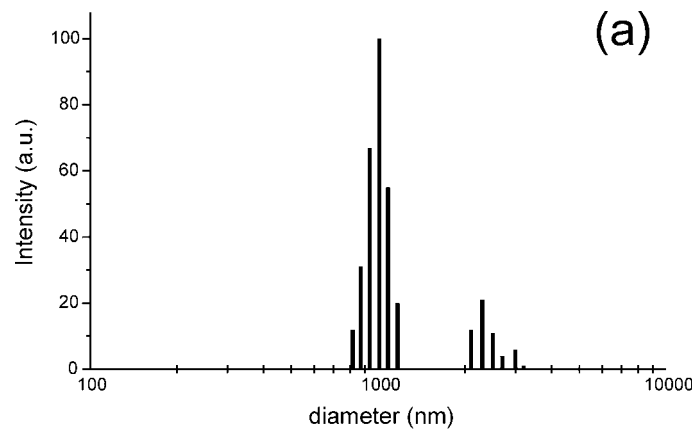


Fig. 3. The particle size distribution of the chalk: (a) natural chalk, (b) chalk ground for 30s, (c) chalk ground for 60 s

Table 2. Mean particle size and polydispersity of the examined unmodified and modified chinks.

Sample	Mean diameter (nm)	Polydispersity
Natural chalk	910	0.112
Chalk ground (30 s)	892	0.099
Chalk ground (60 s)	835	0.092
Maleic acid	1220	0.182
Maleic acid/ grinding	1092	0.167
Acrylic acid	1784	0.211
Acrylic acid/ grinding	1433	0.190
Stearic acid	1447	0.201
Stearic acid/ grinding	1187	0.192

The chinks ground in the electro-magneto-mechano-chemical reactor demonstrated highly uniform granule size usually smaller than 1 μm , which is more uniform than that of the chalk ground in Hicom mill (Braun et al., 2002). Despite a similar granule size distribution, the chinks modified with proadhesive compounds contained in their samples a few granules of the size exceeding even 5 μm , which was not encountered in the ground chalk. In the latter the typical granule size was 1-2 μm . The ASAP2010 sorptometer (Micrometrics) study of adsorption isotherm demonstrated changes in the specific area of the chalk (Figure 4), depending upon the adhesion promoter and the way of modification.

Tribochemical activation, either with or without an adhesion promoter, increased specific area of the chalk. Only difference was observed for tribochemical activation with addition of acrylic acid. In this case, the decrease in the surface area was probably associated with acrylic acid polymerisation in the course of tribochemical processing and agglomeration of particles of the modified chalk. Mean pore size decreased by almost 40% on average, which was linked with filling the pores with the surface modifying substance. One of the methods of testing surface modification was estimation of capacities to absorb water and the plasticiser. Water absorption capacity permitted an evaluation of the extent of surface hydrophobic transformation. Natural chalk is strongly hydrophilic, easily absorbs water, which is unfavourable when it is used as a filler since plasto- and elastomers remain strongly hydrophobic. For this reason the natural chalk has to be modified.

As shown by the water absorption capacity data in Figure 5, the chalk tribochemically modified with acids demonstrated better parameters than that obtained after traditional modification (using deposition of the modifier from the solution). The results obtained in testing the ground chalk without adhesion promoter indicated that tribochemical activation was associated with alteration in the chalk particle

morphology, with the transformation of aragonite into calcite (accompanied by a decrease in hydrophilicity).

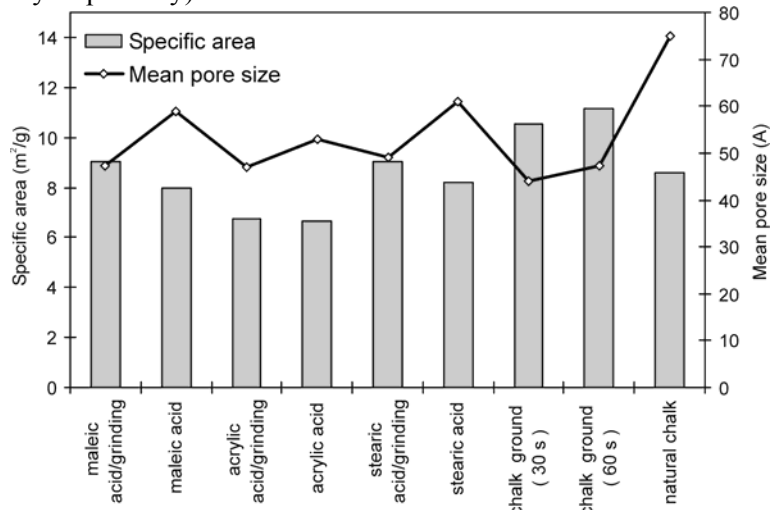


Fig. 4. Distribution of the full isotherm of adsorption

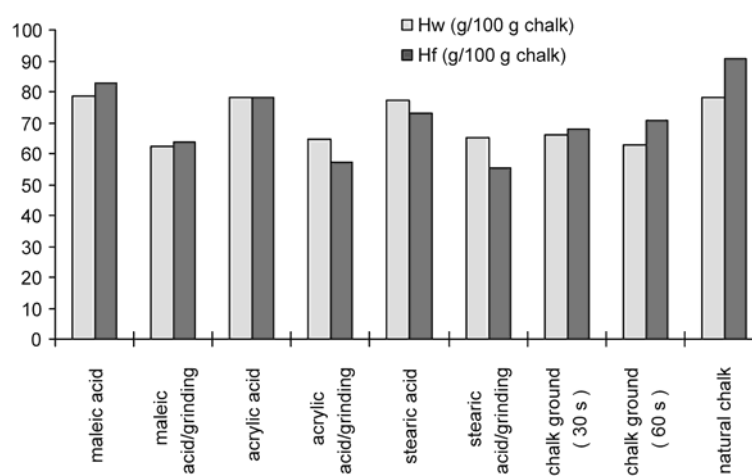


Fig. 5. Water (H_w) and dioctyl phthalate (H_f) absorption capacity

The transformation resulted from shearing and local forces and extensive compressive stresses which acted on various granules. The prolonged mixing might

be accompanied by the appearance of a significant aragonite fraction, in a composition or otherwise, the aragonite might be partly transformed into calcite (Domka, 1979).

Examination of the plastifier absorption capacity involved another way of appraising the surface modification effects. Dioctyl phthalate, the plasticiser used for absorption evaluation, is a hydrophobic substance. The deposited fatty acids accumulating in the chalk micropores, blocked them and changed the surface of the chalk, leading to decreasing plasticiser absorption capacity. The results of the tests clearly indicated a decreased absorption capacity in the samples of the chalks ground with a promoter of adhesion or without it. Tribochemical modification with stearic acid decreased the phthalate absorptive capacity up to 50%. One-minute tribochemical modification with stearic acid markedly increased the hydrophobic character of chalk and increased the phthalate absorption capacity as compared to the samples subjected to 30 s tribochemical activation. Electron microscopy demonstrated that the small fraction of the aragonite form was transformed into the calcite form on the mechanical modification, which resulted in a decreased hydrophilic character.

The presented results have permitted a conclusion that tribochemical activation with the addition of an adhesion promoter is most effective in modification of the natural chalk surface, decreasing the chalk capacity of the water and the plasticiser absorption.

CONCLUSIONS

Chalk, after tribochemical modification in the electro-magneto-mechano-chemical reactor, demonstrated highly uniform granule size, usually smaller than 1 μm . Tribochemical activation, either with or without an adhesion promoter, increased specific area of chalk. Chalk, tribochemically modified with acids, demonstrated better water and plasticizer absorption capacity than that obtained after traditional modification (by deposition of the modifier from the solution).

ACKNOWLEDGMENT

This research was supported in part by a Scientific Grant from the Polish Committee for Scientific Research (2P03B 09919).

REFERENCES

- BINCZYK F., POLECHONSKI W., SKRZYPEK S.J. (2001). *Intensive grinding of powders in an electro-magneto-mechanical mill*. Powder Technology 114, 237-243.
- BRAUN R.M., KOLACZ J., HOYER, D.I. (2002). *Fine dry comminution of calcium carbonate in a Hicom mill with an Inprosys air classifier*. Minerals Engineering, 15, 123-129.
- DEMJÉN Z., PUKÁNSZKY B., FÖLDES E., NAGY, J. (1997). *Interaction of silane coupling agents with CaCO_3* . J. Colloid Interface Sci. 190, 427-436.
- DOMKA L. (1994). *Modification estimate of kaolin, chalk and precipitated calcium carbonate as*

- plastomer and elastomer fillers*, Colloid Polym. Sci. 272, 1190-1202.
- DOMKA L., JESIONOWSKI T., MORAWSKA A., KOZAK M. (2002a). *Influence of pyridinium chlorides on physicochemical character, morphology and particle size distribution of natural chalk*. Tenside Surfactants Detergents 39, 33-39.
- DOMKA L. (1993). *Surface modified precipitated calcium carbonates at a high degree of dispersion*. Colloid Polym. Sci. 271, 1091-1099.
- DOMKA L. (1979). *Effect of experimental conditions on the physicochemical properties of precipitated calcium carbonate used in rubber industry*, (in Polish). UAM Press, Poznań, Poland.
- DOMKA L. (1996). *Modification of Kornica chalk with various proadhesion compounds*. Journal of Adhesion Science and Technology 10, 407-420.
- DOMKA L., URBANIAK W., MORAWSKA A. (1999). Polish Patent Registration.
- GÄCHTER R., MÜLLER H. (1987). *Plastics Additives Handbook*, Hanser Publishers, New York.
- HOYER D.I. (1999). *The discrete element method for fine grinding scale-up in Hicom mills*. Powder Technology 105, 250-256.
- HOYER D.I., MORGAN R.E. (1996). *High-Intensity Size Reduction in the Hicom Mill*. In Chemeca 96 (24th Australian and New Zealand Chem. Eng. Conf.), Sydney, 1996, Sep 30 – Oct 2.
- ISHIDA H. (1988). *Interfaces in polymer, ceramic and metal matrix composites*. Elsevier, New York.
- KATZ H.S., MILEWSKI J.V. (1987). *Handbook of fillers and reinforcements for plastics*. Van Nostrand Reinhold Company, New York.
- MITTAL K.L. (1992). *Silane and other coupling agents*. VSP, Utrecht.
- PLUEDDEMANN E.P. (1991). *Silane coupling agents* (2nd edn.). Plenum Press, New York.
- POLECHONSKI W., POWICHROWSKI J., SZUBERT M. (1996). *Urządzenie z elektromagnetyczną rotacją*, Wzór użytkowy RP, W104656, Poland.
- TABTIANG A., VENABLES R. (2000). *The performance of selected unsaturated coatings for calcium carbonate filler in polypropylene*. European Polymer Journal 36, 137-148.
- WUA W., LU S.C. (2003). *Mechano-chemical surface modification of calcium carbonate particles by polymer grafting*. Powder Technology 137, 41-48.
- WYPYCH G. (1999). *Handbook of fillers*. ChemTec Publishing, Toronto.

Domka L., Kozak M., *Aktywowana trybochemicznie naturalna kreda jako napelniazcz dla plasto- i elastomerów*, Physicochemical Problems of Mineral Processing, 38, (2004) 187-196 (w jęz. ang.).

W prezentowanej pracy przedstawione zostały wyniki analizy fizyko-chemicznej kredy naturalnej poddanej aktywacji trybochemicznej w obecności i bez związków powierzchniowo czynnych z grupy kwasów tłuszczowych (kwas stearynowy, maleinowy i akrylowy). Napelniazcz był modyfikowany przy użyciu reaktora elektro-magneto-mechano-chemicznego. Modyfikacja ta powodowała ewidentne przemiany obejmujące m.in. powstawanie dodatkowych defektów sieciowych, tworzenie nowych, reaktywnych powierzchni oraz wzrost powierzchni właściwej. Efekty modyfikacji mikrostruktury analizowane były z wykorzystaniem techniki skaningowej mikroskopii elektronowej (SEM) oraz dynamicznego rozpraszania światła (DLS). Ponadto zbadano zdolność zmodyfikowanego napelniazcza do absorpcji wody i plastyfikatora – ftalanu dioktylu oraz gęstość nasypową. Analiza SEM wykazała, że cząstki napelniazcza po modyfikacji cechuje jednolity kształt oraz wąski zakres rozmiarów (zwykle zbliżony do 1 µm). Wyniki SEM potwierdzają badania DLS wskazujące na zmniejszenie średnich rozmiarów cząstek po modyfikacji trybochemicznej z 910 nm charakteryzujących kredę niemodyfikowaną do 835 nm po modyfikacji. Widoczne jest także zmniejszenie średnich rozmiarów porów oraz wyraźne zwiększenie powierzchni właściwej.

Filip CIESIELCZYK, Andrzej KRYSZTAFKIEWICZ, Teofil JESIONOWSKI*

INFLUENCE OF PRECIPITATION PARAMETERS ON PHYSICOCHEMICAL PROPERTIES OF MAGNESIUM SILICATES

Received April 30, 2004; reviewed; accepted June 9, 2004

Studies were presented on optimisation of the technique of precipitating magnesium silicate of high dispersion extent so that the obtained product would exhibit possibly best physicochemical parameters. Magnesium silicate was obtained by precipitation reaction using solutions of magnesium sulphate and sodium metasilicate. The variables included temperature, the ways in which the reagents were dosed and addition of modifying substances. Physicochemical parameters of the product were estimated, including bulk density, capacities to absorb water, dibutyl phthalate and paraffin oil, particle diameters, specific surface area and electrokinetic potential.

Key words: magnesium silicate, precipitation process, surface modification, zeta potential

INTRODUCTION

In recent years, synthetic silicates gained increasing importance in several branches of industry. This reflects difficult access to natural deposits of some silicates and problems arising during technological processing of natural silicates. Moreover, synthetic silicates exhibit more pronounced dispersion than the natural materials, which is also an advantageous property. Their increasingly frequent use reflects their broad application potential in various branches (Görlich 1957).

Similarly to natural silicates, synthetic silicates may exhibit crystalline or amorphous structure. In several cases silicates exhibit a similar chemical composition but show distinct physical properties, which is critical for the direction of their application.

* Poznan University of Technology, Institute of Chemical Technology and Engineering
Pl. M. Skłodowskiej-Curie 2, 60-965 Poznan, Poland, Teofil.Jesionowski@put.poznan.pl,

In numerous papers (Krysztafkiewicz 1984, 1986, 1987, 1988) methods were presented of obtaining synthetic silicates of aluminium, zinc and calcium. Principal physicochemical data, decisive for such applications, were also collected.

Basing on the studies, the precipitation process and physicochemical parameters of synthetic magnesium silicate have been analysed in greater detail.

Magnesium silicate surface is partially hydrophobic and partially hydrophilic. The hydrophobic part includes siloxane ($\equiv\text{Si}-\text{O}-\text{Si}\equiv$) groups and the hydrophilic portion contains isolated hydroxy groups ($-\text{Mg}-\text{OH}$), individual silanol groups ($\equiv\text{Si}-\text{OH}$) and hydrogen bonds formed due to close vicinity of hydroxy groups linked to neighbouring silicon atoms (Iler 1979). Surface modification is performed to augment hydrophobicity of silicate surface and, thus, to promote binding of several compounds. The modification takes place by introduction of new organofunctional groups to silicate surface (Krysztafkiewicz 1996, Jesionowski 2001).

Apart from calcium silicate, aluminium silicate and zinc silicate, magnesium silicate is used as adsorbent for purification and decolouring of sugar, products of fermentation industry, mineral oils. Moreover, it is used as an insoluble component of rubber mixtures and similar organic polymers and as a filler of polyurethanes and vinyl polychloride (Domka 1997). The advantages of employing silicates as fillers include not only improved physicochemical properties of the filled plastics but also the fact that silicates belong to the so called light fillers which do not change colour of the material. Several applications of magnesium silicate include also its use as a carrier of drugs or plant protection agents, pesticides and of an inorganic pigment (Krysztafkiewicz 1998) or filler of varnishes (Kotowski 1994).

The so broad applications of magnesium silicate argue for a more detailed analysis of the process of obtaining it and for determination of its basic physicochemical properties. This was the aim of present study.

EXPERIMENTAL

MATERIALS

For production of magnesium silicate, the following substrates were used: 5% solution of magnesium sulphate and sodium metasilicate (5% aqueous solution in respect to SiO_2 content). The sodium metasilicate solution exhibited the following parameters: Na_2O 8.8 %; SiO_2 28.5 %, density 1.38 g/dm^3 and module of 3.33. Surface modification of magnesium silicate was performed using Rokanol K7- oxyethylenated unsaturated fatty alcohol $\text{RO}(\text{CH}_2\text{CH}_2\text{O})_n\text{H}$ (where $\text{R}=\text{C}_{16-22}$, $n_{\text{av}}=7$) and Rokafenol N9 - nonylphenylpolyoxyethyleneglycol ether $\text{C}_9\text{H}_{19}\text{C}_6\text{H}_4\text{O}(\text{CH}_2\text{CH}_2\text{O})_n\text{H}$ (where $n_{\text{av}}=9.7$), produced by Chemical Works „Rokita”.

METHODS OF STUDIES

At the first stage of the studies magnesium silicate was precipitated using 5% solutions of magnesium sulphate and sodium metasilicate. The reaction was conducted

in a three-necked flask of 250 cm³ capacity, equipped with a rapidly revolving stirrer. The reaction system was kept in thermostat-stabilised chamber. In the flask 100 cm³ sodium metasilicate solution was placed and the same amount of magnesium sulphate was dosed to it. The process was conducted at 20, 40, 60 or 80°C.

At the second stage of studies the procedure was repeated but 70 cm³ water was placed in the flask, to which magnesium sulphate and sodium metasilicate solutions were dosed (100 cm³ of each).

Moreover, the second reaction system was modified by addition adequately of 0.5; 1; 3; 5; or 10 weight parts of the Rokanol K7 or Rokafenol N9.

For each sample(s) bulk density as well as capacities to absorb water, dibutyl phthalate and paraffin oil were estimated. Moreover, particle size distribution was tested in the samples. ZetaPlus (Brookhaven Instruments Inc., USA) permitted to establish particle size using the potential of the dynamic light scattering method.

Using the apparatus, the electrokinetic potential (zeta potential) was also estimated, providing a measure of stability of the dispersion systems such as magnesium silicate.

In order to examine images of the obtained magnesium silicate surface, the selected samples were examined in the scanning electron microscope, Philips SEM 515.

For selected samples of the precipitated silicates specific surface area was estimated using BET technique as well as diameter and volume of pores were determined. The measurements took advantage of ASAP 2010 apparatus (Micrometrics Instruments Co., USA).

RESULTS AND DISCUSSION

Principal physicochemical properties of magnesium silicate obtained at the first and the second stage of the studies are listed in Table 1.

Magnesium silicate obtained at the first stage manifested relatively low physicochemical parameters. At any temperature, bulk density of the product was high, while capacities to absorb water, dibutyl phthalate and paraffin oil exhibited similar values. Surface of such a silicate should be more hydrophobic or capacities to absorb the organic compounds should be decisively higher.

The method of precipitation implemented at the second stage of the studies permitted to obtain definitely better parameters of the precipitated magnesium silicate. Bulk densities obtained at any temperature were lower than those obtained at the first stage of the studies. In the case of absorptive capacities, an evident difference appeared between the capacity to absorb water and the capacities to absorb dibutyl phthalate and paraffin oil. The surface of magnesium silicate obtained at the second stage of the studies demonstrated a markedly higher hydrophobic character.

The best parameters were obtained for the sample precipitated at the temperature of 20°C (bulk density 205 g/dm³; capacity to absorb water 300 cm³/100g; capacity to absorb dibutyl phthalate 400 cm³/100g; capacity to absorb paraffin oil 625 cm³/100g).

The results seemed to be corroborated by the data presented in Fig.1, including particle size distribution and SEM microphotograph of magnesium silicate obtained at the second stage of studies, at 20°C.

Table 1. Principal physicochemical properties of obtained magnesium silicate

Bulk density (g/dm ³)	Water absorbing capacity (cm ³ /100g)	Dibutyl phthalate absorbing capacity (cm ³ /100g)	Paraffin oil absorbing capacity (cm ³ /100g)
I stage (magnesium sulphate dosed to sodium metasilicate placed in the flask)			
20°C			
370	200	225	200
40°C			
422	150	200	200
60°C			
370	150	150	200
80°C			
280	150	150	200
II stage (both reagents dosed to water placed in the flask)			
20°C			
205	300	400	625
40°C			
249	225	400	600
60°C			
261	200	425	625
80°C			
245	250	350	550

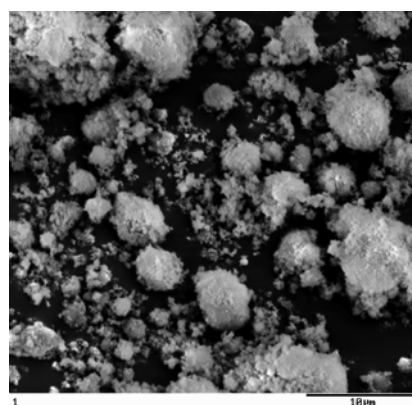
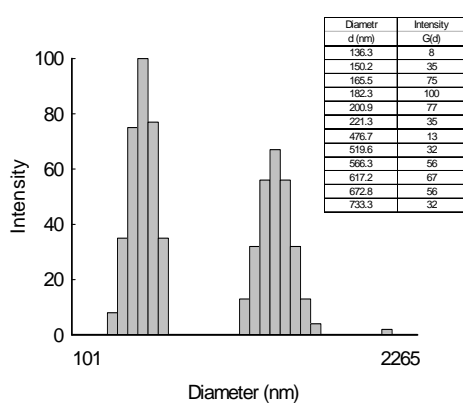


Fig.1. a) Particle size distribution and b) SEM microphotograph of magnesium silicate

The particle size distribution demonstrated three bands. The first band corresponded to silicate particles of the lowest diameters and encompassed the range of 136.3 to 221.3 nm (maximum intensity of 100 corresponded to the particle diameter of 182.3 nm). The second band of lower intensity covered the range of 476.7 to 871.1 nm and represented particles of higher diameters, including aggregates (maximum intensity of 67 corresponded to particles of 617.2 nm in diameter). The third band of a very low intensity corresponded to particles of 1865.8 nm in diameter. The band reflected presence of secondary agglomerates in the studied sample. In the sample, the mean particle diameter was 273.5 nm, and polydispersity amounted to 0.235. SEM microphotograph (Fig.1a) confirmed the presence of particles of low diameter, which bound to each other forming larger clumps of particles (aggregates and agglomerates).

In order to improve chemical parameters and dispersion of the precipitated magnesium sulphate, it was subjected to surface modification using various amounts of Rokanol K7 or Rokafenol N9. Basic physicochemical properties of the modified silicate are shown in Table 2.

Table 2. Principal physicochemical properties of magnesium silicate following modification with Rokanol K7 or Rokafenol N9

Temp. (°C)	Modifying agent	Amount of modifying agent (w/w)	Bulk density (g/dm ³)	Water absorbing capacity (cm ³ /100g)	Dibutyl phthalate absorbing capacity (cm ³ /100g)	Paraffin oil absorbing capacity (cm ³ /100g)
20°C	Rokanol K7	0,5	148	300	475	725
		1	151	275	475	625
		3	134	300	500	700
		5	180	300	425	475
		10	156	325	425	575
20°C	Rokafenol N9	0,5	218	225	425	550
		1	197	275	350	600
		3	178	300	375	625
		5	206	275	375	525
		10	200	275	375	525

Again, the best parameters were obtained at the temperature of 20°C. When 3 weight parts of Rokanol K7 were used, bulk density reached 134 g/dm³, capacity to absorb water was 300 cm³/100g, capacity to absorb dibutyl phthalate 500 cm³/100g, and the capacity to absorb paraffin oil reached 700 cm³/100g. Similar absorptive capacities were obtained for the same amount of Rokafenol N9 used to modification. However, the sample exhibited higher bulk density, of 178 g/dm³.

Particle size distributions and electron micrographs of magnesium silicate modified with 3 weight parts of Rokanol K7 and Rokafenol N9 respectively are presented in Figs.2 and 3. In both cases the graphs demonstrated presence of two bands. In the case

of Rokanol K7, the first band corresponded to particles of small diameters. It fitted the diameter range of 160.9 to 209.0 nm (maximum intensity of 57 corresponded to the particle diameter of 183.4 nm). The other band of higher intensity reflected the presence of silicate aggregates (594.9 to 825.0 nm). Maximum intensity of 100 corresponded to the aggregates diameter of 678 nm. Polydispersity, similarly to the unmodified sample, was relatively high and amounted to 0.274 while the mean particle diameter was 374.1 nm.

For silicate modified with Rokafenol N9 the mean particle diameter was somewhat lower and amounted to 281.3 nm, and polydispersity reached 0.226. The first band fitted the diameter range of 145.3 to 191.9 nm (maximum intensity of 80 corresponded to the particle diameter of 171.7 nm). The other band reflected the presence of aggregates of 441.7 to 583.2 nm in diameter (maximum intensity of 100 corresponded to the aggregates diameter of 493.6 nm).

In each case the results were corroborated by SEM microphotographs, in which clumps of particles of higher diameters (aggregates) prevailed.

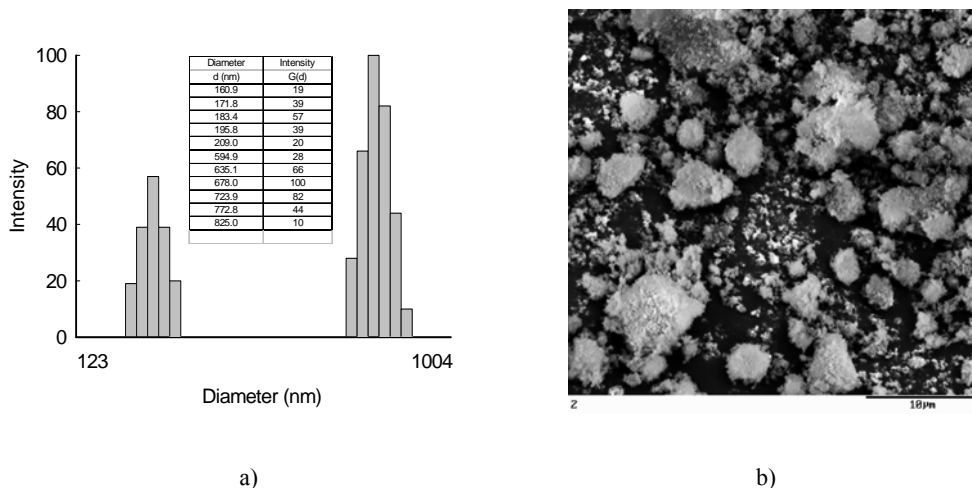


Fig.2. a) Particle size distribution and b) electron micrograph of magnesium silicate following modification with 3 weight parts of Rokanol K7

Electrokinetic potential (zeta potential) represents a significant variable in characteristics of dispersion systems. It serves as a measure of stability of dispersion systems. Its high positive or negative value characterises stable systems, its low value is typical for unstable systems. The relation between zeta potential and pH for the modified and unmodified magnesium silicate (precipitated at 20°C) is presented in Fig.4.

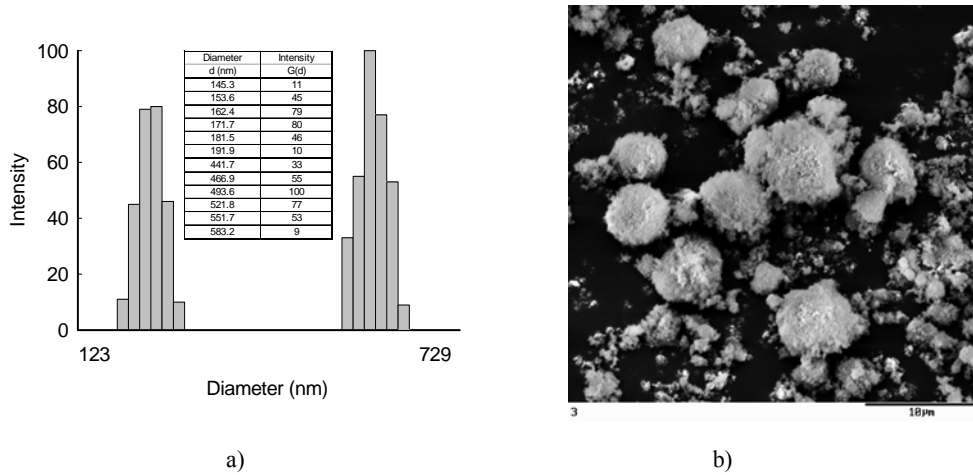


Fig.3. a) Particle size distribution and b) electron micrograph of magnesium silicate following modification with 3 weight parts of Rokafenol N9

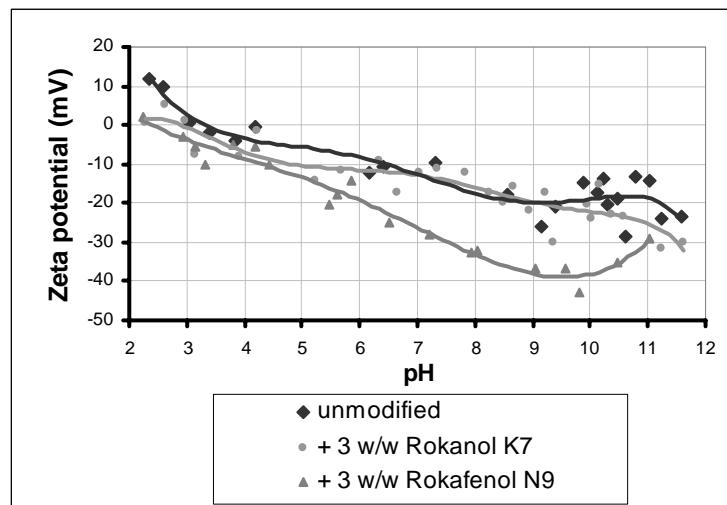


Fig.4. Relation between zeta potential and pH for modified and unmodified magnesium silicate (silicate was precipitated at 20°C)

Eletrokinetic curves for the modified magnesium silicates exhibited a similar course to that for the unmodified silicate. Values of the isoelectric point (or pH at which zeta potential acquires zero value) were as follows: unmodified magnesium silicate 2.29; magnesium silicate modified with 3 weight parts of Rokanol K7 - 2.97;

magnesium silicate modified with 3 weight parts of Rokafenol N9 - 3.16. All the samples in the range of pH from 4 to 12 exhibited negative values of zeta potential.

Isotherms of nitrogen adsorption/desorption for the three precipitated silicates are presented in Fig.3. The isotherms corresponding to silicates modified with three weight parts of Rokanol K7 and Rokafenol N9 exhibited a shape very similar to that of the isotherm for the unmodified silicate. The amount of nitrogen adsorbed by the silicates increased with rising relative pressure and a rapid increase was observed at the pressure range of 0.7 do 1.0. Such course of the curves provided proof for a high activity of the silicates. Observed amount of the adsorbed nitrogen at $p/p_0=1$ reached $400 \text{ cm}^3/\text{g}$ for the unmodified silicate and exceeded $450 \text{ cm}^3/\text{g}$ for magnesium silicate modified with 3 weight parts of Rokanol K7 and Rokafenol N9. The obtained effect provided a significant proof for augmented activity of the silicate precipitated in the presence of non-ionic surfactant. Such a course of the isotherms proved also that the silicates belonged to mesoporous substances (volume of the adsorbed nitrogen did not increase until high relative pressures, exceeding the value of 0.7).

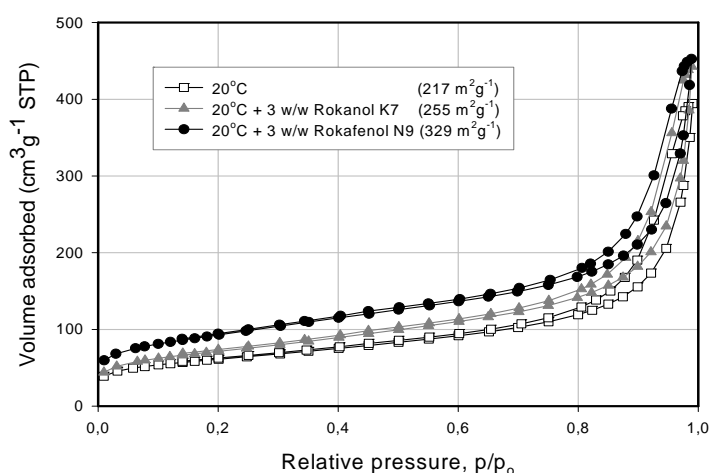


Fig.5. N_2 adsorption/desorption isotherms of the examined magnesium silicates

CONCLUSIONS

The suggested technique of precipitating magnesium silicate according to the second stage procedure yielded better results than the first technique. Introduction of modifying agents additionally improved physicochemical properties of the precipitated silicate. This was particularly evident in cases of bulk density and

capacities to absorb water, dibutyl phthalate and paraffin oil. The shape of electrokinetic curves pointed to a slight effect of modification of the silica surface with Rokanol K7 and Rokafenol N9. The modification did not alter density or charge distribution on the surface of the silicate. On the other hand, effect of the modifiers was evident in isotherms of nitrogen adsorption/desorption. Thus, it could be concluded that they significantly affected activity of the precipitated silicate (best results were obtained for magnesium silicate precipitated in the presence of 3 weight parts of Rokafenol N9 – its specific surface area amounted to 329 m²/g).

REFERENCES

- GÖRLICH E., 1957, *Chemia krzemianów*, Wydawnictwo Geologiczne, Warszawa.
- KRYSZTAFKIEWICZ A., 1984, *Krzemiany wapniowe o dużym stopniu dyspersji jako napelniacze elastomerów*, Przemysł Chemiczny, 63, 312.
- KRYSZTAFKIEWICZ A., 1986, *Krzemian cynkowy – efektywny napelniacz kaucuków*, Przemysł Chemiczny, 65, 667.
- KRYSZTAFKIEWICZ A., 1987, *Modified calcium silicates as active rubber fillers*, J. Mater. Sci., 22, 478.
- KRYSZTAFKIEWICZ A., 1988, *Modified zinc silicate – an active rubber filler*, J. Mater. Sci., 23, 2407.
- ILER R.K., 1979, *The Chemistry of Silica*, John Wiley & Sons, New York, pp. 622-714.
- KRYSZTAFKIEWICZ A., RAGER B., MAIK M., WALKOWIAK J., 1996, *Modified sodium aluminium silicate – a highly dispersed polymer filler and pigment*, Colloids and Surfaces, 113, 203-214.
- JESIONOWSKI T., KRYSZTAFKIEWICZ A., 2001, *Influence of silane coupling agents on surface properties of precipitated silicas*, Applied Surface Science, 172, 18-32.
- DOMKA L., KRYSZTAFKIEWICZ A., GULIŃSKI J., URBANIAK W., MACIEJEWSKI H., 1997, *Krzemionki i krzemiany modyfikowane krajowymi silanowymi związkami proadhezyjnymi – napelniacze poliuretanów i PCW*, Przemysł Chemiczny, 76, 96-99.
- KRYSZTAFKIEWICZ A., MICHALSKA I., JESIONOWSKI T., WIECZOREK M., 1998, *Odpady chromowe i żelazowe – potencjalne źródła do otrzymywania pigmentów*, Fizykochemiczne Problemy Mineralurgii, 32, 77-85.
- KOTOWSKI M., KAMIENSKA E., 1994, *Wypełniacze dolomitowe z Piotrowic wartościowy surowiec lakierniczy*, Farby i Lakiery, 10, 16-20.

ACKNOWLEDGEMENTS

This work was supported by the PUT Research Grant DS No. 32/115/2004.

Ciesielczyk F., Krysztafkiewicz A., Jesionowski T., *Wpływ parametrów strącania na właściwości fizykochemiczne krzemianów magnezu*, Physicochemical Problems of Mineral Processing, 38, (2004) 197-205 (w jęz. ang.).

Przedstawiono badania nad zoptymalizowaniem metody strącania krzemianu magnezu o dużym stopniu dyspersji, tak by uzyskać produkt o jak najlepszych parametrach fizykochemicznych. Krzemian magnezu otrzymywano w reakcji strącania z użyciem roztworów siarczanu magnezu i metakrzemianu sodu. Zmieniającymi się parametrami były: temperatura, sposób dozowania reagentów oraz dodatek substancji modyfikujących. Wyznaczono parametry fizykochemiczne takie jak: gęstość nasypowa, chłonności wody, ftalanu dibutyli i oleju parafinowego, średnice cząstek, powierzchnię właściwą oraz potencjał elektrokinetyczny.

Kazimierz St. SZTABA*

INFLUENCE OF GRAIN SIZE UPON ITS FALLING VELOCITY

Received May 14, 2004; reviewed; accepted June 21, 2004

The problem of determining the theoretically justified method of considering the natural shape of mineral grains in the calculations of their motion velocity in liquid media, especially their falling under the influence of the external mass force, in particular the force of gravity, has not been successfully solved so far. The presented paper shows a possibility of increasing the accuracy of calculations of this velocity with the use of the well-known formulas, discussed in the paper introduction, by means of the appropriate introduction of two different grain shape coefficients into them.

Key words: sedimentation, grain shape, falling velocity, shape coefficient

INTRODUCTION – FALLING VELOCITY OF SPHERICAL GRAINS

The motion velocity of mineral grains (v , $\text{m}\cdot\text{s}^{-1}$) in the liquid medium (liquid or gas) under the effect of the acting external mass force is the principal criterion of their behaviour in the course of flow processes which play an important role in the technology of mineral processing¹. This velocity is the function of the force exerted upon a grain by the mass force (most often gravity force or/and centrifugal force), evoking the grain motion (P_m , $\text{kg}\cdot\text{m}\cdot\text{s}^{-2}$) of surface forces (P_ψ , $\text{kg}\cdot\text{m}\cdot\text{s}^{-2}$), comprising the resistance against the grain moving through the medium, and also, in a significant degree, practically in the initial motion phase – initial velocity (v_p , $\text{m}\cdot\text{s}^{-1}$), given to the grain in the moment of the motion start (Laščenko 1935; Budryk 1936; Barskij *et al.*

*AGH University of Science and Technology, Department of Mineral Processing,
Environment Protection and Waste Utilization, Al. Mickiewicza 30, 30-065 Kraków, Poland,
sztaba@galaxy.uci.agh.edu.pl.

¹ It concerns any technological processes into which the grained materials are subjected. Mineral processing was assumed to set the attention and also due to the significant position played by the flow operations in it.

1974 and others). In the present considerations the following idealized conditions were assumed: a spherical grain of a certain size (d , m) equal to the sphere diameter and density (ρ_z , $\text{kg}\cdot\text{m}^{-3}$), it moves in the liquid (water) of density (ρ_c , $\text{kg}\cdot\text{m}^{-3}$) and dynamic viscosity rate (μ_c , $\text{kg}\cdot\text{m}^{-1}\cdot\text{s}^{-1}$), occupying the unlimited spatial area, by means of free motion, (without possible actions of other objects), caused by gravity force of acceleration value (g , $\text{m}\cdot\text{s}^{-2}$) which is constant in the entire area. The instant velocity of grain in relation to the medium (v , $\text{m}\cdot\text{s}^{-1}$) is studied which is the function of motion duration time (t , s) – $v = v(t)$; the grain initial time is nought ($v_p = v(0) = 0$, $\text{m}\cdot\text{s}^{-1}$)². Such conditions justify the assumption of the fact that the vectors of all forces acting upon the grain lie upon the straight line fixed by the vector of mass force whose sense determines a positive direction and the resultant force (P), acting on the grain, is constituted by the sum

$$P = P_m - P_\psi \quad (1)$$

Force P is the product of grain mass (m_z) – $m_z = V_z \cdot \rho_z$, V_z – grain volume, for sphere $V_z = \frac{1}{6} \cdot \pi \cdot d^3$ – and the values of acceleration of grain motion (dv/dt) – $P = m_z \cdot \frac{dv}{dt} = V_z \cdot \rho_z \cdot \frac{dv}{dt}$ and it has properties of inertial force.

Mass force is the product of grain mass diminished by the value of uplift pressure and acceleration of mass force. In the field of gravity force it is

$$P_m = \frac{\pi \cdot d^3}{6} \cdot (\rho_s - \rho_c) \cdot g \quad (2)$$

Resistance force of the medium (P_ψ) has a general form

$$P_\psi = \Psi \cdot \rho_c \cdot v^2 \cdot d^2 \quad (3)$$

where Ψ – dimensionless resistance coefficient which is a complex function of many factors, especially Reynolds' number characterizing the motion of liquid around the grain in the considered system expressed by the formula

$$\text{Re} = \frac{\rho_c \cdot v \cdot d}{\mu} \quad (4)$$

In general, it can be written that P_ψ is a certain function

$$P_\psi = f(d, v, \rho_c, \text{Re}) \quad (3.1)$$

² accordingly the measurements of the quoted sizes are neglected, assumed in the entire work, according to the SI system of units

Difficulties in precise determining the general function form of the resistance coefficient, and firstly, practical requirements, led to working out, starting from the XVIIth century (Newton), numerous approximate forms of formulas for calculating the resistance force. They can be applied in limited ranges of grain motion conditions, most often defined by means of values of Reynolds' number, characteristic for their highlighted ranges. The advanced work upon the general description of the motion of grains in the described conditions was undertaken as late as in the first half of the XXth century (Laščenko 1935).

Newton's approximations are the oldest and most popular

$$P_d = \frac{1}{3} \cdot F_r \cdot v^2 \cdot \rho_c \quad (5)$$

where F_r – grain projective area – area of the perpendicular projection of the grain upon the plane perpendicular to the tangent to the grain motion track, fixed by its mass centre in the point of the grain instant position; for a sphere in its every position the projective area is equal to the area of the largest cross-section of the sphere:

$$F_r = \frac{\pi}{4} \cdot d^2, \text{ thus}$$

$$P_{d_{sphere}} = \frac{\pi}{12} \cdot d^2 \cdot v^2 \cdot \rho_c \quad (5.1)$$

and by Stokes

$$P_l = 3 \cdot \pi \cdot \mu \cdot v \cdot d. \quad (6)$$

The values of resistance force, expressed by formulas (5) and (6), are characteristic, respectively, to the conditions – turbulent (P_d) and laminar (P_l)³ motions of the medium flowing around the grain. Actually, the resistance force contains always two “components” – a “dynamic” one - P_d - originating from the resistance of inertial liquid and dissipation of energy in turbulent swirls in the conditions and a “laminar” one - P_l - evoked by the friction resistance between liquid layers and the grain surface and liquid in the laminar flow.

The dependence of the resistance force from the grain motion velocity against the medium makes the absolute value of this force increase from the moment of the motion start and the acquisition of increasing velocity v under the effect of force P , and after some time (t_0) (Laščenko 1935 and others) its absolute value becomes so close to the value of mass force that their sum (1), causing the grain motion, aims at

³ it is often assumed (often artificially) that the laminar motion is characterized by the value $Re < \sim 1$ and turbulent one by $Re > \sim 1000$

nought. Then the acceleration of grain motion disappears and it moves on with practically constant speed, called the boundary velocity ($v_0 = v(t \geq \sim t_0) = \sim \text{const}$). Mineral grains of the most popular sizes and densities, subjected to flow operations (flow classification, sedimentation, gravitational enrichment), usually in the water medium, reach as a rule the boundary velocity after very short times t_0 , which contributed to assuming the boundary velocity v_0 , practically constant for given conditions, to be the value characterizing their behaviour in the discussed processes.

Substituting expression for P_ψ corresponding to the present flow conditions ($P_d, P_l, P_d + P_l$ or others) into formula (1) for the balance of forces acting upon the grain, and dividing this formula by two sides by the grain mass ($m_z = V_z \cdot \rho_z$) whereas $\frac{P}{m_z} = \frac{dv}{dt}$,

we obtain the expression for acceleration balance in which the left side describes the acceleration of grain motion – dv/dt . The latter equals nought for the state of boundary velocity and after matching to nought the right side of the acceleration balance we receive an equation in which velocity v is only unknown, now already substituted by boundary velocity v_0 . Solving this equation results in obtaining a formula to calculate the boundary velocity.

Assuming P_ψ according to (5.1) we receive an equation known as Newton-Rittinger's formula⁴

$$v_{0_{NR}} = \sqrt{2 \cdot g} \cdot \sqrt{\frac{(\rho_z - \rho_c) \cdot d}{\rho_c}} \quad (7)$$

which is useful when Reynolds' number assumes large values (large grains, at medium densities, $d \geq \sim 2 \div 5$ mm).

Assuming P_ψ according to (6) results in Stokes' formula

$$v_{0_S} = \frac{g \cdot (\rho_z - \rho_c) \cdot d^2}{18 \cdot \mu} \quad (8)$$

to calculate the boundary velocities of fine and very fine grains ($d \leq \sim 0,2$ mm).

The formal boundary of application of formulas (7) and (8) is determined by the value

$$\text{Re} = \frac{\rho_c \cdot v_0 \cdot d}{\mu} = 36 \quad (9)$$

– v_{0_S} when $\text{Re} \leq 36$

– $v_{0_{NR}}$ when $\text{Re} \geq 36$

⁴ Rittinger derived this formula to be used in designing the operations of coal gravitational enrichment, assuming determining the resistance force according to Newton.

but assuming the permissible relative error of measurement of value Δ (for example, $\Delta = 0.05$) changes the applicability ranges approximately:

- for Stokes' formula (8): into $0 \leq \text{Re} \leq \sim 36 \cdot \Delta$, (for example $0 \leq \text{Re} \leq 1,8$),
- for Newton-Rittinger's formula (7): into $36/\Delta \leq \text{Re}$, (for example $720 \leq \text{Re}$).

A "universal" assumption of resistance force as a sum of $P_d + P_l$ leads to obtaining a formula, given for the first time by Budryk (1936), applicable in a wide range of values of Reynolds' number, characterizing the state of grain round flow

$$v_{0_B} = \frac{18 \cdot \mu}{d \cdot \rho_c} \cdot \left(\sqrt{1 + \frac{g \cdot (\rho_s - \rho_c) \cdot \rho_c \cdot d^3}{162 \cdot \mu^2}} - 1 \right) \quad (10)$$

The quoted formulas (7), (8) and (10) are, due to their simplicity, relatively often applied in cases which are unquestionable as far as a strong predominance of phenomena characteristic for turbulent round flow – Newton-Rittinger's formula (e.g. gravitational enrichment of large and medium grains) or laminar one – Stokes' formula (e.g. sedimentation processes). The most difficult concerns flow classification which concerns in majority of case the materials of grain size distribution $0.1 \div 1$ mm or a little more, of the round flow characteristics through the classification medium about the boundary value $\text{Re} = 36$. Budryk's formula (10), well-fitted for such grains, makes problems resulting from the lack of possibilities of presenting it in the form $v_0 = S \cdot d^n$ where S – constant depending on grain and medium properties, invariable in a given process, n – power exponent at d , characteristic for the given formula (in Newton-Rittinger's formula $n = 1/2$, in Stokes' formula $n = 2$). For the so-called transition range, comprising such grains, many formulas were worked out, including many empirical ones, out of which the most useful is that given by Allen (Barskij *et al.*; Nowak, Sztaba 1986; Zbiorowe 1972 and others).

Assuming in the formerly described approach leading to deriving formulas for v_0 , $P_\psi = \sqrt{P_d \cdot P_l}$ as the value of resistance, Allen's formula is obtained in the form:

$$v_{0_A} = \sqrt[3]{\frac{g^2}{9}} \cdot \sqrt[3]{\frac{(\rho_s - \rho_c)^2}{\rho_c \cdot \mu}} \cdot d \quad (11)$$

As opposed to Budryk's formula of a practically unlimited range of applications, Allen's formula can be used without a too large error, only for falling conditions in the transition range, called also Allen's range, between the ranges of applicability of Stokes' and Newton-Rittinger's formulas. A conclusion may be drawn that it is more relevant to assume P_ψ in the form of a sum, as in Budryk's formula, than as a geometric mean of P_d and P_l resistances, as in the case of Allen's formula.

Among the already mentioned works aiming at working out a uniform way of calculating the boundary velocity, a record generalizing the majority of quoted

formulas is worth mentioning. After solving the general equation (3.1) by means of the dimension analysis and after introducing the resistance coefficient in the form $\Psi = K \cdot \text{Re}^{n-2}$ where:

K – numerical constant

n – coefficient indicating the character of the round flow

$n = 1$	– laminar round flow:	$K = 3 \cdot \pi,$
$1 < n < 2$	– round flow of mixed character (transition range):	$K = \pi/2,$
$n = 2$	– turbulent round flow:	$K = \pi/12,$

in the formerly given way the equation is obtained (Zbiorowe 1972)

$$v_0^n = \frac{4}{3} \cdot \frac{g}{K} \cdot \left(\frac{\rho_z - \rho_c}{\rho_c^{n-1}} \right) \cdot \mu^{n-2} \cdot d^{3-n} \quad (12)$$

as a general formula for the free falling velocity for any flow conditions. Changing value n in the given limits, the formulas for various types of grain motions are obtained, consistent with those given before.

SELECTED DETERMINATIONS OF GRAIN SHAPES APPLIED FOR FLOW PROCESSES

The discussed formulas, important for spherical grains, not occurring in mineral processing, cannot be directly applied in the industry. The problem of considering the shape of grains for calculating the boundary velocity of falling concerned the attention of researchers and engineers for a long time. The collected works and outlooks can be systematically arranged as follows (Zbiorowe 1972 and others).

1. Empirical methods consisting in experimental determining for respective materials (usually minerals) numerical coefficients introduced into the formulas important for spherical grains. These are the oldest methods and are only valuable for the materials tested experimentally, cannot be broadened or generalized, do not use the values directly concerning the shape of grains.
2. Other experimental methods, using coefficients fixed for solids of shapes defined by means of geometric descriptions. In this group special attention should be put upon empirical corrections introduced into formulas for spherical grains and fixed not for the grains of directly defined shapes but of different values of the sphericity coefficient (C_k), discussed further in point 3.b. There are also other coefficients (Zbiorowe 1972), determined for solids of regular shapes, falling at the values of Reynolds' number, characterizing the round flow of the grain by the liquid – classification medium – in ranges $0 \div 0.05$ (correction to Stokes' formula) and over 2000 (correction to Newton-Rittinger's equation). There is no information to prove these empirical dependences for regular grains and no concept to broaden the method into the transition area $\sim 0,05 < \text{Re} < \sim 2000$.

3. Calculation methods based upon introducing the values taking into consideration the non-spherity of real grains into formulas for spherical grains. Real grains can be possibly divided into certain groups (Barskij *et al.* 1974). Out of these the following methods can be differentiated.
- 3.a. Assuming as the grain size the substitute grain diameter (d_z) – a sphere diameter of the volume equal to that of the grain

$$d_z = \sqrt[3]{\frac{6 \cdot V_z}{\pi}} \approx 1.2407 \cdot \sqrt[3]{V_z} \quad (13)$$

For practical purposes d_z is usually fixed as an average value D_z , e.g. for a certain grain class, deducting at random a certain number (N – usually not less than a few hundred) of grains and determining their mass m_N . Knowing the material density ρ_s , it can be calculated:

$$D_{z(N)} = \sqrt[3]{\frac{6 \cdot m_N}{\pi \cdot N \cdot \rho_s}} \approx 1.2407 \cdot \sqrt[3]{\frac{m_N}{N \cdot \rho_s}} \quad (13.1)$$

The application of a substitute diameter has been more and more generally used for a long time in any calculations of flow processes. This principle can be also applied in this paper.

- 3.b. Introducing the coefficients into formulas, which are directly connected with grain geometry (without empirical corrections, as in point 2). The most important ones are given below:
- spherity coefficient (C_k)⁵ – relation of sphere surface (F_k) of the volume equal to the grain (sphere of d_z diameter) to the grain surface (F_z)

$$C_k = \frac{F_k}{F_z} = \frac{\pi \cdot d_z^2}{\pi \cdot d_k^2} = \frac{d_z^2}{d_k^2} \quad (14)$$

where: d_k – diameter of the sphere of the surface equal to the grain (F_z),

- circularity coefficient⁵ (C_c) – relation of the length of outline (c_z) of the perpendicular projection of the grain on the plane on which it is placed in the position in which the centre of the grain mass is situated at the closest of this plane (“the most stable position”) to the length of the circle perimeter (c_k) of the area equal to the area of grain projection (F_p)

$$C_c = \frac{c_z}{c_k} = \frac{c_z}{2 \cdot \sqrt{\pi \cdot F_p}} \quad (15)$$

⁵ Proposed by Wadell in 1934.

the diameter of a circle of the area F_p is the grain projection value (d_p)

$$d_p = 2 \cdot \sqrt{\frac{F_p}{\pi}} \approx 1.1284 \cdot \sqrt{F_p} \quad (16)$$

— grain shape coefficient, given by Nowak (1980)

$$C_{AN} = \frac{d_z^2}{d_p^2} = \sqrt[3]{\frac{9 \cdot \pi}{16} \cdot \frac{V_z^{2/3}}{F_p}} \approx 1.2090 \cdot \frac{V_z^{2/3}}{F_p} \quad (17)$$

3.c. Introducing a coefficient similar to those described in point 3.b. but indirectly considering the change of conditions of the grain round flow depending on its shape in the form of “dynamic shape coefficients” (Barskij *et al.* 1974). This paper does not present examples of such propositions.

Only certain shape coefficients, discussed in point 3.b., are used in the paper. In this domain several significant propositions and elaborations were noted in Poland in the second half of the previous century. Apart from the quoted work by Nowak (1980) there are important investigations by Sysło (1964) on considering the grain shape in calculating the velocity of grains falling for which Stokes’ formula can be applied. Another reason why these works are important is that their final result in the form of corrections to formulas was obtained in both cases by means of heuristic considerations, obtaining then very good results of experimental verification.

FALLING VELOCITY OF NON-SPHERICAL FINE GRAINS

In simplification, it can be stated that the resistance of medium exerted on very fine grains, falling at their purely laminar round flow through the medium, originates as the resistance of friction on the entire surface of grains. Consequently, it should be assumed the value d_k , determined by the grain surface, which can be appropriately assumed to be a representative grain size. Its value can be determined but it is hard to reach. It is, however, connected with the value of substitute diameter d_z , value of sphericity coefficient C_k , assumed for calculations. It results from formula (14):

$$d_k = \frac{d_z}{\sqrt{C_k}} \quad (18)$$

Taking into account this dependence, the force of laminar resistance is written as

$$P'_l = 3 \cdot \pi \cdot \mu \cdot v \cdot \frac{d_z}{\sqrt{C_k}} \quad (6.1)$$

Here and in the subsequent sequence of values, in which the grain shapes were taken into account, they are marked with the ' sign.

Acting in the same way as in deriving Stokes' formula, we obtain the expression, which takes into account the shape of grains:

$$v'_{0s} = \frac{g \cdot \sqrt{C_k} \cdot (\rho_z - \rho_c) \cdot d_z^2}{18 \cdot \mu} \quad (8.1)$$

FALLING VELOCITY OF NON-SPHERICAL LARGE GRAINS

Performing an analogical consideration as in chapter 3. for large grains which are subject mainly to the force of dynamic resistance, it should be observed that the character of this resistance is different from laminar. Especially its value depends upon the front surface area of the grain projective surface F_r – determined in formula (5). This value cannot be measured in relation to the grain falling in the liquid. As assistance we can use a certain phenomenon occurring during the falling of grains on which the dynamic resistance acts significantly. This is a so-called principle of maximum projection, mentioned in some works concerning the motion of solids in liquid media. This phenomenon was analysed in detail also by Sysło (1964).

Descriptively, it consists in the fact that the equilibrium of forces of resistance acting upon the grain leads to setting such spatial position of the falling grain that its projection surface is the largest among all the projections of this grain. Due to that it can be assumed that the projection value d_p (16) is a proper denotation of the grain size. It results from the definition of the shape coefficient C_{AN} (17) that it is connected with a disposable, assumed to be basic, substitute value by the expression

$$d_p = \frac{d_z}{\sqrt{C_{AN}}} \quad (19)$$

Acting as in deriving the modified Stokes, formula and substituting (19) into (5.1) we obtain its modified form

$$P'_d = \frac{\pi}{12 \cdot \sqrt{C_{AN}}} \cdot d_z^2 \cdot v^2 \cdot \rho_c \quad (5.2)$$

which, applied to derive Newton-Rittinger's formula, leads to its form:

$$v'_{0NR} = \sqrt{2 \cdot g \cdot C_{AN}} \cdot \sqrt{\frac{(\rho_z - \rho_c) \cdot d_z}{\rho_c}} \quad (7.1)$$

GENERALIZED FORMULA FOR FALLING VELOCITY
OF NON-SPHERICAL GRAINS

The transformed formulas (7.1) and (8.1) do not solve the problem of considering the grain shape in calculating the boundary falling velocity in a complete way. They do not cover the intermediate range, which is the most important for the needs of flow classification and in which the round flow of grains by the medium occurs at the values of Reynolds' number in the range $(0.05) 0.1 \div 1000 (2000)^6$.

Allen's formula (11), which is applied in this case, complicates greatly a possible repetition of the applied procedure to obtain the formula analogical to (7.1) and (8.1). In this situation this procedure was applied to derive a formula corresponding to Budryk's equation (10). After accepting formulas (5.) and (6.1) to be both components of resistance force and initial assumptions as in Budryk's formula, we achieve its form

$$v'_{0_B} = \frac{18 \cdot \mu}{\rho_c \cdot d_z} \cdot \frac{C_{AN}}{\sqrt{C_k}} \cdot \left(\sqrt{\frac{g}{162} \cdot \frac{C_k}{C_{AN}} \cdot \frac{(\rho_s - \rho_c) \cdot \rho_c}{\mu^2} \cdot d_z^3 + 1} - 1 \right) \quad (10.1)$$

In the works (Nowak, Sztaba 1986, Sztaba 1992) detailed remarks were given about the results of experiments performed to verify the usefulness of formula (10.1) To do this, the range of values of Reynolds' number $1 \div 1000$ was selected. Quartzite of density $2640 \text{ kg} \cdot \text{m}^{-3}$ and grain size distribution $0.06 \div 5 \text{ mm}$ was the tested material, scattered carefully into 20 narrow grain classes.

Average values of the following items were set for each class in precisely determined and controlled conditions:

- D_z – substitute value d_z ,
- D_p – projection value d_p ,
- \bar{F}_z – surface of grains F_z
- \bar{v}_r – real boundary velocity, marked here as v_r to be clearly distinguished, of falling in water at strictly controlled temperature and determining with the corresponding values ρ_c and μ from the tables.

On the basis of these data for each class the average values were calculated:

- \bar{C}_k – spherity C_k ,
- \bar{C}_{AN} – coefficient C_{AN}
- \bar{v}_{0_B} – value of boundary falling velocity (for grains of size D_z) according to Budryk's formula for spherical grains (10),
- \bar{v}_{r_B} – values of boundary falling velocities (for $D_z, \bar{C}_k, \bar{C}_{AN}$) according to formula (10.1),

⁶ according to various authors and also the required calculation accuracy (numbers in brackets concern higher accuracy)

and also, respectively for \bar{v}_{0_B} and \bar{v}_{r_B} , average values of Reynolds' number, not analysed in the present paper.

Figure 1 (Nowak, Sztaba 1976; Sztaba 1992) presents the results of performed investigations.

The figure shows the course of dependence between the mentioned values and values D_z . The use of logarithmic scale results from a large differentiation of grouping of measurement points for fine grains in relation to coarse ones. There is a clear improvement of consistency of calculation results of value \bar{v}_{r_B} according to formula (10.1) as compared to \bar{v}_{0_B} , formula (10), without considering the grain shapes, with the real values of velocity \bar{v}_r . The presented graphs allow us only to formulate quantitative (descriptive) conclusions. To make them precise, the coefficients of linear regression (ρ_k) were calculated of the form:

$$Y = a \cdot X + b \quad (20)$$

obtaining

— for $Y = \bar{v}_{0_B}$, $X = \bar{v}_r$: $a = 0.60555$; $b = -0.00178$; $\rho_k = 0.99638$,

— for $Y = \bar{v}_{r_B}$, $X = \bar{v}_r$: $a = 0.84961$; $b = 0.00234$; $\rho_k = 0.99944$.

Supposing that in case of an ideal compatibility X and Y the presented values would be: $a = 1$, $b = 0$ ($\rho_k = 1$), we can speak about a significant improvement of accuracy of calculations (estimated mostly on the basis of the value of the coefficient a) when we take into account the shape coefficients as compared to the results obtained without taking them into consideration. In another, parallel, series of experiments, the following results were obtained, respectively:

— for \bar{v}_0 (\bar{v}_{0_B}): $a = 0.53025$; $b = 0.00175$,

— for \bar{v}_r (\bar{v}_{r_B}): $a = 0.82095$; $b = 0.00185$

and other similar ones.

Fig. 1 presents also the courses of dependences of coefficients of shape (linear scale) on grain sizes, which reveal certain regularities indicating the need of further research on the methods of determining their values.

Coefficient C_k , decreasing very regularly with the growth of grains up to very small values (below 0.05), indicates that with the growth of grain sizes there are significant, undoubtedly overestimated, results of the measurements of specific surface resulting from the fact that the developed elements of the surface were included in it. In spite of applying the flow methods for the measurements of specific surface (in Tovaroff's apparatus) little sizes of the surface relief elements (in relation to the sizes of large grains) cause significant overestimations of measurement results and, respectively, the decrease of the value of C_k . On the other hand, a regular course of the discussed

dependence is a proof of high accuracy of measurements as such, regardless the discussed limited adequacy of the real measured value to the assumed one.

Respectively, the course of the dependence C_{AN} on D_z reveals the presence of an interesting minimum but, at the same time, a large scatter of points confirms the necessity of significant improvement of the measurement accuracy to be obtained, including the projective diameter D_p .

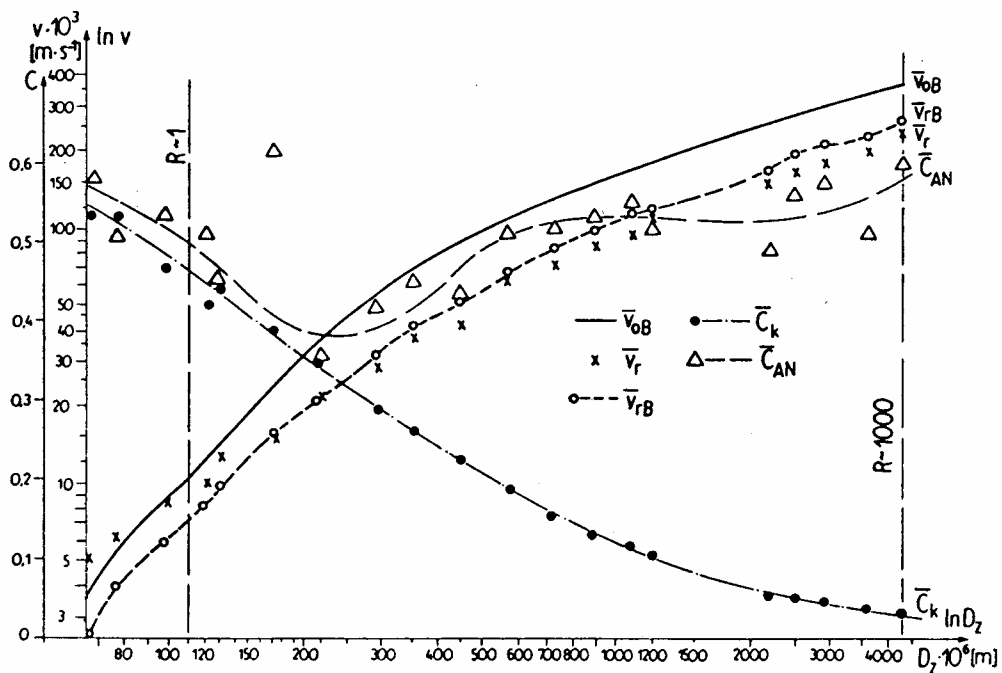


Fig. 1. The calculated and real boundary velocities of quartzite grains falling freely in water (explanations in the text; $R \equiv Re$), according to (Nowak, Sztaba 1986; Sztaba 1992)

In spite of this, the course of the discussed dependence is so much univocal that the final results, already discussed, can be treated in a half-quantitative way. It should be noted that the attempts of improvement of the results of calculations of boundary velocities, with taking into account the coefficients of shape and with the same experimental data, gave worse results or results showing a large scatter than the presented ones.

CONCLUSIONS

1. The investigations confirmed the correctness of the concept of applying several coefficients of shape in the calculations of boundary velocities of non-spherical grains. It seems to be inevitable, especially for the intermediate range ($\sim 1 < Re < \sim 1000$).
2. When the initial assumptions were simplified and formalized, the improvement of the results of calculations of \bar{v}_0 , experimentally confirmed, was obtained. This fact confirms the correctness of the assumed research, though obtaining a possibly total consistence of calculation results and experimental results need further investigations, which are being continued.
3. The methods of measurements determining the values of the coefficients of shape of grains should be perfected (average values of these coefficients in grain sets).
4. It was not planned to provide a general presentation of calculating the boundary velocity which is a special case of grain characteristic velocity ($v_c = v_c(t)$; $v_0 = v_c(\infty)$) in relation to the medium and which is not discussed. The aim of this paper was to present the title possibility of improving the results of calculating the boundary velocity. The author assumed the oldest and most popular methods of calculating this velocity by means of formulas based on the formally considered balance of basic forces acting upon the grain in the liquid medium to constitute the presentation object. The development of the method as well as its applications for the method of calculating the grain velocity in the medium, based upon the most contemporary knowledge about the principles of flow processes are the subject-matter of further investigations.

REFERENCES

- BARSKIJ, M.D., REVNIVCEV, V.I., SOKOLKIN, J.V., 1974 – *Gravitacionnaja klassifikacija zernistych materialov (Gravitational Classification of Grained Materials)*, „Nedra” Moskva (in Russian)
- BUDRYK, W. 1936 – *Contribution à la théorie du lavage, (Contribution to the Theory of Jigging)* – Revue de l'Industrie Minérale, No 374 (in French)
- LAŠČENKO, P.V., 1935 – *Gravitacionnye metody obogaščenija (Gravitational Methods of Enrichment)* – ONTI - SSSR, Moskva – Leningrad (in Russian)
- NOWAK, A. 1980 – *Kornformfaktor für die Bewegung in einem flüssigen Medium, (Coefficient of Shape at the Movement of Grains in a Liquid Medium)*, Freiburger Forschungshefte A 633, Deutscher Verlag für Grundstoffindustrie, Leipzig (in German)
- NOWAK, A., SZTABA, K. 1981 – *Koncepcja uogólnionego ujęcia współczynników kształtu ziarn w określeniu prędkości granicznej opadania (Concept of Generalized Idea of Grains Shape in Determining the Boundary Falling Velocity)* - *Materiały: Seminarium naukowo-techniczne „Klasyfikacja materiałów drobnouziarnionych”*, NOT-AGH, Kraków, komunikat (in Polish)
- NOWAK, A., SZTABA, K. 1986 - *The Influence of Particle Shape on the Falling Velocity in the Allen's Range - Proceedings: 1. World Congress Particle Technology, Part I: Particle Characterisation, Nürnberg (Germany)*
- SYSŁO, M. 1964 – *Uogólnione prawo Stokesa dla brył spójnych, (Generalized Stokes' Law for Compact Solid Bodies)*, Zeszyty Naukowe AGH, Rozprawy vol. 33, Kraków (in Polish)

SZTABA, K. 1992 – *Problems of Taking into Account Shapes of Mineral Grains in Flow Classification – Proceedings: The First International Conference on Modern Process Mineralogy & Mineral Processing*, Beijing (China)

ZBIOROWE 1972 – *Spravočnik po obogaščeniju rud t.1.* (Handbook of Ore Processing vol.1.) – „Nedra” Moskva (in Russian)

Sztaba K., *Wpływ kształtu ziarna na prędkość jego opadania*, Physicochemical Problems of Mineral Processing, 38, (2004) 207-220 (w jęz. ang.).

Problem określenia teoretycznie uzasadnionej metody uwzględniania naturalnego kształtu ziarn mineralnych w obliczeniach prędkości ich ruchu w ośrodkach płynnych – zwłaszcza ich opadania pod wpływem zewnętrznej siły masowej, w szczególności siły ciężkości – nie znalazł dotychczas w pełni zadowalającego rozwiązania ogólnego. Prezentowane opracowanie przedstawia możliwość zwiększenia dokładności obliczeń tej prędkości z zastosowaniem znanych wzorów – omówionych we wstępie opracowania – drogą odpowiedniego wprowadzenia do nich dwóch różnych współczynników kształtu ziarna.

A. Seyfi ERDEM, Ş. Levent ERGÜN, A. Hakan BENZER*

CALCULATION OF THE POWER DRAW OF DRY MULTI-COMPARTMENT BALL MILLS

Received May 6, 2004; reviewed; accepted June 18, 2004

In this paper, a new approach for the calculation of the power draw of cement grinding ball mills is proposed. For this purpose, cement grinding circuit data including the operational and design parameters were collected from 14 industrial ball mills, ranging in diameters from 3.2 to 4.8 m. The ball loads within the mills were measured by different methods proposed in the literature and power draw of each mill were calculated. The results showed that power draw of the cement mills could accurately be predicted by the method proposed in this study.

Key words: power draw, cement, dry grinding, ball mill

INTRODUCTION

Energy is the most important cost item in a cement plant. About 60% of the electricity consumption for cement production is used for grinding the raw material and cement clinker (Zhang et. al., 1988). Annual cement production is approximately 1.6 billion tons and the grinding process consumes nearly 2% of the electricity produced in the whole world (Norholm, 1995).

Grinding of cement clinker has been traditionally performed by the ball mills which can either be open circuit or closed circuit with an air classifier. Selection of right mill for the specified duty is the most critical for circuit design, since it has the highest capital and operating costs.

Bond method has been used for ball mill selection in both mineral and cement industry for 50 years. It is basically rely on determination of grindability of material in a specified laboratory mill. Then, using empirical equations developed by Bond, and later with minor revisions by Rowland, the mill size is determined (Rowland, 1985; Napier-Munn et. al., 1996; Man, 2000). Once, the size and ball load is determined, the power draw for a given mill is calculated using Equation 1.

* Hacettepe University, Department of Mining Engineering, Ankara, Turkey, lergun@hacettepe.edu.tr

$$KW_b = 4.879 \times D^{0.3} \times (3.2 - 3V_p) \times fC_s \times \left(1 - \frac{0.1}{2^{9-10C_s}}\right) + S_s \quad (1)$$

where

- KW_b – Kilowatts per metric ton of balls
 D – Mill diameter inside liners in meters
 V_p – Fraction of mill volume loaded with balls
 fC_s – Fraction of critical speed
 S_s – Ball size factor

To determine the power that a dry grinding needs, full grate discharge mill Equation 1 is multiplied by the factor of 1.08. A multi-compartment ball mill consists of two or more grate discharge ball mills in series. The same equation is used to calculate the power that each ball mill compartment should draw. The total power is the sum of the power calculated for each of the separate compartments.

Although, Bond's method has been widely used, the required link to classification is missing. Therefore, it is not possible to calculate circuit performance when any of the design and operational parameters are changed (Napier-Munn et. al., 1996; Man, 2000). Model based methods has becoming popular to overcome these deficiencies (Herbst and Fuerstenau, 1980; Austin and Klimpel, 1982; Kavetsky and Whiten, 1982; Morrell and Man, 1997).

Morrell and Man (1997) proposed a model based approach using the results of the Bond ball mill grindability test for overflow wet ball mills. An approach was proposed by Erdem (2002) for dry multi-component cement grinding ball mills, using the results of the Bond ball mill grindability test.

For all model based methods, a reliable method to calculate mill power draw for a given mill is required for the calculation of power draw. Morrell (1996) proposed a mathematical model for autogenous, semi-autogenous and ball mills which is based on the motion of grinding charge inside the mill. He also verified his approach with various plant data (Napier-Munn et. al., 1996).

In this study, power draw of 14 multi-compartment cement grinding mills were calculated based on Morrell's approach. Design and operational parameters for the mills were collected from operating plants. With this respect, ball load within the mill which is the most determining factor for power draw was determined by several methods proposed in the literature (Austin et. al., 1984; Napier-Munn et. al., 1996).

MORRELL'S C-MODEL (1996)

The charge is treated as a continuum, which allows analytical solutions to the equations that are developed. The model can be expressed as:

$$\text{Gross power} = \text{no-load power} + (k \times \text{charge-motion power}) \quad (2)$$

Where gross power is the power input to the motor, no-load power is the power input to the motor when the mill is empty, charge-motion power is the power associated with the movement of the charge, and (k x charge-motion power) is the total power input to the charge. k is a lumped parameter that allows for heat losses and energy consumed. In this model, there are three principal equations for calculating the power draws associated with the charge in the cylindrical and conical end-sections of a wet tumbling mills. Power draw of cylindrical section is calculated using Equation 3, Power draw of conical section is calculated using Equation 4, and no-load power is calculated using Equation 5 (Morrell, 1996). Schematic diagram of cone-end of a wet system ball mill seen in Figure 1 is not so same shape as the dry system multi-compartment ball mill. This area covers too small place of all grinding surface due to design form, so power draw of conical section is negligible when calculating the gross power of tube mills.

$$P_t = \left[\frac{\pi \cdot g \cdot L \cdot N_m \cdot r_m}{3(r_m - z \cdot r_i)} \right] \times \left[2r_m^3 - 3z \cdot r_m^2 \cdot r_i + r_i^3 (3z - 2) \right] \times \left[\rho_c \cdot (\sin \theta_S - \sin \theta_T) + \rho_p \cdot (\sin \theta_T - \sin \theta_{TO}) \right] + \left[L \cdot \rho_c \cdot \left(\frac{N_m \cdot r_m \cdot \pi}{(r_m - z \cdot r_i)} \right)^3 \times \left[(r_m - z \cdot r_i)^4 - r_i^4 \cdot (z - 1)^4 \right] \right] \quad (3)$$

$$P_c = \left[\frac{\pi \cdot g \cdot L_d \cdot N_m}{3(r_m - r_i)} \times \left[r_m^4 - 4r_m \cdot r_i^3 + 3r_i^4 \right] \right] \times \left[\rho_c (\sin \theta_S - \sin \theta_T) + \rho_p (\sin \theta_T - \sin \theta_{TO}) \right] + \left[\frac{2\pi^3 \cdot N_m^3 \cdot L_d \cdot \rho_c}{5(r_m - r_i)} \times (r_m^5 - 5r_m \cdot r_i^4 + 4r_i^5) \right] \quad (4)$$

$$p_y = 1.68 \cdot D^{2.05} \times \left[\phi \cdot (0.667 \cdot L_d + L) \right]^{0.82} \quad (5)$$

- P_t – Power draw of cylindrical section, kW
- P_c – Power draw of conical section, kW
- L – Length of cylindrical section of mill inside liners, m
- L_d – Length of cone-end, m
- N_m – Rotational rate of mill, rev/s
- g – Acceleration due to gravity, m/s²
- ρ_c – Density of total charge, t/m³
- ρ_p – Density of discharge, t/m³
- Z – Parameter
- D – Diameter of cylindrical section of mill inside liners, m
- r_m – Radius of mill inside liners, m
- r_i – Radial location of inner surface of charge, m
- r_t – Radius of discharge trunnion, m

- ϕ – Fraction of theoretical critical speed, %
 θ_S – Angular displacement of shoulder location at mill shell, radians
 θ_T – Angular displacement of toe location at mill shell, radians
 θ_{TO} – Angular displacement of surface of slurry pool at toe, radians

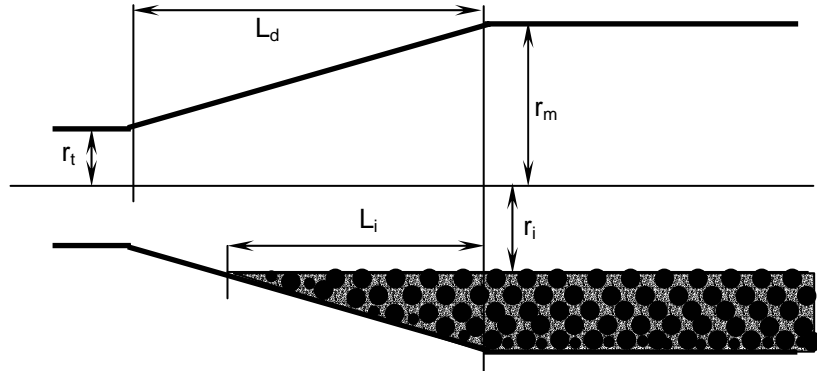


Figure 1. Schematic diagram of cone-end of a wet system ball mill

EXPERIMENTAL WORK

To verify the new power draw approach, detailed surveys of the 14 ball mill circuits at 6 different plants were carried out. The ball mills sampled in this study are ranging in diameters from 3.2 m to 4.8 m. Design and operational parameters of the ball mills sampled are given in Table 1.

Table 1. Sampled ball mill's design and operational parameters range

Operating and Design Variables	Values
Mill diameter	3.2 – 4.8 m
1 st chamber length	3.15 – 4.25 m
2 nd chamber length	5.18 – 10.00 m
Total fractional mill filling of 1 st chamber length	29.00 – 32.98 %
Total fractional mill filling of 2 nd chamber length	27.20 – 34.90 %
Mill rotational speed	14.87 – 17.34 rev/min
Fraction critical speed	71.89 – 77.02 %
Specific gravity of ore	2.90 – 3.10 tons/m ³
Bulk density of ore	1.54 – 2.07 tons/m ³
Mill Power	1450 – 5200 kW

The mill load that is the volume of charge in the mill is the principal determinant of power draw. Estimation of the ball load that is mixed with the cement charge is difficult and can be highly erroneous. So direct measurement must be taken for calculation of mill load. A direct measurement of the load entails the crash stopping of the ball mill under load whilst the mill is running under steady state conditions. Before taking measurement steady state conditions were verified by the plant staff, then the mills were crash stopped so that required measurements could be taken from the both compartments along the grinding path inside the mills. The load within the mills was determined by measuring the width and length of the charge and perpendicular distance between the charge and liner surface at various points in each compartment as seen in Figure 2. At the same time, all variables measured were recorded in the control room during these operations.

From these measurements the load volume can be calculated with using simple geometry and different equation proposed by Morrell and Allis Chalmers Company. Mill load volume can be also calculated with using Equation 9 if total ball tonnage value is known. All of the equations used to calculate the load volume are given below. Mathematical equation using X, Y measurements and geometry relations to calculate the load volume is given in Equation 6, proposed by Morrell in Equation 7, and proposed by Allis Chalmers Company in Equation 8. Basic notation used in calculations is given in Figure 3.

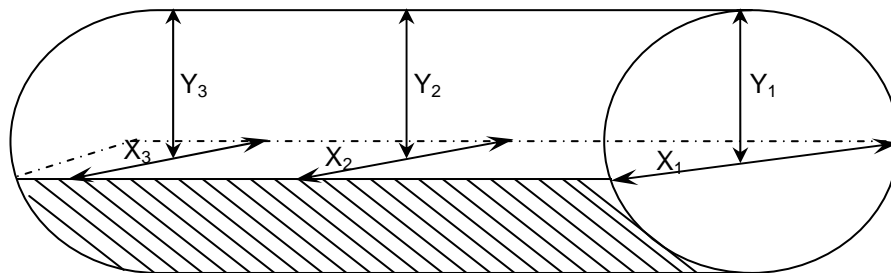


Figure 2. Mill inside measurement points

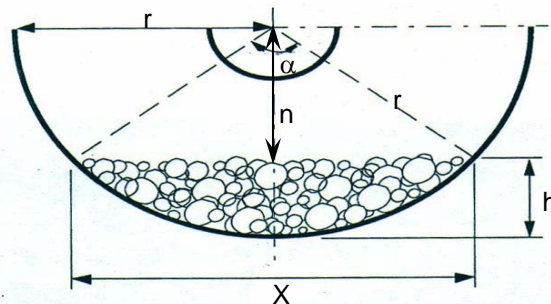


Figure 3. Cross section view of ball mill

$$\% \text{ mill load} = \frac{(A_{\alpha} - A_{ii})}{A_d} \times 100 \quad (6)$$

$$\% \text{ mill load} = \frac{\left(\frac{h}{6X} \cdot (3h^2 + 4X^2) \right)}{A_d} \times 100 \quad (7)$$

$$\% \text{ mill load} = 113 - \left(\frac{Y}{D} \times 126 \right) \quad (8)$$

$$\% \text{ mill load} = \frac{\left(\frac{10 m_d}{6 \rho_b} \right)}{A_d \cdot L} \times 100 \quad (9)$$

A_{ii} – Area of triangle with h height and X base length, m^2

A_{α} – Area of arc with α angle, m^2

A_d – Area of circle with r radius, m^2

h – Height of mill load, m

X – Width of the charge, m

Y – Perpendicular distance between the charge and liner surface, m

m_d – Tonnage of ball in each compartment, ton

ρ_b – Density of ball, ton/m^3

L – Length of compartment, m

D – Radius of mill, m

POWER DRAW CALCULATIONS AND DISCUSSION

In a cement plant mill load value calculated with different approaches are given in Table 2.

Table 2. Calculated mill load volume with using different calculation method for Çorum cement mill

Calculation Method	Mill Load Volume	
	1 st Chamber	2 nd Chamber
Geometric equation (Using measured horizontal (X) value)	32.04	24.55
Geometric equation (Using measured vertical (Y) value)	27.48	26.63
Allis Chalmers equation	27.19	26.30
Morrell equation	28.10	26.25
Mathematical equation (Using total ball tonnage value)	25.44	29.66

Representative samples were also taken from the material being ground in the mill to determine the bulk and specific gravity of the material after a crash stop of the mill. Specific gravity and bulk density of the materials were determined by using air-pycnometer and a graduated vessel respectively.

After these required measurements and mill load volume calculation which will be used in power model were obtained no-load power, charge motion power for first and second compartment and finally gross power were calculated separately. To illustrate the calculation steps a worked example is given for a cement ball mill. To execute the calculation certain design and operating data are required. These are summarized in Table 3.

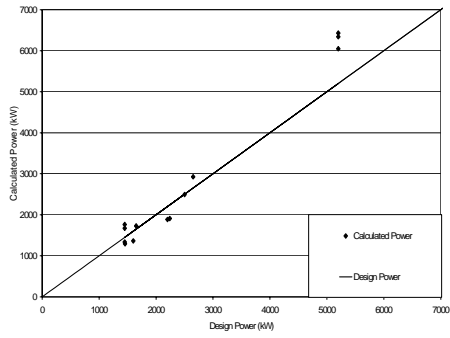
Table 3. Operating and design data for calculation

Operating and Design Variables [units]	Values
Mill diameter, [m]	3.27
1 st chamber length, [m]	3.60
2 nd chamber length, [m]	7.00
Total fractional mill filling of 1 st chamber length, [%]	27.48
Total fractional mill filling of 2 nd chamber length, [%]	26.63
Ball and void fractional mill filling of 1 st chamber length, [%]	19.98
Ball and void fractional mill filling of 2 nd chamber length, [%]	19.36
Mill rotational speed, [rev/min]	17.00
Fraction critical speed, [%]	72.67
Specific gravity of ore, [tons/m ³]	2.93
Bulk density of ore, [tons/m ³]	2.00
Specific gravity of balls, [tons/m ³]	7.80
Fractional porosity of charge	0.40

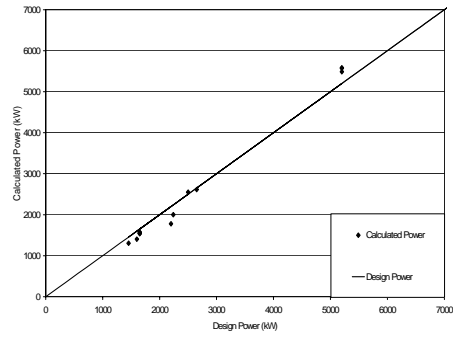
Calculation steps:

1. Calculate the charge motion power for first and second compartment. From Equation 3 first compartment charge motion power: 341.97 kW and second compartment charge motion power: 650.69kW.
2. Calculate the no-load power for first and second compartment. From Equation 5 first compartment no-load power: 41.94kW and second compartment no-load power: 72.35kW.
3. Calculate the gross power. Total power draw due to charge motion in the mill is 992.66kW, no-load power is 114.29kW and calibration factor that allows for heat losses and other energy consumed, k , is 1.26. From Equation 2: gross power (power input to the motor): 1365.04kW.

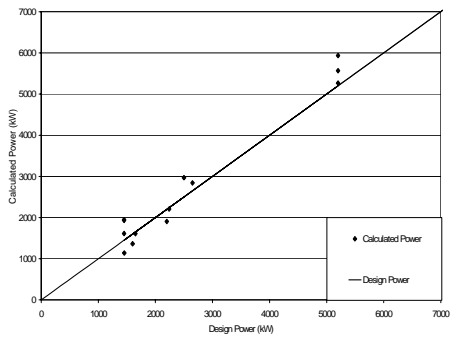
Graphically the accuracy of this new approach to calculate power draw of dry ball mills used in cement grinding is illustrated in comparisons of the observed and predicted power draws in Figure 4.



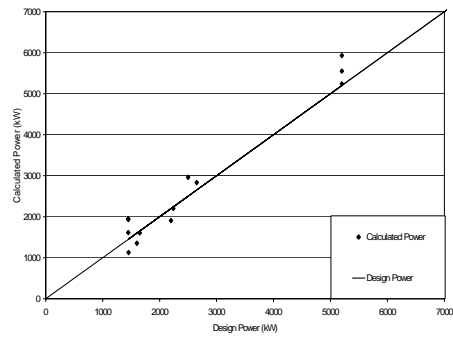
a – Calculated and design power values (Using measured horizontal (X) value mill load)



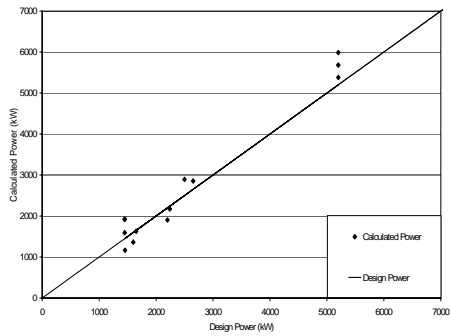
d – Calculated and design power values (Using Allis Chalmers equation mill load)



b – Calculated and design power values (Using measured horizontal (X) value mill load)



e – Calculated and design power values (Using total ball tonnage value mill load)



c – Calculated and design power values (Using Morrell equation mill load)

Figure 4. Observed vs design power consumption of ball mills

In order to design a ball mill and to calculate the specific energy of grinding, it is necessary to have equation(s) law which relates mill power and mill size and mill operating conditions.

Power draw varies as a function of ball loading and rotational speed. Lifter design is another parameter for the power draw of the mills. Although the cement mills sampled in this study have got similar ball loading, rotational speed and lifter design, different mill power draws were recorded. The data give the opportunity to set the exact relationship between the mill diameter and power draw for the cement mills.

As mentioned in the context, there are some several ways of determining the load in the mill. Ball milling operations start with a design charge and under normal operating conditions. It is necessary to add the make up charge. This will cause losing the mill load data at the sepecific circuit. Therefore, it is the best way to calculate the mill load is to get the measurements. In order to achieve the most efficient operation, mill conditions should be optimized and the choice of mill conditions are dependent on the economics of ball loading and wear.

In this exercise the success of the calculation methods are compared with the ball tonnage recorded during the plant survey. As given in Figure 4 the predictions give very good fit with the measured data.

CONCLUSIONS

A new approach based on Morrell's C model is used to calculate the power draw of dry multi-compartment ball mills. Calculated power draws were in good agreement with the measured values. Volumetric mill load calculated using different equations gave similar results. Increasing the number of measurements taken along the width and length of the mill would improve the accuracy of the calculation.

It was found that the power draw of dry multi-compartment ball mills used in cement grinding could successfully be predicted using this approach. However, this method needs to be validated with more data sets including variation of other operating parameters such as critical speed and lifter design.

REFERENCES

- AUSTIN L. G. KLIMPEL R. R., LUCKIE P. T. AND ROGERS R. S. C., (1982), *Simulation of grinding circuits for design, Design and Installation of Comminution Circuits*, American Institute of Mining, Metallurgical and Petroleum Engineers Inc, New Jersey, 1982, Editor; Mular, A. L., Jergensen, G. V., Chapter 19, pp. 301-324.
- AUSTIN L. G., KLIMPEL, R. R. AND LUCKIE, P. T. (1984), *Process engineering of size reduction: ball milling*, American Institute of Mining, Metallurgical and Petroleum Engineers Inc, New Jersey, 1984, pp. 1-556.
- ERDEM A. S. 2002, *Modelleme yardımıyla kamaralı bilyalı değirmen tasarımı ve tane boyu dağılımlarının belirlenmesi*, Hacettepe Üniversitesi Maden Mühendisliği Anabilim Dalı Yüksek Mühendislik Tezi, 2002.
- HERBST J. A., FUERSTENAU D. W. (1980), *Scale-up procedure for continuous grinding mill design using population balance models*, International Journal of Mineral Processing, 7, 1980, pp. 1-31.

- MAN Y. T. (2000), *A model-based procedure for scale-up of wet, overflow ball mills*, Julius Kruttschnitt Mineral Research Centre Department of Mining, Minerals and Materials Engineering, Degree of Doctor of Philosophy, The University of Queensland, February 2000.
- MORRELL S. (1996), *Power draw of wet tumbling mills and its relationship to charge dynamics, part 1: A continuum approach to mathematical modelling of mill power draw*, Transaction of Institute of Mining and Metallurgy, Section C: Mineral Processing and Extractive Metallurgy, 105, January-April 1996, pp. 43-53.
- MORRELL S., MAN Y. T. (1997), *Using modelling and simulation for the design of full scale ball mill circuits*, Minerals Engineering, 1997, Volume 10, No. 12, pp. 1311-1327.
- NAPIER-MUNN T. J., MORRELL S., MORRISON R. D., KOJOVIC T., (1996), *Mineral comminution circuits their operation and optimisation*, Editor; Napier-Munn, T. J, pp. 1-413.
- NORHOLM A. (1995), *Notes on energy conservation*, FL Smidth and Co. Seminar, September 1995, İstanbul, Turkey,
- ROWLAND C. A. (1982), *Selection of rod mills, ball mills, pebble mills and regrind mills*, *Design and Installation of Comminution Circuits*, American Institute of Mining, Metallurgical and Petroleum Engineers Inc, New Jersey, 1982, Editor; Mular, A. L., Jergensen, G. V., Chapter 23, pp. 393-438.
- ROWLAND C. A. (1985), *Ball mills*, *SME Mineral Processing Handbook*, American Institute of Mining, Metallurgical and Petroleum Engineers Inc, New York, 1985, Editor; Weiss, N. L., Section 3C.
- WHITEN W. J., KAVETSKY A. (1984), *Studies on scale-up of ball mills*, Minerals and Metallurgical Processing, May 1984, pp. 23-28.
- ZHANG Y. M., NAPIER-MUNN T. J., KAVETSKY A. (1988), *Application of comminution and classification modelling to grinding of cement clinker*, Transactions of Institute of Mining and Metallurgy, Section C: Mineral Processing and Extractive Metallurgy, 97, December 1988, pp.207-214.

Erdem A.S., Ergün Ş.L., Benzer A.H., *Zużycie energii przez pracujące „na sucho”, wielokomorowe młyny kulowe*, Physicochemical Problems of Mineral Processing, 38, (2004) 221-230 (w jęz. ang.).

W pracy zaproponowano nowe podejście do problemu kalkulacji zużycia energii przez młyny kulowe pracujące „na sucho”, stosowane do otrzymywania cementu. Dla realizacji tego zamierzenia, zgromadzone zostały dane operacyjne i projektowe z 14 instalacji przemysłowych, które zawierają młyny kulowe o średnicy w przedziale od 3,2 do 4,8 m. Załadunek kulami każdego młyna został zmierzony przy wykorzystaniu różnych metod, proponowanych w literaturze. Zużycie energii przez każdy z badanych młynów, zostało wyliczone. Otrzymane wyniki wskazują, że zużycie energii przez młyny do produkcji cementu można dokładnie przewidzieć stosując metodę zaproponowaną w pracy.

Levent ERGÜN, Zafir EKMEKÇİ, Özcan GÜLSOY, Hakan BENZER*

MODELLING AND SIMULATION OF GRINDING CIRCUIT IN MADNEULI COPPER CONCENTRATOR

Received May 11, 2004; reviewed; accepted June 28, 2004

In this study, modelling and simulation studies to improve the performance of grinding circuit of Madneuli Copper Flotation Plant in Georgia were presented. After detailed sampling surveys, size distribution and solids content of the samples were determined. Then, mass balance of the circuit was calculated using these data. The results showed that the existing performance of the plant was not good and required to be improved. Using the data obtained, the models were developed for the mills and classifiers used in the circuits. Finally, several alternatives for a better performance were evaluated by using computer simulation. The results showed that the performance of the circuit could be improved and energy consumption in the grinding circuit could also be decreased.

Key words: grinding, modelling, simulation, classification

INTRODUCTION

Madneuli concentrator has a design capacity of 1610000 tons per annum consists of three parallel grinding circuits. While two of them are identical and have an annual capacity of 680000 ton., third circuit has annual capacity of 250000 tons.

A performance evaluation study in a flotation plant indicated that the flotation feed fineness should be increased to improve the flotation performance (Ergün et al, 2000).

Simulation of the grinding circuits using mathematical models of the mills and classifiers is a technique which is being used increasingly in comminution because of its low cost and its ability to consider many variables simultaneously (Lynch 1977, Napier-Munn et al., 1996).

Simulation would provide the quantified information about the effects of the proposed changes on the circuit performance in terms of size distribution, solid and water flowrates etc. Such information could then be used to check the suitability of the existing equipment to the modified conditions, and for equipment selection.

* Hacettepe University, Department of Mining Engineering, Ankara, Turkey, lergun@hacettepe.edu.tr

The aim of the study was to develop mathematical models of ball mills and classifiers used in the grinding circuit and to investigate the effects of the proposed modifications on the circuit performance using simulation. For this purpose, sampling surveys were carried out around the circuit. The size distributions of the samples formed the main data basis for the following simulation studies. The raw data was first mass balanced. Then, they were used for the calibration of the equipment models for the circuit. Finally, the effects of a number of flowsheet changes as well as the effects of changing operating parameters on the circuit performance were investigated by computer simulations using calibrated models.

SAMPLING AND LABORATORY STUDIES

To evaluate the performance of grinding circuits and to obtain the data required for the modelling studies, samples were taken from the points marked in Figure 1. Because of the similarity of the three different circuits, sampling and performance evaluation was only applied to the second circuit in the plant.

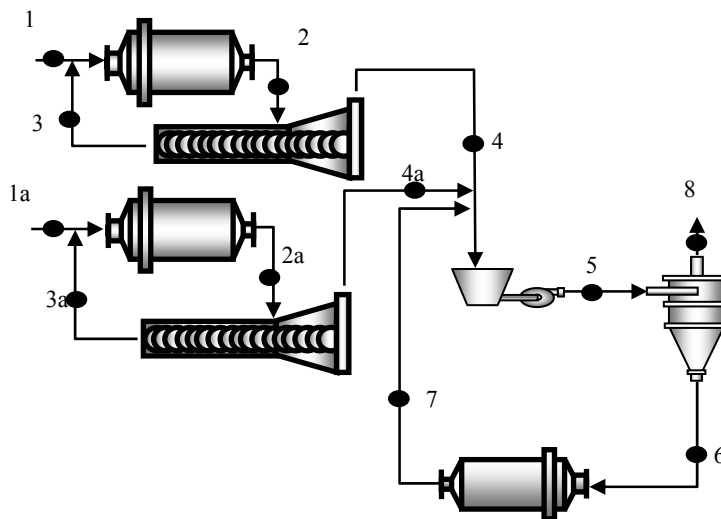


Fig. 1. The simplified flowsheet and sampling points around the circuit

For this purpose, pulp samples were taken from grinding circuits. All samples were dried, weighed and sieved. Size distribution of each sample was determined down to 6 μm . Mass balancing of grinding circuits were performed to calculate the flowrates in each stream.

All the size distributions of the samples taken were determined. In order to characterize the breakage characteristics of the ores at the mine Work index and drop weight breakage function were measured.

Work indices of the samples were determined by using standard Bond Work index test. The results are given in Table 1.

Table 1. Bond work indices of the different ore types in Madneuli deposit.

	Plant feed	Oxidised ore	Sulphide ore	Complex ore
Wi (kWh/ton)	10.1	6.27	12.53	13.84

Despite the major variations among the work indices of the different ore types, the plant feed prepared by blending the three ores gives a mean value. Breakage functions of the ore were also measured to expose the breakage behaviour of the ores. These data give us the opportunity to reflect different breakage characteristics to the model structure. Breakage functions of the three different ores are illustrated in Figure 2.

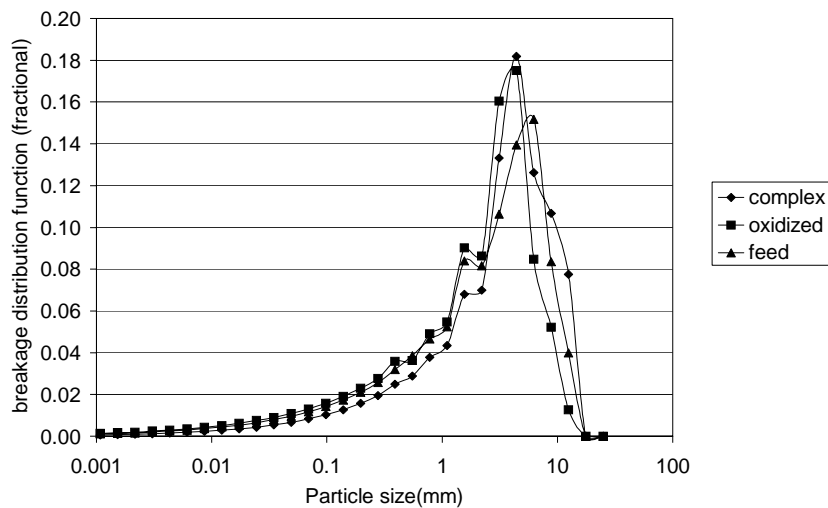


Fig. 2. Breakage functions of different ores mined in Madneuli ore deposit

MASS BALANCING

To evaluate the existing performance of the grinding circuit mass balancing studies were carried out by using the plant survey data. The flow rates are given in Figure 3. During the sampling survey the plant capacity was measured as 84.5 tph. The measured value of the flotation feed fineness was found to be only about 43-45% - 74 μ m in the circuit. After mass balancing, to compare the measured and calculated values, the size distributions of the measured and calculated data were plotted. The following figures show this comparison for each point in the circuit (Figure 4-5).

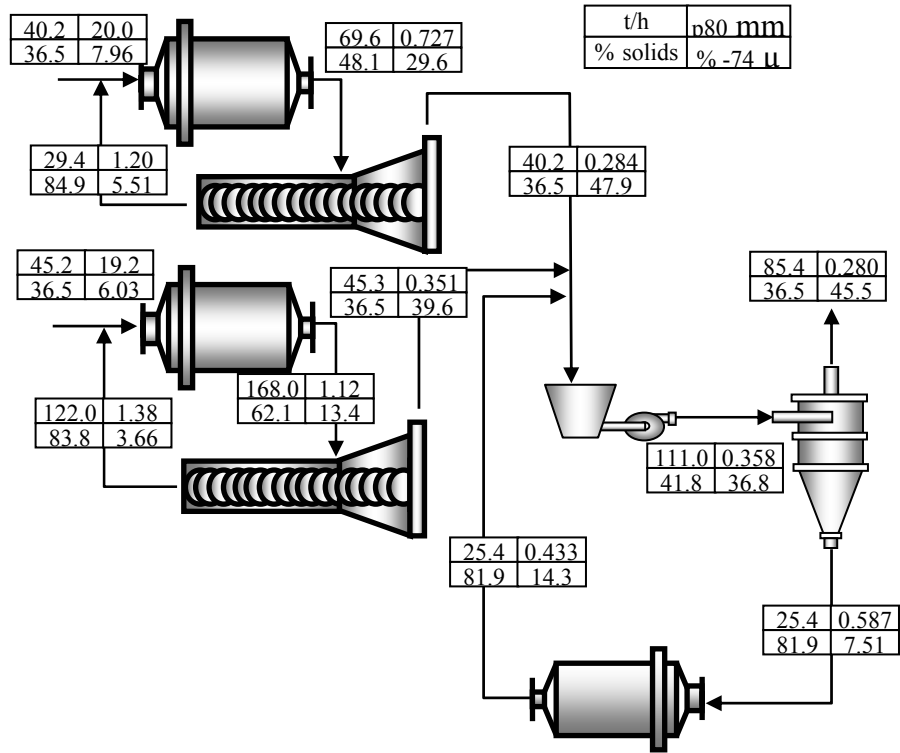


Fig. 3. Flow rates after mass balancing

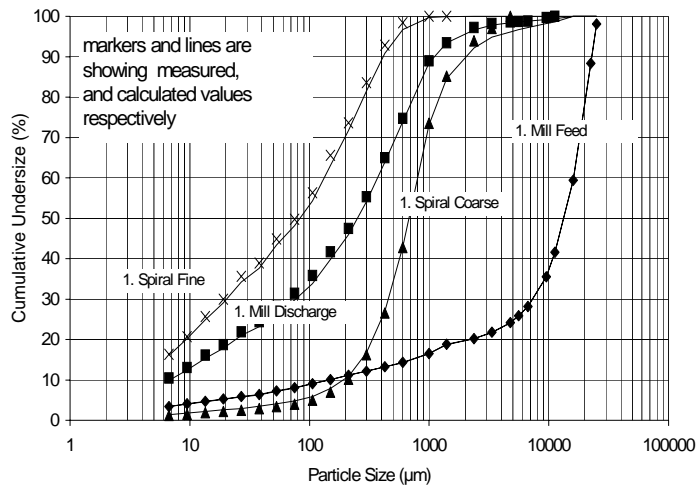
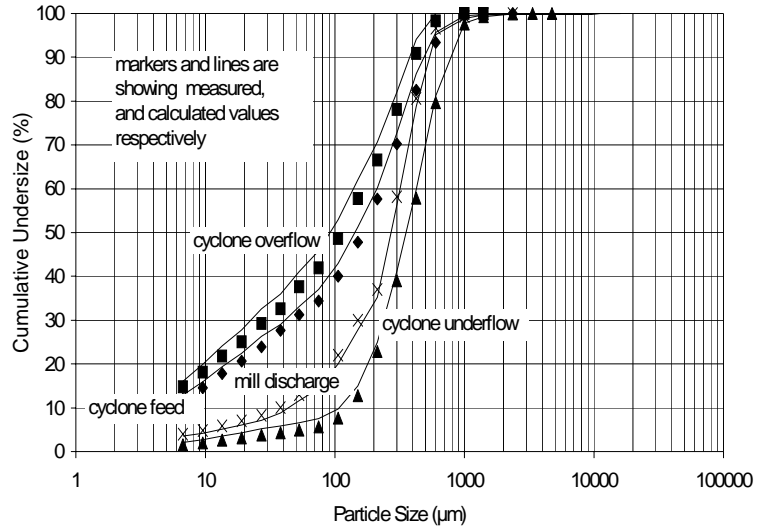
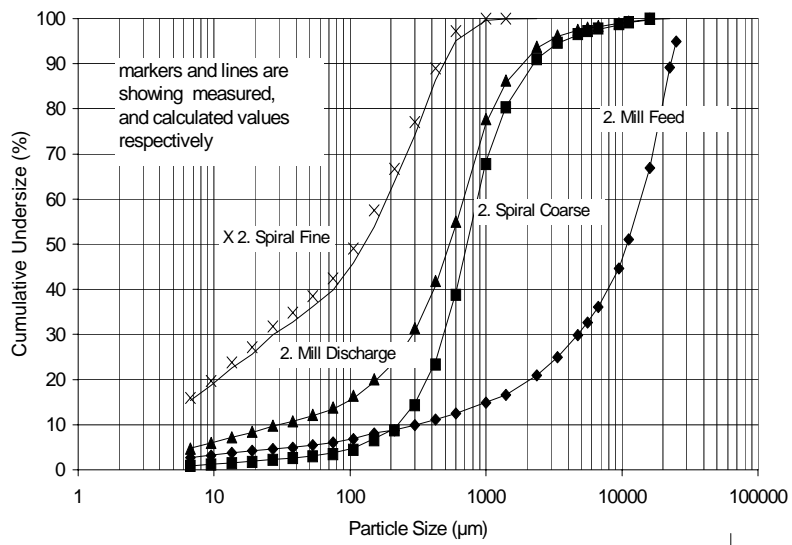


Fig. 4. Measured and mass balanced values around 1st, 2nd primary grinding circuit



(a)



(b)

Fig. 5 a, b. Measured and mass balanced values around secondary grinding circuit

MODELLING STUDIES

As shown in the figures, mass balance of each stream was obtained without any significant correction on the measured data. Therefore, the data obtained from mass balance could be used for modelling of the grinding circuit. Then, models for each unit in the circuit were developed by using mass balanced data.

The models used are the perfect mixing model for ball mills and the efficiency curve model for separators.

Ball mill model for steady state operations includes two sets of model parameters, i. e. the breakage function (a_{ij}) and a combined breakage/discharge rate (r_i/d_i) function.

$$f_i - r_i \frac{p_i}{d_i} + \sum_{j=1}^i a_{ij} r_j \frac{p_j}{d_j} - p_i = 0 \quad (1)$$

Calibration of a ball mill model is the calculation of r/d values using the feed and product size distributions obtained under particular operating conditions.

Classifiers are modelled using efficiency curve approach (Napier-Munn *et al*, 1996). The mathematical model selected for the study is capable of defining the fish hook type efficiency curves. The general form of the equation is presented below.

$$E_{oa} = C \left[\frac{(1 + \beta \cdot \beta^* \cdot X)(\exp(\alpha) - 1)}{\exp(\alpha \cdot \beta^* \cdot X) + \exp(\alpha) - 2} \right] \quad (2)$$

where

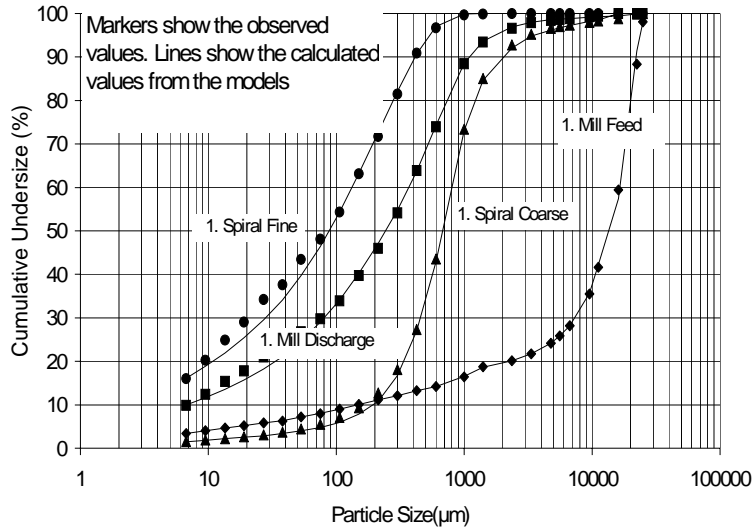
$$X = \frac{d_i}{d50_c} \quad (3)$$

In cases where the efficiency curve does not exhibit fish hook behaviour, the parameter β is equal to zero and a simplified form of this equation is obtained:

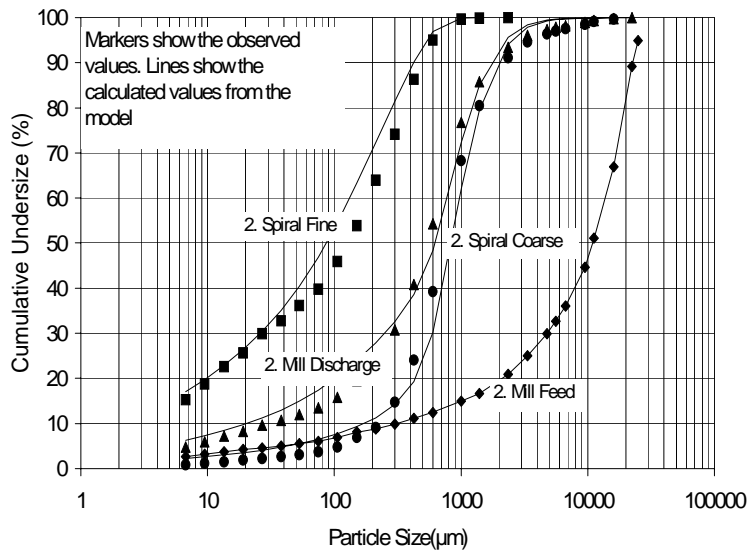
$$E_{oa} = C \left[\frac{\exp(\alpha) - 1}{\exp(\alpha \cdot X) + \exp(\alpha) - 2} \right] \quad (4)$$

The classifier performance can be modelled in terms of $d50(\text{corr})$, by-pass (1-C), the "fish hook" (β), and the sharpness of the curve (α).

In order to control the accuracy of the models, size distributions of each stream were calculated by using only the size distribution of the feed. The following figures show the comparison of measured and predicted size distributions (Figures 6-7).



(a)



(b)

Fig. 6 a, b. Measured and predicted values around 1st and 2nd primary grinding circuit

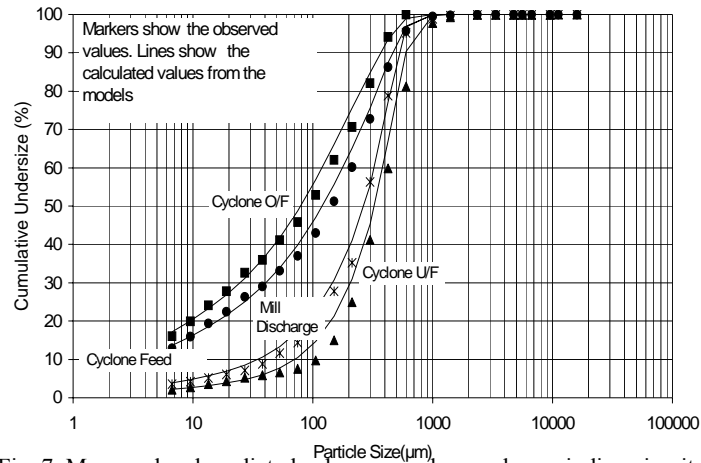


Fig. 7. Measured and predicted values around secondary grinding circuit

The figures show clearly that the plant conditions can be simulated perfectly by the models derived. Thus, several operation alternatives were tested during simulation studies to obtain optimum conditions.

SIMULATION STUDIES

Mass balance studies indicated that the circuit was operating under its design capacity which is 100 tph. Therefore, during simulation studies first the performance of 100 tph and 110 tph were predicted. As expected, the flotation feed became coarser. These figures provided a basis for further simulation studies. Then, simulation studies were performed by modifying ball size, cyclone geometry, feed size and % solids in the primary ball mill to obtain optimum conditions for the existing and alternative flowsheets. Simulation results are summarised in Table 2.

Table 2. The results of the simulation studies

	Feed rate (t/h)	1 st & 2 nd primary grinding circulating loads (t/h)	Secondary grinding circulating load (t/h)	Final product fineness % -74 µ
Existing conditions	100	42.5 & 145	31.0	42.9
Existing conditions	110	49.9 & 170	35.1	42.2
Optimum conditions	100	34.8 & 35.7	17.2	62.0
Optimum conditions	110	74.1 & 74.4	19.7	60.6
Hard ore (Wi:13.84)	100	41.0 & 42.2	19.2	58.3
Cyclone diameter:500 mm	100	34.8 & 35.7	80.6	69.3
Cyclone diameter:650mm	100	34.8 & 35.7	82.8	68.7
Cyclone diameter:700 mm	100	34.8 & 35.7	85.2	67.4
Cyclone diameter:750 mm	100	34.8 & 35.7	81.5	67.7

During the simulation studies, an alternative grinding circuit was also proposed. In this alternative, primary ball mills was replaced by a rod mill of which model parameters are known. The rod mill parameters were taken from another study (Ergün et al., 2000). Instead of using the three ball mills each having a motor power of 630 kW in the circuit, a rod mill with 400 kW motor power and a ball mill operating in series would provide the same fineness at higher capacities with the power savings of 45 %. The flowsheet of the existing and this alternative grinding circuit is given in Figure 8.

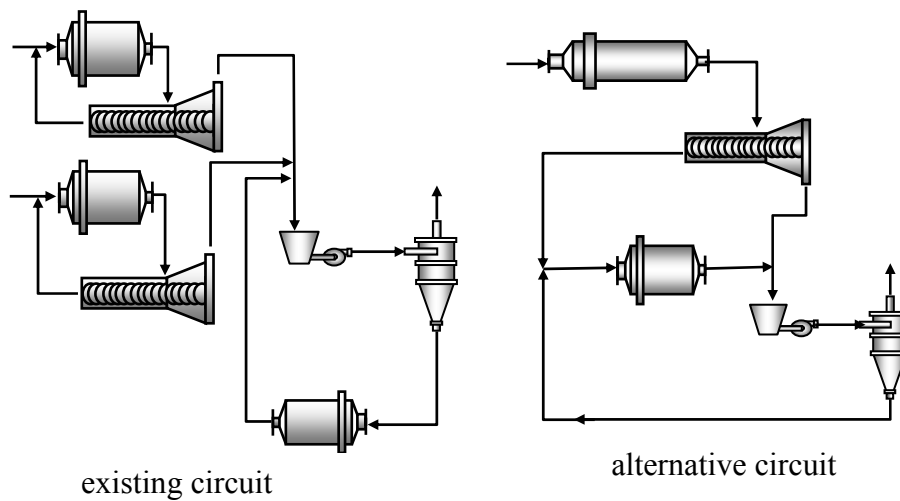


Fig. 8. The flowsheet of the alternative circuit in which rod mill is used

On this alternative circuit, the effects of various operation conditions on circuit performance were also predicted. The results of these simulation studies are summarised in Table 3.

Table 3. The results of these simulation studies

	Feed rate (t/h)	Ball mill circulating load (t/h)	Final product fineness % -74 μ
Optimum conditions	100	154	64.0
Optimum conditions	110	174	62.9
Cyclone diameter:500 mm	100	102	66.1
Cyclone diameter:650mm	100	106	65.5
Cyclone diameter:700 mm	100	109	64.0
Cyclone diameter:750 mm	100	105	64.4
Hard ore (Wi:13.84)	100	142	59.9

CONCLUSIONS

In this study, the performance of the existing grinding circuit in Madneuli copper plant was determined. The results showed that the existing performance of the grinding circuit could be improved and the fineness of the flotation feed could be increased to the desired value.

Two alternatives were proposed. First, optimisation of the existing circuit to produce finer product and second using combination of rod and ball mill instead of the existing two stage ball mill grinding. These alternatives will provide finer product with higher capacity and flexibility to increase the capacity. Besides production of finer product, rod and ball mill combination will reduce the energy consumption significantly.

Bond tests indicated that the different ore types in the plant have got different work indices. Therefore, it can be concluded that blending of the plant would provide a consistent feeding to the plant. The breakage tests showed that the material have got a brittle structure and can easily be broken under impact mechanism.

REFERENCES

- ERGÜN, L., EKMEKÇİ, Z., GÜLSOY, Ö., BENZER, H. AND ASLAN, A. (2000), *Performance evaluation studies in Madneuli (Georgia) copper flotation plant and optimization of grinding circuit by using modelling and simulation*, Project Report, (unpublished), pp. 189.
- LYNCH, A.J. (1977). *Mineral crushing and grinding circuits: their simulation, optimisation, design and control*, Elsevier, pp. 340.
- NAPIER-MUNN, T.J., MORRELL, S., MORRISON, R.D. and KOJOVIC, T. 1996. *Mineral comminution circuits: their operation and optimisation*. JKMRRC., pp. 413.
- ERGÜN, L., EKMEKÇİ, Z., GÜLSOY, Ö., CAN N.M., ORHAN E. C., DİKMEN S., OBUT A., (2000), *Investigations on the alternatives to obtain finer flotation feed at Küre grinding circuit by simulation*, Mineral Processing on the verge of the 21st Century, Özbayoğlu Eds, Balkema, Rotterdam.

Ergün L., Ekmeççi Z., Gülsoy Ö., Benzer H., *Modelowanie i symulacja węzła mielenia w zakładach wzbogacania miedzi Madneuli*, Physicochemical Problems of Mineral Processing, 38, (2004) 231-240 (w jęz. ang.).

W pracy zostały przedstawione modelowe badania symulacyjne mające na celu poprawę parametrów ruchowych sekcji mielenia w zakładzie wzbogacania rud miedzi Madneuli w Gruzji. Instalacja mielenia i klasyfikacji została opróbowana. Skład ziarnowy i zawartość części stałych w pobranych próbach zostały określone. Na podstawie zebranych danych został wykonany bilans masowy instalacji. Otrzymane z bilansu wyniki wskazują, że działający węzeł mielenia i klasyfikacji nie działa prawidłowo i wymaga poprawy. Został zoptymalizowany układ mielenia i klasyfikacji. Kilka alternatywnych rozwiązań wynikających z symulacji komputerowej zostało zaproponowanych. Otrzymane wyniki wskazują, że praca węzła mielenia i klasyfikacji może zostać poprawiona a zużycie energii w procesie mielenia także obniżone.

Ömürden GENÇ^{*}, Levent ERGÜN^{*}, Hakan BENZER^{*}

SINGLE PARTICLE IMPACT BREAKAGE CHARACTERIZATION OF MATERIALS BY DROP WEIGHT TESTING

Received May 28, 2004; reviewed; accepted June 30, 2004

A drop weight tester was designed for the purpose of analyzing single particle impact breakage characteristics of different materials. Test results were evaluated through the breakage distributions of different size fractions at various impact energy levels. Breakage parameter t_{10} (Narayanan, 1986) is used to represent the degree of size reduction which is assumed to be representative of the breakage product size distribution obtained from drop-weight tests. Relation between specific comminution energy level and breakage index number (t_{10}) was established on the size fractional base so that the variation in impact breakage characteristics of different materials can be evaluated. It can be concluded that, drop-weight test method is a useful and practical way of evaluating the impact strengths of various materials on the size fractional base and results of which can be used in the mathematical modelling of autogenous and ball milling.

Key words: grinding, modelling, breakage function, drop weight test.

INTRODUCTION

Breakage distribution of a material can be simply defined as the distribution of the fragments appearing after the breakage of single particles of different sizes. Although many methods are suggested in the literature for the measurement of breakage distributions experimentally, it is usually difficult to represent the breakage of materials by a standard method due to the mathematical formulation and non-normalizable breakage such as in the traditional approach of Austin (1984). Models of comminution equipments require the determination of breakage distributions known as breakage or appearance functions for the characterization of the material breakage. For example ball mills can be modelled by the perfect mixing model given in Equation 1.

^{*} Hacettepe University, Dept. of Mining Engineering, 06532, Ankara-Turkey
ogenc@hacettepe.edu.tr

$$f_i - p_i \left(\frac{r_i}{d_i} \right) + \sum_{j=1}^i a_{ij} p_j \left(\frac{r_j}{d_j} \right) - p_i = 0 \quad (1)$$

In this comminution model, f_i and p_i are the feed rates (t/h) of size fraction i , a_{ij} is the mass fraction of particle of size j that appear at size i after breakage, and (r_i/d_i) is a combined model parameter where r_i is the breakage rate of particle size i (h^{-1}) and d_i is the discharge rate of particle size i (h^{-1}). Determination of breakage distribution functions experimentally will enable the calculation of model parameter (r_i/d_i) if the feed and product size distributions are measured at the steady state conditions of the ball mill.

For the determination of breakage distributions and understanding of complex nature of particle breakage took in industrial grinding mills, single particle breakage characterization test methods can be used which are grouped into three main classes depending on the breakage mechanism; single impact, double impact (dynamic loading) and slow compression. These tests were used by many researchers for the investigation of input energy-size reduction relationships on the basis of energy utilization. Test results provide practical informations on the impact strengths of individual particles of different ores types. Beside the traditional approach of Austin (1984), it was stated that, tumbling action in a ball mill can be simulated in the double impact tests such as drop weight and pendulum methods although the energy available for particle breakage can only be obtained from pendulum tests (Lynch et al, 1986). Thus these type of tests were widely used for the characterization of ore particles ground in wet or dry ball mills for many years. A general review of single particle test applications and their results were presented by Narayanan (1986). Applications of pendulum tests and corresponding results were explained in the literature (Narayanan, 1985; Narayanan 1987; Munn et al, 1996; Weedon 2001).

On the other hand, various kinds of drop-weight testers were developed by which the breakage distribution and energy utilisation during breakage of different materials were investigated (Gross, 1938; Piret, 1953; Fairs, 1954; Schönert, 1972; Rumpf, 1973; Narayanan and Whiten, 1983; Pauw and Marè, 1988). In a classical drop-weight breakage set up, a single particle is subjected to breakage between two solid surfaces where the drop weight can be a steel ball or a plate. Narayanan (1985) used a ball shaped drop-weight in his breakage set-up to characterize chalcopyrite and lead-zinc ores ranging in size 9.5mm and 2.36mm. Andersen (1988), Man (2000) studied the breakage of +8mm ore particles by using the drop-weight apparatus developed at the Julius Kruttschnitt Mineral Research Centre which was described in detail by Napier Munn et al (1996). Man (2000) carried out single particle breakage tests by using the JKMRC drop-weight tester to characterize basalt which was considered to be relatively homogenous material. Man used two types of drop-weight testers namely, larger drop weight for the breakage of basalt particles ranging in size 45mm and 8 mm and a smaller one for the breakage of particles ranging between 8mm and 2.8mm in

which the dropping weights are steel plate and steel ball respectively. Test results showed that, breakage characteristics change with particle size and ore type on the otherhand at finer size fractions breakage product distributions do not vary. A different version of a drop weight tester was used by Asim (1984) for conducting bed breakage tests of clinker particles. In the drop-weight set up a bed of clinker, formed between four steel balls, was subjected to impact progressively by dropping a steel ball onto the centre of particle bed. Impact breakage of clinker was also studied by a twin pendulum device (Zhang, 1992).

Drop-weight tests have many recorded advantages compared to other single particle tests such as an extended input energy range, extended particle size range, shorter test duration, possibility to conduct particle bed breakage tests although they do not give any information about the actual energy consumed during the breakage of single particle. In order to understand the fracture and deformation characteristics of particles under impact loading, a different version of a drop weight tester known as the ultra-fast load cell was used by Tavares and King (1998) for the measurement of particle fracture energy, particle strength and particle stiffness. Many other studies concerning the investigation of breakage distributions of single particles in microscale with the aid of impact load cells were done by Weichert and Herbst (1986), Frandrich et.al (1998), Briggs (1997), Bourgeois and Banini (2002).

Evaluation of single particle breakage data through a single parameter is useful in the understanding of the main breakage characteristics namely size and input energy level dependency. Breakage characteristics of different size fractions can be examined at various impact energies expressed in kWh/ton or joules by determining the product size distribution of broken particle size at the selected energy level. A practical way of analysing single particle breakage data was given by Narayanan (1986). In that well-known approach, product size distributions are defined by a series of size distribution parameters such as t_2 , t_4 , t_{10} , t_{25} , t_{50} and t_{75} correspondingly expressing the cumulative per cent passing size of $x/2$, $x/4$, $x/10$, $x/25$, $x/50$, and $x/75$ where x is the geometric mean of the size interval for the test particles. t_{10} is selected in a traditional way as a breakage fineness comparison parameter.

Narayanan and Whiten (1983;1988) investigated the breakage test results quantitatively by plotting out t_{10} values as a function of specific input energy level. By this means, material strength to impact breakage can be determined through a single distribution parameter and the power demand to achieve the desired product fineness can also be predicted.

Relationship between t_{10} and specific comminution energy is represented by the comminution model given in Equation 2 (Leung,1987) where A and b are the material specific impact breakage parameters and E_{cs} is the specific comminution energy level in kWh/t.

$$t_{10} = A[1 - \exp(-bE_{cs})] \quad (2)$$

Value of A gives the maximum value of t_{10} , whereas the slope of the t_{10} versus E_{cs} plot gives the value of b. This relation was verified for different ore types broken by a twin-pendulum device (Leung et.al.,1987) and drop weight tester (Napier Munn et al, 1996 ; Man 2000).

The aim of this research was to investigate single particle impact breakage characteristics of different materials by the drop-weight test method.

BREAKAGE SET-UP AND EXPERIMENTAL STUDIES

SINGLE PARTICLE BREAKAGE SET-UP

Drop weight tester manufactured for the purpose of breakage study at the Mineral Processing Laboratory of Hacettepe University. A photograph of the drop weight apparatus is shown in Figure 1. It mainly comprises a steel anvil made from steel alloy, plate shaped drop weight head, an electromagnet through which an electromagnetic field is formed so that weights can be hold or released from desired heights. Drop weight head mass has a series of lead weights which can be added or removed when required. Drop weight apparatus is fitted with a 5.870 kg fixed head mass which can be extended to 44.16 kg with a maximum drop height of 51.50cm. representing a wide energy range. In this experimental set up, plate shaped drop weight is raised to a known height through a mechanical arm and then subjected to free fall onto a particle that is placed on the center of the steel anvil so that the impact breakage of particles are achieved. Breakage area is enclosed by an aluminium casing in order to prevent the losing of the broken fragments during the test. Drop weights of the breakage set up is tabulated in Table 1.

Table 1. Drop weights

	Drop weights
Fixed head weight	5.870 kg
Lead weights	11.690kg-10.550kg-9.300kg-4.421kg
Steel weights	1.429-3x4kg-11 kg-4.5kg
<i>Extra weights added during the test: 0.624kg-0.3956kg-Small bolt:0.0535 kg-Big bolt:0.1150kg</i>	

Tests were conducted on various size fractions of colemanite, quartz, copper ore, trass, limestone, gypsum, clay and cement clinker samples. Samples were dry sieved to the desired narrow size intervals and representative samples were taken from each size interval for each breakage energy level. For the calculation of breakage energy level, number of particles in each set of sample was counted to determine the mean mass of the particles. To achieve the desired specific comminution energy levels for each size, appropriate height and drop weights were calculated. Impact energy supplied by the plate shaped weight is calculated from the equations given by Napier-Munn et al (1996).



Fig. 1. A photograph of the drop weight apparatus

$$E_i = m_d g (h_i - h_f) \quad (3)$$

where,

- E_i : Impact breakage energy ($\text{m}^2 \text{kg}/\text{sec}^2$)
- m_d : Mass of drop weight head (kg)
- h_i : Initial height of the drop-weight above the anvil (m)
- h_f : Final height of the drop-weight above the anvil (m)

$$E_{cs} = E_i / m_p \quad (4)$$

where,

- E_{cs} : Specific comminution energy in kWh/t
- m_p : Mean particle mass in g.

Single particle breakage tests were conducted on each set of sample at the required energy levels and the broken fragments were collected from each set of particles, and dry sieved on a root 2 sieve series on a ro-tap sieve shaker for 15 minutes. Finally, breakage product size distributions of each sample was determined. Size fractions, average number of particles broken in each size fraction and experimental breakage energy levels are summarized in Table 2.

Table 2. Experimental conditions

Size fractions (mm)	Nominal particle size (mm)	Number of particles broken in each energy level	E _{input} levels (Joule)	E _{cs} levels (kWh/t)
Material: Colemanite				
-28+25.4	26.67	8	36.98 - 23.4 - 4.99	0.33 - 0.20 - 0.09
-22.4+19	20.63	15	37.16 - 23.67 - 9.85	0.59 - 0.38 - 0.16
-16.0+13.2	14.53	30	23.96 - 10.21	1.42 - 0.60
Material: Quartz Type I				
-63+55	58.86	2	140.37-222.25	0.11-0.17
-45+38	41.35	4	45.49-226.58-106.14	0.10-0.48-0.22
-31.5+25	28.06	10	38.99-167.23-228.75	0.25-1.03-1.44
-22.4+19	20.63	17	51.78-119.25-13.30	1.08-2.52-0.26
-16+13.2	14.53	35	39.36-16.71-4.09	2.52-1.07-0.26
Material: Quartz Type II (Bergama)				
-13.2+11.2	12.16	33	2.07-3.08-3.73	0.24-0.35-0.43
-9.5+8.0	8.72	58	2.04-2.71-3.85	0.49-0.67-0.92
-8.0+6.7	7.32	150	1.96-2.99-4.09	0.86-1.32-1.77
-5.6+4.75	5.16	233	1.96-4.09	2.47-5.16
Material: Copper ore				
-16+13.2	14.53	30	27.88	1.10
-13.2+11.2	12.16	60	17.88	1.07
-9.5+8.0	8.72	100	5.91	1.05
-5.6+4.75	5.16	175	4.09	3.15
Material : Trass Type I (cement additive)				
-16+13.2	14.53	30	4.94-10.04-15.43-15.36	0.39-0.80-1.22-1.79
-13.2+11.2	12.16	50	4.94-10.32-15.58	0.60-1.28-1.89
-9.5+8.0	8.72	70	4.91-10.56-15.58	1.72-3.87-5.61
Material : Trass Type II (cement additive)				
-9.5+8.0	8.72	100	3.57	1.04
Material : Limestone Type I (cement additive)				
-16+13.2	14.53	25	4.10-9.89-15.15	0.22-0.52-0.80
-13.2+11.2	12.16	40	4.25-10.17-15.22	0.34-0.81-1.21
-9.5+8.0	8.72	60	4.78-10.44-15.63	1.19-2.67-3.90
Material : Limestone Type II (cement additive)				
-9.5+8.0	8.72	100	3.80	1.00
Material : Gypsum Type I (cement additive)				
-16+13.2	14.53	26	15.70-10.32-4.76	1.09-0.72-0.34
-13.2+11.2	12.16	36	15.70-4.91-10.44	1.92-0.59-1.26
-9.5+8.0	8.72	70	15.82-10.56-5.03	5.73-3.82-1.82
Material : Clay				
-9.5+8.0	8.72	100	3.80	0.95
Material: Cement clinker typeI				
-22.6+16	19.02	20	13.95-35.73-67.11-90.19	0.47-1.06-2.01-3.04
-9.5+8.0	8.72	80	4.15-7.16-9.66-10.67-11.56-14.92-16.17	1.07-1.97-2.86-3.00-3.32-4.14-4.4
Material: Cement clinker typeI				
-13.2+11.2		40	3.04-2.25-3.85	0.32-0.25-0.42
-9.5+8.0	8.72	100	2.87-2.11-3.74	0.90-0.61-1.20
-5.6+4.75	5.16	265	1.96-3.74	2.89-5.53

RESULTS AND DISCUSSION

Impact breakage test results were evaluated through the size distributions of the breakage products. Breakage distributions of some of the test materials are presented in Figures 2, 3, 4, 5, 6, 7 and 8. 80% passing particle sizes (P80) of breakage distributions are tabulated in Tables 3 and 4.

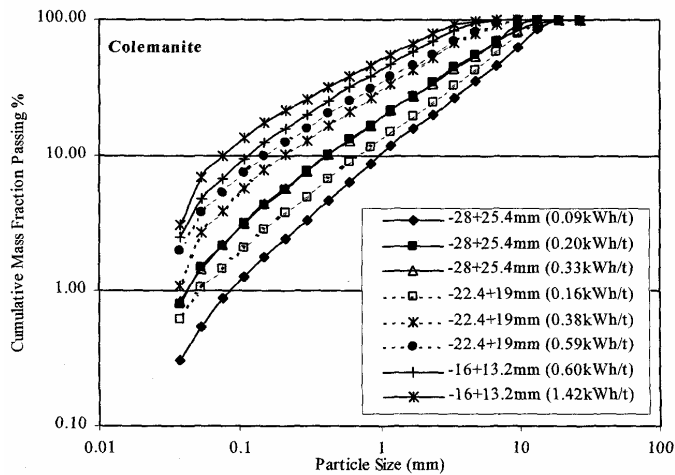


Fig. 2. Cumulative impact breakage distributions of colemanite ore at different energy levels

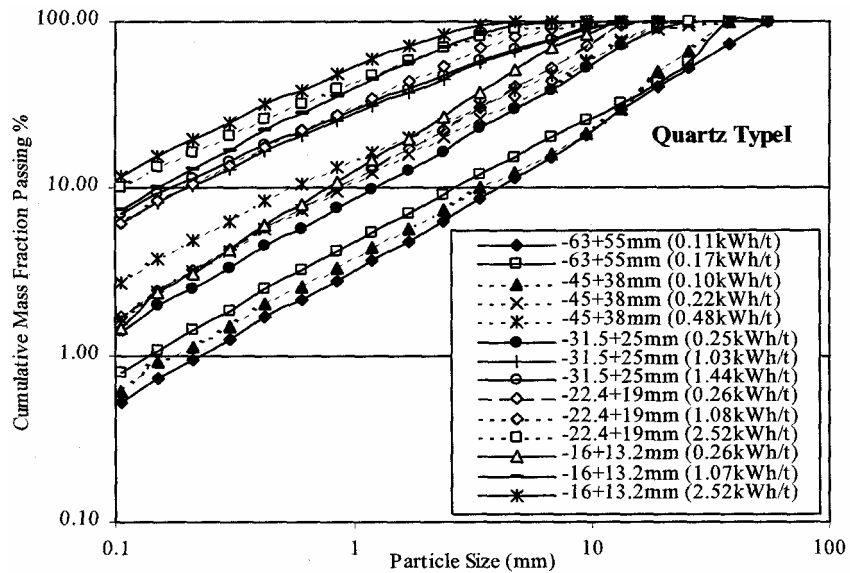


Fig. 3. Cumulative impact breakage distributions of quartz at different energy levels

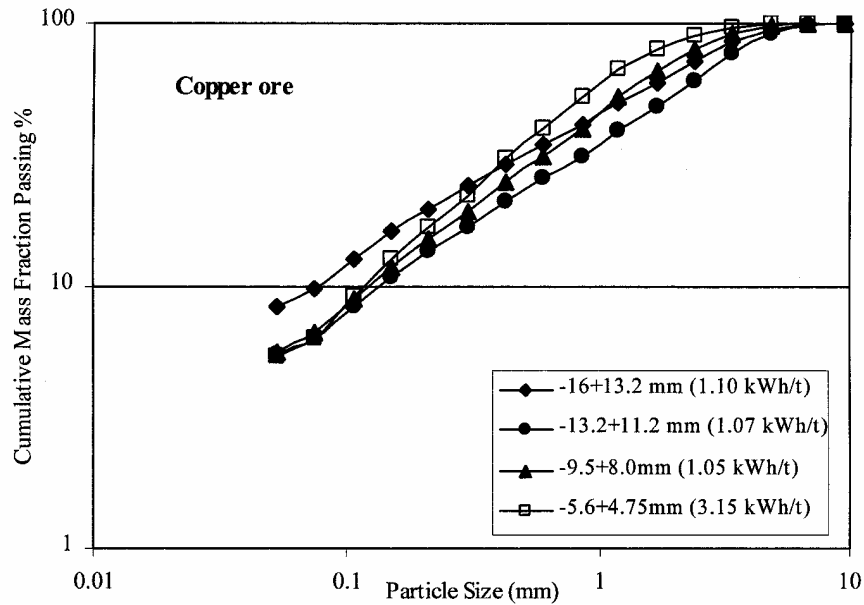


Fig. 4. Cumulative impact breakage distributions of copper ore at different energy levels

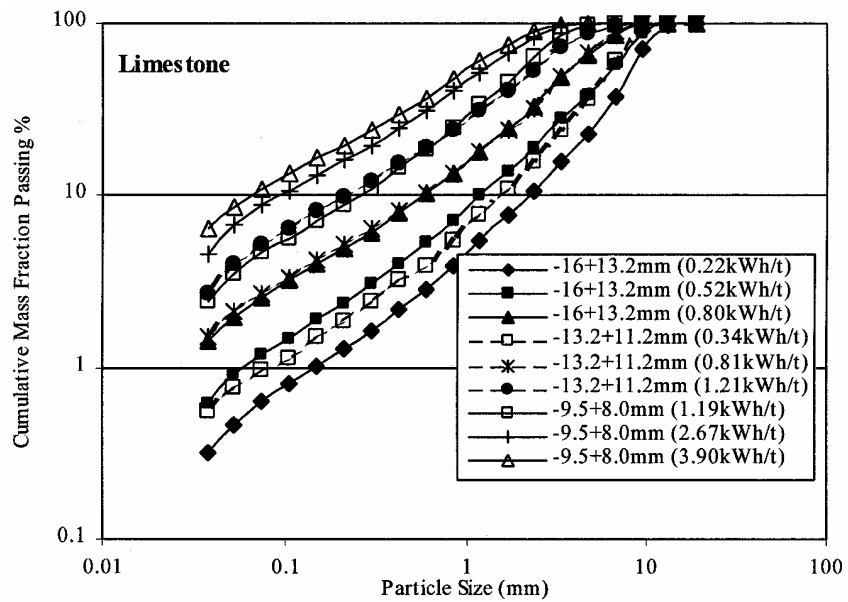


Fig. 5. Cumulative impact breakage distributions of limestone at different energy levels

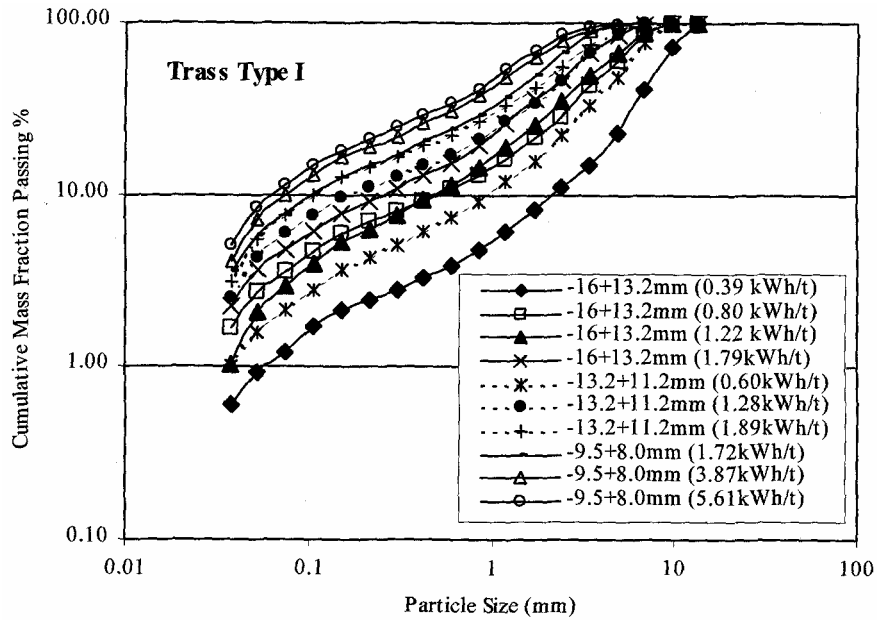


Fig. 6. Cumulative impact breakage distributions of trass at different energy levels

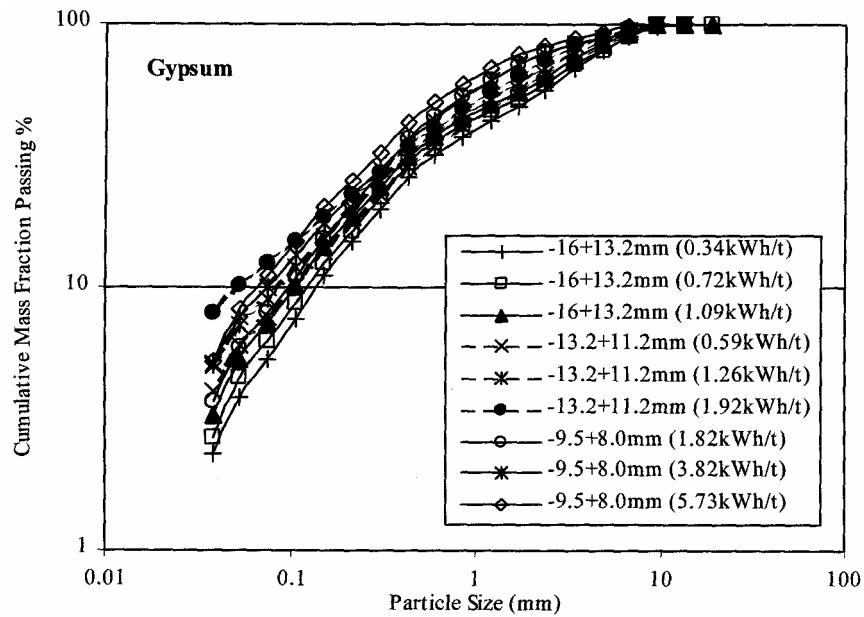


Fig. 7. Cumulative impact breakage distributions of gypsum at different energy levels

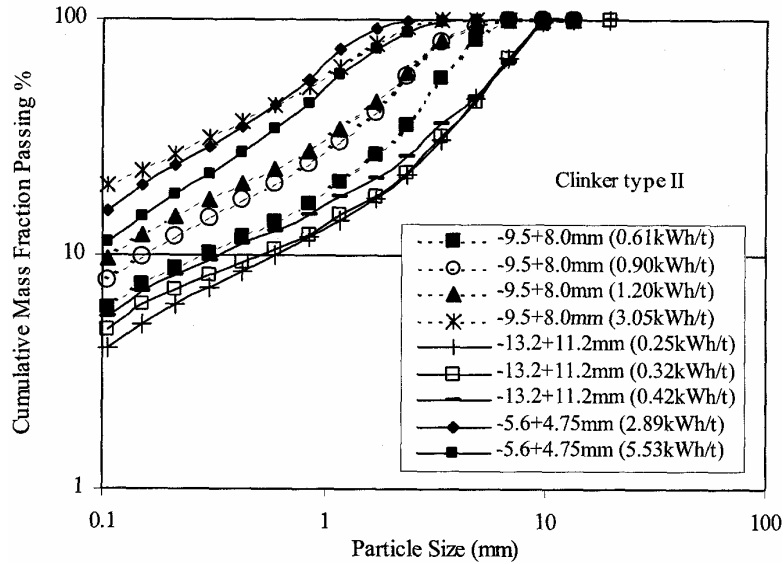


Fig. 8. Cumulative impact breakage distributions of clinker type II at different energy levels

Breakage product size distributions indicated that, increase in breakage energy level increases the fineness of the breakage distributions whereas, size distributions start to become closer at higher energy levels indicating no more size reduction would occur such as in case of $-13.2+11.2\text{mm}$ and $-9.5+8.0\text{mm}$ particles of limestone sample (Figure 5).

Table 3. Breakage product fineness variations with size and breakage energy level

Quartz Type I	$-22.4+19\text{mm}$			$-16+13.2\text{mm}$				
Ecs (kWh/t)	0.26	1.08	2.52	0.26	1.07	2.52		
P80 (mm)	10.47	4.56	3.23	8.54	2.98	2.09		
Quartz Type I	$-63+55\text{mm}$		$-45+38\text{mm}$			$-31.5+25\text{mm}$		
Ecs (kWh/t)	0.11	0.17	0.10	0.22	0.48	0.25	1.03	1.44
P80 (mm)	39.15	28.14	27.16	14.34	14.01	15.29	6.95	7.03
Colemanite	$-28+25.4\text{mm}$			$-22.4+19\text{mm}$			$-16+13.2\text{mm}$	
Ecs (kWh/t)	0.09	0.20	0.33	0.16	0.38	0.59	0.60	1.42
P80 (mm)	12.17	7.77	8.79	9.75	4.83	4.50	2.99	2.41
Copper ore	$-16+13.2\text{mm}$		$-13.2+11.2\text{mm}$		$-9.5+8.0\text{mm}$		$-5.6+4.75\text{mm}$	
Ecs (kWh/t)	1.1		1.07		1.05		3.15	
P80 (mm)	2.9		3.53		2.39		1.68	

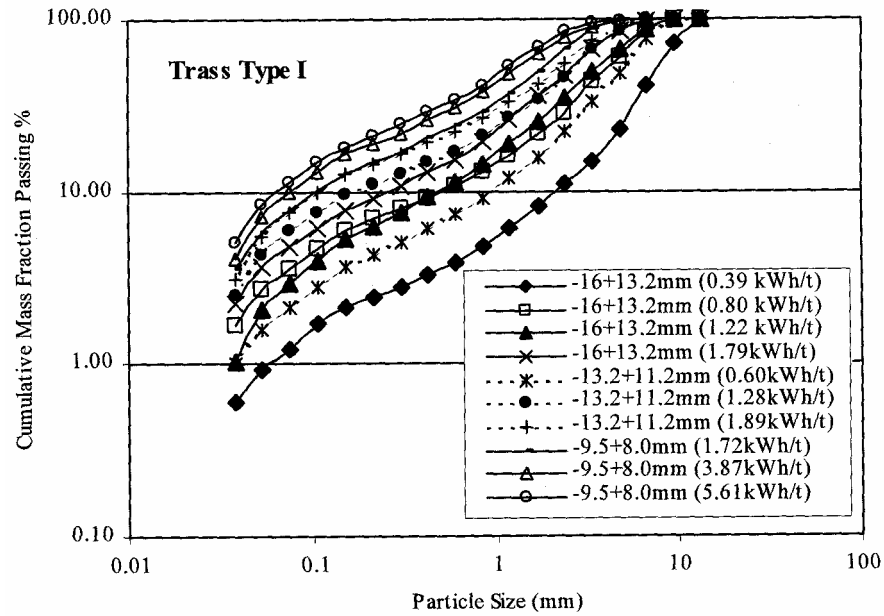


Table 4. Breakage product fineness variations with size and breakage energy level for clinker and cement additive materials

Limestone	<i>-16+13.2mm</i>			<i>-13.2+11.2mm</i>			<i>-9.5+8.0mm</i>		
Ecs (kWh/t)	0.22	0.52	0.80	0.34	0.81	1.21	1.19	2.67	3.90
P80 (mm)	10.30	8.57	5.99	7.87	5.65	3.91	3.02	2.16	1.86
Trass type I									
Ecs (kWh/t)	0.39	0.80	1.22	0.60	1.28	1.89	1.72	3.87	5.61
P80 (mm)	9.84	6.25	5.77	7.02	4.32	3.73	2.90	2.40	2.13
Gypsum									
Ecs (kWh/t)	0.34	0.72	1.09	0.59	1.26	1.92	1.82	3.82	5.73
P80 (mm)	0.34	4.89	4.14	4.38	3.60	3.01	2.59	2.77	2.05
Clinker typeII									
	<i>-13.2+11.2mm</i>			<i>-9.5+8.0mm</i>			<i>-5.6+4.75mm</i>		
Ecs (kWh/t)	0.25	0.32	0.42	0.61	0.90	1.20	3.05	2.89	5.53
P80 (mm)	7.40	7.48	7.54	4.63	3.34	3.23	1.73	1.30	1.91

Fineness of the breakage products was represented by the t10 values and the relation between specific comminution energy level and t10 was established for the test materials. Typical relations between Ecs and t10 parameter are given for some of the test materials in Figure 9. It was observed that, colemanite ore was broken easily compared to the other materials. Highest resistance to impact breakage was observed in the breakage event of quartz type II which belongs to a gold deposit. Impact

breakage result of gypsum showed that, selected energy levels are so high that small deviations in t_{10} values are obtained at energy levels higher than 0.3kWh/t indicating the mineral softness. Maximum or limiting value of breakage index (t_{10}) which is defined by the parameter A in the $E_{cs}-t_{10}$ model (Leung, 1987) is obtained at lower energy levels for coarse size fractions of the test materials.

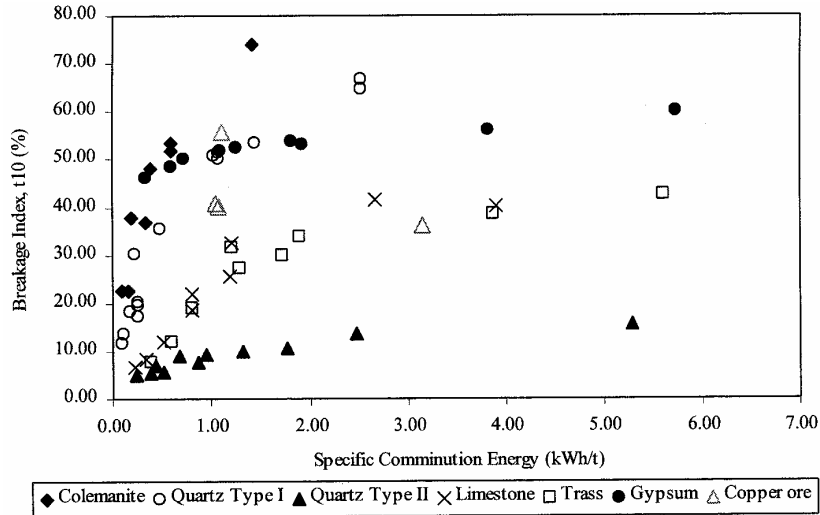


Fig. 9. Comparison of $E_{cs}-t_{10}$ relation for different materials

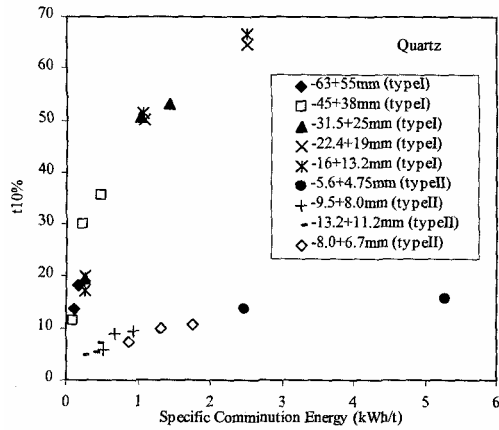


Fig. 10. Comparison of $E_{cs}-t_{10}$ relation for two different quartz

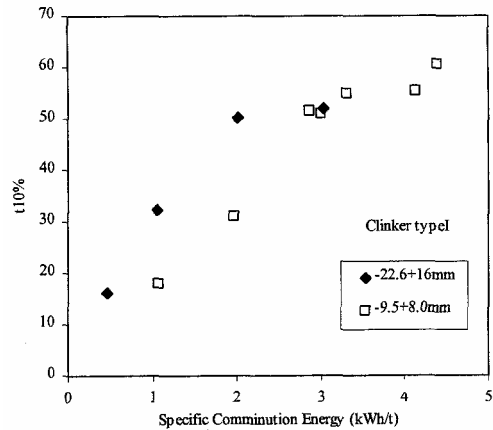


Fig. 11. Comparison of $E_{cs}-t_{10}$ relation for test size fractions of clinker type I

Breakage index values of both quartz types and clinker type II were compared on the size fractional base in Figures 10 and 11 respectively. It was observed that, strength of particles vary with particle size at the same level of specific comminution energy such as in case of approximately 0.2kWh/t for particles of -63+55mm (t10%:18.33) and -45+38mm (t10%:30.15). On the other hand excluded of -45+38mm size fraction, impact breakage of other size fractions produced the same amount of fines at 0.25kWh/t. Overall breakage resistance of both quartz types are completely different leading to have different grindability values with variations in breakage distributions of some particle sizes. Clinker also showed a size dependent breakage behaviour.

In case of complex copper ore, which is not a homogeneous material, size independent breakage behaviour was observed for size fractions of -9.5+8.0mm (t10%:40.83) and -13.2+11.2mm (t10%:40.29) whereas -16+13.2mm (t10%:55.71) particles broke in a different manner. Result of such variations in breakage strengths of different size fractions of the same material can be due to the microstructure, mineralogical composition and the included probable microcracks.

At the same level of specific comminution energy, breakage result of -9.5+8.0mm size fraction was compared for different materials through breakage index value of t10 in Figure 12. Results showed that impact strength of copper ore is the lowest among the test materials on the considered size fraction. Clinker and limestone samples of different plants also showed variation in their breakage characteristics.

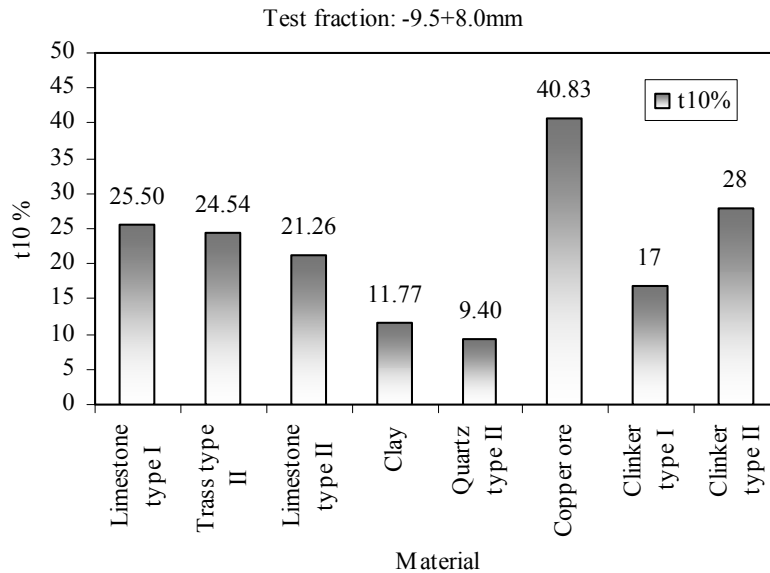


Fig. 12. Breakage index values of different materials at an impact energy level of around 1kWh/t

CONCLUSION

Drop weight test results can be used to evaluate the single particle breakage strengths of materials on the size fractional base. Results of such tests can then be used in the comminution models of autogeneous and ball mills. Size dependent breakage behaviour of materials is an important problem in terms of grinding modelling studies since the breakage distributions of the mill feed materials are commonly determined by using the breakage data of single particle size broken at an appropriate specific comminution energy level. In most of the modelling studies, breakage distribution function of materials are assumed to be independent of particle size just to ease the grinding modelling work which is not true for most of the materials. In order to achieve more reliable grinding simulation results, a detailed breakage study should be carried out in such a way that, different size fractions of the same material should be broken from the same level of specific energies. In fact breakage distribution of each size fraction should be defined in comminution models in some way.

REFERENCES

- ASIM M.E. (1984), *Investigations of Cement Clinker Grindability Using Drop-Weight Tests and its Relation to Tube Mill Performance*, Zement-Kalk-Gips, No.11, pp.577-584.
- ANDERSEN J.S (1988), *Development of a cone crusher model*, M.Eng.Sc., Thesis, University of Queensland (JKMRC).
- AUSTIN L.G., KLIMPEL R.R., LUCKIE P.T. (1984), *Process Engineering of Size Reduction:Ball Milling*, AIME Publ., NY
- BOURGEOIS F.S., BANINI G.A., 2002, *A portable load cell for in-situ ore impact breakage testing.*, Int J. Miner. Process. 65, pp.31-54
- BRIGGS C.A., BEARMEN R.A., 1997, *An Investigation of Rock Breakage and Damage in Comminution Equipment*, Minerals Engineering, Vol.9, No.5, January, pp.489-497.
- FAIRS G.L. (1954), *A Method of Predicting the Performance of Commercial Mills in the Fine Grinding of Brittle Materials.*, Trans Inst Min. Metall, Vol 63, pp.211-240.
- FANDRICH R.G., CLOUT J.M.F., BOURGEOIS F.S., 1998., *The CSIRO Hopkinson Bar Facility for Large Diameter Particle Breakage.*, Minerals Engineering, Vol. 11, No 9, pp. 861-869
- GROSS J. (1938), *Crushing and Grinding*, US Bureau of Mines Bulletin, Vol 402, pp.1-148.
- LYNCH A.J., WHITEN W.J., NARAYANAN S.S. (1986), *Ball mill Models: Their evolution and present status*, Advances in Mineral Processing, Advance in mineral Processing, S.M.E./A.I.M.E. pp.48-63.
- LEUNG K. (1987), *An energy based ore specific model for autogeneous and semiautogenous grinding*, PhD thesis, University of Queensland, Australia.
- MUNN N, MORRELL S., MORRISON R.D., KOJOVIC T. (1996)., *Mineral Comminution Circuits Their Operation and Optimization*, JKMR, Brisbane, pp.413. .
- MAN Y.T. (2000), *A Model-based scale-up procedure for Wet, Overflow Ball Mills.*, Julius Kruttschnitt Mineral Research Centre., Department of Mining, Minerals and Materials Engineering, The University of Queensland, February.
- NARAYANAN S.S., WHITEN W.J. (1983), *Breakage characteristics of ores for ball mill modelling*, Proceedings of AusIMM, 286, June, pp.31-39.
- NARAYANAN S.S. (1985), *Development of a laboratory single particle breakage technique and its application to ball mill modelling and scale-up*. PhD thesis, University of Queensland, Australia.
- NARAYANAN S.S. (1986), *Single particle breakage tests: A review of principles and applications to comminution modeling.*, Bull Proc. Australas. Inst. Min. Metall., Vol 291, No. 4, pp.49-58.

- NARAYANAN S.S., (1987), *Modelling the performance of industrial ball mills using single particle breakage data*, Int. J. mineral Process., 20, pp.211-28
- NARAYANAN S.S., WHITEN W.J. (1988), *Determination of comminution characteristics from single particle breakage tests and its application to ball-mill scale-up*, Trans. Inst Min.Metall., 97, pp.115-124
- PAUW O.G., MARÈ M.S., (1988), *The determination of optimum impact-breakage routes for an ore*, Powder Technology, Vol 54, pp.3-13.
- PIRET E.L., (1953), *Fundamental aspects of grinding*, Chem Eng Prog, Vol. 49, pp.56-63.
- RUMPF H., (1973), *Physical aspects of comminution and new formulation of a law of comminution*, Powder Technology, Volume 7, pp.145-159.
- SCHÖENERT K., (1972), *Role of fracture physics in understanding comminution phenomena*, Transactions of Society of Mining Engineers AIME, Vol.252, March, pp.21-26.
- WEEDON D.M., (2001), *A perfect mixing matrix model for ball mills.*, Minerals Engineering, Vol 14, No.10, pp.1225-1236.
- WEICHERT R, HERBST J.A., (1986), *An ultrafast load cell device for measuring particle breakage*, Prepr. 1st World Congr. Particle Technology, Nürnberg II, pp.3
- TAVERES L.M., KING R.P., *Single-particle fracture under impact loading.*, 1998., Int. J. Miner. Process., 54., pp.1-28
- ZHANG Y.M., 1992, *Simulation of comminution and classification in cement manufacture*, Ph.D.Thesis, South University B.E. (Central-South University of Technology, China), pp.252.

Genç Ö., Ergün L., Benzer H., *Zastosowanie testu rzutu ciężaru do opisu kruszenia udarowego pojedynczego ziarna*, Physicochemical Problems of Mineral Processing, 38, (2004) 241-255 (w jęz. ang.).

Analizowano skutki kruszenia udarowego pojedynczego ziarna różnych materiałów za pomocą metody rzutu ciężaru. Wyniki badań oceniano drogą analizy rozkładów kontrolowanych klas ziarnowych przy różnych poziomach energii udaru. Stopień pomniejszenia ziarn w teście zrzutowym odpowiadający rozkładowi rozmiarów ziarn produktu skruszonego reprezentował parametr rozkruszenia t10 zaproponowany w pracy Natarayanana (1986). Zależność pomiędzy właściwą energią rozdrabniania i indeksem skruszenia t10 oceniano na podstawie rozmiaru ułamkowego, co umożliwiła szacowanie zmienności charakterystyki kruszenia udarowego różnych materiałów. Stwierdzono, że metoda testu rzutu ciężaru jest użytecznym narzędziem oceny naprężeń udarowych różnych materiałów na podstawie rozmiaru ułamkowego i może być wykorzystana w modelowaniu matematycznym procesów mielenia w młynach autogenicznych i kulowych.

Piotr WODZIŃSKI*

CRUDE ORE SCREENING IN COPPER INDUSTRY

Received March 15, 2004; reviewed; accepted May 15, 2004

This study was stimulated by the problems with crude ore screening in the “Polska Miedź” SA. company. The process of screening preceding ore crushing is performed using screens which do not guarantee a desired process efficiency. The existing single-plane screens do not ensure proper segregation of crude ore layer on the sieve, and consequently, not all particles which represent undersize fraction have a chance to fall into mesh and pass through it.

In this situation the problem should be solved using various means, i.e. a variety of actions should be undertaken to obtain proper characteristics of the screening process. The first one is to propose a new schematic of screening which should be carried out on 4, and in an extreme case on 3 sieve levels. Another action should encompass the application of a linear-elliptic screen. The third innovation can be the use of cascade (stepped) sieves, in particular for two lowest screens on which the proper ore classification is performed. The last one seems to be the application of a feeder which supplies the feed to the sieves of screening machines.

Key words: screening, screen, copper ore, screening efficiency, sieve

INTRODUCTION

In the “Polska Miedź” SA company crude copper ore is classified on sieves after its previous crushing. The crude ore screening is far too much inefficient because of a too high mass flow rate at which ore stream is supplied to screens. A too thick granular layer is formed on the sieves which prevents efficient separation of the undersize fraction from the oversize. A proper mine run classification, according to the present technology, is carried out according to a scheme in which two sieves $l_1=40$ mm, and $l_2=12-16$ mm are used.

It is proposed to carry out this task with the use of a modern linear-elliptic screen [Wodzinski 1997] which is a single-plane screen [Banaszewski 1990, Dietrych 1962, Schmidt 1984, Sztaba 1993, Wodziński 1997, 2001], i.e. in which plane motion takes place in the main plane Π of the machine (Fig. 1). The main plane determines cross

* Technical University of Łódź, Faculty of Process and Environmental Engineering, Department of Process Equipment, wodzinski@wipos.p.lodz.pl

section symmetry of the machine, which is a longitudinal plane perpendicular to the sieve. Sieve trajectories specific for a single-plane screen can be linear, circular, elliptic and complex. The latter are characteristic of drives with double frequency. Single-plane screens, called also vibrating screens (which seems to be incorrect), Wurfsiebe, Schwingsiebmaschinen, etc., are built in Poland and they are considered to be well developed.

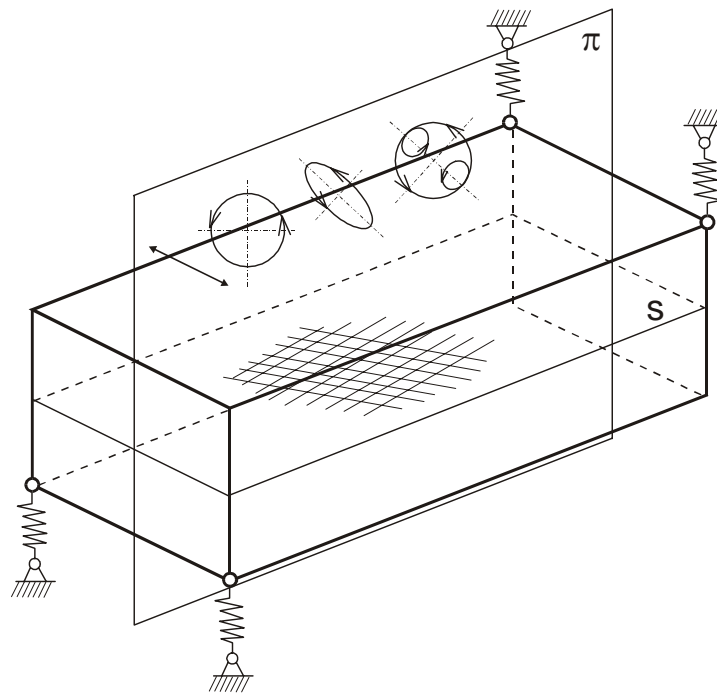


Fig. 1. Single-plane screen

This paper was prepared on the basis of the study on “Modern problems of copper ore processing in Poland” published in the proceedings of a seminar that was held in the headquarters of the “Polska Miedź” SA company on 16 November 2000. It follows from this source (pp. 77-78, 93-99), that the main cause of problems related to copper ore screening is a too big stream of feed Q [t/h , $t/h m^2$] directed to the process of sieve classification. The problem can be solved in many ways and the situation can be improved only when several conditions are satisfied. These conditions are as follows:

- 1) application of feeders in the screens,
- 2) application of a linear-elliptic screen,
- 3) application of a new schematic of screening,
- 4) optimised selection of mesh with reference to proper sieves,
- 5) application of cascade sieves.

SCREENING PROCESS

As mentioned above, the existing screens' efficiency is very insufficient and so the screens do not separate the whole undersize fraction contained in the feed. According to the suggestions of the company "Polska Miedz" SA, crude ore screening should be performed on two sieves (Fig. 2) with mesh dimensions $\Phi_3=40$ mm and $\Phi_4=12-16$ mm. As a result, using this scheme two oversize products X_1 and X_2 , and one undersize product Y is obtained. This is an indisputable opinion on the types of sieves which should be used. At present, there is a tendency that polyurethane sieves are applied in mineral raw material processing. Such sieves are extremely resistant to grinding as compared to woven sieves made from metal (wire). However, it should be remembered that the application of polyurethane sieves much decreases the sieve clearance coefficient A_0 , defined as the ratio of mesh surface to the surface of the entire sieve. So, if in the case of normalised woven sieves $A_0 \approx 36\%$, in the case of polyurethane sieves $A_0 \approx 10\%$. This means such a proportional decrease of screening efficiency. Thus, the application of polyurethane sieves brings about a significant decrease of screening efficiency when compared to woven sieves which would have been used in the same screen and in the same conditions (e.g. when screening the same feed).

Hence, in order to increase screening efficiency it is proposed to apply two preliminary sieves whose mesh size would be bigger than that in sieves 3 and 4 (Fig. 2). It is proposed to use grates or polyurethane sieves. The task of sieves 1 and 2 is to "extract" big particles that cause resistance of the layer from the feed as quickly as possible. These particles disturb small particles (undersize fraction) to get near the sieve and then to be screened off. Next, the oversize products from sieves 1, 2 and 3 are joined in one granular stream denoted as X_1 .

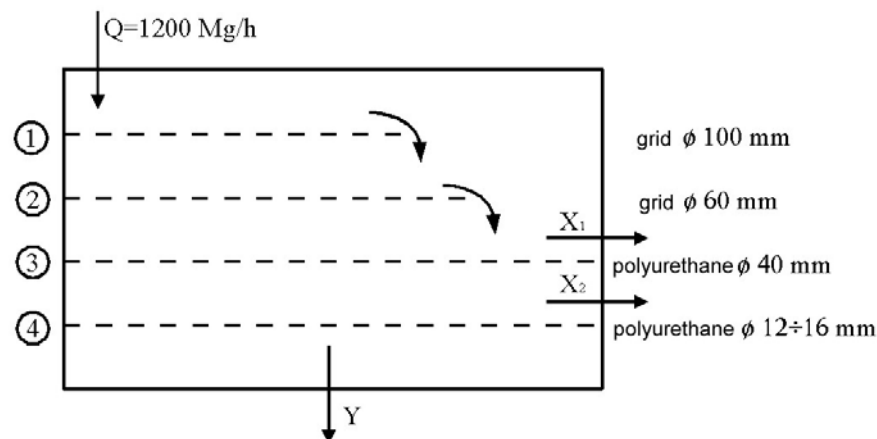


Fig. 2. Schematic of crude ore screening

Selection of mesh size, both for preliminary and proper sieves, should be carried out taking into account diagrams of crude ore particle size distribution: Figs. 3 to 8. Figure 3 shows a diagram of the curve of particle size fractions occurrence frequency in the feed. This diagram is prepared in a normal system. Since this diagram is difficult to interpret, the same function was presented in a two-log system (Fig. 4) and bar diagram of the particle composition of the feed in a one-log system (Fig. 5). Typical granulometric curves of particle size distribution are shown in Fig. 6, where curve P is the curve of sieve residues, and curve R – screening through a sieve. Next, in Fig. 7 the same curves are presented in a one-log system, and in Fig. 8 – in a two-log system.

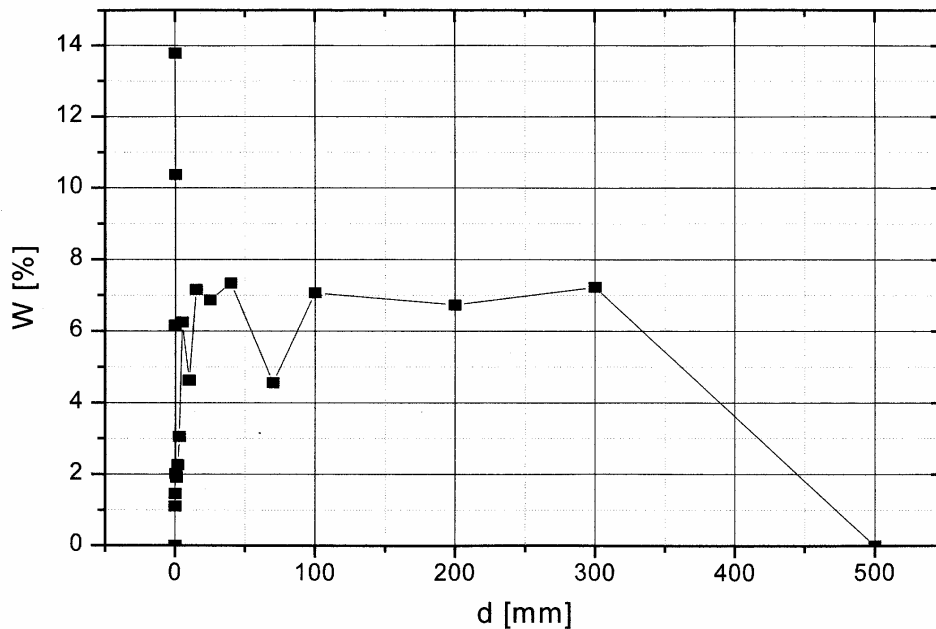


Fig. 3. Diagram of frequency curve for feed size grade fractions

On the basis of the graphic material characteristic mesh sizes (or grate slots) were determined for preliminary sieves 1 and 2. Assuming $\Phi=100$ mm for sieve 1 means that 20% feed (the biggest particles) is separated on it and $\Phi=60$ mm for sieve 2 that further 10% feed is separated. So, on both preliminary sieves 30% feed will be separated and these will be the particles that hamper most seriously the process of screening.

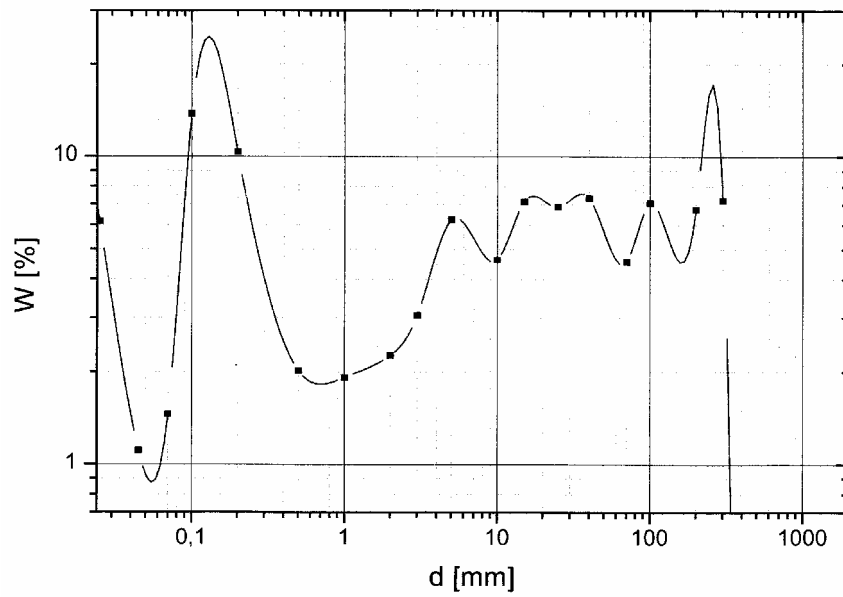


Fig. 4. Diagram of frequency curve for feed size grade fractions

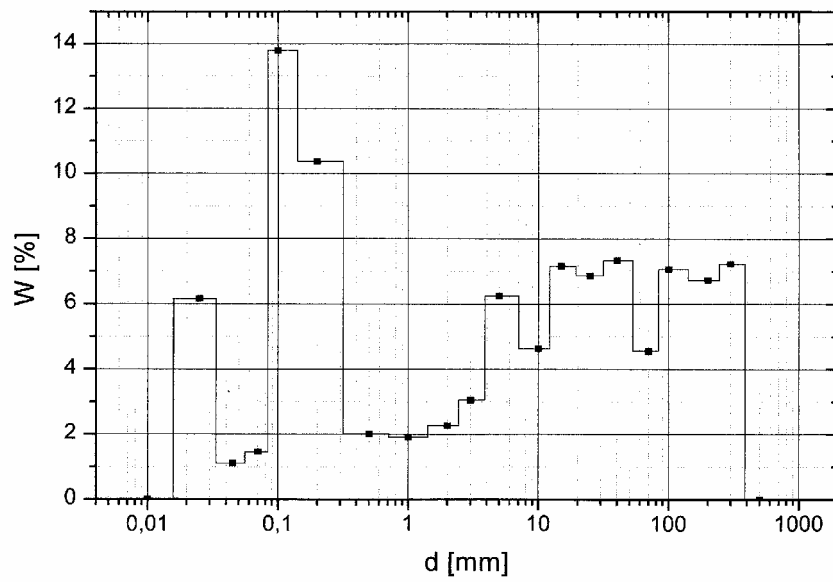


Fig. 5. Bar chart of feed size analysis

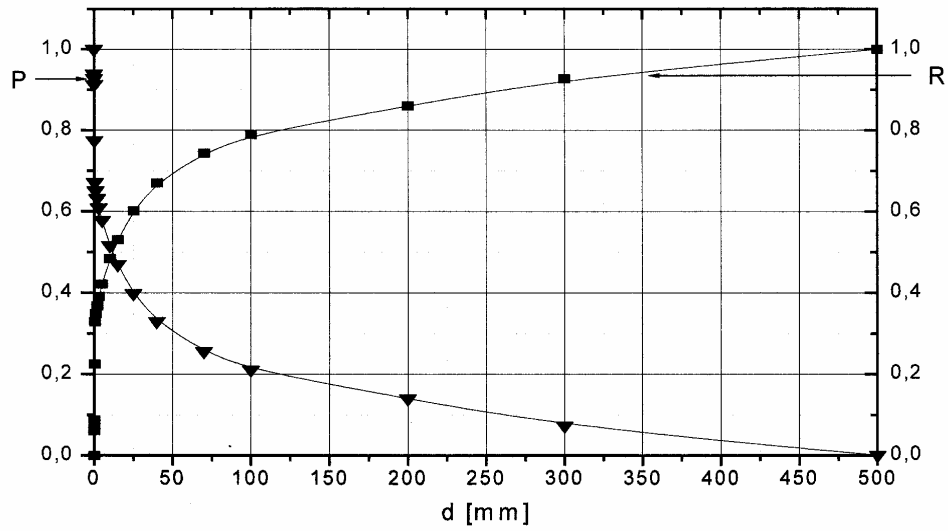


Fig. 6. Particle size distribution of crude ore, P – sieve residue, R – sieve dumping

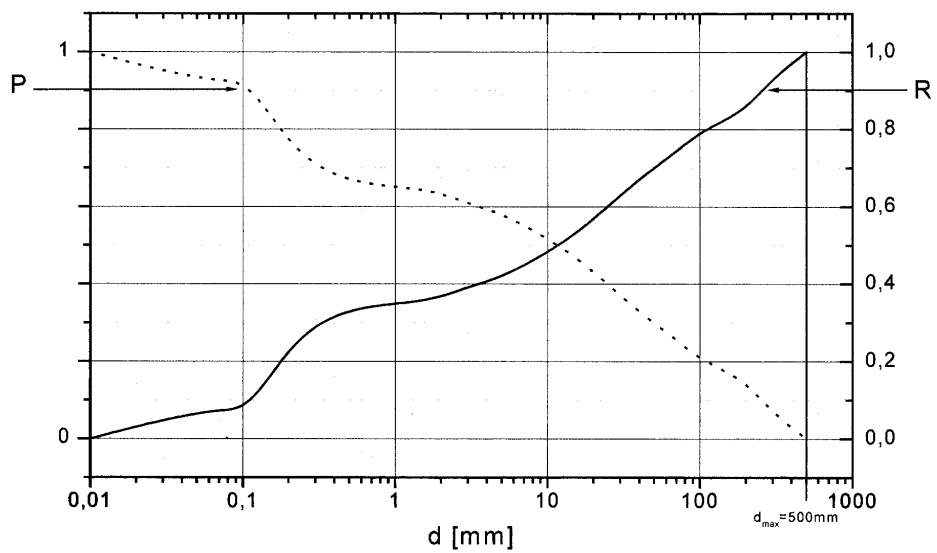


Fig. 7. Particle size distribution of crude ore, P – sieve residue, R – sieve dumping

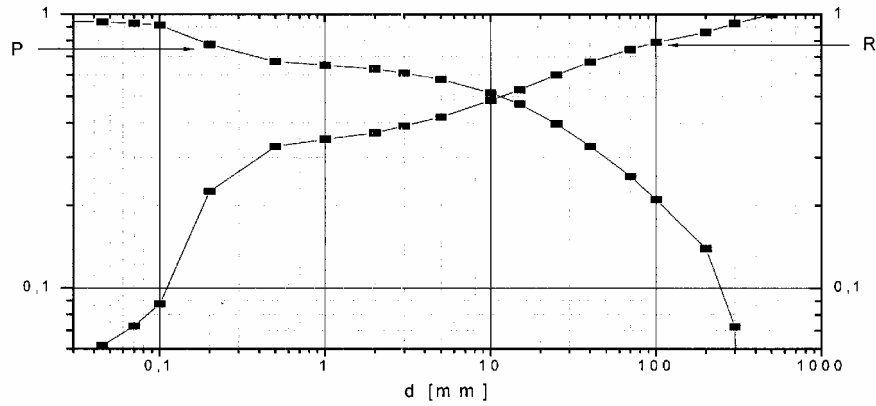


Fig. 8. Particle size distribution of crude ore, P – sieve residue, R – sieve dumping

LINEAR-ELLIPTIC SCREEN

To carry out the process of screening it is proposed to use a modern linear-elliptic screen [Wodziński 1997; Wodziński 2001] that can replace machines working in the ore processing plant. The machine has been described in detail in literature, so here we will deal with it very briefly. A linear-elliptic screen can be either inclined ($\alpha=8^\circ-10^\circ$) (Fig. 9) or horizontal ($\alpha=0^\circ$) (Fig. 10).

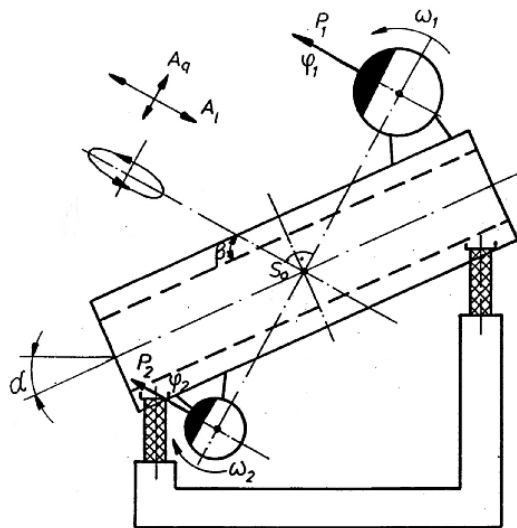


Fig. 9. Inclined linear-elliptic screen

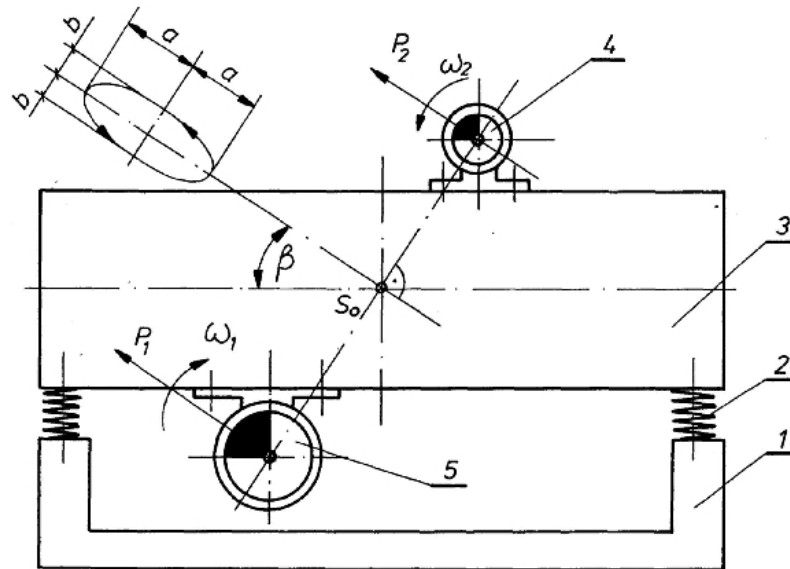


Fig. 10. Horizontal linear-elliptic screen

In both cases the screen is composed of a rectangular riddle, it contains typical elements that are known in other screens, i.e. riddle, springs, main frames, the mechanisms of sieve mounting, the sieves themselves, and also rotary vibrators which drive the screen. As compared to the existing screens, the difference is in drive system configuration (Figs. 9 and 10). If through a centre of mass of the whole riddle S_0 a line of sieve oscillations (the line of driving force action) is drawn and oriented at the angle β to the sieve surface, then the line perpendicular to the line of sieve oscillations in point S_0 is a straight line combining centres of unbalanced shafts that drive the screen. This machine can oscillate in different conditions of drive system operation. The static moments of shafts (or unbalanced engines) can be equal or different. The same refers to rotational speed of drive shafts. Additionally, these shafts can work in the conditions of dynamic concurrent or backward self-synchronisation. So, the linear-elliptic screen can work in different drive systems and consequently move along various trajectories [6]. This is important because the shape of screen trajectory and distribution of oscillation amplitudes on the whole sieve surface determine the screen efficiency.

Figure 11 shows different positions of drive shafts in the linear-elliptic screen. Displacement of shaft axes results in an increase of sieve trajectory angle β . Figure 12 shows different, possible variants of drive system operation in the linear-elliptic screen. Attention is focussed on the application of various static moments of drive shafts, different types of self-synchronisation: concurrent and backward, different values of exciting force (3 values) and different angles of sieve trajectories β .

Subsequent figures show vibrating sieve trajectories in the linear-elliptic screen. The real sieve trajectories are different than the trajectories being a result of calculations (computer simulation), e.g. trajectories of the end and beginning of the sieve (Fig. 13), are straight lines, and their real shape is shown in the figure. The trajectory of sieve centre (Fig. 14) should be circular, its real shape is illustrated in the figure.

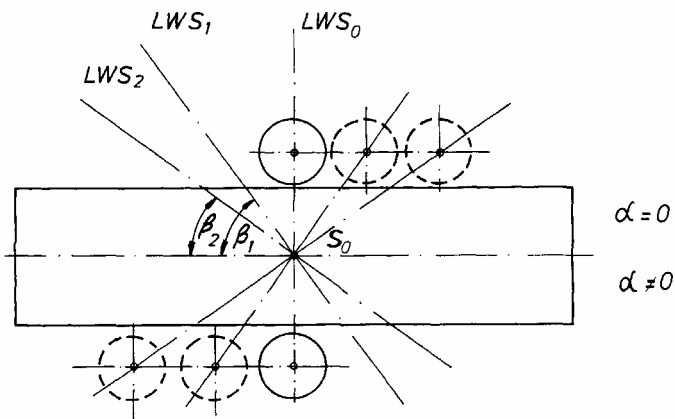


Fig. 11. Position of drive shaft axes in a linear-elliptic screen

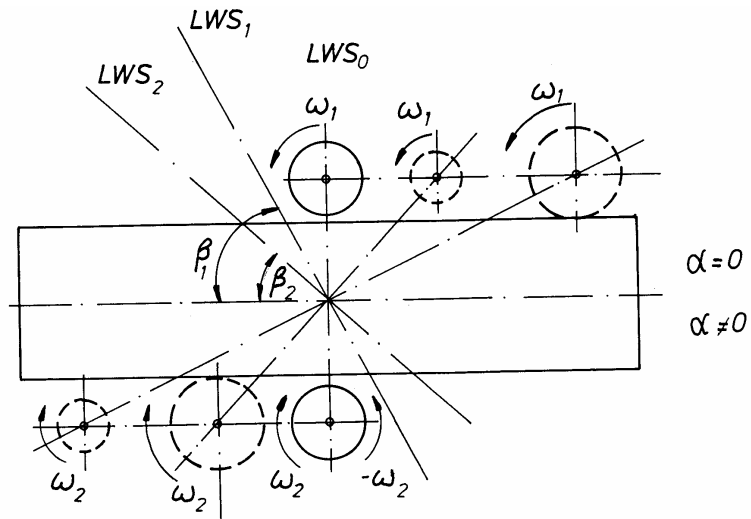


Fig. 12. Types of drive system operation in the linear-elliptic screen

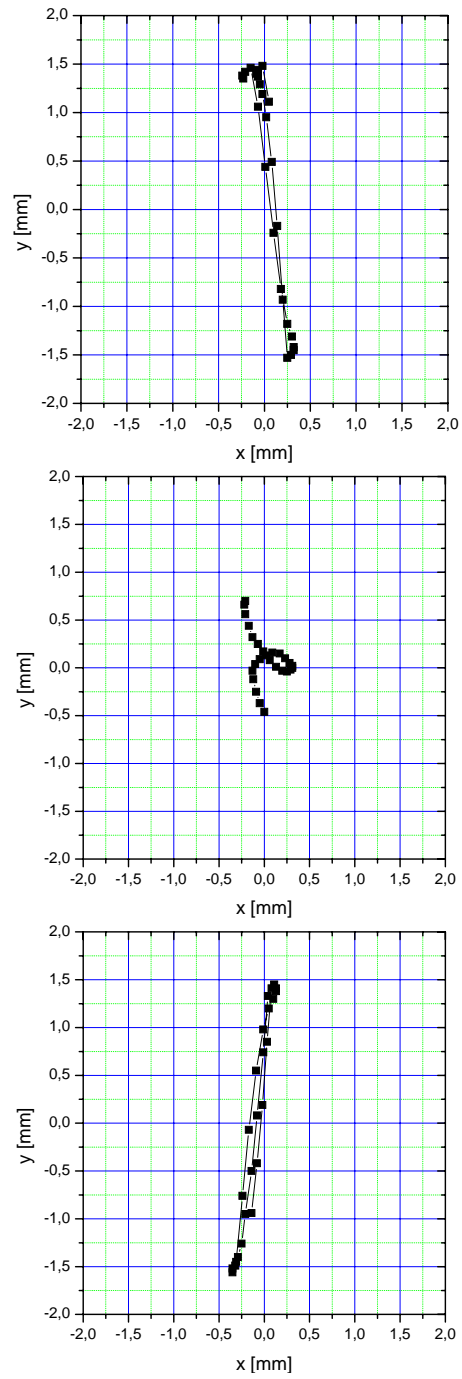


Fig. 13. Screen trajectories for medium force and co-current synchronisation

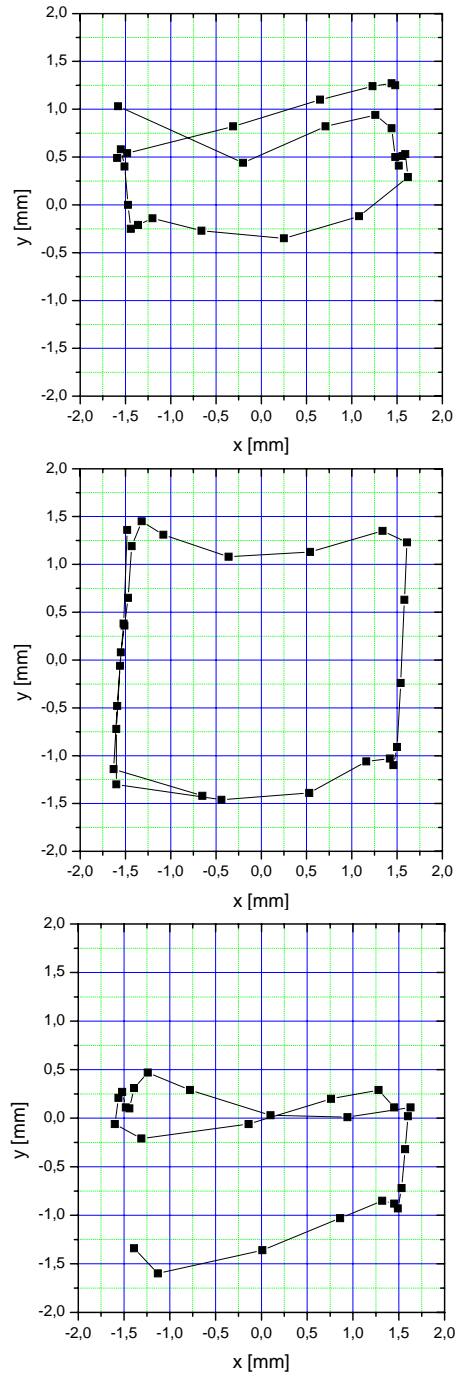


Fig. 14. Screen trajectories for maximum force and co-current synchronisation

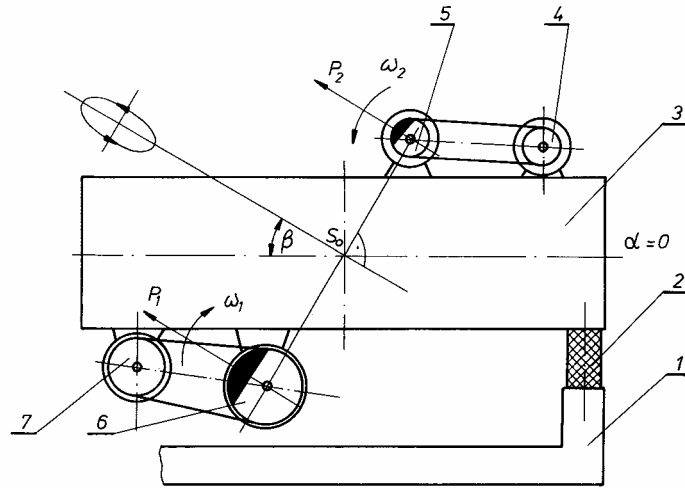


Fig. 15. Variant of a linear-elliptic screen with drive engines on the riddle

Figure 15 illustrates design solutions of the linear-elliptic screen different from the existing ones, in which drive engines were located immediately on the riddle. However, the most proper solution of the drive system is shown in Figs. 16, 17 and 18. This is a so-called module drive system where constant (known) modules of unbalanced shafts are used. Electric drive engines are on immobile frames mounted on a common base with a supporting frame of the screen. Elastic shafts are used for driving. They combine unbalanced modules with each other and with a drive engine. Elements shown in Figs. 16-18 are known from other constructions of screens and they have been thoroughly verified in industrial practice.

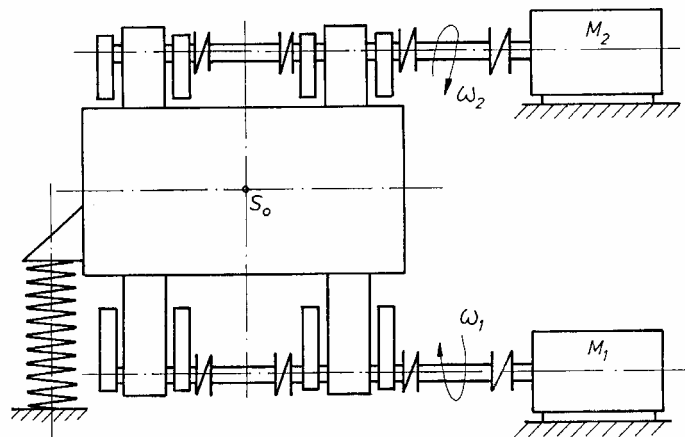


Fig. 16. Drive system of the linear-elliptic screen with stable engines

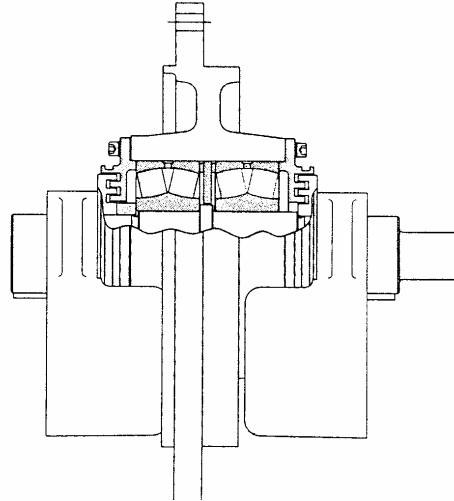


Fig. 17. Vibrating module

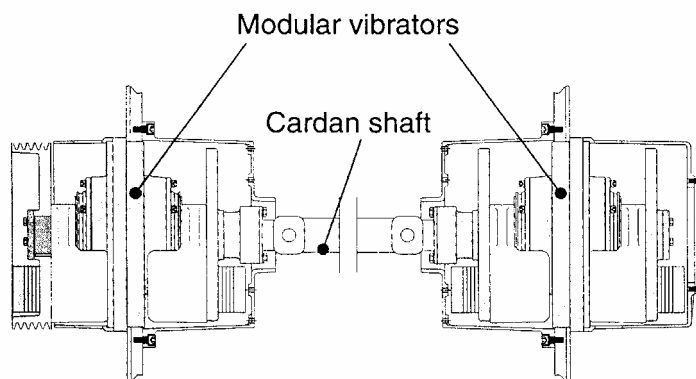


Fig. 18. Module drive

In Poland it is believed that particularly big machines (e.g. screens working in mining and processing industries) should be driven by unbalanced shafts, with bearings directly in sides of the screen riddle. Also in the case of a linear-elliptic screen this solution is possible (Fig. 19), and additionally it was proposed to apply a cascade sieve. The cascade sieves can be one-sided (Fig. 20) or two-sided (Fig. 21). An advantage of the cascade sieve is screening of the feed which is additionally mixed and hence small particles that constitute undersize fraction, can find their way to the sieve more easily which is a condition to pass through the mesh. In segments SO_{AB} , SO_{CD} , SO_{EF} the most intensive feed discharge from the layer on the sieve takes place because this is the initial segment of the kinetic curve of screening, i.e. a so-called outflow function.

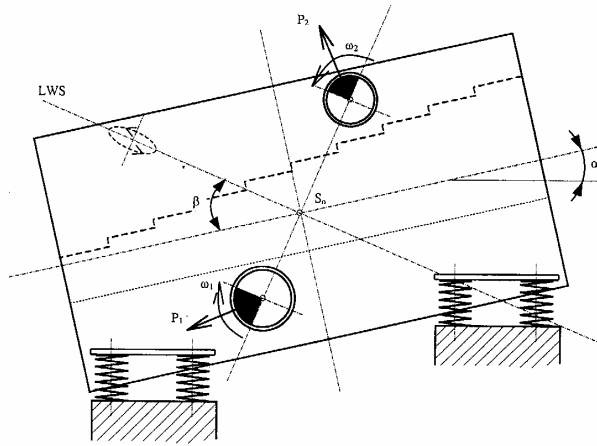


Fig. 19. Linear-elliptic screen with a stepped sieve

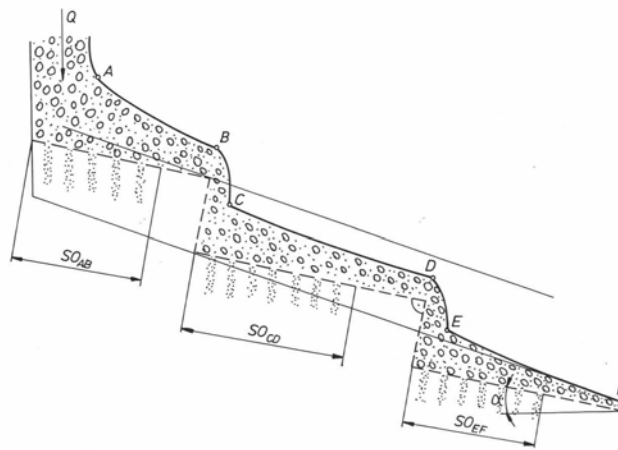


Fig. 20. One-sided cascade sieve

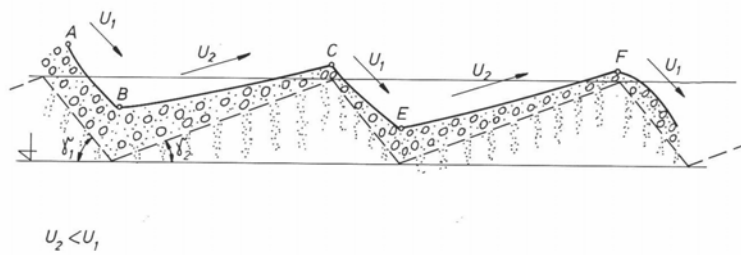


Fig. 21. Two-sided cascade sieve

Screening on a two-sided cascade sieve (Fig. 21) is performed on both surfaces of the cascade. On the AB segment of discharge curve, material moves at velocity u_1 , and on the segment BC – u_2 , and so on. A cascade placed in this way constitutes an “obstacle” for small particles which due to low kinetic energy cannot leap over the step and are held up. Owing to this, the probability that they will be screened off increases.

As we can see, the linear-elliptic screen is a universal screen in which advantage is taken of experience gained so far in the area of constructing and exploiting screening machines. This screen is characterised by a relatively uniform arrangement of vibrating masses, a feature unknown in the constructions known so far.

SUPPLY OF FEED TO THE SCREEN

The methods of feed supply to the screen were discussed in literature [Wodziński 2001]. One of possible design variants of such a feeder (with a horizontal trough) was also shown. The feeder can be driven by:

1. an electromagnetic vibrator placed usually below the feed transporting trough,
2. one rotating vibrator (in such a case the trough must be inclined),
3. two backward-synchronised rotating vibrators (unbalanced engines). Then, the most advantageous arrangement of the vibrators is on the side walls of the feeder (Fig. 22).

Design recommendations obligatory for mines referring to such feeders (Fig. 22) were discussed [Wodzyński 2001] and presented in a feeder schematic diagram.

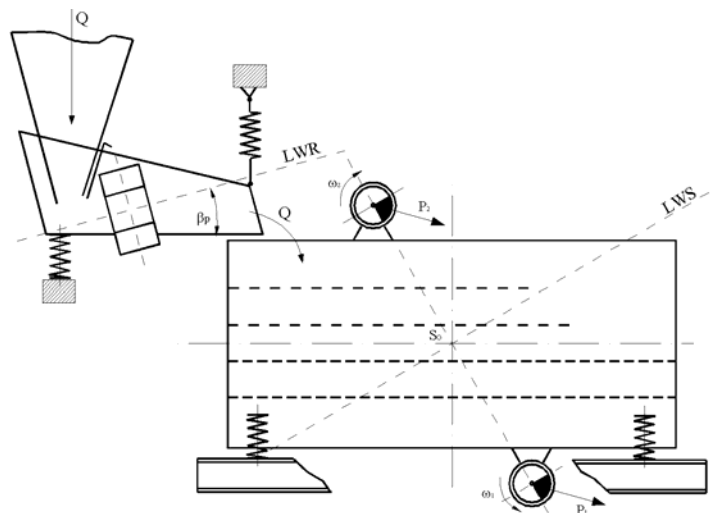


Fig. 22. Screen with a feeder

CONCLUSIONS

1. On the basis of the analysis of the state of the art in the area of crude ore screening in the "Polska Miedź" SA company, a linear-elliptic screen with a new sieve system was proposed.
2. There is still an open problem of optimal selection of mesh size and sieves to carry out the process of ore screening before crushing.
3. An important issue is a correct feed supply to the screen and this problem refers to almost all screening processes, in particular on rectangular sieves and with linear flow of material through the screen.

REFERENCES

- T. BANASZEWSKI, 1990, *Przesiewacze*, Śląsk, Katowice.
J. DIETRZYCH, *Teoria i budowa przesiewaczy*, 1962, WGH, Katowice.
D. SCHMIDT, *Das Siebklassieren*, 1984, Chem. Ing. Techn. 56, nr. 12,
K. SZTABA, *Przesiewanie*, 1993, Śląsk, Katowice.
P. WODZIŃSKI, *Przesiewanie i przesiewacze*, 1997, Łódź.
P. WODZIŃSKI, *Klasyfikacja rud miedzi na sitach*, 2001, ICNOP.

Wodziński P., *Wstępne przesyłanie rudy w przemyśle miedziowym*, Physicochemical Problems of Mineral Processing, 38, (2004) 257-272 (w jęz. ang.).

Bodźcem do powstania niniejszego opracowania były problemy, jakie są związane z procesem przesiewania rudy surowej w KGHM "Polska Miedź" SA. Proces przesiewania poprzedzający kruszenie rudy, jest realizowany na przesiewaczach, nie zapewniających wymaganej skutecznej wydajności procesowej. Istniejące przesiewacze jednopłaszczyznowe nie zapewniają odpowiedniej segregacji warstwy rudy surowej na sicie, a co za tym idzie nie wszystkie ziarna reprezentujące swym wymiarem klasę dolną, mają szansę wpaść w otwory sitowe i następnie przejść przez te otwory.

W tej sytuacji rozwiązanie problemu powinno być prowadzone wielotorowo, tzn. powinny być wykonane różne działania, które razem doprowadzą do uzyskania właściwych charakterystyk procesu przesiewania. Pierwszym z nich jest zaproponowanie nowego schematu procesu przesiewania, który powinien być prowadzony na 4, a w skrajnym przypadku na 3 pokładach sitowych. Drugim działaniem powinno być zastosowanie przesiewacza liniowo-eliptycznego. Trzecią innowacją może być zastosowanie kaskadowych (schodkowych) pokładów sitowych, w szczególności dla dwóch najniższych sit, na których odbywa się właściwa klasyfikacja rudy. Ostatnim wydaje się być zastosowanie podajnika zasilającego, podającego nadawę na sita maszyn przesiewających.

Jadwiga FARBISZEWSKA-KICZMA **, Teresa FARBISZEWSKA *,
Mirosław BAŁ **

BIOLEACHING OF METALS FROM POLISH BLACK SHALE IN NEUTRAL MEDIUM

Received May 25, 2004; reviewed; accepted June 30, 2004

The black shale present in Polish ores (Lubin region) differs from others in mineralogical and chemical properties and in susceptibility to enrichment. The ores are characterized by high content of copper and others metals like silver. Some metals in the shale ore are present as bituminous organo-metallic compounds such as porphyrins. The presence of these compounds, reduces metals recovery by classical acid bioleaching methods. This study has been undertaken in order to determine possibilities of metals bioleaching from the sandwich compounds occurred in black shale. The bioleaching process was carried out in neutral medium using *Bacillus cereus* and *Bacillus amyloliquefaciens* strains. The progress of this process was followed by analysis of copper, zinc and nickel bioleaching kinetics. The bioleaching experiments with copper suggest different organic forms of this metal in the shale ore. Some of them are highly susceptible to bioleaching by heterotrophic bacteria. Organic compounds of the nickel appeared to be more resistant to bioleaching than copper compounds. Bioleaching of zinc was negligible. Also, the bioleaching process was carried out on a batch scale using "Biomel" reactor.

Key words: bioleaching, black shale ore, Bacillus cereus, Bacillus amyloliquefaciens

INTRODUCTION

The Lubin deposits of a cupriferous ore consist of three lithological forms: carbonate, sandstone and shale. Shale ores containing a bituminous component are called the black shale. Main components of the black shale are loams, carbonate minerals, organic compounds and detrital minerals [Kucha et al., 1996; Łuszczkiewicz, 2000]. In the black shale some organic matter occurs in a shape of laminas, small inclusions, loamy interlayers and organic remnants. The contents of the

* University of Opole, Faculty of Natural and Technical Sciences, Molecular and Experimental Biology Department, ul. Kominka 4, 45-035 Opole

** University of Opole, Faculty of Natural and Technical Sciences, Process Engineering Department, ul. Dmowskiego 7-9, 45-365 Opole, gaga@uni.opole.pl

organic matter fluctuate from 1% to 30% with 6% on average; however, the contents of bitumen range from 1% to 11% [Speczik et al., 1996]. The black shale ores differ from others in mineralogical and chemical properties and in a susceptibility of recovery. They are characterized by high content of copper (5.5 %) and other metals like silver (0.01 %). In the bituminous shale ore the content of metals is from 3 to 10 times greater than that in carbonate and sandstone forms [Łuszczkiewicz, 2000]. Therefore this ore can be treated as a natural polymetallic concentrate.

Some metals in the shale ore are present as bituminous organo-metallic compounds as porphyrins. The presence of these compounds, reduces the metals recovery by using classical methods of ore enrichment. [Łuszczkiewicz, 2000]

This study has been undertaken to determine the possibilities of bioleaching of metals from sandwich compounds occurring in Lubin (Poland) black shale. The bioleaching process was carried out in neutral medium with *Bacillus* bacteria strains. The progress of this process was followed by analysis of bioleaching kinetics of copper, zinc and nickel recovery.

MATERIALS AND METHODS

MATERIAL

Cupriferous black shale ore was obtained from the Lubin region in Poland. The shale was initially subjected to acid bioleaching, then after extensive washing with distilled water the second bioleaching step was performed under neutral pH condition. Material prepared by this means contained 1.58% Cu, 0.67% Pb, 0.27% Zn and 0.006% Ni.

ISOLATION OF MICROORGANISMS

The bioleaching process was carried out using autochthonous bacteria. *Bacillus* bacteria strains were isolated by our team from the investigated shale samples. Microorganisms were washed out from black shale with physiological solution. The suspended matter was diluted by Lister method from 10^{-1} to 10^{-6} . About 0.1 cm³ of diluted fluid (10^{-5} and 10^{-6}) was taken from test-tubes and placed on nutrient agar. After 24 hour of aerobic incubation at 30°C, the grown bacterial culture was transferred into flasks with enriched broth.

In order to select *Bacillus* bacterial strains with spores, flasks with bacterial culture were pasteurized [Chmiel, 1998; Kunicki-Goldfinger, 1998]. In the next step of experiment we screened them on the solid medium and transferred onto a thiolignin medium, specific for *Bacillus*, followed by 24 hour aerobic incubation at 30°C. As a result two aerobic, *Bacillus* strains (designed as B₁ and B₂) were obtained and identified. The first step in identification process involved staining using Gram method [Singleton, 2000]. In all cases Gram (+) batch were observed and then tested on a microanalyzer API. The isolated B₁ and B₂ strains were identified as *B. cereus* and designed as B.c.-04, and *B. amyloliquefaciens* designed as B.a.-04, respectively.

This identification was confirmed using Moseley medium. In the case of the B₁ strain the plates were colored red indicating the *Bacillus cereus* strain. Next the cultures were grown on the enriched broth.

BACTERIAL STRAINS CHARACTERISTICS

Bacillus cereus is an aerobic or relatively aerobic, Gram(+) bacterium that can produce resting spores. This bacillary bacterium (3-5 µm in length and 1.0 -1.2 µm wide) has a flagellum and tends to form chain-like colonies. It grows from 5° to 50°C of pH 5.5-8.5 with a water activity of $a_w = 0.95$. Our *B. cereus* strain hydrolyzes casein, starch, gelatin and decomposes glucose and tyrosine. Extracellular products of the bacterium contain hemolysins, lytic (included proteolytic) enzymes, and phospholipase. Some strains of this bacterium under certain conditions produce red or fluorescent yellow-green pigment. [Bergley, 1986]. *B. cereus* strains are frequently found in soil, water and sewage. This bacterium can contaminate food-products and during their growth in food or intestines produce poisonous endotoxins [Prescott et al., 1999; Libudzisz et al., 2000].

Bacillus amyloliqueficiens strain was isolated and identified as a different *Bacillus subtilis* strain by Welker and Campbell in 1967. They found the difference between mole% G+C in DNA of *B. amyloliqueficiens* (43.5-44.9) and DNA of *B. subtilis* (42.0-43.0). The DNA hybridization of these species shows only 15% of homology explaining some different properties of the species. They contain an inducible amylase gene that can produce great amounts of active α -amylase enzyme. *B. amyloliqueficiens* cells are 2-3 µm in length and 0.7-0.8 µm wide. This strain is an aerobic or relatively aerobic, Gram(+) bacteria strain, with resting spores. The temperature of the bacterium growth is in the range 5°-50°C, pH = 6-8 [Bergley, 1986].

BIOLEACHING EXPERIMENTS

Bioleaching of metals from black shade was carried out in Erlenmayer flasks on a small laboratory scale. The leaching medium contained 0.75% KNO₃, 0.1% K₂HPO₄ and 0.05% MgSO₄ * H₂O. The active bacteria strains found in the culture were *B.c.-04* and *B.a.-04*, in ratio 1:1 and the solid phase to liquid phase ratio was 5:1. Experiments were performed during 28 days in three batches at 10°, 20° and 40°C. The pH value was brought close to pH 7. Three control systems, with thymol as a bacteriostatic substance, were simultaneously prepared.

The progress of the extraction process was monitored by measurements of the concentration of following ions: Cu²⁺ every three-four days, Ni²⁺ in the third and the last day and Zn²⁺ at the end of the experiment. All these measurements were performed using ASA method. An acidity of systems were checked twice a day and adjusted to pH 7 with 10% NaOH.

The bioleaching process was carried out over 24 days in the „Biomel” batch reactor, at 25°C with a continuous aeration and mixing (300 r.p.m.). Samples of 400

g black shale ore were placed into 3400 cm³ leaching medium containing Mg²⁺, SO₄²⁻, K⁺, HPO₄²⁻, NO₃⁻ and 600 cm³ inoculated broth. The active bacteria strains in the culture were *B. cereus* - B.c.-04 and *B. amyloliquefaciens* - B.a.-04, mixed in a ratio of 1:1. The pH value was brought close to pH 7.0 with 10% NaOH. Simultaneously, we prepared control reaction mixtures that contained 400 g black shale and 4000 cm³ leaching medium with 20 g thymol as a bacteriostatic agent. The concentration of ions was determined every 3-4 days as follows: Cu²⁺ by ASA method, concentration Fe²⁺ and Fe³⁺ by a compleximetric titration, and Ni²⁺ by ASA method when process was finished.

RESULTS AND DISCUSSION

We studied bioleaching of copper, nickel and zinc ions from the black shale during 28 days of process duration. The extension of the leaching process in the studied and control systems at three temperatures is shown in Figure 1, 2 and 3.

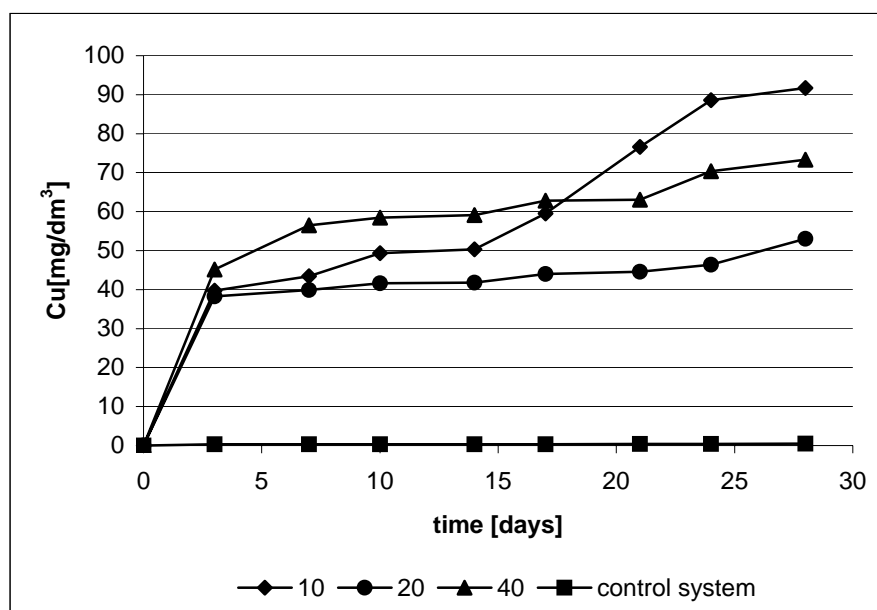


Fig. 1. The effect of temperature on the copper bioleaching during 28 days of process (10°, 20° and 40°C)

In the first three days of leaching, the concentration of copper increased quickly up to 40 mg/dm³ at the three temperatures. For the next seven days, bioleaching process was not observed (Figure 1) at 10°C. After 20 days the process started again and the concentration of Cu²⁺ ions increased up to 55 mg/dm³ (1.7% copper contained in the studying shale). At 20°C, the leaching of copper stopped after seven days (leaching concentration 59 mg/dm³). Some leaching was observed again after 20th day of the

process duration (Figure 1). In the last day of studies the concentration of Cu^{2+} ions reached 75 mg/dm^3 (2.4%). The maximum concentration of copper (90 mg/dm^3) was found in the 28th day of the leaching, at 40°C . We were able to extract 2,8% copper contained in the black shale (Figure 1). In all control systems, no leaching of copper was observed that indicating only biological leaching (Figure 1) in the studied samples.

The concentrations of nickel ions were measured only in the third and the last day of the process duration. Figure 2 shows the values obtained for nickel leaching. As can be seen, bioleaching process was not observed in the first three days (at the same time the quantity of leached Cu^{2+} ions was greatest). In the 28th day bioleaching of nickel was highest at 40°C and reached up to level 1.2 mg/dm^3 (10% nickel contained in the studying shale). The levels of leached nickel at 10° and 20°C were 6% and 9%, respectively (Figure 2).

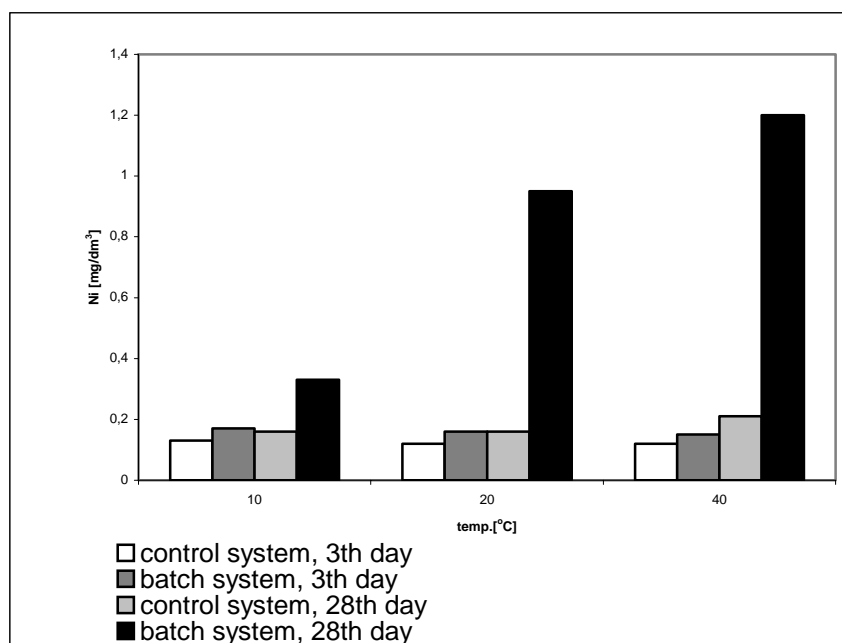


Fig. 2. The effect of temperature on Ni bioleaching during 28 days of process

The concentrations of zinc ions were determined only in the 28th day of process duration (Figure 3). Bioleaching was highest at 40°C but only 0,007% zinc was released.

In order to obtain more information, the bioleaching experiment was carried out on a bench scale. The conditions for bioleaching process were similar with the condition used in laboratory experiments (neutral medium, heterotrophic bacteria *B. cereus* - B.c.-04 and *B. amyloliquefaciens* - B.a.-04). The results are shown in Figure 4.

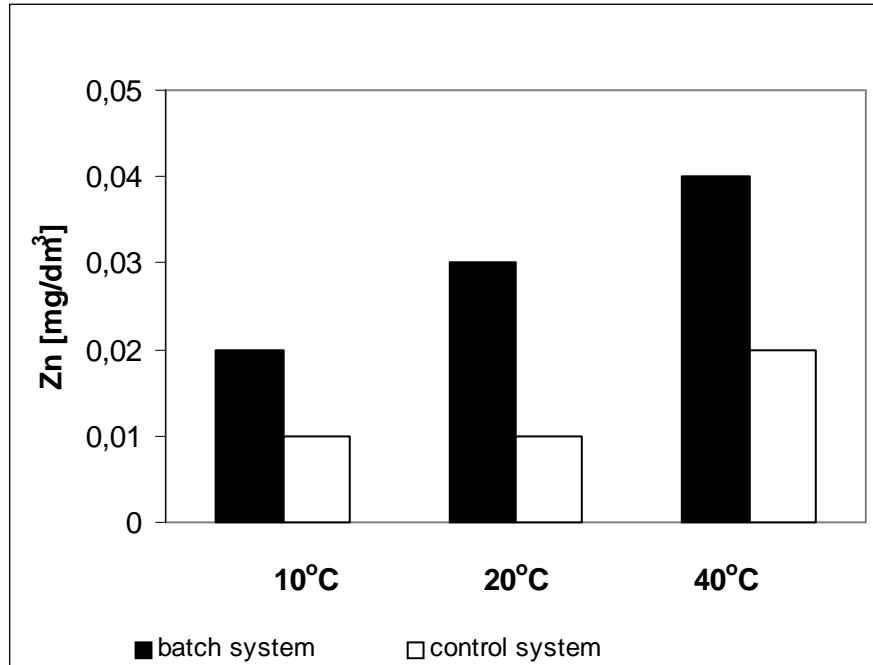


Fig. 3. The bioleaching of Zn during 28 days of process at 10°, 20° and 40 °C

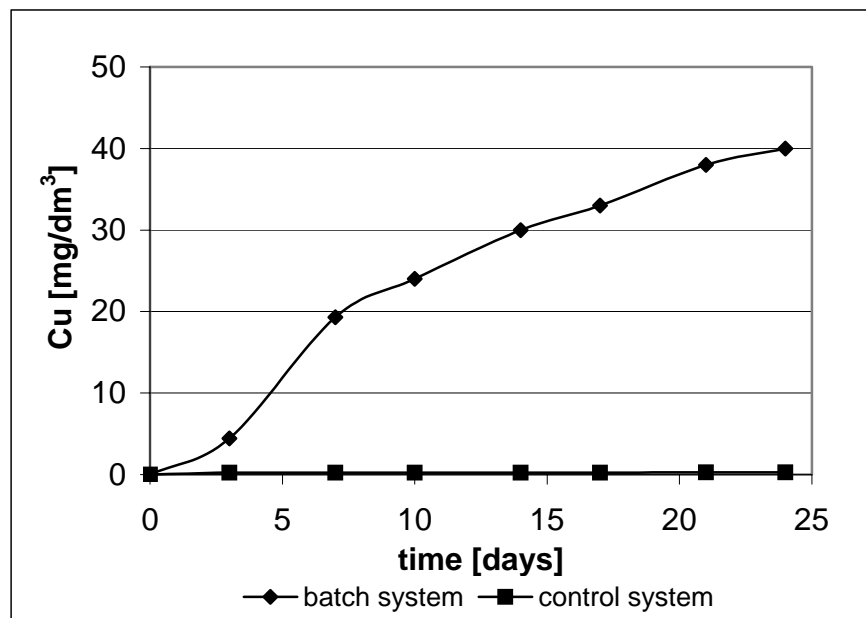


Fig. 4. The bioleaching of copper during 24 days of process

The process of copper leaching started in the 3th day and ran most intensely between the 3rd and 7th day. As shown in Figure 4 the slope of the curve decreases after 7 days indicating that the rate of extraction process decrease after that time. However, there was a significant overall rate of copper production between the 7th and 21st day. In the last three days the reaction was very slow. The first three days represent an adaptation period for microflora. The microflora adapted well to gentle mixing, however it was shocked by intensive mixing in a bioreactor. The intensive mixing was necessary for keeping an uniform ore suspension.

The bioleaching and leaching data are presented in Table 1.

Table 1 Bioleaching and leaching copper and nickel extraction

Process	Recovery , [%]	
	Copper	Nickel
Bioleaching	2.5	9.3
Leaching	0.15	0.22

CONCLUSIONS

The results of our experiments have confirmed predications that copper, nickel and zinc contained in Polish black shale appear in organo-mettalic compounds, because they can be extracted by bioleaching with *B. cereus* and *B. amyloliquefaciens* strains. The bioleaching experiments with copper (Figure 1) suggest different organic forms of this metal in the shale ore. Some of them are highly susceptible to bioleaching by heterotrophic bacteria during the first three days. The others extracted only after 14 days of the process duration at 40°C (Figure 1). We have also found that up to 10% of nickel still remaining in the black shale after acid bioleaching is an organic nickel. The organic compounds of the nickel appeared to be more resistant to bioleaching than the quickly dissolving copper compounds (Figure 2).

REFERENCES

- BERGLEY L.C., 1986, *Manual of Systematic Bacteriology*, Williams & Wikins, volume 2.
 CHMIEL A., 1998, *Biotechnologia. Podstawy mikrobiologiczne i biochemiczne*, PWN, Warszawa.
 KUCHA H., MAYER W., 1996, *Geochemia skał zmineralizowanych*, in: Monografia KGHM Polska Miedź S.A., Lubin, pp. 237-247.
 KUNICKI-GOLDFINGER W., 1998, *Życie bakterii*, PWN, Warszawa, pp. 53-59.
 LIBUDZISZ Z., KOWAL K., 2000, *Mikrobiologia techniczna*, Wyd. Pol. Łódzkiej, volume 1., Łódź, pp. 336.
 ŁUSZCZKIEWICZ A., 2000, *Wykorzystanie frakcji czarnych tutek miedzionośnych z rud z rejonu lubińsko-głogowskiego*, Współczesne problemy przeróbki rud miedzi w Polsce, Pachowica, pp. 137-152.
 PRESCOTT L., HARLEY J., KLEIN D. 1999, *Microbiology*, WCB/McGraw-Hill, International Edition.
 SINGLETON P., 2000, *Bakterie w biologii, biotechnologii i medycynie*, PWN 2000, pp. 18-20.

SPECZIK S., SAWŁOWICZ Z. 1996, *Substancja organiczna i jej rola w procesach złóżotwórczych*, w: Monografia KGHM Polska Miedź S.A., Lubin 1996, pp. 252-258.

Farbiszewska-Kiczma J., Farbiszewska T., Bąk M., *Bioługowanie metali z polskiego łupka miedzionośnego w środowisku obojętnym*, Physicochemical Problems of Mineral Processing, 38, (2004) 273-280 (w jęz. ang.).

W artykule przedstawiono wyniki izolacji, z polskiego łupka miedzionośnego, autochtonicznych szczepów bakterii heterotroficznych oraz wyniki badań nad bioługowaniem tegoż łupka w środowisku obojętnym, przy współdziałaniu wyizolowanych bakterii. Proces prowadzono w małej skali laboratoryjnej, w trzech różnych temperaturach. Dla porównania, proces bioługowania w większej skali został przeprowadzono w bioreaktorze. Proces prowadzony był w bioreaktorze przez 24 dni w temperaturze 25°C.

Małgorzata PACHOLEWSKA*

BIOLEACHING OF GALENA FLOTATION CONCENTRATE

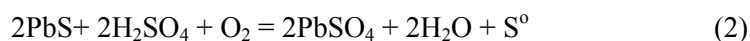
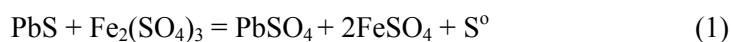
Received May 13, 2004; reviewed; accepted June 30, 2004

The results of the bioleaching process of the galena flotation concentrates from ZGH Boleslaw S.A. by *Acidithiobacillus ferrooxidans* bacteria have been presented. It has been recorded that the final level of conversion of S_S into S_{SO4} in bioleaching process is about 48% and it is two-fold higher than in the control examinations. However, in the course of reaction there is a gradual passivation of the galena surface caused by sparingly soluble PbSO₄. The analysis of raw materials and the products by X-ray analysis proved that there are differences in the composition of reaction products after the process of bioleaching and control leaching. The tested bacteria have been identified on the surface of the examined raw materials by scanning electron microscopy.

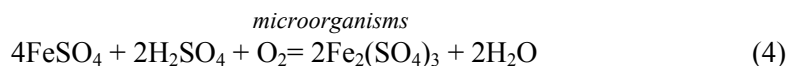
Key words: Bioleaching, galena concentrate, x-ray analysis, passivation

INTRODUCTION

Galena is a sulphide mineral of great importance for lead metallurgy. Lead can be recovered from galena applying hydrometallurgical method, i.e. leaching by oxidant solutions, namely by iron(III) salt in the form of FeCl₃ (Dutrizac, 1986). In the process of bioleaching chloride anion, which is toxic for microorganisms, is replaced by sulphate anion. The course of reaction of chemical and biological leaching of galena in acid medium by Fe₂(SO₄)₃ can be presented by the following equations (Bang et al. 1995, Gonzales-Chaves et al. 2000):



* Silesian University of Technology, Faculty of Materials Science and Metallurgy
Department of Metallurgy, 40 019 Katowice, Krasinskiego 8, malg@mail.polsl.katowice.pl



Using $\text{Fe}_2(\text{SO}_4)_3$ as an oxidant in H_2SO_4 solution, acid medium produces sparingly soluble PbSO_4 (the product of the reaction). Therefore, hydrometallurgical process of lead recovery from sulphides should be modified and chloride solutions ought to be used again for lead extraction. Although this technology is considered as highly impractical, recent scientific reports present quite favourable opinions on the use of microorganisms for bioleaching of galena together with sphalerite in sulphide ores (Santhiya et al. 2001, Liao et al. 2004). *Acidithiobacillus ferrooxidans* bacteria are used in bioleaching process of lead and zinc sulphide minerals. This kind of bacteria can easily oxidize sulphur in reduced form (sulphide sulphur and elemental sulphur) into S_{SO_4} and they are also able to regenerate and reproduce in the process of leaching the Fe^{3+} ion (Karavaiko 1985, Torma, Bang et al., 1995). Another kind of sulphur bacteria which can be used as well are *Acidithiobacillus thiooxidans*, however they are able to oxidize only the reduced sulphur compounds (Santhiya et al. 2001). The effect of forming a passive film of elemental sulphur in the course of reaction is prevented by the action of *Acidithiobacillus thiooxidans* (reaction 3). Electrochemical interaction of Zn and Pb minerals in the process of biological leaching (da Silva et al. 2003) and their properties and functioning in the flotation process preceded by bioleaching have been examined as well (Santhiya et al. 2001).

The aim of this paper is to analyse and define suitability and applicability of *Acidithiobacillus ferrooxidans* bacteria for bioleaching of lead sulphide flotation concentrates, produced by mine Boleslaw (Poland). At this time, galena concentrate (PbS) has been used as a raw material for producing lead, applying pyrometallurgical methods.

EXPERIMENTAL METHODS

MATERIALS

Table 1 presents the chemical constitution of the examined flotation galena concentrate which was used in the bioleaching experiments. X-ray analysis revealed that raw concentrate of flotation galena was composed mainly of PbS (~80%). The percentage of other components was as follows: hydrocerusite (~5%), marcasite (~5%), sphalerite (~5%), pyrite (~4%) and minute quantities of gypsum and quartz (~2% in total).

Synthetic lead sulphide PbS (100%) of high purity made by IMN Gliwice has been used for a comparison.

Table 1. Constitution of flotation galena concentrate from ZGH Boleslaw S.A.

Constituent	H ₂ O	Zn	Pb	S _{total}	Fe	CaO	MgO	Sso ₄	Ss	SiO ₂	Cd
Contents [%]	7.5	2.44	69.3	18.4	6.21	0.77	0.22	0.33	18.09	0.50	0.02

BACTERIAL CULTURE

Strain of F3-02 *Acidithiobacillus ferrooxidans* bacteria of high activity in the oxidation process of iron(II) and reduced sulphur compounds have been used in the experiments. The strain of bacteria has been separated from ferruginous mineral water (Piwniczna-Lomnica). In preparation for the experiment the bacteria have been cultivated in a modified 2K medium. 2K liquid medium has got the following composition: (NH₄)₂ SO₄-3,0; KCl-0,1; MgSO₄ · 7H₂O-0,5; Ca(NO₃)₂-0,01; K₂ HPO₄-0,5; FeSO₄ · 7H₂O - 9,84 (g/dm³) (Silverman 1959). The concentration of Fe(II) in 2K medium was 2,0 g/dm³ and the application of 2M H₂SO₄ solution allowed to obtain pH 2 medium which actually became the leaching solution for galena concentrate. The bacteria used in the experiments were not initially adapted to be with lead compounds.

BIOLEACHING EXPERIMENTS

The experiment was carried out in Erlenmeyer's flask of 300 cm³ capacity. The quantity of galena concentrate was 5% weight/volume, the volume of solution was 100 cm³, whereas the strain of bacteria was 10 cm³. Laboratory shaker was used to aerate the leached samples, the number of cycles was 130 revolutions/min and the temperature was 25°C. Pb, Zn, Fe(II) concentration, oxidizing-reducing potential, pH, S_{total} and S_{SO4} contents in the residue after leaching have been analysed in the solution during the experiments. The method of spectral atomic absorption was applied to determine Zn and Pb concentration, whereas Fe(II) concentration was determined by manganometry method. S_{SO4} was determined by weigh method, S_{S²⁻} was calculated as the difference between S_{total} contents determined by weigh method and S_{SO4}. The residue was analysed by X-ray method. The surface analysis were carried out by scanning microscopy method (SEM). The obtained results were verified by the examinations performed in sterile conditions.

X-RAY ANALYSIS

The examinations of phase composition of flotation galena samples before and after leaching process were carried out using PW 3710 X-ray diffractometer (produced by Philips). It was realised at the following measurement conditions: radiation Cu α_1 ; graphitoidal monochromator, 40kV voltage, 35mA intensity, counting time of the impulses - 2s, rate of meter shift - 0.02.

STRUCTURAL ANALYSIS

The examinations of samples microstructure were performed using HITACHI S-4200 scanning microscope, which was coupled with EDS X-ray spectrometer and Voyager microanalysis system. The bioleaching residues were dried outdoors on the filter. The samples were prepared for analysis on a copper pad and were covered (sprayed) by gold.

RESULTS AND DISCUSSION

EXTRACTION OF METALS, Eh CHANGE, pH CHANGE

Table 2 presents the results which are the proof that in the process of bioleaching of flotation galena concentrate at the period of 288 h. As can be seen, *Acidithiobacillus ferrooxidans* bacteria caused rapid oxidation of Fe(II) into Fe(III) in biological leaching. It was resulted in growth of oxidizing-reducing potential measured in the slurry. This potential was increased from +408,6 mV to 560,8 mV after 288 h of bioleaching. The value of oxidizing-reducing potential (redox) in the control experiment was 286,5 mV at the same period of time. The increase of Fe(II) oxidation in the control solutions was entirely spontaneous due to atmospheric oxygen. For both the biological and control processes the total oxidation of Fe(II) ions was noticed after 384 h. It was found that there was a decrease of potential redox and it was connected with pH changes of the slurry.

The analysis of pH changes showed that the initial pH 2 of the slurry rises quite rapidly up to pH 4-5 which has been caused by abrupt course of chemical reaction of oxidizing PbS into PbSO₄ and sulphur S⁰ (reaction 2). The next stage of reaction was possible due to the presence of *A. ferrooxidans* microorganisms and the biological reaction of oxidizing S⁰ into H₂SO₄ (reaction 3) which led to a gradual increase of acidity and a decrease of pH to lower values. In practice, it can indicate the progress of the reaction of biological oxidizing of sulphide PbS since in the control examinations no process of rapid acidifying of the solution is observed which means that the reaction of biological oxidizing of elemental sulphur into H₂SO₄ does not take place.

It was found that there was an increase of the concentration of zinc released into the solution from 0,0 to 0,196 g/dm³. To compare, the zinc concentration in control experiments increased only up to 0,040 g/dm³. The function of zinc in the examined set was to indicate how the process precedes (progress of the reaction). The lead concentration in the solution in the presence of sulphate ions ranged from 0,0019 to 0,0033 g/dm³ but in the control examinations it was from 0,0021 to 0,0036 g/dm³. The highest concentration of Pb was reached in the leaching process of synthetic galena – 0,0098 g/dm³.

Table 2 presents, just for comparison, the results of biological oxidizing of pure synthetic sulphide PbS. It can be noticed that the initial rapid processs of neutralizing the solution as a result of chemical oxidation of PbS into PbSO₄ was the reason of

bacterial activity decline. The surface of galena is then covered with a passive film of lead sulphate, which makes further process of galena oxidizing impossible. The redox potential stays at low unchangeable level which indicates that there is no oxidizing of Fe(II). At the same time pH growth caused hydrolytic precipitation of iron salts which got down to the sediment.

Table 2. The results of bioleaching flotation galena concentrates by *A. ferrooxidans* F3-02 in 2K solutions. Marking: (b) - biological, (ktr) - control, (cz) - biological leaching of pure PbS

Nr	Czas [h]	PH	Eh, [mV] vs Ag/AgCl	Fe(II) [g/dm ³]	Zn [g/dm ³]	Pb [g/dm ³]
PbS1 (ktr)	0	2.2	413.4	2.159	0.00	0.00
PbS4 (b)		2.2	408.6	2.159		
PbS10(cz)		2.2	410.2	2.159		
PbS1 (ktr)	48	4.7	157.6	2.159	0.022	0.0036
PbS4(b)		3.2	433.2	1.127	0.025	0.0033
PbS10(cz)		5.2	130.1	1.985	0.005	0.0074
PbS1(ktr)	96	4.9	151.0	1.961	0.021	0.0030
PbS5(b)		3.3	415.0	0.392	0.090	0.0030
PbS10(cz)		5.1	130.6	2.00	0.005	0.0038
PbS1(ktr)	192	4.2	181.5	1.796	0.023	0.0032
PbS6(b)		3.2	428.8	0.561	0.091	0.0027
PbS10(cz)		5.0	133.9	1.904	0.005	0.0041
PbS2(ktr)	288	3.4	286.5	1.113	0.024	0.0022
PbS7(b)		2.7	560.8	0.00	0.157	0.0021
PbS11(cz)		5.0	156.4	1.041	0.003	0.0035
PbS3(ktr)	384	3.4	478.3	0.00	0.040	0.0021
PbS8(b)		2.2	534.5	0.00	0.196	0.0019
PbS12(cz)		5.4	174.0	0.555	0.004	0.0098

The best pH conditions for *A. ferrooxidans* bacteria are pH 2-3 [Karavaiko 1985]. Therefore, the alkaline medium is inappropriate for them. Lead sulphide in natural galena is not easily accessible in the process of biological oxidizing contrary to PbS in chemical reagent which is present there, thus there are differences in activity and state of the samples. These conclusions are similar to those presented in the paper by Cisneros-Gonzales, (1999).

THE LEVEL OF S_S CONVERSION INTO S_{SO4}

Chemical analysis of residues after bioleaching and control leaching regarding time relations has been presented in Table 3. The results prove that the dynamics of conversion reaction of sulphide sulphur S_S into sulphate sulphur S_{SO4} was higher in the case of bioleaching. The conversion of S_S into S_{SO4} amounted up to 42,39% after 192

h. The level of sulphide sulphur conversion into an oxidized form was 47,99% after 288 h of duration of leaching process by *A. ferrooxidans* bacteria but the level of conversion was only 27,25% in control leaching. Further biological oxidation of galena surface is quite different because of gradual passivation of its surface by lead sulphate, which has also been confirmed by other examination results [Bang et al. 1995, Gonzales-Chaves et al. 2000].

Table 3. Composition of residues after leaching of flotation galena in [%]

Serie	S _{SO4}	S _S	Zn	Pb	Fe	S _{SO4} /(S _{tot.} -S _{O4})*	Time, [h]
Control leaching	2.70	16.10	2.01	63.4	7.40	1.7	0
	2.72	15.07	1.91	63.4	7.94	18.05	96
	3.67	13.47	1.69	61.9	6.30	16.73	192
						27.25	288
Biological leaching	3.52	15.48	1.82	60.6	7.81	22.74	96
	5.32	12.55	1.59	57.8	8.37	42.39	192
	5.51	11.48	1.43	57.9	8.15	47.99	288
	5.54	11.13	1.40	56.9	7.41	49.78	384

* The level of S_S conversion into S_{SO4}

There is a layer of PbSO₄ as a product of the reaction, on the grains of galena as shown in microscope pictures (Fig.2). *A. ferrooxidans* bacteria dipped in the base, partly covered with lead sulphate can be seen as well. Prolonging the time of leaching up to 384 h does not make any difference in the progress of oxidizing reaction of galena and the level of sulphide sulphur conversion into sulphate sulphur S_{SO4}/(S_{total} - S_{SO4}) remains unchanged in biological examinations. Bacterial colonies were not present in bioleaching examinations of pure synthetic galena but its surface was covered with fine PbSO₄ crystals, which were formed by chemical reaction (2).

PHASE ANALYSIS OF RESIDUES

The analysis of X-ray radiography (Fig.1) showed that in the sample of galena flotation concentrate after the process of bioleaching by *A. ferrooxidans* microorganisms for 288h, the phase composition of the sample is as follows: galena PbS (~43%), anglesite PbSO₄ (~40%), pyrite FeS₂(~8%), jarosite (H₃O)Fe₃(OH)₆(SO₄)₂(~6%), sulphur admixture (~3%).

In the sample of flotation galena after control leaching (288h) in iron salts (II) the following stages could be distinguished: galena PbS(~62%, anglesite PbSO₄ (~25%), pyrite (~6%), jarosite of mixed and difficult to identify composition (with H₃O⁺, Pb²⁺, K⁺, Na⁺?) (~4%), marcasite FeS₂ (~3%). Trace amount of sulphur is also quite possible.

The composition of galena flotation concentrate in the process of biological leaching indicates that there is the higher concentration of oxidized sulphur compounds in the sample compared to the control tests.

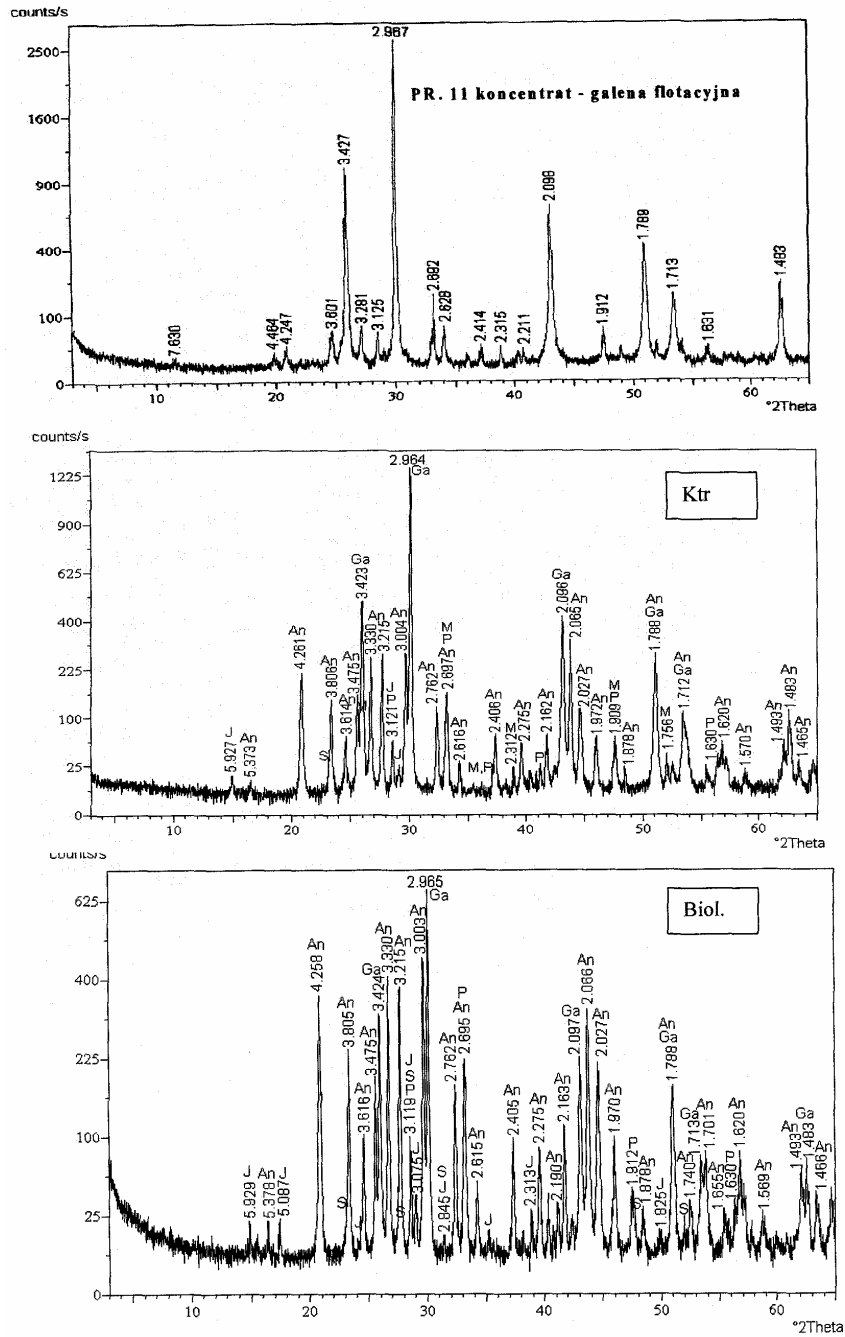


Fig. 1. Radiography of PbS flotation galena and control leaching residues (Ktr), biological leaching residues (Biol). Marking: J-jarosite, An-anglesite, Ga-galena, P-pyrite, M-marcasite

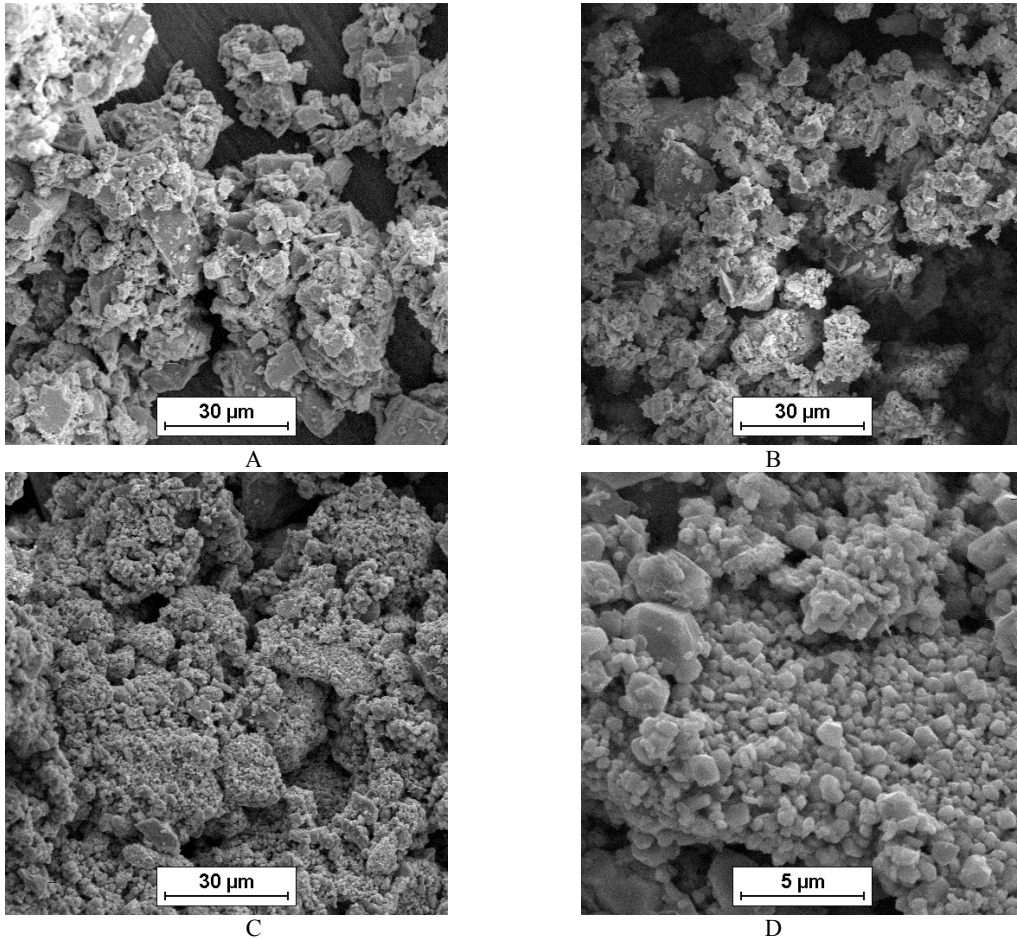


Fig. 2. SEM microphotographs of galena: A-raw galena flotation concentrate and B-after sterile control leaching (288h), 500x; C-galena flotation concentrate after bioleaching using *Acidithiobacillus ferrooxidans* (288 h) 500x, and D-3000x

MICROSCOPE ANALYSIS

The picture of the surface of raw concentrate of flotation galena after the process of bioleaching and control leaching in the solutions of iron salts has been presented in Fig. 2 and Fig.3. The method of scanning microscopy was applied. It can be noticed that the morphology of galena has been changed by the leaching solution. The surface of grains becomes covered and coated with a film of reaction products (Fig. 2). The film of reaction products (PbSO_4 and most likely S^0) can also be responsible for making the surface of galena passive as well as reducing the penetration of solution components and oxygen inside the grain. On the surface of galena in the process of bioleaching there were *Acidithiobacillus ferrooxidans* bacteria cells stuck to the surface and dipped in the leached base (Fig. 3).

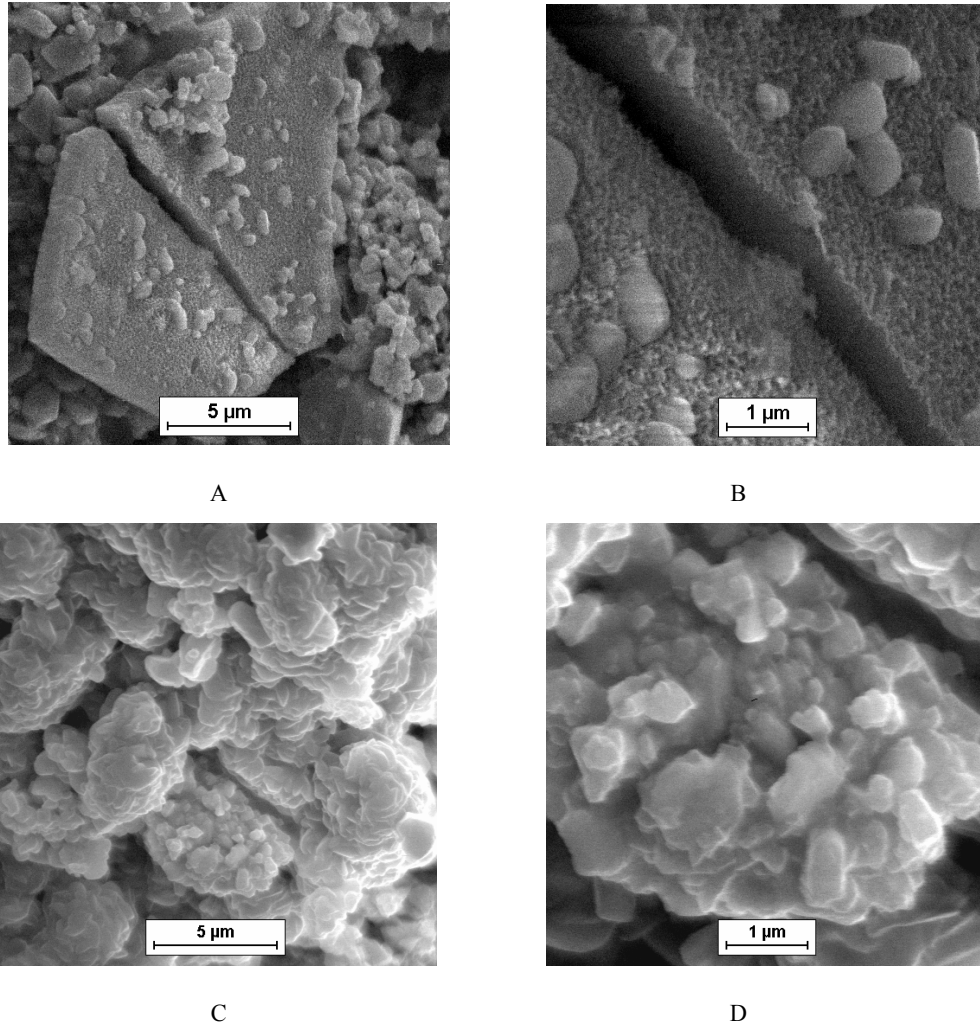


Fig. 3. SEM microphotographs of galena flotation concentrate surface after bioleaching using *Acidithiobacillus ferrooxidans*: (288 h) - A-3000x, B-10000x; and (384h) - C-3000x, D-10000x

SUMMARY

The examinations on bioleaching of natural galena flotation concentrate in iron(II) salt solutions by *Acidithiobacillus ferrooxidans* bacteria allowed to draw some conclusions that the bacteria have an impact on higher yield in the course of reaction of oxidizing PbS into PbSO₄ as compared to the control data. The level of conversion of S_S into S_{SO4} after 288h of bioleaching amounted up to 47,99% whereas in the control examinations it was only 27,25%. After a period of time (384 h) though, there is a definite inhibiting of the course of S_S oxidizing reaction. The possible cause of

inhibiting the reaction is the formation of passive film of products of galena oxidizing - lead sulphate - on the surface of leached galena and the fact that the access of the leaching agent and microorganisms inside the grain is made difficult.

ACKNOWLEDGEMENTS

The work was supported by the State Committee for Scientific Research in Poland, project No.7 To9D 0021

REFERENCES

- BANG S., DESHPANDE S., HAN K.(1995), *The oxidation of galena using Thiobacillus ferrooxidans*, Hydrometallurgy 37, nr2, 181-192.
- CISNEROS-GONZALEZ I., OROPEZA-GUZMAN M.I., GONZALEZ I., (1999), *Cyclic voltammetry applied to the characterisation of galena*, Hydrometallurgy, 53, 133-144
- CWALINA B. (1994), *Metabolizm siarki u Thiobacillus ferrooxidans w procesie ługowania metali z mineralów siarczkowych*. Wyd. UŚ, Katowice.
- DA SILVA , LASTRA M.R., BUDDEN J.R. (2003), *Electrochemical passivation of sphalerite during bacterial oxidation in the presence of galena*, Minerals Engineering 16, 199-203.
- DUTRIZAC J.E.(1986), *The dissolution of galena in ferric chloride media*, Metallurgical Transactions B, vol.17B, March, 5-17.
- GONZALEZ-CHAVEZ J.L., GONZALEZ F., BALLESTER A., BAZQUEZ M.L.(2000), *Effect of mesophilic microorganisms on the electrochemical behavior of galena*, Minerals and metallurgical processing, vol.7, no2, May, 116-120.
- KARAVAIKO G.I (1985), *Microbiological Processes for Leaching of metals from ores*. Ed Torma A.E. Moscow.
- LIAO M.X., DEN T.L.(2004), *Zinc and lead extraction from complex raw sulfides by sequential bioleaching and acidic brine leach*, Minerals Engineering 17, 17-22.
- MIKHLIN YU., KUKLINSKIY A. MIKHLINA E., KARGIN V., ASANOV I. (2004), *Electrochemical behaviour of galena (PbS) in aqueous nitric acid and perchloric acid solutions*, J. Appl. Electrochem., 34, 37-46.
- SANTHIYA D., SUBRAMANIAN S., NATARAJAN K.A., HANUMANTHA RAO K., FORSSBERG K.S.E.(2001), *Bio-modulation of galena and sphalerite surfaces using Thiobacillus thiooxidans.*, Int. J. Miner. Process. 62, 121-141.
- SILVERMAN M.P., LUNDGREN D.G. (1959), *Studies on the Chemoautotrophic Iron Bacterium Ferrobacillus ferrooxidans*, J. Bacteriol., vol.77., 642-647.
- TORMA A. (1988) Leaching of metals, Chapter 12 [in:] Biotechnology – A Comprehensive Treatise in 8 Volumes, ed.H.-J. Rehm, G.Reed, vol.6 b, Weinheim.

Pacholewska M., *Biologowanie galenowego koncentratu flotacyjnego*, Physicochemical Problems of Mineral Processing, 38, (2004) 281-290 (w jęz. ang.).

W pracy przedstawiono wyniki procesu biologowania przy udziale bakterii *Acidithiobacillus ferrooxidans* naturalnych siarczkowych koncentratów ołowiu z ZGH” Bolesław” S.A. Stwierdzono, że końcowy stopień konwersji siarki Ss do Sso₄ w procesie biologowania wynosi około 48% i jest dwukrotnie wyższy w porównaniu z próbami kontrolnymi. W miarę postępu reakcji zachodzi jednak stopniowa pasywacja powierzchni galeny przez trudno rozpuszczalne produkty (prawdopodobnie PbSO₄, S⁰). Analiza fazowa surowców i produktów metodą rentgenograficzną potwierdziła różnice w składzie produktów reakcji po ługowaniu biologicznym i kontrolnym. Na powierzchni badanych surowców zidentyfikowano testowane bakterie przy użyciu elektronowej mikroskopii skaningowej.

A. URYGA, Z. SADOWSKI*, A. GROTOWSKI**

BIOLEACHING OF COBALT FROM MINERAL PRODUCTS

Received May 20, 2004; reviewed; accepted June 30, 2004

A kinetic approach to study cobalt, copper and arsenic bioleaching has been proposed and discussed. Two flotation by-products from the Lubin mine have been used. *Acidithiobacillus ferrooxidans* bacteria isolated from water from the "colour" lakes of Boguszow (Lower Silesia), was adopted to metal leaching. Semi-empirical model has been proposed to describe the metal extraction from collected samples. This model originated from the shrinking core and it was able to fit the experimental data. This model is an useful tool to investigate and compare ore bioleaching process for different size fractions.

Key words: bioleaching, cobalt, kinetic model, biomining

INTRODUCTION

Bioleaching of mineral products from KGHM Polska Miedz has been a subject of research for over three decades (Sadowski, 1998, 2002). This process has been used to extract metal from low-grade ores and more recently there is an increasing interest in metal leaching from cobalt-bearing products.

There are two mechanisms of bioleaching: one is indirect leaching, in which microbial (*A. ferrooxidans*) acts on iron(II) ions in solution producing iron(III) ions, and the other, direct mechanism, in which microbial cells interact directly with the solid surface. For both of the above mechanisms, the rate of leaching makes a biologically assisted process economically attractive to conventional roasting or pressure oxidation process.

Many authors have assumed that kinetic model of bioleaching is related to the kinetic of ferrous iron oxidation (Boon et al., 1999, Nemati et al., 1998). Veglio

* Wroclaw University of Technology, Department of Chemical Engineering
Zygmunt.Sadowski@pwr.wroc.pl

** CBPM Cuprum Sp z o.o. OBR, Wroclaw, a.grotowski@cuprum.wroc.pl

(Beolchini et al., 1999, Veglio et al., 2000), suggested that the pyrrhothite ore leaching process kinetics is controlled by the chemical reaction. It was confirmed by the activation energy of the process equal to about 100 kJ/mol.

Small quantities of cobalt (101 ppm) occur in the copper ores, which are actually exploited by KGHM Polska Miedz S.A. The highest concentration of cobalt has been observed at the Lubin mine. The beneficiation of cobalt from copper ore is (70.8%). The copper flotation concentrate contains 1055 ppm of cobalt. In the smelting process, cobalt goes towards a converter slag. The conventional production of cobalt from copper deposits is uneconomic. For this reason alternative technology must be developed.

The objective of the present study was to examine the bioleaching process of two by-products from the Lubin copper mine. The bioleaching data will be fit to a simple bioleaching kinetic model, which will be able to describe the cobalt extraction from cobalt bearing sulphide minerals.

The aim of the present work was to compare the bioleaching kinetics between two particle size groups and establish a correlation between the leaching kinetic and the particle size.

MATERIAL AND METHODS

CULTURE OF MICROORGANISM

A pure culture of microorganism, *Acidithiobacillus ferrooxidans* was used in this study. These acidiphilic bacteria were selected from water taken from "colour" lakes of Boguszow (Lower Silesia). The strain was routinely cultured in 2K liquid medium. An inoculum age of about 3 days was used in the experimental trials.

MINERALS

Two kinds of cobalt-bearing mineral samples were obtained from the flotation plant of ZWR Lubin mine (Poland). Before experiments these samples were sieved using a 0.315 mm sieve. Table 1 provides the chemical composition of the cobalt-bearing flotation samples used in these studies.

Table 1. The composition of the cobalt-bearing samples

Sample No	Sample	Weight [g]	Weight Recovery [%]	Element [mg/kg]		
				Cu	Co	As
1	ZWR Lubin I -0.315 mm	1630	52.67	12.25	0.126	0.347
2	ZWR Lubin I +0.315 mm	1465	47.33	20.45	0.191	0.812
3	ZWR Lubin II -0.315 mm	2014	65.20	12.35	0.135	0.325
4	ZWR Lubin II +0.315	1075	34.80	22.35	0.121	0.81

BIOLEACHING BIOREACTOR

The biooxidation studies were carried out in a 12-dm³ bioreactor at constant temperature (30°C). Bioleaching experiments were performed with 1 kg sample. The pH of the solution in the bioreactor was maintained by addition of sulphuric acid. The pH was adjusted to 2.5 for mesophilic bacteria. A bioleaching run was started, when 2.5 dm³ of an active culture of the microorganisms was added. Samples of solid particle were regularly analysed using BET method.

ANALYTICAL TECHNIQUE

Solution samples were collected at various times during the bioleaching experiment runs. The concentrations of copper, cobalt, and arsenic were measured by atomic-absorption spectrophotometry. Metal leaching recovery was expressed as the fraction of original metal extracted into solution.

RESULTS AND DISCUSSION

The chemical leaching of samples in the absence of microorganism was realised during the pH adjust procedure. Typical bioleaching process started when an inoculum was added. Bioleaching kinetic data are presented in Figures 1-4.

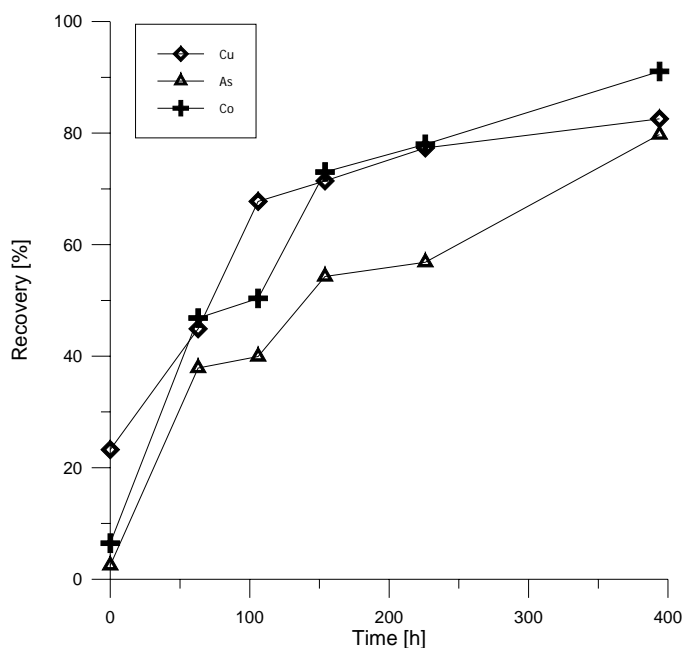


Fig. 1. Recovery of Cu, Co and As from sample I (-0.315mm)

Figure 1 presents the metal recovery evolution as a function of leaching time. As can be seen the solution concentration of Cu, As and Co obtained from the biooxidation of tested mineral sample systematically increased. Experimental cobalt, copper and arsenic recovery (R) is calculated following the standard formula:

$$R = \frac{Q_n}{Q_0} 100$$

where Q_n and Q_0 are masses of solids during and before leaching, respectively.

Bioleaching is a particulate process, which is dependent on the size distribution of leached particles. The microbiological profiles of Cu, Co and As for +0.315 mm fraction were presented at Fig. 2.

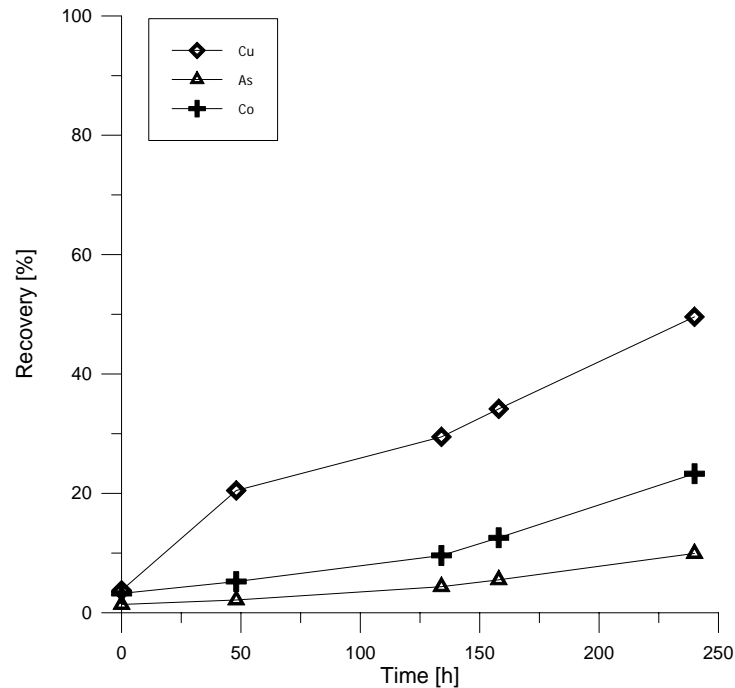


Fig. 2. Copper, cobalt and arsenic extraction in the bacterial leaching of sample I (+ 0.315 mm)

Figures 3 and 4 show the experimental kinetic curves for each size fraction of the second sample, respectively.

As can be seen from Fig 3, copper, cobalt and arsenic extraction after 240 hours of bioleaching were 73.09, 79.20 and 59.01%, respectively. Copper, cobalt and arsenic extractions after 240 hours of bioleaching of + 0.315 mm fraction are shown at Fig. 4.

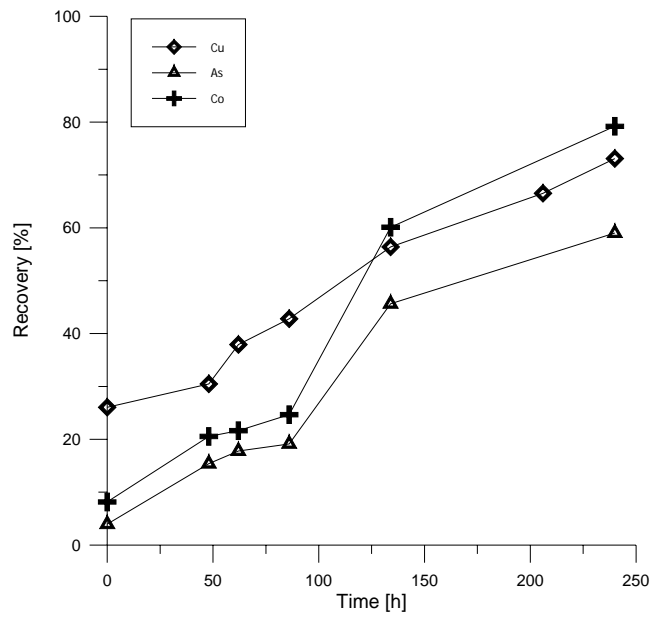


Fig. 3. Bioleaching of -0.315 mm fraction of cobalt bearing sample II

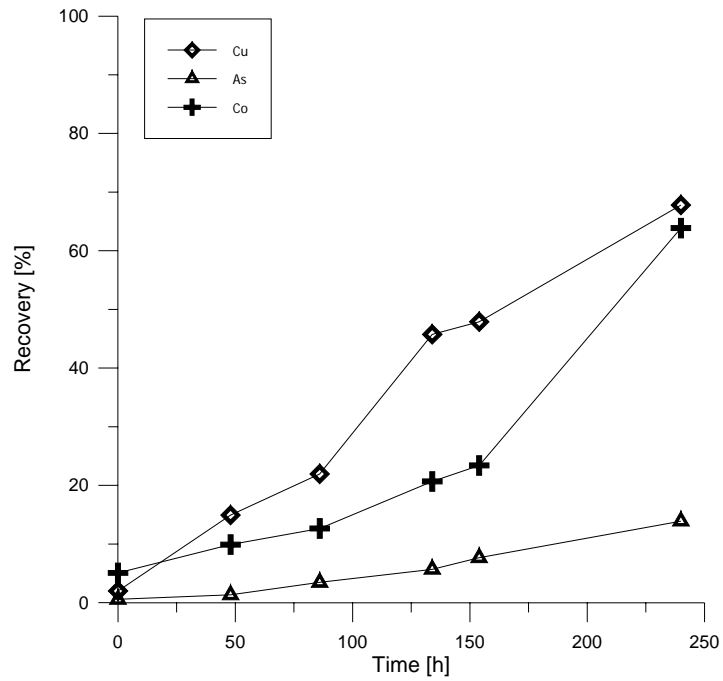


Fig. 4. Bioleaching of +0.315 mm fraction of cobalt bearing sample II

Final recovery of metals at the end of the bioleaching tests are summarised in Table 2.

Table 2. Summary of the metal recoveries obtained in these experiments

Sample	Recovery [%]		
	Cu	Co	As
Sample I -0.310 mm	82.2258	91.07	79.74
Sample I +0.310 mm	49.58	23.30	9.92
Sample II -0.310 mm	73.09	79.2	59.01
Sample II +0.310 mm	67.79	63.85	13.90

According to the shrinking core model (Lizama et al. 2003) the leaching kinetic involves a surface reaction and pore diffusion transport. The kinetics of leaching can be described by the equation:

$$1 - \left(\frac{2}{3}\right)\alpha_{Co} - (1 - \alpha_{Co})^{\frac{2}{3}} = kt$$

where: α_{Co} is the cobalt recovery, k is the rate constant and, t is time (day) of bioleaching.

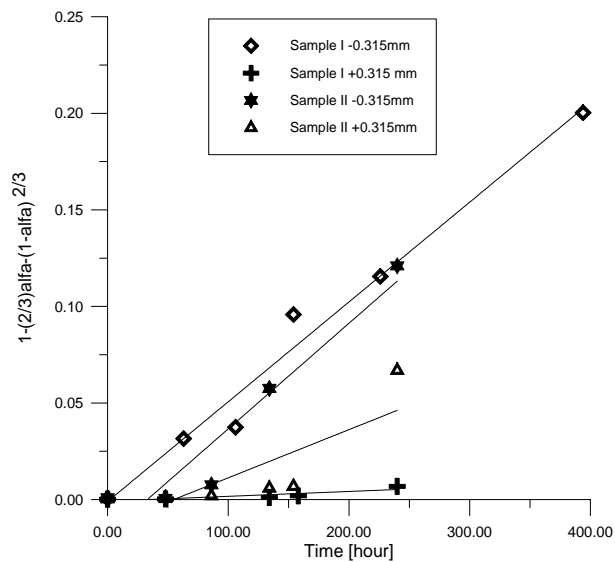


Fig. 5. Experimental data for cobalt according to the shrinking core model

The shrinking core rate constant “k” is related to the surface area of leaching samples and should be constant over time. If the particle shrinks at a uniform rate, the leaching rate is proportional to the surface area of the mineral particle. The bioleaching process has been controlled by the change of the surface area. Table 3 presents the initial and final surface areas of bioleached samples.

Table 3. Surface areas of samples before and after bioleaching

Sample	Surface area [m ² /g]	
	before bioleaching	after bioleaching
Sample I (+0.315mm)	3.88	7.35
Sample I (-0.315 mm)	5.50	8.21
Sample II (+0.315 mm)	3.36	6.64
Sample II (-0.315 mm)	4.89	7.44

The kinetics of dissolution of single particles can be expressed by the following equation:

$$\frac{dM}{t} = 3\alpha\rho D_p^2 \frac{d(dD_p)}{dt}$$

where M is the mass particle and dD_p is the diameter of the particle (Haddadin et al., 1995). This model can predict the evolution of particle size as a function of leaching time:

$$\frac{dD_p}{dD_{p0}} = \left(1 - \frac{at^b}{f_c c_0}\right)^{\frac{1}{3}}$$

where: a and b are constants.

Based on the evolution of cobalt concentration in solution for each particles size treated, the evolution of cobalt recovery (and other metals) has been calculated and fitted using a first order kinetic function (Brochot et al., 2004, d’Hugues at al.,1997):

$$R = R_{\max} \left(1 - e^{-kt}\right)$$

where: R recovery at time t; R_{max} maximum recovery; k, kinetic constant.

It was observed that kinetic constant k linearly depends on 1/D, the inverse of the particle diameter (Brochot et al., 2003). The particle diameter is decreasing during the bioleaching process with a constant rate. According to the shrinking core model, the quantity of material reacting is proportional to the available surface of unreacted core. At the shrinking core model, the diameter of leaching particle decreases during the

bioleaching process. If this happens, for a population of particles, the size fraction must be a function of an initial size distribution and leaching time.

The leaching phenomenon is governed by the particle surface developed. The reduction of particle size is realised with a constant rate $dx/dt = -k^*$. Where, x is the particle diameter (m) and k^* is the kinetic constant expressed as the diameter decrease rate (m/s). Table 4 shows a comparison between the parameter k (shrinking core rate constant) and the surface area increase (Δs) during bioleaching process.

Table 4. Comparison between estimated kinetic parameter and surface area increase

Sample	Size [mm]	$k \cdot 10^{-4}$	Δs	Sample	Size [mm]	$k \cdot 10^{-4}$	Δs
I	- 0.315	5.16	2.71	I	+ 0.315	2.54	3.47
II	- 0.315	5.46	2.55	II	+0.315	2.49	3.28

It is evident, as can be expected, an increase of surface area is inversely proportional to the bioleaching rate constant. However, we must remember that, the overall leaching kinetics is a result of a multiplicity of elementary processes, of which three are the most important:

- i. Adhesion of microbial cells to the mineral surface and their detachment
- ii. Direct oxidation of the mineral by the attached bacteria
- iii. Chemical oxidation of the sulphide mineral with iron(III)
- iv. For these reasons, the shrinking core model should be rebuilt for both bacterial growth and colonisation kinetics.

CONCLUSION

The bacterial leaching tests of two cobalt-bearing samples showed a cobalt leaching ability of these samples. The most important parameter affecting the cobalt, copper and arsenic extraction from investigated samples is the initial mineral particle size. Decreasing the initial mineral particle size gives rise to an increase in copper, cobalt and arsenic recovery.

The results of preliminary leaching experiments reveal that the shrinking core model can represent the bioleaching process of cobalt-bearing samples.

REFERENCES

- BEOLCHINI F., VEGLIO F., 1999, *Kinetic modeling of pyrrhotite ore leaching by ferric iron and related statistical analysis*, Ind. Eng. Chem. Res., 38, pp. 3296-3299.
- BOON M., BRASSER J.H., HANSFORD S.G., HEIJNEN J.J., 1999, *Comparison of the oxidation kinetics of different pyrites in the presence of Thiobacillus ferrooxidans or Leptospirillum ferrooxidans*, Hydrometallurgy, 53, pp. 57-72.

- BROCHOT S., DURANCE M.V.M., VILLENEUVE J., d'HUGUES P., MUGABI M., 2004, *Modelling of the bioleaching of sulphide ores: application for the simulation of bioleaching/gravity separation of the Kasese Cobalt Company Ltd process plant*, Minerals Engineering, 17, pp. 253-260.
- d'HUGUES P., CEZAC P., CABRAL T., BATTAGLIA F., TRUONG-MEYER X.M., MORIN D., 1997, *Bioleaching of cobaltiferous pyrite: a continuous laboratory-scale study at high solids concentration*, Minerals Engineering, 10 (5), pp. 507-527.
- HADDADIN J., DAGOT Ch., FICK M., 1995, *Models of bacterial leaching*, Enzymes Microbial Technology, 17, pp. 290-305.
- LIZAMA M.H., FAIRWEATHER J.M., DAI Z., ALLEGRETTO D.T., 2003, *How does bioleaching start?*, Hydrometallurgy, 69, pp.109-116.
- NEMATI M., HARRISON L.T.S., HANSFORD S.G., WEBB C., 1998, *Biological oxidation of ferrous sulphate by Thibacillus ferrooxidans: a review on the kinetic aspects*, Biochemical Engineering J., 1, pp.171-190.
- SADOWSKI Z., 1998, *Wstępna analiza możliwości wykorzystania procesów obróbki biologicznej surowców mineralnych dla potrzeb KGHM Polska Miedź S.A.*, Opracowanie na zlecenie KGHM Polska Miedź S.A.
- SADOWSKI Z., 2002, *Analiza możliwości zastosowania procesów bioługowania w przeróbce produktów z bogacania rud miedzi*, Opracowanie na zlecenie KGHM Polska Miedź S.A.
- VEGLIO F., BEOLCHINI F., NARDINI A., TORO L., 2000, *Bioleaching of a pyrrhotite ore by a sulfooxidans strain: kinetic analysis*, Chemical Engineering Sci., 55, pp.783-795.

Uryga A., Sadowski Z., Grotowski A., *Bioługowanie kobaltu z produktów mineralnych*, Physico-chemical Problems of Mineral Processing, 38 (2004) 291-299 (w jęz. ang.).

Badania kinetyki procesu bioługowania kobaltu, miedzi i arsenu zostały przeprowadzone w warunkach laboratoryjnych. Do badań użyto dwa półprodukty otrzymane z procesu flotacji z ZWR Lubin. Bakterie *Acidithiobacillus ferrooxidans*, które zostały wykorzystane w tych badaniach, były wyizolowane z kwaśnych wód pobranych z "kolorowych" jezior w okolicy Boguszowa (Dolny Śląsk). Do opisu procesu ekstrakcji badanych próbek został zastosowany półempiryczny model. Model ten zakłada istnienie warstwy półprzepuszczalnej nad ługowaną powierzchnią mineralną. Zastosowanie tego modelu okazało się odpowiednie dla opisu procesu bioługowania ziaren o różnych wymiarach.

Özcan Y. GÜLSOY*, Eren Caner ORHAN*

IMPORTANCE OF MAGNET-STEEL CONFIGURATION IN DRY HIGH INTENSITY PERMANENT MAGNETIC ROLLS: THEORETICAL AND PRACTICAL APPROACH

Received May 12, 2004; reviewed; accepted June 28, 2004

Permanent magnetic rolls have found wide area of applications in separation of paramagnetic minerals from diamagnetics especially after the development of neodymium-iron-boron magnets. Their simple separation principles together with relatively high magnetic induction values and relatively low capital and operational costs made them preferable in industrial minerals processing. Besides the magnetic field and induction values of the magnets, another important factor is the magnet-steel configuration where the magnet:steel width ratio is the key factor that should carefully be selected depending on the feed particle size. In this study, the effects of magnet-steel configurations on the removal of iron-bearing impurities from a feldspar sample are investigated.

Key words: magnetic separation, permanent magnetic rolls, magnet-steel configuration

INTRODUCTION

Enrichment of minerals depending on the difference in their magnetic susceptibilities is being used since the beginning of 20th century. However, the use of permanent magnets in treating minerals is comparatively recent (Parker, 1977). Parallel to the advances in materials sciences and technologies, permanent magnets have been used in mineral processing since 1970's (Fig. 1). However, due to relatively high cost, low magnetic field and/or induction levels, permanent magnets such as Alnico 5 and cobalt-samarium (Co-Sm) had found limited area of applications. The development of neodymium-iron-boron (Nd-Fe-B) ceramic magnets in mid 80's made permanent magnets possible to be used in separation of weakly paramagnetic minerals (i.e. mica minerals, hornblende, etc.).

* Hacettepe University, Department of Mining Engineering, 06532, Beytepe, Ankara, Turkey;
email: ogulsoy@hacettepe.edu.tr

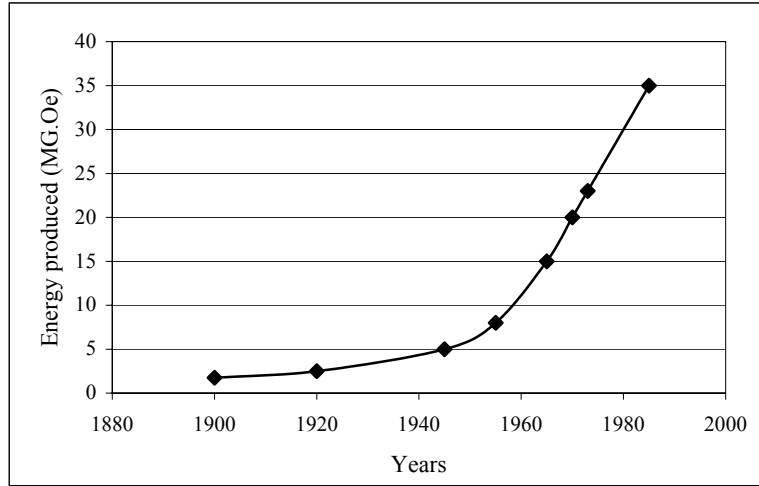


Fig. 1. Advances in magnet manufacturing (modified from Arvidson, 1990)

This development has been appreciated by the industrial minerals industry as Nd-Fe-B magnets offer relatively high magnetic induction and low capital and operating cost. Hence they have been used in beneficiation of industrial minerals (i.e. feldspar, magnesite, etc.) successfully since 1990's.

Dry high intensity permanent magnetic rolls are manufactured using series of Nd-Fe-B magnetic disk - steel disk combinations assembled along a steel roll. Besides the magnetic field and induction properties of the magnets, the magnet:steel width ratio has a considerable importance in this simple design. Although without experimental support, Kopp (1984) theoretically mention the importance of the separator configuration where he derived the physical equations governing the magnetic separation in permanent magnetic rolls.

The magnetic force in a field B and field gradient ∇B is given with the well-known equation as

$$F_m = \mu_0 m \chi B \nabla B \quad (1)$$

where m is the mass of the particle in the field (kg), χ is the mass susceptibility (m^3/kg) and μ_0 is the permeability of free space (Henry/m) which is equal to $4\pi \times 10^{-7}$. In permanent magnetic rolls, the equations for calculation of B and $B \nabla B$ is derived by Kopp (1984) as

$$B = B_0 \exp(-z/t) \quad (2)$$

$$B \nabla B = \frac{B_0^2}{t} \exp\left(\frac{-2z}{t}\right) \quad (3)$$

where B_0 is the magnetic field at the edge of the magnet, z is the distance of the particle from the magnet surface (m) and t is the width of the steel between magnets (m). Eq. 3 shows that magnetic force term $B \nabla B$ takes its largest value at $z = t/2$ which is the distance from the magnet surface magnitude being half the width of the steel disk. This suggests that the feed particle size should match with this value or the magnetic separator should be designed according to the particle size at which the separation will be carried out.

In this study, the effects of magnet:steel width ratio configurations of permanent magnetic rolls on the separation of coloring impurities from a feldspar ore at different particle sizes are investigated.

MATERIALS AND METHODS

The feldspar ore used in the experiment is a titanium bearing, micaceous albite ore and is supplied from Cine Akmaden Mining Co. The chemical composition of the ore is given in Table 1. Thin section analysis together with the chemical analysis showed that the sample is composed mainly of sodium feldspar with mica minerals (mainly biotite) and minor amount of hematite as paramagnetic impurities. Chemical analysis of carefully handpicked grains of mica minerals showed that they contain approximately 2% TiO_2 probably as a $Ti^{+4} \leftrightarrow Al^{+3}$ substitution product. This case agrees well with the mineralogical observations of Deer et.al. (1974) and experimental evidences of Bayraktar et.al. (2001). Hence, a decrease in TiO_2 content should be expected in the concentrate.

Table 1. The chemical composition of the feldspar sample used in the experiments

Component	Content, %
SiO_2	64.97
Al_2O_3	20.50
Fe_2O_3	0.335
TiO_2	0.350
CaO	1.97
MgO	0.88
Na_2O	9.92
K_2O	0.68
P_2O_5	0.15
LOI	0.25
Total	100.005

The experiments are carried out using laboratory scale dry high intensity permanent magnetic rolls (Permroll) with 3 different magnet-steel configurations. Each configuration is achieved by the combination of different number of Nd-Fe-B disc magnets (4 mm width, 10 mm diameter) and steel discs (1 mm width, 10 mm diameter). The magnet-steel configurations

investigated and built-in the magnetic separator are: (a) 4mm magnetic disks with 1 mm steel disks, (b) 8 mm magnetic disks with 2 mm steel disks, (c) 12 mm magnetic disks with 3 mm steel disks (Fig. 2). **Blad!**

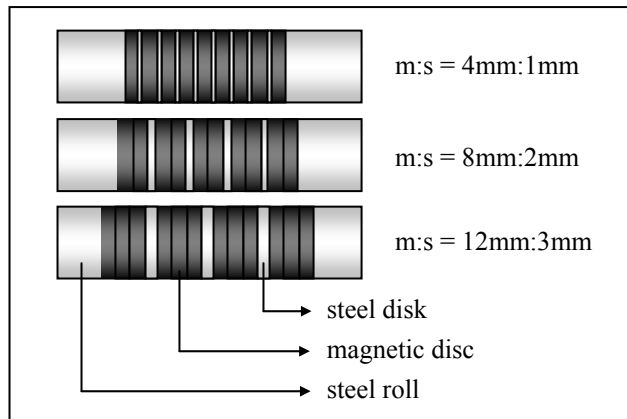


Fig. 2. Magnet-steel configurations

The effects of magnet-steel configurations are studied on three different size fractions being -2 mm, -1 mm and -0.5 mm. The sample preparation flowsheet is given in Fig. 3 and particle size distributions of the prepared samples are given in Fig. 4. Prior to the experiments, -0.075 mm fraction that deteriorates the separation (due to particle-particle and particle-belt electrostatic interactions) is removed from the feed.

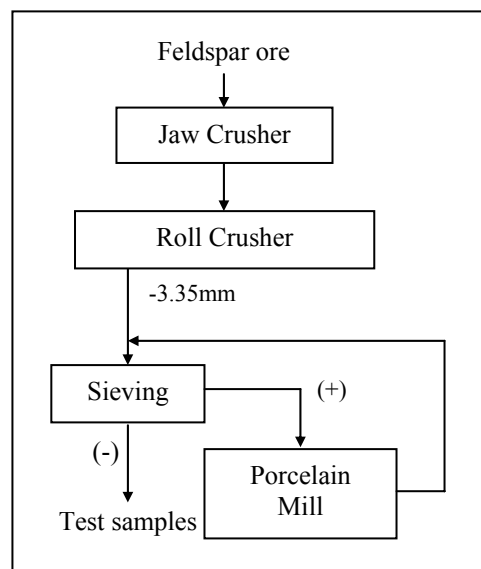


Fig. 3. Sample preparation flowsheet

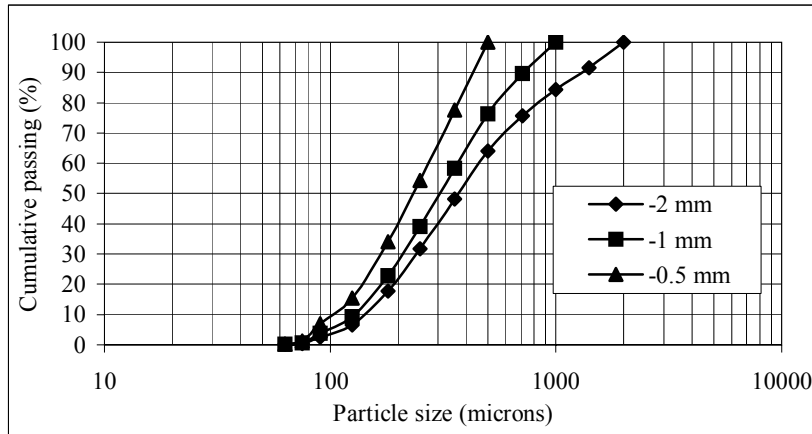


Fig. 4. Particle size distributions of test samples

In order to examine the change of magnetic field in each magnet-steel configuration, the magnetic induction values along the magnetic roll is measured. Then the magnetic induction change apart from the surface of the magnet is examined.

RESULTS AND DISCUSSION

The surface magnetic induction measurements show that maximum magnetic induction values (B_{max}) obtained is approximately 1.05 Tesla where magnet:steel = 4:1, 1.24 Tesla where magnet:steel = 8:2 and 1.27 Tesla where magnet:steel = 12:3 (Fig. 5).

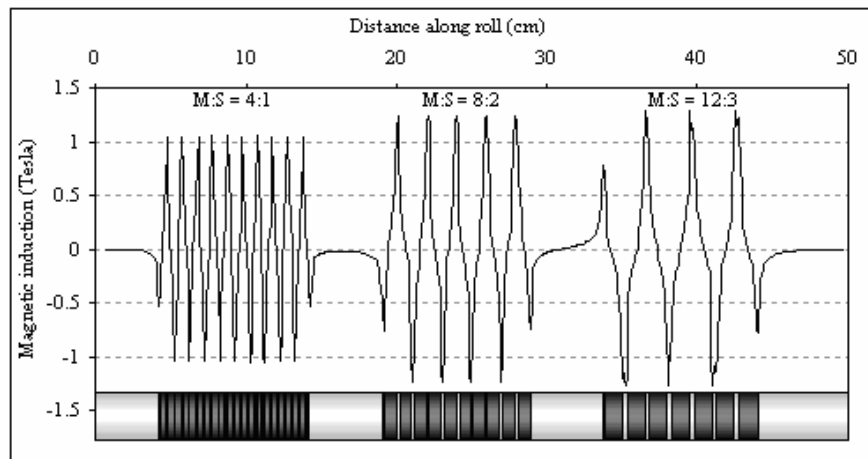


Fig. 5. Change in magnetic induction along the magnetic roll and different magnet-steel configurations

It is clearly seen in Fig. 5 that although the same magnets and steels are used in the configurations, B_{\max} values increase in magnet:steel ratio order of $12:3 > 8:2 > 4:1$. The same case is also valid for the magnetic induction values measured apart from the roll surface (Fig. 6) and $m:s = 12:3$ configuration provides the largest magnetic induction value at all distances. Fig. 6 (a) and (b) shows that the measured and calculated values from Eq. 3 agrees well with acceptable variations and that Eq. 3 is valid for practical cases. Although it provides the largest magnetic induction value, it is not always the best case for all feed sizes as is mentioned in Eq. 3.

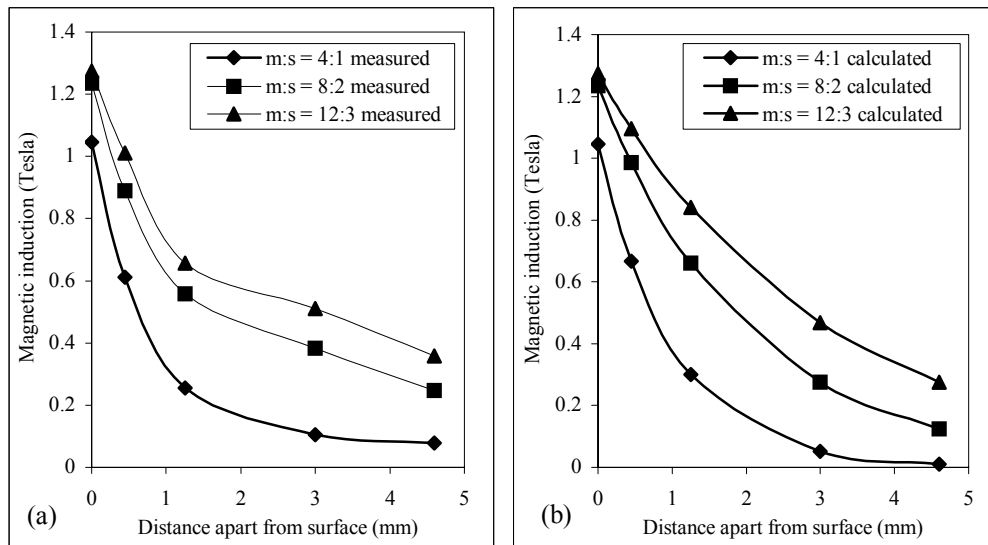


Fig. 6. (a) measured, (b) calculated, magnetic induction (B_{\max}) change apart from roll surface for different magnet:steel width ratios

The magnetic separation test results of $-2+0.075$ mm, $-1+0.075$ mm and $-0.5+0.075$ mm size fractions at three different magnet-steel configurations are given in Tables 2, 3 and 4 respectively.

Table 2. Magnetic separation test results of $-2+0.075$ mm size fraction

Weight	Magnet:steel width ratio		
	4:1	8:2	12:3
Tailings (%)	7.55	8.29	16.8
Concentrate (%)	92.45	91.71	83.20
Concentrate chemical composition			
SiO ₂	65.71	65.71	65.74
Al ₂ O ₃	20.50	20.50	20.20
Fe ₂ O ₃	0.119	0.113	0.090
TiO ₂	0.310	0.320	0.280

Table 2. - continuation			
CaO	2.03	2.02	2.04
MgO	0.31	0.32	0.24
Na ₂ O	10.31	10.35	10.38
K ₂ O	0.38	0.37	0.34
P ₂ O ₅	0.14	0.13	0.14
LOI	0.19	0.17	0.15
Total	99.999	100.003	99.600

Table 3. Magnetic separation test results of -1+0.075 mm size fraction

Weight	Magnet:steel width ratio		
	4:1	8:2	12:3
Tailings (%)	8.22	9.09	25.72
Concentrate (%)	91.78	90.91	74.28
Concentrate chemical composition			
SiO ₂	66.13	65.82	66.09
Al ₂ O ₃	20.60	20.50	20.50
Fe ₂ O ₃	0.041	0.046	0.060
TiO ₂	0.220	0.230	0.240
CaO	2.04	2.04	2.06
MgO	0.12	0.12	0.15
Na ₂ O	10.36	10.36	10.37
K ₂ O	0.26	0.28	0.30
P ₂ O ₅	0.14	0.13	0.14
LOI	0.09	0.47	0.09
Total	100.001	99.996	100.000

Table 4. Magnetic separation test results of -0.5+0.075 mm size fraction

Weight	Magnet:steel width ratio		
	4:1	8:2	12:3
Tailings (%)	9.98	13.07	14.00
Concentrate (%)	90.02	86.93	86.00
Concentrate chemical composition			
SiO ₂	66.26	66.25	66.20
Al ₂ O ₃	20.50	20.50	20.40
Fe ₂ O ₃	0.026	0.030	0.050
TiO ₂	0.200	0.200	0.219
CaO	1.92	1.93	1.94
MgO	0.06	0.07	0.13
Na ₂ O	10.53	10.46	10.50
K ₂ O	0.24	0.25	0.28
P ₂ O ₅	0.19	0.18	0.16
LOI	0.07	0.13	0.12
Total	99.996	100.000	99.999

The chemical analysis show that the magnetic separation provide high amount of reduction in iron content, the lowest content certainly existing in the finest fraction due to liberation. Besides, considerable amount of TiO_2 is also removed with biotite. Changes in concentrate Fe_2O_3 content and Fe_2O_3 removal recovery depending on magnet-steel configuration are given in Fig. 7.

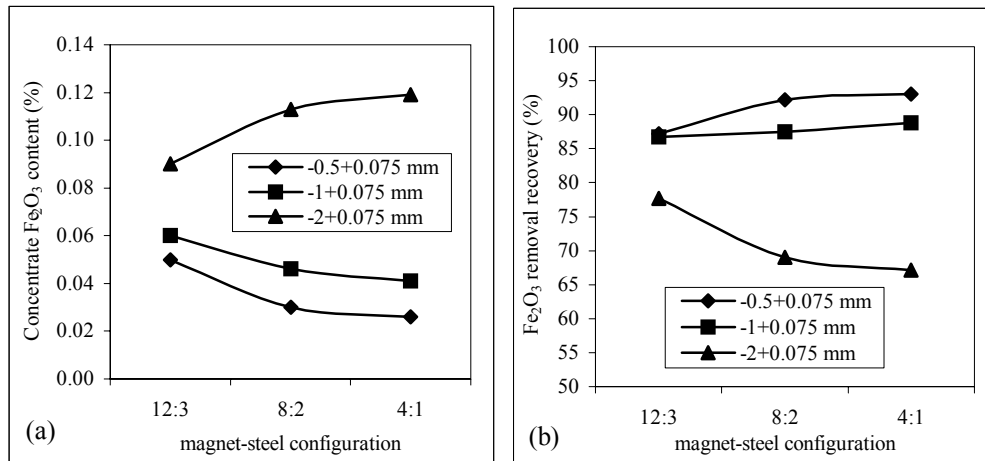


Fig. 7. (a) Concentrate Fe_2O_3 contents, (b) Fe_2O_3 removal recoveries, obtained in different magnet-steel configurations

Concentrate Fe_2O_3 content and Fe_2O_3 removal recovery values (Fig. 7) of different particle sizes should not be compared with each other, as naturally the liberation is the fact that causes the differences in content and recovery values. However, the important point is the change in the trends of the curves in different particle sizes. Concentrate Fe_2O_3 contents of -1+0.075mm and -0.5+0.075 mm size fractions decrease in the order of 12:3 > 8:2 > 4:1 (Fig. 7a). On the contrary, the Fe_2O_3 content of -2+0.075 mm concentrate exhibits the reverse order as 12:3 < 8:2 < 4:1 of which the liberation could not be responsible. Same relations also apply for Fe_2O_3 removal recovery values (Fig. 7b) but in reverse orders for all size fractions. The values show that 4:1 configuration provides the lowest Fe_2O_3 content and highest recovery for -1+0.075mm and -0.5+0.075mm size fractions where as 12:3 configuration provides lowest Fe_2O_3 content and highest recovery for -2+0.075mm fraction.

This behavior clearly indicates the importance of selection of suitable magnet:steel ratio configuration and that highest B_{max} values does not always provide the best separation for all particle sizes. Although Eq. 3 suggests that the average particle size should be half the steel width of the separator, in most cases it is not always possible to determine the average particle size of a distribution. However, it is evident that higher magnetic induction and m:s configurations are required as the feed gets coarser.

CONCLUSIONS

The results clearly show that magnet:steel width ratio has a considerable effect on concentrate Fe_2O_3 content and Fe_2O_3 removal recovery in feldspar concentration. It is clear that the suitable size fraction should be fed to a specific magnetic separator or the magnetic separator should be designed specifically for the material that is to be concentrated.

Although the theory suggests equations for the selection of the optimum magnet:steel configuration, they are not practically applicable as the average particle size cannot be determined exactly for a particle size distribution. However, the theory can provide reasonable solutions where feed with very narrow size distribution is to be separated.

Nevertheless, obtaining the best solutions for a specific ore always requires thorough studies on both the ore and the magnetic separator.

REFERENCES

- ARVIDSON, B. (1990), *Recent developments in dry high intensity magnetic separation*, Australian IMM 1990 Annual Conference, March 1990.
- BAYRAKTAR, İ., GÜLSOY, Ö.Y., CAN, N. M., ORHAN, E.C., (2001), *Concentration of feldspars*, 4th Industrial Minerals Symposium, pp.97-105, Chamber of Mining Engineers of Turkey, İzmir, Turkey.
- DEER, W.A., HOWIE, R.A., ZUSSMAN, J., (1974), *An Introduction to the Rock Forming Minerals*, Longman, p. 193-203, London.
- KOPP, J., (1984), *Permanent magnet disk separators*, IEEE Transactions on Magnetics, Vol. MAG-20, No.5, September.
- PARKER, M.R., (1977), *The physics of magnetic separation*, Contemporary Physics, Vol. 18, No. 3, pp. 279-306.

Gülsoy Ö.Y., Orhan E.C., *Teoretyczne i praktyczne aspekty konfiguracji dysków magnetycznych i stalowych w separatorach rolkowych ze stałymi magnesami*, Physicochemical Problems of Mineral Processing, 38, (2004) 301-309 (w jęz. ang.).

Separatory magnetyczne rolkowe ze stałymi magnesami znalazły szerokie zastosowanie do rozdziału minerałów o właściwościach słabo magnetycznych po wprowadzeniu ceramicznych magnesów Nd-Fe-B. Zaletą tych urządzeń są proste zasady operacji przy względnie wysokiej wartości indukcji magnetycznej i niskich kosztach operacyjnych i inwestycyjnych. Obok wysokiego natężenia pola magnetycznego ważnym parametrem tych separatorów jest wzajemna konfiguracja dysków stalowych i dysków magnetycznych w wałku roboczym. Konfiguracja to powinna być ściśle dobrana m.in. w zależności od uziarnienia nadawy. W pracy badano wpływ konfiguracji dysków stalowych i magnetycznych na skuteczność usuwania zażelazionych zanieczyszczeń z surowca skaleniowego.

M.H. KHEDR*

EFFECT OF FIRING TEMPERATURE AND COMPACTING PRESSURE ON THE MAGNETIC AND ELECTRICAL PROPERTIES OF NICKEL FERRITE

Received March 15, 2004; reviewed; accepted May 15, 2004

Spinel ferrites have attracted considerable attention and efforts continue to investigate them for their technological importance to the microwave industries, high speed digital tape or disk recording and magnetic refrigeration system. NiFe_2O_4 was prepared by mixing pure nickel oxide and iron oxide, dried, pressed at 150, 200, and 250 kg/cm^2 , then fired at 1273, 1373 and 1473 K for 10 hours. X-ray diffraction was used to assess the formation of NiFe_2O_4 .

Results showed that density increases with increasing either hydraulic pressing and firing temperature. Magnetic properties are measured and an isoperm hysteresis loop is obtained, remanent magnetic flux induction, saturation magnetic flux induction and coercive force are calculated and found to be density dependant.

Electrical properties of NiFe_2O_4 were measured and it was found that it has low electrical conductivities (10^{-6} - $10^{-8} \Omega^{-1}\text{cm}^{-1}$), and values of dielectric constant, and dielectric loss are consistent with semiconductors properties.

Key words: ferrite, preparation, magnetic properties, electrical properties

INTRODUCTION

Ferrite spinels have attracted wide attention because of their remarkably high electrical and high magnetic flux induction. They form very good dielectric materials and have therefore found many technological applications. Large scale application of ferrites have prompted the development of various chemical methods which includes hydrothermal, co-precipitation, freeze drying, spray drying, precursor and sol-gel for the preparations of the stoichiometric and chemically pure spinel ferrites (Komarneni

* Chemistry Department, Faculty of Science, (Benisuef Branch), Cairo University,
akhedr@yahoo.com

et. al 1988), (Morrish et. al. 1981), (Johnson 1981), (Marcilly et. al. 1970) and (Upadhyay et. al. 2003).

These methods are characterized by high cost with respect to conventional ceramic powders prepared by solid – state reaction of mechanically mixed and calcined starting materials. The present investigation deals with the synthesis of NiFe_2O_4 by solid – state reaction of mechanically mixed, pressed and uncalcined iron(III) oxide and Ni(II) oxide powder. (Randhawa et al. 1997) studied the preparation of NiFe_2O_4 from thermolysis of nickel hexa (ferrate) ferrate(III) hexahydrate which shows a very well saturation magnetization (4440 G) and its potential to function at high frequencies. Seema et al. 1998 investigated the magnetic properties of nanosized NiFe_2O_4 particles synthesized by the citrate precursor technique, single domain particles were found to form linear chain like clusters because of strong magnetic dipole interactions, the low saturation magnetization values were attributed to the spin non collinearity predominantly at the surface. The Hopkinson effect is exhibited by an assembly of non interacting single domains particles and is explained within mathematical formation given by the Stonerad Wohlfarh model.

Hana et al.1999 studied the preparation of NiFe_2O_4 by ceramic and wet methods. They found that AC resistivity, dielectric constant decreased with increasing frequency while dielectric loss and loss tangent went through peak values at the relaxation frequency.

EXPERIMENTAL

A mixture (1:1 mole ratio) of analar grade NiO and Fe_2O_3 were employed as raw materials, wet milled with ethanol in a ball mill for 8 hours to ensure homogeneity. Samples were dried for 4 hours at 353 K and then equal wights of approximately 1.5 g powder mixture were pressed in a cylindrical mould of 10 mm inner diameter into cylindrical briquette at 150, 200 and 250 kg/cm^2 . The dry samples were gradually heated in air using a muffle furnace at 1273, 1373 and 1473 K for 10 hours. The fired samples were left to cool gradually to avoid cracking due to thermal shocks. XRD powder patterns were obtained using SHIMADZU – 610-XD diffractometer. The x-ray generating was equiped with Co filter and generates a beam of CuK_α radiation ($\lambda = 1.5418\text{\AA}$). The operational settings for all XRD scans voltage: 40 kV, current 30 mA, Scanning speed 8° min^{-1} . The structure changes of different samples were examined by reflected light microscope and porosity measurments.

Magnetic flux density and remnant magnetic flux density were calculated from hysteresis loop measured by 6900-VS magnetometer. The dielectric properties were measured using a Philips RCL bridge (digital and computerized) at frequency range $60\text{-}10^5$ Hz.

RESULTS AND DISCUSSION

Figure 1-a shows a standard X-ray diffraction pattern (Williams et. al. 1994) for NiFe_2O_4 , pure Fe_2O_3 and pure NiO . X-ray diffraction pattern for NiFe_2O_4 prepared by firing at 1273 K and compacting pressure 150 kg/cm^2 is shown in Fig. 1-b where peaks corresponds to NiFe_2O_4 and others of lower intensity referred to Fe_2O_3 and NiO are observed.

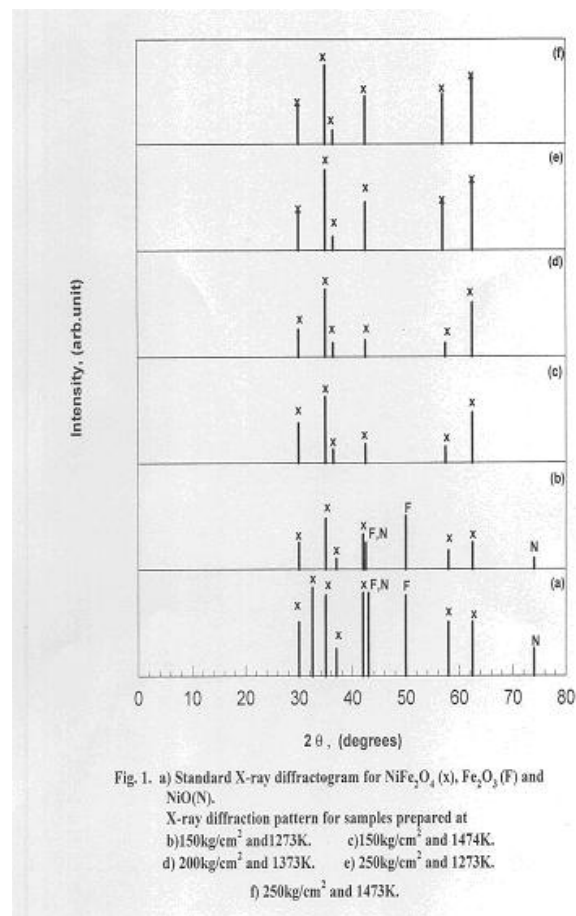


Fig. 1. Standard X-ray diffractogram for NiFe_2O_4 , Fe_2O_3 and NiO

From diffractograms in Figures 1 c-f as can be noticed are very similar showing NiFe_2O_4 phase only with the absence of Fe_2O_3 and NiO phases, the only observation is the increase in the intensity of peaks due to crystallization as results of increasing temperature and or compacting pressure. Spectra of other samples are not mentioned as they are basically the same.

POROSITY AND DENSITY MEASUREMENTS

Table 1 shows the effect of changing compacting pressure and firing temperature on the density of the prepared samples of NiFe_2O_4 . It is clear that increasing the temperature causes an increase in density which is attributed to sintering (Rosales et al.1995). At compacting pressure 250 Kg/cm^2 density changes from 2.8 to 4.02 g/cm^3 for a change in temperature from 1273 to 1473 K (Figure 2). On the other hand compacting pressure has a very small effect on density. Figures 3 a-c show the photomicrographs of samples compacted at 250 Kg/cm^2 and fired at 1273,1373 and 1473 K, respectively. Figure 3-a shows a highly porous structure with a small number of large ferrite grains, at 1373 K (Fig. 3-b) a densification is observed leading to larger grains of NiFe_2O_4 , by increasing the firing temperature to 1473 K (Fig. 3-c) a dense matrix of connected ferrite grains are observed with the decrease in porosity (Table 1).

Table 1. Effect of compacting pressure and firing temperature on density of the prepared NiFe_2O_4

Compacting pressure, Kg/cm^2	Firing temperature, K		
	1273	1373	1473
150	2.682	3.049	3.584
200	2.773	3.014	3.314
250	2.809	2.929	4.027

MAGNETIC PROPERTIES

The desired technological properties of ferrites depends on stoichiometry, density and crystal structure of ferrite in order to know the distribution of the ions over the available sites in the compound.

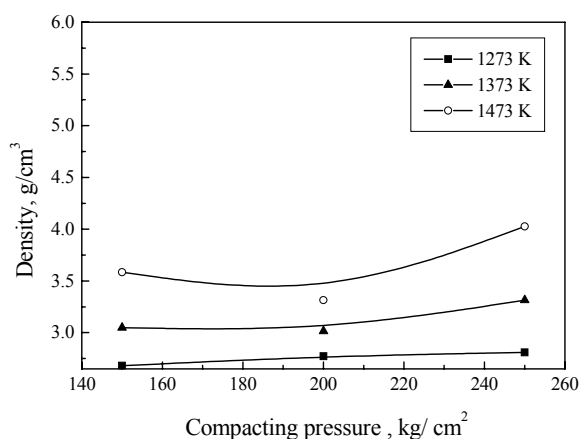


Fig. 2. Effect of Compacting pressure on the density of the prepared NiFe_2O_4

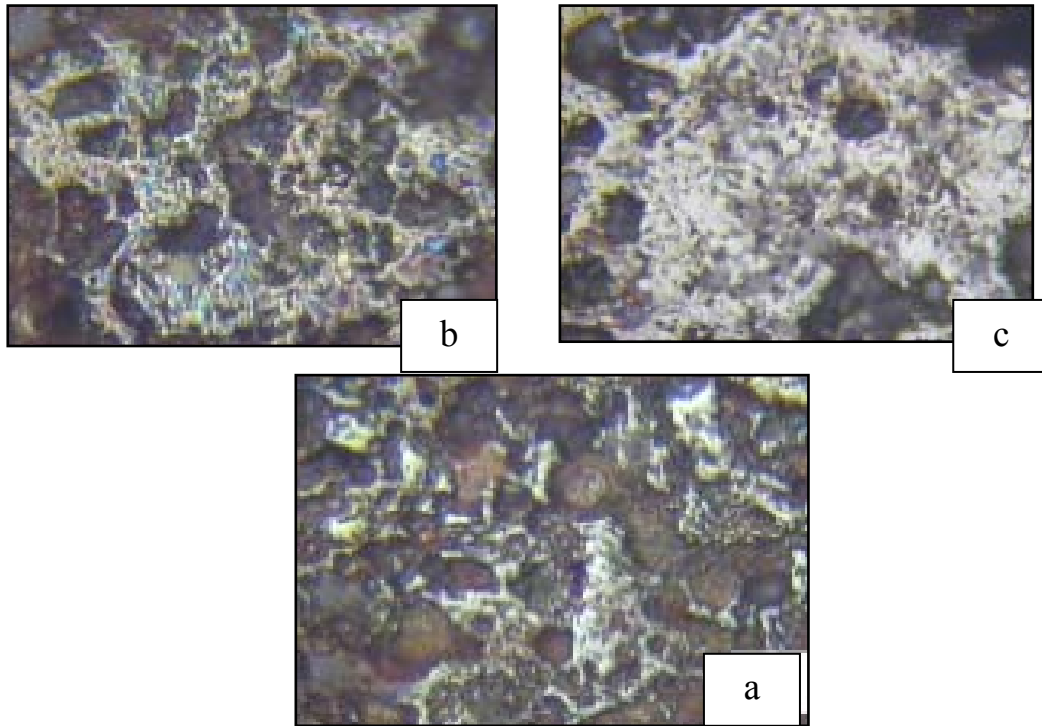


Fig. 3. Photomicrograph of NiFe_2O_4 prepared by compacting at 250 Kg/cm^2 at
 a) 1273 K b) 1373 K c) 1473 K, X 600

NiFe_2O_4 has an inverse spinel structure, in natural spinel the eight divalent ions are in the eight available tetrahedral sites and the sixteen trivalent ions in the sixteen octahedral, in case of NiFe_2O_4 the order is changed and the eight divalent ions (Ni^{2+}) in eight of the sixteen available octahedral sites and the sixteen trivalent (Fe^{3+}) ions uniformly distributed over the remaining sites (Bhise et. al. 1991). Magnetic properties for NiFe_2O_4 samples were measured, all samples show isoperm (of relatively equal permeability) hysteresis loops which describes the relation between external magnetic field H and magnetic flux induction B (Figure 4). Table 2 shows values of saturation magnetic flux induction (B_s), remnant magnetic flux induction (B_r) and coercive force (H_c) for samples prepared at different conditions.

Figure 4 shows hysteresis loops for samples prepared at compacting pressure 200 Kg/cm^2 , firing temperature 1273, 1373 and 1473 K, it is clear that increasing temperature has a pronounced effect on the size of the hysteresis loop which is arising from the change in B_r , B_s and H_c . Figure 5 shows the dependence of B_r , B_s and H_c on temperature for this sample. Saturation magnetic flux density increases with increasing temperature which is attributed to the decrease in the inter and intragranular pores resulting from increasing firing temperature (Fig. 3-c). The presence of such

pores causes a discontinuity which prevents the movement of domain walls. Remnant magnetic induction shows a very small change with temperature.

On the other hand the coercive force decreases clearly with increasing temperature (Fig. 5). If remenance simply corresponds to a return of the magnetization vectors to the nearest easy direction, while each grain reactions saturated, then remnance and saturation should retains approximately close B_s/B_r value. The pores gives rise to demagnetizing fields which could either cause rotation of the magnetization away from the easy direction or the nucleation of reverse domains in which case it is surprising that B_s/B_r should be greater for the more porous sample (Heck 1967), (Table 2). However the denser sample, when prepared by firing at higher temperature, will also contain larger grains in which nucleation is more probable.

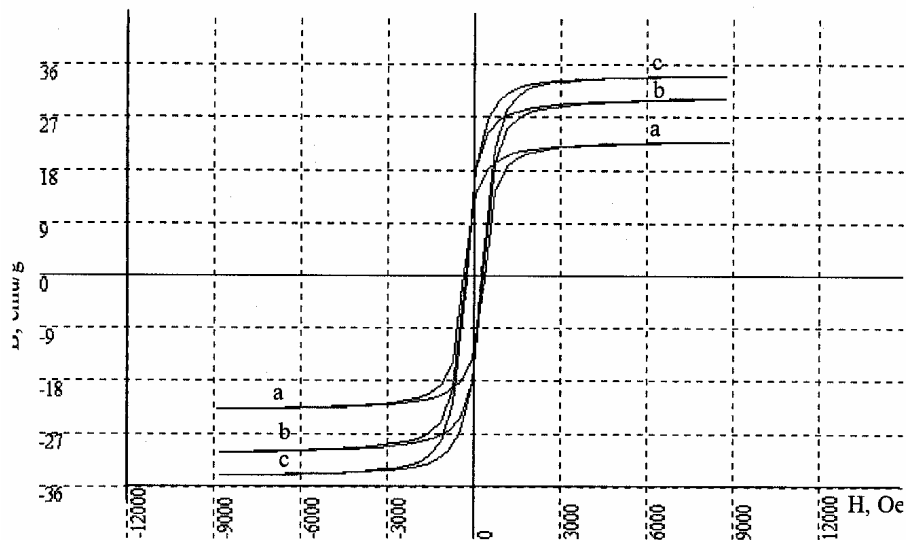


Fig. 4. B-H Hysteresis loops for NiFe_2O_4 prepared by compacting at 250 kg/cm^2
at a) 1273K. b) 1373K c) 1473K

Fig. 4. B-H Hysteresis loops for NiFe_2O_4 prepared by compacting at 250 Kg/cm^2
at a) 1273K. b) 1373K c) 1473K

The effects of intragranular pores on the corecivity arises from the impedance of the motion of the domain wall. It has been noted that the magnetization processes in NiFe_2O_4 consists of discontinuous movements of walls over considerable distances of the sudden rearrangements of the structures within entire grains, indicating the presence of large-scale discontinuities which may have been groups of pores. The direct interaction of domain walls with pores, including the formation subsidiary tie-domains, has been demonstrated by Knowle (Heck 1967).

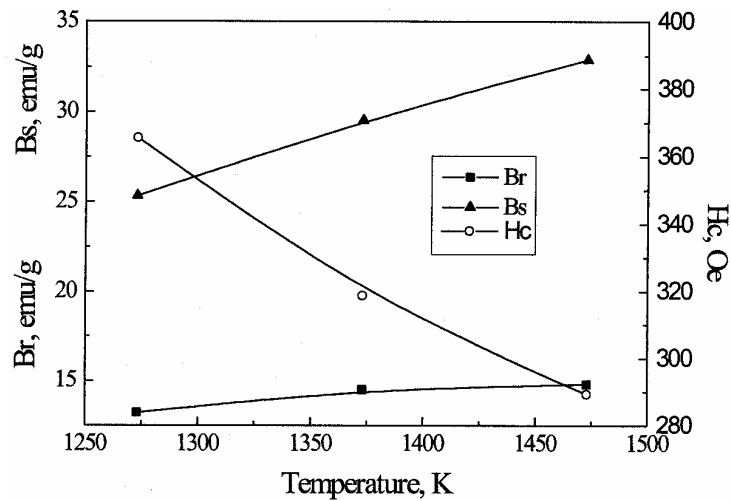
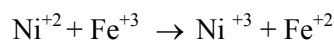
Fig. 5. Dependence of magnetic properties on the firing temperature of NiFe₂O₄

Table 2. Variation of the magnetic properties for samples prepared at different conditions

Preparation conditions		B _s , emu/g	B _r , emu/g	B _s /B _r	H _c , Oe
Compacting pressure	Firing Temp., K				
150 Kg/cm ²	1273	23	12.1	1.9	365
	1373	29.8	14.4	2.06	306.8
	1473	33.4	13.94	2.39	273.6
200 Kg/cm ²	1273	25.34	13.22	1.91	365.5
	1373	29.57	14.51	2.03	318.8
	1473	32.95	14.81	2.20	289.3
250 Kg/cm ²	1273	22.86	11.99	1.90	353
	1373	30.1	14.98	2.00	317
	1473	34.11	14.78	2.30	276

ELECTRICAL PROPERTIES

The AC electrical conductivity were studied as a function of frequency for a series of NiFe₂O₄ samples prepared at different conditions of firing temperature and compacting pressure. All samples showed a conductivity ranging from 10⁻⁶ to 10⁻⁸ Ω⁻¹cm⁻¹, this is explained by the fact that NiFe₂O₄ forms a cubic close-packed oxygen lattice with the metal ions situated at the tetrahedral (A) and octahedral (B) sites. Electronic conduction in these ferrites can be explained in terms of the verwey mechanism (Yajie et. al. 1995) which consists of electrons exchange between ions of the same element present in more than one valency state distributed randomly over crystallographically equivalent lattice sites. The expected hopping mechanism is



Because Fe^{+2} ions preferentially occupies the B site, A-A hopping therefore does not take place. Moreover, as the B-B distance is smaller than A-B distance, electron hopping between B-B ions becomes the main mechanism of conduction.

The logarithmic relation between electrical conductivity and frequency as represented in Figure 6 indicates that conductivity increases slightly on increasing frequency. The small value at low frequencies and their increase as frequency increases can be explained on the basis of Maxwell-Wagner theory (Koops 1951), which is a result of the inhomogenous nature of dielectric structure. The dielectric structure was supposed as composed of two layers. The first is the large ferrite grains of fairly well conducting materials which are separated by the second thin layer (grain boundaries) of relatively poor conducting substances. These grain boundaries were formed by superficial reduction or oxidation of the crystallites in the porous material as a result of their direct contact with firing atmosphere. The resistive grain boundaries were found to be more effective at lower frequencies while the conductive ferrite grains are more effective at higher frequencies. For all samples the same trend was observed, the effect of firing temperature and compacting pressure shows a very small difference in conductivity with frequency.

Figure 7 shows the effect of changing frequency with dielectric constant ϵ' , the general trend for all investigated samples is the decrease in its value with increasing frequency which is a normal dielectric behaviour in ferrites. This decrease in dielectric polarization is due to the fact that beyond a certain frequency, the hopping of electrons between Fe^{+3} and Fe^{+2} can not follow the frequency of the alternating electric field. In other word, the low frequency helps in aligning more dipoles in the field direction with the result of an increase in the polarization as well as ϵ' , while by increasing frequency, the dipoles are distributed and ϵ' decreases (Reddy et. al. 1999).

The dependence of dielectric loss ϵ'' on frequency at room temperature is shown in Figure 8. It is clear that ϵ'' (energy dissipated per cycle) decreases with increasing frequency. It is very important to emphasize that the ac dielectric response of concentrated charge – carriers-containing materials is strongly affected by the charge contribution to the total sample polarizability, mainly at lower frequencies (Dias et. al. 1998).

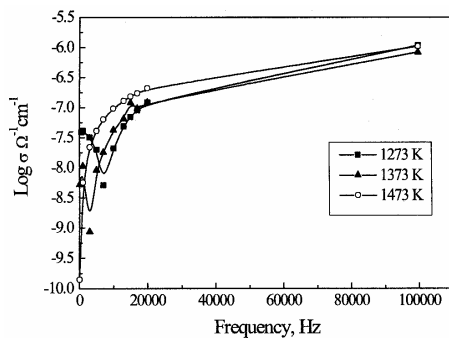


Fig. 6. Frequency dependence of $\log \sigma$ for NiFe_2O_4 prepared by compacting at 200 Kg/cm^2 at
a) 1273K b) 1373K c) 1473K

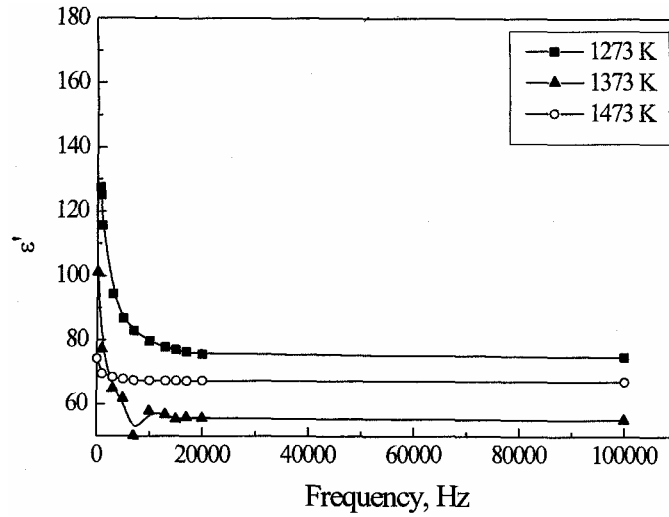


Fig. 7. Frequency dependence of dielectric constant (ϵ') for NiFe_2O_4 prepared by compacting at 200 Kg/cm^2 at a) 1273K b) 1373K c) 1473K

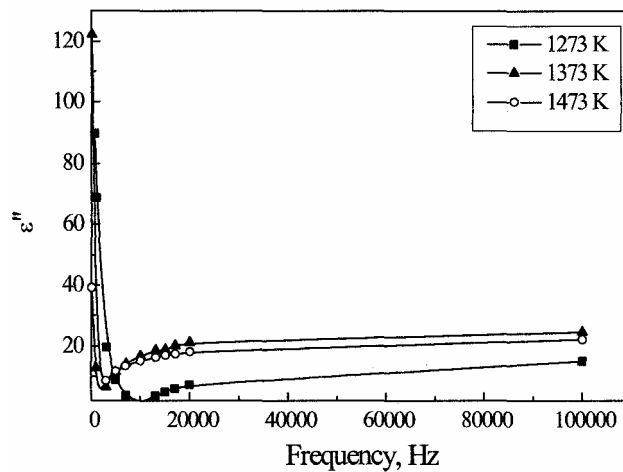


Fig. 8. Frequency dependence of dielectric loss (ϵ'') for NiFe_2O_4 prepared by compacting at 250 kg/cm^2 at a) 1273K b) 1373K c) 1473K

CONCLUSION

The density of NiFe_2O_4 prepared by mixing pure nickel oxide and iron oxide with no calcination was found to be strongly affected by firing temperature and compacting pressure.

The increase in density causes a great improvement in the magnetic properties: isoperm hysteresis loop is obtained, saturation magnetic flux induction increased while coercive force decreased.

Electrical properties of samples shows low electrical conductivities (10^{-6} - $10^{-8} \Omega^{-1}\text{cm}^{-1}$). Values of dielectric constant, dielectric loss and magnetic properties indicates that it could be used in many technological application.

REFERENCES

- BHISE B., DONGAR M., PATIL S., SAWANT S. (1991), *Mater. Sci. Lett.* Vol. 10, pp. 992.
- DIAS A., MOREIRA R. (1998), *Mater. Res.*, Vol. 8, pp. 2190.
- Heck C. (1967), *Magnetic materials and their applications*, London, Butterworths, pp. 579.
- JOHNSON D. W. (1981), *Am. Ceram. Soc. Bull.*, Vol. 60, pp. 221.
- KOMARNENI S., FREGEAU E., BREVAL E. (1988), *J. Am. Ceram. Soc. Commun.*, Vol. 71, pp. 26.
- KOOPS C. (1951), *Phys. Rev.*, Vol. 38, pp. 216.
- MARCILLY C.H., COURTY P., DELMON B. (1970), *J. Am. Ceram. Soc.*, Vol. 53 pp. 56.
- MORRISH A.H., HANEDA K. (1981), *J. Appl. Phys.*, Vol. 52, pp. 2696.
- MOUSTAF I. (1999), *Ph.D. Thesis, Faculty of Engineering, Cairo Univ.*, pp. 68.
- PARASAD S., GAJBHIYE N.S (1998), *Alloys and compounds*, Vol. 265, pp. 87.
- RANDHAWA B., SINGH R. (1997), *De-Physique, IV*; Vol. 7, pp. 89.
- REDDY A.R., MOHN G. R., RAVINDER D., BOYANOV B. (1999), *Mater. Sci. J.*, Vol. 34, pp. 3169.
- ROSALES M.I., PLATA A.M., NICHU M.E., BRITO A., PONCE M., CASTANO V. (1995), *Mater. Science J.*, Vol. 30 pp. 4446.
- UPADHYAY C., MISHRA D., VERMA H.C., ANAND S., DAS R.P. (2003), *Magnet. and Mag. Mater.*, Vol. 260 pp. 188.
- WILLIAMS C.M., ABE M., ITOH T., LUPITZ P. (1994), *IEEE Trans. on Magnet.*, Vol. 30, pp. 4896.
- YAJIE C., PEISHENG L., ZONGMING J. (1995), *Mater. Sci. Lett.* Vol. 14, pp. 998.

Khedr M.H., *Wpływ temperatury wypalania i ciśnienia sprasowania na magnetyczne i elektryczne właściwości ferrytu niklowego*, Physicochemical Problems of Mineral Processing, 38, (2004) 311-320 (w jęz. ang.).

Spinele ferrytowe ciągle wzbudzają duże zainteresowanie oraz wymagają dalszych intensywnych badań z uwagi na ich znaczenie technologiczne. Znajdują one liczne zastosowanie w przemyśle do produkcji urządzeń mikrofalowych, taśm magnetycznych do szybkiego zapisu, dysków do komputerów oraz magnetycznych układów chłodzących. NiFe_2O_3 był otrzymany przez zmieszanie tlenku niklu z tlenkiem żelaza, ogrzanie mieszaniny pod ciśnieniem 150, 200 i 250 kg/cm^2 , następnie, materiał był wyprażany w temperaturach 1273, 1373 i 1473 K przez 10 godzin. Analizę otrzymanego materiału dokonano metodą dyfrakcji rentgenowskiej. Otrzymane wyniki badań wskazują, że gęstość materiału wzrasta wraz ze wzrostem ciśnienia i temperatury stosowanej w syntezie. Właściwości magnetyczne otrzymanego produktu zostały zbadane. Określono histerezę magnetyczną dla badanego materiału. Wyliczone zostały inne parametry magnetyczne jak szczątkowy i nasycony strumień indukcji magnetycznej. Wszystkie te parametry okazały się być zależne od gęstości otrzymanych ferrytów. Podobnie zostały zmierzone właściwości elektryczne NiFe_2O_3 . Okazało się, że spinele miały małe przewodnictwo elektryczne (10^{-6} - $10^{-8} \Omega^{-1}\text{cm}^{-1}$), a stała dielektryczna była zgodna z wartościami odpowiadającymi półprzewodnikom.

Zeynep ÖZDEMİR*, Gülhan ÖZBAYOĞLU*, Meral KIZILYALLI**,
Ayşen YILMAZ**

SYNTHESIS AND CHARACTERIZATION OF LITHIUM TRIBORATE

Received March 15, 2004; reviewed; accepted June 30, 2004

Lithium triborate (LBO) is a newly developed ideal nonlinear optical (NLO) crystal used in laser weapon, welder, radar, tracker, surgery, communication and etc. In this study, lithium triborate was synthesized from the solid state reaction of Li_2CO_3 and H_3BO_3 at 750°C . X-ray diffractometer was used to characterize and identify the products. According to the experimental results conducted up to now, lithium triborate was produced successfully with minor amount of side products. The preliminary results of this study will be presented here, the studies for the removal of side products are underway.

Keywords: lithium triborate, synthesis, solid state reaction, non-linear optical material

INTRODUCTION

Research on borates provides distinctive opportunities for the discovery and identification of new compounds having certain physical properties that are unattainable with any other type of material. In large measure, these properties come from the unique crystal and electronic structures that result from the very small B atom in an oxide matrix (Keszler 1999).

Borates find widespread use as phosphors: $\text{Eu}:\text{SrB}_4\text{O}_7$ in UV-emitting medical lamps, $\text{Ce},\text{Tb}:\text{GdMgB}_5\text{O}_{10}$ as the green-emitting component in high-efficacy fluorescent lamps and $\text{Eu}:(\text{Y},\text{Gd})\text{BO}_3$ as the red-emitting component in plasma display panels for high-definition television. Borate crystals such as $\beta\text{-BaB}_2\text{O}_4$ (BBO), LiB_3O_5 (LBO), and CsLiB_3O_5 (CLBO) have made possible the reliable production of laser light at wavelengths and power levels that were preciously unattainable with solid-state systems. Due to these performance characteristics including excellent nonlinear

* Mining Eng. Dept., Middle East Technical University, 06531 Ankara/TURKEY, gulhano@metu.edu.tr

** Chemistry Dept., Middle East Technical University, 06531 Ankara/TURKEY

properties as well as good mechanical and chemical parameters borates find widespread use in materials processing, medicine, and R&D (Keszler 1999; Moryc and Ptak 1999).

Ultraviolet lasers are viewed as clean energy sources for the synthesis and processing of materials. They have been strongly demanded for various applications such as high density optical disk mastering, photolithography, material processing and medical treatment. However, for many applications, no convenient source exists for the direct production of laser light having the proper frequency and power characteristics. For these uses, the requisite frequency and power may be generated by passing a laser beam through a suitable nonlinear optical crystal. Only an excimer laser (e.g. XeCl, KrF, and ArF) practically meets these requirements today. However, these bulky lasers use corrosive gases, require high voltage gaseous discharges and regular maintenance. A compact, maintenance free, all-solid-state alternative is therefore desired (Furukawa and Sato 1995; Sugawara et al. 1998; Takatomo et al. 2001; Mori et al. 2002)

High polarizability and excellent transparency in ultraviolet region of planar $[\text{BO}_3]^{3-}$ imply that borates are attractive candidates in the search for new nonlinear optical materials. The fundamental features of NLO borate materials are: i) a crystal structure with an advantageous arrangement of highly NLO active structural units, ii) suitable linear optical properties, and iii) the availability of crystals of sufficient optical quality and size through crystal growth processes. So a great deal of research interest has been focused on the synthesis and characterization of inorganic borates during the past decades (Becker 1998; He et al. 2002a).

$\text{K}[\text{B}_5\text{O}_6(\text{OH})_4] \cdot 2\text{H}_2\text{O}$ (KB₅) (Dewey et al. 1975) is the first NLO crystal discovered in the series of borates in 1975. After that various borate crystals, including β -BaB₂O₄ (BBO) (Liebertz and Stahr 1983), LiB₃O₅ (LBO) (Chen et al. 1989), Sr₂B₂Be₂O₇ (SBBO) (Chen et al. 1995), BiB₃O₆ (BiBO) (Helwing et al. 1999), and the latest Ca₄LnO (BO₃)₃ (CLnOB) (Aka et al. 1996) have been studied as promising NLO crystals (Xue et al. 2000). A review on borate crystals is recently reported by Becker in 1998.

Although there are many reports on the applications of Li₂B₄O₇ and LiB₃O₅ in surface acoustic wave (SAW) and non-linear optical (NLO) devices, respectively, the data on the unit cell parameters, density, solubility in water, thermal stability and thermal expansion characteristics etc. of these compounds are incomplete and scantily reported. A detailed study on the Li₂O-B₂O₃ system were undertaken by Mathews et al., in 1998.

Recently LBO has been proposed to be a promising scintillator for neutron detection. The elements Li and B both have large neutron capturing capacity. This possibility has been reported mainly for glass and ceramic materials by Van Eijk with the details of adsorption and cross-section of neutrons, their different products and energies derived from these elements (Senguttuwan et al. 2002).

Kim et al. studied the growth of the nonlinear optical crystals of lithium triborate and beta barium borate in 1997. The crystal growth and optical properties of rare earth aluminum borates were investigated by Lee et al., in 1998.

In 2001, He et al., synthesized a new compound, LiAlB_2O_5 , by solid state reaction and they give hint for researcher exploring new non-linear optical materials (He et al. 2001a).

A new compound, dilithium aluminum pentaborate, $\text{Li}_2\text{AlB}_5\text{O}_{10}$ has been synthesized by solid state reaction and its structure determined by single crystal X-ray diffraction by He et al. in 2001(b).

The ternary system, $\text{Li}_2\text{O}-\text{Al}_2\text{O}_3-\text{B}_2\text{O}_3$ have been investigated by many researchers. However they left a lot of uncertainties in their work. In order to synthesize new borates and search for new optical materials, He et al., reinvestigated this system with solid state reaction and X-ray powder diffraction technique to clarify some long-standing uncertainties (He et al. 2002a).

$\text{Li}_3\text{AlB}_2\text{O}_6$ is another new compound synthesized by solid state reaction. Its structure was also solved and refined from single-crystal and powder X-ray diffraction data (He et al. 2002b).

LITHIUM TRIBORATE (LBO, LiB_3O_5)

Lithium triborate, LiB_3O_5 , is one of the most known lithium borates. It is a newly developed nonlinear optical crystal. It offers the following advantages: extremely high damage threshold, large phase matching acceptance angle, very wide transparency range and chemical stability. So it is particularly useful for making doubler or tripler for such as Nd: YAG lasers where high power density, high stability, and long time operation are required. It is an ideal nonlinear optical crystal used in laser weapon, welder, radar, tracker, surgery, communication and etc..

LiB_3O_5 was first discovered in 1926 by Mazzetti and Carli, Rollet and Bouaziz (1955) and it was found that it crystallizes according to the phase diagram of the $\text{Li}_2\text{O}-\text{B}_2\text{O}_3$ system by a peritectic reaction at 834°C (Sastry et al. 1958). The structure of LBO was discovered by Konig and Hoppe (1978) 20 years later. Chen discovered the possible application of LBO crystals in nonlinear optics in 1989.

According to Konig and Hoppe, LiB_3O_5 crystallizes in the orthorhombic system with the space group $\text{Pna}2_1-\text{C}_{2v}$. The unit cell parameters are given as: $a = 8.446 \text{ \AA}$, $b = 5.13 \text{ \AA}$, $c = 7.38 \text{ \AA}$. At 595°C , LiB_3O_5 decomposes to $\text{Li}_2\text{B}_4\text{O}_7$ and $\text{Li}_2\text{B}_8\text{O}_{13}$, but this reaction is reported to take long period of time, so crystals of LiB_3O_5 cooled at moderate rates ($30\text{-}40^\circ\text{C/h}$) remain stable. The first successful growth of small crystals was achieved by the solid-state reaction of B_2O_3 glass covered with LiF powder and reaction at 750°C for 10 h by Konig and Hoppe in 1978.

Zhong and Tang studied the growth units and morphology of lithium triborate crystals in 1996. They have investigated the solution structures for compositions with different ratios of Li_2O and B_2O_3 using Fourier infrared-spectrum analysis of samples quenched in liquid nitrogen.

In 1997, Betourne and Touboul attempted to obtain LiB_3O_5 starting from a stoichiometric mixture of the hydrated borates $\text{LiB}_2\text{O}_3(\text{OH})\cdot\text{H}_2\text{O}$ and $\text{LiB}_5\text{O}_8\cdot 5\text{H}_2\text{O}$. LiB_3O_5 . Cell parameters have been refined from those known using the X-ray powder diagram: $a = 8.456 \text{ \AA}$, $b = 7.376 \text{ \AA}$, $c = 5.133 \text{ \AA}$, the space group is $\text{Pna}2_1$.

Moryc and Ptak studied the infrared absorption spectra of lithium triborate (LBO) in the form of polycrystalline sample. The LiB_3O_5 samples were made from lithium carbonate, natural boric acid, boric acid containing isotope ^{10}B (94.4%) and ^{11}B (98.4%) and hydrated lithium hydroxide with ^6Li isotope.

Effect of highest temperature invoked on the crystallization of LiB_3O_5 from boron rich solution was studied in 2003 by Sabharwal et al. The polycrystalline LBO was synthesized by solid-state sintering method. The same authors were carried out investigations on the growth of LiB_3O_5 by top-seeded solution growth technique in 2004 (Sabharwal et al. 2004).

EXPERIMENTAL

Lithium triborate was prepared from the starting materials Li_2CO_3 and H_3BO_3 both of analytical grade. After mixing appropriate quantities of these materials, they were finely powdered by agate mortar. Finally, the homogenized mixture was heated in a porcelain crucible at 750°C for 7, 14 and 21 hours.

In order to identify the compounds obtained at the end of each heat treatment period, powder XRD patterns were recorded by using monochromatic $\text{CoK}\alpha$ radiation on Philips X-ray Diffractometer, Model PW 1320. The obtained powders will also be examined by IR technique in future studies.

RESULTS

The XRD pattern of the LiB_3O_5 obtained from the solid state reaction of Li_2CO_3 and H_3BO_3 at 750°C , 7 hours is given in Figure 1. It is clear that, at the end of 7 hours heat treatment, all the LiB_3O_5 line with respect to JCDPS File No: 32-549 were observed. The literature given by Betourne and Touboul (1997) confirmed this result also. Li_2CO_3 at this temperature turns into Li_2O which then reacted with H_3BO_3 . Besides strong $\text{Li}_2\text{B}_4\text{O}_7$ (JCPDS File No: 18-717) lines, some weak lines of H_3BO_3 were still present in the pattern.

Figure 2 shows the XRD pattern of the LiB_3O_5 obtained from the solid state reaction of Li_2CO_3 and H_3BO_3 at 750°C , 14 hours. LiB_3O_5 lines were observed again together with the lines of H_3BO_3 and $\text{Li}_2\text{B}_4\text{O}_7$.

XRD pattern of LiB_3O_5 produced at 750°C for 21 hours were given in Figure 3. It can be observed from this figure that, $\text{Li}_2\text{B}_4\text{O}_7$ lines were still present in the pattern but the intensities were very weak. All the lines of LiB_3O_5 with respect to JCPDS File No: 32-549 were produced successfully and confirmed by the literature (Betourne and Touboul 1997) also.

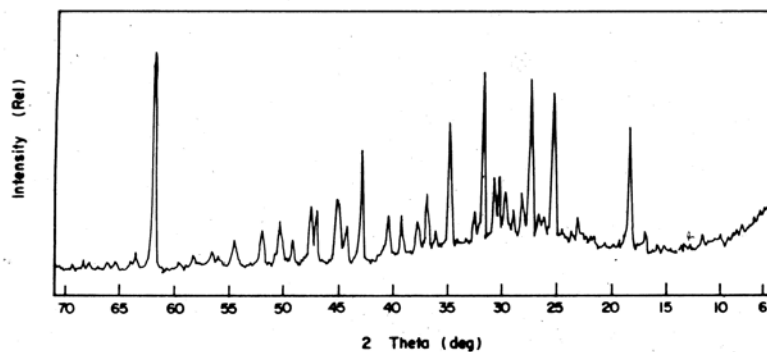


Fig. 1. The XRD pattern of LiB_3O_5 produced at 750°C for 7 hours (x: LiB_3O_5)

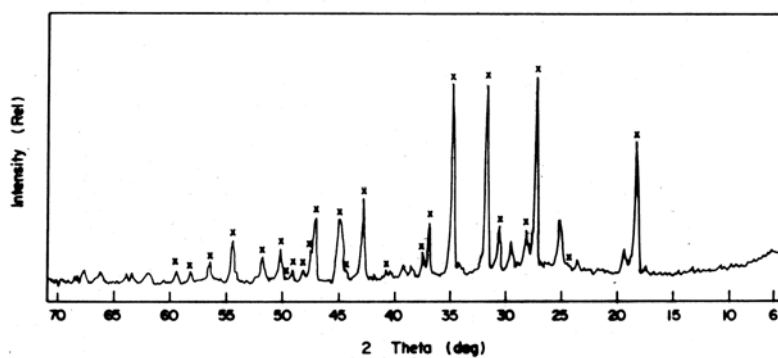


Fig. 2. The XRD pattern of LiB_3O_5 produced at 750°C for 14 hours (x: LiB_3O_5)

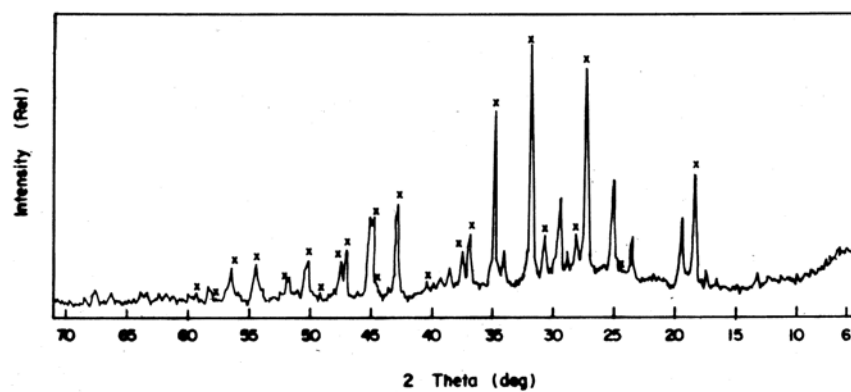


Fig. 3. The XRD pattern of LiB_3O_5 produced at 750°C for 21 hours (x: LiB_3O_5)

CONCLUSION

The interest in the use of borate crystals in nonlinear optics has increased during the past decade due to increase in the demand for solid-state short wave length lasers obtained with NLO. Lithium triborate is one of the most known lithium borates and it has become one of the most important crystals for NLO applications since it was first developed in 1989.

It was found from this study that, the LiB_3O_5 was produced successfully from the solid state reaction of Li_2CO_3 and H_3BO_3 at 750°C together with a side product. Characterization of LiB_3O_5 and the side products will be completed by means of IR, DTA and TGA besides XRD in future studies.

REFERENCES

- AKA G., HARARI K., VIVIEN D., BENIETZ J.M., SALIN F., GODARD J. J. (1996), *Solid State Inorg. Chem* 33, p. 727.
- BECKER P. (1998), *Borate Materials in Nonlinear Optics*, *Advanced Materials* 10 (13), p. 979.
- BETOURNE E., TOUBOUL M. (1997), *Synthesis of lithium borates ($B/Li \geq 3$) as LiB_3O_5 by dehydration of hydrated precursors*, *Journal of Alloys and Compounds* 255, p. 91.
- CHEN C., U Y., JIANG A., BOCHANG W., YOU G., LI R., LIN S. (1989), *Journal of the Optical Society of America B: Optical Physics* 6(4), p. 616.
- CHEN C., WANG Y., WU B., WU K., ZENG W., YU L. (1995), *Nature* 373, p. 322.
- DEWEY C.F., COOK Jr. W.R., HODGSON Jr. R.T., WYNNE J.J. (1975), *Appl. Phys. Lett.* 26, p. 714.
- FURUKAWA Y., SATO M. (1995), *Lithium triborate and optical device using it*, *Jpn. Kokai Tokkyo Koho* 1995, 3 pp, Patent written in Japanese, Application JP 94-103966 19940518.
- HE M., CHEN X.L., GRAMLICH V., BAERLOCHER Ch., ZHOU T., and HU B.Q. (2002b), *Synthesis, structure and thermal stability of $\text{Li}_3\text{AlB}_2\text{O}_6$* , *Journal of Solid State Chemistry* 163(2), pp. 369-376.
- HE M., CHEN X.L., HU B.Q., ZHOU T., XU Y.P., and XU T. (2002a), *The ternary system $\text{Li}_2\text{O}-\text{Al}_2\text{O}_3-\text{B}_2\text{O}_3$: Compounds and phase relations*, *Journal of Solid State Chemistry* 165, pp. 187-192.
- HE M., CHEN X.L., LAN C.H., LI H., and XU Y.P. (2001a), *Ab initio structure determination of new compound LiAlB_2O_5* , *Journal of Solid State Chemistry* 156, pp. 181-184.
- HE M., LI H., CHEN X., XU Y., XU T. (2001b), *$\text{Li}_2\text{AlB}_5\text{O}_{10}$* , *Acta Crystallographica Section C, Crystal Structure Communications*, 57(Pt 9) 1010-1.
- HELWING H., LIEBERTZ J., BOHATU L. (1999), *Solid State Commun.* 109, p. 249.
- KESZLER D.A. (1999), *Synthesis, crystal chemistry, and optical properties of metal borates*, *Current Opinon in Solid State and Materials Science* 4, p. 155-162, 1999.
- KIM H.G., KANG J.K., PARK S.J. (1997), *Growth of the nonlinear optical crystals of lithium triborate and beta barium borate*, *Optical Materials* (accepted).
- KÖNIG H., HOPPE R. (1978), *Z.Anorg. Allg. Chem.* R439 p. 71.
- LEE S.M., CHOI D.Y., CHUNG S.J., KOR J. (1998), *Crystal growth and optical properties of rare earth aluminum borates*, *Phys. Soc.*, Vol. 32, pp. 443-445.
- LIEBERTZ J., STAHR S. (1983), *Z. Kristallogr* 165, p. 91.
- MATHEWS M.D., TYAGI A.K., and MOORTHY P.N. (1998), *High temperature behaviour of lithium borates: Part I: Characterization and thermal stability*, *Thermochimica Acta* 320, pp. 89-95.
- MAZZETTI C., CARLI F.D. (1926), *Gazz. Chim. Ital.* 56, p. 146.
- MORI Y., YAP Y.K., KAMIMURA T., YOSHIMURA M., Sasaki T. (2002), *Recent development of nonlinear optical borate crystals for UV generation*, *Optical Materials* 19, p.1.
- MORYC U., and PTAK W.S. (1999), *Infrared spectra of $\beta\text{-BaB}_2\text{O}_4$ and LiB_3O_5 : new nonlinear optical materials*, *Journal of Molecular Structure* 511-512, pp. 241-249, 1999.

- Powder Diffraction File No. 18-717 JCPDS-ICDD, USA.
Powder Diffraction File No. 32-549 JCPDS-ICDD, USA.
ROLLET A.P., BOUAZIZ R. (1955), *Comp. Rend. (Paris)* 240, p. 2417.
SABHARWAL S.C., SANGEETA B. T. (2004), *J. of Crystal Growth* 263, p. 327.
SABHARWAL S.C., SANGEETA B.T. (2003), *J. of Crystal Growth* 249, p. 502.
SASTRY B.S.R., HUMMEL F.A. (1958), *J. Am. Ceram. Soc.* 41, p. 11.
SENGUUTUVAN N., ISHII M., SHIMOYAMA M., KOBAYASHI M., TSUTSUI N., NIKL M., DUSEK M., SHIMIZU H.M., OKU T., ADACHI T., SAKAI K., and SUZUKI J. (2002), *Crystal growth and luminescence properties of Li₂B₄O₇ single crystals doped with Ce, In, Ni, Cu and Ti ions*, *Nuclear Instruments and Methods in Physics Research A* 486, pp. 264-267.
SUGAWARA T., KOMATSU R., and UDA S. (1998), *Linear and nonlinear optical properties of lithium tetraborate*, *Solid State Communications* 107, No.5, pp. 233-237, 1998.
TAKATOMO S., YUSUKE M., MASASHI Y. (2001), *Development of new NLO borate crystals*, *Journal of Nonlinear Optical Physics and Materials* 10(2), pp. 249-263, 2001.
VAN EIJK C.W.E. (1997), *Proceedings of the International Conference on Inorganic Scintillators and Their Applications*, Shanghai, Peoples Republic of China, September 22-25, p.3.
XUE, D., BETZLER K., HESSE H., and LAMMERS D. (2000), *Nonlinear optical properties of borate crystals*, *Solid State Communications* 114, pp. 21-25.
ZHONG W., TANG D. (1996) *Journal of Crystal Growth* 166, p. 91.

Özdemir Z., Özbayoğlu G., Kızılyallı M., Yılmaz A., *Synteza i charakterystyka trójboranu litu*, *Physicochemical Problems of Mineral Processing*, 38, (2004) 321-327 (w jęz. ang.).

Trójboran litu jest idealnie nieliniowym kryształem optycznym odkrytym w ostatnich latach. Jego szerokie zastosowanie obejmuje takie dziedziny jak broń laserowa, radary, spawalnictwo, chirurgia, komunikacja i wiele innych. Przeprowadzone w pracy badania dotyczyły syntezy trójboranu litu. Synteza została przeprowadzona w temperaturze 750⁰C. Substancjami były węglan litu (Li₂CO₃) i kwas borowy (H₃BO₃). Dla scharakteryzowania otrzymanego produktu zastosowano metodę dyfrakcji promieni X. Zgodnie z danymi eksperymentalnymi, synteza trójboranu litu zachodzi w sposób zadawalający z małą ilością produktów ubocznych. W pracy zostały przedstawione jedynie wstępne wyniki badań. W następnym etapie badań zostanie opracowany problem usuwania produktów ubocznych.

Antoni MUSZER*

MINERALOGICAL CHARACTERISTICS OF METALLURGICAL DUST IN THE VICINITY OF GŁOGÓW

Received May 10, 2004; reviewed; accepted June 25, 2004

The investigations of the atmospheric dusts in the Głogów-Żukowice area detected the presence of unaltered grains and fragments of ore minerals characteristic of the ore from the Legnica Głogów Copper District. Industry in the Żukowice area emits not only sulphides and arsenides of such metals as Cu, Pb, Zn, and Ni but also alloys of Pb and Pb-Cu as well as precious metals. Size of the dust particles varies considerably from submicroscopic grains to several hundreds of micrometers. The particles are usually xenomorphic grains or crystals and ore fragments (mainly shale ore). Intergrowths of ore minerals are rare. The biggest grains consist of semigraphite blades and unaltered fragments of bituminous shale. Bornite, chalcopyrite, goethite, chalcocite, hematite, covellite, marcasite, arsenides of Ni-Co (rammelsbergite-safflorite), fragments of Bessemer and shaft furnace slag, metallic silver and copper, metallic iron, ilmenite, magnetite, malachite, cuprite, pyrrhotite, metallic lead and lead alloys were detected in the polished samples.

Key words: metallurgical dust, ore minerals, silver, ore microscopy, sulphides, metals alloy

INTRODUCTION

The research aimed mainly at characterising the mineralogical composition of metallurgical dusts falling in the neighbourhood of the copper smelters and refineries Głogów I and II near the Żukowice village. It has been carried out systematically since 1999 and the results were presented in several MSc thesis (Gruszka 2001, Grech 2002, Wójcik 2003). The observations allow evaluating the efficiency of filters installed on the factories' chimneys.

Dusts are generated on various technological stages of extracting copper and accompanying metals and carried out by smelter gases as well as air that are pumped out of the factory buildings. The dusts are mobilised mechanically by a stream of

* University of Wrocław, Department of Geological Science, Poland, amus@ing.uni.wroc.pl

ventilation air from materials under processing (transport, mixing, drying etc.) and by smelter gases in roasting and sintering devices as well as in furnaces (Krupkowski 1974, Byrdziak 1996). They are also generated as a result of partial escaping and subsequent condensation of some constituents of metallurgical load.

The investigations of the atmospheric dusts, which fall on the ground and vegetation in the Głogów-Żukowice area, detected the presence of unaltered grains and fragments of the ore minerals characteristic of the Legnica Głogów Copper District metal deposits. The presence of various alloys was also detected. Not only sulphides and arsenides of such metals as Cu, Pb, Zn, and Ni but also alloys of Pb, Pb-Cu and precious metals are emitted from the smelters and refineries near Żukowice. Presence of metallic compounds in the atmospheric dusts is an indicator of pollution that was not eliminated entirely in the last period of the factories activity. Most of all the research was to answer the problem to what extent Głogów is subjected to falls of metallurgical dusts from the Żukowice area and how far anthropogenic dusts generated during smelting activity in the Głogów area may travel.

METHODS

Sampling of the dusts was carried out in autumn – winter and spring – summer cycles. The dusts were caught in basins with a diameter of 40 cm. The investigations presented in the article cover the period of time from 1999 to 2003. Depending on the place in which the basins were installed collecting of the dusts took about 4-8 weeks in autumn-winter and spring. The basins were installed in various distances from the Głogów smelter and refinery in accordance with wind directions dominating in the area. Material for the investigations comes from Żukowice (in the proximity of the metallurgical complex) Bogomice, Biechów, Głogów, Drozów and Nielubia (Fig. 1).



Fig. 1. Location of sampling points

It was sifted on the 250 µm and 125 µm Fritz sieves. Polished samples for reflectance microscopy and electron microscopy were then prepared. Reflectance microscopy was performed using an Optiphot 2-Pol Nikon microscope equipped with a Photometr 100 for reflectance measurements. Ore identification followed a standard procedure based on reflectance microscopy observations (Ramdohr 1975, Piestrzyński 1992, Muszer 2000). They were carried out at the Laboratory of Ore Minerals Microscopy, University of Wrocław. Chosen polished samples abundant in metallic compounds were coated with graphite and analysed with a scanning microscope Philips-515 equipped with a microprobe and an EDX spectrometer at the Institute of Low Temperature and Structure Research, Polish Academy of Sciences in Wrocław.

Chosen polished samples abundant in metallic compounds were coated with graphite and analysed with a scanning microscope Philips-515 equipped with a microprobe and an EDX spectrometer at the Institute of Low Temperature and Structure Research, Polish Academy of Sciences in Wrocław.

SOURCES OF POLLUTION

Industry in the Żukowice area generates various dust wastes depending on a technological process. During copper smelting convective gases (N_2 , SO_2 , O_2) mobilise fine silica grains, cold solid additions, and fragments of slag and metallic copper. Together with these particles some volatile metals (Zn, Pb, As, Bi etc.) are ejected. According to Chodkowski (1976) the amount of dust generated in technological processes constitutes about 0,5 to 1 % of the volume of the processed material. According to Byrdziak (1996) on the other hand, after application of methods of wet de-dusting of gases in 1970-1980's and installation of bag and cassette filters (in 1995) operating at 99,9 % efficiency the amount of dusts does not exceed 5 mg/Nm^3 .

During drying of copper concentrate in the "Głogów I" smelter and refinery the "Mikropul" wet de-dusting installation operates with the efficiency of 94.7 % and in the "Głogów II" electrofilters reach the efficiency of 98 %. In "Głogów I" de-dusting systems were not installed in reloading sections, which are not attended by workers, but bag filters were applied and operate at 99.9 % efficiency in loading sections of shaft furnaces. In "Głogów II" hermetisation of the technological line was applied instead of de-dusting. Shaft furnace gases are de-dusted with a Venturi tube with a regulated valve. Then all the shaft furnace gases are transported to the heat plant and combusted. In emergency shaft furnace gas is released through 150 m high chimneys and in case of de-dusters malfunctioning untreated gas is emitted through the technological chimney of a shaft furnace. Furnace loading is done through a bell shaped valve. Filters (e.g. in "Głogów II") de-dust with 99,9 % efficiency reaching the level of 5 mg/Nm^3 of dust in the gases. Flush furnace gases are de-dusted with the efficiency of 99,9 %. According to the data presented by KGHM Polska Miedź S.A. converter gases do not contain dusts after application of converter flaps.

CHARACTERISTICS OF ANTHROPOGENIC DUSTS

Dusts generated during metallurgical activity are not homogeneous and depend on the character of the technological process of copper extraction and solid wastes generated in this process (Muszer 1996, 1998). Their abundance and composition depend on the season of a year and distance from the smelter and refinery in Żukowice. Dusts collected in the basins installed in the same places but in different time periods show different mineralogical compositions. Size of the dust particles varies considerably from submicroscopic grains to particles with a diameter of several hundred micrometers. They are represented mostly by separate xenomorphic grains or crystals and fragments of ore (mainly shale ore). Intergrowths of ore minerals are rare (Fig. 2). The biggest fragments consist of semigraphite blades and unaltered parts of bituminous shale. However semigraphite and graphite were not taken into account in the current work as their presence results from the activity of heat plants operating in the Głogów area.

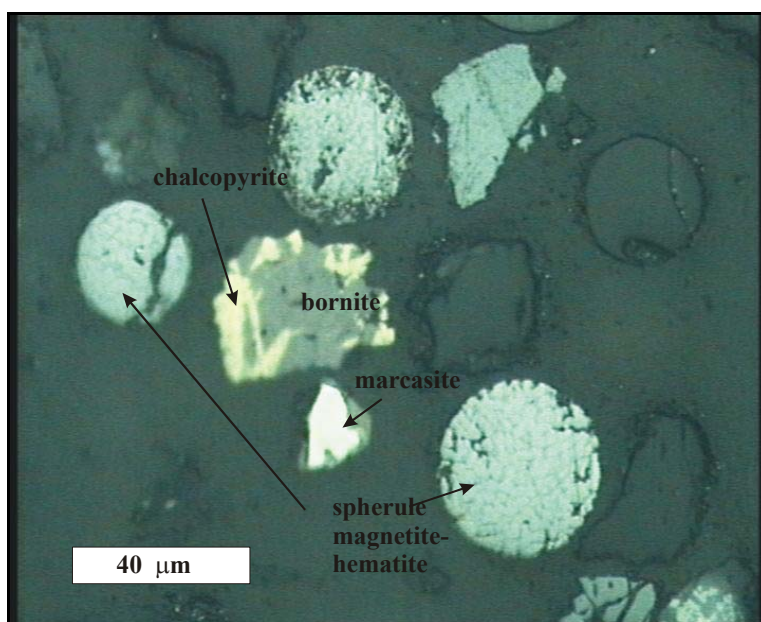


Fig. 2. Forms of anthropogenic dusts near Bogomice. Reflected light, uncrossed nicols. Grey minerals: quartz and silicates of metals

The greatest concentration of metallurgical dusts was observed in Żukowice (in the protective zone of the copper smelter and refinery) and northeastwards, in Bogomice and Biechów. In the other places the amount of the material collected in the basins decreased with the distance from the smelter and refinery. In the polished samples the

following phases were detected: Ni-Co arsenides (rammelsbergite-safflorite), bornite, chalcopyrite, goethite, chalcocite, hematite, covellite, marcasite, silver and metallic copper, fragments of Bessemer and shaft furnace slag, metallic iron, ilmenite, magnetite, malachite, cuprite, pyrrhotite, metallic lead and lead alloys.

The greatest fall of anthropogenic dust occurs near the Głogów I and II smelters and refineries, i.e. at the fences, northeastwards towards the Odra River and in the forested protective zone. The material collected in this area resembled rich ore concentrate with minor amount of wind-blown quartz (Fig. 3). In the polished samples from this area the following phases were detected: chalcocite, chalcopyrite, metallic copper, cuprite, covellite, bornite, magnetite, sphalerite, chromite, goethite, pyrite, marcasite, Pb-Cu alloys, metallic lead, fragments of Bessemer and shaft furnace slag. The size of the ore phases varies from 0,1 μm to 75 μm in diameter. The copper ore minerals display structures typical of copper ores. This indicates the lack of thermal influence. Lead and lead-copper alloys show irregular forms up to 20 micrometers in diameter. Exsolutions of lead are present within the spheres of metallic copper. Lead, together with metallic copper, iron and traces of gold are also present in cristobalite spheres (Fig. 4). Those spheres contain 50 wt.% of lead and 26,45 wt. % of copper.

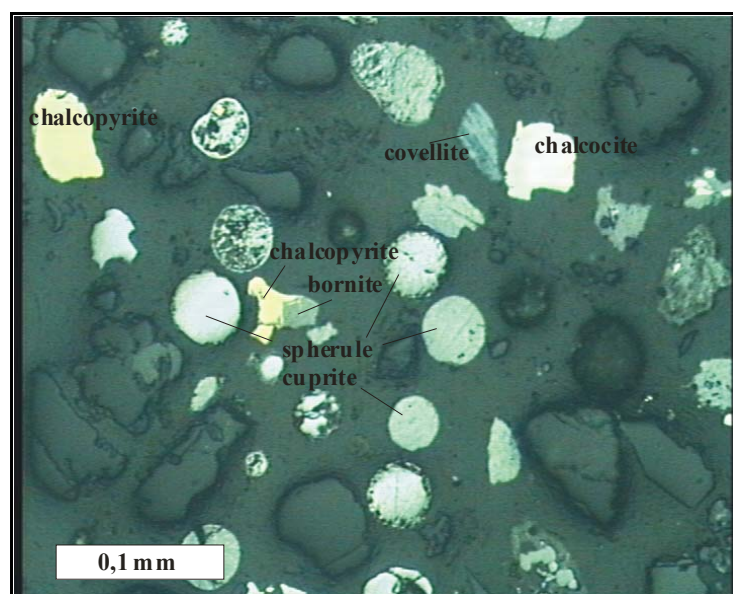


Fig. 3. Forms of anthropogenic dusts near Żukowice. Reflected light, uncrossed nicols. Grey minerals: quartz and silicates of metals

Apart from cristobalite spheres also silicate spheres with diameters below a hundred micrometers fall around the smelter and refinery. They contain steel metals, i.e. Ni up to 4,5 wt. %, Co up to 6,5 wt. %, Cr up to 24,5 wt. % and non-ferrous metals: Zn up to 3,5 wt. %, Cu up to 1,5 wt. % (Fig. 5).

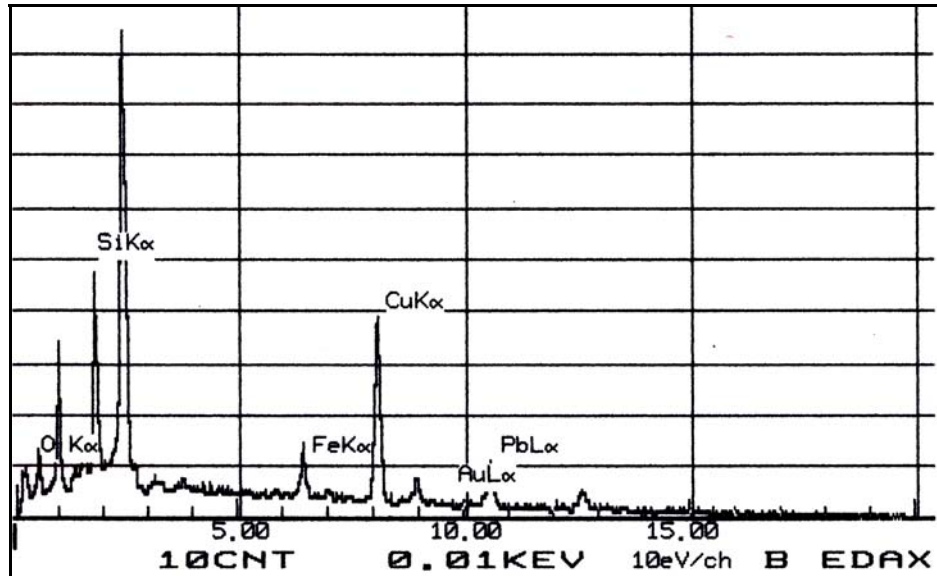


Fig. 4. EDS spectrum of a cristobalite sphere with exsolutions of Pb, Cu, Fe and Au alloys

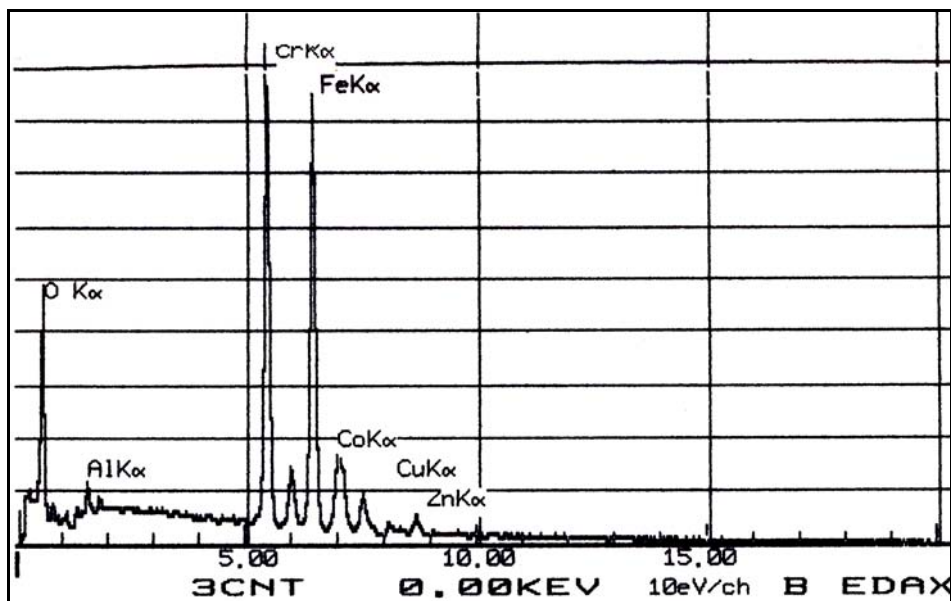


Fig. 5. EDS spectrum of a silicate sphere with exsolutions of metallurgical alloys

The distribution of the atmospheric dust is similar in the areas of Biechów (Fig.6) and Bogomice (Fig. 7). Hematite, covellite, goethite, marcasite, chalcopyrite, bornite, metallic copper, alloys of Pb and magnetite occur in both places. The main difference between the places lies mostly in the presence of fragments of Bessemer slag and metallic iron in the Bogomice area. Main ore minerals are represented by copper phases unaltered by influence of high temperature. Their structures and intergrowths are typical of the processed copper ore. The size of ore dust particles rarely exceeds 40 μm . The diameter of the main ore grains varies from 2 to 35 μm .

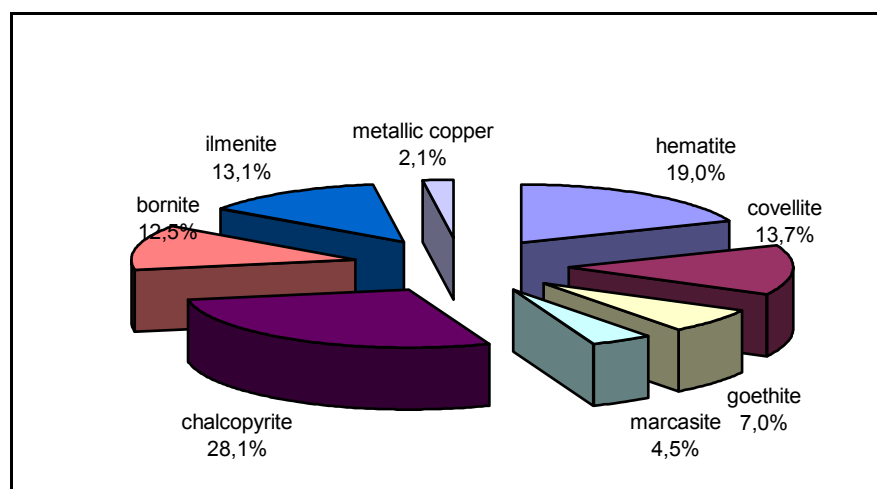


Fig. 6. Percentages of ore minerals in the Biechów area.

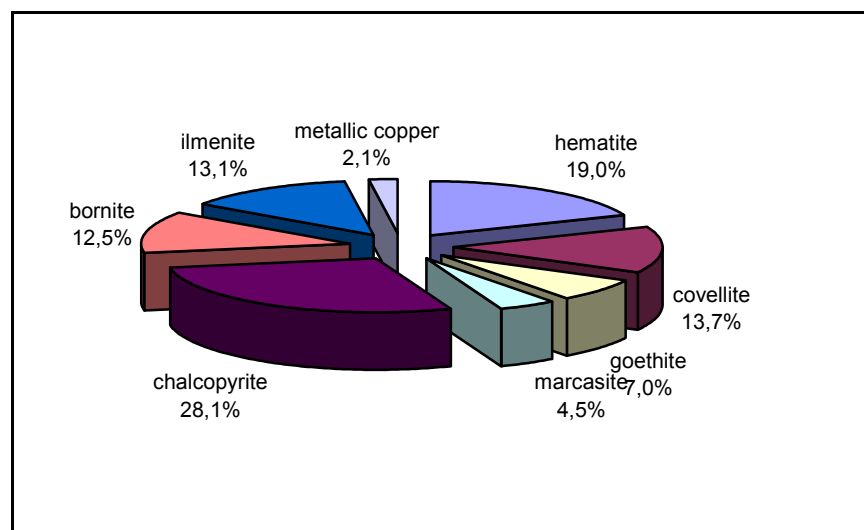


Fig. 7. Percentages of ore minerals in the Bogomice area.

In the Głogów area there are ore minerals of Fe: goethite, magnetite, hematite, and Cu: covellite, bornite, chalcopyrite, chalcocite, metallic copper, cuprite, malachite as well as marcasite, pyrite framboids, Bessemer slag, pyrrhotite, metallic iron, ilmenite and metallic silver. The biggest grains in the collected materials consist of goethite and reach 250 μm in diameter. The other ore minerals do not exceed 70 μm and their average diameter is 16 μm . The copper ore minerals do not reveal signs of melting opposite to metallic copper, cuprite, magnetite and metallic iron. The copper phases of cuprite and metallic copper are related to each other. Cuprite is usually present as rims around metallic copper spheres (Fig. 8). Metallic iron on the other hand forms tiny, below twenty micrometers in diameter, spheres in silicates (pyroxenes).

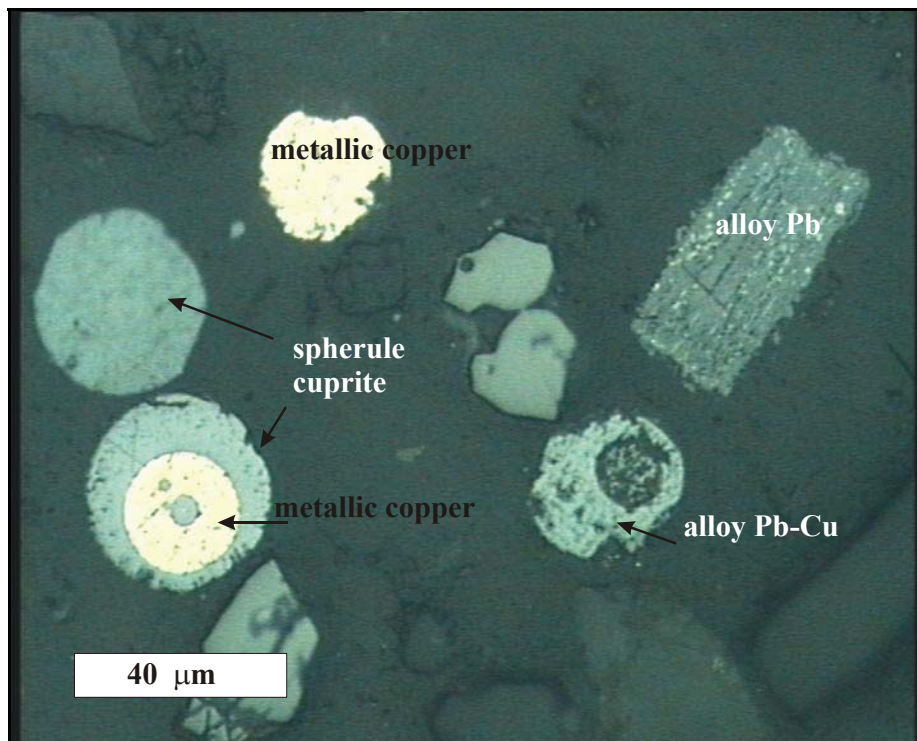


Fig. 8. Forms of anthropogenic dusts near Głogów. Reflected light, uncrossed nicols. Grey minerals: quartz and silicates

In the Głogów area a clear difference in the character of dust falls between autumn-winter and spring-summer periods (Fig 9). In autumn-winter the main ore minerals are covellite, goethite and metallic iron with bornite while during spring-summer the relative percentage changes and hematite and covellite become major constituents (Fig. 9).

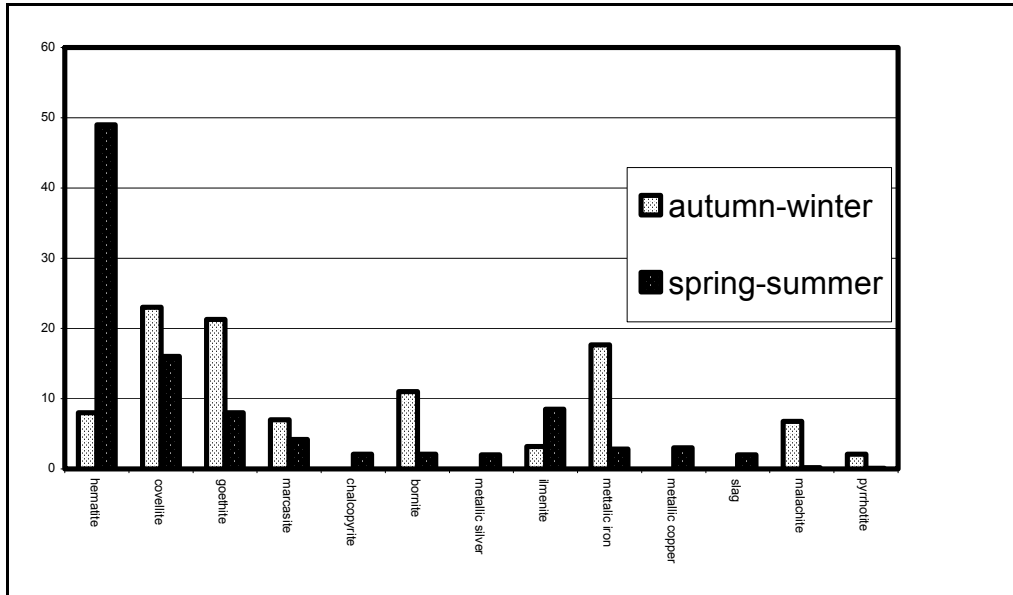


Fig. 9. Percentages of ore minerals in the investigated samples from the Głogów area

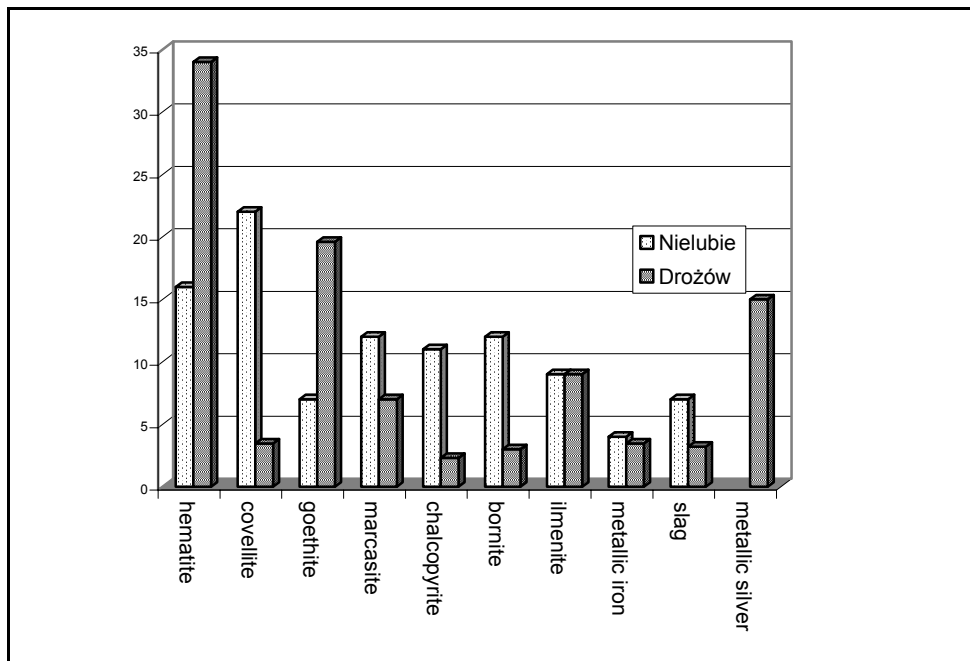


Fig. 10. Percentages of ore minerals in samples from Nielubie and Drożów

Villages of Nielubie and Drożów lie North of the metallurgical complex of Żukowice. They are located about 5 and 10 km respectively away from the metallurgical complex. Identical composition of ore minerals was detected in both places in summer 2002 and 2003. The collected dusts are dominated by fragments and spheres of hematite, ilmenite, goethite, marcasite, metallic iron, chalcopyrite, bornite, covellite, granulated (Bessemer) slag and pyrite framboids. Moreover the presence of metallic silver was detected near the Drożów village. Southern direction of metallic silver transportation was already confirmed four times since 2000. All ore minerals, except metallic iron, show typical forms. Usually they are xenomorphic due to ore milling. Only iron and metallic silver display forms different from the other phases. Metallic iron is present as spheres in magnetite or silicates while metallic silver forms broken dendrites or flat blades. Statistic relations between ore minerals are depicted in Figure 10.

SUMMARY AND CONCLUSIONS

Pollution resulting from metallurgical processes poses a threat not only on a local but also regional scale as it may be seen in the areas around metallurgical complexes in Mancziegorsk in the Kola Peninsula (Ni-Cu smelter and refinery) and Karabash (Ni-Cu smelter and refinery in the Ural Mts.). These areas belong to the most polluted zones in Europe.

According to the published data (Byrdziak et al. 1996) the main source of dust emission in the whole area of the Legnica Głogów Copper District is the HM Głogów heat plant. It emits 700Mg of dusts a year. Those dusts display a characteristic composition (Piestrzyński, Ratajczak 2000). The dusts analysed with a microscope in the present study are not related to the heat plant but to metallurgical activity. It seems however that a part of hematite observed in the polished samples may come from magnetite weathered during transport in the air. Hematite spheres display sieve structure with preserved relicts of magnetite. Such spheres are typical of coal burning processes. Structures of the other ore minerals and their chemical composition suggest their formation either as a result of copper concentrate melting or forceful ejection of milled ore fragments. The presences of intergrowths of framboidal pyrite and covellite or intergrowths of chalcopyrite with bornite clearly indicate that they are grains of copper concentrate.

Due to migration of elements in nature pollution of water, soil and air affects eventually plants and human. In the case of dust fall from metallurgical industry contamination will last in the near surface zone of the earth crust much longer than gaseous pollution. This a result of slow migration of elements incorporated in the minerals that build dust particles. The process of releasing the elements and their entering the biozone was treated in detail in geochemical publications (Polański, Smulikowski 1969; Kabata-Pendias 1993). These processes however are mostly governed by pH and Eh of the environment and proceed according to the diagrams for

individual element systems (Garrels 1960; Garrels, Christ 1965; Barnes 1982, Bułach et al. 1995). Knowledge of the crystallographic form of the dust substance may allow determining the rate of migration of such pollution to the environment. The rate is related to resistance of mineral phases to weathering processes. Metals shielded by silicate cover will be cumulated in the environment longer. If however dusts are composed of fragments of ore exploited from a deposit, they will oxidise immediately, transform into soluble phases, migrate to aquifers and will be incorporated by plants. In the cases presented in the article all forms of ore minerals are unstable and disintegrate easily.

Wide spread of metallic silver on great distances from the smelter and refinery in Żukowice (Głogów, Drożów) is noteworthy. The presence of gold and silver in lead alloys from the metallurgical dusts has been monitored since 1999. The investigations carried out in the same places in 2004 confirmed that the situation had not changed. Nevertheless it still remains not clear which of the two metallurgical complexes, "Legnica" or "Głogów", is responsible predominantly for the metallic silver emission to the atmosphere.

REFERENCES

- BARNES H.L. (1982) - *Geochemistry of hydrothermal ore deposits*. New York-Toronto.
- BUŁACH A.G., Kriwiczew W.G., Zołotariw A.A. (1995) - *Formuły minerałów. Termodinamiczeskij analiz w mineralogii i geochemii*. Petersburg (in Russian).
- BYRDZIAK H. (1996) - *Ochrona środowiska. Hutnictwo*. Monografia HGHM Polska Miedź S.A.
- CHODKOWSKI Sz. (1976) - *Metalurgia metali nieżelaznych w zarysie*. Wyd. WGH. Warszawa.
- GARRELS R.M. (1960) - *Mineral equilibria at low temperature and pressure*, New York.
- GARRELS R.M., Christ Ch.L. (1965) - *Solutions, Minerals and Equilibria*. New York.
- GRECH G., (2002) - *Analiza antropogenicznych pyłów powstających w rejonie Huty Miedzi „Głogów”*. Praca magisterska. Arch. Uni. Wroc.
- GRUSZKA A., 2001- *Charakterystyka i wpływ wybranych odpadów metalurgicznych z Huty Miedzi „Głogów” na skażenie środowiska naturalnego*. Praca magisterska. Arch. Uni. Wroc.
- KABATA-PENDIAS A. (1993) - *Biogeochemia pierwiastków śladowych*. Wyd. PWN. Warszawa.
- KRUPKOWSKI A. (1974) - *Podstawowe zagadnienia teorii procesów metalurgicznych*. PWN.
- MUSZER A. (1996) - *Charakterystyka petrograficzno-mineralogiczna żużli metalurgicznych z Huty Miedzi Głogów*. Fizyk. Probl. Miner, nr 30. s. 193-205.
- MUSZER A. (1998) — *Metale ciężkie w żużlach szybowych z Huty Miedzi „Głogów”*. In. Wybrane zagadnienia z zakresu ochrony litosfery. Wrocław, s. 48-55.
- MUSZER A., 2000 – *Zarys mikroskopii kruszców*. Wyd. Uni. Wroc.
- POLAŃSKI A., SMULIKOWSKI K. (1969) - *Geochemia*. Wyd. Geol. Warszawa.
- PIESTRZYŃSKI A., 1992 – *Wybrane materiały do ćwiczeń z petrografii rud*. Wyd. AGH. Kraków.
- PIESTRZYŃSKI A., RATAJCZAK T. (2000) - *Skład fazowy frakcji magnetycznej popiołów lotnych pochodzącej ze spalania polskich węgla kamiennych i brunatnych*. PTM. Prace Spec. z 16.
- RAMDOHR P. (1975) - *Die Erzminerale und ihre Verwachsungen*. Akademie Verlag. Berlin.
- WÓJCIK R., 2003 – *Charakterystyka pyłów atmosferycznych pomiędzy LGOM a Wrocławiem na podstawie badań w świetle odbitym*. Praca magisterska. Arch. Uni. Wroc.

Muszer A., *Charakterystyka mineralogiczna pyłów hutniczych z okolic Głogowa*, Physicochemical Problems of Mineral Processing, 38, (2004) 229-340 (w jęz. ang.).

Głównym celem badań było scharakteryzowanie składu mineralogicznego pyłów hutniczych, opadających w rejonie hut miedzi Głogów I i II, położonych w okolicy wsi Żukowice. Badania pyłów atmosferycznych wykonane w rejonie Głogowa-Żukowic wykazały obecność niezmiennych ziarn i okruchów kruszców charakterystycznych dla rud znajdujących się w złożu LGOM. Z zakładów przemysłowych w rejonie Żukowic nie tylko wydostają się siarczki i arsenki metali: Cu, Pb, Zn, Ni ale także stopy Pb, Pb-Cu oraz metale szlachetne. Wielkość pyłów waha się w szerokich granicach od ziarn submikroskopowych do kilkuset mikrometrów średnicy. Badane pyły są niejednorodne. Najczęściej są to pojedyncze ksenomorficzne ziarna lub kryształy oraz fragmenty rudy łupkowej. Rzadziej spotykane są zrosty kruszców ze sobą. Największe okruchy składają się z blaszek semigrafitu i niezmiennych fragmentów łupka smolistego. W preparatach polerowanych stwierdzono obecność: bornitu, chalkopirytu, goethytu, chalkozynu, hematytu, kowelinu, markasytu, arsenków Ni-Co (ramelsbergitu-safflorytu), fragmentów żużla konwertorowego i szybowego, srebra i miedzi metalicznej, żelaza metalicznego, ilmenitu, magnetytu, malachitu, kuprytu, pirotynu, ołowiu metalicznego oraz różnych stopów ołowiowych. Struktury kruszców oraz ich skład pierwiastkowy świadczy o tym, że powstały albo w wyniku przetopienia koncentratu miedziowego, albo w wyniku wyrzucenia w powietrze z dużą siłą zmieszanych okruchów rudy.

Tadeusz CHRZAN*

INFLUENCE OF MINERAL COMPOSITION OF MELAPHYRE GRITS ON DURABILITY OF MOTORWAY SURFACE

Received April 4, 2004; reviewed; accepted June 5; 2004

The surface layer of the Konin-Września motorway section was made between July and November of 2001. Although the tests of melaphyre aggregates against grade and class requirements had confirmed that grits were the first class and grade according to the Polish standards, the motorway has been wearing rapidly with the first repairs being carried out as early as 2003. The motorway surface has been excessively worn and looks as if it were used for at least 5 years. The paper explains why the motorway surface has been worn so rapidly.

Key words: motorway, melaphyre grit, weathering

INTRODUCTION

The surface layer of the Konin-Września motorway section was made during the period from July to November 2001. The layer was made with granulated aggregate 0-20 mm in diameter from Borówko and Grzędy melaphyre quarry, bounded with modified bituminous mass. The tests of melaphyre aggregates against grade and class requirements had confirmed that the grits were the first class and grade (Chrzan, 1997; Wysokowski, 2000/2001) according to the Polish Standards (PN-11112:96, PN-11110:96, PN-EN 1097-2).

The binding layer of asphaltic concrete made and tested on samples that were taken from the completed motorway also conformed to the standard requirements according to Polish Standards (PN-S/96025, PN-74/S-96022). Also, the adhesion of asphalt to the melaphyre grit conformed to the standard (PN-84/B-6714/22).

After the wintertime, in spring 2002, on the surface of the roadway, distinct signs of scaling and weathering were observed on the surface of larger melaphyre grit grains. In August 2002, it was found that the number of weathered grains had

* Institute of Environmental Engineering, University of Zielona Góra, Poland

increased and some of them lost their compactness and disintegrated (Ruttmar, 2002). Between September and November of 2003, due to the above reason, which threatened the safety of moving vehicles, partial repairs were carried out covering 1600 square metres. The surface of motorway has been excessively worn and looks as if it were used for at least 5 years.

In this paper, it is explained why the motorway has been worn so quickly.

ANALYSIS OF DECREASE OF ASPHALTIC CONCRETE STRENGTH OF MOTORWAY A2 BINDING LAYER IN RESPECT TO MINERAL COMPOSITION OF ROCKS

DESCRIPTION OF MELAPHYRE DEPOSIT (Radziszewska-Jargosz, 1982;
Szuszkiewicz I Król, 1988)

The melaphyre used for road construction come from deposit that was formed from basalt-type volcanic rocks in the Permian period around 350 mln million years ago. The volcanic rocks created trachyte-basalt, trachyte and tuff-type rocks. The melaphyre deposit is exploited in the quarries of Borówno, Grzędy and Rybnica Leśna. The trachyte basalts are of two types. The first one includes rocks coloured cherry-brown, cherry-brick and grey-violet. They have chaotic structure and aphanitic texture. Cracks are filled with the ferruginous and carbonate substance.

The second type is the rock ranging from grey-brown through grey-greenish to nearly black in colour. The structure is aphanitic and the texture is dense. Course-grained breccia of chaotic texture is also found. Volcanic spalls are cemented with the ferruginous and carbonate binder. The rock spalls are grey-brown and are of various size and aphanitic structure.

The tuffs are cherry-brown, have aphanitic structure and chaotic, texture. They disintegrate into irregular small blocks. Numerous quartz grains and carbonate veins are visible.

The sedimentary rocks are cherry-brown in colour and have fine-grained structure with directional texture. They disintegrate into irregular small blocks. Rocks of lava-mudstone fraction are found in the deposit which may have been the result of lava flooding during volcano eruption of weathered layers from the previous outflow.

The exploited rock is melaphyre-type aphanite lava ranging from dark grey to black in colour; solid but intensely cracked rock. The cracks make it vulnerable to weathering and 0-10 mm sized rock is dumped as waste (Kancler, 2002a) in amount of 21% at Borówno quarry, and 15% at Grzędy quarry (Kancler, 2002b). This gives evidence that malaphyre in the Borówno quarry is built from minerals that are subject of stronger weathering than that in the Grzędy quarry. The melaphyre (Kancler, 2002a and 200b) in both quarries is built from minerals that disintegrate under the influence of temperature, air and water.

PETROGRAPHIC ANALYSIS OF MELAPHYRE

The petrographic analysis of Grzędy deposit (Radziszewska-Jargosz, 1982) shows that plagioclases are found in the form of small phenocrysts. Feldspars undergo the process of sericitization and carbonization, and weathering processes lead to kaolinization. The ferruginous substance infiltrates the strips of plagioclases. Dark minerals were completely transformed. They were replaced with hydrated iron oxides accompanied by concentrations of carbonates, and in place of olivine there is a substance that is difficult to identify. Chlorite is rarely found. Pores are refilled with calcite accompanied by ferruginous pigment. In the pores there are concentrations of chalcedony. Concentrations of limonite are often found. Apatite, ilmenite and magnetite are accessory minerals. Volcanic glass, brown or orange in colour is also found. The rock groundmass consists of heavily carbonatized glass, perches of plagioclases, ash fraction and iron oxides.

PROPERTIES OF MINERALS FOUND IN THE MELAPHYRE DEPOSIT [Bolewski I Manecki, 1993; Bolewski, 1972; Chrzan, 1997)

On the basis of geological documentation [8] on melaphyre deposit of the Borówno quarry, the mineralogical composition of fresh samples collected from the deposit is as follows: plagioclase 45.2-75.0 %, pyroxene 0-5.81 %, oxides and hydroxides 6.1-38.7 %, carbonates 0-8.3 %, chlorite 0-4.7 %, clayey minerals 0-5.2 %, quartz 0-3.0 %, iddingsite 0-9.7%, and unidentified 0-1.0 %.

Feldspars (plagioclases)

Plagioclases are sodium-calcium (Ca, Na) feldspars. Also found, there are potassium (K), white (Na) and lime (Ca) feldspars. The feldspars, more generally called aluminosilicates, form mixed crystals where K, Na, and Ca combined in different proportions among themselves and silica. Specific density of feldspars ranges from 2.5-2.8 Mg/m³. With an increase of calcium (Ca) content, plagioclases disintegrate easier into clay minerals, in particular into kaolinite. The kaolinization of plagioclases is commonly known among geologists. The weathering product of plagioclases that are rich in calcium is also calcite (CaCO₃) coloured yellowish or brown. Kaolinite is the basic component of clayey minerals coloured red or brown and with specific density 2.5-2.6 Mg/m³, which is found in the form of dense or scaly concentrations. Wet kaolinite becomes plastic.

The clayey minerals also include montmorillonite with specific density 2.0 Mg/m³ and in the form of white dense or scaly concentrations, which intensely swells in water, and decolourises denatured alcohol or methylene blue solution.

Bentonite of the same colour and density behaves in a similar way; it is a mixture of clay minerals of the montmorillonite group.

Feldspars also undergo the processes of sericitization and carbonisation. From the potassium feldspars, sericite is formed of scaly structure, and chlorite of scaly structure.

Micas, such as muscovite, are found in the form of lamellas or lamella concentrations. These are minerals, formed of Na, K, Al, Fe, Mg, Si elements in various combinations. Mica is found in the magma rocks rich in SiO₂ such as granites. In sedimentary rocks, it transforms into hydro-muscovite. They are green and black, yellow or brown in colour.

Sericite has the form of tiny scales and is created at low hydrothermal temperatures. Sericitization takes place when feldspar turns to sericite.

Pyroxenes

Pyroxenes belong to aliphatic silicates and aluminosilicates. Group 1 consists of Mg-Fe, Mn-Mg, Ca, Ca-Na, Na-type pyroxenes. Pyroxenes is an important group of rock-forming minerals, which are created at high temperatures and at low water pressure. They are components of magma rocks and metamorphic rocks. They are not resistive to climatic factors, therefore are rarely found in sedimentary rocks.

The colour of pyroxenes depends on iron and titanium content. At small content, it ranges from white to greenish, with larger content, it is olive, brown or dark green. Orthorhombic pyroxenes form the isomorphous series from Mg to Fe, with distinguished enstatite, bronzite, hypersthene, ferrohypersthene, eulite. Monoclinic pyroxenes include four minerals creating a diopside-hedenbergite series built from Ca, Mg, Fe, SiO₂.

Iron oxides and hydroxides

Hematite (Fe₂O₃) has a cherry colour in variety of shades. It is insoluble. It may instantly oxidize in weak acids. In small quantities, it is found in magma rocks, especially those coloured red. It is a component of hydrothermal formations.

Goethite (FeOOH) ranges from brown to is red in colour. It is a product of hydrothermal activity at low temperature. It often occurs as an admixture colouring other rocks and in melaphyre vacuum. It is a product of iron mineral oxidation.

Carbonates

Calcite (CaCO₃) is ranging from white to brown in colour. A component of sedimentary rocks, such as limestone, chalk, marls. It is formed in the hydrothermal activity zone independently fills rock crevices.

Aragonite (CaCO₃) is from white to brown in colour and is found in granular or dripstone crevices of melaphyres and basalts. It is a mineral of hydrothermal zone.

Dolomite (CaMg(CO₃)₂) is a sedimentary rock mineral ranging from white to black in colour with density 2.8-2.9 Mg/m³ and is found in granular or dense form.

Magnesite (MgCO₃) is from white to black in colour and is found in granular or dense form. It is created through metamorphism of rocks. It fills crevices in serpentinites and is a product of hydrothermal activity.

Siderite (FeCO_3). Its colour is ranging from grey to brown. It is a product of warm hydrothermal water activity. It turns to iron hydroxides under the influence of water and oxygen.

Chlorites

Chlorites are minerals of hydrothermal zone and may crystallize in ultra-alkaline rocks as primary minerals. They are also found in weathering zone. It is a group of package silicate minerals, containing mainly magnesium and iron, and magnesium and chromium.

They also form chlorite slates – metamorphic rocks. Chlorite is a mineral of magnesium and iron, and is dark green in colour.

Clayey minerals

Clayey minerals is kaolinite ranging from white to red or greenish in colour. It is commonly found as a product of feldspar and aluminosilicate weathering. It becomes plastic under the influence of water.

Illite. It is a products of feldspar and kaolin weathering. Commonly found as components of clay rocks such as kaolin, clay, silt, and rocks that are formed in sea environment. These minerals are chemically related and do not differ in macroscopic properties. Their colour depends on iron admixture.

Montmorillonites. They form dense wax concentrations. Their colour depends on iron admixture and ranges from white to black-brown. They swell when flooded with water. They discolour methylene blue solution. Components of sedimentary rocks and hydrothermal formations of low temperature. Montmorillonites are created as the products of magma glaze weathering in alkaline and heavily salted environment. Montmorillonite's colour depends on iron content

Quartz SiO_2

Rock forming mineral, very durable, weatherproof. It may also be found as tridymite and cristobalite. Its colourless form is called mountain crystal, other forms are yellow, violet, black, pink, green.

Iddyngsite

It is a product of olivine metamorphosis. It has a lamellar structure. Its red colour suggests that it is a serpentine with high iron content.

A serpentine subgroup is formed by clay minerals similar to the kaolin subgroup. Mg serpentines include antigorite, lizardite and chryzotile with density 2.5-2.6 Mg/m^3 . Serpentinization of magma rocks occurs at the temperature below 400 °C under the influence of water. As a result serpentinite minerals which are MgO rich (olivine) and Al_2O_3 poor rocks are formed.

Amphiboles

Amphiboles are important rock-forming ribbon silicates and aluminosilicates minerals. Four groups of amphiboles are distinguished: 1) Fe-Mg-Mn, 2) Ca, 3) Na-Ca, and 4) Na. Amphiboles also include the hornblende group usually containing Na, Ca, K, Fe, Si, Al, SiO₂ ranging from light green to dark green in colour, with density 2.9-3.4 Mg/m³. Hornblende usually occurs in magma rocks of any type from neutral, acid to alkaline.

OXIDATION UNDER ALKALINE CONDITIONS FOUND ON THE MOTORWAY SURFACE AND FORMATION OF NEW MINERALS (Bolewski I Manecki, 1993; Bolewski, 1972)

Plagioclases

According to the geological documentation of the deposit, there is from 45.2 to 75.0 % of plagioclases in melaphyre. These minerals are sodium-calcium feldspars, which with increasing calcium content, due to the weathering process, disintegrate into kaolin, which is a clay mineral.

It may not be ruled out that the weathering process in melaphyre grits, which has begun in the deposit, will continue on the surface of the motorway.

Pyroxenes (0-5.8 %)

Pyroxene minerals are not weatherproof. It is visible in Table 1.

Table 1. Content of minerals in samples taken for the Borówno quarry (Strasser, 2002)

	Weathered samples		Fresh samples	
	BO-4	BO-2	BO-3	BO-5
(Clayey minerals, montmorillonites)	60	50	32	13
Quartz	7	3	-	-
Plagioclases	13	45	58	76
Calcite	15	-	-	-
Goethite	5	-	-	-
Amphiboles	-	2	-	-
Pyroxenes	-	-	10	11

Oxides and hydroxides

These kinds of minerals occur in melaphyre with the content ranging from 6 to 39%. They may be iron compounds, which are components of magma rocks. Goethite (FeOOH), a product of iron mineral oxidation, may be also found, which is also a product of low temperature hydrothermal activity. The minerals undergo considerable

oxidation during one-year period (visible change in aggregate colour in the storage yard). The impact of their content on grit strength in the motorway surface is difficult to determine. However, the iron oxidation process certainly reduces the strength of rock components in asphaltic concrete.

Carbonates (0-8.3 %)

Carbonate minerals such as calcite, aragonite, dolomite and magnesite are products of hydrothermal formations and are found in melaphyre. They do not undergo oxidation or weathering process. However, siderite (FeCO_3) is a product of hydrothermal waters, and under the influence of water and oxygen, that is possible on the motorway surface, it transforms into iron hydroxides. It can also contain admixtures of clay minerals and calcite. That carbonate mineral may have a great impact on the strength of grits in the motorway surface.

Chlorite (0-4.7 %)

Chlorites are minerals of hydrothermal zone and ultra-alkaline magma. Chlorite is a manganese and iron mineral coloured dark green. It does not undergo oxidation and weathering. It has no influence on the reduction of grit strength of the motorway surface.

Clay minerals (0-5.2 %)

Clay minerals include kaolinite, which is a product of weathering of feldspars and plagioclases that make up 75% of the deposit. Feldspar weathering products also include illite and hydro-muscovite. Montmorillonite is a product of magma glaze weathering in alkaline and heavily salted environment. The natural weathering process that has begun in the deposit may have accelerated in alkaline environment during the winter usage of salt for motorways and roads. These minerals swell when submerged in water. Their colour is red-brown. Taking the above into account, it must be stated that the clay minerals have a great impact on the strength of grits in the motorway surface.

Quartz 0-3.0 %

Very hard mineral, weatherproof. It does not reduce the strength of grits in the motorway surface. A small content in the rock causes the rock not to be resistant to weather conditions.

Iddyngsite (0-9.7% - product of olivine serpentinization)

Iddyngsite is a serpentinite with a high iron content. It is a clay-type mineral and it has a great impact on the strength of grits in the motorway surface.

Unidentified minerals (1.0 %)

They may not have a positive impact on melaphyre strength.

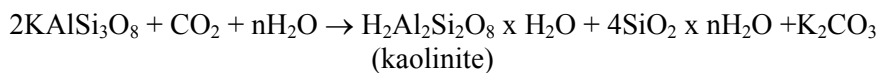
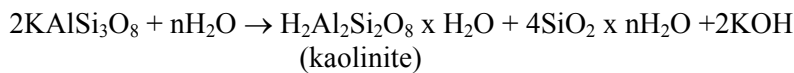
The above data shows that the following minerals have unquestionable impact on the reduction of melaphyre grit strength:

- plagioclases (content 45-75 %),
- carbonates (content 0-8 %),
- clay minerals (content 0-5 %),
- pyroxene with content (0-6 %).

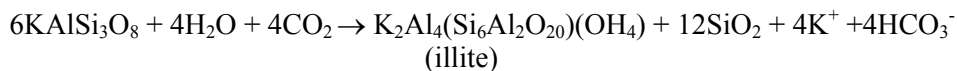
This makes from 45 to 94 % of minerals vulnerable to weather conditions. Therefore, they have considerable impact on the reduction of strength and compactness of melaphyre grit applied to the upper layer of the motorway surface.

Reactions of mineral hydration are as follows:

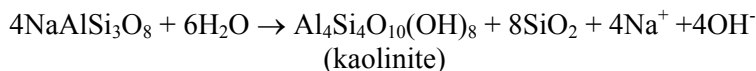
1) Orthoclase



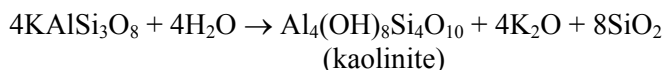
2) Orthoclase



3) Albite



4) Potassium feldspar



MINERALOGICAL TESTS

The testing of samples collected from the Borówno quarry was carried out both on fresh solid, not weathered samples, and on weathered, low-cohesion samples in a laboratory in Austria (Strasser, 2002). The petrographic study (Strasser, 2002) determined, as it is specified in the Polish geological documentation of Borówno melaphyre deposit (Szuszkiewicz i Król, 1988), that in the melaphyre there are clayey minerals and plagioclases which undergo weathering into silica and clayey minerals. The contents of plagioclases in both cases were very high in samples from Borówno

(58 to 76 % according to Austrian study and from 45 to 75 % according to the Polish study).

Samples were collected from the Borówno quarry and were designated as:

- BO-2 -brittle grains taken from key aggregate 16/22, brown, able to be ground with fingers,
- BO-3- sample taken from fresh grain,
- BO-4- sample able to be ground with fingers,
- BO-5- sample from 2nd production level, BO-6- sample from 2nd level at the road.

In brittle and weathered samples, higher percentage of clayey minerals was found, which form as a result of plagioclase disintegration. During the weathering process, clayey mineral such as kaolinite and quartz are formed from plagioclases (potassium feldspars). Hence, an average content of clayey minerals, quartz and plagioclases in weathered samples BO-4 and BO-2 equals to the average sum of clayey minerals and plagioclases in fresh samples BO-3 and BO-5.

Weathered samples:

BO-4 = 80%
BO-2 = 98%
average 89.0%

Fresh samples:

BO-5 = 89%
BO-3 = 90%
average 89.5%

Table 1 shows that montmorillonite and quartz are formed from plagioclases. In alkaline environment montmorillonite is formed, and kaolinite is formed in the acidic environment. In the weathering process, iron hydroxides are formed (such as goethite), which is not present in samples taken from the fresh rocks. The study shows that pyroxenes also disintegrate into iron hydroxides and calcite, which were not present in the fresh samples.

On the basis of tests and analysis, it may be stated that melaphyre and its minerals, used for the top layer have undergone oxidation and weathering processes that cause rapid disintegration of melaphyre and compactness of the motorway top layer.

FINAL DISCUSSION AND CONCLUSIONS

The petrographic analysis shows that melaphyre is built from the minerals, which undergo weathering and oxidation under the influence of water, temperature and air, and therefore it should not be used for top layers of roads and motorways.

In the melaphyre deposit of Borówno quarry, the intense and developed processes of weathering and oxidation take place, which is obvious, considering 21% of waste being dumped. This 21% of waste confirms the petrographic appearance of the rock in which there are minerals not resistant to weathering and oxidation processes. The rock is not weatherproof, and this is a reason of rapid disintegration of melaphyre grits contained in asphalt. The mineralogical analysis of the rock applied to asphalt mass

makes it possible to explain the reason of rapid deterioration of the new motorway surface. It can be said that the rocks containing more than 45% of minerals that are not resistant to oxidation and weathering processes despite conforming to all standard requirements should not be used for the top layers of motorways. This type of rock includes melaphyres and gabbros.

LITERATURE

- BOLEWSKI A., MANECKI A. (1993), *Mineralogia szczegółowa*, Wydawnictwo PAE, Warszawa.
- BOLEWSKI A. (1972), *Rozpoznawanie mineralów*, Wydawnictwa Geologiczne, Warszawa.
- CHRZAN T. (1997), *Autostrady i surowce do ich budowy*, Politechnika Wroclawska, Wrocław.
- KANCLER M. (2002), *Operat ewidencyjny zasobów złoza melafiru „Borówno” Kopalnia Melafiru „Borówno”*, Wałbrzych.
- KANCLER M. (2002), *Operat ewidencyjny zasobów złoza melafiru „Grzędy” Kopalnia Melafiru „Grzędy”*, Wałbrzych.
- RADZISZEWSKA-JAGOSZ E. (1982), *Opracowanie petrograficzne skal ze złoza Grzędy*, Przedsiębiorstwo Geologiczne. Wrocław.
- RUTTMAR I. (2002), *Degradacja grysów melafirowych na nawierzchni autostrady A-2*, Raport nr. 02/A2/EW/SW/IR/05 Instytut Badań Technicznych, TPA, Poznań.
- SZUSZKIEWICZ K., KRÓL J. (1988), *Dokumentacja geologiczna złoza melafiru Borówno*, Przedsiębiorstwo Geologiczne. Wrocław.
- STRASSER M. (2002), *Badania petrograficzne melafiru Czarny Bór*, Laboratorium, TPA, sprawozdanie nr.57/02, Wiedeń, Austria.
- WYSOKOWSKI A. (2001), *Orzeczenie o jakości kruszywa*, Instytut Badawczy Dróg i Mostów, Filia Wrocław, Ośrodek badań mostów betonów i kruszyw, Żmigród-Węglewo.

Polish Standards

- PN-B-11112: 1996 Kruszywa łamane do nawierzchni drogowych.
- PN-B-11110 Surowce skalne lite dla produkcji kruszyw łamanych stosowanych w budownictwie drogowym.
- PN-84/B-06714/22 Oznaczanie przyczepności do bituminów.
- PN-EN 1097-2 Badanie mechanicznych własności kruszyw.
- PN-S/96025 Badanie mieszanek mineralnych i betonów asfaltowych.
- PN-74/S-96022 Badanie masy z betonu asfaltowego przy układaniu i wykonaniu.

Chrzan T., *Wpływ składu mineralnego na stan nawierzchni autostrad*, Physicochemical Problems of Mineral Processing, 38, (2004) 341-350 (w jęz. ang.).

W artykule podano skład mineralny melafiru i omówiono trwałość zawartych w skale minerałów pod kątem wpływu czynników atmosferycznych. W wyniku analizy stwierdzono, że badany melafir zawiera ponad 50% minerałów nieodpornych na czynniki atmosferyczne. Zaistniałe szybkie zużycie powierzchni górnej warstwy autostrady wytłumaczono nadmierną zawartością minerałów szybko ulegającym przemianom w warunkach panujących na powierzchni górnej warstwy autostrady.

Zygmunt SADOWSKI, Izabela POLOWCZYK, Ewa JAŹDŹYK,
Agnieszka SZUBERT*

EFFECT OF POLYMER-SURFACTANT INTERACTION ONTO THE SPHERICAL AGGLOMERATION

Received May 20, 2004; reviewed; accepted June 30, 2004

The effect of polymer-surfactant interaction has been studied at the solid surface. The flotation tailings from KGHM Polska Miedz S.A. were used for both the adsorption and spherical agglomeration investigations. The adsorption isotherms of sodium oleate suggest a competition between polymer and surfactant. The preadsorption of polymer causes the increase of sodium oleate adsorption onto the mineral surface. The agglomeration results partially agree with the sodium oleate adsorption in the polymer presence. Polymer excess causes a decrease of agglomerate size.

Key words: polymer-surfactant interaction, spherical agglomeration, adsorption, surfactant, polymer

INTRODUCTION

The polymer-surfactant interaction occupies an increasingly important place among the available cosmetic, pharmaceutical and oil technology (Goddard and Grubert 1999, Hackey et al., Sakar and Somasundaran 2002). Water soluble polymers often interact strongly with surfactants in aqueous solution. The strong interaction of polymer-surfactant shows two break points at a surface tension curve. These points attributed to the formation of the micelles on the polymer chain, called the critical aggregation concentration (cac), and the second point corresponds to the normal micellisation of the surfactant (cmc) (Kwak 1998, Adler et al., 2000). The properties of a variety of polymer-surfactant mixtures in water have been extensively studied (Shimabayashi, et al., 1997, Langevin, 2001, Torn et al., 2003).

* Wroclaw University of Technology, Department of Chemical Engineering, Wroclaw, Poland
Zygmunt.Sadowski@pwr.wroc.pl

In contrast, there is little information about the polymer-surfactant interaction at the solid-solution interface. In the case of poly(ethylene oxide), PEO, and sodium dodecyl sulphate, SDS, the experimental data show a competitive adsorption between surfactant and polymer at the solid-water interface. For this reason the adsorption of both polymer and surfactants used to modify the surfaces to impart desired chemical properties. For instance: integration of cationic surfactant (CTAB) with polymer onto the silica surface (Shubin, 1994, Magny et al., 1994). If the surfactant was preadsorbed onto silica surface and then the polymer was added, surfactant was desorbed from the silica surface. When the surfactant polymer ratio approached 1:1 creation of the complex occurred and substantial increase in adsorption was observed (Dedinaite et al., 2000).

In this paper, we present a part of investigations of polymer-surfactant interaction onto the mineral surface and the effect of this interaction on the spherical oil agglomeration. We compare the behavior of mineral suspensions when the order, in which the surfactant and polymer were added, is changed.

EXPERIMENTAL

MATERIAL AND METHODS

The commercial polymers used in this investigation were PAM (polyacrylamide) and PEO (poly(ethylene oxide) samples, with the molecular weight of 5 000 000. PEO was obtained from BDH Chemicals Ltd., (England) and PAM was purchased from Aldrich Chemical, Inc., (USA). Both reagents were used without any further purification. Sodium oleate (SOL) was purchased from Riedel-de Haen (Germany) and it was used as received. Cationic surfactants CTAB and DDA HCl were purchase from POCH-Gliwice (Poland). n-heptane and kerosene were also obtained from POCH-Gliwice.

Adsorption isotherms were measured using the depletion methods. Approximate 1 g of mineral sample was transfer to the each of the flasks having 100 ml of aqueous SOL or polymer solution of the different initial concentration. The flasks were shaken for 24 hours. The supernatant was separated and centrifuged. The final concentration of both PEO and PAM in the supernatant was determined by complexation with tannic acid. The adsorption density was calculated from the residual concentration.

The agglomeration tests were carried out in a special designed mixing unit. In each experiment, 2 g mineral sample were used. These samples were suspended in 50 ml of sodium oleate solution. Then an appropriate 50 ml of water emulsion (n-heptane and kerosene) was added. The cationic surfactant (CTAB) was added to the emulsion as an emulsifier reagent. The mineral water suspension and emulsions were extensive mixed for 50 s. at 10000 rpm. The agglomerated material was recovered on a 100 μm sieve and dried in an oven and weighed.

RESULTS AND DISCUSSION

The adsorption of polymers and surfactants onto the solid surface should be considered a delicate balance on polymer-surfactant, polymer-solid and surfactant-solid interactions. The adsorption polymer and surfactant can be additive, cooperative and competitive (Persson et al., 2000). Adsorption isotherms, given in Figures 1 and 2, presented the effect of polymer addition onto the sodium oleate adsorption. These experiments were carried out at the constant pH (pH=8.0).

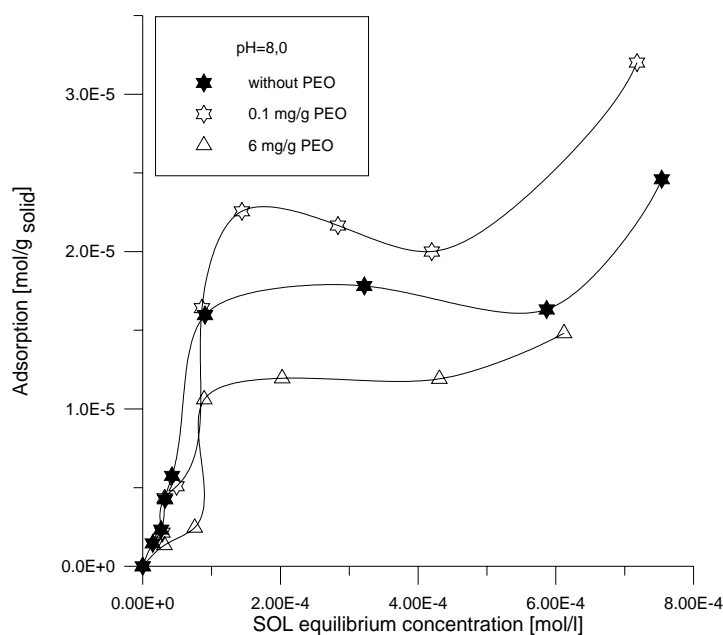


Fig. 1. Adsorption isotherms of SOL on the flotation tailings in the presence of preadsorbed PEO

One can see that preadsorption of PEO on the surface of flotation tailings caused that the adsorbed amount of SOL increased at the low concentration of preadsorbed PEO. The adsorbed amount of SOL was decreased at the high PEO concentration (6 mg/g PEO).

Fig. 2 shows the adsorption isotherms of SOL on the flotation tailings in the presence of PAM.

The SOL isotherms also showed a decrease in the presence of preadsorbed PAM. In this case, the degree of SOL adsorption depends on the quantity of preadsorbed polymer.

Effect of surfactant pretreatment on the polymer adsorption was investigated. The results of these investigations are presented in Fig. 3 and Fig. 4.

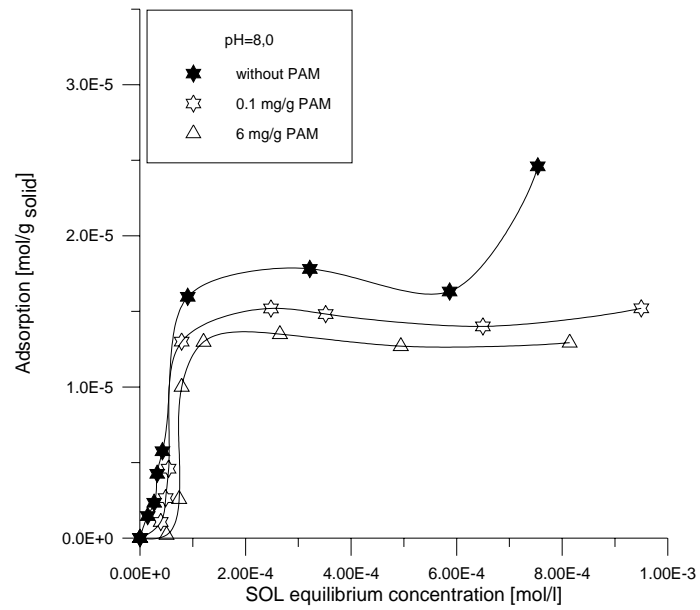


Fig. 2. Adsorption isotherms of SOL on the flotation tailings in the presence of preadsorbed PAM

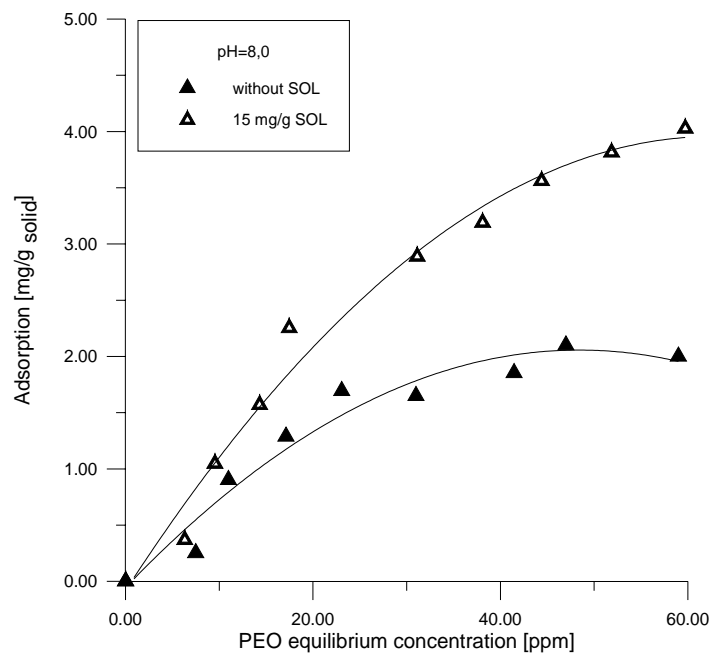


Fig. 3. Adsorption isotherms of PEO on the flotation tailings in the presence of preadsorbed SOL

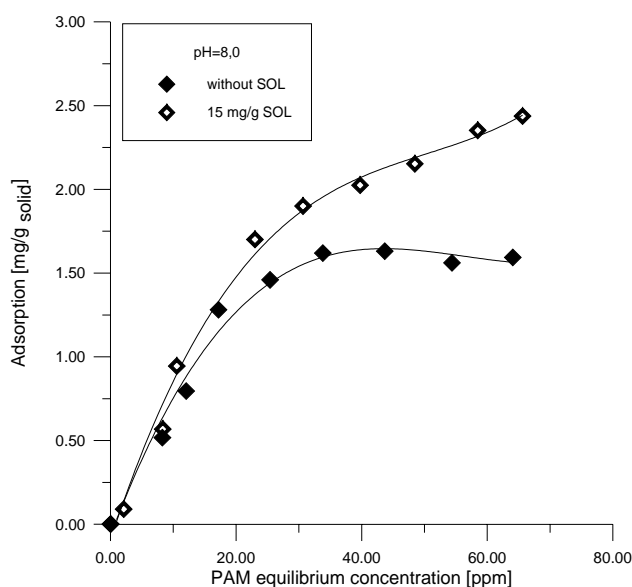


Fig. 4. Adsorption isotherms of PAM on the flotation tailings in the presence of preadsorbed SOL

Pretreatment of the mineral suspension with sodium oleate (15 mg/g) causes a substantial enlargement of the polymer adsorptions. The same behaviour was observed for the kaolin suspension with the presence of nonionic polymer (PAM-A) and three surfactant reagents (Besra et al, 2002 a,b,c).

In order to elucidate the structure and hydrophobicity of adsorbed layer on the mineral surface, the following agglomeration experiments were carried out.

Table 1. Agglomeration of flotation tailings with n-heptane and kerosene

SOL concentration (mole/l)	CTAB concentration (mole/l)	Volume of oil (ml)	Results
$2 \cdot 10^{-3}$	$2.5 \cdot 10^{-4}$	n-heptane 0.4	Flocculation
$2 \cdot 10^{-3}$	$1.75 \cdot 10^{-4}$	n-heptane 0.5	Flocculation
$2 \cdot 10^{-3}$	$2.5 \cdot 10^{-4}$	n-heptane 0.5	Spherical agglom.
$2 \cdot 10^{-3}$	$2.5 \cdot 10^{-4}$	n-heptane 0.6	Spherical agglom.
$2 \cdot 10^{-3}$	$2.5 \cdot 10^{-4}$	n-heptane 0.8	Paste
$2 \cdot 10^{-3}$	$1.75 \cdot 10^{-4}$	Kerosene 0,5	Flocculation
$2 \cdot 10^{-4}$	$2.5 \cdot 10^{-4}$	Kerosene 0.2	Spherical agglom.
$2 \cdot 10^{-3}$	$2.5 \cdot 10^{-4}$	Kerosene 0.3	Spherical agglom.
$2 \cdot 10^{-3}$	$2.5 \cdot 10^{-4}$	Kerosene 0.6	Paste

The agglomeration process may be considered as a collision between hydrophobic particle and hydrophobic oil droplet. These collisions lead to adhesion as a result of the formation of pendular oil bridges (Kawashima and Capes, 1974). A further factor

of importance for spherical agglomeration was a quantity of cationic surfactant added to the oil-water emulsion. The process pre-emulsification of the oil phase is important for spherical oil agglomeration. From both investigated cationic surfactants (CTAB and DDA HCl) dodecylammonium hydrochloride seem be much better.

Agglomerate size is controlled by the balance between agglomerate interaction determined by capillary forces and the destructive forces determined by the shear regime. The shears forces were constant at our experiments (stirrer speed and mixing time were constant). It means that size agglomeration was controlled by chemical factors.

The changes in the medium diameter of agglomerates for the polymer-surfactant systems are presented in Figure 5 and Figure 6.

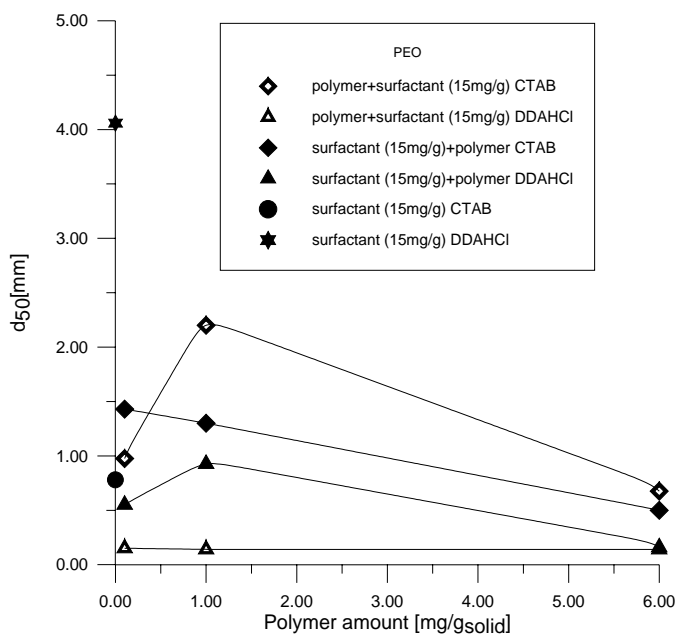


Fig. 5. Influence of surfactant-polymer interaction (SOL-PEO) on the agglomerate size

Figure 5 shows the effect of increasing polymer quantity on agglomerate diameter. Generally, the size agglomerates decrease at high polymer addition and it does not depend on the order of a polymer addition versus surfactant. The same behaviour can be observed for SOL-PAM system (Fig. 6).

From the data presented in Figs 5 and 6 can be seen that the agglomerates resulting from a polymer pretreatment of the mineral surface are large than those produced from a surfactant pretreatment. It may be tentatively concluded that for the small quantity of polymer (1.00 mg/g of powder) the preadsorption of polymers would be preferable to produce large agglomerates.

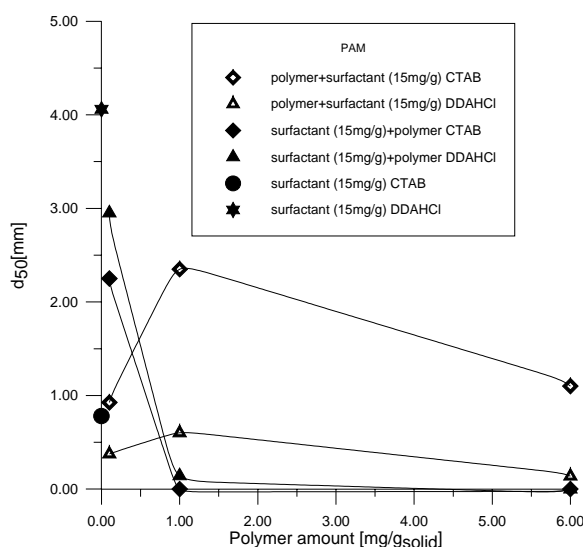


Fig. 6. Influence of surfactant-polymer interaction (SOL-PAM) on the agglomerate size

From the practical point of view (solid paste creation) the presented data represent the initial stage of developing a suitable process optimisation procedure. For this task completes a number of quantitative conclusions must be draw.

CONCLUSION

The experimental data presented here clearly demonstrate the importance of understanding the role of polymer-surfactant interaction for the spherical agglomeration of mineral suspensions. It is shown here that, it is possible to control the size of aggregates by controlling both the order and quantity of polymer and surfactant addition. The adsorption isotherm reveals the difference in the polymer-surfactant interactions onto the mineral surface. The surfactant initially binds on the mineral surface can be impeded the polymer adsorption. On the other hand, a small quantity preadsorbed PEO caused an increase of the sodium oleate adsorption. It was found that the polymer-surfactant interactions have been facilitated the spherical agglomeration process in the range of low polymer dosage.

REFERENCES

- ADLER J.J., SINGH K.P., PATIST A., RABINOVICH I.Y., SHAH O. D., MOUDGIL M. B., (2000), *Correlation of particulate dispersion stability with the strength of self-assembled surfactant films*, Langmuir, 16, 7255-7262.
- BASRA I., SENGUPTA D.K., ROY K.S., AY P., (2002a), *Studies on flocculation and dewatering of kaolin suspensions by anionic polyacrylamide flocculant in the presence of some surfactants*, Int. J. Miner. Process., 66 1-8.

- BASRA L., SENGUPTA K.D., ROY K.S., AY P., (2002b), *Polymer adsorption: its correlation with flocculation and dewatering of kaolin suspension in the presence and absence of surfactants*, Int. J. Miner. Process., 66, 183-202.
- BASRA L., SENGUPTA K.D., ROY K.S., AY P., (2002c), *Flocculation and dewatering of kaolin suspension in the presence of polyacrylamide and surfactants*, Int. J. Miner. Process., 66, 203-231.
- BREMMELE E.K., JAMESON J.G., BRIGGS S., (1999), *Forces between surfaces in the presence of a cationic polyelectrolyte and an anionic surfactant*, Colloid Surfaces, 155, 1-10.
- DEDINAITE A., CLASSON M.P., BERSTROM M., (2000), *Polyelectrolyte-surfactant layers; Adsorption of preformed aggregates versus adsorption of surfactant to preadsorbed polyelectrolyte*. Langmuir 2000, 5257-5266.
- GODDARD E. D., GRUBER V.J. (1999), *Principles of polymer science and technology in cosmetics and personal care*, Marcel Dekker Inc., New York.
- HACKLEY A.V., SOMASUNDARAN P., LEWIS A.J., (2002), *Polymers in particulate systems. Properties and applications*, Marcel Dekker Inc., New York.
- KAWASHIMA Y., CAPES E.C., (1974), *An experimental study of kinetics of spherical agglomeration in a stirred vessel*, Powder technology, 10 85-92.
- KWAK C.J., (1998), *Polymer-surfactant systems*, Marcel Dekker, Inc., New York,
- LANGVIN D., (2001), *Polyelectrolyte and surfactant mixed solution. Behavior at surfaces and in thin film*, Adv. Colloid Interface Sci., 89-90, 467-484.
- MAGNY B., ILIOPOULOS I., ZANA R., AUDEBERT R., (1994), *Mixed micelles formed by cationic surfactants and anionic hydrophobically modified polyelectrolytes*, Langmuir 10, 3180-3187.
- PERSSON B., HUGERTH A., CARAM-LELHAM N., SUNDELOF O-L., (2000), *Dextran surface-amphiphile interaction; Effect of polyelectrolyte charge density and amphiphile hydrophobicity*, Langmuir, 16. 313-137.
- SARKAR D., SOMASUNDARAN P., (2003), *Polymer surfactant kinetics using surface plasmon resonance spectroscopy dodecyltrimethylammonium chloride/polyacrylic acid system*, J. Colloid Interface Sci., 261, 197-205.
- SHIMABAYASHI S., UNO T., NAKAGAKI M., (1997), *Formation of a surface complex between polymer and surfactant and its effect on the dispersion of solid particles*, Colloid Surfaces, 123-124, 283-295.
- SHUBIN V., (1994), *Adsorption of cationic polymer onto negatively charged surfaces in the presence of anionic surfactant*, Langmuir, 10, 1093-1100.
- TORN H.L., de KEIZER A., KOOPAL K.L., LYKLEMA J., (2003), *Mixed adsorption of poly(vinylpyrrolidone) and sodium dodecylbenzenesulfonate on kaolinite*, J. Colloid Inter. Sci., 260, 1-8.

Sadowski Z., Polowczyk I., Jażdżyk E., Szubert A., *Wpływ oddziaływania polimer-surfaktant na sferyczną aglomerację*, Physicochemical Problems of Mineral Processing, 38, (2004) 351-358 (w jęz. ang.).

W pracy badano wpływ wzajemnego oddziaływania między cząsteczkami polimeru i surfaktantu, które mają miejsce na powierzchni ciała stałego, na proces adsorpcji i sferycznej aglomeracji. Badania przeprowadzono na odpadach po flotacji siarczkowych rud miedzi, otrzymanych z ZWR Lubin. Do modyfikacji powierzchni mineralnej użyto poliakryloamidu oraz politlenku etylenu oraz oleinianu sodu. Stwierdzono, na podstawie pomiarów adsorpcyjnych, że wstępna adsorpcja polimeru na powierzchni minerału poprawia wyniki adsorpcji oleinianu sodu. Wyniki wstępnych testów aglomeracyjnych wskazały, że nafta nadaje się lepiej jako ciecz apolarna niż n-heptan. Do emulgacji fazy olejowej lepiej stosować DDA HCl niż CTAB, Wyniki sferycznej aglomeracji w części są zgodne z wynikami adsorpcji. Nadmiar użytego polimeru zmniejsza w wyraźny sposób średnią wielkość powstających sferycznych aglomeratów.

Our books are available in the following bookshops:
„Politechnika”, Wybrzeże Wyspiańskiego 27,
50-370 Wrocław, budynek A-1 PWr, tel. (071) 320 25 34
„Tech”, plac Grunwaldzki 13,
50-377 Wrocław, budynek D-1 PWr, tel. (071) 320 32 52
Orders can also be sent by post.

ISSN 0137-1282
Physicochemical Problems of Mineral Processing, 38 (2004)